Making Gold from Waste:
Catalytically-active Inclusion Bodies as biologically-produced Immobilizates for Biocatalysis

Inaugural-Dissertation

zur Erlangung des Doktorgrades
der Mathematisch-Naturwissenschaftlichen Fakultät
der Heinrich-Heine-Universität Düsseldorf

vorgelegt von

Vera D. Jäger
aus Krefeld

Jülich, Februar 2019

aus dem Institut für Molekulare Enzymtechnologie
der Heinrich-Heine-Universität Düsseldorf

Gedruckt mit Genehmigung der
Mathematisch-Naturwissenschaftlichen Fakultät der
Heinrich-Heine-Universität Düsseldorf

Referent: Prof. Dr. Karl-Erich Jaeger
Korreferentin: Prof. Dr. Martina Pohl
Tag der mündlichen Prüfung: 3.6.2019

It is known that knowledge is power,
and power is energy,
and energy is matter,
and matter is mass,

and therefore, large accumulations of knowledge distort time and space.

Sir Terry Pratchett, from 'The Science of Discworld'

for Lisa
my sister, my friend, my everyday heroine

I. ABSTRACT

The awareness of today's humanity about overpopulation and climate change along with rising economic standards have prompted the promotion of more environmentally benign processes in modern industry. Biocatalysis, as a 'green' alternative, has gained rising popularity during the last decades, not least due to the high chemo-, regio-, and stereoselectivity of biocatalysts, especially for the production of fine chemicals. On the other hand, the classical biotechnology often needs harsh reaction conditions such as high temperature, extreme pH values, or the use of organic solvents. In many cases this results in the rapid inactivation of the biocatalyst, which however can be partly compensated for by enzyme immobilization. Enzyme immobilization, e.g. classically defined as binding to, or encapsulation of enzymes in carrier materials, requires tedious and thereby expensive purification and immobilization steps. Therefore, simple, generic, and if possible, carrier-free methods for enzyme immobilization are needed to fulfil the industry's need for stable, cheap, yet pure enzyme preparations.

The here extensively characterized catalytically-active inclusion bodies (CatIBs), as biologically produced, carrier-free immobilizates, fulfil those requirements. CatIB-formation is achieved by genetic fusion of a coiled-coil domain to a target enzyme/ protein, which induces the formation of intracellular proteinaceous aggregates, so-called inclusion bodies (IBs), which retain a certain degree of activity. The production of CatIBs is remarkably easy and economical, since after production in the well-established production host *Escherichia coli* and subsequent cell lysis, only one washing step is needed. The result is an immobilized, cell-free biocatalyst, which can directly be applied for biocatalysis.

In this thesis a 'toolbox' of fusion proteins consisting of ten different target enzymes and proteins, as well as two coiled-coil domains, as aggregation-inducing tag, was established. Target enzymes were chosen to cover a broad range of different enzyme classes of variable complexity. Target enzymes, that were repeatedly used throughout this thesis to address certain issues of the CatIB strategy, were e.g. the benzaldehyde lyase of *Pseudomonas fluorescens* (*Pf*BAL), the *Ralstonia* sp. alcohol dehydrogenase (*R*ADH), and the constitutive lysine decarboxylase of *Escherichia coli* (*Ec*LDC). For all ten targets, catalytically-active or functional inclusion bodies (CatIBs or FIBs) could be obtained after optimization. Gene fusions were designed to investigate the potential for optimization of the CatIB-formation process and to systematically address the biotechnological relevant properties of CatIBs. As optimization approaches, the presence/absence of linker polypeptides, the site of coiled-coil fusion (N- *vs*. C-terminal), and the use of alternative coiled-coil domains were identified. In particular, the use of different coiled-coil domains resulted in the formation of morphologically distinct CatIBs/FIBs, being either of compact or diffuse nature. The latter property seems to be correlated with residual activity of the respective CatIB preparation, with diffuse CatIBs

showing much higher residual activity than their corresponding compact counterparts. Utilizing the toolbox dataset, structure-function relations were studied to address the predictability of the CatIB/FIB strategy, revealing that sequence and structure-based computational methods can be used to predict the aggregation propensity of a given target.

The influence of the expression conditions on CatIB production was studied, demonstrating the robustness of the current production method, while suggesting ways for CatIB-yield optimization, i.e. by pH control, reduction of expression temperature and cultivation time. The stability and activity of *Pf*BAL-CatIBs under different reaction conditions was explored, which revealed that, (i) regardless of the employed coiled-coiled domain, CatIBs are stabilized compared to the soluble purified enzyme in aqueous buffer and (ii) depending on the employed coiled-coil domain, CatIBs can be tailored for the use in biphasic or monophasic reaction systems.

The biotechnological application of *Ec*LDC-CatIBs for the production of 1,5-diaminopentane (DAP), an important precursor for the production of bio-based polyamides, was demonstrated, resulting in space-time yields for DAP production that were competitive to the best described processes from literature.

Last but not least, the CatIB strategy was extended to the co-immobilization of multiple proteins and enzymes to create Co-FIBs and Co-CatIBs. Co-FIBs of the fluorescent reporter proteins YFP and mCherry were utilized to demonstrate co-localization of two proteins within IB particles. Finally, a two-enzyme, one-pot cascade for the production of (1*R*,2*R*)-1-phenylpropane-1,2-diol, an important precursor for the calcium channel blocker diltiazem, was realized with (Co-)CatIBs of *Pf*BAL and *R*ADH, again demonstrating the competitiveness of CatIB (co-)immobilizates. The improved stability of the (Co-)CatIBs, compared to the soluble purified enzymes, suggests that the use of CatIBs and Co-CatIBs can be beneficial for the realization of cascade reactions, i.e. under conditions where enzyme stability is a limiting issue.

In conclusion, the results presented in this thesis advance our understanding of the CatIB/IB formation process and reveal the generic applicability of the CatIB-immobilization strategy, rendering CatIBs a promising, new enzyme preparation for application in synthetic chemistry and biocatalysis.

II. ZUSAMMENFASSUNG

Das heutige Bewusstsein einer stetig wachsenden Bevölkerung über Klimawandel und steigende ökonomische Anforderungen begünstigt die Förderung umwelt-schonenderer Prozesse in der modernen Industrie. Die Biokatalyse als „grüne“ Alternative erlangt, nicht zuletzt wegen ihrer hohen Chemo-, Regio- und Stereoselektivität, besonders in der Produktion von Feinchemikalien, zunehmende Popularität. Andererseits erfordert die klassische Biotechnologie oft schwierige Reaktionsbedingungen, wie hohe Temperaturen, extreme pH-Werte oder die Verwendung organischer Lösemittel. Dies resultiert häufig in einer Inaktivierung der Biokatalysatoren, was jedoch durch Enzymimmobilisierung teilweise kompensiert werden kann. Enzymimmobilisierung, also die Bindung an oder der Einschluss des Enzyms in Trägermaterialien, bedarf aufwendiger und dadurch teurer Reinigungs-, und Immobilisierungsschritte. Aus diesem Grund werden einfache, universelle und nach Möglichkeit trägerfreie Methoden zur Enzymimmobilisierung benötigt, um dem industriellen Anspruch nach stabilen, einfach zu produzierenden, sauberen Enzympräparationen gerecht zu werden.

Die in dieser Arbeit intensiv charakterisierten katalytisch aktiven *inclusion bodies* (CatIBs), als biologisch produzierte, trägerfreie Immobilisate, erfüllen eben diese Ansprüche. CatIB-Bildung basiert auf der Fusion einer *coiled-coil* Domäne an ein Zielenzym/-protein, wodurch die Bildung intrazellulärer Proteinaggregate, sogenannter *inclusion bodies* (IBs) induziert wird, die jedoch einen gewissen Anteil an Aktivität besitzen. Die Herstellung von CatIBs ist ausgesprochen einfach und ökonomisch, da nach der Produktion in *Escherichia coli* und dem anschließenden Zellaufschluss nur ein Waschschritt notwendig ist. Als Ergebnis wird ein immobilisierter, zellfreier Biokatalysator erhalten, der direkt für die Biokatalyse eingesetzt werden kann.

In dieser Arbeit wurde eine „*Toolbox*“, von Fusionsproteinen, bestehend aus zehn unterschiedlichen Zielenzymen und -proteinen, sowie zwei *coiled-coil* Domänen als Aggregationsvermittler, etabliert, mit denen eine große Bandbreite verschiedener Enzymklassen mit variierenden Komplexitäten abgedeckt werden konnte. Zielenzyme, mit deren Hilfe bestimmte Fragen der CatIB Methode untersucht wurden, waren z.B. die Benzaldehydlyase aus *Pseudomonas fluorescens* (*Pf*BAL), die Alkoholdehydrogenase aus *Ralstonia* sp. (*R*ADH) und die konstitutiv exprimierte Lysin-decarboxylase aus *Escherichia coli* (*Ec*LDC). Für alle Zielenzyme/-proteine konnten nach Optimierung katalytisch aktive oder funktionale *inclusion bodies* (CatIBs oder FIBs) gewonnen werden. Genfusionen wurden so konzipiert, dass das Optimierungspotential der CatIB Bildung ausgeschöpft und biotechnologisch relevante Eigenschaften der CatIBs systematisch überprüft werden konnten. Als Optimierungswege wurden die An- bzw. Abwesenheit eines Polypeptidlinkers, die Position der *coiled-coil* Fusion (N- *vs*. C-terminal) sowie die Verwendung alternativer *coiled-coil* Domänen identifiziert. Insbesondere die Verwendung alternativer *coiled-coil* Domänen resultierte in der Bildung

morphologisch unterschiedlicher CatIBs/FIBs, die entweder eine kompakte oder diffuse Natur aufwiesen. Diese Eigenschaft scheint zudem mit der Restaktivität der jeweiligen CatIB Präparation zu korrelieren, wobei diffuse CatIBs eine deutlich höhere Restaktivität aufwiesen, als die entsprechenden kompakten CatIBs. Durch Verwendung der CatIB/FIB Datensätze konnten Beziehungen zwischen Struktur und Funktion untersucht werden, mit denen die Vorhersagbarkeit der CatIB/FIB Methode adressiert wurde. Diese Analyse legen nahe, dass aufgrund von sequenz- und struktur-basierten, computergestützten Berechnungen die Aggregationstendenz eines jeweiligen Zielenzyms/-proteins prognostiziert werden kann.

Untersuchungen zum Einfluss der Expressionsbedingungen auf die CatIB Produktion demonstrierten einerseits, wie robust das aktuelle Verfahren ist, zeigten jedoch gleichzeitig Optimierungsmöglichkeiten für eine höhere CatIB Ausbeute auf; wie pH Kontrolle oder Verringerung von Expressionstemperatur und -zeit. Des Weiteren wurde die Stabilität und Aktivität von *Pf*BAL-CatIBs unter verschiedenen Reaktionsbedingungen untersucht. So wurde nachgewiesen, dass (i) unabhängig von der *coiled-coil* Domäne CatIBs in wässrigem Puffer stabiler sind als die entsprechenden löslichen Enzyme, und dass (ii) CatIBs, abhängig von der verwendeten *coiled-coil* Domäne, für den Einsatz in Ein- oder Zweiphasensystemen angepasst werden können.

Der biotechnologische Einsatz von *Ec*LDC-CatIBs zur Produktion von 1,5-Diaminopentan (DAP), einem wichtigen Baustein zur Produktion von Biopolyamiden, resultierte in Raum-Zeit-Ausbeuten konkurrenzfähig zu den besten literaturbeschriebenen Prozessen.

Schließlich wurde die CatIB Methode um die Möglichkeit der Co-Immobilisierung mehrerer Proteine und Enzyme in Co-FIBs und Co-CatIBs erweitert. Dazu wurde mit Co-FIBs der Fluoreszenzreporterproteine YFP und mCherry die Co-Lokalisierung zweier Proteine in IB Partikeln demonstriert. Schließlich wurde mit (Co-)CatIBs von *Pf*BAL und *R*ADH eine simultane Zweienzym-Eintopf-Synthese zur Produktion von (1*R*,2*R*)-1-phenylpropan-1,2-diol, einer wichtigen Vorstufe für Arzneimittel, entwickelt. Dabei konnte die Konkurrenzfähigkeit von CatIB-basierten (Co-)Aggregaten erneut demonstriert werden. Die erhöhte Stabilität von (Co-)CatIBs im Vergleich zu löslichen gereinigten Enzymen, deutet darauf hin, dass unter Bedingungen, bei denen Enzymstabilität ein limitierender Faktor ist, die Verwendung von CatIBs und Co-CatIBs vorteilhaft für die Realisierung von Reaktionskaskaden sein kann.

Zusammenfassend konnten aufgrund der in dieser Arbeit erzielten Ergebnisse Fortschritte im Verständnis des CatIB/IB Bildungsprozesses erlangt, und gleichzeitig die allgemeine Eignung der CatIB-Immobilisierungsmethode nachgewiesen werden. Somit stellen CatIBs eine vielversprechende, neue Methode zur Herstellung von Enzymimmobilisaten, für die Anwendung in der synthetischen Chemie und Biokatalyse, dar.

III. TABLE OF CONTENTS

I. Abstract I
II. Zusammenfassung III
III. Table of Contents V
IV. Conference Contributions VII
a. Poster Presentations VII
b. Oral Presentations VIII
V. List of Publications IX
VI. Abbreviations X
VII. List of Figures XII
VIII. List of Tables XIII
1 Introduction 1
1.1 Biocatalysis and biotechnology 1
1.1.1 Historical summary and definition 1
1.1.2 Advantages and drawbacks of biocatalysts 3
1.2 Immobilization of enzymes for biotechnological application 6
1.2.1 Immobilization on a carrier 7
1.2.2 Encapsulation or entrapment in a carrier 8
1.2.3 Bioconjugation 9
1.3 Catalytically-active Inclusion Bodies 11
1.3.1 The changing perception of inclusion bodies 11
1.3.2 Inclusion bodies allow for diverse applications 13
1.3.3 Immobilization *via* self-assembling protein tags 15
1.3.4 Additional approaches to produce biocatalytic inclusions 18
1.3.5 Coiled-coil domains as IB-inducing tag 20
1.3.5.1 Design of superhelical structures in coiled-coil domains 20
1.3.5.2 TDoT and 3HAMP as coiled-coil domains for CatIB-formations 22
1.4 Targets used for research on CatIBs 24
1.4.1 Fluorescent proteins 24
1.4.1.1 Yellow fluorescent protein from *Aequorea victoria* 25
1.4.1.2 mCherry from *Discosoma striata* 25
1.4.2 Alcohol dehydrogenases 25
1.4.2.1 Alcohol dehydrogenase from *Ralstonia* sp 26
1.4.2.2 Alcohol dehydrogenase from *Lactobacillus brevis* 26
1.4.3 Thiamine diphosphate-dependent decarboxylases 26
1.4.3.1 Benzaldehyde lyase from *Pseudomonas fluorescens* 27
1.4.3.2 Benzoylformate decarboxylase from *Pseudomonas putida* 28
1.4.4 Lysine decarboxylase from *Escherichia coli* 28
1.5 Scope and outline of the thesis 30
2 Results 31
2.1 Publication I 33
2.1.1 Publication I: Supporting Information 53
2.2 Publication II 63
2.2.1 Publication II: Supporting Information 79
2.3 Publication III 81
2.3.1 Publication III: Supporting Information 93
2.4 Publication IV 101
2.4.1 Publication IV: Supporting Information 113

2.5 Publication V 117
2.5.1 Publication V: Supporting Information 132
2.6 Publication VI 137
2.6.1 Publication VI: Supporting Information 149
3 General Discussion 159
3.1 General set-up of a 'CatIB toolbox' 160
3.1.1 Strategies for CatIB optimization 161
3.1.2 Optimizing the expression conditions for CatIBs and FIBs 163
3.2 Understanding IB formation - lessons learned from CatIBs and FIBs 166
3.2.1 Morphologically-distinct CatIBs/FIBs are formed depending on the fused aggregation-inducing tag 167
3.2.2 3HAMP and TDoT CatIBs possess distinct functional properties 168
3.2.3 CatIB-formation results in activation of the protein quality control machinery 170
3.2.4 Two proteins can be co-localized within the same IB particles 171
3.2.5 Influence of the surface hydrophobicity of the target on (Cat)IB formation 173
3.2.6 A unified model for IB and CatIB formation? 175
3.3 Biotechnological application of CatIBs 178
3.3.1 Stability of *Pf*BAL CatIBs in different reaction systems 178
3.3.2 *Ec*LDC CatIBs allow the competitive production of 1,5-diamino-pentane 181
3.3.3 Realization of a two-enzyme cascade reaction with CatIBs and Co-CatIBs 183
3.4 CatIBs in comparison to other immobilization strategies 187
3.4.1 CatIBs produced by fusion of small, artificial peptides or aggregation-prone proteins 187
3.4.2 CatIBs, CLEAs, and HaloTag®-immobilizates: similarities and differences 188
3.4.3 Immobilization of multiple enzymes for cascades 190
3.5 Conclusions: CatIBs as a new method for enzyme immobilization 193
3.5.1 Evaluation of CatIBs under economical aspects 194
3.6 The future of CatIBs 196
4 References 199
5 Appendix 211
5.1 Additional information to support the General Discussion 211
5.2 DNA and amino acid sequence of all fusion constructs 215
6 Acknowledgement 227
7 Erklärung 229

IV. CONFERENCE CONTRIBUTIONS

a. Poster Presentations

V. D. Jäger, R. Kloss, K.-E. Jaeger, M. Pohl, and U. Krauss. Catalytically-active inclusion bodies – promising, novel biomaterials for bioeconomy. *Gordon Research Conference - Synthetic Biology*. Waterville Valley, NH, USA. **2019**.

R. Lamm, **V. D. Jäger**, R. Kloss, M. Pohl, U. Krauss, K.-E. Jäger, and J. Büchs. Catalytically-active inclusion bodies: Application of high-throughput cultivation technologies to study innovative enzyme aggregates. *DECHEMA-Himmelfahrtstagung*, Madgeburg, Germany. **2018**.

V. D. Jäger, S. Longerich, R. Kloß, A. Grünberger, M. Pohl, K.-E. Jaeger, and U. Krauss. Towards the realization of an enzyme cascade in Catalytically-active Inclusion Bodies. *13th International Symposium on Biocatalysis and Biotransformations, Biotrans*. Budapest, Hungary. **2017**.

R. Lamm, **V. D. Jäger**, R. Kloss, M. Pohl, U. Krauss, K.-E. Jäger, and J. Büchs. Catalytically-active inclusion bodies: Application of high-throughput cultivation technologies to study innovative enzyme aggregates. *HTPD: High-Throughput Process Development Conference*. Toledo, Spain. **2017**.

V. D. Jäger, R. Kloß, M. Diener, M. Dietrich, M. Pohl, K.E. Jaeger, and U. Krauss. Catalytically-active Inclusion Bodies (CatIBs) – Biologically-produced enzyme immobilizates. *"Future Bioeconomy" PhD-Day NRW*, Düsseldorf, Germany. **2016**

V. D. Jäger, R. Kloß, M. Diener, M. Dietrich, M. Pohl, K.-E. Jaeger, and U. Krauss. Catalytically-active Inclusion Bodies (CatIBs) New Carrier-free Enzyme Immobilizates for Biocatalysis. *Biocat*. Hamburg, Germany. **2016**. (awarded with poster prize).

R. Kloß, **V. D. Jäger**, M. Diener, U. Krauß, and M. Pohl. Catalytically active Inclusion Bodies: A new Carrier-free Enzyme Immobilisation Method. *ProcessNet*. Aachen, Germany. **2016**. (awarded with poster prize).

b. Oral Presentations

V. D. Jäger[#], R. Kloß, R. Lamm, J. Büchs, M. Pohl, K.-E. Jaeger, and U. Krauss. CatIBs - Catalytically active inclusion bodies: New carrier-free enzyme immobilizates for biocatalysis. *4th BioSC Forum*. Köln, Germany. **2017**.

V. D. Jäger, R. Kloß, M. Diener, B. Kopka, M. Kaschner, T. Fettweiss, O. Schillinger, A. Fulton, A. Stadler, B. Strodel, M. Pohl, K.-E. Jaeger, and Ulrich Krauss[#]. Artificial multi-domain proteins – engineering enzyme function, stability and immobilization. *13th International Symposium on Biocatalysis and Biotransformations, Biotrans*. Budapest, Hungary. **2017**.

R. Kloß[#], M. Limberg, **V. D. Jäger**, U. Mackfeld, T. Karmainski, A. Grünberger, U. Krauß, and M. Pohl. Catalytically active inclusion bodies: A novel carrier-free enzyme immobilisation method. *13th International Symposium on Biocatalysis and Biotransformations, Biotrans*. Budapest, Hungary. **2017**.

R. Kloß[#], **V. D. Jäger**, M. Diener, U. Krauß, and M. Pohl. Catalytically active Inclusion Bodies: A new Carrier-free Enzyme Immobilisation Method. *ProcessNet*. Aachen, Germany. **2016**.

D. Rother[#], D. Johannes, R. Kloß, **V. D. Jäger**, U. Krauß, and M. Pohl. Enzyme toolboxes & reaction engineering – Solutions for applied biocatalysis. *ProcessNet*. Aachen, Germany. **2016**.

[#]presenting author

V. LIST OF PUBLICATIONS

U. Krauss, **V. D. Jäger**, M. Diener, M. Pohl, and K.-E. Jaeger. Catalytically-active inclusion bodies - Carrier-free protein immobilizates for application in biotechnology and biomedicine. *Journal of Biotechnology*. **2017**. 258: 136-147.

doi: 10.1016/j.jbiotec.2017.04.033

R. Kloss*, M. H. Limberg*, U. Mackfeld, D. Hahn, A. Grünberger, **V. D. Jäger**, U. Krauss, M. Oldiges, and M. Pohl. Catalytically active inclusion bodies of *L*-lysine decarboxylase from *E. coli* for 1,5-diaminopentane production. *Scientific Reports*. **2018**. 8(1):5856.

doi: 10.1038/s41598-018-24070-2, *both authors contributed equally

V. D. Jäger, R. Lamm, R. Kloß, E. Kaganovitch, A. Grünberger, M. Pohl, J. Büchs, K.-E. Jaeger, and U. Krauss. A synthetic reaction cascade implemented by co-localization of two proteins within catalytically-active inclusion bodies. *ACS Synthetic Biology*. **2018**. 7(9): 2282-2295

doi: 10.1021/acssynbio.8b00274

R. Kloss, T. Karmainski, **V. D. Jäger**, D. Hahn, A. Grünberger, M. Baumgart, U. Krauss, K.-E. Jaeger, W. Wiechert, and M. Pohl. Tailor-made catalytically active inclusion bodies for different applications in biocatalysis. *Catalysis Science and Technology*. **2018.** 8(22):5816-5826

doi: 10.1039/C8CY01891J

V. D. Jäger*, R. Kloss*, A. Grünberger, S. Seide, D. Hahn, T. Karmainski, M. Piqueray, J. Embruch, S. Longerich, U. Mackfeld, K.-E. Jaeger, W. Wiechert, M. Pohl, and U. Krauss. Tailoring the properties of (catalytically)-active inclusion bodies. *Microbial Cell Factories*. **2019.** 18(1):33

doi: 10.1186/s12934-019-1081-5, *both authors contributed equally

V.D. Jäger, M. Piquaray, S. Seide, M. Pohl, W. Wiechert, K.-E. Jaeger, and U. Krauss. An Enzymatic 2-Step Cofactor and Co-Product Recycling Cascade towards a Chiral 1,2-Diol. Part II: Catalytically Active Inclusion Bodies. *Advanced Synthesis and Catalysis*. **2019.** 361(11).

doi: 10.1002/adsc.201900189

R. Lamm, **V.D. Jäger**, B. Heyman, C. Berg, C. Cürten, U. Krauss, K.-E. Jaeger, and J. Büchs. Crucial cultivation parameters for fluorescent inclusion body production induced by a tetrameric coiled-coil domain. *Manuscript in preparation*.

VI. ABBREVIATIONS

3HAMP	part of the receptor protein Aer2 from *Pseudomonas aeruginosa*
6-APA	6-aminopenicillanic acid
aa	amino acid
ADH	alcohol dehydrogenase
*At*HNL	hydroxy nitrile lyase from *Arabidopsis thaliana*
ATP	adenosine triphosphate
BCoA	Burtyryl-CoA
BLAST	Basic Local Alignment Search Tool
*Bs*LA	lipase A from *B. subtilis* lipase A
BZ	bait zipper
bzw	beziehungsweise
CadA	see LDCi
CatIB	catalytically-active inclusion body
CBD	cellulose binding domain
CCE	crude cell extract
CD	circular dichroism
CLEA	cross-linked enzyme aggregate
CLEC	cross-linked enzyme crystal
CLIB	crosslinked inclusion body
Co-CatIBs	co-immobilized enzymes in CatIBs
Co-FIBs	co-immobilized proteins in FIBs
CPME	cyclopentyl methyl ether
DAP	1,5-diaminopentane or cadaverine
DMBA	3,5-dimethoxybenzaldehyde
DMSO	dimethyl sulfoxide
DNA	deoxyribonucleic acid
DPA	dextran polyaldehyde
*Ds*Red	red fluorescent protein from *Discosoma striata*
EC	enzyme classes
*Ec*LDC	lysine decarboxylase from *E. coli*
*Ec*MenD	2-succinyl-5-enol-pyruvyl-6-hydroxy-3-cyclohexene-1-carboxylate synthase from *E. coli*
e.g.	*exempli gratia*
EG-NHS	ethylene glycol-bis [succinic acid N-hydroxy succinimide]
EMR	enzyme membrane reactor
EPA	Environmental Protection Agency
et al.	*et aliae/alii*
EYFP	enhanced YFP
FbFP	FMN-binding fluorescent protein
FIB	fluorescent inclusion bodies
FP	fluorescent proteins
FRET	Förster resonance energy transfer
FTIR	Fourier-transform infrared spectroscopy
GFP	green fluorescent protein from *Aequorea Victoria*
GLA	glutaraldehyde
GMO	genetically modified organism
GRAS	generally regarded as safe
HAMP	histidine kinases, adenylyl cyclases, methyl-accepting chemotaxis proteins, and phosphatases
HCoA	hydroxybutyryl-CoA
HPP	(*R*)-2-hydroxy-1-phenylpropanone
HTP	high-throughput
IB	inclusion body
Ibp	inclusion body associated protein
i.e.	*id est*
IUPAC	International Union of Pure and Applied Chemistry
k_{cat}	turnover number
*Lb*ADH	alcohol dehydrogenase from *Lactobacillus brevis*
LDC	lysine decarboxylase
LDCc	constitutive LDC from *E. coli*
LDCi,	inducible LDC from *E. coli*, also called CadA
LZ	leucine zipper
mCherry	FP from *Discosoma striata*
MOPS	3-(*N*-morpholino)propanesulfonic acid
mRFP	monomeric red fluorescent protein from *Discosoma striata*
MTBE	methyl *tert*-butyl ether
MTP	microtiter plate
NAD(P)H/$^+$	cofactor nicotinamide adenine dinucleotide (phosphate)
n.d.	not determined
n.i.	no information provided
NMR	nuclear magnetic resonance
Omp	outer membrane protein
P	pellet
P(3HB)	poly(3-hydroxybutyrate)
PEG	polyethylene glycol
*Pf*BAL	benzaldehyde lyase from *Pseudomonas fluorescens*
pH	negative decadic logarithm of the concentration of protons
PHA	polyhydroxyalcanoate
PLP	pyridoxal-5'-phosphate
pNIPAM	poly(*N*-isopropylacrylamide)

PP	pyrophosphate domain
*Pp*BFD	benzoylformate decarboxylase from *Pseudomonas putida*
PPD	(1*R*,2*R*)-1-phenylpropan-1,2-diol
P_{T7}	T7 promotor
PYR	pyrimidine domain
PZ	prey zipper
R^2	coefficient of determination values
*R*ADH	alcohol dehydrogenase from *Ralstonia* sp. DSM 6428
RBS	ribosome binding site
rpm	revolutions per minute
SASA	solvent accessible surface area
SDR	short-chain dehydrogenase/reductase
SDS-PAGE	sodiumdodecylsufate polyacrylamide gel electrophoresis
SEM	scanning electron microscopy
sHsps	small heat shock proteins
SN	supernatant
STY	space time yield
TB	terrific broth
TDoT	tetramerization domain of the cell-surface protein tetrabrachion from *Staphylothermus marinus*
TEA	triethanolamine
TEED	Thiamine diphosphate dependent Enzyme Engineering Database
ThDP	thiamin diphosphate
TMBZ	(*R*)-(3,3',5,5')-tetramethoxybenzoin
U	unit
UV	ultraviolet
vis	visible
vs.	*versus*
v/v	volume per volume
YFP	yellow fluorescent protein from *Aequorea victoria*

VII. List of Figures

Figure 1-1 A selection of important mile-stones in biocatalysis from 4000 BC until today 2
Figure 1-2 The 24 principles of green engineering and green chemistry 4
Figure 1-3 Different strategies of enzyme immobilization 6
Figure 1-4 Protein aggregation within bacterial cells 12
Figure 1-5 Protein extraction from (active) IBs 14
Figure 1-6 Different approaches to produce *in situ* protein inclusions 19
Figure 1-7 Structure of coiled-coils to illustrate the heptad repeat 21
Figure 1-8 Superhelical structures of the coiled-coil domains 23
Figure 1-9 Chromophores of (a): YFP and (b): mCherry 25
Figure 1-10 General mechanism proposed for ThDP-dependent lyases 27
Figure 1-11 Mechanism of the PLP-dependent A-amino acid decarboxylation 29

Figure 3-1 Target proteins used to set-up the 'CatIB toolbox', shown in order of increasing complexity .161
Figure 3-2 Strategies for the optimization of CatIB-formation 162
Figure 3-3 Cultivation of *E. coli* BL21(DE3) producing TDoT-YFP FIBs (left) or soluble YFP (right) at different temperatures 165
Figure 3-4 (Fluorescence) Microscopy (a) and SEM (b) images illustrating the formation of FIBS 168
Figure 3-5 Comparison of TDoT (top) and 3HAMP (bottom) fusions with regard to CatIB/FIB-formation efficiency 169
Figure 3-6 SDS-PAGE analysis of contaminant bands in TDoT-*Pf*BAL CatIB (left), soluble *Pf*BAL (right), and TDoT-*Pf*BAL CatIBs preparations 170
Figure 3-7 Co-localization of TDoT-YFP and TDoT-mCherry in FIBs 171
Figure 3-8 Computational analysis of (a, b) target protein amino acid sequences and (c, d) structural determinants of CatIB/FIB formation 174
Figure 3-9 Different theories about CatIB formation 176
Figure 3-10 Two-enzyme, one-pot cascade reaction 184
Figure 3-11 PPD production observed in the two-enzyme, one-pot cascade reactions 185
Figure 3-12 Production of CatIBs by a simple standardized protocol 193

Figure 4-1 Microscopy images illustrating the exceptions from the diffuse/compact morphology distinction between 3HAMP and TDoT CatIBs 211
Figure 4-2 FIB-formation efficiency of Co-FIBs A-D and the single TDoT FIBs of YFP and mCherry 212
Figure 4-3 Hydrophobic patch analysis of TDoT (left, PDB: 1FE6) and 3HAMP (right PDB: 3LN3) 212
Figure 4-4 Time course of co-expression and co-localization of TDoT-L-YFP and TDoT-mCherry in *E. coli* 213

VIII. List of Tables

Table 1-1 Overview of different fusion-tags used for induction of CatIB formation 17

Table 3-1 Comparison of activity, yield, and composition of different Co-CatIBs 172
Table 3-2 Half-lives [h] of *Pf*BAL CatIBs and purified soluble *Pf*BAL determined under different conditions 179
Table 3-3 Comparison of *Pf*BAL CatIBs to different *Pf*BAL immobilizates from literature 180
Table 3-4 Comparison of 1,5-diaminopentane production by CatIBs and other approaches from literature 182
Table 3-5 Half-lives [h] of different *Pf*BAL/*R*ADH (Co-)CatIBs and of the corresponding purified soluble enzymes within the two enzyme, one-pot cascade reactions under various conditions 186
Table 3-6 Comparison of residual activities of CatIBs obtained by fusion of different CatIB-formation inducing tags. 188
Table 3-7 Comparison of selected CLEA and HaloTag® immobilized enzymes in comparison to CatIBs. 189
Table 3-8 Examples of different strategies to co-immobilize enzymes in comparison to Co-CatIBs. 192
Table 3-9 Calculation of activity yield and production costs for *Pf*BAL and *R*ADH when produced as TDoT and 3HAMP CatIBs or as soluble enzyme 195

Table 4-1 Example calculation of activity yield and production costs 214

1 Chapter 1 Introduction

1.1 Biocatalysis and biotechnology

1.1.1 Historical summary and definition

Biocatalysis has a long tradition throughout history. Enzymes are the oldest industrial catalysts, even though unknown for most of the time (Figure 1-1): Already over 6000 years ago, in ancient Egypt and Mesopotamia, microorganisms like yeast were used for bread baking and beer brewing [1]. Yet, the period between first usage and scientific definition was extreme: Only 184 years ago, the word 'catalyst', derived from the ancient greek word 'κατάλυσις', meaning 'to annul', was coined by Berzelius [2, 3]. Not long after, in 1857, Pasteur identified microorganisms as the origin of lactic acid fermentation, broadly suggesting that all fermentative processes are caused by microorganisms [1, 4], while in 1878 Kühne proposed the term 'enzyme', from the ancient greek words 'ἐν' and 'ζύμη', meaning 'in the yeast' [5]. Shortly after, in 1897, Buchner observed that not only whole-cells, but enzymes alone have catalytic properties, a discovery, for which he was awarded with the Nobel prize in Chemistry in 1907 [6]. Around this time the so-called first wave of biocatalysis, as e.g. used by Bornscheuer *et al.*, began [7].

Despite late discovery, catalysis has become one of the most important processes in today's industry, where worldwide about 85-90% of all chemical processes are performed catalytically [8], with a global demand forecasted to US$ 34.3 billion until 2024 [9]. The deciphering of the DNA-structure in 1953 by Franklin, Wilkins, Watson, and Crick [10] as well as the invention of *in vitro* DNA recombination techniques and the construction of plasmid vectors in 1972 by Cohen and Boyer [11] paved the way for modern biotechnology. Until the 1980s, when those technological developments sparked the second wave of biotechnology [7], several hundred industrial processes, that utilized enzymes and whole-cells with only marginal genetic alterations [12], already existed [13]. During this time, first protein engineering technologies emerged that were used to extend, for example, the substrate spectrum of enzymes towards non-natural substrates, i.e. for the production of pharmaceutical intermediates and fine chemicals [7].

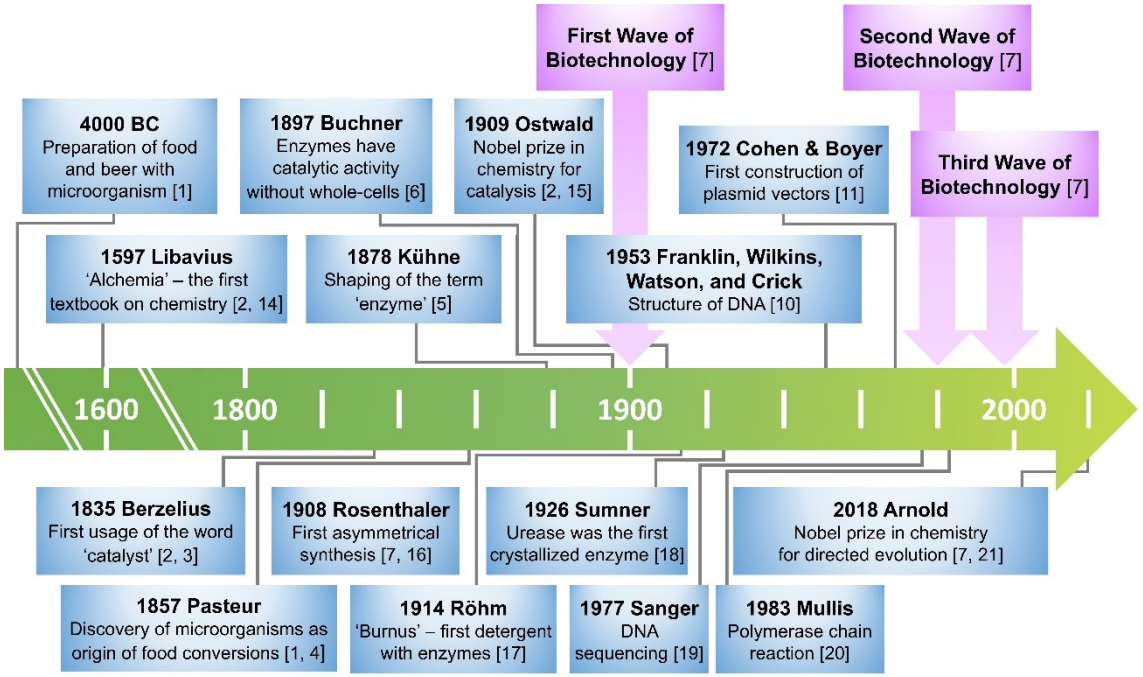


Figure 1-1 A selection of important mile-stones in biocatalysis from 4000 BC until today [1-7, 10, 11, 14-21]. Based loosely on a figure seen in [22].

Over the years, enzymatic catalysis became more and more popular. The third, and present, wave of biocatalysis defined to have started in the late 1990s, when Arnold and Stemmer invented new protein engineering methods like directed evolution and gene shuffling. This brought the power or Darwinian evolution to the laboratory and enabled the rapid modification of biocatalysts towards a desired trait [7]. Moreover, the major advances in DNA technologies and bioinformatics, at the beginning of the new millennium, have shaped today's biocatalysis research. While the costs for sequencing one human genome was around US$ 70 million in 2002, the 1000-dollar genome program at the National Human Genome Research Institute, today, states the price at US$ 1121 [23]. Furthermore, ultra-high-throughput screening technologies, e.g. for elucidation of protein sequence-function relationships [24], whole-gene DNA synthesis, and bioinformatic tools, like the Basic Local Alignment Search Tool (BLAST) [25] and the availability of databases, such as GenBank [26] and UniProt [27], or the RCSB Protein Data Bank [28], severely accelerated the discovery and engineering of new enzymes for industrial applications. Apart from accelerating research, those technological advances also allowed for the development of enzymes with capabilities not found in nature. These days, the transformation of previously-believed inert substrates is possible, e.g. using promiscuous catalyst. Along those lines, for example, a promiscuous cytochrome *c* oxidase was optimized by directed evolution to enable the efficient formation of carbon-silicon bonds, a reaction not known to exist in nature [29]. Using those methods, enzymes can nowadays rapidly be adapted or tailored to match demanding process conditions, like high temperature, extreme pH values, or the addition of organic solvents. While in enzyme engineering campaigns of the early 2000s one to five mutations where normal,

in 2010 enzymes with 30 or 40 mutations were produced [7]. To honour these ground-breaking technological inventions, just last year, the Nobel prize in Chemistry was awarded to Arnold, for her work on directed evolution [21]. Furthermore, these developments steadily move biotechnology forward, potentially heralding a fourth wave of biocatalysis [30].

Currently, more than 130 biocatalytic processes have been commercialised [31], often to replace chemical catalysis. A popular example is the hydrolysis of penicillin G [32]. Until the mid-1980s, the product 6-aminopenicillanic acid (6-APA) was chemically produced from penicillin G at -40 °C, involving dichloromethane, a harmful and possible carcinogenic reactant. Today the process employs a penicillin-acylase, using 37 °C and only ammonium for pH adjustment. Thereby, several thousand tons of 6-APA are produced worldwide every year [33].

In conclusion, since the definition of the terms 'catalyst' and 'enzyme' by Berzelius and Kühne in the late 19th century, (bio)catalysis research has come a long way.

The definition of (bio-)catalysis is nowadays strictly specified. The International Union of Pure and Applied Chemistry (IUPAC) defines a 'catalyst' as 'A SUBSTANCE THAT INCREASES THE RATE OF A REACTION WITHOUT MODIFYING THE OVERALL STANDARD GIBBS ENERGY CHANGE IN THE REACTION […]. THE CATALYST IS BOTH A REACTANT AND PRODUCT OF THE REACTION.'[1]

And a 'biocatalyst' is set to be 'AN ENZYME OR ENZYME COMPLEX CONSISTING OF, OR DERIVED FROM, AN ORGANISM OR CELL CULTURE (IN CELL-FREE OR WHOLE-CELL FORMS) THAT CATALYSES METABOLIC REACTIONS IN LIVING ORGANISMS AND/OR SUBSTRATE CONVERSIONS IN VARIOUS CHEMICAL REACTIONS'[2].

1.1.2 Advantages and drawbacks of biocatalysts

The awareness of today's humanity about overpopulation and climate change along with rising economic standards have favoured the promotion of more environmentally friendly processes in modern industry. In 1998, the United States Environmental Protection Agency (EPA) emphasised the *12 Principles of Green Chemistry* [34], which consider environmental factors and energy efficiency alongside occupational safety to create a roadmap how to implement green chemistry in industrial processes. This was later modified and extended by the *Principles of Green Engineering* to be summarized in the mnemonic IMPROVEMENTS PRODUCTIVELY (Figure 1-2) [35, 36].

[1] PAC, 1981, 162, Symbolism and terminology in chemical kinetics (IUPAC Technical Reports and Recommendations) http://iupac.org/publications/pac/pdf/1981/pdf/5303x0753.pdf

[2] PAC, 1992, 64, 147 Glossary for chemists of terms used in biotechnology (IUPAC Recommendations) http://dx.doi.org/10.1351/pac199264010143

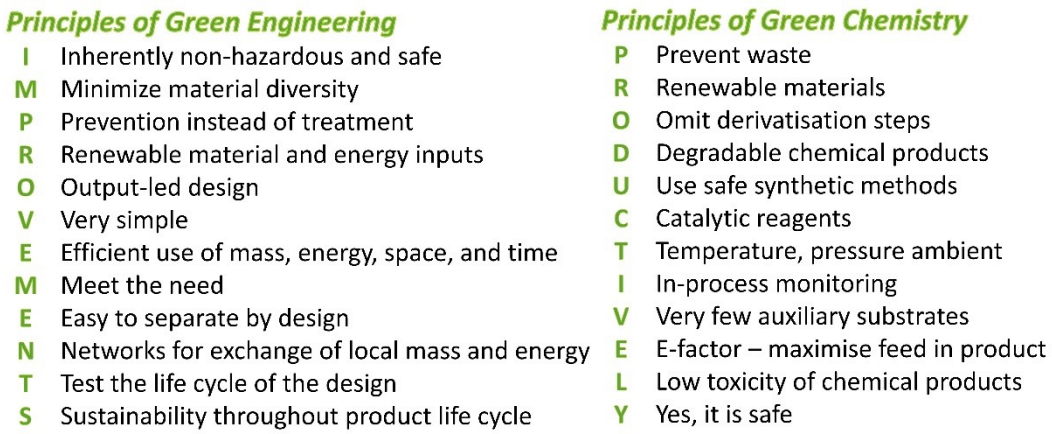


Figure 1-2 The 24 principles of green engineering and green chemistry as proposed originally by Anastas and Warner [34] and summarized in a mnemonic by Tang *et al.* [35, 36].

Based on these principles, the advantages of enzymatic over classical chemical catalysts become apparent:

- HIGH CATALYTIC ACTIVITY: Enzymatic catalysis operates at rates by far exceeding those of chemical catalysts. Consequently, enzymes are typically employed at a catalyst loading of 0.01 to 0.001 mol%, while chemical catalysts are used at concentrations up to a magnitude higher [8].
- USE OF SOLVENT: In contrast to most chemical catalysts, enzymes usually operate in aqueous media. However, since 85% of the total mass of chemicals, produced by pharmaceutical industry, are obtained by using organic solvents with a recovery rate of 50 to 80% [33, 37], it is important to promote reactions with nontoxic, non-hazardous, and not inflammable or corrosive solvents. In addition to that, it was shown that enzymes can retain activity in solvents other than water, enabling the use of enzymes in applications that require non-aqueous reaction media, i.e. for substrates with poor water solubility [38-40].
- REACTION CONDITIONS: Most enzymes work under mild conditions, like physiological pH, temperatures, and atmospheric pressure, thus greatly reducing energy input and the risk for industrial staff [8, 41]. Furthermore, extremophilic enzymes, like the alcohol dehydrogenase from *Flavobacterium frigidimaris* with a temperature optimum at 70 °C, can be used under harsh reaction conditions [42].
- ENVIRONMENTAL COMPATIBILITY: Enzymes themselves contribute to the sustainable management of resources, since they are built from renewable sources, are usually non-toxic, and are completely biodegradable [7].
- STEREOSELECTIVITY: One of the greatest advantages of enzymes is their high chemo-, regio-, and stereoselectivity, compared to conventional chemical catalyst. Thereby, the use of enzymes mostly circumvents the need for functional group activation and group protection, reduces unwanted side products, and simplifies the purification of the desired enantiomer [33]. This advantage is particularly

important for the production of fine chemicals and pharmaceuticals [8].

– BROAD APPLICATION: For every chemical reaction there is probably an enzyme that can do the same job [8]. By 2017 almost 84 000 proteins in over 7000 enzyme classes (EC) were known, highlighting the enormous biological variety of enzymes [43]. Furthermore, it is known today that one enzyme can possess different promiscuous activities, e.g. with regard to substrate spectrum or reaction conditions [8]. They can also be used in multi-enzyme cascades, which can simplify a reaction comprised of several steps or force an unfavourable equilibrium towards the desired product [33].

Nevertheless, the application of biocatalysts has also several bottlenecks, which need to be mentioned. Likely the biggest is the price for enzymes. Especially for the production of pharmaceuticals, enzymes should be applied in highly pure form, for which the costs can easily exceed 1000 € kg^{-1} [44]. This however, becomes less problematic as the price of the product increases. Enzymes are commonly considered as sensitive and unstable, i.e. compared to chemical catalysts [45]. Furthermore, enzymes often contain cofactors that, with few exceptions [46], cannot be replaced with more economical artificial substitutes [8]. Another challenge is posed by the limited choice of suitable solvents. Even though water is commonly considered the 'greenest' option, certain organic substrates and products are hardly soluble in water. The resulting waste water is difficult to recycle and needs to be purified before it can be released to the environment, which poses a problem in itself. Replacing water with organic solvents to increase the availability of hydrophobic substrates is often associated with a huge loss of catalytic activity [8]. Also, the mild conditions under which enzymes usually work, normally regarded as an advantage, can turn into a bottleneck, as there is often only a narrow window for adjustment, e.g. with regard to the temperature range in which enzymes can be used [8]. Finally, even if enzymatic engineering today is much faster than 20 years ago, it still requires large research teams and/or robotic equipment. Moreover, rational enzyme engineering often relies on structural information obtained from crystallized enzymes. Such crystals, which only form under very specific conditions, provide structural information, which does not necessarily reflect the enzyme structure under reaction conditions accurately. These problems, however, might be solved in the coming decades by advancing research and improved scientific methods [7]. Given these problems, an urgent requirement for the industrial application of enzymes appears to be the availability of highly-pure, cheap-to-produce, and stable enzyme preparations.

1.2 Immobilization of enzymes for biotechnological application

For application in biotechnology, enzymes are often used in immobilized form: they are attached to, bound to, entrapped in, or assembled (conjugated) into an insoluble preparation (Figure 1-3). The first scientific description of enzyme immobilization dates back to 1916, where an invertase was shown to possess activity when adsorbed on a charcoal surface [47]. Until today, more than 5000 publications and patents comprising immobilization techniques have been published, several hundred enzymes have been immobilized, and numerous enzyme-based large-scale processes have been developed [48]. This success is largely based on the considerable advantages of immobilized enzymes over soluble ones, such as the possibility for recycling, together with the rapid termination of reactions by enzyme removal, thus preventing product contamination with enzymes. For pharmaceutical products, enzyme removal is instrumental for the reduction of potential allergenic effects caused by enzymatic contaminations [48, 49]. Other points are the long-term stability, the possibility to use unconventional reaction media, such as organic solvents, supercritical fluids, and ionic liquids, and the extended variety of suitable bioreactor designs [45, 48, 49].

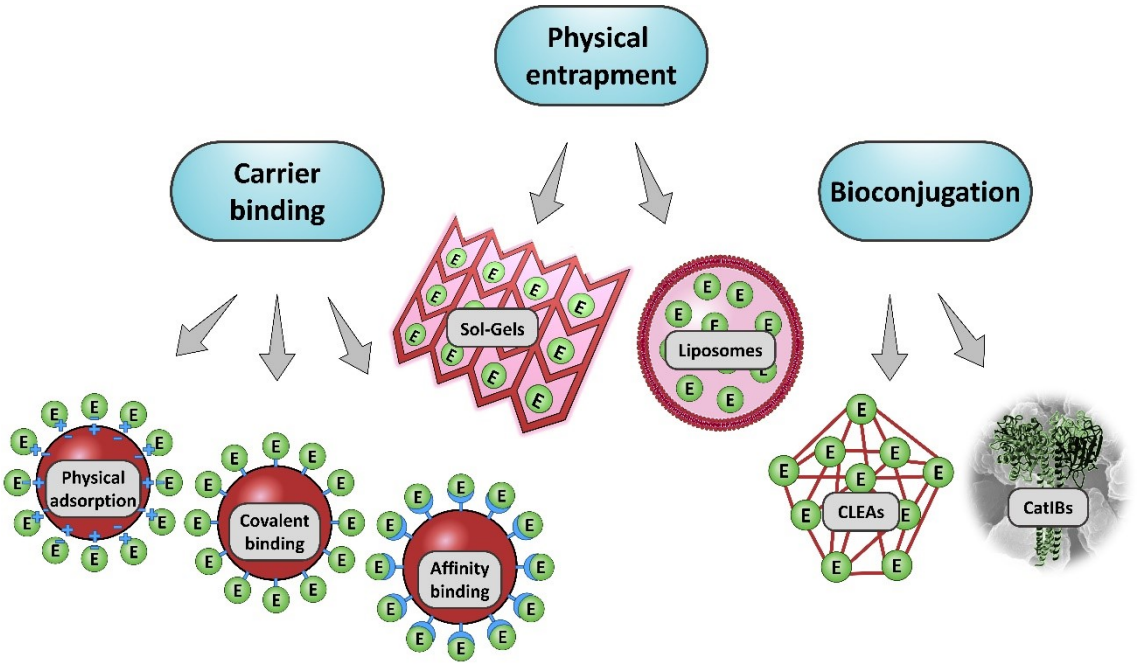


Figure 1-3 Different strategies of enzyme immobilization. Carrier binding is achieved through physical adsorption, e.g. based on hydrophobic, ionic, or van-der-Waals interactions, by covalent- or affinity binding. Physical entrapment includes encapsulation in sol-gels or liposomes. The third immobilization category is bioconjugation, a carrier-free form of immobilization, exemplified by cross-linked enzyme aggregates (CLEAs) or catalytically-active inclusion bodies (CatIBs).

Enzyme immobilization techniques can roughly be grouped into in three categories: (i) binding of the enzyme to a carrier, (ii) physical entrapment or encapsulation of the enzyme, and (iii) bioconjugation of enzymes (Figure 1-3). For every immobilization strategy several considerations are vital. Among them, the most important ones are

efficiency and yield, recovered activity and enzyme loading, diffusion limitations and robustness, as well as the reactor type and the mode of downstream processing that can be used [49]. In the following the different possibilities for enzyme immobilization are presented in more detail.

1.2.1 Immobilization on a carrier

The immobilization of enzymes on carrier materials was developed in the 1950s. Since the late 1960s this method constituted the most popular method for three decades [49]. As the easiest immobilization strategy, carrier-based immobilizates are even nowadays still hugely popular, as recently reviewed by Barbosa *et al*. [50]. Depending on the nature of the enzyme-carrier interaction, two general principles are predominant: physical 'adsorption' and 'covalent' attachment (Figure 1-3).

Physical adsorption represents the simplest method for immobilization, since it generally does not require pre-treated or chemically modified enzymes and in some cases is even possible for crude cell extract [45]. It can be achieved through weak, non-specific forces, like hydrophobic interactions, hydrogen bonds, or van-der-Waals interactions, which, however, often cannot prevent enzyme leakage, or with much stronger ionic interactions [45, 49]. Other popular examples of this category are affinity-based adsorption methods, which are commonly used for enzyme purification, but can also be employed for immobilization [50, 51]. Thereby, matrix-bound ligands are used, displaying affinities for a peptide or protein, called 'tag', which has to be fused to the target protein. The most commonly used tag for protein purification is the polyhistidine-tag, a repetitive unit of four to ten histidine residues, which form chelate complexes with bivalent transition metal ions, like Ni^{2+}, Cu^{2+}, or Co^{2+} [52]. Other commonly used tags are the FLAG-tag with affinity to a monoclonal antibody or the Strep-tag with affinity to the protein streptavidin [53, 54]. Even bigger domains or whole proteins can be used, like carbohydrate-binding domains or the maltose-binding protein [51, 54].

In contrast to physical adsorption, covalent binding between enzyme and carrier is very tight. Therefore, this immobilization method considerable reduces enzyme leaching, which renders it favourable for applications like the immobilization of biosensors in a biomedical setting, where contaminations of the medium with the sensor must be avoided at all costs. Covalent bonds between carrier and enzymes are typically formed by functional groups of amino-acid side chains on the enzyme surface, like amino groups of lysins, thiol groups of cysteines, or carboxy groups of glutamic and aspartic acid. Thereby, enzymes are either directly linked to the carrier or *via* cross-linking agents, such as *N*-hydroxysuccinimide or glutaraldehyde. Furthermore, links can be formed with oligosaccharides of post-translationally glycosylated amino acids. In some cases links are highly specific, making it possible to engineer the orientation of the enzyme [48]. An interesting example is the covalent immobilization with the commercially available

HaloTag® system, a protein-based tag, consisting of a modified haloalkane dehalogenase from *Rhodococcus rhodochrous*, which forms a covalent bond with a chloroalkane ligand present on a synthetic carrier. By genetic fusion of this tag to a target enzyme, the direct immobilization from crude cell extracts is enabled [55].

Since the invention of carrier-based immobilization methods, a wide variety of carrier materials for enzyme immobilization have been described. Examples range from natural polymers (e.g. chitin [56] or cellulose, as used in the Tanabe process for the production of *L*-amino acids [57]) and synthetic organic polymers (e.g. amberlite XAD-7, industrially used in Novozyme 435 [58], Eupergit C [59], or sepabeads [60]) over inorganic polymers (e.g. zeolites [61], sol-gels [62], and mesoporous silicas [63]) to even more exotic carrier materials (e.g. protein-coated microcrystals [64], enzyme-magnetic nanoparticles [65], or gold nanoparticles [66]). More recently, smart polymers have been employed. These stimulus responsive polymers dramatically change their conformation in response to small environmental changes [67]. For example, liquid poly(*N*-isopropylacrylamide) (pNIPAM) changes its physical state and becomes solid above a certain temperature, allowing for enzyme recovery, which was e.g. used for the immobilization of penicillin G amidase [49, 68].

1.2.2 Encapsulation or entrapment in a carrier

A much gentler immobilization strategy than covalent binding is the physical entrapment of enzymes inside a carrier, called encapsulation (Figure 1-3). A special characteristic thereby is the synthesis of the polymer network in presence of the enzyme. Encapsulation is beneficial for retaining enzymes in their active form, since it creates an aqueous microenvironment around the enzyme, containing buffer salts and, if necessary, cofactors [48]. Therefore it is the preferred method for immobilization of whole-cells [49]. As for carrier-based adsorption, a frequent problem encountered with encapsulation-based immobilizates is enzyme leakage, which however can be prevented by additional covalent attachments or cross-linking [49]. On the other hand, encapsulation can result in diffusional limitations for highly polar molecules [45, 48, 69]. Encapsulation matrices are commonly sol-gels (e.g. based on silicon or *N*-isopropylacrylamide [49, 69, 70]) or natural hydrogels [48, 70], but also include membranes, like hollow fibres or microcapsules [49].

Silica sol-gels are chemically inert glasses, build from partly hydrolysed and partly polymerised tetramethoxylsilane ($Si(OR)_4$) or methyltrimethoxylsilane ($RSi(OR)_3$) [49]. They are thermally and mechanically very stable, but also brittle [45, 48]. With different drying methods distinct morphologies can be achieved (aqua-, xero-, aero-, ambi-, or cryogels) [45, 48, 49]. As silica sol-gels often require extreme preparation conditions, they are rather used for simple adsorptive immobilization. Commercially available are LentiKats, from partially dried polyvinyl alcohol hydrogels [49]. They were successfully

employed for whole-cells as well as enzymes [71] and can even be combined with cross-linked enzyme aggregates (CLEAs, see 1.2.3) [72].

Another form of encapsulation uses liposomes, a form of lipid vesicle, built of bilayer-forming molecules (e.g. phospholipids) in aqueous solution. Depending on the fabrication method, liposomes can be multi-, oligo, or unilamellar, covering a large size range (about 25 nm up to 15 μm). They always possess a hydrophobic interphase and an aqueous core [73]. Apart from multilamellar ones, liposomes do not form spontaneously, since on the chemical level they are not thermodynamically but only kinetically stable and present a 'trapped' system [48, 74]. Production therefore relies on dispersion, extrusion, sonication, or filtration [48, 73]. Other vesicle-based encapsulation systems have been described, e.g. based on alginate [75], poly(lactic acid) [76], lignin [77], or polymeric nanogels [73]. In addition to the use in biocatalysis, liposomes are commonly used as drug delivery systems [78], as biosensors [79], or in the food industry [80].

1.2.3 Bioconjugation

Apart from binding on or encapsulation in a carrier, there are also other techniques available that completely circumvent the need for expensive carrier materials. Instead they rely on the forced, unordered interaction between enzyme molecules, which results in their aggregation. Most widely known here might be cross-linked enzyme aggregates (CLEAs) [81]. Likewise, other carrier-free immobilizates depending on self-assembling polypeptides, for example catalytically-active inclusion bodies (CatIBs, see 1.3), also belong to this category. Just like for carrier-based immobilizates, the interactions between enzyme molecules within the aggregate can either be covalent, as for CLEAs.

CLEAs originally have been adapted from the earlier invented cross-linked enzyme crystals (CLECs) first described in 1961 [82]. CLECs are constituted of enzyme crystals, which become highly stable and active by cross-linking. Althus Biologies commercialised this system in the 1990s, but since the production of CLECs has to start with tedious to prepare and hence expensive crystallized enzymes, they are no longer available [83]. In contrast, CLEAs are prepared in two easy steps. First, the enzyme is precipitated from aqueous solution with chaotrophic agents, non-ionic polymers, or water-miscible organic solvents, ideally resulting in active enzyme aggregates. Thereby the structure of the enzymes is assumed to be only minimally disturbed. In a second step, covalent bonds are formed between amino groups of amino-acid side chains on the enzyme surface and a cross-linker, to form a Schiff's base, which is further reduced to a stable amine bond, e.g. by sodium borohydride. CLEAs are prepared from purified enzymes or even crude cell extract [49]. A common cross-linker is the rather cheap glutaraldehyde, but also others, e.g. dextran polyaldehyde, have been used [84]. The resulting particles are generally 5-50 mm in size, so they can be recovered by filtration or centrifugation [49].

The CLEA technology is widespread in biotechnological research, since it presents a fast and economic way of immobilization, for e.g. the immobilization of hydrolases, oxidoreductases, or lyases [49]. Additionally, they can be combined with other materials, like nanoparticles or polymers. For example, a composite of CLEAs and silica sol-gels was described, which possessed fundamentally different properties compared to solely sol-gel immobilized enzyme, most notably featuring less leaching [81]. Alcalase-CLEAs, prepared with proteases, have been used for amino acid (aa) and drug synthesis [85]. Smart magnetic CLEAs, with functionalized magnetic nanoparticles have been employed for magnetic decantation or magnetically stabilized fluidized bed reactors [81]. Capillary reactors have been used, with CLEAs immobilized on the inner walls of microchannels [86]. In addition, combi-CLEAs, co-immobilized CLEAs of two or more enzymes, have been developed [49]. The first application of CLEAs was with the above mentioned penicillin G amidase (see 1.1.1) [33, 87]. In 2002 the CLEA technique was commercialised by CLEA Technologies B. V. (Delft, Netherlands), the company, however, declared insolvency in 2017. Based on the CLEA principle, so-called 'spherezymes' have been described, which are formed from a water-in-oil emulsion of surfactant and enzyme that is subsequently cross-linked. This resulted in a hyperactive lipase, but has also been shown to work for other enzyme classes, like laccases [69].

Admittedly, while the CLEA technology has many advantages, its use has also several drawbacks. Often the activity of enzymes is strongly reduced after cross-linking, due to loss of flexibility [81] or impaired active sites [84]. The latter can also be caused by the cross-linker glutaraldehyde, which is assumed to penetrate into active sites, a process that can be circumvented by using the bigger dextran polyaldehyde instead [84]. Moreover, it is always necessary to fine tune every step of the CLEA preparation process, which is a challenging and time-consuming task. If there is not enough attention paid to parameters, like cross-linking agent and duration, as well as adjustment of the protein concentration, CLEA formation can result in a huge decrease of activity or stability [69, 84]. It has also been reported that these parameters can influence the enantioselectivity of CLEAs [69]. Furthermore, since cross-linking depends on lysine residues of surface exposed amino acids, every enzyme behaves differently and the process is less effective with enzymes that lack a sufficient number of such residues. This, however, can be compensated by co-precipitation with polymers containing amino groups, like polyethylene imine or poly-*L*-lysine [49]. These disadvantages demonstrate that CLEA production, although being a potentially economic and simple method, definitely requires needs individual case-to-case optimization.

1.3 Catalytically-active Inclusion Bodies

1.3.1 The changing perception of inclusion bodies

Insoluble protein aggregates are oligomeric complexes consisting of non-native conformers, assumed to arise from non-native interactions of protein-folding intermediates. This makes them an inevitable consequence of protein production (Figure 1-4a) [88]. In unstressed cells, protein aggregation is prevented by the cellular quality control machinery, encompassing so-called chaperones which assist in protein folding along with proteolytic enzymes that degrade misfolded polypeptides before they accumulate [88, 89]. Inclusion bodies (IBs), as a final stage of protein aggregation, are generally formed due to stress in host cells, most commonly caused by overproduction of recombinant/heterologous proteins, although cases of IBs of homologous proteins have been reported, too [90]. Bacteria in general have a rather simple protein folding and degradation machinery and also lack compartmentation. This means that overproduction of heterologous proteins can quickly lead to an overload of the quality control machinery and generally results in improper folding conditions, like high protein concentration, missing cofactors, or wrong environmental conditions, e.g. oxidative *vs*. reductive, which in turn leads to an accumulation of thermodynamically more stable protein folding intermediates and ultimately to the formation of IBs [70, 88, 91].

IBs have mostly been observed in the Gram-negative bacterium *Escherichia coli*, but have also been reported to occur in the Gram-positive bacteria *Corynebacterium glutamicum* [92], *Lactococcus lactis* [93], and *Bacillus subtilis* [94], as well as in some yeasts, such as *Schizosaccharomyces pombe* [95] and *Saccharomyces cerevisiae* [96]. In mammalian cells, IBs, called aggresomes, can be sequestrated by microtubules. Aggresomes are closely associated with degenerative diseases like Alzheimer, Parkinson, and Huntington [88]. The shape of IBs depends on host organism and culture conditions, in *E. coli* they are typically spherical or rod shaped, with a length of 0.05 to over 1 µm [70, 97]. For a long time, it was the common opinion that IBs only consist of misfolded, inactive protein, although already in 1989 IBs with catalytic activity have been described [90]. The long-believed model for IB-formation assumes only a single or limited number of nucleation sites from which a giant amorphous aggregate grows (Figure 1-4b, top) [88, 98]. Contradictory to this, in 2005 amyloid-like structures were shown to be present in IBs [99], highlighting their more complex structure. This promoted a new view of the IB-formation process, where a number of small proto-aggregates coalescence into an ‘aggregate-of-aggregates’ (Figure 1-4b, bottom) [88, 91]. This not only accommodates the amyloid-like structures observed for IBs, but also accounts for the possibility of partially correct folded, and hence active, protein within the aggregates. Even though the exact composition and structure of IBs needs yet to be deciphered, it becomes more and more apparent that they are not just amorphous particles, but instead possess an inner

molecular organization [99]. Moreover, amyloid-like structures seem to play a big role, as they are now believed to be a common feature of all IBs, regardless of the IB-constituting protein [99]. Proteolytic digestion of IBs with proteinase K yielded amyloid fibers about the same size and shape as the IBs, but with reduced density that would make up for 20% of the IBs [100]. This suggests that an amyloidal network acts as a skeleton, surrounding partially correct folded protein and simultaneously accounting for the characteristic stability of IBs (Figure 1-5) [99].

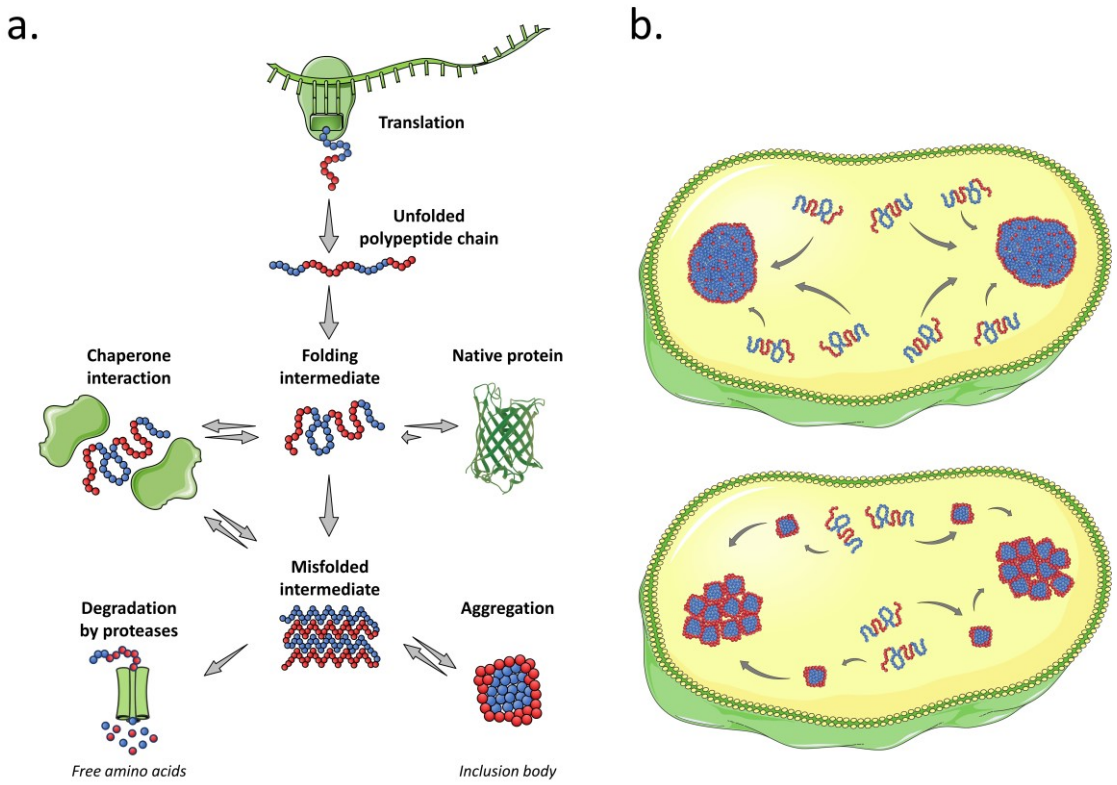


Figure 1-4 Protein aggregation within bacterial cells. (a): Protein folding machinery and quality control. Proteinaceous aggregates are assumed to be formed from polypeptide chains present in kinetically trapped conformations that can only be refolded by chaperones or are degraded by proteases. If those quality control mechanisms are overloaded due to strong overexpression of heterologous genes, the resulting misfolded polypeptide aggregate forming IBs. (b): Two models of inclusion body formation adapted from [88]. Top: Model starting from a limited number of aggregation sites, resulting in a giant amorphous IB aggregate. Bottom: Model starting from small proto-aggregates, yielding IBs as aggregates-of-aggregates.

Bacterial IBs are formed in the cytoplasm, accumulating as dense, refractile particles at the cell poles, whereas each cell often contains only one or two IBs. Although sometimes they can be associated with the cell membrane and in isolated cases have been reported to be present in the periplasm [101]. The accumulation at the cell poles can simply be explained by a process termed nucleoid occlusion [102]. Bacterial cell poles are characterized as being largely free of chromosomal DNA (nucleoid). Hence, in contrast to the central region of the cell, where most of the DNA is located and where cell division takes place, enough space is available at the poles to allow for the formation of

bulky structures such as IBs [99]. This also accounts for the observation that most of the major disintegration chaperones are also located at the cell poles [103]. Until today it is unclear, whether the transport of misfolded protein or small proto-aggregates to the growing IB at the cell pole is a purely passive process, depending only on diffusion and physical interactions or whether active transport processes are involved [99]. The bacterial cytoplasm can either be fluid or of a glass-like consistency that impedes movement of larger particles and could prevent the formation of IBs. The shift from glass-like to fluid is an energy-driven process (hydrolysis of ATP), meaning that passive IB-formation can only occur when biochemical processes disturb the glass-like structure of the cytoplasm [104]. However, protein folding and degradation by the different chaperones and heat-shock proteins clearly is also energy-dependent [99]. This facilitates a balance of IB formation and degradation which during strong overproduction of recombinant proteins favours IB growths, by overloading the capacity of chaperones and proteases. However, in aging or biosynthetic arrested cultures it is also possible that IBs are actively or passively disintegrated [99].

Regardless of their formation, IBs predominantly consist of the recombinant protein (up to 90%) [105]. Contaminations arise mostly from interacting chaperones, but also from diverse polypeptides, traces of macromolecules, like nucleic acids, and even cell wall components, that associate with the IB during cell disruption [99]. IBs are mechanically and chemically extremely stable and show poor solubility in water or detergents. Their production is simple and after cell disruption, they can easily be retrieved by centrifugation. This renders IBs an excellent choice for the preparation of stable biomaterials, e.g. as source for refolding studies or in case of active IBs, as enzyme immobilizate (1.3.3).

1.3.2 Inclusion bodies allow for diverse applications

The combination of high purity and easy purification renders the production of target proteins as IBs a fast and simple way of gaining access to the recombinant target. Nevertheless, their use has long been neglected as in most studies dealing with the production of recombinant proteins IBs were considered as waste, or at most were employed for renaturation and refolding studies, with often considerably low yields [88]. To address this problem, a form of mild extraction was developed, where the correctly folded part of the IB, containing an epimerase, is separated from the amyloid-like scaffold (Figure 1-5a), omitting tedious protein refolding steps [106].

In recent years, the discovery of activity in certain IBs opened a whole new chapter, as this allows for their direct use as carrier-free enzyme immobilizates in biotechnology. These catalytically-active inclusion bodies (CatIBs) offer a range of benefits. The production of large IB quantities is not only simple but also economic, since no expensive and complex chromatographic purification steps are needed. The use of biocatalysts for

industrial applications is often impeded simply by the production costs. Purification of enzymes can easily increase these costs by an order of magnitude compared to crude cell lysates [44]. Moreover, as (Cat)IBs are insoluble in water and organic solvents [107], no subsequent immobilization or cross-linking is needed that would further raise production costs. As carrier-free enzyme immobilizates formed *via* bioconjugation (see Figure 1-3), they can best be compared to CLEAs (see 1.2.3). CatIBs are generally produced in *E. coli* [107], but also in *Pichia pastoris* [108], both classified as GRAS organisms (generally regarded as safe), so they could potentially be employed for food and drug production. Additionally, CatIBs can in principle be produced as cell-free immobilizates, i.e. free of genetically modified organisms (GMO-free), e.g. by inactivating remaining cells during or after CatIB purification [109]. Another interesting aspect is that IBs of heterologous proteins can be used to produce small peptides in bacteria (about 30 to 100 aa), since they are stable under physiological conditions. These are often unstable and susceptible to degradation by the host. However, they can be safely produced in IBs, where they are protected from proteolytic degradation and can easily be recovered after cell disruption by cleavage of the IB-inducing element, e.g. by using a self-cleaving *Mxe* GyrA intein, fused between target and IB-inducing tag. After CatIB purification, the tag is cleaved autocatalytically (by pH-shift or thiol-containing buffers). When CatIBs instead of conventional inactive IBs are used, refolding of the target peptide might even be dispensable (Figure 1-5b) [110].

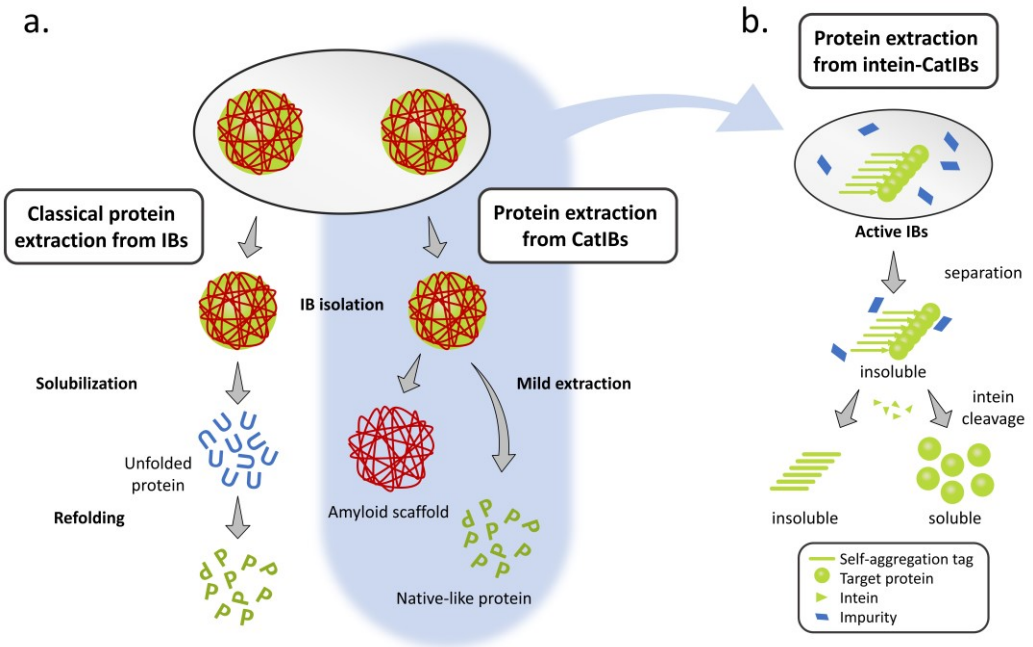


Figure 1-5 Protein extraction from (active) IBs. (a): Classical protein extraction *vs.* protein extraction from (Cat)IBs. Classical extraction always requires solubilization through strong chaotropic reagents and subsequent protein refolding, whereas mild extraction separates the amyloid scaffold from the correctly folded protein, for example with detergents or at high pH-values [106]. Picture adapted from [99]. (b): Mild protein extraction from CatIBs by self-cleavage of intein fusion proteins. CatIB formation is induced by aggregation-prone peptides, which are fused to the target *via* an *Mxe* GyrA intein. After isolation, self-cleavage is induced by pH-shift or thiol-containing buffers, releasing the soluble protein in native-like form. Picture adapted from [110].

Apart from the use in biocatalysis, IBs have also been employed in material science and biomedicine as highly stable novel biomaterials, because they display no apparent toxicity for mammalian cells. They show good results in studies about long-term storage at different conditions [111, 112]. Their size is controllable by selecting the harvesting time, since they progressively grow during protein biosynthesis [99]. Additionally, they can be absorbed by mammalian cells, e.g. by anchoring them to the cell membrane, followed by cellular uptake as macropinosomes [113]. This renders them an interesting novel type of nanostructured therapeutic agent, being used as a long-term *in vivo* depot or for direct drug delivery as protein releasing agents, which has already been tested *in vitro* for cell growth restoration and to counteract oxidative stress [114] and *in vivo* as immuno-stimulant [115]. Nevertheless, the protein releasing mechanism of IBs is yet poorly understood and probably also involves intracellular molecular chaperones [99].

An additional biomedical application for IBs is found in tissue engineering, where the regeneration of damaged tissue is facilitated by scaffold matrices. These scaffolds must be mechanically stiff but also biocompatible and biodegradable. Furthermore, having amyloid-like properties, IBs can be studied as a model for amyloidosis and prion propagation [116].

1.3.3 Immobilization *via* self-assembling protein tags

Until today it is impossible to judge, whether activity is an intrinsic feature of all IBs or whether it is only observed for certain targets. Since IBs have been regarded as waste for a long time, the activity of most IB-forming proteins was probably never measured, eventually dismissing their high potential for application [97]. The study of CatIBs is still a niche area and most studies do not go beyond measuring activity as a proof-of-concept. First attempts have been made to predict the aggregation propensity of different IB-inducing tags by computational means and compare it to collected functional data [97]. This, though, remains a challenging task, since it is at present unclear which structural factors, such as polypeptide-chain composition, quaternary structure, and surface composition of target and tag dominate the (Cat)IB-formation process [97].

To this day only a few cases of naturally formed CatIBs are known (without IB-inducing elements), even though there are presumably noticeably more. The first active IBs ever discovered where those of a β-galactosidase, homologously produced in *E. coli* [90]. Other hydrolase family examples include a β-galactosidase from *Pyrococcus furiosus* [117], an endoglucanase D from *Clostridium thermocellum* [118], and the lipase A from *Serrataia marcescens* [119], which can all be produced as CatIBs in *E. coli*. Further examples are a human dihydrofolate reductase [120], a pyruvate oxidase from *Paenibacillus polymyxa* [121], and a diguanylate cyclase from *Thermatoga maritima* [122]. All of these enzymes show activity in insoluble form to a greater or lesser extent.

Besides these naturally occurring CatIBs, different strategies to artificially induce CatIB-formation have been presented, whereby different IB-forming elements are genetically fused to a target (Table 1-1), facilitating the aggregation of the fusion protein in insoluble, yet active form. The elements used for this purpose can generally be divided into two categories: (i) small artificial peptides, and (ii) larger, aggregation-prone proteins or protein-domains. Artificial IB-inducing peptide tags were intensively studied by the group of Lin [123-126]. These tags possess quite different structural properties, ranging from α-helical peptides (18A), over β-sheet structures (ELK16 and GFL8), to surfactant-like tags (L_6KD). Nevertheless, they all induce CatIB formation, with in some cases quite high residual activity. For example, some variants of the 18A-tag when fused to a lipase showed 4-times higher activity in CatIBs than the corresponding soluble lipase [126]. Furthermore, with these tags, CatIBs can be used for mild extraction to obtain the native target enzyme (Figure 1-5b). Since the target, at least partially, retains its quaternary structure within the IBs, no expensive and tedious refolding steps are needed [110].

From the second category, cellulose binding domains (CBDs) have been widely used as aggregation-inducing tag. These protein domains are known for their tendency to self-aggregate during heterologous expression and can be used to induce CatIB formation for chimeric CBD/target-protein fusions [127]. Additionally, CBDs generally display little interference with folding and function of their fusion partners, thus helping to preserve the native structure of the target protein [127]. For example, CatIBs of sialic acid aldolase, fused to a CBD from *Clostridium cellulovorans* (CBDclos), showed about the same activity as the soluble protein and could be recycled 19-times without loss of activity. However, here the CatIBs were further stabilized by cross-linking, resulting in crosslinked inclusion bodies (CLIBs), in analogy to the above-described CLEAs (see 1.2.3).

Further aggregation-prone proteins, used to induce CatIB-formation, are the capsid protein (VP1) of the foot-and-mouth disease virus that is known to be prone to aggregation, and a variant of the human Aβ-amyloid peptide (Aβ42(F19D)) [120]. Both were studied by the group of Villaverde, and resulted in catalytically-active or fluorescent IBs. In case of VP1, β-galactosidase CatIBs with a specific activity 1.6-times higher than the soluble protein could be generated [120]. The by far biggest aggregation-prone protein used for CatIB-induction, is the 574 aa big pyruvate oxidase (PoxB) from *Paenibacillus polymyxa* that resulted in CatIBs with 2-fold volumetric activity compared to the soluble target enzyme, when fused to an amylase [121]. Additionally, another rather large aggregation-prone protein, used to induce CatIB formation, is a folding-deficient variant of the maltose binding protein MalE31 from *E. coli*, which consists of 396 aa. Here, fusion to an alkaline phosphatase or a β-lactamase resulted primarily in periplasmic CatIBs, which is the native location of the soluble maltose binding protein, in contrast to most described cytoplasmic CatIBs [128].

Table 1-1 Overview of different fusion-tags used for induction of CatIB formation as adapted from [97]. 1 N- *vs.* C-terminal fusion: Means the fusion site (C- or N-terminal). 2: For this peptide, a range of variants was studied. 3: Residual specific fluorescence. 4: Volumetric activity. 5: Abbreviation for 2-succinyl-5-enol-pyruvyl-6-hydroxy-3-cyclohexene-1-carboxylate synthase. n.i.: No information provided. n.a.: Not applicable.

Name and Fusion site[1] (Origin) and length		Target enzyme/protein	Target origin	Expression host	IB formation efficiency [%]	residual activity [%]	Ref.
I. Artificial peptides							
L6KD (artificial)	C **8**	lipase A	*B. subtilis*	*E. coli* BL21(DE3)	80	30	[123]
		amadoriase II	*A. fumigatus*		61	93	
		xylosidase	*B. pumilus*		84	26	
		GFP	*A. victoria*		n.i.	n.a.	
GFIL8 (artificial)	C **8**	lipase A	*B. subtilis*	*E. coli* BL21(DE3)	89	43	[124]
		amadoriase II	*A. fumigatus*		93	54	
		Ulp1 protease	*S. cerevisiae*		n.i.	40	[129]
ELK16 (artificial)	C **16**	amadoriase II	*A. fumigatus*	*E. coli* BL21(DE3)	120	88	[125]
		xylosidase	*B. pumilus*		94	77	
		GFP	*A. victoria*		n.i.	n.a.	
18A[2] (artificial)	C **18**	lipase A	*B. subtilis*	*E. coli* BL21(DE3)	90	150	[126]
		amadoriase II	*A. fumigatus*		n.i.	n.i.	
		xylosidase	*B. pumilus*		n.i.	n.i.	
		GFP	*A. victoria*		n.i.	n.a.	
II. Aggregation-prone proteins and protein domains							
Aβ42(F19D) (*Homo sapiens*)	N **42**	BFP	*A. victoria*	*E. coli* MC4100	61-65	31[3]	[120]
TDoT (*S. marinus*)	N **53**	hydroxynitrile lyase	*A. thaliana*	*E. coli* BL21(DE3)	80	11	[107]
		MenD[5]	*E. coli*		90	n.i.	
		lipase A	*B. subtilis*		100	n.i.	
		YFP	*A. victoria*		80	n.a.	[22]
CBDclos (*C. cellulovorans*)	N **156**	D-amino acid oxidase	*T. variabilis*	*E. coli* BL21(DE3)	>90	42	[127]
		sialic acid aldolase	*E. coli* K12		100	100	[130]
		maltodextrin phosphorylase	*P. furiosus*		83	n.i.	[131]
		cytidylate kinase	*E. coli*	n.i.	n.i.	n.i.	[132]
		polyphosphate kinase PPK3	*S. pomeroyi*		n.i.	n.i.	
VP1 capsid protein (*foot-and-mouth disease virus*)	N **209**	β-galactosidase	*E. coli*	*E. coli* MC4100	36-46	166	[120]
		GFP	*A. victoria*		n.i.	n.a.	
MalE31 (*E. coli*)	N **396**	alkaline phosphatase	*E. coli*	*E. coli* pop6499	>95	n.i.	[128]
		β-lactamase	*E. coli*		>95	n.i.	
CBDcell (*C. fimi*)	C **484**	β-glucuronidase	*E. coli* MG1665	*E. coli* BL21(DE3)	92	19	[133]
		β-glycosidase	*T. caldophilus*		93	n.i.	
		*Ds*Red	*D. striata*		n.i.	n.a.	
		GFP-leucine zipper	*A. victoria*	n.i.	n.i.	n.a.	
PoxB (*P. polymyxa E681*)	N **574**	GFP	*A. victoria*	*E. coli* BW25113	n.i.	n.a.	[121]
		amylase	*B. subtilis*		77	200[4]	
Cry3Aa (*Bacillus thuringiensis*)	N **625**	lipase A	*B. subtilis*	*Bacillus thuringiensis*	n.i.	221	[134]
		esterase	*B. subtilis*		n.i.	101	
		deformylase	*Borrelia burgdorferi*		n.i.	48	

Recently, the group of Ulrich Krauss could identify another aggregation-prone protein domain suitable for CatIB production, namely TDoT, a coiled-coil domain from *Staphylothermus marinus* (see 1.3.5) [107]. All of the mentioned aggregation-prone peptides or proteins induce the formation of CatIBs, although with variable efficiency. Moreover, not in all cases the activity of the CatIB-based immobilizate was thoroughly studied or compared to their soluble counterparts.

Another recently developed method, that resembles the CatIB approach, is the use of Cry3Aa, a crystalline toxin from *Bacillus thuringiensis*, as fusion partner [134]. With 625 aa it is even bigger than PoxB. In contrast to the CatIB approach, the Cry3Aa method relies on encapsulation of the fused target within a supposedly crystalline lattice formed by Cry3Aa molecules. The group of Chan demonstrated that a fusion protein consisting of Cry3Aa and the lipase A of *B. subtilis* forms crystal-like particles with high residual activity, which could be repeatedly used for the conversion of triacylglycerols to fatty acid methyl ester biodiesel [134].

1.3.4 Additional approaches to produce biocatalytic inclusions

Apart from the fusion of aggregation-prone peptides and proteins for CatIB-formation, some entirely different strategies have been described, which also achieve immobilization through intracellularly formed inclusions. Thereby, the intracellular inclusion serves only as a scaffold for target immobilization, but displays no activity itself, and in some cases is not even composed of proteins or peptides. Therefore, these scaffolds will not be called IBs, but for the sake of completeness, they will be briefly described here.

Inclusions of lipid polyhydroxyalkanoates (PHAs) are commonly produced in prokaryotes as a source of energy and as carbon storage deposit [135]. They display a lipophilic core, but are surrounded by an amphiphilic protein shell that can be used for intracellular enzyme immobilization (Figure 1-6a) [70]. PHA granules are formed primarily by three enzymes. The first two, a β-ketothiolase (PhaA) and an acetoacetyl-CoA reductase (PhaB), convert Acetyl-CoA, originating from glycolysis, into the activated form 3-hydroxy-butyryl-CoA, which is then polymerised by PhaC, a PHA synthase. These amphipathic PhaC-PHA complexes can self-assemble into inclusions. Genetically fusing a target enzyme to PhaC results in PHA granules, coated with the target enzyme. The covalent binding of the PhaC fusion enzyme within the PHA prevents leakage during cell disruption. This strategy has already been tested for several enzymes, like an α-amylase and a lipase [70]. These PHA-particles could further be made fluorescent by additional fusion of GFP to PhaC, resulting in fluorescent PHA-immobilizates [136].

Another strategy relies on the intracellular capture of target enzymes by inclusion bodies (Figure 1-6b) [137]. Similar to CatIBs, this approach also uses CBDs for particle

formation, but instead of directly fusing the target gene to the CBD gene, leucine zipper (LZ) heterodimer interactions are used for enzyme capture. The employed LZ consists of two monomers: a bait zipper (BZ) and a prey zipper (PZ) forming a stable antiparallel heterodimeric structure. The BZ is genetically fused to the CBD resulting in CBD particles coated with BZ, while the PZ is genetically fused to the target enzyme. Thereby, the capture of the independently produced soluble PZ-enzyme fusions on the IB surface is possible. In this way, a reaction cascade was set up, reconstituting the metabolic pathway for 1-butanol production (starting from acetyl-CoA) *in vivo* and *in vitro*, facilitated by the collective immobilization of four different enzymes on CBD-IB particles [137]. Similarly, the LZ strategy is also applicable to PHAs-based immobilizates by genetically fusing an LZ to PhaC, thereby enabling the *in situ* capture of the LZ-tagged target enzymes on PHA particles [138].

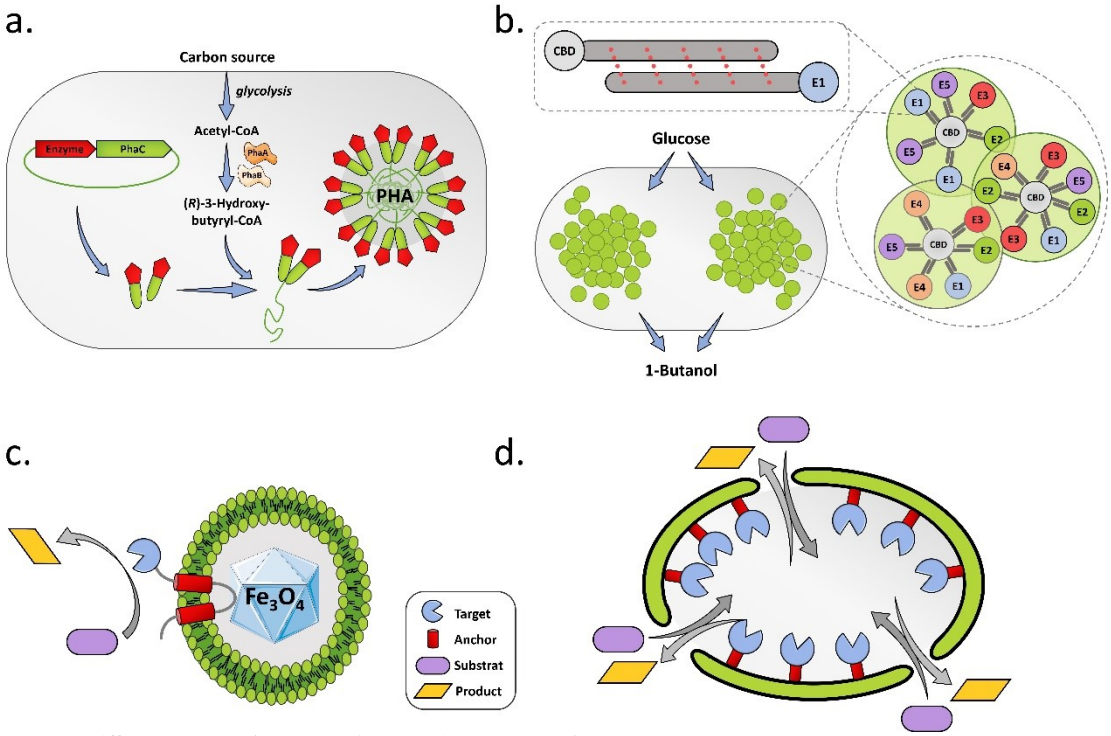


Figure 1-6 Different approaches to produce *in situ* protein inclusions. (a): Inclusions of polyhydroxyalkanoates (PHAs) coated with target enzymes can be achieved using three enzymes. PhaA: β-ketothiolase, PhaB: acetoacetyl-CoA reductase, PhaC: PHA synthase. To display a target enzyme on the surface of PHA particles, the target enzyme is genetically fused to PhaC. The corresponding enzyme-PhaC-PHA complexes self-assemble into amphipathic inclusions. Adapted from [70]. (b): Enzyme immobilization on the surface of IBs with the help of a leucine zippers (LZ). IB-forming CBD and target enzymes are each genetically fused to antiparallel LZ domain pairs. After expression, IBs of CBD are formed that display the target enzyme on their surface. Adapted from [137]. (c): For enzyme immobilization on magnetosomes, the target enzyme is anchored on lipid-coated magnetite crystals by fusion to a membrane anchor protein. Adapted from [139]. (d): Use of the cell membrane as immobilization scaffold. The target enzyme is fused to a membrane anchor and inserted at the inner membrane of *E. coli*. Subsequent expression of lytic phage protein results in pore formation and cell death, leaving a cellular envelope with immobilized enzymes and pores for diffusion. Adapted from [140].

The use of special intracellular structures, called 'magnetosomes', are another way to achieve intracellular protein immobilization (Figure 1-6c). They are naturally formed in certain bacteria and composed of a magnetite (Fe_3O_4) or greigite (Fe_3S_4) crystals enveloped in a lipid membrane [70]. The presence of these nano-sized protein-and-lipid-

coated vesicles allows magnetotactic bacteria orientation by passive alignment along the geomagnetic field [141]. Enzyme immobilization on the surface of magnetosomes is possible by genetically fusing a target protein to an anchor protein that can double-pass the lipid bilayer membrane of the vesicle and bind tightly to the magnetic core. After cell disruption they can easily be separated by applying a magnetic field. This strategy was used, e.g. for the immobilization of an organophoshydrolase [139] as well as for the co-immobilization of an endoglucanase and a β-glycosidase [142].

Even simple membrane anchors can be used for *in situ* immobilization, as was demonstrated for a β-galactosidase that was genetically fused to a membrane anchor originating from rabbit liver cytochrome b_5 and subsequently inserted into the cell membrane. The expression of a lytic phage protein caused cell lysis and release of the cytosol, resulting in cellular envelopes with immobilized enzymes and lysis pores (Figure 1-6d) [140].

A rather exotic approach, which resembles the CatIB approach, is the immobilization of target enzymes within forisomes, plant-derived mechanoproteins. Forisomes are self-assembled multiprotein complexes that are naturally present in the phloem of fabacean plants, where they are involved in wound healing. The 10 to 40 µm long superstructures are about 10- to 80-times bigger than IBs and are therefore produced in *Saccharomyces cerevisiae*. A genetical fusion of a target enzyme to forisomes results in CatIB-like structures called 'forizymes' [143]. However, this approach has not been studied intensively up to now.

1.3.5 Coiled-coil domains as IB-inducing tag

A few years ago, it was demonstrated that the fusion of a FMN-binding fluorescent protein from *Bacillus subtilis* (FbFP) to a hydroxy nitrile lyase from *Arabidopsis thaliana* (*At*HNL) significantly enhanced the stability of the fusion protein in the weakly acidic pH range, most likely by targeted oligomerization *via* the FbFP domain [144]. It was assumed that this was partly caused by the N- and C-terminal α-helical coiled-coil structures, which contribute to dimerization in the employed FbFP. Therefore, in a subsequent study, another peptide, solely consisting of a coiled-coil motif, was chosen to further extend this strategy. However, the outcome was not a more stable enzyme, but instead the formation of IBs that after a while were discovered to still be catalytically-active and hence were called CatIBs [22, 107].

1.3.5.1 Design of superhelical structures in coiled-coil domains

Coiled coils present a unique structural motif, widespread in many proteins. Structurally, they form a superhelix consisting of at least two α-helices, slightly shifted and twisted around each other, just like the winding of ropes (Figure 1-7) [145, 146]. The primary polypeptide-chain is hereby generally comprised of heptad repeats $(abcdefg)_n$,

where *a* and *d* are usually hydrophobic amino acids and the residues *e* and *g* are charged. The positions *b*, *c*, and *f*, are most commonly occupied by polar amino acids. The hallmark of coiled coils is the tightly packed hydrophobic core, formed by the *a* and *d* residues in a knobs-into-holes manner. Thereby, the residues of one helix (knob) pack into a space formed by the adjacent helix (hole). The periodically repetition however, is only possible, when the right handed α-helix gets a left-handed twist, thus reducing the number of residues to 3.5 per turn (in contrast to approximately 3.6 in undistorted helices). This results in a left-handed supercoil composed of right-handed α-helices that roughly winds around once every 15 heptad repeats [147].

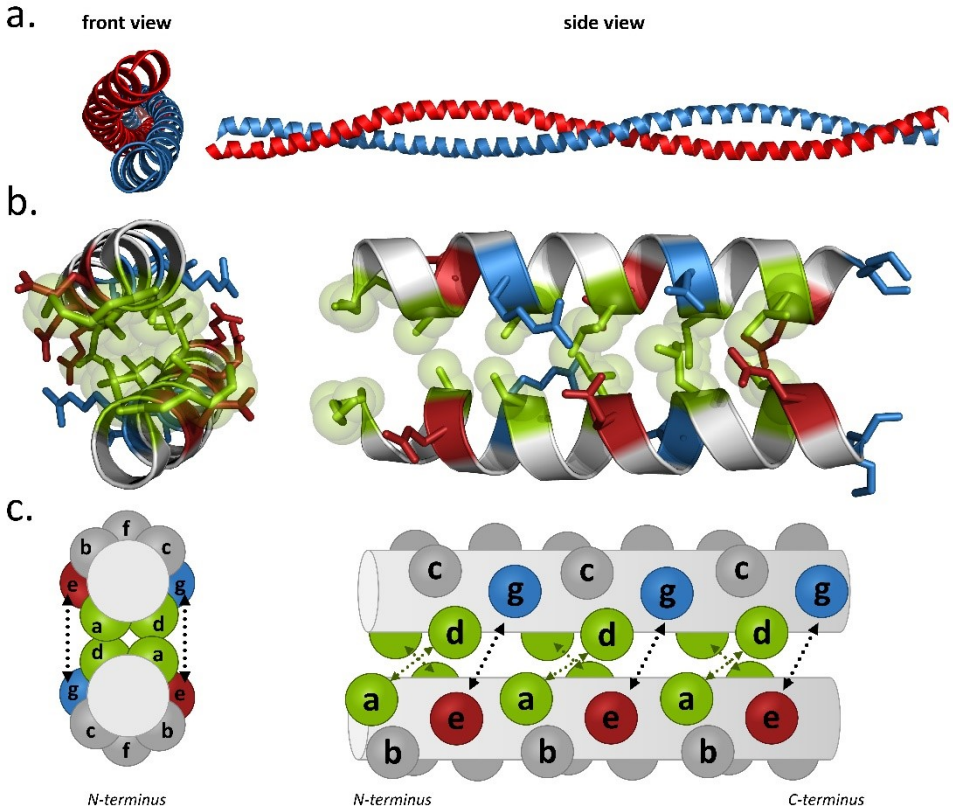


Figure 1-7 Structure of coiled-coils to illustrate the heptad repeat. As an example, the dimeric coiled-coil structure of tropomyosin (PDB: 1C1G) is shown. (a): Overall structure of the tropomyosin coiled coil (residues 1 to 126). The two subunits of the dimeric coiled coil are shown as red and blue cartoon, respectively. (b and c): Closer up view of three heptad repeats of the tropomyosin coiled coil (residues 29-49) in cartoon representation (b) and as schematic illustration (c). The side chains are colored as follows: green represents hydrophobic side chains at positions *a* and *d* of the heptad, while residues with opposing charge at positions *e* and *g* are colored in red and blue. Furthermore, in b, the spatial expansion of the hydrophobic core is illustrated by showing side chain atoms as spheres. Hydrophobic or ionic interactions are symbolized by arrows in c. Remaining amino acids that are not involved in the formation of this molecular Velcro are shown in grey without side chains.

Further stabilization of the supercoil is achieved *via* solvent-exposed residues at positions *e* and *g* of the heptad. These residues usually display opposite charge and thus create salt bridges, which stabilize the quaternary structure of the coiled coil [148]. They become increasingly important with higher oligomeric state, converging to the extreme, where these positions also fit into each other in a knobs-into-holes manner [146]. Contrary to the conserved heptad repeat, most coiled coils show discontinuities by insertion of three

residues (stammers) or four residues (stutters), whereby an irregular turn of the helix is added, resulting in an over- or underwinding of the supercoil and a disturbance in hydrophobic core packaging [145, 148].

The structure of coiled coils was independently postulated by Crick and Pauling in late 1952 [149, 150]. Nowadays, they are known to be ubiquitous in nature, occurring in many different combinations including parallel and antiparallel structures of homo- or hetero-oligomers, and various oligomeric states, up to the formation of α-helical barrels [145, 146]. In cells, long coiled coils, often over several hundred amino acids long, result in rod-like supramolecular structures and form two- or three-dimensional networks. For example, the cytoskeletal protein spectrin, forms a layer on the inner surface of all cell membranes in animal cells. Spectrin, an exceptional big protein, is largely assembled by multiple 106 aa long α-helices, which interact to form intramolecular coiled-coil trimers. In bacterial cells, crescentin, an equivalent coiled coil could be identified [151]. Coiled coils often act as a cellular Velcro that holds together all molecules and subcellular structures attached to it [147, 148], e.g. tropomyosin in the cytoskeleton and muscle fibers [152]. Furthermore, coiled coils can possess dynamic or regulatory functions, especially in motor proteins and sensory receptors, such as histidine kinases and transcription factors like bZIP [153]. Thereby intramolecular domain movements are triggered or relayed *via* conformational changes in coiled coils, e.g. enabling transcriptional regulation [154, 155].

1.3.5.2 TDoT and 3HAMP as coiled-coil domains for CatIB-formations

The first coiled-coil domain used for CatIB formation was the tetramerization domain of the cell-surface protein tetrabrachion from the archaeon *Staphylothermus marinus*, called TDoT (Figure 1-8a, Table 1-1, 1.3.3) [22, 97, 107]. This coiled-coil domain is already well characterized with regard to structure and stability [156, 157]. The outstanding stability it displays under extreme conditions, leads back to its origin from the archaeon *S. marinus*, which originates from black smoker vents in the deep sea, where it lives under strict anaerobic conditions at an optimal temperature of 92 °C [158, 159]. In correspondence to this, TDoT resists heat denaturation up to 130 °C and has a broad pH stability between 1 and 11. Contrary to most natural coiled coils, the supercoil structure of the homo-tetrameric TDoT is right-handed, instead of left-handed. As proposed for right-handed supercoils, the 53 aa of each monomer are organized in a 11-residue repeat $(abcdefghijk)_n$, rather than the classical heptad repeat of left-handed supercoils (see above). Additionally, a stutter in the α-helix leads to an extra twist. Since the positions *a*, *e*, and *h* are strictly hydrophobic, the supercoil is stabilized by more hydrophobic interactions and the hydrophobic cavities become larger, and are partially filled with water. Together with a complex networks of surface salt bridges, this results in an extremely thermostable coiled coil [156, 157].

So far, three different enzymes and one fluorescent reporter protein have been

immobilized in CatIBs by N-terminal fusion of the TDoT domain, always resulting in mainly insoluble, yet catalytically-active or functional protein assembled as IBs [22, 107]. Especially a hydroxynitrile lyase from *Arabidopsis thaliana* (*At*HNL) was studied extensively, retaining about 11% residual activity, relative to the purified soluble *At*HNL, while remaining stable at much more acidic pH values compared to the soluble enzyme. Furthermore, *At*HNL CatIBs could be recycled several times for the synthesis of chiral cyanohydrins in a micro-aqueous organic-solvent based reaction system [107]. Likewise, MenD, a carboxylate synthase from *E. coli*, could be recycled multiple times from an aqueous buffer-based reaction system without significant loss of activity [107]. The easy and economical immobilization method presented by CatIBs is now also part of a patent application [160].

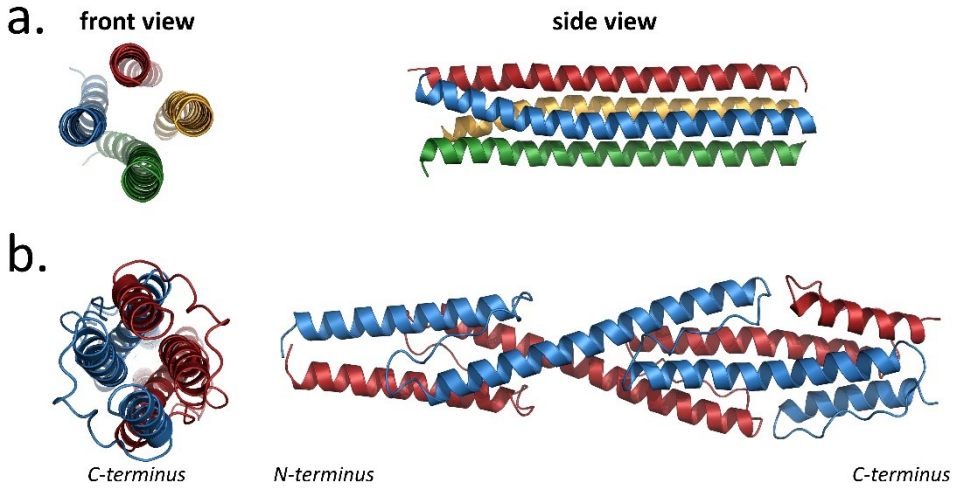


Figure 1-8 Superhelical structures of the coiled-coil domains. Front (left) and side view (right) of (a): TDoT (PDB: 1FE6) and (b): 3HAMP (PDB: 3LN3). The different subunits are shown in different color. TDoT is 53 aa long and forms a parallel homo-tetramer, while the 172 aa long 3HAMP domain forms as parallel homo-dimer.

Another coiled-coil domain, which was already employed for CatIB formation in preliminary unpublished studies is 3HAMP (Martin Diener, personal communication), derived from the oxygen sensor protein Aer2 from *Pseudomonas aeruginosa* (Figure 1-8b) [161]. The name 3HAMP originates from the types of proteins, where HAMPs were originally identified (histidine kinases, adenyl cyclases, methyl-accepting chemotaxis proteins, and phosphatases) [162]. The 3HAMP coiled coil forms a stable homo-dimeric structure consisting of parallel monomers, each with a length of 172 aa. The monomers are ordered in three successive domains (HAMP1, 2, and 3), each about 50 residues long and bridged by flexible linkers. The domains adopt a unique four-helix bundle, in which each monomer contributes two parallel α-helices (AS1 and 2). The residues are ordered in a classical heptad repeat but with a stutter at the end of AS2. Therefore, AS1 and AS2 in-register in HAMP1 and HAMP3 (sidechains that form the hydrophobic core are in the same plane) but offset in HAMP2, thus providing the possibility for signal transduction by movement from an in-register four-helix bundle to a distorted structure [161].

1.4 Targets used for research on CatIBs

1.4.1 Fluorescent proteins

For biotechnological application, CatIBs should ultimately be used for the immobilization of (catalytically-active) enzymes. Nevertheless, for proof-of-principle studies, i.e. aiming at verifying cellular localization and the proof of IB formation, fluorescent proteins (FPs), as easy-to-detect model proteins, are perfectly suited.

Nowadays the most commonly used FPs derive from the green fluorescent protein (GFP) or relatives thereof. GFP was isolated from the jellyfish *Aequorea victoria* in the early 1970s [163-165]. In the early 1990s [166-168], the huge application potential of GFP as a genetically-encoded fluorescent reporter, caused the development of an avalanche of different FPs obtained by site-directed mutagenesis and directed evolution. Eventually Shimomura, Tsien, and Chalfie were awarded with the Nobel prize in Chemistry 'for the discovery and development of the green fluorescent protein, GFP' in 2008 [165]. Furthermore, mining other marine organisms for FPs and using additional methods, like iterative somatic hypermutation [169], computational designed libraries, and *in silico* screening [170], filled essential gaps in the FP color palette. Thus today, a color range of excitation-emission wavelengths from 384-448 nm (Azurite [171]) to far-red FPs at even 598-675 nm (TagRFP675 [172]) is covered by more than hundred different FP variants.

All GFP-like FPs possess similar structures composed of a tightly interwoven 11-stranded β-barrel cylinder [165, 167, 168]. The cyclic chromophore is formed autocatalytically from a tripeptide and is buried within the core of the protein. For chromophore synthesis and maturation, no additional components other than molecular oxygen are required. Substituting the residues, which constitute the GFP chromophore, hereby results in different colors of the FP. A further advantage of GFP and its derivatives is the fact that N- and C-terminus of the protein protrude from the β-barrel and are thus freely available for genetic fusion to a target protein. These facts render GFP-based FPs genetically encoded probes for *in vivo* fluorescence labeling in the field of cell biology, medicine, and physiology [165]. Furthermore, pairs of suitable FPs can be used for Förster resonance energy transfer (FRET) to study the radiation-free energy transfer between donor and acceptor in living cells [173, 174], essentially yielding distance information for the donor and acceptor pair. This effect has for example been utilized to study protein-protein interactions in living cells [175].

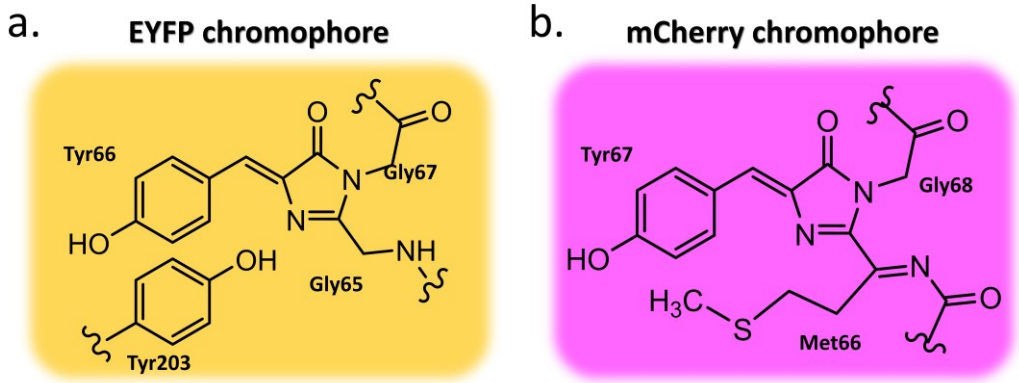


Figure 1-9 Chromophores of (a): YFP and (b): mCherry. The color of GFP-like FPs is determined by the delocalized π-electron system of the chromophore. No additional compounds other than O_2 are needed for the autocatalytic cyclization of the residues Gly65, Tyr66, and Gly67 in EYFP and Gln66, Tyr67, and Met66, Tyr67, and Gly68 in mCherry, respectively, to form the chromophore. In YFP the residue Tyr203 induces red-shifted spectral properties by further π-orbital stacking interaction with the chromophore.

1.4.1.1 Yellow fluorescent protein from *Aequorea victoria*

The 238 aa long yellow fluorescent protein (YFP) is a GFP variant, generated by introducing the mutation T203Y, which facilitates π-orbital stacking interactions between the phenol ring of the introduced tyrosine and the chromophore, thereby shifting the extinction-emission wavelengths of GFP from 488-507 to about 514-527 nm (Figure 1-9a) [163, 165]. YFP is the most red-shifted derivative, achievable from GFP [176]. Further important mutations are S65G, resulting in enhanced YFP (EYFP) with a drastically increased brightness, and A206K, which diminishes the weak tendency of GFP to form dimers [177].

1.4.1.2 mCherry from *Discosoma striata*

The original FP found in the Anthozoa *Discosoma striata* was a tetrameric FP named *Ds*Red [178]. A total of 33 substitutions were needed to generate the monomeric variant mRFP [179] that heralded the start of the mFruit series, which is the umbrella term for a whole series of FP with variations in the residues Gln66 and Tyr67 of *Ds*Red (Figure 1-9b) [169, 180]. All these derivatives are called after the fruit whose color they resemble, ranging from mHoneydew to mPlum. Of these mFruits, mCherry with a excitation-emission wavelength of 587-610 nm is the most promising candidate with regard to brightness, maturation time of the chromophore, and photostability [165].

1.4.2 Alcohol dehydrogenases

Alcohol dehydrogenases belong to the class of oxidoreductases (ADH, EC 1.1.1.1.) and occur in many organisms, e.g. in yeast and bacteria. ADHs catalyze the reversible reaction of alcohols to aldehydes/ketones and *vice versa*. The direction of these usually highly stereospecific reactions is determined by the reaction parameters [181]. The reducing equivalents, usually hydride ions (H^-), are transferred within the catalytic cycle by the cofactor nicotinamide adenine dinucleotide (phosphate) (NAD(P)H /$NAD(P)^+$) [181, 182], which is bound to the enzyme within a typical Rossmann fold [183, 184].

Since these cofactors, especially NADPH, are very expensive, they are generally applied only in catalytic amounts and recycled during the reaction [8] by different approaches, like the substrate-coupled and the enzyme-coupled approach [185]. In the substrate-coupled approach the same enzyme catalyzes both the desired conversion as well as a cofactor regeneration reaction, in which a second, usually cheap co-substrate is converted to regenerate the cofactor. In the enzyme-coupled approach a second enzyme is used for cofactor regeneration, e.g. glucose dehydrogenase [186], or formate dehydrogenase [187]. In all cases the equilibrium of the cofactor regeneration reaction has to be considered. Therefore, co-substrates are preferred that impede the reverse reaction. For example, formate is reduced to the gaseous carbon dioxide [187] or 1,4-butandiol is converted to a chemically inert lactone [188].

1.4.2.1 Alcohol dehydrogenase from *Ralstonia* sp.

The alcohol dehydrogenase from *Ralstonia* sp. DSM 6428 (*R*ADH), with a subunit size of 27 kDa, belongs to the short-chain dehydrogenase/reductase (SDR) family [189]. SDRs have usually 250 to 350 amino acids per subunit and a highly conserved catalytic tetrad of Asn-Ser-Tyr-Lys [190]. *R*ADH is a homo-tetramer, in which one NADP(H) molecule is bound within each monomer [191]. *R*ADH shows remarkable high reduction rates for bulky-bulky ketones, usually with high (*R*)-selectivity, following Prelog's rule [189, 191, 192]. The pH-optimum for the reduction lies between pH 6 and 9.5 and for the oxidation between pH 10 and 11.5 [193]. Furthermore, the stability of *R*ADH can significantly be enhanced by the addition of divalent calcium ions [193].

1.4.2.2 Alcohol dehydrogenase from *Lactobacillus brevis*

Quite similar to *R*ADH, the alcohol dehydrogenase from *Lactobacillus brevis* (*Lb*ADH), with a subunit size of also 27 kDa, is an SDR, too. Like *R*ADH, it forms a homo-tetramer with one active site per subunit, requiring NADP(H) as cofactor. In contrast to *R*ADH, *Lb*ADH requires divalent magnesium ions for its structural integrity and catalytic activity [194, 195]. A considerable rare fact is the (*R*)-selectivity of *Lb*ADH, due to its anti-Prelog selectivity [192, 194, 195], while most ADHs exhibit Prelog selectivity [196].

1.4.3 Thiamine diphosphate-dependent decarboxylases

Thiamin diphosphate (ThDP)-dependent enzymes are found in all organisms and constitute a very diverse protein family. It is classified into nine superfamilies, all belonging to oxidoreductases, transferases, or lyases [197, 198]. They all possess highly similar reaction mechanisms with the mutual cofactor ThDP, the biologically active form of vitamin B_1, acting as actual catalyst. Since they catalyze the formation or cleavage of C-C, C-O, C-N, or C-S bonds with a broad range of substrates, ThDP-dependent enzymes are of utmost importance for the synthesis of chiral building blocks by asymmetric

synthesis [199, 200].

A comprehensive database of the diverse ThDP-dependent enzymes has been set up to systematically explore the relation between sequence, structure, and function (TEED: Thiamine diphosphate dependent Enzyme Engineering Database) [197]. They all share two conserved domains: the pyrophosphate domain (PP) and the pyrimidine domain (PYR), which are both essential for binding and activation of ThDP [201]. In the decarboxylase superfamily of ThDP-dependent enzymes, for example, the active site is sandwiched between PYR and PP of different subunits, resulting in a functional dimer of an inter-subunit/PYR-PP-type [198]. The cofactor is bound *via* its diphosphate moiety to a bivalent magnesium or calcium ion, which in turn is chelated in the active site by a highly conserved motif, including two aspartate or an aspartate and an asparagine residue [202]. The first step in the catalytic cycle always starts with the activation of ThDP. Thereby, ThDP is deprotonated at its C_2 atom by a highly conserved glutamic acid in PYR to yield a ThDP-ylide (Figure 1-10a) [198, 202, 203].

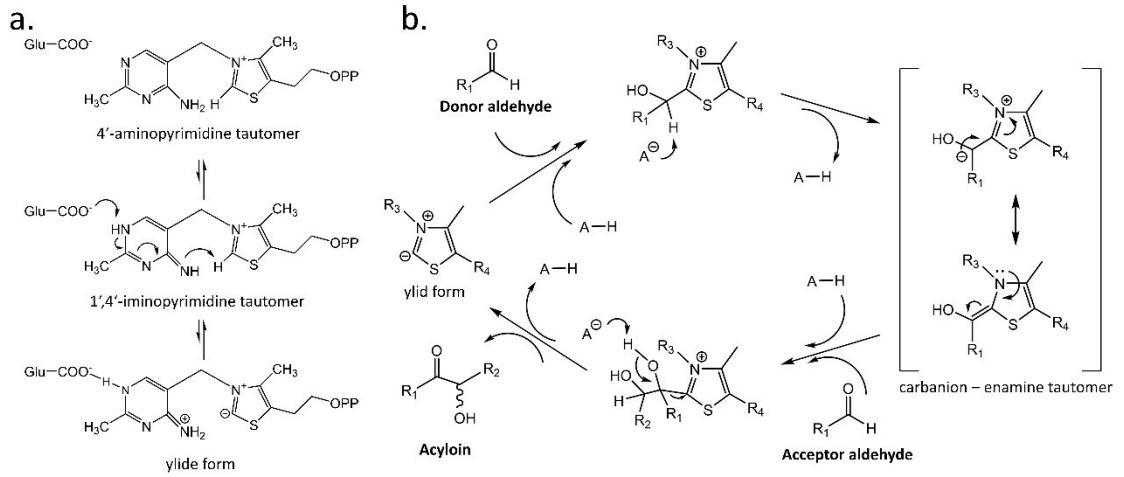


Figure 1-10 General mechanism proposed for ThDP-dependent lyases. (a): Formation and stabilization of the ThDP ylide, as adapted from [200]. (b): General mechanism for the catalyzation of acyloin as proposed by [204].

ThDP-dependent decarboxylases catalyse acyloin condensation-like reactions between an aldehyde and a suitable donor, thus generating enantiomerically enriched α-hydroxy ketones [204]. The key step of this reaction is the nucleophilic attack of the ThDP-ylide on the carbonyl carbon of the donor aldehyde, which results in an enamine-carbanion intermediate. In a second step, the now nucleophilic carbon of the enamine attacks an acceptor aldehyde, forming an α-hydroxy ketone (Figure 1-10b) [200, 204].

1.4.3.1 Benzaldehyde lyase from *Pseudomonas fluorescens*

The benzaldehyde lyase from *Pseudomonas fluorescens* Biovar I (*Pf*BAL, EC 4.1.2.38) was first described in 1989 [205]. It forms a homo-tetramer with a subunit size of 60 kDa, where the ThDP is located at the bottom of a narrow channel [206-208]. *Pf*BAL catalyzes the enantioselective formation of C-C bonds between aromatic aldehyde donors and aromatic or even aliphatic aldehyde acceptors to form strictly (*R*)-specific

benzoins and acyloins. Additionally, *Pf*BAL is also able to catalyze the reverse cleavage reaction, displaying a particularly high C-C bond cleavage activity [204, 206]. Thereby, a broad range of substrates distinguishes the *Pf*BAL from other carboligases, which extend from *ortho*-, *para*-, or *meta*-substituted aromatic aldehydes over heteroaromatic aldehydes to even small aliphatic aldehydes [204, 207, 208]. Only sterically hindered aldehydes and pyridine derivates are not easily accepted as substrates [204, 208].

1.4.3.2 Benzoylformate decarboxylase from *Pseudomonas putida*

Another ThDP-dependent enzyme is the benzoylformate decarboxylase from *Pseudomonas putida* ATCC 12633 (*Pp*BFD, EC 4.1.1.7), which is structurally quite similar to *Pf*BAL, despite only 24% sequence identity, and also forms a homo-tetrameric structure with a subunit size of 57 kDa [206, 209]. The natural reaction is the non-oxidative decarboxylation of benzoylformate to benzaldehyde as part of the mandelate pathway [210]. Like the *Pf*BAL, *Pp*BFD is able to catalyze enantioselective acyloin- and benzoin condensations [204, 211]. However, one significant difference is the narrower binding site compared to *Pf*BAL, resulting in a slightly smaller substrate spectrum, excluding *ortho*-substitutes aldehydes, as well as an absence of C-C bond cleavage activity [204, 206]. Another difference is the stereo specificity. While *Pf*BAL forms only (*R*)-enantiomers, a small extra binding pocket in *Pp*BFD allows for an inverse orientation of the acceptor aldehyde, thus resulting in formation of the (*S*)-enantiomer, but only for small acceptors, like acetaldehyde [206]. Therefore, the stereoselectivity of *Pp*BFD reactions is highly dependent on the structure of substrate aldehydes [204].

1.4.4 Lysine decarboxylase from *Escherichia coli*

As the name implies, the lysine decarboxylase from *E. coli* (*Ec*LDC, EC 4.1.1.18) catalyzes the decarboxylation of L-lysine to 1,5-diaminopentane, also known as cadaverine. Thereby, it uses pyridoxal-5'-phosphate (PLP, vitamin B_6) as cofactor and releases carbon dioxide as coproduct. In fact, *E. coli* possesses two lysine decarboxylases: one is inducible (LDCi, also called CadA) the other is constitutive (LDCc) [212]. Their high sequence similarity of 69% identical and 84% similar amino acids [212], is also reflected in the quaternary structure, as both enzymes form a homo-decameric complex, built of five functional dimers, with the active site sandwiched between two monomers [213, 214].

In its host *E. coli*, the inducible LDCi counteracts acid stress, e.g. in the very acidic environment of the human stomach [215]. Therefore, its gene expression is inducible at low pH values as 5.5 with an optimum at pH 5.7. In comparison, LDCc is only weakly expressed in *E. coli*, as part of the polyamine synthesis pathway, in which cadaverine is substituted to aminopropyl cadaverine, an essential factor in vegetative cell growth [216]. LDCc displays a broader pH-optimum of 6.2 to 8 [217]. At these pH values (≥ 8) LDCi already loses its native quaternary structure: the decamer disintegrates into dimers [215].

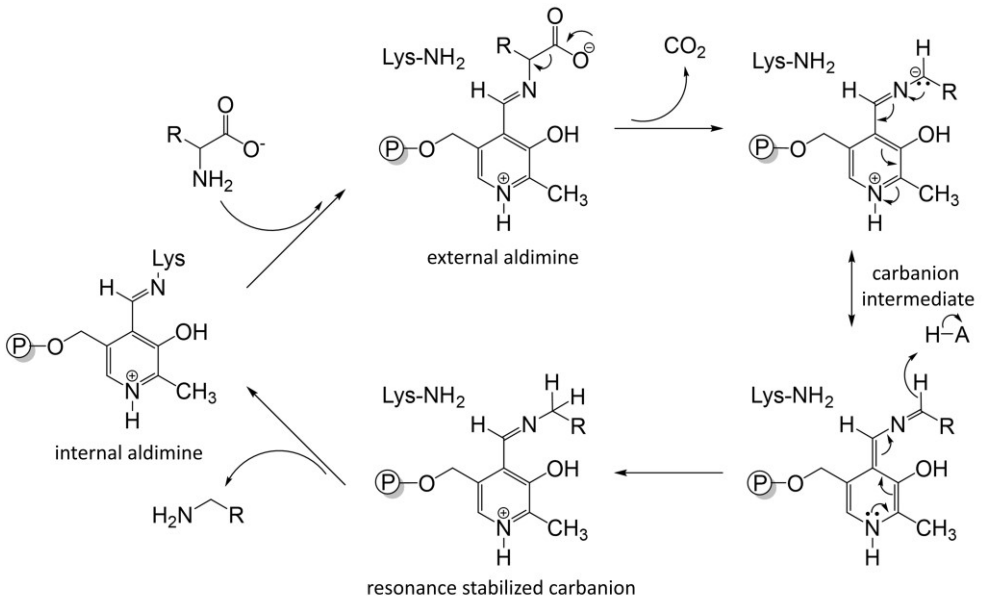


Figure 1-11 Mechanism of the PLP-dependent α-amino acid decarboxylation, as adapted from [218].

As common for PLP-dependent enzymes, PLP forms a covalent enzyme-PLP complex with a highly conserved lysine that protects the aldehyde group of PLP by forming an 'internal aldimine' or Schiff base (Figure 1-11) [218]. This stabilized enzyme-PLP complex can then react with the α-amino group of a substrate in a transimination, to form an 'external aldimine'. This aldimine withdrawing group in β-position provides the necessary driving force to release CO_2 and leaving a resonance-stabilized carbanion. After protonation, the decarboxylated product is released by reforming the 'internal aldimine'.

1.5 Scope and outline of the thesis

The rapid development of modern biotechnology increases the need for new economical ways to prepare stable and reusable biocatalysts/enzyme immobilizates for industrial applications (see 1.1.2). Catalytically-active inclusion bodies (CatIBs) essentially represent a naturally-produced enzyme immobilizate that fulfills those requirements (1.3). However, their full potential for biotechnology has not been comprehensively investigated.

The aim of this thesis was to broaden the scope of the initial CatIB strategy by generating CatIBs and fluorescent inclusion bodies (FIBs) of additional enzymes and fluorescent proteins and to investigate the potential for optimization of the CatIB formation process. Thus, a so-called 'CatIB toolbox' was generated using a set of variably complex enzymes and fluorescent proteins (1.4) as well as different coiled-coil domains as CatIB-formation inducing tags (1.3.3). This toolbox was further utilized to

i) comparatively analyze biotechnologically relevant properties such as activity, yield, and protein content; and to address the predictability of CatIB properties by computational means (2.1).

ii) address issues related to CatIB formation due to the employed expression conditions (2.2).

iii) study the interplay between CatIB stability, activity, and morphology under different reaction conditions (2.3).

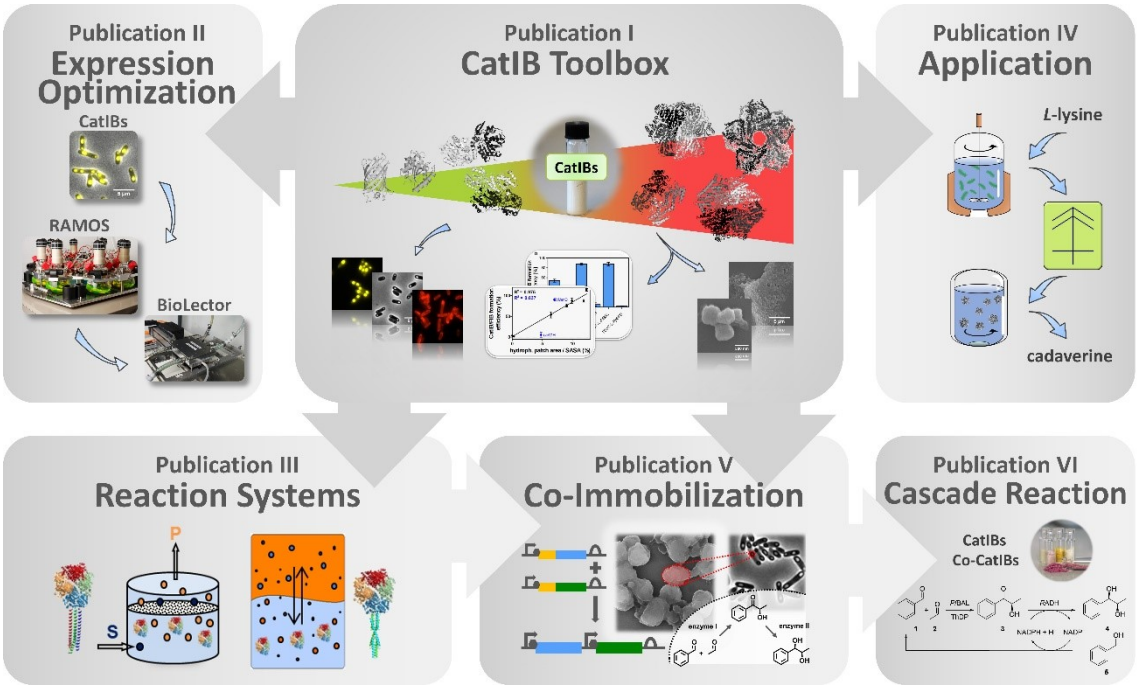
iv) demonstrate a possible biotechnological application by using CatIBs under industrial relevant conditions (2.4).

v) expand the CatIB strategy by analyzing the possibility to co-immobilize multiple enzymes and proteins in IBs (Co-CatIBs) (2.5).

vi) realize an efficient two-enzyme, one-pot cascade by using CatIBs and Co-CatIBs, thereby extending their application range (2.6).

In this way a better understanding of the applicability and predictability of the CatIB strategy is expected to be gained, while at the same time the application potential of CatIB-based immobilizates will be demonstrated.

2 Chapter 2
Results



In the following section, three already published and three submitted manuscripts are compiled that portray the results of this thesis. Most of the work was performed in close collaboration with the 'Biocatalysis' group of the Institute for Bio- and Geoscience (IBG-1) at the Forschungszentrum Jülich and in part together with the 'Biochemical Engineering' group of the Aachener Verfahrenstechnik (AVT) at the RWTH Aachen University. Contributions of all authors are specified on the cover page of every manuscript.

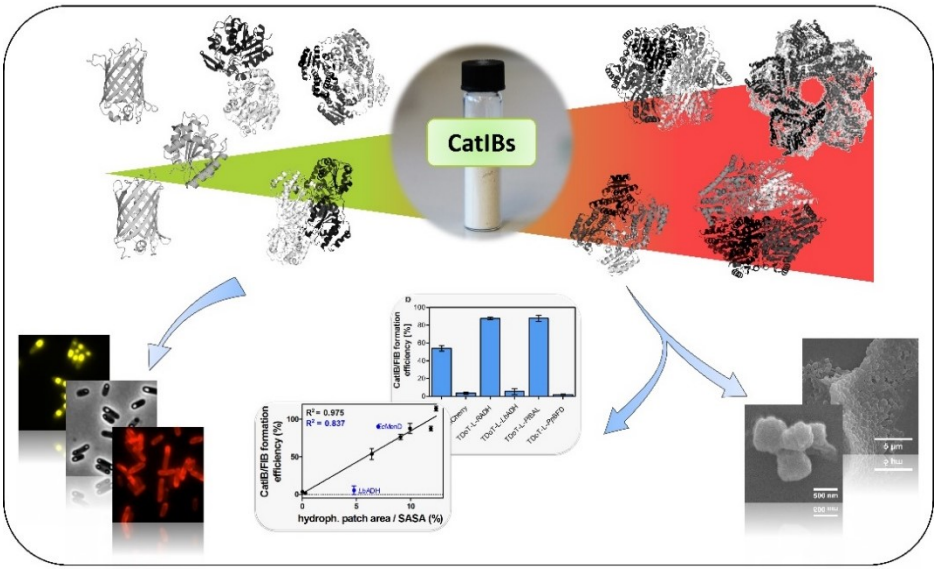
2.1 Publication I

Tailoring the properties of (catalytically)-active inclusion bodies

Vera D. Jäger[+], Ramona Kloss[+], Alexander Grünberger, Selina Seide, Doris Hahn, Tobias Karmainski, Maja Piqueray, Jochen Embruch, Stefanie Longerich, Ursula Mackfeld, Karl-Erich Jaeger, Wolfgang Wiechert, Martina Pohl, and Ulrich Krauss[*]

[+]both authors contributed equally; [*]corresponding author

Microbial Cell Factories, 2019, 18(1):33



Contributions:

VDJ and RK contributed equally: both wrote the manuscript, planed, supervised, analyzed, and assisted the experiments. VDJ optimized plasmid constructs, generated different expression vectors and created the fusion proteins. RK, assisted by UK, planned and generated the genetic construct for the C-terminal LDC-3HAMP/TDoT fusion. VDJ characterized fluorescent proteins, measured distributions and activities for *R*ADH and *Pf*BAL, optimized *R*ADH activity assays and performed scanning electron microscopy. RK optimized activity assays for *Pf*BAL, *Pp*BFD, and *Lb*ADH and supervised the characterization of these enzymes and *Ec*LDC. VDJ, RK, and AG performed live-cell imaging. UK performed bioinformatic and computational structural analyses. SS, DH, TK, MPiqueray, UM, JM, and SL performed experiments that were planned and supervised by RK and VDJ under the coordination and supervision of MPohl and UK. WW, KE-J, MPohl, and UK planned the CatIB project and corrected the manuscript.

Copyright: Creative Commons Attribution 4.0 International License.
(https://microbialcellfactories.biomedcentral.com/articles/10.1186/s12934-019-1081-5)

Microbial Cell Factories

RESEARCH Open Access

Tailoring the properties of (catalytically)-active inclusion bodies

V. D. Jäger[1,4†], R. Kloss[2,4†], A. Grünberger[2,3], S. Seide[2], D. Hahn[2], T. Karmainski[2], M. Piqueray[1], J. Embruch[2], S. Longerich[1], U. Mackfeld[2], K.-E. Jaeger[1,2,4], W. Wiechert[2,4], M. Pohl[2,4] and U. Krauss[1,4*]

Abstract

Background: Immobilization is an appropriate tool to ease the handling and recycling of enzymes in biocatalytic processes and to increase their stability. Most of the established immobilization methods require case-to-case optimization, which is laborious and time-consuming. Often, (chromatographic) enzyme purification is required and stable immobilization usually includes additional cross-linking or adsorption steps. We have previously shown in a few case studies that the molecular biological fusion of an aggregation-inducing tag to a target protein induces the intracellular formation of protein aggregates, so called inclusion bodies (IBs), which to a certain degree retain their (catalytic) function. This enables the combination of protein production and immobilization in one step. Hence, those biologically-produced immobilizates were named catalytically-active inclusion bodies (CatIBs) or, in case of proteins without catalytic activity, functional IBs (FIBs). While this strategy has been proven successful, the efficiency, the potential for optimization and important CatIB/FIB properties like yield, activity and morphology have not been investigated systematically.

Results: We here evaluated a CatIB/FIB toolbox of different enzymes and proteins. Different optimization strategies, like linker deletion, C- versus N-terminal fusion and the fusion of alternative aggregation-inducing tags were evaluated. The obtained CatIBs/FIBs varied with respect to formation efficiency, yield, composition and residual activity, which could be correlated to differences in their morphology; as revealed by (electron) microscopy. Last but not least, we demonstrate that the CatIB/FIB formation efficiency appears to be correlated to the solvent-accessible hydrophobic surface area of the target protein, providing a structure-based rationale for our strategy and opening up the possibility to predict its efficiency for any given target protein.

Conclusion: We here provide evidence for the general applicability, predictability and flexibility of the CatIB/FIB immobilization strategy, highlighting the application potential of CatIB-based enzyme immobilizates for synthetic chemistry, biocatalysis and industry.

Keywords: Immobilization, Biocatalysis, Inclusion bodies, Protein aggregates, Protein engineering, Structure–function relations, Enzymes

*Correspondence: u.krauss@fz-juelich.de
†V. D. Jäger and R. Kloss contributed equally to this work
[1] Institut für Molekulare Enzymtechnologie, Heinrich-Heine-Universität Düsseldorf, Forschungszentrum Jülich, 52425 Jülich, Germany
Full list of author information is available at the end of the article

© The Author(s) 2019. This article is distributed under the terms of the Creative Commons Attribution 4.0 International License (http://creativecommons.org/licenses/by/4.0/), which permits unrestricted use, distribution, and reproduction in any medium, provided you give appropriate credit to the original author(s) and the source, provide a link to the Creative Commons license, and indicate if changes were made. The Creative Commons Public Domain Dedication waiver (http://creativecommons.org/publicdomain/zero/1.0/) applies to the data made available in this article, unless otherwise stated.

Background

For sustainable application, enzyme preparations have to face several requirements, such as long-term stability under process conditions and the possibility of recycling [1]. In order to stabilize enzymes, e.g. towards organic solvents or harsh reaction conditions, immobilization is often the preferred strategy, for which a variety of methods are available [2–5]. Enzymes can be bound onto a carrier material by non-covalent adsorption with the risk of enzyme leakage, or by covalent binding, which mostly requires chemical modification using crosslinking agents. An example are cross-linked enzyme aggregates (CLEAs) [6], which do not require any carrier material and stabilize precipitated enzyme aggregates using glutaraldehyde as a crosslinking agent. Another method is encapsulation of the biocatalyst in polymeric matrices, e.g. in a highly porous sol–gel [7]. All of these methods, however, need case-to-case optimization, since at present no general-purpose strategy for immobilization is available. Moreover, most of the presented immobilization methods require previous (chromatographic) purification of the biocatalyst, which may raise production costs enormously and thus hampers industrial application [8].

We and others have previously shown that the molecular biological fusion of coiled-coil domains [9–11], small artificial peptides [12–15] and aggregation-prone proteins and domains [16–22] to a target protein, induces the intracellular formation of protein aggregates, so called inclusion bodies (IBs) [23], which, in contrast to the long held view of IBs as inactive intracellular waste deposits [24], can to a certain degree retain their function or, in case of enzymes, their catalytic activity (reviewed recently in [2, 11]. This strategy enables the combination of protein production and immobilization, resulting in (in situ) biologically-produced immobilizates, which we coined catalytically-active IBs (CatIBs) [9–11] or in case of proteins without catalytic activity, functional IBs (FIBs) [25]. Like IBs, CatIBs/FIBs contain predominantly the recombinant target protein [26]. Furthermore, they can be produced fast and cost-efficiently, because any previous purification and subsequent cross-linking steps are dispensable. These properties render the resulting particles beneficial for the application in synthetic chemistry, biocatalysis [9, 16, 27], and biomedicine [28–30].

In contrast to most of the above-mentioned strategies that employed artificial peptides or aggregation-prone proteins, our recently presented strategy relies on the fusion of a naturally-occurring coiled-coil domain for the targeted production of CatIBs/FIBs [9–11]. In these studies the tetrameric coiled-coil domain of the cell-surface protein tetrabrachion (tetramerization domain of tetrabrachion; TDoT) from *Staphylothermus marinus* [31] was fused to a variety of different target enzymes with different complexity: the lipase A from *Bacillus subtilis* (*Bs*LA), a hydroxynitrile lyase from *Arabidopsis thaliana* (*At*HNL), the thiamine-diphosphate (ThDP)-dependent enzyme MenD (2-succinyl-5-enol-pyruvyl-6-hydroxy-3-cyclohexene-1-carboxylate synthase) from *E. coli* (*Ec*MenD), and the pyridoxal 5′-phosphate (PLP)-dependent lysine decarboxylase from *E. coli* (*Ec*LDC), as well as the yellow fluorescent protein (YFP) [9–11]. Thus, we already demonstrated that the fusion strategy is applicable to a broad spectrum of enzymes as well as fluorescent proteins of the GFP family. In these recent studies, the application of CatIBs in biocatalysis was addressed in more detail, e.g. it could be demonstrated that *At*HNL–CatIBs revealed a higher stability at acidic pH values compared to the soluble enzyme, and could be recycled several times for the production of chiral cyanohydrins in a mono-phasic micro-aqueous reaction system consisting of the buffer-saturated organic solvent, methyl *tert*-butyl ether (MTBE) [9]. CatIBs of the constitutive L-lysine decarboxylase of *E. coli* were employed for the efficient biocatalytic production of 1,5-diaminopentane (trivial name: cadaverine) [10]. Moreover, very recently we employed the CatIB strategy for the coimmobilization of two enzymes, namely a benzaldehyde lyase from *Pseudomonas fluorescens* (*Pf*BAL) and an alcohol dehydrogenase from *Ralstonia* sp. (*R*ADH), to facilitate the realization of an integrated enzymatic two-step cascade for the production of (1*R*,2*R*)-1-phenylpropane-1,2-diol, a building block of the calcium channel blocker diltiazem [25]. The resulting *Pf*BAL/*R*ADH Co-CatIBs showed improved stability in the cascade reaction as compared to the soluble enzymes [25]. Improved stability, compared to soluble, purified *Pf*BAL, was also demonstrated for the isolated *Pf*BAL-CatIBs, while additionally it could be shown that, depending on the employed coiled-coil domain, CatIBs can be tailored for the application in different reaction systems [32]. For example, the use of the 3HAMP coiled coil, which was derived from the oxygen sensor protein Aer2 from *Pseudomonas aeruginosa*, as aggregation-inducing tag, resulted in CatIBs that were better suited for the use in biphasic aqueous-organic reaction systems, e.g. with cyclopentyl methyl ether (CPME) as organic phase [32]. In contrast, TDoT-*Pf*BAL CatIBs appeared to be better suited for the use in monophasic buffer/dimethyl sulfoxide (DMSO) mixtures [32]. While demonstrating the application potential of CatIBs, these studies did not fully address differences in aggregation (CatIB/FIB formation) efficiency and characteristics, such as the overall activity compared to the soluble purified enzyme, the composition of the particles, the final yield, or their morphology. Moreover, the flexibility of the approach,

i.e. in terms of optimization potential by fusion–protein redesign, and the structural basis for CatIB/FIB formation remain unaddressed.

To fill this gap, in the present contribution we applied our fusion strategy to different fluorescent reporter proteins and various differently complex enzymes and empirically analyzed the properties of already established CatIBs. Using this strategy, for three out of seven target proteins, CatIB/FIB formation was successful, revealing variable CatIB/FIB formation efficiency. Based on this initial success, we set out to evaluate the optimization potential for our strategy by generating redesigned fusion constructs by (i) deleting intradomain linkers, (ii) considering C-terminal instead of N-terminal TDoT fusion and (iii) by employing an alternative coiled-coil domain as aggregation-inducing tag. Employing those simple genetic optimization steps, all of the target proteins that initially failed to produce active aggregates or only did so inefficiently, could successfully be produced as CatIBs/FIBs. Using this wealth of different CatIBs/FIBs, we systematically characterized biotechnologically-relevant properties like residual activities compared to the soluble purified enzyme, yield, particle composition, and morphology. Interestingly, (electron) microscopic studies revealed differences in particle/immobilizate morphology, which could be correlated to different CatIB/FIB properties such as activity retention, yield and composition. Last but not least, we show evidence that aggregation (CatIB/FIB formation) efficiency appears to be correlated to the solvent-accessible hydrophobic surface area of the target enzyme, providing a structure-based rationale for our strategy and opening up the possibility to predict its efficacy for any given target protein.

Results and discussion

The toolbox strategy

As outlined in the introduction, our previously presented immobilization strategy relies on the molecular biological fusion of a tetrameric coiled-coil domain to a target enzyme, which induces the formation of catalytically-active inclusion bodies (CatIBs) that in case of non-catalytically-active target proteins, such as fluorescent proteins (FPs), are called functional inclusion bodies (FIBs). In its physiological context, this coiled-coil domain forms a strong superhelix [33, 34] and induces the formation of CatIBs/FIBs by a currently unknown mechanism [11]. The initial gene-fusion-containing expression plasmid was constructed from separate modules so that every part could be easily exchanged or deleted (Additional file 1: Figure S5, A). In all previous constructs the fusion protein contained an N-terminal hexahistidine (His_6) tag, followed by the TDoT domain fused N-terminally to the target enzyme, via a linker region consisting of a flexible $(GGGS)_3$-motif and a protease Factor Xa cleavage site. In contrast to our initial study [9], the starting vector used in this study did not possess the coding sequence for an N-terminal His_6 tag, as also described recently [10]. To rule out any effect of His_6-tag removal on the aggregation behaviour, quantified here as the efficiency of CatIB/FIB formation, we compared FIB formation for a TDoT-L-YFP construct with and without N-terminal His_6-tag (Additional file 1: Figure S1). CatIB/FIB formation efficiency is hereby defined as the activity, or in case of FPs, fluorescence, of the insoluble IB-containing pellet fraction (P) relative to the activity/fluorescence of the crude cell extract (CCE, set to 100%). For both constructs, similar fluorescence was detected in the insoluble IB-containing fraction of the corresponding lysates, suggesting that the His_6 tag has no influence on the aggregation inducing behaviour of the TDoT domain (Additional file 1: Figure S1). Therefore, to simplify the previous vector design, all further constructs were generated without His_6 tag.

To further validate the broad applicability of our CatIB/FIB strategy, we here employed simple FPs, for easy detection and microscopic observation of FIB formation, and generated CatIBs of various differently complex target enzymes to enable catalytic characterization. As target FPs we selected a monomeric version of the enhanced yellow fluorescent protein [35, 36] (YFP; 27.1 kDa) (for details regarding the employed YFP version see "Methods") and mCherry (26.7. kDa), a monomeric red fluorescent protein [37]. As target enzymes, two alcohol dehydrogenases (*R*ADH from *Ralstonia* sp. and *Lb*ADH from *Lactobacillus brevis*) and two ThDP-dependent enzymes [benzoylformate decarboxylase from *Pseudomonas putida* (*Pp*BFD) and benzaldehyde lyase from *Pseudomonas fluorescence* (*Pf*BAL)] were added to the CatIB toolbox. *R*ADH and *Lb*ADH are NADPH-dependent tetrameric enzymes with a subunit size of about 27 kDa [38–40]. *R*ADH requires Ca^{2+}-ions for its stability [41], whereas Mg^{2+}-ions are important for *Lb*ADH to maintain its structural integrity and catalytic activity [42]. *Pf*BAL [43] and *Pp*BFD [44–47] are thiamine-diphosphate (ThDP) and Mg^{2+}-ion dependent tetrameric enzymes with a subunit size of 60 kDa (*Pf*BAL) and 56 kDa (*Pp*BFD). CatIBs of *Pf*BAL as well as *R*ADH have recently been described [25]. For *Pp*BFD, we used the variant L476Q with enhanced carboligation activity [48]. The by far biggest enzyme tested as CatIBs is *Ec*LDC, the constitutive lysine decarboxylase from *Escherichia coli* [49]. This pyridoxal 5′-phosphate (PLP)-dependent enzyme forms a decamer that comprises five dimers with a subunit size of 80.6 kDa. The biocatalytic application of *Ec*LDC-CatIBs was recently demonstrated [10].

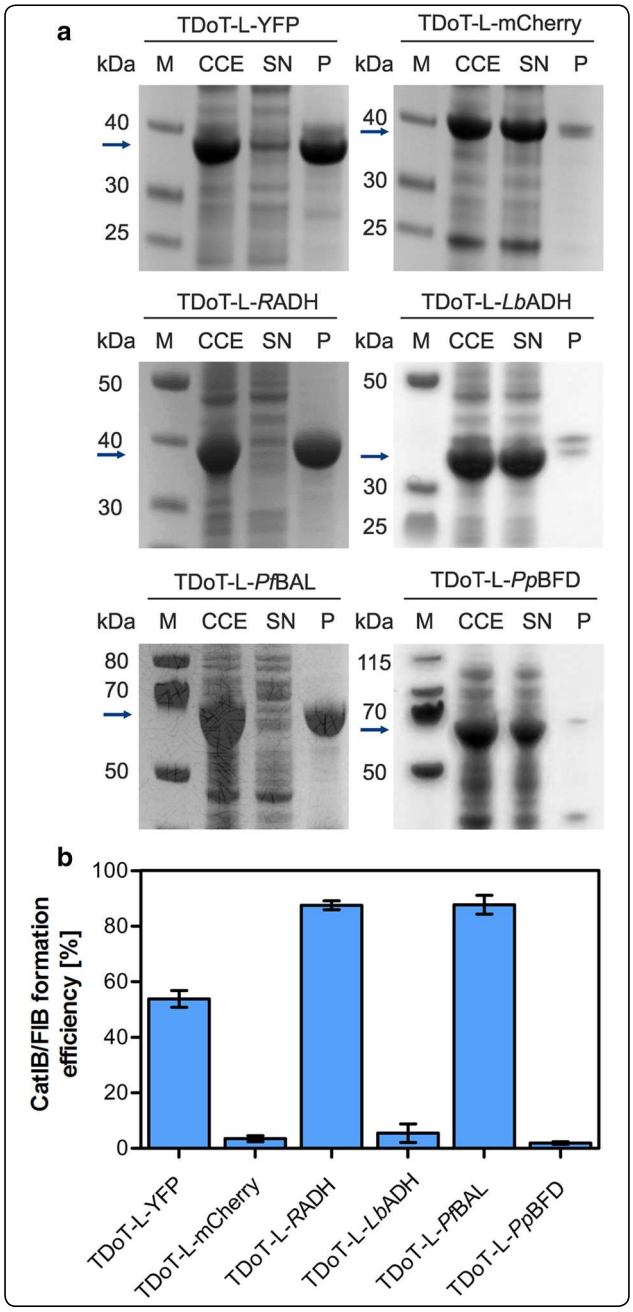


Fig. 1 Evaluation of the CatIB/FIB strategy by **a** SDS-PAGE analysis of CatIB/FIB-production and **b** CatIB/FIB formation efficiency for TDoT-L-YFP (Data taken from [25]), TDoT-L-mCherry, TDoT-L-*R*ADH (Data taken from [25]), TDoT-L-*Lb*ADH, TDoT-L-*Pf*BAL (Data taken from [25]), and TDoT-L-*Pp*BFD. After cell disruption, the crude cell extract (CCE) was separated by centrifugation into the soluble protein containing supernatant (SN) and the insoluble IB-containing pellet (P) fractions. **a** SDS-PAGE analysis of the respective protein/enzyme fractions: CCE, SN, and P. The molecular mass of the respective fusion proteins is indicated by arrows (TDoT-L-YFP: 34.6 kDa, TDoT-L-mCherry: 34.3 kDa, TDoT-L-*R*ADH: 34.3 kDa, TDoT-L-*Lb*ADH: 34.3 kDa, TDoT-L-*Pf*BAL: 66.5 kDa, TDoT-L-*Pp*BFD: 65.3 kDa). The protein content in the SN was measured using the Bradford method [87]. **b** CatIB/FIB formation efficiency quantified as the activity/fluorescence in P fractions expressed relative to the activity/fluorescence of the CCE (set to 100%). The complete datasets illustrating the distribution of activity/fluorescence in the CCE, SN and P fractions can be found in Additional file 1: Figure S2. Note: the P fraction was washed once with water and centrifuged again before the activity/fluorescence measurement. The initial rate activities of the ADHs were measured by reduction of 1-phenylethanol (TDoT-L-*Lb*ADH) or cyclohexanone (TDoT-L-*R*ADH) under the consumption of NADPH (Additional file 1: Figure S13a and b). Initial rate activities of the TDoT-L-*Pf*BAL CatIBs and the TDoT-L-*Pp*BFD CatIBs were measured by following the carboligation of 3,5-dimethoxybenzaldehyde (DMBA) to the respective benzoin or by following the decarboxylation of benzoylformate to benzaldehyde (Additional file 1: Figure S13c and d). Error bars correspond to the standard deviation of the mean derived from at least three biological replicates

Formation of CatIBs/FIBs by N-terminal TDoT fusion

Our previous design concept for immobilization of additional target proteins was validated by fusing the TDoT-domain N-terminally to the above described target proteins following the fusion strategy depicted in Additional file 1: Figure S5a. CatIBs/FIBs were produced and purified using a standardized protocol [9, 10]. This protocol included standardized expression of the gene fusions in *E. coli* BL21(DE3), cell disruption and fractionation of the resulting crude cell extract (CCE) by centrifugation to separate the soluble protein containing fraction (supernatant, SN) from the insoluble, CatIB/FIB-containing fraction (pellet, P). To remove any eventually present soluble protein from the IB pellet, the pellet was resuspended in water, and subsequently centrifuged to separate again the supernatant from the CatIB/FIB containing pellet. All fractions were analyzed by SDS-PAGE (Fig. 1a) and CatIB/FIB formation efficiency was quantified as the activity, or in case of FPs the fluorescence of the once washed IB-containing pellet faction (P) relative to the activity/fluorescence of the CCE (set to 100%) (Fig. 1b). For clarity, only the relative activity in the washed CatIB/FIB-containing pellet fraction is shown in Fig. 1b. The complete datasets illustrating the distribution of activity/fluorescence in the CCE, SN and P fractions can be found in Additional file 1: Figure S2).

Whereas for both TDoT-L-*R*ADH and TDoT-L-*Pf*BAL >80% of the CCE activity was found in the pellet fraction, only 40% of the YFP fluorescence was detected in the pellet, indicating that, our strategy works less efficient for YFP (Fig. 1b). For TDoT-L-mCherry, TDoT-L-*Lb*ADH, and TDoT-L-*Pp*BFD, this effect was even more pronounced, as for these fusions barely any activity/fluorescence could be detected in the IB-containing pellet fraction (Fig. 1b), whereas the majority of the CCE activity was present in the soluble (SN) fraction (Additional

file 1: Figure S2). The same overall trend was also seen in the corresponding SDS-PAGE analyses. The TDoT-L-*Ec*LDC fusion formed large amounts of insoluble aggregates (Additional file 1: Figure S6), which, however, did barely possess any detectable activity ($k_{cat} = 6.2*10^{-7}\ s^{-1}$). In conclusion, our previously presented fusion strategy, relying on the N-terminal fusion of the TDoT coiled-coil domain, was successful for three out of seven of the tested target proteins/enzymes. To evaluate the potential for optimization, we modified our initial strategy generating redesigned fusion constructs by (i) deleting intra-domain linkers, (ii) considering C-terminal instead of N-terminal TDoT fusion and (iii) by employing an alternative coiled-coil domain as aggregation inducing tag.

Concepts to improve the CatIB/FIB formation efficiency

Deletion of the linker region

From previous studies it is known that the linker employed for fusion protein design can have a large impact on fusion protein functionality [50, 51]. Therefore, as a first optimization approach, the influence of deleting the linker polypeptide that in our fusion proteins connect the TDoT coiled-coil domain with the target enzyme/protein, was exemplarily tested for the TDoT-L-mCherry fusion protein, which almost exclusively remained in the supernatant (SN) after cell disruption (96.8%) (Additional file 1: Figure S2a) and barely any fluorescence was detectable in the insoluble FIB-containing pellet (Fig. 1b). Additionally, the same optimization strategy was tested for TDoT-L-YFP, for which only 40% of the total fluorescence of the CCE was found in the pellet fraction (Fig. 1b and Additional file 1: Figure S2a). Therefore, the fusion variants TDoT-YFP and TDoT-mCherry were generated, which lack the $(GGGS)_3$ linker motif as well as the Factor Xa cleavage site (Additional file 1: Figure S5a). Deletion of the linker resulted in about 10% increased fluorescence in the FIB-containing pellet fraction (P) of TDoT-YFP. The improvement was more pronounced for TDoT-mCherry. Here, the fluorescence in the pellet fraction increased by almost 30% (Fig. 2), which is also apparent from the corresponding SDS-PAGE analysis (Fig. 2a; compare to Fig. 1a; TDoT-L-mCherry).

This improvement of the FIB-formation efficiency might hereby be related to a higher rigidity of the fusion protein, due to deletion of the linker. In conclusion, linker deletion appears to be one suitable strategy to improve the CatIB/FIB formation efficiency for difficult target proteins.

C-terminal TDoT-domain fusion

When designing N-terminal or C-terminal fusion proteins of multimeric proteins, it is instrumental to consider

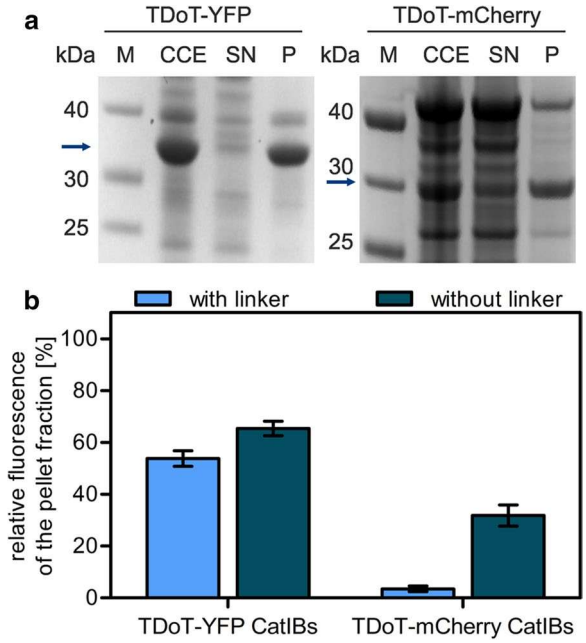


Fig. 2 Optimization of the CatIB strategy by excision of the linker region. CatIB formation was evaluated by **a** SDS-PAGE analysis and **b** FIB formation efficiency for TDoT-YFP and TDoT-mCherry (Data taken from [25]) without linker (dark blue bars) compared to TDoT-L-YFP (Data taken from [25]) and TDoT-L-mCherry with linker (light blue bars). After cell disruption, the crude cell extract (CCE) was separated by centrifugation into the soluble protein containing supernatant (SN) and the insoluble FIB-containing pellet (P) fraction. Sample preparation for SDS-PAGE analysis and determination of the FIB formation efficiency was carried out as described in Fig. 1. **a** SDS-PAGE analysis of the respective protein fractions: CCE, SN, and P. The molecular mass of the target fusion proteins is indicated by arrows (TDoT-YFP: 33.1 kDa, TDoT-mCherry: 32.7 kDa). **b** FIB formation efficiency quantified as the fluorescence in P fractions expressed relative to the fluorescence of the CCE (set to 100%). The complete datasets illustrating the distribution of fluorescence in the CCE, SN and P fractions can be found in Additional file 1: Figure S3. Error bars correspond to the standard deviation of the mean derived from at least three biological replicates

steric constrains imposed by the quaternary structure, i.e. with regard to the location of the termini. We therefore analyzed the structures of all our multimeric target proteins (*R*ADH, *Lb*ADH, *Pf*BAL, *Pp*BFD and *Ec*LDC) for the accessibility of the N- and C-terminus (Additional file 1: Figure S4). For *R*ADH, *Lb*ADH, *Pf*BAL and *Pp*BFD, the N-termini are localized at the protein surface facing outwards and should thus be accessible for TDoT fusion (Additional file 1: Figure S4a–d) without impacting the formation of the multimer. Thus, C-terminal TDoT fusion was not considered in these cases. In contrast, in *Ec*LDC, the N-termini are buried within the decameric structure of the *Ec*LDC multimer, whereas the C-terminus is located at the protein surface [52] (Additional file 1: Figure S4e). Therefore, N-terminal fusion of the TDoT tag appears not

Table 1 Characteristics of CatIBs/FIBs All constructs were characterized regarding CatIB/FIB formation efficiency, quantified as the relative activity of the insoluble CatIB/FIB-containing pellet fraction compared to the crude cell extract (set to 100%), the initial rate activity (k_{cat}; $\mu mol_{Product}$ s^{-1}, per subunit) of the lyophilized CatIB preparation, activity retention compared to the soluble enzyme, the relative protein and lipid content based on the initial weight of the lyophilizate and the yield of CatIBs obtained from 100 g wet *E. coli* cells

Construct	CatIB/FIB formation efficiency [%]	Activity k_{cat} [s^{-1}]	Residual activity [%][d]	Rel. protein content lyophilizate [%]	Yield $\frac{g_{lyophilizate}}{100 g_{cells}}$ g	Lipid content [%]
Constructs showing robust CatIB/FIB formation efficiency						
TDoT fusions						
TDoT-L-YFP	53.8 ± 7.4 (6)[b]	na	na	70.0 ± 5.3 (4)	4.9 ± 0.6 (3)	nd
TDoT-YFP	65.4 ± 4.9 (3)	na	na	69.2 ± 6.8 (2)	5.5 (1)	nd
TDoT-mCherry	31.8 ± 8.2 (4)[b]	na	na	85.7 ± 8.3 (2)	3.2 (1)	nd
TDoT-L-*Bs*LA[a]	114.1 ± 3.1 (1)	nd	nd	79 (1)	8.6 (1)	nd
TDoT-L-*At*HNL[a]	76.4 ± 3.5 (1)	4.3 ± 0.2 (1)	11.1	85 (1)	7.3 (1)	nd
TDoT-L-*Ec*MenD[a]	90.3 ± 0.2 (1)	nd	nd	93 (1)	12.2 (1)	nd
TDoT-L-*R*ADH	87.5 ± 3.2 (4)[b]	0.054 ± 0.008 (3)[b]	2.0[b]	84.6 ± 3.9 (3)[b]	9.7 ± 1.7 (4)[b]	14.3 ± 0.3 (1)
TDoT-L-*Pf*BAL	87.7 ± 6.8 (4)[b]	0.77 ± 0.12 (4)[b,c]	1.0[b,c]	71.9 ± 4.5 (4)[b,c]	8.8 ± 1.0 (8)[b]	16.4 ± 1.0 (1)[c]
TDoT-*Ec*LDC	nd	$6.2*10^{-7}$ (1)	nd	nd	nd	nd
*Ec*LDC-L-TDoT	nd	0.71 (1)[e]	nd	67.9 ± 5.9 (3)[e]	12.4 ± 3.0 (3)	12.9 ± 3.2 (1)
3HAMP fusions						
3HAMP-L-*R*ADH	75.4 ± 3.7 (4)	0.33 ± 0.02 (3)	12.0	50.9 ± 7.6 (3)	3.8 ± 0.5 (3)	30.6 ± 8.3 (1)
3HAMP-L-*Pf*BAL	75.8 ± 8.0 (5)	13.9 ± 2.9 (3)[c]	18.1[c]	33.8 ± 5.2 (3)[c]	3.3 ± 0.5 (4)	30.1 ± 4.7 (1)[c]
3HAMP-L-*Lb*ADH	67.0 ± 21.7 (3)	0.60 ± 0.20 (3)	1.0	54.6 ± 8.0 (3)	8.1 ± 1.3 (3)	34.7 ± 1.36 (1)
3HAMP-L-*Pp*BFD	61.3 ± 35.4 (3)	23.4 ± 6.1 (4)	10.3	35.5 ± 6.7 (4)	6.6 ± 1.4 (3)	27.9 ± 3.7 (1)
*Ec*LDC-L-3HAMP	nd	0.80 (1)	nd	56.5 ± 6.5 (2)	7.5 ± 6.5 (4)	17.7 ± 0.6 (1)
Constructs showing low CatIB/FIB formation efficiency						
TDoT-L-mCherry	3.5 ± 1.9 (3)	na	na	15.8 ± 0.5 (1)	2.8 (1)	nd
TDoT-L-*Lb*ADH	5.4 ± 5.9 (3)	3.63 ± 0.90 (3)	5.8	43.4 ± 5.5 (3)	2.5 ± 0.4 (3)	25.2 ± 0.73 (1)
TDoT-L-*Pp*BFD	1.2 ± 0.6 (3)	9.2 ± 4.7 (4)	4.1	26.9 ± 4.1 (4)	1.6 ± 0.7 (3)	19.1 ± 0.8 (1)
3HAMP-L-YFP	6.3 ± 3.2 (4)	na	na	49.0 ± 5.7 (3)	5.4 ± 1.0 (3)	nd
3HAMP-L-mCherry	5.5 ± 0.2 (5)	na	na	36.4 ± 4.1 (4)	3.0 ± 0.9 (4)	nd

[a] Data taken from [9]

[b] Data taken from [25]

[c] Data taken from [32]

[d] Residual activity (k_{ca}, µmol product, per subunit) relative to the activity of the corresponding soluble purified enzyme: (*R*ADH: $k_{cat} = 2.76 \pm 0.04\ s^{-1}$; *Pf*BAL: $k_{cat} = 76.7 \pm 2.3\ s^{-1}$; *Lb*ADH: $k_{cat} = 62.2 \pm 6.7\ s^{-1}$; *Pp*BFD: $k_{cat} = 226 \pm 40\ s^{-1}$)

[e] Data given in or derived from [10]. Numbers in brackets refer to the numbers of the biological replicates that were used to obtain error estimates. na: not applicable; nd: not determined

to be feasible for *Ec*LDC, which is corroborated by the observation that the resulting TDoT-L-*Ec*LDC CatIBs, although formed in large amounts, showed barely any activity ($k_{cat} = 6.2*10^{-7}\ s^{-1}$; vide infra, Table 1). At least dimerization of *Ec*LDC is necessary to form the active site [52, 53]. Thus, it is likely that the N-terminal fusion of the TDoT domain impairs the formation of a correctly folded active site. To improve activity and potentially the CatIB-formation efficiency, we modified our initial TDoT-L-*Ec*LDC construct (Additional file 1: Figure S5a) by shifting the TDoT domain from the N-terminus to the C-terminus of *Ec*LDC (Additional file 1: Figure S5b), resulting in *Ec*LDC-L-TDoT. SDS-PAGE analysis of the resulting *Ec*LDC-L-TDoT CatIBs revealed, similar to the N-terminal fusion, large amounts of protein in the insoluble IB-containing pellet fraction (Additional file 1: Figure S6). However, in contrast to the N-terminal fusion, the activity of the final *Ec*LDC-L-TDoT-CatIB lyophilizate was increased by six orders of magnitude ($k_{cat} = 0.71\ s^{-1}$). In conclusion, for target proteins for which structural information is available, the position and accessibility of the N- and C-termini should be considered when generating TDoT fusion proteins to induce CatIB formation, whereas

for target proteins with unknown structure both, N-and C-terminal fusions may be considered.

Fusion to a different coiled-coil domain

To improve the CatIB/FIB formation efficiency, the exchange of the TDoT-domain by another coiled-coil domain was considered as further optimization option. As an alternative to TDoT, the 3HAMP-domain [HAMP: histidine kinases, adenylyl cyclases, methyl-accepting chemotaxis proteins (MCPs), and phosphatases], which is part of the soluble oxygen sensor Aer2 of *P. aeruginosa* [54], was selected. The 3HAMP domain was chosen because of its larger size (172 amino acids) compared to the rather short TDoT coiled-coil domain (52 amino acids), with the rationale in mind that for larger target proteins larger coiled-coils might be needed to facilitate efficient CatIB/FIB formation. Therefore, as the next logical optimization step, we generated fusion proteins for *Lb*ADH and *Pp*BFD, which instead of TDoT were fused to the 3HAMP domain. As in case of our initial fusion strategy and in light of the above described structure analyses (Additional file 1: Figure S4; see chapter "*C-terminal TDoT-domain fusion*"), the 3HAMP domain was fused to the N-terminus of the respective target enzyme, resulting in the constructs 3HAMP-L-*Lb*ADH and 3HAMP-L-*Pp*BFD. Interestingly, for both target enzymes N-terminal 3HAMP-fusion drastically increased the CatIB-formation efficiency, as evidenced by both SDS-PAGE analysis (Fig. 3a; compare to TDoT-L-*Lb*ADH and TDoT-L-*Pp*BFD in Fig. 1a) and activity measurements of the CatIB-containing pellet fraction after fractionation of the corresponding crude cell extracts (Fig. 3b). Compared to the corresponding TDoT fusions (see also Fig. 1b), the CatIB-formation efficiency was increased 12- and 51-fold for 3HAMP-L-*Lb*ADH and 3HAMP-L-*Pp*BFD, respectively.

Prompted by these results, we also generated 3HAMP fusions of the remaining target proteins and quantified CatIB formation efficiency (Fig. 3c, d). While for YFP and mCherry the FIB formation efficiency was low, i.e. compared to the corresponding best performing TDoT construct (Fig. 2), clear CatIB formation was observed for 3HAMP-L-*Pf*BAL and 3HAMP-L-*R*ADH (Fig. 3c, d). In conclusion, the 3HAMP domain apparently can replace TDoT as a tag to induce CatIB/FIB formation and appears to be a valid alternative for difficult targets, for which the TDoT fusion approach fails.

Comparative characterization of TDoT and 3HAMP CatIBs/FIBs

As shown above, we were able to successfully produce CatIBs/FIBs for all of the seven tested target enzymes/proteins by optimizing our initial TDoT fusion strategy. To elucidate potential differences between CatIBs/FIBs produced by TDoT and 3HAMP fusion, we characterized all obtained CatIBs and FIBs with regard to yield ($g_{lyophilizate}$ per 100 g wet *E. coli* cells), composition (relative protein and lipid content), specific activity (k_{cat}), and residual activity compared to the respective soluble purified target enzymes, where possible. The corresponding data is summarized in Table 1 (see also Additional file 1: Figure S8 for details). Some of this data has been presented before, e.g. as part of CatIB application studies [10, 25, 32]. For comparison we also included the respective values (if available) from our first CatIB study, in which we demonstrated CatIB formation by TDoT fusion to the lipase A from *Bacillus subtilis* (*Bs*LA), a hydroxynitrile lyase from *Arabidopsis thaliana* (*At*HNL), and the thiamine-diphosphate (ThDP)-dependent enzyme MenD (2-succinyl-5-enol-pyruvyl-6-hydroxy-3-cyclohexene-1-carboxylate synthase) from *E. coli* (*Ec*MenD) [9].

To provide a better overview, we grouped the different constructs into two categories (i) TDoT and 3HAMP fusion constructs showing robust CatIB/FIB formation and (ii) constructs that only showed low CatIB/FIB formation efficiency (< 10%), irrespective of whether they were fused with TDoT or 3HAMP. The latter category contained constructs of the initial round of experiments, where the TDoT domain was fused N-terminally to the target protein/enzyme (TDoT-L-mCherry, TDoT-L-*Lb*ADH, TDoT-L-*Pp*BFD; see chapter "*Formation of CatIBs/FIBs by N-terminal TDoT fusion*") as well as constructs fused with the 3HAMP domain (3HAMP-L-YFP and 3HAMP-L-mCherry; see chapter "*Fusion to a different coiled-coil domain*"). Compared to the constructs with robust CatIB/FIB formation efficiency those preparations showed low to moderate protein content (16–49%) and lyophilizate yields (1.6–5.4 g lyophilizate per 100 g wet cells) as well as low lipid content (19–25%). In terms of yield and composition those values likely derive from cellular constituents, which remain in the insoluble pellet after cell lysis and centrifugation, i.e. non-lysed cells, cell debris, membrane proteins, and membrane lipids. Surprisingly, the CatIB preparations of TDoT-L-*Lb*ADH and TDoT-L-*Pp*BFD, for which we only observe low CatIB formation efficiency (1.2–5.4% of the overall crude cell extract activity), still showed activities that correspond to 5.8% (TDoT-L-*Lb*ADH) and 4.1% (TDoT-L-*Pp*BFD) of the activity of the corresponding soluble purified enzymes. Several explanations could account for this phenomenon. First, the observed activities result from intact non-lysed cells, containing the respective soluble produced fusion protein, which would require that the substrates used for the activity assays can be taken up by these cells. Likewise, those intact cells could become

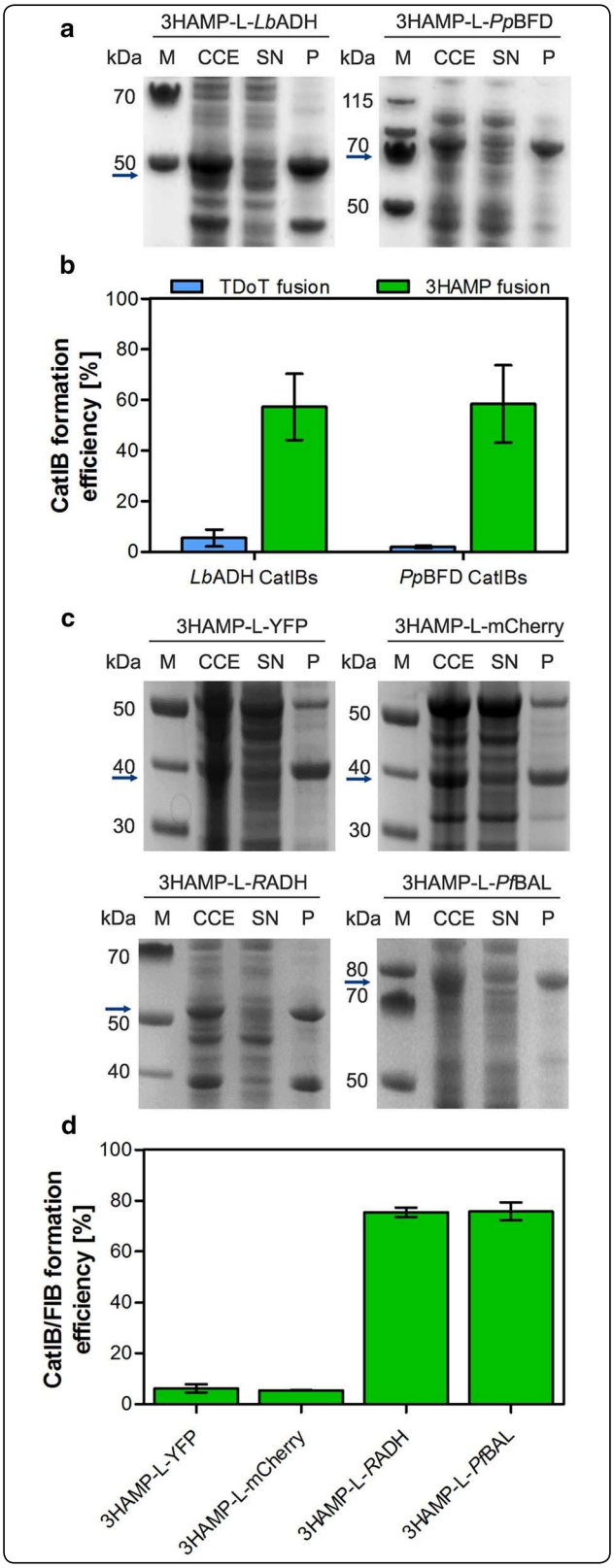


Fig. 3 Optimization of the CatIB strategy by variation of coiled-coil domains using 3HAMP instead of TDoT fusions. CatIB formation was evaluated by **a** SDS-PAGE analysis and **b** CatIB formation efficiency for 3HAMP-L-*Lb*ADH- and 3HAMP-L-*Pp*BFD (green bars) compared to TDoT-L-*Lb*ADH and TDoT-L-*Pp*BFD (blue bars). Panels c) and d) contain the equivalent data for 3HAMP-L-YFP, 3HAMP-L-mCherry, 3HAMP-L-*Pf*BAL and 3HAMP-L-*R*ADH. After cell disruption, the crude cell extract (CCE) was separated by centrifugation into the soluble protein containing supernatant (SN) and the insoluble IB containing pellet (P) fraction. Sample preparation for SDS-PAGE analysis and the determination of the CatIB/FIB formation efficiency was carried out as described in Fig. 1. **a**, **c** SDS-PAGE analysis of the respective protein fractions: CCE, SN, and P. The molecular mass of the target fusion proteins is indicated by arrows (3HAMP-L-*Lb*ADH: 47.1 kDa; 3HAMP-L-*Pp*BFD: 77.0 kDa, 3HAMP-L-YFP: 47.4 kDa, 3HAMP-L-mCherry: 47.1 kDa, 3HAMP-L-*R*ADH: 47.1 kDa and 3HAMP-L-*Pf*BAL: 79.3 kDa). **b**, **d** CatIB/FIB formation efficiency determined as described in Fig. 1. The complete datasets illustrating the distribution of activity in the CCE, SN and P fractions can be found in Additional file 1: Figure S7. Initial rate activities were measured as described in Fig. 1

(partially) lysed during lyophilization of the washed pellet, which would result in the release of the soluble produced fusion protein and hence could account for the observed activity. Secondly, those constructs might indeed form intracellular CatIBs, which, however, disintegrate or are solubilized during the washing step of the CatIB preparation procedure. The latter hypothesis should be observable by SDS-PAGE analyses, i.e. by the appearance of target fusion protein bands in the soluble wash fractions retrieved during the CatIB preparation procedure. Indeed, compared to TDoT-L-*Pf*BAL (Additional file 1: Figure S9c), increased solubilization/leakage of the fusion proteins is observed during the preparation of the TDoT-L-*Lb*ADH and TDoT-L-*Pp*BFD CatIBs (Additional file 1: Figure S9a and b).

Among the constructs showing robust CatIB/FIB formation, all CatIBs/FIBs produced by TDoT fusion, with the exception of the FPs, which showed FIB formation efficiencies between approx. 32% (TDoT-mCherry) and 65% (TDoT-YFP), showed higher CatIB/FIB formation efficiencies [between 76% (TDoT-L-*At*HNL) and 114% (TDoT-L-*Bs*LA)] compared to the 3HAMP fusions [between 61% (3HAMP-L-*Pp*BFD) and 76% (3HAMP-L-*Pf*BAL)]. Here, either less efficient CatIB/FIB formation or partial solubilization/leakage of the fusion protein during the CatIB/FIB preparation procedure might be potential causes. The latter is supported by SDS-PAGE analysis (Additional file 1: Figure S10), where for both 3HAMP-L-*Lb*ADH as well as 3HAMP-L-*Pp*BFD increased leakage/solubilization is observed during the washing steps performed for CatIB/FIB preparation (Additional file 1: Figure S10, compare to TDoT-*L*-*Pf*BAL, Additional file 1: Figure S9c).

Interestingly, in terms of activity (expressed as k_{cat} to account for the differences in molecular mass between the TDoT and 3HAMP fusions and the respective soluble purified enzymes) and residual activity (compared to the respective soluble enzyme), the 3HAMP CatIBs generally seem to outperform the TDoT CatIBs. With the exception of TDoT-L-*At*HNL the TDoT CatIBs showed residual activities of 1–2% of the respective soluble purified enzyme, while the 3HAMP CatIBs possessed residual activities between 10% (3HAMP-L-*Pp*BFD) and 18% (3HAMP-L-*Pf*BAL). For example, the direct comparison between equivalent TDoT and 3HAMP fusions revealed a 6- and 18-fold increase in k_{cat} and residual activity for the 3HAMP-*R*ADH and 3HAMP-*Pf*BAL CatIBs, respectively (Table 1).

The observed differences in activity between TDoT and 3HAMP CatIBs are also manifested in differences in CatIB/FIB composition. Here, the relative protein content of the respective lyophilizates was higher for the TDoT CatIBs/FIBs (between 66% [*Ec*LDC-L-TDoT) and 93% (TDoT-L-*Ec*MenD)] compared to the corresponding 3HAMP CatIBs/FIBs [between 34% (3HAMP-L-*Pf*BAL) and 57% (*Ec*LDC-L-3HAMP)]. The lower protein content of the 3HAMP CatIBs/FIBs, however, was accompanied by increased lipid content (approx. 2-fold higher than for the tested TDoT CatIBs/FIBs).

With the exception of the FPs, in terms of yield we routinely obtain 7.3–12.2 g of CatIB lyophilizate per 100 g wet cells of TDoT CatIBs, while for the 3HAMP CatIBs somewhat lower yields of 3.3–8.1 g of CatIB lyophilizate per 100 g wet cells were obtained.

In conclusion, CatIBs/FIBs derived from TDoT or 3HAMP fusion appear to possess different characteristics. Most interestingly the here described 3HAMP CatIBs showed much higher residual activities than the TDoT-derived CatIBs, which would be advantageous for application. This might be related to a less dense packing of the 3HAMP CatIBs, which would enable better substrate access and could result in higher activities. This hypothesis is supported by the observation that 3HAMP CatIBs more easily disintegrate during CatIB preparation (vide supra, see Additional file 1: Figure S10). As a carrier-free immobilization method, CatIBs can be best compared to cross-linked enzyme aggregates (CLEAs), which showed residual activities of 6–100% based on the initial activity of the enzyme preparation (usually crude cell extracts) before immobilization [55–63]. In the case of CatIBs, as in situ produced immobilizates, we cannot determine the initial total activity before the immobilization process but can only refer to k_{cat} of the purified soluble enzyme. Although a direct comparison of residual activities is not possible, it can be concluded that 3HAMP CatIBs possess residual activities that are at least comparable to certain CLEA preparations. However, compared to CLEAs, CatIBs can be produced more easily and more straightforward involving only cell lysis, centrifugation, and washing steps, i.e. not requiring tedious and expensive enzyme purification, precipitation, and/or cross-linking.

Morphology of the CatIBs

The distinct characteristics observed here for the TDoT and 3HAMP CatIBs/FIBs hint at distinct molecular differences, which might be observable as different CatIB/FIB morphologies. We therefore comparatively investigated the morphology of the different CatIBs/FIBs by conventional (fluorescence) microscopy and scanning electron microscopy (SEM). Hereby, IBs are known to form dense refractive particles at the cell poles in *E. coli*, which can be observed by conventional microscopy [64]. Previous SEM studies of isolated IBs revealed round or barrel like shapes with a size between 300 nm and 1 µm [9, 30, 65, 66].

As a first step, microscopic images of *E. coli* cells after production of different CatIBs/FIBs were taken (Fig. 4). Phase-contrast images were acquired for all preparations and fluorescence detection was used to directly visualize FIB formation for the YFP and mCherry FIBs (Fig. 4a–f); the latter providing additional insight into the localization and morphology of the resulting IB particles. Therefore, we first focused on the different FIB producing constructs. For all TDoT-fusions of YFP and mCherry (with or without the linker region), defined particles were visible at the cell poles, in both phase-contrast and fluorescence images. Interestingly, the construct TDoT-L-mCherry, which showed only low FIB formation efficiency (Fig. 1; Table 1), still shows intracellular FIB formation (Fig. 4d), indicating that the particles are less stable/compact and thus disintegrate more or less completely during cell lysis or later CatIB preparation steps. The same, although to a lesser degree, might be the case for TDoT-L-YFP, as also lower than average FIB formation efficiencies were observed here (Fig. 1, Table 1). In contrast, the 3HAMP-FIBs of YFP and mCherry show no distinct cell-pole localized IB particles in phase-contrast. The corresponding fluorescence images, however, reveal that the fusion proteins are partly distributed throughout the cytoplasm and are partly membrane associated (Fig. 4c, f). In a few cells, less well-defined bright fluorescent spots are found at the cell poles. This is in accordance to the low FIB formation efficiency observed for 3HAMP-L-YFP and 3HAMP-L-mCherry (Fig. 3), and indicates that, indeed, the 3HAMP-derived CatIBs/FIBs might possess a different morphology.

To address this issue, we next acquired phase-contrast images for the remaining 3HAMP and TDoT fusion

constructs (Fig. 4g–k). Here, only the TDoT-fusion of *R*ADH (g), *Pf*BAL (i), and *Ec*LDC (k) as well as the 3HAMP-fusion of *Ec*LDC (k), which also showed robust CatIB formation efficiencies (Fig. 1, Table 1), gave visible CatIB formation. With the exception of the *Ec*LDC-L-3HAMP fusion, which clearly showed intracellular IB formation, all 3HAMP fusions did not show distinct IB particles in the corresponding phase-contrast images.

At the first glance, this appears contradictory to the robust CatIB formation efficiency and the high specific activity (Table 1) observed for e.g. 3HAMP-L-*R*ADH and 3HAMP-L-*Pf*BAL (Fig. 3, Table 1). In principle, two explanations could account for this discrepancy. First, although unlikely, the respective 3HAMP CatIBs are not formed inside the cell and only aggregate into particles after cell disruption. Secondly, the particles are formed within the cell but possess a less dense and more diffuse structure, so that they are not detectable as refractive particles in phase-contrast images. The observed membrane association and the presence of bright fluorescent spots at the cell poles of the 3HAMP mCherry and YFP fusions (Fig. 4c, f) would support the latter possibility. A more diffuse, less densely packed structure would also account for the higher activities observed for the 3HAMP CatIBs, as such particles would enable better substrate accessibility. Likewise, partial membrane association would also explain the increased lipid content of the 3HAMP CatIBs, as membrane lipids might become co-purified together with the CatIBs.

Further, more detailed insight into those morphological features might be gained by scanning SEM. Therefore, we exemplarily acquired SEM images for a set of TDoT and 3HAMP CatIBs (Fig. 5).

As expected, the TDoT-YFP and the TDoT-L-*Pf*BAL CatIBs form classical IBs with round or barrel-like shapes and a size between 500 nm and about 1 µm (Fig. 5a, c). Interestingly, the structures of the corresponding 3HAMP CatIBs appear less well ordered, forming sheets of micrometer-sized flakes, which, however, appear to consist of smaller substructures (Fig. 5b, d).

In conclusion, the TDoT and 3HAMP CatIBs, which possess different characteristics such as residual activity

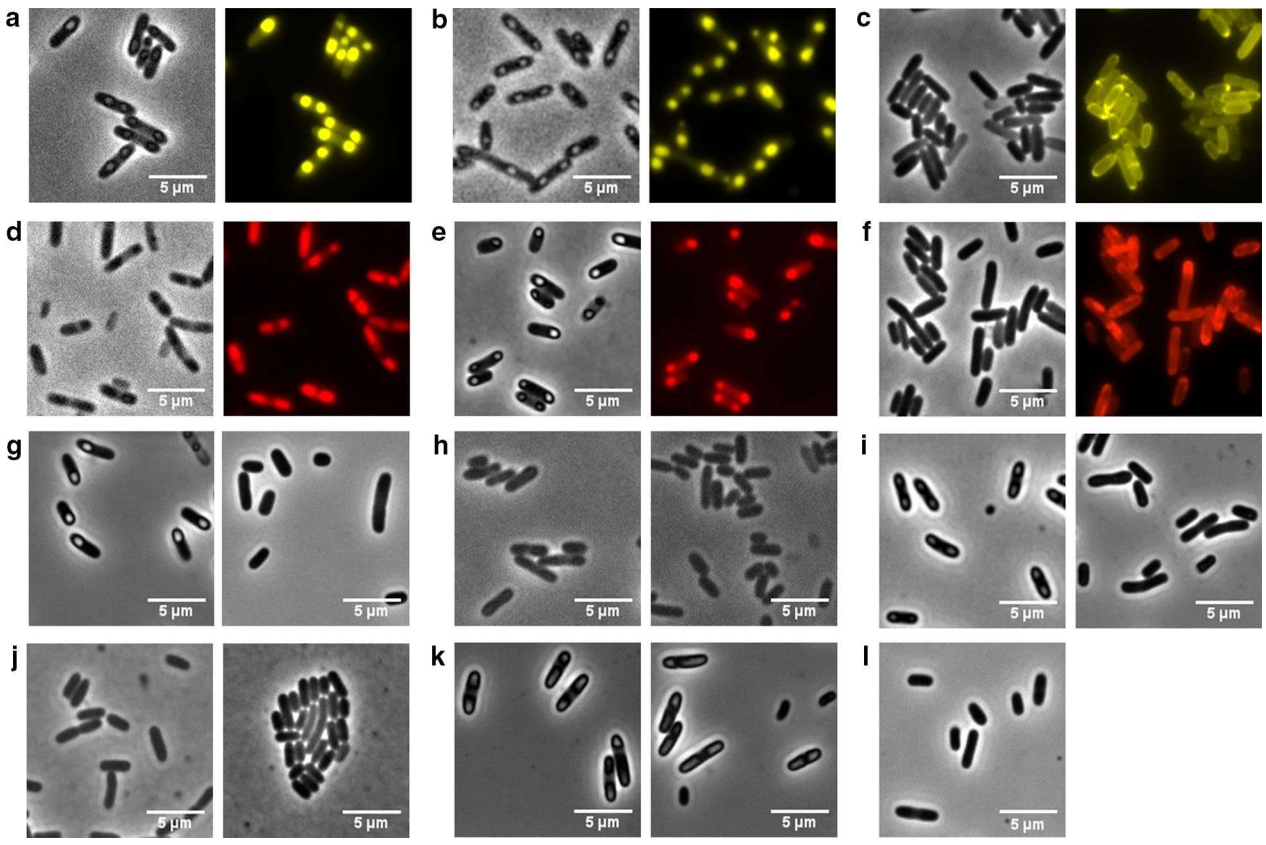


Fig. 4 Microscopy images illustrating CatIB/FIB formation in *E. coli*. **a**–**f** Phase-contrast and fluorescence images of *E. coli* cells expressing **a** TDoT-L-YFP, **b** TDoT-YFP, **c** 3HAMP-L-YFP, **d** TDoT-L-mCherry, **e** TDoT-mCherry, and **f** 3HAMP-mCherry. **g**–**k** phase-contrast images of TDoT fusion (left) and 3HAMP fusion (right) expressing *E. coli* cells containing **g** *R*ADH, **h** *Lb*ADH, **i** *Pf*BAL, **j** *Pp*BFD, **k** *Ec*LDC (here, the coiled-coil domain is fused C-terminally), and **l** *E. coli* BL21(DE3) with empty pET-28a vector. All strains were grown under standard growth conditions as described in "Methods" section

and composition, also show clearly distinct morphology. Moreover, the more diffuse, less densely packed structure of the 3HAMP CatIBs could account for the improved activity compared to the compact, well ordered TDoT CatIBs. To the best of our knowledge this morphological distinction has not been observed before.

Relationship between target sequence, structure, and CatIB formation

The fact that fusing the TDoT coiled-coil domain to certain target proteins resulted in low CatIB/FIB formation efficiencies (Fig. 1, Table 1), while others showed robust aggregate formation (although with variable efficacy), indicates that certain sequence- or structural-features are a prerequisite for CatIB/FIB formation and/or determine the efficiency of the aggregation process. This rationale includes the observation that certain CatIBs/FIBs appear to more easily disintegrate during CatIB/FIB preparation, as this phenomenon likewise results in lower apparent CatIB/FIB formation efficiencies.

We therefore initially analyzed the here employed target proteins as well as the corresponding TDoT fusions for their propensity to aggregate using sequenced-based predictions, as recent studies have indicated that the propensity for IB formation is linked to certain aggregation-prone sequence stretches [11, 67–69]. Hereby, the aggregation propensity of unfolded polypeptide chains appears to be correlated to physicochemical properties like hydrophobicity, secondary structure propensity and charge [70], which can be inferred from the amino acid sequence of both the target protein and the fusion [71]. We here used AGGRESCAN, one of the more widely employed tools for the prediction of aggregation hot spots [72]. In Fig. 6a, the CatIB/FIB formation efficiency (Table 1) of all TDoT fusions was plotted against the AGGRESCAN-derived Na^4vSS score (for further explanations see "Methods"; Additional file 1: Table S1). With the exception of *Lb*ADH and the *Pp*BFD (which both did not form classical, compact CatIBs when fused to the TDoT domain; Fig. 4h, j), there seems to be a weak linear relationship between the Na^4vSS values of the target proteins and the CatIB-formation propensity (outliers were *Lb*ADH and *Pp*BFD; $R^2 = 0.735$ when excluding outliers and $R^2 = 0.353$ when including outliers). Here, target proteins that yield low Na^4vSS values (mCherry, YFP; Additional file 1: Table S1) also yield lower activities/fluorescence in the insoluble fraction. Such low aggregation propensities (i.e. high negative Na^4vSS values) have been for example inferred for intrinsically disordered proteins (IDPs) [72], which are generally very resistant to aggregation and often remain soluble even after boiling [73, 74]. In contrast, the majority of the here employed target proteins showing robust CatIB-formation yield Na^4vSS values between −5 and +5 (Additional file 1: Table S1). Thus, they show aggregation propensities well within the range reported for globular, soluble, and IB-forming polypeptides [72].

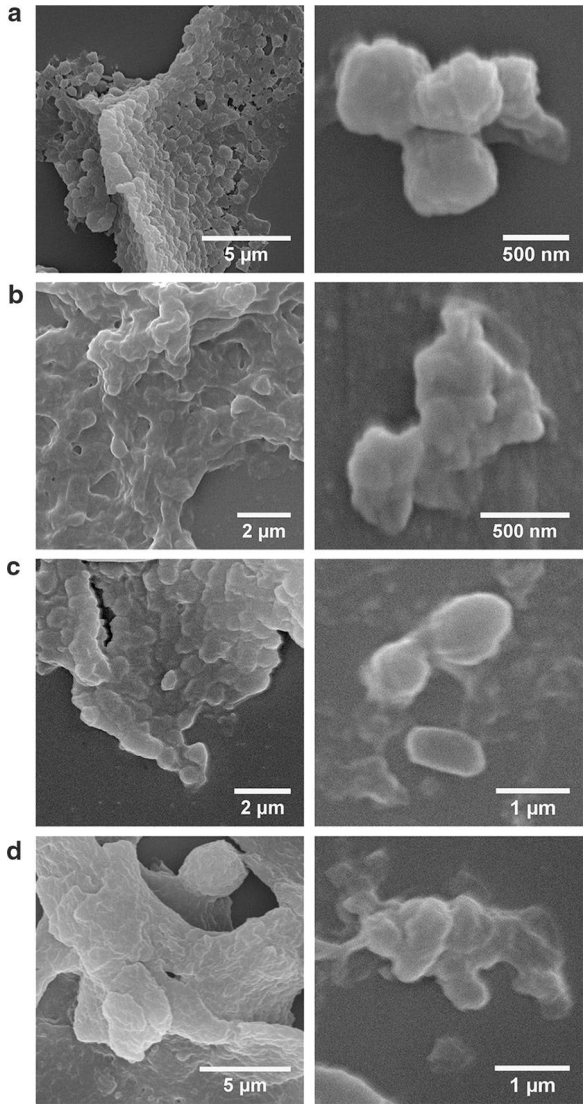


Fig. 5 SEM images of **a** TDoT-YFP, **b** 3HAMP-L-YFP, **c** TDoT-L-*Pf*BAL, and **d** 3HAMP-L-*Pf*BAL CatIBs/FIBs at different magnification. Overview images are shown on the left and detailed images at higher magnification illustrating the smallest particles found in the corresponding preparations are shown on the right. SEM samples were prepared from the final lyophilized CatIB/FIB preparations. Samples were prepared and SEM images were acquired as described in "Methods" section

We next tried to address the influence of fusing the TDoT coiled-coil domain to any given target by calculating the relative change of the Na^4vSS value due to

addition of the TDoT domain (ΔNa^4vSS) (Fig. 6b; Additional file 1: Table S1). Here, no clear trend was observed. On the contrary, while some of the targets that show little aggregation or no classical compact CatIBs (mCherry, *Lb*ADH, *Pp*BFD, YFP) exhibit low positive or low negative ΔNa^4vSS values, the *Bs*LA and *At*HNL fusions, which display robust CatIB formation, show the most prominent (−275% and −51%) change in Na^4vSS by addition of the TDoT domain. This suggests that the TDoT fusion should increase their solubility, which however was not observed experimentally (Additional file 1: Table S1). In conclusion sequence-based predictions can be used in a first approximation to predict the aggregation propensity of a given target protein, however, the consequences of TDoT fusion (i.e. the efficacy of the resulting CatIB-formation process) cannot be directly inferred or understood only based on those predictions.

Since CatIBs/FIBs, in contrast to conventional IBs, retain a certain degree of activity, it seems reasonable to assume that the corresponding enzymes/proteins retain their native (quaternary) structure in CatIBs/FIBs (at least to some extend). Therefore, it seems likely that in CatIBs/FIBs aggregation does not solely occur from the unfolded state (as the previous sequence-based predictions assume) but also involves the aggregation or co-aggregation of already folded (i.e. native) protein species. Hereby, the presence/absence of hydrophobic surface patches on a given target could determine the efficiency of aggregation. To address this issue, we evaluated the available target protein structures for the presence of large hydrophobic surface patches by using the Rosetta protein design software (see "Methods" for details; Additional file 1: Figure S11, Table S2) [75, 76]. For five out of nine of the target proteins, the plot of the CatIB/FIB formation efficiency against the percentage of the hydrophobic patch area on the overall solvent accessible surface area (SASA) yielded a good linear relation (excluding outliers: $R^2 = 0.995$; including *Ec*MenD, *R*ADH, YFP, and *Lb*ADH: $R^2 = 0.286$) (Additional file 1: Figure S12). When we consider the presence of alternative oligomeric assemblies (inferred by using the PISA webserver; see "Methods"; Additional file 1: Table S2), the correlation is significantly improved for *R*ADH and YFP (excluding outliers: $R^2 = 0.975$; including *Ec*MenD and *Lb*ADH: $R^2 = 0.837$) (Fig. 6c). Here, it appears that the presence of large hydrophobic surface patches clearly relates to the efficacy of CatIB formation, thus providing a structural rationale, why certain highly soluble proteins like mCherry fail to form insoluble FIBs or form only FIBs that disintegrate during cell lysis or are solubilized during CatIB/FIB preparation.

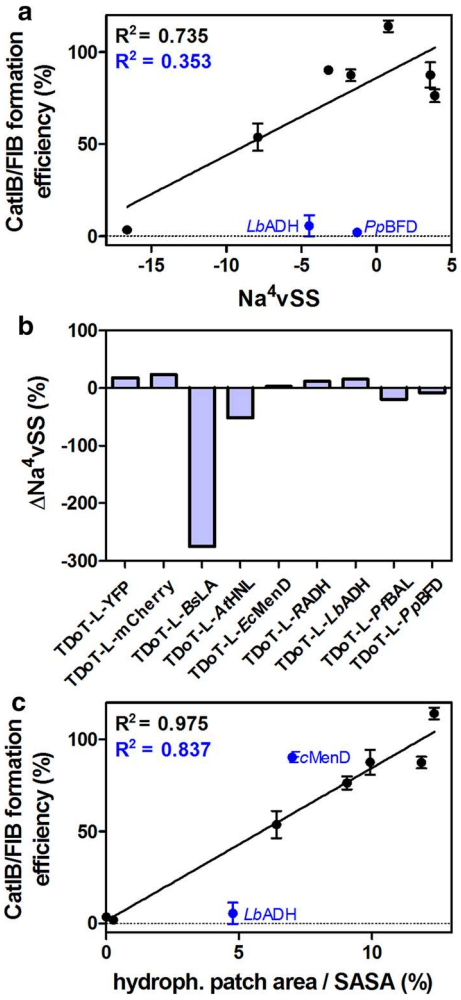


Fig. 6 Computational analysis of the **a**, **b** sequence-based and **c** structural determinants of CatIB/FIB formation analyzed based on the TDoT dataset. **a** Sequence-based aggregation propensities were inferred using the AGGRESCAN webserver [72] and the average aggregation-propensity values per amino acid (a^4v) normalized to a 100-residue protein (Na^4vSS) were used as indicator for aggregation. Low (negative) Na^4vSS are an indicator for low aggregation propensity as for example demonstrated for intrinsically disordered proteins (IDPs) [72]. **b** The relative change of the Na^4vSS value due to addition of the TDoT domain $\left(\Delta Na^4vSS = \left(\frac{(Na^4vSS_{fusion} - Na^4vSS_{target})}{|Na^4vSS_{target}|}\right) \times 100\right)$ has in the past been used for the computation of the effects of point mutations on aggregation [72]. Positive values suggest increased and negative values decreased aggregation due to addition of the TDoT domain. **c** The presence/absence of large hydrophobic surface patches for the corresponding target protein structures was quantified using the hpatch tool implemented in Rosetta [75, 76, 94]. Surface areas were quantified using Pymol 1.7.0.0 (Schrödinger, LCC, New York, NY, USA). In a and c CatIB-formation was plotted as the relative activity in the insoluble fraction (Additional file 1: Table S1). Coefficient of determination (R^2) values are always given excluding the blue-highlighted outliers (black) and including the outliers (blue)

Conclusions

The generation of catalytically-active inclusion bodies (CatIBs) represents a recently developed, promising strategy for the solely biological production of carrier-free enzyme immobilizates. This strategy relies on the molecular biological fusion of a coiled-coil domain to target enzymes/proteins to induce the formation of intracellular aggregates (inclusion bodies, IBs) which retain a certain degree of activity. While this strategy has already been proven successful in multiple cases, the efficiency, the potential for optimization, and important CatIB properties like yield, activity, and morphology have not been investigated systematically. In this contribution, different optimization strategies, like linker deletion, C- versus N-terminal fusion, and the fusion of alternative aggregation-inducing tags have been evaluated. While linker deletion and C-terminal instead of N-terminal fusion successfully yielded CatIBs/FIBs for certain target proteins for which our initial N-terminal fusion strategy failed, the use of the 3HAMP coiled-coil domain as alternative aggregation-inducing tag resulted in CatIBs with superior activity and altered composition. Using conventional microscopy and scanning electron microscopy, we provide evidence for the distinct morphology of 3HAMP-derived CatIBs. The latter appears moreover to be linked to their superior performance. Last but not least, we demonstrated that CatIB formation efficiency can be correlated to the solvent-accessible hydrophobic surface area of the target enzyme, providing a structure-based rationale for our strategy and opening up the possibility to predict its efficiency for any given target protein. In conclusion, we here provide evidence for the general applicability, predictability, and flexibility of the CatIB immobilization strategy, highlighting its application potential for synthetic chemistry and industry.

Methods

Reagents and chemicals

Chemicals were purchased from Sigma-Aldrich, Fluka, Roth, KMF, Biosolve, Alfa Aesar, AppliChem, and Merck. Enzymes for molecular biology were purchased from Thermo Scientific (Waltham, MA, USA). Enantiopure (*R*)-(3,3‘,5,5‘)-tetramethoxy benzoin (TMBZ) for the calibration of HPLC analysis was taken from a stock prepared as described elsewhere [10, 25, 77].

Construction of expression plasmids

The general design strategy for the construction of the respective TDoT gene fusions has been described before [9] (Additional file 1: Figure S5a). If not stated otherwise, all gene fusions consisted of gene fragments coding for a coiled-coil domain (here TDoT or 3HAMP), a linker polypeptide, consisting of a protease Factor Xa cleavage site and a triple $(GGGS)_3$ and the respective target proteins/enzymes cloned into a pET-28a vector (Novagen, Merck KGaA, Frankfurt, Germany). As target FPs YFP (27.1 kDa), a monomeric version of the enhanced yellow fluorescent protein (eYFP) from *Aequorea victoria* was used. This YFP contains the A206K exchange for the monomerization [36] but lacks the Q69K substitution, which renders it less sensitive in the neutral pH [78, 79]. As a second FP target, the monomeric red fluorescent protein mCherry from *Discosoma striata* (26.7 kDa) [37] was chosen. As target enzymes, two alcohol dehydrogenases (*R*ADH from *Ralstonia* sp. and *Lb*ADH from *Lactobacillus brevis* [38–40]) and two ThDP-dependent enzymes [benzoylformate decarboxylase from *Pseudomonas putida* (*Pp*BFD) [43] and benzaldehyde lyase from *Pseudomonas fluorescence* (*Pf*BAL)] [46, 47] were used. To simplify the toolbox vector, the N-terminal His_6-tag was removed from pTDoT-Linker-YFP [9], resulting in the pTDoT-L-YFP vector, as described before [25]. All in the following described constructs were based on this simplified toolbox vector and hence lacked the N-terminal His_6 tag.

The pTDoT-YFP and pTDoT-mCherry vectors lacking the linker polypeptide, consisting of the Factor Xa protease cleavage site and the triple $(GGGS)_3$ motif, were created as described before [25]. For the exchange of the coiled-coil domain, the pTDoT-L-YFP plasmid was digested with *Nde*I and *Spe*I to release the *tdot* fragment. A codon-optimized *3hamp* gene fragment, containing 5′-*Nde*I and 3′-*Spe*I restriction sites, was synthesized and supplied on a plasmid (pEX-A-3HAMP-Linker, Eurofins Genomics, Ebersberg, Germany). After restriction, the corresponding *3hamp* gene fragment was ligated into the initial plasmid, lacking the *tdot* gene fragment, to attain the p3HAMP-L-YFP vector. Genes coding for mCherry, *R*ADH, *Lb*ADH, *Pf*BAL, *Pp*BFD, and *Ec*LDC were amplified by standard PCR utilizing oligonucleotide primers containing a 5′-*BamH*I and a 3′-*Sal*I (mCherry, *R*ADH, *Lb*ADH, *Ec*LDC) or 3′-*Not*I (*Pf*BAL, *Pp*BFD) site. PCR products were digested with respective restriction endonucleases and ligated into similarly hydrolyzed pTDoT-L-YFP or p3HAMP-L-YFP. The vectors containing the TDoT-L-*R*ADH and TDoT-L-*Pf*BAL fusion as well as the vector containing the 3HAMP-L-*Pf*BAL fusion has been constructed as described in [25] and [32], respectively. The construction of the plasmid p*Ec*LDC-L-TDoT, for C-terminal fusion of TDoT to *Ec*LDC, has also been described before [10]. The plasmid containing the gene fusion encoding for the C-terminal *Ec*LDC-L-3HAMP fusion (p*Ec*LDC-L-3HAMP) was constructed similarly to the N-terminal 3HAMP-vectors by digesting p*Ec*LCD-L-TDoT with *Bam*HI and *Not*I and ligating the resulting linear DNA with a PCR amplified *3hamp* gene fragment

utilizing oligonucleotide primers containing a 5′-*BamH*I and a 3′-*Not*I restriction site, originated from the pEX-A-3HAMP-Linker vector. All sequences were verified by sequencing (Seqlab GmbH, Göttingen, Germany and LGC genomics, Berlin, Germany). For information about all plasmids and oligonucleotide primers see Additional file 1.

Production and purification of inclusion bodies (IBs)

The target gene fusions were heterologously expressed in *E. coli* BL21(DE3) using autoinduction medium [80] for 69 h at 15 °C as described recently [9, 10, 25]. Cell disruption was performed from a 10% (w/v) suspension in lysis buffer (50 mM sodium phosphate buffer, 100 mM NaCl, pH 8.0) with an Emulsiflex-C5 high-pressure homogenizer (Avestin Europe GmbH, Mannheim, Germany) as described before [10, 25]. To separate the IB-containing pellet from the soluble supernatant, the crude cell extract was centrifuged (30 min at 4 °C and 15,000×*g*) and frozen at −20 °C in a freezer. The pellet was washed once with the initial volume of MilliQ water and was again centrifuged. The obtained pellet was lyophilized for 72 h from a frozen (−80 °C) 10% (w/v) suspension in MilliQ water (Christ ALPHA 1-3 LD Plus, Martin Christ Gefriertrocknungsanlagen GmbH, Osterode, Germany). The dried CatIBs were grounded and stored as a fine powder at −20 °C until further use [10, 25].

Production and purification of soluble enzymes

Soluble *R*ADH, encoded on a pET-22b vector [81], was produced in *E. coli* BL21(DE3) according to the expression protocol used for the CatIB production. Soluble *Lb*ADH, encoded on a pET-21a vector, was produced in *E. coli* BL21(DE3) as described elsewhere [82, 83]. Soluble *Pf*BAL was fused to a C-terminal hexahistidine tag and was encoded on a pkk233_2 vector [84]. The protein was produced in *E. coli* SG 13009 according to a protocol described elsewhere [77, 84] using a 40 l Techfors fermenter (Infors AG, Bottmingen, Swiss) at 30 °C in fed-batch mode [85]. Soluble *Pp*BFD-L476Q (fused to a C-terminal hexahistidine tag) encoded on the pkk233_2 vector was produced in *E. coli* SG 13009 according to a protocol described elsewhere [48].

Cells were harvested, centrifuged and the remaining pellet was frozen at −20 °C. The frozen cells were suspended in a 25% (w/v) suspension in the respective equilibration buffer used for purification. Cell disruption was performed on ice by sonication (UP200 s, Hielscher Ultrasonics GmbH, Teltow, Germany) 10-times for 1 min at an amplitude of 70% and a cycle of 0.5, followed by a 1 min break. The soluble enzyme was separated from the cell debris by centrifugation for 30 min (18,000×*g*, 4 °C).

Purification of soluble *R*ADH was performed by anion exchange chromatography according to the protocol described previously [81]. The first step included a desalting by gel filtration with a Sephadex-G25 (GE Healthcare, Little Chalfont, United Kingdom) column with 10 mM TEA-buffer (pH 7.5, 0.8 mM $CaCl_2$). In the second step the desalted protein fraction was purified via anion exchanger (Q-Sepharose Fast Flow column, GE Healthcare, Little Chalfont, United Kingdom) starting with equilibration buffer (50 mM TEA, pH 7.5, 0.8 mM $CaCl_2$), followed by an application of a linear NaCl-gradient up to 200 mM NaCl (50 mM TEA, pH 7.5, 0.8 mM $CaCl_2$, 200 mM NaCl) within 150 min at a flow of 1 ml min^{-1}. Desalting was performed again by gel filtration on a Sephadex-G25 (GE Healthcare, Little Chalfont, United Kingdom) column with 10 mM TEA-buffer (pH 7.5, 0.8 mM $CaCl_2$).

Soluble *Lb*ADH was purified by anion-exchange chromatography [82, 83] by an anion exchanger (Q-Sepharose Fast Flow column, GE Healthcare, Little Chalfont, United Kingdom) starting with equilibration buffer (50 mM TEA, pH 7.2, 1 mM $MgCl_2$). This was followed by an application of a linear NaCl-gradient up to 1 M NaCl (50 mM TEA, pH 7.2, 1 mM $MgCl_2$, 1 M NaCl) within 150 min at a flow of 1 ml min^{-1}. Desalting was performed by gel filtration on a Sephadex-G25 (GE Healthcare, Little Chalfont, United Kingdom) column with 10 mM TEA-buffer (pH 7.5, 1 mM $MgCl_2$).

The soluble *Pf*BAL was purified by metal ion affinity chromatography as described earlier [46, 86]. For the purification with the Ni–NTA-Sepharose column (QIAGEN, Hilden, Germany) the following buffers were used: equilibration buffer (50 mM TEA, pH 7.5, 2.5 mM $MgSO_4$, 0.5 mM ThDP, 300 mM NaCl), washing buffer (50 mM TEA, pH 7.5, 50 mM imidazole, 300 mM NaCl), elution buffer (50 mM TEA, pH 7.5, 250 mM imidazole, 300 mM NaCl). For the final desalting step with Sephadex-G25 (GE Healthcare, Little Chalfont, United Kingdom) column, 10 mM TEA-buffer (pH 7.5, 2.5 mM $MgSO_4$, 0.1 mM ThDP) was employed.

The soluble *Pp*BFD-L476Q was purified by metal ion affinity chromatography as described earlier [45, 46, 48]. For the purification with Ni–NTA-Sepharose column (QIAGEN, Hilden, Germany) the following buffers were used: equilibration buffer (50 mM KPi, pH 7.0, 2.5 mM $MgSO_4$, 0.1 mM ThDP), washing buffer (50 mM TEA, pH 7.0, 50 mM imidazole), elution buffer (50 mM TEA, pH 7.5, 250 mM imidazole). For the final desalting step with Sephadex-G25 (GE Healthcare, Little Chalfont, United Kingdom) column, 10 mM TEA-buffer (pH 6.5, 2.5 mM $MgSO_4$, 0.1 mM ThDP) was employed.

The enzyme solutions were lyophilized (Christ ALPHA 1-3 LD Plus, Martin Christ Gefriertrocknungsanlagen GmbH, Osterode, Germany) from frozen (−20 °C), maximal 2 mg ml^{-1} protein solutions (in the respective storage buffer) and stored at −20 °C until further use.

Sodium dodecyl sulfate-polyacrylamide gel electrophoresis (SDS-PAGE) and determination of protein concentration

The distribution of the recombinant fusion proteins in *E. coli* cell extract fractions, crude cell extract (CCE), soluble supernatant (SN), and insoluble IB-containing pellet (P), as well as the success of the IB-purification was analyzed by SDS-PAGE as described recently [10, 25]. For SDS-PAGE NuPAGE™ 4–12% Bis–Tris Protein Gels with MES SDS running buffer (50 mM MES, 50 mM TRIS, 0.1% SDS, 1 mM EDTA, pH 7.3) and PageRuler Prestained Protein ladders or PageRuler Plus Prestained Protein ladders (both: ThermoFisher Nunc, Waltham, MA, USA) were used. The total protein content in the supernatant was determined, using the Bradford assay [87]. SDS-PAGE samples of the supernatant fraction contained 10 µg protein, all other samples were prepared relative to the supernatant fractions by using the same sample volume [10, 25].

The protein content of lyophilized CatIBs was determined by the absorption at 280 nm. Therefore, lyophilized CatIBs were dissolved in 6 M guanidine hydrochloride, incubated for 30 min at 30 °C under constant shaking at 1000 rpm (Thermomixer comfort, Eppendorf, Germany), and centrifuged for 20 min at 4 °C and 16,060×*g*. The absorption of the protein solution was measured at 280 nm. The protein content was estimated using the molar extinction coefficient as calculated based on the amino acid composition using the ProtParam Tool (http://web.expasy.org/protparam [88] (Additional file 1: Table S6).

Cell fractionation and determination of the CatIB/FIB formation efficiency

Inclusion body production was evaluated by determining the distribution of functional recombinant fusion proteins in different *E. coli* cell extract fractions. Therefore, the fluorescence or activity of the respective target protein was measured in all fractions: crude cell extract (CCE), supernatant (SN), and pellet (P) as described before [25]. Suitable dilutions of the CCE in lysis buffer (50 mM sodium phosphate buffer, 100 mM sodium chloride, pH 8.0) were separated into the soluble supernatant (SN) fraction and insoluble IB-containing pellet fraction (P) by centrifugation (2 min, 7697×*g*, room temperature). The P fraction was washed once with lysis buffer and was resuspended in the initial volume of lysis buffer before measuring. The fluorescence/activity in P (IBs) and SN (soluble protein) was expressed relative to the activity of the crude cell extract (set to 100%). CatIB/FIB formation efficiency was defined as the relative activity, or in case of FPs fluorescence, of the insoluble IB-containing pellet fraction.

For the fluorescent proteins YFP and mCherry distribution in different fractions [crude cell extract (CCE), soluble protein-containing supernatant (SN), and IB-containing pellet (P)] was determined by fluorescence spectroscopy, as described recently [25].

The distribution of the enzymes *R*ADH, *Lb*ADH, *Pf*BAL, and *Pp*BFD in different cell fractions was determined by continuous photometric activity assays in 10 × 4 mm quartz-glass cuvettes with a volume of 1 ml (4 mm light path in excitation) using a Fluorolog3-22 spectrofluorometer (Horiba Jobin–Yvon, Bensheim, Germany) in front-face angle according to the *Pf*BAL initial rate activity assay developed by Schwarz [77].

*R*ADH activity was measured by following the reduction of cyclohexanone to cyclohexanol (Additional file 1: Figure S13a) by detecting the consumption of the cofactor NADPH. The reaction was monitored for 90 s at 30 °C by excitation at λ_{ex} 350 nm and emission at λ_{em} 460 nm (bandwidth 1.4 nm in excitation and emission) using TEA-buffer (50 mM TEA, 0.8 mM CaCl2, pH 7.5) with 100 mM cyclohexanone, 0.2 mM NADPH, and 200 µl sample suspension in suitable dilutions. Measurements of all distributions were performed at least as four technical replicates of biological triplicates.

*Pf*BAL activity was measured using the carboligation of 3,5-dimethoxybenzaldehyde (DMBA) to (*R*)-(3,3′,5,5′)-tetramethoxy benzoin (TMBZ) (Additional file 1: Figure S13c). DMBA consumption was monitored for 90 s at 25 °C by excitation at λ_{ex} 350 nm and emission at λ_{em} 460 nm (bandwidth 1.3 nm in excitation and emission) in TEA-buffer (50 mM TEA, 0.5 mM ThDP, 2.5 mM $MgSO_4$, pH 8.0) with 3 mM DMBA [in DMSO, final concentration 20% (v/v)] and 200 µl sample suspension in suitable dilutions.

The *Lb*ADH and *Pp*BFD activity distribution in different *E. coli* cell extract fractions was measured as described in the activity assays section below.

Phase-contrast and fluorescence image acquisition

Microscopy imaging was performed as described before [25]. After cultivation of *E. coli* BL21(DE3) containing CatIBs/FIBs, a culture volume of 1 ml was removed and the cells were harvested by centrifugation for 2 min at 15,800×*g*. The resulting cell pellet was suspended in lysis buffer (50 mM sodium phosphate buffer, 100 mM NaCl, pH 8) to an OD_{600} of approx. 10. A volume of 1.5 µl was

applied on a microscope slide with a 1% (w/v) agarose base, covered with a coverslip and placed in the microscope setup for imaging. An inverted Nikon Eclipse Ti microscope (Nicon GmbH, Düsseldorf, Germany) was used, equipped with an Apo TIRF 100× Oil DIC N objective (ALA OBJ-Heater, Ala Scientific Instruments, USA), an ANDOR Zyla CMOS camera (Andor Technology plc., Belfast, UK), and an Intensilight (Nicon GmbH, Düsseldorf, Germany) light source for fluorescence excitation, and fluorescence filters for YFP (excitation: 520/60 nm, dichroic mirror: 510 nm, emission: 540/40 nm) and mCherry (excitation: 575/15 nm, dichroic mirror: 593 nm, emission: 629/56 nm) (AHF Analysentechnik, Tübingen, Germany). The filter spectra are given in nm as peak/peak width. The dichroic mirror serves as longpass filter for wavelengths larger than the given value. Fluorescence and camera exposure was 200 ms for both filters at 25 or 12.5% lamp intensity. Analysis of cell images were performed with Fiji [89].

Lipid content determination

For the gravimetric determination of the lipid content [90] approx. 100 mg lyophilized CatIBs were weighted and transferred into a 50 ml falcon tube. After mixing with 14 ml chloroform and 7 ml methanol, the suspension was incubated for 2 h at 60 °C and 750 rpm in a thermomixer (Thermomixer comfort, Eppendorf, Hamburg, Germany). After incubation, the complete suspension was transferred to a 50 ml separating funnel for washing with 5.6 ml 0.73% (w/v) NaCl solution. After collecting the lower organic phase, the remaining aqueous phase was extracted with 14 ml chloroform. The organic phase was pooled, dried over $MgSO_4$, and concentrated by a rotating evaporator (Rotavapor R-100, Büchi Labortechnik GmbH, Essen, Germany). The remaining liquid was transferred to a glass vessel and organic solvent was removed by evaporation first under the hood and then under high vacuum (0.2 mbar) over 24 h. The lipid amount was gravimetrically determined. The lipid content was calculated based on the initial weight. All measurements were performed in three technical replicates of one biological sample.

Activity assays

The initial rate activity of *R*ADH and *R*ADH-CatIBs was measured by using a discontinuous photometric assay in which the consumption of the cofactor NADPH was measured at 340 nm, during the enzyme-catalyzed reduction of cyclohexanone to cyclohexanol (Additional file 1: Figure S13a). The reaction was performed in a polypropylene reaction tube (2 ml safe-lock tube) in a reaction volume of 1750 µl containing 100 mM cyclohexanone and 0.4 mM NADPH in TEA-buffer (50 mM, pH 7.5, 0.8 mM $CaCl_2$) which was pre-incubated at 30 °C. The reaction was started with 300–500 µg ml^{-1} *R*ADH-CatIBs or 10–20 µg ml^{-1} soluble *R*ADH (pre-incubated for 5 min at 30 °C). Reactions were performed for 5 min at 30 °C and 1000 rpm in a thermomixer (Thermomixer comfort, Eppendorf, Germany). Every minute (0–5 min) samples of 250 µl were taken and diluted 1:3 in MeOH to stop the reaction. Samples were centrifuged for 5 min (7697×*g*, room temperature) and measured in standard disposable cuvettes. The amount consumption of NADPH was quantified employing a molar extinction coefficient of $\varepsilon_{340nm} = 1.975\ M^{-1}\ cm^{-1}$ as determined in the reaction system.

For initial rate activity determination of *Pf*BAL-CatIBs and soluble *Pf*BAL, the carboligation of 3,5-dimethoxy benzaldehyde (DMBA) to (*R*)-(3,3‘,5,5‘)-tetramethoxy benzoin (TMBZ) (Additional file 1: Figure S13c) was followed to a conversion of 10% by a discontinuous HPLC assay. The reaction was carried out in polypropylene reaction tubes in 1 ml reaction volume comprised of 80% (v/v) TEA-buffer (50 mM, pH 7.5, 2.5 mM $MgSO_4$, 0.1 mM ThDP), 20% (v/v) DMSO and 10 mM DMBA, This solution was incubated at 30 °C before the reaction was started by addition of the enzyme (0.017–0.30 mg ml^{-1} *Pf*BAL-CatIBs, 3–6 µg ml^{-1} soluble *Pf*BAL, initial protein weight) The reaction was performed for 5 min at 30 °C and 1000 rpm in a thermomixer (Thermomixer comfort, Eppendorf, Germany) under sampling (20 µl) every minute. Subsequently, the sample was diluted 1:10 with 180 µl methanol (incl. 0.1‰ (v/v) *p*-methoxy benzaldehyde as internal standard) to stop the reaction and to prepare the sample for HPLC analysis (see below).

The initial rate activity of *Ec*LDC-CatIBs was measured for the decarboxylation of 10 mM L-lysine in potassium phosphate buffer (50 mM, pH 8.0) containing 0.1 mM PLP at 30 °C and 1000 rpm by a discontinuous HPLC-based assay according to the protocol described previously [10].

*Lb*ADH and *Pp*BFD initial rate activities were measured by continuous photometric activity assays in 10 × 4 mm quartz-glass cuvettes with a volume of 1 ml (4 mm light path in excitation) using a Fluorolog3-22 spectrofluorometer (Horiba Jobin–Yvon, Bensheim, Germany) in front-face angle [77].

*Lb*ADH activity was measured for the reduction of acetophenone to 1-phenylethanol (Additional file 1: Figure S13b) under the consumption of the cofactor NADPH [83], which was detected by excitation at λ_{ex} 350 nm and emission at λ_{em} 460 nm (bandwidth 1.5 nm in excitation and emission). The reaction was started by addition of 500 µl sample suspension in suitable dilutions (protein amount of approx. 0.07–0.4 mg ml^{-1} soluble

*Lb*ADH and 2–25 mg ml^{-1} *Lb*ADH-CatIBs) to the preheated TEA-buffer (50 mM pH 7.0, 0.8 mM $MgCl_2$) containing 10.7 mM acetophenone, and 0.2 mM NADPH, and was followed for 90 s at 30 °C. For NADPH calibration, NADPH, in concentrations between 0.1 mM and 0.20 mM, was dissolved in TEA-buffer and measured under the same conditions.

*Pp*BFD activity was followed by a coupled two-step assay reaction beginning with *Pp*BFD-catalyzed decarboxylation of phenylglyoxylic acid (PGA) to benzaldehyde, which was followed by the reduction to benzyl alcohol by horse liver (HL-)ADH under the oxidation of NADH (Additional file 1: Figure S13d). The reaction was started by the addition of 500 µl sample suspension in suitable dilutions (protein amount of approx. 0.05–0.35 mg ml^{-1} soluble *Pp*BFD and 0.4–2.5 mg ml^{-1} *Pp*BFD-CatIBs) to the preheated reaction solution containing TEA-buffer (50 mM TEA, 0.5 mM ThDP, 2.5 mM $MgSO_4$, pH 6.5) with 5 mM PGA, 0.25 mM NADH, and 0.25 U ml^{-1} HL-ADH. NADH consumption was monitored for 90 s at 30 °C by excitation at λ_{ex} 350 nm and emission at λ_{em} 460 nm (bandwidth 1.4 nm in excitation and emission). For NADPH calibration, NADPH concentrations between 0.1 mM and 0.25 mM were dissolved in TEA-buffer and measured under the same conditions.

Measurements of the initial rate activities were performed at least as three technical replicates of the respective biological triplicates. Activity was calculated as turn over number k_{cat} [s^{-1}] referring to the amount of enzyme (in µmol and referring to one subunit, calculated based on the protein content) which catalyzes the formation of 1 µmol product per second from the respective substrate under the applied reaction conditions.

HPLC analysis

For *Ec*LDC activity determinations the concentration of L-lysine and 1,5-diaminopentane (DAP) was determined as described recently [10].

The concentration of DMBA and TMBZ, the substrate and reaction product of the *Pf*BAL activity assay, were determined by high performance liquid chromatography (HPLC). The samples were prepared for HPLC analysis by centrifugation at 15,800×*g* for 1 min. Subsequently, the supernatant was transferred to HPLC vials equipped with inlets. For analysis, 10 µl of samples were injected into a Thermo Scientific Dionex Ultimate 3000 HPLC system containing a diode-array detector DAD-3000 (ThermoFisher Scientific, Waltham, MA, USA). As stationary phase, a Chiralpak® IE column was used (4,6 µm × 250 mm, 5 µm particle size column, Daicel, Tokyo, Japan), which was combined with a pre-column of the same material (Chiralpak® IE 4 mm x 10 mm; Daicel, Tokyo, Japan). The columns were tempered to 20 °C. Separation was achieved under isocratic elution (flow rate 1 ml min^{-1}) using a binary mobile phase consisting of 50% (v/v) dd H_2O and 50% (v/v) acetonitrile. The analytes eluted at retention times of 6.1 min for *p*-MBA (270 nm), 7.6 min for DMBA (215 nm); and 9.4 min for (*R*)-TMBZ (215 nm). To quantify substrate and product, a calibration of DMBA and TMBZ was performed [32].

Scanning electron microscopy

Scanning electron microscopy images of CatIBs were taken by Steffen Köhler from the Center for Advanced Imaging (CAi) at the Heinrich-Heine University Düsseldorf with a Leo 1430 VP scanning electron microscopy (Carl Zeiss AG, Oberkochen, Germany). For sample preparation, 2 mg ml^{-1} lyophilized TDoT-CatIBs or 4 mg ml^{-1} 3HAMP-CatIBs were used. CatIB solutions (2.5 µl) were fixed on a silicon disk (VWR, Radnor, Pennsylvania, USA) with 2.5% (v/v) glutaraldehyde in 100 mM sodium phosphate buffer, pH 7.2 for 2 h at 25 °C and 250 rpm and rinsed three times for 10 min with buffer [91]. Afterwards, the samples were dehydrated through a graded ethanol series (30, 50, 70, 95, and 100%) for 15 min, respectively. Samples were dried by critical point method and coated with gold at the CAi before images were taken at an accelerating voltage of 15 or 19 kV.

Computational analysis of sequence-based and structural determinants of CatIB formation

The aggregation propensity of the target proteins, as well as of the corresponding TDoT fusions, was inferred from their amino acid sequence by using the AGGRESCAN tool (http://bioinf.uab.es/aggrescan) [72] (see Additional file 1: Table S1). Implementation tests and details about the algorithm employed by AGGRESCAN have been provided elsewhere [11, 72]. The program provides several parameters that serve as a global indicator for the aggregation propensity of a given amino acid sequence. The average aggregation-propensity values per amino acid (a^4v) normalized to a 100-residue protein (Na^4vSS) were employed as quantitative descriptors for aggregation propensity. Those values have previously been shown to be good indicators for changes in aggregation properties, due to the introduction of point mutations, and have also been employed for the differentiation of soluble, unfolded, amyloid- and IB-forming proteins [72].

Alternatively, the presence/absence of large hydrophobic surface patches was considered as structural proxy for the aggregation propensity of a given target protein. Therefore, for each target protein, the pdb coordinates representing the most likely native oligomer were obtained from the pdb data bank (https://www.rcsb.org) [92]. Alternative oligomeric assemblies were derived using the PISA webserver ['Protein interfaces, surfaces

and assemblies' service PISA at the European Bioinformatics Institute (http://www.ebi.ac.uk/pdbe/prot_int/pistart.html)] [93]. All solvent molecules and heteroatoms were removed before surface calculations were performed. The surface properties of the target proteins were evaluated by using the Rosetta protein design software [75, 76] by employing the hpatch tool [94]. The hpatch tool identifies surface localized clusters of hydrophobic atoms (hydrophobic patches) and provides a Pymol selection term for visualization of each identified patch. The overall patch area was calculated by summation over all identified patches. Patch areas and the overall solvent accessible surface area (SASA) were calculated with Pymol 1.7.0.0 (Schrödinger, LCC, New York, NY, USA). PDB-IDs and additional information about the employed structures and assemblies is provided in Additional file 1: Table S2.

Additional file

Additional file 1. Additional information containing Additional Results, Methods, DNA and amino acid sequences of the fusion proteins and Additional references.

Abbreviations

IBs: inclusion bodies; CatIBs: catalytically-active inclusion bodies; FIBs: functional inclusion bodies; *E. coli*: *Escherichia coli*; CLEAs: cross-linked enzyme aggregates; FPs: fluorescent proteins; TDoT: coiled-coil tetramerization domain of tetrabrachion; HAMP: histidine kinases, adenylyl cyclases, methyl-accepting chemotaxis proteins, and phosphatases; 3HAMP: coiled-coil HAMP domain of the Aer2 oxygen sensor; SEM: scanning electron microscopy; SASA: solvent accessible surface area.

Authors' contributions

VDJ and RK contributed equally: both wrote the manuscript, planed, supervised, analyzed, and assisted the experiments. VDJ optimized the plasmids constructs, generated the different expression vectors and created the fusion proteins. RK, assisted by UK, planned and generated the genetic construct for the C-terminal fusion. VDJ characterized the fluorescent proteins, measured the distributions and activities for *R*ADH and *Pf*BAL, optimized the *R*ADH activity assays and performed scanning electron microscopy. RK optimized the activity assays for *Pf*BAL, *Pp*BFD, and *Lb*ADH, and supervised the characterization of these enzymes and *Ec*LDC. VDJ, RK, and AG performed live-cell imaging. UK performed bioinformatic and computational structural analyses. SS, DH, TK, M. Piqueray, UM, JM, and SL performed experiments, that were planned and supervised by RK and VDJ under the coordination and supervision of M. Pohl and UK. WW, KE-J, M. Pohl, and UK planned the CatIB project and corrected the manuscript. All authors commented on the manuscript. All authors read and approved the final manuscript.

Author details

[1] Institut für Molekulare Enzymtechnologie, Heinrich-Heine-Universität Düsseldorf, Forschungszentrum Jülich, 52425 Jülich, Germany. [2] IBG-1: Biotechnology, Forschungszentrum Jülich GmbH, 52425 Jülich, Germany. [3] Multiscale Bioengineering, Bielefeld University, Universitätsstraße 25, 33615 Bielefeld, Germany. [4] Bioeconomy Science Center (BioSC), c/o, Forschungszentrum Jülich, 52425 Jülich, Germany.

Acknowledgements

The scientific activities of the Bioeconomy Science Center were financially supported by the Ministry of Innovation, Science and Research within the framework of the NRW Strategieprojekt BioSC (No. 313/323-400-002 13). BioSC is a research cluster of RWTH Aachen University, the universities of Düsseldorf and Bonn, and Forschungszentrum Jülich. The authors thank the Institute for Bioorganic Chemistry (IBOC, Heinrich-Heine University/FZ Jülich) for performing ^{1}H-NMR analysis, Steffen Köhler of the Center for Advanced Imaging (Heinrich-Heine University Düsseldorf) for the scanning electron microscopy pictures, and Christoph Westerwalbesloh and Eugen Kaganovitch from the Microscale Bioengineering Group (IBG-1, Forschungszentrum Jülich) for taking phase-contrast and fluorescence images of *E. coli* cells containing CatIBs/FIBs.

Competing interests

The authors declare that they have no competing interests.

Availability of data and materials

All data generated or analyzed during this study are included in this article and it's Additional file 1.

Consent for publication

Not applicable.

Ethics approval and consent to participate

Not applicable.

Funding

This research was funded by the Ministry of Innovation, Science and Research within the framework of the NRW Strategieprojekt BioSC (No. 313/323-400-002 13).

Publisher's Note

Springer Nature remains neutral with regard to jurisdictional claims in published maps and institutional affiliations.

Received: 4 December 2018 Accepted: 30 January 2019
Published online: 07 February 2019

References

1. Castro GR, Knubovets T. Homogeneous biocatalysis in organic solvents and water-organic mixtures. Crit Rev Biotechnol. 2003;23:195–231.
2. Rehm FB, Chen S, Rehm BH. Enzyme engineering for in situ immobilization. Molecules. 2016;21:1370. https://doi.org/10.3390/molecules21101370.
3. Hanefeld U, Gardossi L, Magner E. Understanding enzyme immobilisation. Chem Soc Rev. 2009;38(453–46):8.
4. Sheldon RA, van Pelt S. Enzyme immobilisation in biocatalysis: why, what and how. Chem Soc Rev. 2013;42:6223–35.
5. Es I, Vieira JD, Amaral AC. Principles, techniques, and applications of biocatalyst immobilization for industrial application. Appl Microbiol Biotechnol. 2015;99:2065–82.
6. Sheldon RA. Characteristic features and biotechnological applications of cross-linked enzyme aggregates (CLEAs). Appl Microbiol Biotechnol. 2011;92:467–77.
7. Pierre AC. The sol-gel encapsulation of enzymes. Biocatal Biotransform. 2004;22:145–70.
8. Tufvesson P, Lima-Ramos J, Nordblad M, Woodley JM. Guidelines and cost analysis for catalyst production in biocatalytic processes. Org Process Res Dev. 2011;15:266–74.
9. Diener M, Kopka B, Pohl M, Jaeger KE, Krauss U. Fusion of a coiled-coil domain facilitates the high-level production of catalytically active enzyme inclusion bodies. Chemcatchem. 2016;8:142–52.
10. Kloss R, Limberg MH, Mackfeld U, Hahn D, Grünberger A, Jäger VD, Krauss U, Oldiges M, Pohl M. Catalytically active inclusion bodies of L-lysine decarboxylase from *E. coli* for 1,5-diaminopentane production. Sci Rep. 2018;8:5856.

11. Krauss U, Jäger VD, Diener M, Pohl M, Jaeger KE. Catalytically-active inclusion bodies—carrier-free protein immobilizates for application in biotechnology and biomedicine. J Biotechnol. 2017;258:136–47.
12. Zhou B, Xing L, Wu W, Zhang X-E, Lin Z. Small surfactant-like peptides can drive soluble proteins into active aggregates. Microb Cell Fact. 2012;11:10.
13. Lin Z, Zhou B, Wu W, Xing L, Zhao Q. Self-assembling amphipathic alpha-helical peptides induce the formation of active protein aggregates in vivo. Faraday Discuss. 2013;166:243–56.
14. Wu W, Xing L, Zhou B, Lin Z. Active protein aggregates induced by terminally attached self-assembling peptide ELK16 in *Escherichia coli*. Microbial Cell Fact. 2011;10:9.
15. Wang X, Zhou B, Hu W, Zhao Q, Lin Z. Formation of active inclusion bodies induced by hydrophobic self-assembling peptide GFIL8. Microb Cell Fact. 2015;14:88.
16. Nahálka J, Nidetzky B. Fusion to a pull-down domain: a novel approach of producing *Trigonopsis variabilis* D-amino acid oxidase as insoluble enzyme aggregates. Biotechnol Bioeng. 2007;97:454–61.
17. Nahálka J, Patoprstý V. Enzymatic synthesis of sialylation substrates powered by a novel polyphosphate kinase (PPK3). Org Biomol Chem. 2009;7:1778–80.
18. Choi S-L, Lee SJ, Ha J-S, Song JJ, Rhee YH, Lee S-G. Generation of catalytic protein particles in *Escherichia coli* cells using the cellulose-binding domain from *Cellulomonas fimi* as a fusion partner. Biotechnol Bioprocess Eng. 2011;16:1173–9.
19. García-Fruitós E, González-Montalbán N, Morell M, Vera A, Ferraz RM, Arís A, Ventura S, Villaverde A. Aggregation as bacterial inclusion bodies does not imply inactivation of enzymes and fluorescent proteins. Microb Cell Fact. 2005;4:27.
20. Hrabárová E, Achbergerová L, Nahálka J. Insoluble protein applications: the use of bacterial inclusion bodies as biocatalysts. Methods Mol Biol. 2015;1258:411–22.
21. Nahálka J, Mislovicová D, Kavcová H. Targeting lectin activity into inclusion bodies for the characterisation of glycoproteins. Mol BioSyst. 2009;5:819–21.
22. Park S-Y, Park S-H, Choi S-K. Active inclusion body formation using *Paenibacillus polymyxa* PoxB as a fusion partner in *Escherichia coli*. Anal Biochem. 2012;426:63–5.
23. Kopito RR. Aggresomes, inclusion bodies and protein aggregation. Trends Cell Biol. 2000;10:524–30.
24. Baneyx F, Mujacic M. Recombinant protein folding and misfolding in *Escherichia coli*. Nat Biotechnol. 2004;22:1399–408.
25. Jäger VD, Lamm R, Kloss R, Kaganovitch E, Grünberger A, Pohl M, Büchs J, Jaeger K-E, Krauss U. A synthetic reaction cascade implemented by co-localization of two proteins within catalytically-active inclusion bodies. ACS Synth Biol. 2018;7:2282-95. https://doi.org/10.1021/acssynbio.8b00274.
26. Steinmann B, Christmann A, Heiseler T, Fritz J, Kolmar H. In vivo enzyme immobilization by inclusion body display. Appl Environ Microbiol. 2010;76:5563–9.
27. Li S, Lin K, Pang H, Wu Y, Xu J. Production, characterization, and application of an organic solvent-tolerant lipase present in active inclusion bodies. Appl Biochem Biotechnol. 2013;169:612–23.
28. Ratera I, Peternel S, Seras-Franzoso J, Cano-Garrido O, García-Fruitós E, Cubarsí R, Vazquez E, Corchero JL, Rodríguez-Carmona E, Veciana J, Villaverde A. Biomedical applications of bacterial inclusion bodies. In Doglia SM, editor. Protein Aggregation in Bacteria: Functional and structural properties of inclusion bodies in bacterial cells. Lotti M2014. p. 203–20.
29. Rueda F, Gasser B, Sánchez-Chardi A, Roldán M, Villegas S, Puxbaum V, Ferrer-Miralles N, Unzueta U, Vázquez E, Garcia-Fruitós E, et al. Functional inclusion bodies produced in the yeast *Pichia pastoris*. Microb Cell Fact. 2016;15:166.
30. Vázquez E, Corchero JL, Burgueño JF, Seras-Franzoso J, Kosoy A, Bosser R, Mendoza R, Martínez-Láinez JM, Rinas U, Fernández E, et al. Functional inclusion bodies produced in bacteria as naturally occurring nanopills for advanced cell therapies. Adv Mater. 2012;24:1742–7.
31. Stetefeld J, Jenny M, Schulthess T, Landwehr R, Engel J, Kammerer RA. Crystal structure of a naturally occurring parallel right-handed coiled coil tetramer. Nat Struct Biol. 2000;7:772–6.
32. Kloss R, Karmainski T, Jäger VD, Hahn D, Grünberger A, Baumgart M, Krauss U, Jaeger K-E, Wiechert W, Pohl M. Tailor-made catalytically active inclusion bodies for different applications in biocatalysis. Catal Sci Technol. 2018;8:5816–26.
33. Lupas AN, Gruber M. The structure of α-helical coiled coils. Adv Protein Chem. 2005;70:37–78.
34. Woolfson DN, Bartlett GJ, Bruning M, Thomson AR. New currency for old rope: from coiled-coil assemblies to α-helical barrels. Curr Opin Struct Biol. 2012;22:432–41.
35. Wachter RM, Elsliger MA, Kallio K, Hanson GT, Remington SJ. Structural basis of spectral shifts in the yellow-emission variants of green fluorescent protein. Structure. 1998;6:1267–77.
36. Zacharias DA, Violin JD, Newton AC, Tsien RY. Partitioning of lipid-modified monomeric GFPs into membrane microdomains of live cells. Science. 2002;296:913–6.
37. Shaner NC, Campbell RE, Steinbach PA, Giepmans BN, Palmer AE, Tsien RY. Improved monomeric red, orange and yellow fluorescent proteins derived from *Discosoma* sp. red fluorescent protein. Nat Biotechnol. 2004;22:1567–72.
38. Hummel W. Large-scale applications of NAD(P)-dependent oxidoreductases: recent developments. Trends Biotechnol. 1999;17:487–92.
39. Schlieben NH, Niefind K, Muller J, Riebel B, Hummel W, Schomburg D. Atomic resolution structures of *R*-specific alcohol dehydrogenase from *Lactobacillus brevis* provide the structural bases of its substrate and cosubstrate specificity. J Mol Biol. 2005;349:801–13.
40. Lavandera I, Kern A, Ferreira-Silva B, Glieder A, de Wildeman S, Kroutil W. Stereoselective bioreduction of bulky-bulky ketones by a novel ADH from *Ralstonia* sp. J Org Chem. 2008;73:6003–5.
41. Kulig J, Frese A, Kroutil W, Pohl M, Rother D. Biochemical characterization of an alcohol dehydrogenase from *Ralstonia* sp. Biotechnol Bioeng. 2013;110:1838–48.
42. Niefind K, Muller J, Riebel B, Hummel W, Schomburg D. The crystal structure of *R*-specific alcohol dehydrogenase from *Lactobacillus brevis* suggests the structural basis of its metal dependency. J Mol Biol. 2003;327:317–28.
43. Gonzalez B, Vicuna R. Benzaldehyde lyase, a novel thiamine PPi-requiring enzyme, from *Pseudomonas fluorescens* biovar I. J Bacteriol. 1989;171:2401–5.
44. Tsou AY, Ransom SC, Gerlt JA, Buechter DD, Babbitt PC, Kenyon GL. Mandelate pathway of *Pseudomonas putida*: sequence relationships involving mandelate racemase, (*S*)-mandelate dehydrogenase, and benzoylformate decarboxylase and expression of benzoylformate decarboxylase in *Escherichia coli*. Biochemistry. 1990;29:9856–62.
45. Iding H, Dünnwald T, Greiner L, Liese A, Muller M, Siegert P, Grotzinger J, Demir AS, Pohl M. Benzoylformate decarboxylase from *Pseudomonas putida* as stable catalyst for the synthesis of chiral 2-hydroxy ketones. Chemistry. 2000;6:1483–95.
46. Gocke D, Walter L, Gauchenova E, Kolter G, Knoll M, Berthold CL, Schneider G, Pleiss J, Muller M, Pohl M. Rational protein design of ThDP-dependent enzymes-engineering stereoselectivity. ChemBioChem. 2008;9:406–12.
47. Hegeman GD. Benzoylformate decarboxylase (*Pseudomonas putida*). In: Methods in Enzymology, vol 17. Academic Press; 1970. p. 674–8.
48. Lingen B, Kolter-Jung D, Dünkelmann P, Feldmann R, Grötzinger J, Pohl M, Müller M. Alteration of the substrate specificity of benzoylformate decarboxylase from *Pseudomonas putida* by directed evolution. ChemBioChem. 2003;4:721–6.
49. Kind S, Jeong WK, Schroder H, Wittmann C. Systems-wide metabolic pathway engineering in *Corynebacterium glutamicum* for bio-based production of diaminopentane. Metab Eng. 2010;12:341–51.
50. Arai R, Ueda H, Kitayama A, Kamiya N, Nagamune T. Design of the linkers which effectively separate domains of a bifunctional fusion protein. Protein Eng. 2001;14:529–32.
51. Chen X, Zaro JL, Shen WC. Fusion protein linkers: property, design and functionality. Adv Drug Deliv Rev. 2013;65:1357–69.
52. Kandiah E, Carriel D, Perard J, Malet H, Bacia M, Liu K, Chan SW, Houry WA, Ollagnier de Choudens S, Elsen S, Gutsche I. Structural insights into the Escherichia coli lysine decarboxylases and molecular determinants of interaction with the AAA + ATPase RavA. Sci Rep. 2016;6:24601.
53. Kanjee U, Gutsche I, Alexopoulos E, Zhao B, El Bakkouri M, Thibault G, Liu K, Ramachandran S, Snider J, Pai EF, Houry WA. Linkage between the bacterial acid stress and stringent responses: the structure of the inducible lysine decarboxylase. EMBO J. 2011;30:931–44.

54. Airola MV, Watts KJ, Bilwes AM, Crane BR. Structure of concatenated HAMP domains provides a mechanism for signal transduction. Structure. 2010;18:436–48.
55. Alvarenga AE, Amoroso MJ, Illanes A, Castro GR. Cross-linked α-l-rhamnosidase aggregates with potential application in food industry. Eur Food Res Technol. 2014;238:797–801.
56. Chmura A, van der Kraan GM, Kielar F, van Langen LM, van Rantwijk F, Sheldon RA. Cross-linked aggregates of the hydroxynitrile lyase from *Manihot esculenta*: highly active and robust biocatalysts. Adv Synth Catal. 2006;348:1655–61.
57. Cui J, Zhao Y, Feng Y, Lin T, Zhong C, Tan Z, Jia S. Encapsulation of spherical cross-linked phenylalanine ammonia lyase aggregates in mesoporous biosilica. J Agric Food Chem. 2017;65:618–25.
58. Cui JD, Sun LM, Li LL. A simple technique of preparing stable CLEAs of phenylalanine ammonia lyase using co-aggregation with starch and bovine serum albumin. Appl Biochem Biotechnol. 2013;170:1827–37.
59. Kumar VV, Sivanesan S, Cabana H. Magnetic cross-linked laccase aggregates—bioremediation tool for decolorization of distinct classes of recalcitrant dyes. Sci Total Environ. 2014;487:830–9.
60. Mateo C, Palomo JM, van Langen LM, van Rantwijk F, Sheldon RA. A new, mild cross-linking methodology to prepare cross-linked enzyme aggregates. Biotechnol Bioeng. 2004;86:273–6.
61. Park SH, Soetyono F, Kim HK. Cadaverine production by using cross-linked enzyme aggregate of *Escherichia coli* lysine decarboxylase. J Microbiol Biotechnol. 2017;27:289–96.
62. Talekar S, Waingade S, Gaikwad V, Patil S, Nagavekar N. Preparation and characterization of cross linked enzyme aggregates (CLEAs) of *Bacillus amyloliquefaciens* alpha amylase. J Biochem Technol. 2012;3:349–53.
63. Zhou LY, Mou HX, Gao J, Ma L, He Y, Jiang YJ. Preparation of cross-linked enzyme aggregates of nitrile hydratase ES-NHT-118 from *E coli* by macromolecular cross-linking agent. Chin J Chem Eng. 2017;25:487–92.
64. Rokney A, Shagan M, Kessel M, Smith Y, Rosenshine I, Oppenheim ABE. *E. coli* transports aggregated proteins to the poles by a specific and energy-dependent process. J Mol Biol. 2009;392:589–601.
65. Cano-Garrido O, Sánchez-Chardi A, Parés S, Giró I, Tatkiewicz WI, Ferrer-Miralles N, Ratera I, Natalello A, Cubarsi R, Veciana J, et al. Functional protein-based nanomaterial produced in microorganisms recognized as safe: a new platform for biotechnology. Acta Biomater. 2016;43:230–9.
66. Wang L. Towards revealing the structure of bacterial inclusion bodies. Prion. 2009;3:139–45.
67. Lopez de la Paz M, Serrano L. Sequence determinants of amyloid fibril formation. Proc Natl Acad Sci USA. 2004;101:87–92.
68. Esteras-Chopo A, Serrano L, Lopez de la Paz M. The amyloid stretch hypothesis: recruiting proteins toward the dark side. Proc Natl Acad Sci USA. 2005;102:16672–7.
69. Teng PK, Eisenberg D. Short protein segments can drive a non-fibrillizing protein into the amyloid state. Protein Eng Des Sel. 2009;22:531–6.
70. Chiti F, Stefani M, Taddei N, Ramponi G, Dobson CM. Rationalization of the effects of mutations on peptide and protein aggregation rates. Nature. 2003;424:805–8.
71. Hamodrakas SJ. Protein aggregation and amyloid fibril formation prediction software from primary sequence: towards controlling the formation of bacterial inclusion bodies. FEBS J. 2011;278:2428–35.
72. Conchillo-Sole O, de Groot NS, Aviles FX, Vendrell J, Daura X, Ventura S. AGGRESCAN: a server for the prediction and evaluation of "hot spots" of aggregation in polypeptides. BMC Bioinform. 2007;8:65.
73. Tompa P. Intrinsically unstructured proteins. Trends Biochemical. Science. 2002;27:527–33.
74. Kalthoff C. A novel strategy for the purification of recombinantly expressed unstructured protein domains. J Chromatogr B Anal Technol Biomed Life Sci. 2003;786:247–54.
75. Kuhlman B, Baker D. Native protein sequences are close to optimal for their structures. Proc Natl Acad Sci. 2000;97:10383.
76. Rohl CA, Strauss CE, Misura KM, Baker D. Protein structure prediction using Rosetta. Methods Enzymol. 2004;383:66–93.
77. Schwarz M. Einflussfaktoren auf die Stabilität und Aktivität der Benzaldehydlyase aus *Pseudomonas fluorescens* in Carboligasereaktionen mit aromatischen Aldehyden. Forschungszentrum Jülich GmbH, IBG-1, Forschungszentrum Jülich; 2010.
78. Miyawaki A, Griesbeck O, Heim R, Tsien RY. Dynamic and quantitative Ca^{2+} measurements using improved cameleons. Proc Natl Acad Sci USA. 1999;96:2135–40.
79. Shaner NC, Steinbach PA, Tsien RY. A guide to choosing fluorescent proteins. Nat Methods. 2005;2:905–9.
80. Studier FW. Protein production by auto-induction in high density shaking cultures. Protein Expr Purif. 2005;41:207–34.
81. Kulig J, Simon RC, Rose CA, Husain SM, Hackh M, Ludeke S, Zeitler K, Kroutil W, Pohl M, Rother D. Stereoselective synthesis of bulky 1,2-diols with alcohol dehydrogenases. Catal Sci Technol. 2012;2:1580–9.
82. Kulishova L, Dimoula K, Jordan M, Wirtz A, Hofmann D, Santiago-Schübel B, Fitter J, Pohl M, Spiess AC. Factors influencing the operational stability of NADPH-dependent alcohol dehydrogenase and an NADH-dependent variant thereof in gas/solid reactors. J Mol Catal B Enzym. 2010;67:271–83.
83. Kulishova L. Analysis of factors influencing enzyme activity and stability in the solid state Heinrich-Heine Universität Düsseldorf, Institut für Molekulare Enzymtechnologie; 2010.
84. Janzen E, Muller M, Kolter-Jung D, Kneen MM, McLeish MJ, Pohl M. Characterization of benzaldehyde lyase from *Pseudomonas fluorescens*: a versatile enzyme for asymmetric C-C bond formation. Bioorg Chem. 2006;34:345–61.
85. Korz DJ, Rinas U, Hellmuth K, Sanders EA, Deckwer WD. Simple fed-batch technique for high cell density cultivation of *Escherichia coli*. J Biotechnol. 1995;39:59–65.
86. Pohl M, Müller M, Demir AS. Nucleotide sequence encoding a benzaldehyde lyase, and process for stereoselectively synthesizing 2-hydroxyketones. vol. US 7,045,334 B2 2006.
87. Bradford MM. A rapid and sensitive method for the quantitation of microgram quantities of protein utilizing the principle of protein-dye binding. Anal Biochem. 1976;72:248–54.
88. Gasteiger E, Hoogland C, Gattiker A, Duvaud SE, Wilkins MR, Appel RD, Bairoch A. Protein identification and analysis tools on the ExPASy server. In: Walker JM, editor. The proteomics protocols handbook. Totowa: Humana Press; 2005. p. 571–607.
89. Schneider CA, Rasband WS, Eliceiri KW. NIH Image to ImageJ: 25 years of image analysis. Nat Methods. 2012;9:671–5.
90. Morschett H, Wiechert W, Oldiges M. Automation of a Nile red staining assay enables high throughput quantification of microalgal lipid production. Microb Cell Fact. 2016;15:34.
91. White SL, Wise RR. Anatomy and ultrastructure of *Wolffia columbiana* and *Wolffia borealis,* two nonvascular aquatic angiosperms. Int J Plant Sci. 1998;159:297–304.
92. Berman HM, Westbrook J, Feng Z, Gilliland G, Bhat TN, Weissig H, Shindyalov IN, Bourne PE. The protein data bank. Nucleic Acids Res. 2000;28:235–42.
93. Krissinel E, Henrick K. Inference of macromolecular assemblies from crystalline state. J Mol Biol. 2007;372:774–97.
94. Jacak R, Leaver-Fay A, Kuhlman B. Computational protein design with explicit consideration of surface hydrophobic patches. Proteins. 2012;80:825–38.

Ready to submit your research? Choose BMC and benefit from:

- fast, convenient online submission
- thorough peer review by experienced researchers in your field
- rapid publication on acceptance
- support for research data, including large and complex data types
- gold Open Access which fosters wider collaboration and increased citations
- maximum visibility for your research: over 100M website views per year

At BMC, research is always in progress.

Learn more biomedcentral.com/submissions

BMC

2.1.1 Publication I: Supporting Information

The here presented Supporting Information of the Manuscript 'Tailoring the properties of (catalytically)-active inclusion bodies' was shortened for clarity of the thesis. The original Supporting Information additionally contain DNA and amino acid sequences of all fusion constructs. They can be found in the Appendix (5.2).

Supporting Results

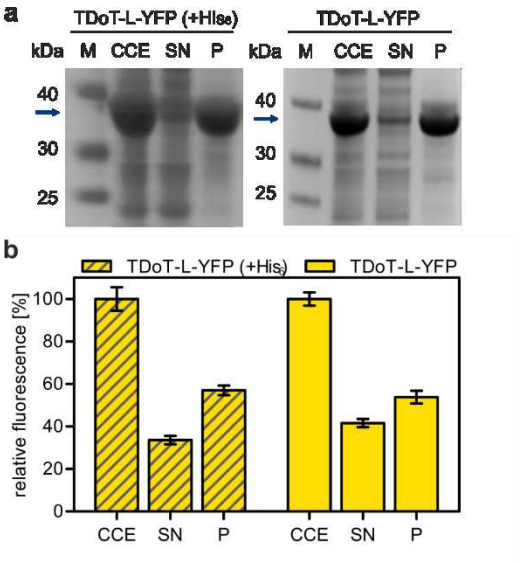


Fig. S1 Improving the CatIB strategy by deleting the Hex histidine-tag (His_6-tag) from the original vector **[1]**. Evaluation by (a) SDS-PAGE analysis and (b) fluorescence distribution for TDoT-L-YFP (+His) (36.8 kDa) and TDoT-L-YFP (34.6). After cell disruption, the crude cell extract (CCE) was separated by centrifugation into the soluble protein containing supernatant (SN) and the insoluble IB containing pellet (P) fraction. (a) SDS-PAGE analysis of the respective protein fractions: CCE, SN, and P. The molecular mass of the respective fusion protein is indicated by arrows. The protein content in the SN was measured according to Bradford **[2]**. (b) Normalized fluorescence in the CCE, SN, and P fractions of the respective proteins. Note, that the P fraction was washed once with water and centrifuged again before the fluorescence measurement. The fluorescence in CCE, SN, and P fractions was calculated relative to the activity in the CCE, which was set to 100%. Error bars correspond to the standard deviation of the mean derived from at least three technical replicates.

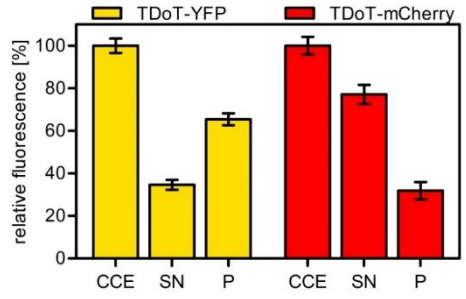


Fig. S3. The fluorescence distribution of the linker-free variants TDoT-YFP- and TDoT-mCherry-FIBs. Sample preparation was done as in Figure S1. Error bars correspond to the standard deviation of the mean derived from at least three biological replicates.

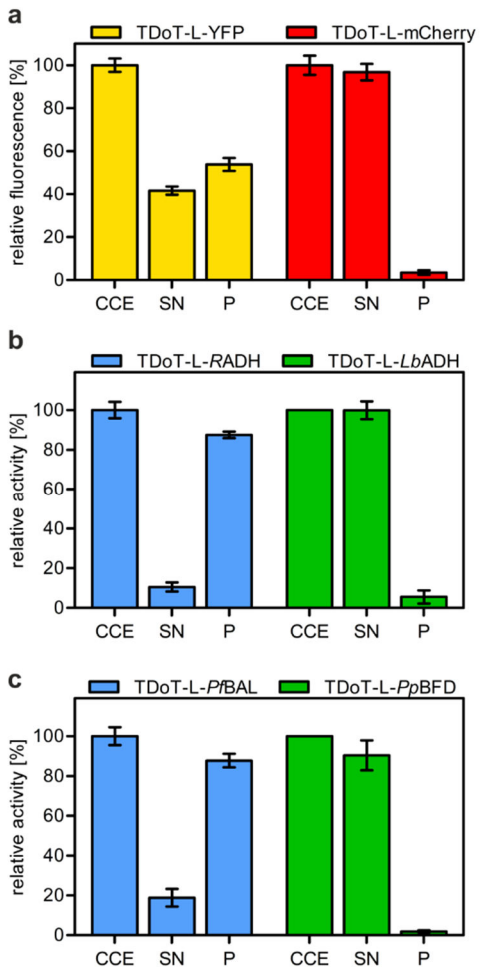
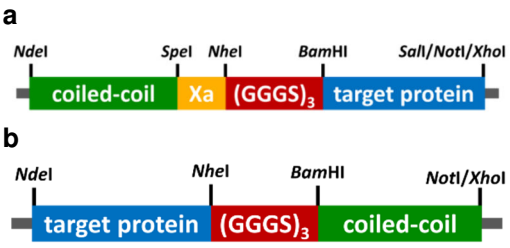


Fig. S2 The fluorescence/activity distribution of (a) TDoT-L-YFP-, TDoT-L-mCherry-, (b) TDoT-L-*R*ADH-, TDoT-L-*Lb*ADH-, (c) TDoT-L-*Pf*BAL- and TDoT-L-*Pp*BFD-CatIB. Sample preparation was done as in Figure S1. Initial rate activities were measured by carboligation of 3,5-dimethoxybenzaldehyde (DMBA) to the respective benzoin catalyzed by TDoT-L-*Pf*BAL-CatIBs and decarboxylation of benzoylformate to benzaldehyde by TDoT-L-*Pp*BFD-CatIBs, which was followed by the reduction to benzyl alcohol by horse liver HL-ADH under the oxidation of NADH. Initial rate activities of the ADH enzymes were measured by reduction of 1-phenylethanol (TDoT-L-*Lb*ADH) or cyclohexaone (TDoT-L-*R*ADH) under the consumption of NADPH. For reaction equations see Figure S13. Error bars correspond to the standard deviation of the mean derived from at least three biological replicates. Controls expressing the corresponding soluble versions of YFP, mCherry, *R*ADH, and *Pf*BAL (with TDoT tag) have been presented before [3].



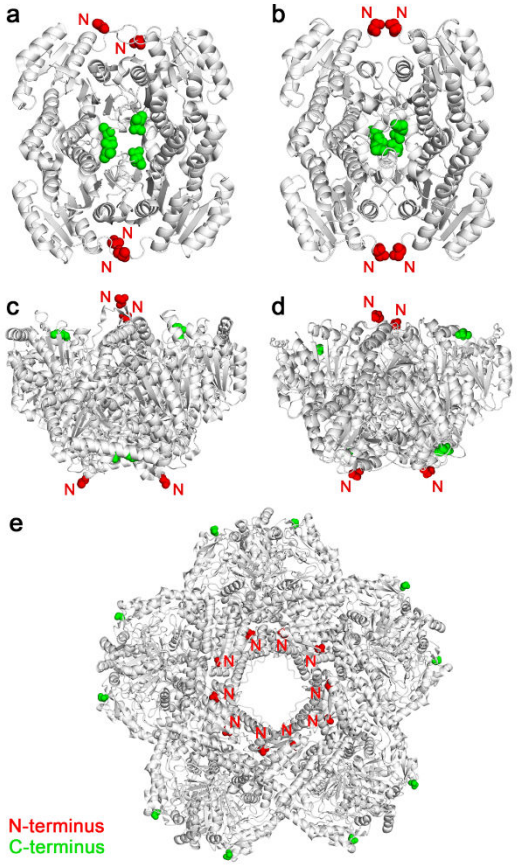


Fig. S4 Structures of the multimeric target enzymes of this study: (a) *R*ADH (PDB: 4BMN), (b) *Lb*ADH (PDB: 1ZK4), (c) *Pf*BAL (PDB: 2UZ1), (d) *Pp*BFD (PDB: 5DEI) and (e) *Ec*LDC (PDB: 5FKZ). All subunits are shown in grey cartoon representation, while the N- and C-terminal amino acids are shown as spheres in red (N-terminus) and green (C-terminus). For clarity, only the N-terminus is labelled in each panel. The N-terminus is accessible in *R*ADH, *Lb*ADH, *Pf*BAL, and *Pp*BFD. In contrast, it is buried within the decameric structure in the N-terminal wing domain of the *Ec*LDC multimer, whereas the C-terminus is located at the outer part in the C-terminal domain **[4]** and hence should be accessible for tag fusion.

Fig S5 Schematic illustration of the N-terminal (a) and C-terminal (b) fusion strategy employed for the generation of CatIBs/FIBs. All expression vectors/gene fusions are constructed modularly, so that every element can be easily exchanged or deleted, by the use of the depicted restriction sites. Gene fusions consist of coding sequences for: the respective target protein (blue), a coiled-coil domain (green), for which we used the TDoT coiled-coil domain (52 amino acids) of the cell-surface protein tetrabrachion of *Staphylothermus marinus* **[5]** or the 3HAMP coiled coil (172 amino acids) of the soluble oxygen sensor Aer2 of *Pseudomonas aeruginosa* **[6]**. Whenever mentioned gene fusions additionally contained a linker region, comprising a cleavage site of the Factor Xa protease (orange, 4 amino acids) and a $(GGGS)_3$-motif (red, 12 amino acids). The gene fusion design shown in (b) was chosen only for the enzyme *Ec*LDC **[4].**

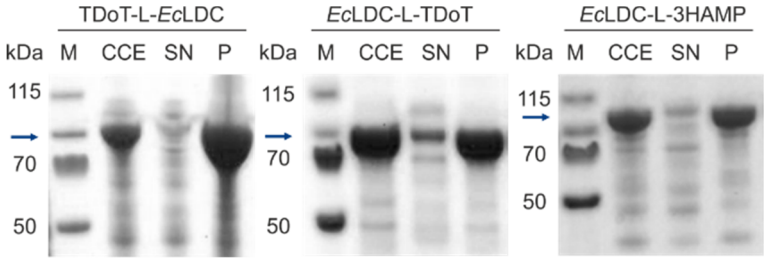


Fig S6 SDS-PAGE analysis of the respective protein fractions of TDoT-L-*Ec*LDC-CatIBs (90.3 kDa), *Ec*LDC-L-TDoT-CatIBs (87.5 kDa) and *Ec*LDC-L-3HAMP-CatIBs (100.5 kDa): crude cell extract (CCE), supernatant (SN), and pellet (P). The target protein is indicated by arrows. Sample preparation was done as in Figure S1.

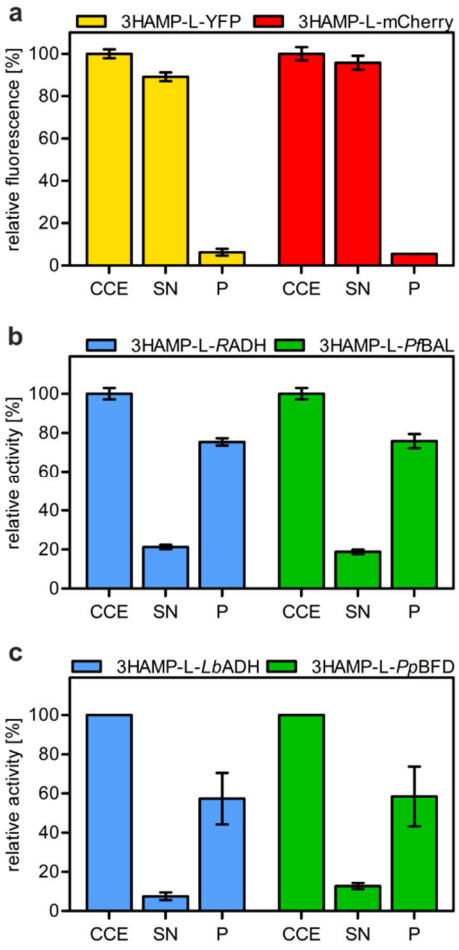


Fig. S7 The fluorescence/activity distribution of (a) 3HAMP-L-YFP-, 3HAMP-L-mCherry-, (b) 3HAMP-L-*R*ADH-, 3HAMP-L-*Pf*BAL-, (c) 3HAMP-L-*Lb*ADH-, and 3HAMP-L-*Pp*BFD-CatIBs. Sample preparation was done as in Figure S1. Initial rate activities were measured by carboligation of 3,5-dimethoxybenzaldehyde (DMBA) to the respective benzoin catalyzed by 3HAMP-L-*Pf*BAL-CatIBs and decarboxylation of benzoylformate to benzaldehyde by 3HAMP-L-*Pp*BFD-CatIBs, which was followed by the reduction to benzyl alcohol by horse liver HL-ADH under the oxidation of NADH. The initial rate activities of the ADH enzymes were measured by reduction of 1-phenylethanol (3HAMP-L-*Lb*ADH) or cycloheaxone (3HAMP-L-*R*ADH) under the consumption of NADPH. For reaction equations see Figure S13. Error bars correspond to the standard deviation of the mean derived from at least three biological replicates.

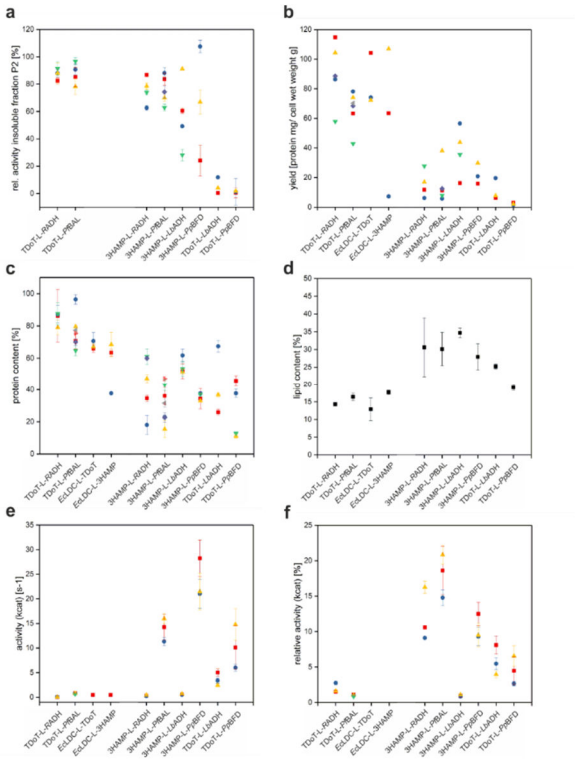


Fig S8 Mean values for each biological replicate with standard deviation (A) for the activity in the pellet compared to CCE, (B) yield (mg protein for 1 g wet cell weight), (C) protein content, and (D) lipid content, based on the dry weight of lyophilized CatIBs, (E) initial rate activity (k_{cat}) and (F) residual activity compared to the soluble enzyme.

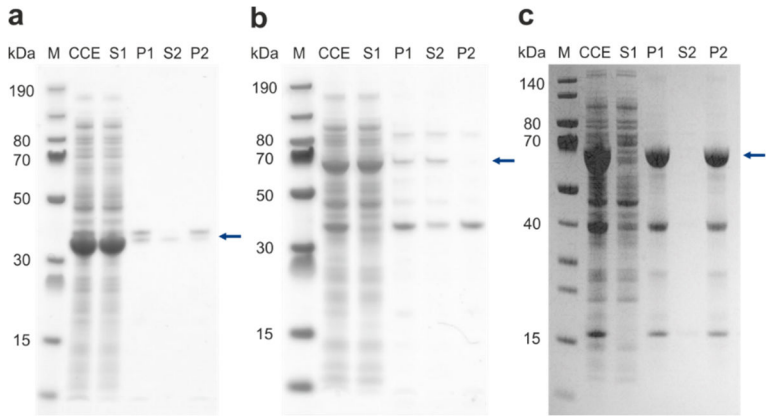


Fig S9 Evaluation of the CatIB strategy by SDS-PAGE analysis of the respective protein fractions of (a) TDoT-L-*Lb*ADH (34.3 kDa), (b) TDoT-L-*Pp*BFD (64.2 kDa) and (c) TDoT-L-*Pf*BAL CatIBs (66.5 kDa): crude cell extract (CCE), supernatant (SN), and pellet (P). The target protein is indicated by arrows. Sample preparation was done as in Figure S1.

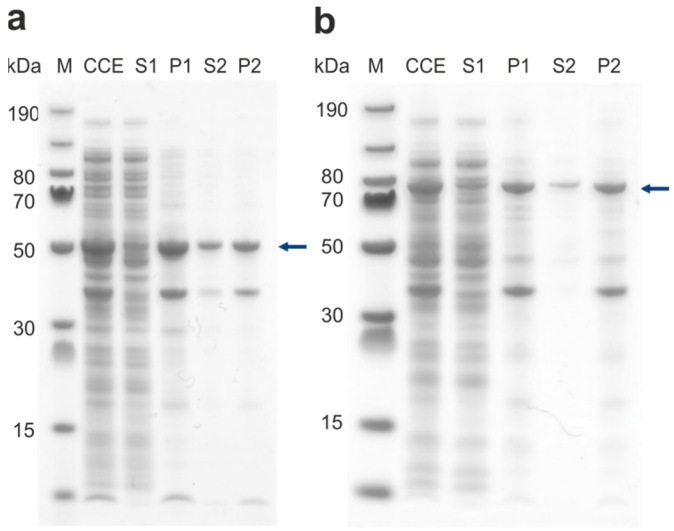


Fig S10 Evaluation of the CatIB strategy by SDS-PAGE analysis of the respective protein fractions of (a) 3HAMP-L-*Lb*ADH- (47.1 kDa), (b) 3HAMP-L-*Pp*BFD-CatIBs (77.0 kDa): crude cell extract (CCE), supernatant (SN), and pellet (P). The target protein is indicated by arrows. Sample preparation was done as in Figure S1.

Tab S1 Sequence-based aggregation-propensity prediction for each target protein and the corresponding TDoT fusion. All predictions were carried out using the AGGRESCAN web server (http://bioinf.uab.es/aggrescan) [7]. Displayed are the average aggregation-propensity values per amino acid (a^4v) normalized to a 100-residue protein (Na^4vSS) and the relative change in Na^4vSS (ΔNa^4vSS) due to fusion of the TDoT domain.

target protein	Na^4vSS	TDoT-target-protein fusion	Na^4vSS	ΔNa^4vSS*
YFP	-7.9	TDoT-L-YFP	-6.5	17.7
mCherry	-16.6	TDoT-L-mCherry	-12.6	24.1
*Bs*LA	0.8	TDoT-L-*Bs*LA	-1.4	-275.0
*At*HNL	3.9	TDoT-L-*At*HNL	1.9	-51.3
*Ec*MenD	-3.2	TDoT-L-*Ec*MenD	-3.1	3.1
*R*ADH	-1.7	TDoT-L-*R*ADH	-1.5	11.8
*Lb*ADH	-4.5	TDoT-L-*Lb*ADH	-3.8	15.6
*Pf*BAL	3.6	TDoT-L-*Pf*BAL	2.9	-19.4
*Pp*BFD	-1.3	TDoT-L-*Pp*BFD	-1.4	-7.7

*calculated according to: $\Delta Na^4vSS = \left(\frac{(Na^4vSS_{fusion} - Na^4vSS_{target})}{|Na^4vSS_{target}|}\right) \times 100\right)$ [7].

Tabb S2 Surface properties of the target proteins used in this study. The presence/absence of large hydrophobic surface patches for the corresponding target protein structures was quantified using the hpatch tool implemented in Rosetta [8-10]. Surface areas were quantified using Pymol 1.7.0.0 (Schrödinger, LCC, New York, NY, USA).

target protein	PDB-ID	comments	hydrophobic patch area [A^2]	solvent accessible surface area (SASA) [A^2]	hydrophob. patch area / overall SASA [%]
YFP	1YFP	asu, monomer, chain A and B	1000	9467	10.6
YFP*	1YFP	1st PISA dimer	1085	16914	6.4
mCherry*	2H5Q	asu, monomer	0	9493	0
*Bs*LA*	1ISP	asu, monomer	972	7867	12.4
*At*HNL*	3DQZ	asu, dimer, chain A and B	1692	18662	9.1
*Ec*MenD	2JLC	asu, dimer	1566	34022	4.6
*Ec*MenD*	2JLC	1st PISA tetramer	3797	54278	7.0
*R*ADH	4BMN	tetramer	1183	27318	4.3
*R*ADH*	4BMN	1st PISA dimer	2068	17423	11.9
*Lb*ADH	1ZK4	1st PISA tetramer	2748	27590	9.9
*Lb*ADH*	1ZK4	2nd PSIA dimer	874	18316	4.8
*Pf*BAL*	2UZ1	asu, tetramer	5194	52235	9.9
*Pp*BFD*	5DEI	asu, tetramer	185	69766	0.27

* final data used in Figure 6c; main paper; asu: the pdb coordinates present in the asymmetric unit were used for surface calculations.

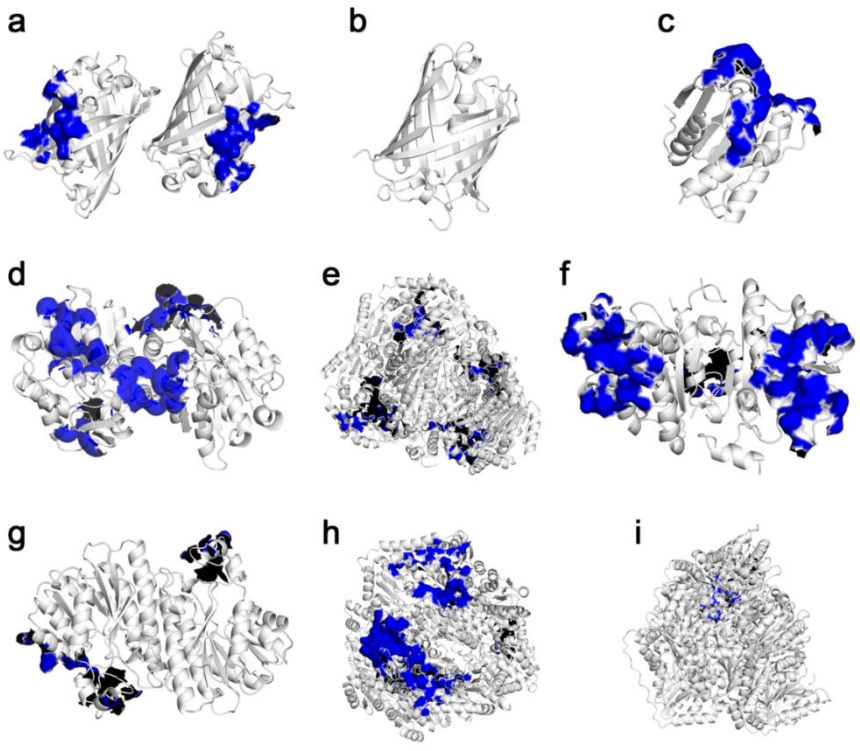


Fig S11 Hydrophobic patch analysis of (a) YFP, (b) mCherry, (c) *Bs*LA, (d) *At*HNL, (e) *Ec*MenD, (f) *R*ADH, (g) *Lb*ADH, (h) *Pf*BAL, and (i) *Pp*BFD. Structures are shown in cartoon representation in grey with the Rossetta-identified hydrophobic surface patches shown as blue surfaces [9, 10]. PDB-IDs were as follows YFP (1YFP), mCherry (2H5Q), *Bs*LA (1ISP), *At*HNL (3DWZ), *Ec*MenD (2JLC), *R*ADH (4BMN), *Lb*ADH (1ZK4), *Pf*BAL (2UZ1) and *Pp*BFD (5DEI).

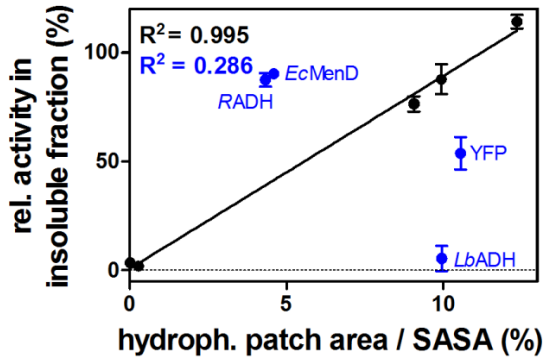


Fig S12 Computational analysis of the structural determinants of CatIB formation. The presence/ absence of large hydrophobic surface patches for the corresponding target protein structures was quantified using the hpatch tool implemented in Rosetta [8-10]. Surface areas were quantified using Pymol 1.7.0.0 (Schrödinger, LCC, New York, NY, USA). CatIB-formation was plotted as the relative activity in the insoluble fraction (Table S6). Coefficient of determination (R^2) values are always given excluding the blue-highlighted outliers (black) and including the outliers (blue)

Supporting Methods

Cloning and sequences

Tab S3 Plasmids used in this study. DNA and amino acid sequences of all gene fusions are given in the annex.

Vector	Genotyp	Description
pET28a	*ColE1 lacZ'* Kan^R P_{T7} P_{tac}	Merck (Darmstadt, Germany)
pTDoT-Linker-YFP	pET-28a, P_{T7}, gene fusion [*His-tag- tdot*-factor Xa recognition site- *(GGGS)₃ linker-yfp*]	[11]
pTDoT-L-YFP	pET-28a, P_{T7}, gene fusion [*tdot*-factor Xa recognition site-*(GGGS)₃ linker-yfp*]	pTDoT-Linker-YFP derivative, insertion of a 40 bp *Xba*I/*Nde*I RBS containing fragment of pET28a in pTDoT-Linker-YFP; without the 99 bp fragment containing RBS and *His-tag* [3]
pTDoT-YFP	pET-28a, P_{T7}, gene fusion [*tdot-yfp*]	pTDoT-L-YFP derivative, insertion of a 155 bp *Nde*I/*Bam*HI *tdot*-containing fragment in pTDoT-L-YFP; without the 215 bp fragment containing *tdot*, factor Xa recognition site and *(GGGS)₃ linker*
p3HAMP-L-YFP	pET-28a, P_{T7}, gene fusion [*3hamp*-factor Xa recognition site-*(GGGS)₃ linker-yfp*]	pTDoT-L-YFP derivative, insertion of a 518 bp *Nde*I/*Spe*I *3hamp*-containing fragment in pTDoT-L-YFP; without the 155 bp fragment containing *tdot*,
pTDoT-L-mCherry	pET-28a, P_{T7}, gene fusion [*tdot*-factor Xa recognition site-*(GGGS)₃ linker-mcherry*]	pTDoT-L-YFP derivative, insertion of 717 bp PCR-amplified *Bam*HI/*Sal*I *mcherry* fragment in pTDoT-L-YFP; without the 726 bp fragment containing *yfp* [3]
pTDoT-mCherry	pET-28a, P_{T7}, gene fusion [*tdot-mcherry*]	pTDoT-L-mCherry derivative, insertion of 155 bp *Nde*I/*Bam*HI *tdot*-containing fragment in pTDoT-L-mCherry; without the 215 bp fragment containing *tdot*, factor Xa recognition site and *(GGGS)₃ linker* [3]
p3HAMP-L-mCherry	pET-28a, P_{T7}, gene fusion [*3hamp*-factor Xa recognition site-*(GGGS)₃ linker-mcherry*]	pTDoT-L-mCherry derivative, insertion of a 518 bp *Nde*I/*Spe*I *3hamp*-containing fragment in pTDoT-L-mCherry; without the 155 bp fragment containing *tdot*,
pET22b-*R*ADH	pET22b, P_{T7}, *radh* gene	[12]
pTDoT-L-*R*ADH	pET-28a, P_{T7}, gene fusion [*tdot*- factor Xa recognition site-*(GGGS)₃ linker-radh*]	pTDoT-L-YFP derivative, insertion of 756 bp PCR-amplified *Bam*HI/*Sal*I *radh* fragment in pTDoT-L-YFP; without the 726 bp fragment containing *yfp* [3]
p3HAMP-L-*R*ADH	pET-28a, P_{T7}, gene fusion [*3hamp*-factor Xa recognition site-*(GGGS)₃ linker-radh*]	pTDoT-L-*R*ADH derivative, insertion of a 518 bp *Nde*I/*Spe*I *3hamp*-containing fragment in pTDoT-L-*R*ADH; without the 155 bp fragment containing *tdot*
pET21a-*Lb*ADH	pET21a, P_{T7}, *lbadh* gene	[13]
pTDoT-L-*Lb*ADH	pET-28a, P_{T7}, gene fusion [*tdot*-factor Xa recognition site-*(GGGS)₃ linker-lbadh*]	pTDoT-L-YFP derivative, insertion of 766 bp PCR-amplified *Bam*HI/*Sal*I *lbadh* fragment in pTDoT-L-YFP; without the 726 bp fragment containing *yfp*
p3HAMP-L-*Lb*ADH	pET-28a, P_{T7}, gene fusion [*3hamp*-factor Xa recognition site-*(GGGS)₃ linker-lbadh*]	p3HAMP-L-*R*ADH derivative, insertion of 766 bp PCR-amplified *Bam*HI/*Sal*I *lbadh* fragment in p3HAMP-L-*R*ADH; without the 756 bp fragment containing *radh*
pKK233_2-*Pf*BAL-*His*	pKK233_2 P_{trc}, gene fusion [*pfbal, His-tag]*	[14]

pTDoT-L-*Pf*BAL	pET-28a, P_{T7}, gene fusion [*tdot*-factor Xa recognition site-*(GGGS)$_3$ linker- pfbal*]	pTDoT-L-YFP derivative, insertion of 1699 bp PCR-amplified *Bam*HI/*Not*I *pfbal* fragment in pTDoT-L-YFP; without the 739 bp fragment containing *yfp* [3, 15]
p3HAMP-L-*Pf*BAL	pET-28a, P_{T7}, gene fusion [*3hamp*-factor Xa recognition site-*(GGGS)$_3$ linker-pfbal*]	pTDoT-L-*Pf*BAL derivative, insertion of a 518 bp *Nde*I/*Spe*I *3hamp*-containing fragment in pTDoT-L-*Pf*BAL; without the 155 bp fragment containing *tdot* [15]
pKK233_2-*Pp*BFD *L476Q-His*	pKK233_2 P_{trc}, gene fusion [*ppbfd, His-tag]*	[16]
pTDoT-L-*Pp*BFD *L476Q*	pET-28a, P_{T7}, gene fusion [*tdot*-factor Xa recognition site-*(GGGS)$_3$ linker-ppbfd*]	pTDoT-L-YFP derivative, insertion of 1600 bp PCR-amplified *Bam*HI/*Not*I *ppbfd* fragment in pTDoT-L-YFP; without the 739 bp fragment containing *yfp*
p3HAMP-L-*Pp*BFD *L476Q*	pET-28a, P_{T7}, gene fusion [*3hamp*-factor Xa recognition site-*(GGGS)$_3$ linker-pphbfd*]	p3HAMP-L-*Pf*BAL derivative, insertion of 766 bp PCR-amplified *Bam*HI/*Not*I *ppbfd* fragment in p3HAMP-L-*Pf*BAL; without the 1699 bp fragment containing *pfbal*
pTDoT-L-*Ec*LDC	pET-28a, P_{T7}, gene fusion [*tdot*-factor Xa recognition site-*(GGGS)$_3$ linker-ecldc*]	pTDoT-L-YFP derivative, insertion of 2148 bp PCR-amplified *Bam*HI/*Sal*I *ecldc* fragment in pTDoT-L-YFP; without the 726 bp fragment containing *yfp*
p*Ec*LDC-L-TDoT	pET-28a, P_{T7}, gene fusion [*ecldc-(GGGS)$_3$ linker-tdot*]	pTDoT-L-*Pf*BAL derivative, i) insertion of 2144 bp PCR-amplified *Nde*I/*Nhe*I *ecld* fragment in pTDoT-L-*Pf*BAL; without the 173 bp fragment containing *tdot-Xa*, ii) insertion of 160 bp PCR-amplified *Bam*HI/*Not*I *tdot* fragment in p*Ec*LDC-L-*Pf*BAL, without the 1699 bp fragment containing *bfbal* [17]
p*Ec*LDC-L-3HAMP	pET-28a, P_{T7}, gene fusion [*ecldc-(GGGS)$_3$ linker-3hamp*]	p*Ec*LDC-L-TDoT derivative, insertion of 526 bp PCR-amplified *Bam*HI/*Not*I *3hamp* fragment in p*Ec*LDC-L-TDoT; without the 160 bp fragment containing *tdot*

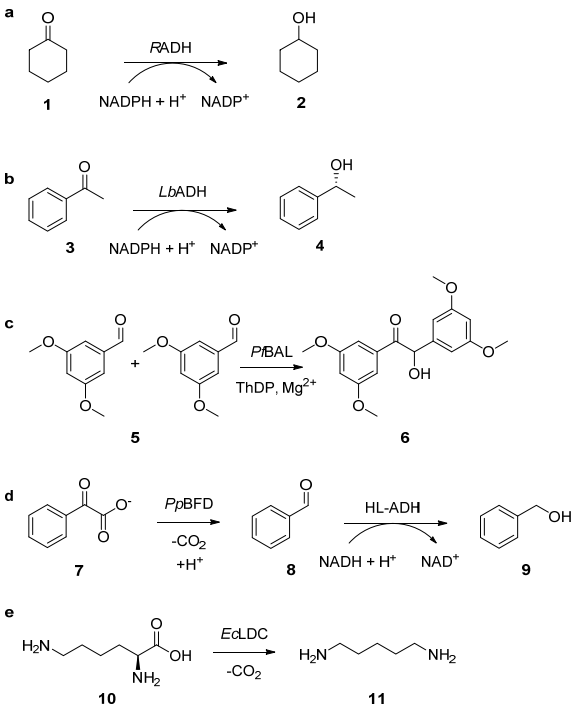
Tab S4 Oligonucleotide primers used in this study. Restriction endonuclease cleavage sites are underlined.

Name	Sequence (5' - 3')	Application
*Bam*HI_YFP_fw	ATATATGGATCCATGGTGAGCAAGGGCGAG	PCR amplification of *yfp*
YFP_*Sal*I_rv	ATATATGTCGACTTACTTGTACAGCTCGTCCATG	
*Bam*HI_mCherry_fw	ATATATGGATCCATGGTGAGCAAGGGCGAGGAGG	PCR amplification of *mcherry*
mCherry_*Sal*I_rv	ATATATGTCGACTTACTTGTACAGCTCGTCCATGCCGC	
*Bam*HI_*Pf*BAL_fw	ATATATGGATCCATGGCGATGATTACAGGCGGCGAAC	PCR amplification of *pfbal*
*Pf*BAL_*Not*I_rv	ATATATGCGGCCGCTTATGCGAAGGGGTCCATG	
*Bam*HI_*R*ADH_fw	ATATATGGATCCATGTATCGTCTGCTGAATAAAACCGC	PCR amplification of *radh*
*R*ADH_*Sal*I_rv	ATATATGTCGACTTAAACCTGGGTCAGACCACCATC	
*Nde*I_ TDoT_fw	ATATATCATATGATCATTAACGAAACTGCCGATGAC	Removal of factor Xa recognition site and $(GGGS)_3$ linker
TDoT_*Bam*HI_rv	TATATAGGATCCAATGCTCGCGAGAATGGTG	
RBS_Oligo_fw	CTAGAAATAATTTTGTTTAACTTTAAGAAGGAGATATACA	Removal of His-Tag
RBS_Oligo_rv	TATGTATATCTCCTTCTTAAAGTTAAACAAAATTATTT	
*Bam*HI_*Lb*ADH_fw	ATATATGGATCCATGTCTAACCGTTTGGATGGTAAGGTAG	PCR amplification of *lbadh*
*Lb*ADH_*Sal*I_rev	ATATATGTCGACTCTATTGAGCAGTGTAGCCACCG	
*Bam*HI_BFD_fw	ATATATGGATCCATGGCTTCGGTACACGGCACCAC	PCR amplification of *ppbfd*
BFD_*Not*I_rev	ATATATGCGGCCGCTTAAGATCTCTTCACCGGGCTTAC	
*Bam*HI_LDC_fwd	ATATATGGATCCATGAACATCATCGCTATCATGGGCCC	PCR amplification of *ecldc*
LDC_*Sal*I_rev	ATATATGTCGACTTAGCCTGCCATCTTAAGGACGCG	
*Nde*I_LDC_fw	ATATATCATATGATGAACATCATCGCTATCATGGGCCC	PCR amplification of *ecldc*
LDC_*Nhe*I_rv	ATATATGCTAGCGCCTGCCATCTTAAGGACG	
*Bam*HI_TDot_fw	ATATATGGATCCATCATTAACGAAACTGCCGATGACATCG	PCR amplification of *tdot*
TDot_*Not*I_rv	ATATATGCGGCCGCTTAAATGCTCGCGAGAATG	
*Bam*HI_3HAMP_fw	ACGTATGGATCCATGGGCCTGTTTAACGCCCATGCAGTTG	PCR amplification of *3hamp*
3HAMP_*Not*I_rev	ACATATGCGGCCGCTTAATTGTAGGCGGCTGTGGCCAGC	

Tab S5 The used strains are given with genotype and reference or source.

strains	genotype	reference or source
E. coli BL21 (DE3)	*F- ompT hsdSB(rB- mB -) gal dcm (λIts857ind1 Sam7 nin5 lacUV5-T7 gene1)*	[18] Invitrogen (Carlsbad, USA)
E. coli DH5α	*supE44 ΔlacU169 (Φ80lacZDM15) hsdR17 recA1 endA1 gyrA96 thi-1 relA1*	Invitrogen (Carlsbad, USA)
E. coli SG 13009	*F- ompT hsdS_B (rB-mB-) dcm gal* (DE3)	Qiagen (Hilden Germany)

Reaction equations



Extinction coefficients and molecular weight for protein concentration determination at 280 nm

Tab S6 Extinction coefficient and molecular weight of all used enzymes and proteins in soluble and CatIB form calculated with ExPASy ProtParam Tool (http://expasy.org/tools/protparam [19].

Protein	Extinction coefficient [L·mol^{-1}·cm^{-1}]	Molecular weight [kDa]
TDoT-L-YFP	26 485	34.6
TDoT-YFP	26 485	33.1
3HAMP-L-YFP	34 965	47.4
TDoT-L-mCherry	37 360	34.3
TDoT-mCherry	37 360	32.7
3HAMP-L-mCherry-	45 840	47.1
soluble *R*ADH	14 440	26.7
TDoT-L-*R*ADH	17 420	34.3
3HAMP-L-*R*ADH	25 900	47.1
soluble *Lb*ADH	19 940	26.8
TDoT-L-*Lb*ADH	22 920	34.3
3HAMP-L-*Lb*ADH	31 400	47.1
soluble *Pf*BAL	52 160	60.0
TDoT-L-*Pf*BAL	55 140	66.5
3HAMP-L-*Pf*BAL	63 620	79.3
soluble *Pp*BFD	62 340	57.4
TDoT-L-*Pp*BFD	65 320	64.2
3HAMP-L-*Pp*BFD	73 800	77.0
TDoT-L-*Ec*LDC	109 210	90.3
*Ec*LDC-L-TDoT	109 210	87.5
*Ec*LDC-L-3HAMP	117 690	100.5

Fig S13 Reactions to measure the initial rate activities of the enzymes used in this study. (a) *R*ADH-CatIBs catalyze the reduction of cyclohexanone **1** to cyclohexanol **2** under the consumption of NADPH. (b) *Lb*ADH-CatIBs catalyze the reduction of acetophenone **3** to (*R*)-1-phenylethanol **4** under the consumption of NADPH. (c) *Pf*BAL-CatIBs catalyze the carboligation of 3,5-dimethoxybenzaldehyde (DMBA, **5**) to the respective benzoin (*R*)-(3,3´,5,5´)-tetramethoxybenzoin (TMBZ, **6**). (d) *Pp*BFD-CatIBs catalyze the decarboxylation of benzoylformate **7** to benzaldehyde **8** followed by the reduction to benzyl alcohol **9** by horse liver (HL-)ADH under the oxidation of NADH. (e) *Ec*LDC-CatIBs catalyze the decarboxylation of L-lysine **10** to cadaverine (1,5-diaminopentane, **11**)

References

1. Diener M, Kopka B, Pohl M, Jaeger KE, Krauss U: **Fusion of a coiled-coil domain facilitates the high-level production of catalytically active enzyme inclusion bodies.** *Chemcatchem* 2016, **8:**142-152.
2. Bradford MM: **A rapid and sensitive method for the quantitation of microgram quantities of protein utilizing the principle of protein-dye binding.** *Analytical Biochemistry* 1976, **72:**248-254.
3. Jäger VD, Lamm R, Kloss R, Kaganovitch E, Grünberger A, Pohl M, Büchs J, Jaeger K-E, Krauss U: **A synthetic reaction cascade implemented by co-localization of two proteins within catalytically-active inclusion bodies.** *ACS Synthetic Biology* 2018, **[Epub ahead of print] doi: 10.1021/acssynbio.8b00274**.
4. Kandiah E, Carriel D, Perard J, Malet H, Bacia M, Liu K, Chan SW, Houry WA, Ollagnier de Choudens S, Elsen S, Gutsche I: **Structural insights into the *Escherichia coli* lysine decarboxylases and molecular determinants of interaction with the AAA+ ATPase RavA.** *Scientific Reports* 2016, **6:**24601.
5. Stetefeld J, Jenny M, Schulthess T, Landwehr R, Engel J, Kammerer RA: **Crystal structure of a naturally occurring parallel right-handed coiled coil tetramer.** *Nature Structural Biology* 2000, **7:**772-776.
6. Airola MV, Watts KJ, Bilwes AM, Crane BR: **Structure of concatenated HAMP domains provides a mechanism for signal transduction.** *Structure* 2010, **18:**436-448.
7. Conchillo-Sole O, de Groot NS, Aviles FX, Vendrell J, Daura X, Ventura S: **AGGRESCAN: a server for the prediction and evaluation of "hot spots" of aggregation in polypeptides.** *BMC Bioinformatics* 2007, **8:**65.
8. Jacak R, Leaver-Fay A, Kuhlman B: **Computational protein design with explicit consideration of surface hydrophobic patches.** *Proteins* 2012, **80:**825-838.
9. Kuhlman B, Baker D: **Native protein sequences are close to optimal for their structures.** *Proceedings of the National Academy of Sciences* 2000, **97:**10383.
10. Rohl CA, Strauss CE, Misura KM, Baker D: **Protein structure prediction using Rosetta.** *Methods Enzymol* 2004, **383:**66-93.
11. Diener M: **Von gezielter Oligomerisierung zu katalytisch aktiven *inclusion bodies* – Eine alternative Strategie zur Stabilisierung und Immobilisierung von Biokatalysatoren.** Heinrich-Heine University Düsseldorf, Institut für Molekulare Enzymtechnologie; 2014.
12. Kulig J, Simon RC, Rose CA, Husain SM, Hackh M, Ludeke S, Zeitler K, Kroutil W, Pohl M, Rother D: **Stereoselective synthesis of bulky 1,2-diols with alcohol dehydrogenases.** *Catalysis Science & Technology* 2012, **2:**1580-1589.
13. Weckbecker A, Hummel W: **Cloning, expression, and characterization of an (*R*)-specific alcohol dehydrogenase from *Lactobacillus kefir*.** *Biocatalysis and Biotransformation* 2006, **24:**380-389.
14. Janzen E, Muller M, Kolter-Jung D, Kneen MM, McLeish MJ, Pohl M: **Characterization of benzaldehyde lyase from *Pseudomonas fluorescens*: A versatile enzyme for asymmetric C-C bond formation.** *Bioorganic Chemistry* 2006, **34:**345-361.
15. Kloss R, Karmainski T, Jäger VD, Hahn D, Grünberger A, Baumgart M, Krauss U, Jaeger K-E, Wiechert W, Pohl M: **Catalytically active inclusion bodies of benzaldehyde lyase from *Pseudomonas fluorescens* for application in biocatalysis.** *??? to be submitted*.
16. Lingen B, Kolter-Jung D, Dünkelmann P, Feldmann R, Grötzinger J, Pohl M, Müller M: **Alteration of the substrate specificity of benzoylformate decarboxylase from *Pseudomonas putida* by directed evolution.** *ChemBioChem* 2003, **4:**721-726.
17. Kloss R, Limberg MH, Mackfeld U, Hahn D, Grünberger A, Jäger VD, Krauss U, Oldiges M, Pohl M: **Catalytically active inclusion bodies of L-lysine decarboxylase from *E. coli* for 1,5-diaminopentane production.** In *Scientific reports*, vol. 8. pp. 58562018: 5856.
18. Studier FW, Moffatt BA: **Use of bacteriophage T7 RNA polymerase to direct selective high-level expression of cloned genes.** *J Mol Biol* 1986, **189:**113-130.
19. Gasteiger E, Hoogland C, Gattiker A, Duvaud Se, Wilkins MR, Appel RD, Bairoch A: **Protein identification and analysis tools on the ExPASy server.** In *The Proteomics Protocols Handbook*. Edited by Walker JM. Totowa, NJ: Humana Press; 2005: 571-607.

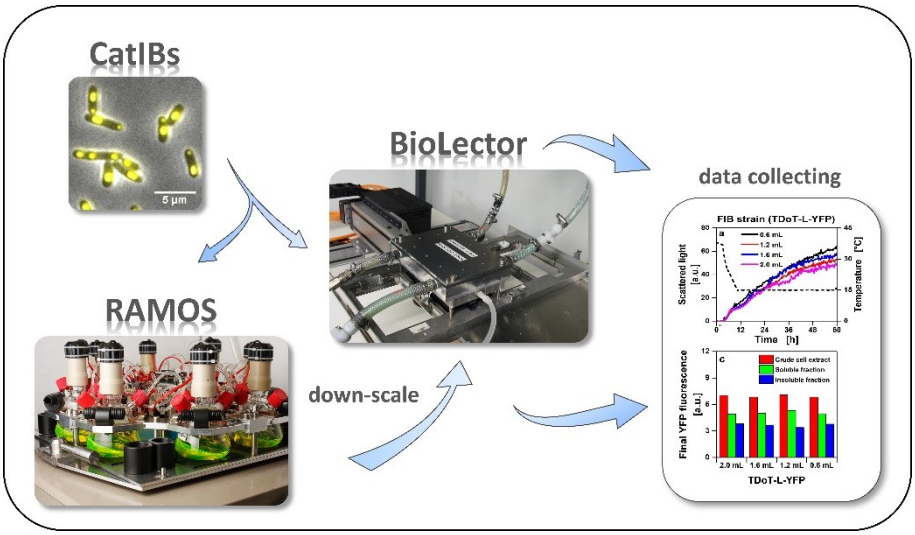
2.2 Publication II

Crucial cultivation parameters for fluorescent inclusion body production induced by a tetrameric coiled-coil domain

Robin Lamm, Vera D. Jäger, Benedikt Heyman, Christoph Berg, Christin Cürten, Ulrich Krauss, Karl-Erich Jaeger, Jochen Büchs*

*corresponding author

Manuscript in preparation



Contributions:

RL designed the study, performed the cultivation experiments, interpreted the data and drafted the manuscript. VDJ generated the expression constructs and carried out microscopic analyses. BH assisted in data interpretation and experiment design. CC performed HPAEC-PAD analyses and interpreted data regarding complex media compounds. UK, KEJ, and JB initiated and coordinated this study. JB supervised this study, participated in data interpretation and assisted in drafting the manuscript. All authors read, commented, and approved the manuscript.

Crucial cultivation parameters for fluorescent inclusion body production induced by a tetrameric coiled-coil domain

Robin Lamm[1,3] · Vera D. Jäger[2,3] · Benedikt Heyman[1] · Christoph Berg[1] · Christin Cürten[1,3] · Ulrich Krauss[2,3] Karl-Erich Jaeger[2,3,4] · Jochen Büchs[1,3]

Abstract

During heterologous protein production with *E. coli*, the formation of inclusion bodies (IBs) is often a major drawback as these aggregated proteins are usually inactive. However, different strategies for the generation of IBs consisting of catalytically active proteins have recently been described. In this study, the archaeal tetrameric coiled-coil domain of the cell-surface protein tetrabrachion was fused to a target reporter protein to produce fluorescent IBs (FIBs). As the cultivation conditions severely influence IB formation, the entire cultivation process resulting in the production of FIBs were thoroughly studied. First, the cultivation process was scaled down based on the maximum oxygen transfer capacity, combining online monitoring technologies for shake flasks and microtiter plates with offline sampling. The evaluation of culture conditions in complex terrific broth autoinduction medium showed strong oxygen limitation and leaky expression. Furthermore, strong acetate formation and pH changes from 6.5 to 8.8 led to sub-optimal cultivation conditions. However, in minimal Wilms-MOPS autoinduction medium defined culture conditions and a tightly controlled expression was achieved. The production of FIBs is strongly influenced by the induction strength. With increasing induction strength lower total amounts of active protein but higher amounts of active IBs are obtained. Furthermore, to prevent the formation of conventional inactive IBs, a temperature shift from 37°C to 15°C is crucial to generate FIBs. Finally, the gained insights were transferred to a stirred tank reactor batch fermentation. Hereby, 12 g/L FIBs were produced, making up 43 % (w/w) of the total generated biomass.

Keywords Active inclusion bodies · Fluorescent protein · Online monitoring · Process characterization High-throughput technologies

1 Introduction

The application of enzymes in biocatalysis and synthetic chemistry is a promising approach due to their high specificities and stereoselectivities that are often not achieved by chemical catalysts [1, 2]. Nevertheless, enzymes often lack stability under harsh process conditions like extreme pH, high temperatures, or in non-conventional reaction media that are commonly applied to enable economically feasible processes [3]. Immobilization represents a common strategy to increase enzyme stability and recyclability [4-8]. However, due to chromatographic purification steps during enzyme isolation and subsequent immobilization protocols, enzyme immobilization is usually laborious and therefore costly [9]. Hence, it is highly important to develop generic methods for the simple and cost-efficient production of stable enzyme immobilizates.

✉ Jochen Büchs
Jochen.buechs@avt.rwth-aachen.de

1 AVT – Aachener Verfahrenstechnik, Chair of Biochemical Engineering, RWTH Aachen University, Germany

2 Institute of Molecular Enzyme Technology, Heinrich-Heine-Universität Düsseldorf, Forschungszentrum Jülich GmbH, Germany

3 Bioeconomy Science Center (BioSC), Jülich, Germany

4 Institute of Bio- and Geosciences IBG-1: Biotechnology, Forschungszentrum Jülich GmbH, D-52425 Jülich, Germany

Bacterial inclusion bodies (IBs) are protein aggregates that are often formed intracellularly during high-level heterologous protein production [10]. These IBs can easily be purified from the culture broth. However, their lack of activity hinders utilization in biocatalysis and synthetic chemistry [11]. Recently, it was demonstrated that under certain conditions, IBs can retain catalytic activity [9, 12]. Amongst other strategies, the fusion of aggregation-prone tags to enzymes can induce the formation of catalytically active inclusion bodies (CatIBs). Besides CatIBs, fluorescent IBs (FIBs) have often been produced by using a fluorescent reporter protein as a target protein. Garcia-Fruitos *et al.* [13] fused different aggregation-prone tags to a galactosidase and two fluorescent proteins and obtained active IBs with all fusion proteins. Similarly, Nahalka and Nidetzky [14] showed that the fusion of the cellulose-binding domain of Clostridium cellulovorans to a target enzyme leads to formation of CatIBs. In the fusion strategy described by Diener *et al.* [15], the small (53 amino acids), tetrameric coiled-coil domain of the cell-surface protein tetrabrachion (TDoT) of the deep-sea archaeon *Staphylothermus marinus* is fused to different proteins. Additionally, a short flexible linker peptide is fused between the coiled-coil domain and the target protein. The linker consists of a $(GGGS)_3$ motif and a cleavage site for the protease factor Xa (hereafter referred to as L). Diener *et al.* [15] showed that at least 80 % of the

overall measured activity was found in CatIBs for three enzymes of increasing structural complexity (monomeric lipase A of *Bacillus subtilis*, dimeric *Arabidopsis thaliana* hydroxy nitrile lyase and a dimeric thiamine diphosphate dependent synthase of *E. coli*).

Existing studies comprise the engineering of aggregation-prone tags, computational predictions of polypeptide aggregation and investigations about the morphology and structure of IBs (See reviews by Krauss *et al*. [9], Rinas *et al*. [12] and de Marco *et al*. [16]). In a few studies, the impact of different cultivation parameters on CatIB formation has been investigated [17-22]. However, depending on the aggregation-prone tag and the fusion strategy, the impact of cultivation parameters can vary regarding the amount and activity of IBs. Furthermore, most studies focus on one specific cultivation parameter, which hampers the comparability.

For the fusion strategy described by Diener *et al*. [15], which was recently applied and extended in multiple studies [23-27], the impact of the cultivation process on IB activity has not been investigated yet. Therefore, we have characterized the cultivation process for FIBs production with *E. coli* and investigated the impact of important cultivation parameters (medium composition, oxygen availability, temperature, induction strength) for active IBs production. To enable online monitoring and a higher degree of parallelization, the cultivation protocol published by Diener *et al*. [15] was scaled down from 5 L shake flasks to 250 mL shake flasks and 48-deepwell microtiter plates (MTPs) [28]. Thereby, for the first time, the production of FIBs was in-depth characterized using the Respiration Activity MOnitoring System (RAMOS) [29] and the BioLector technology [30] at defined cultivation conditions. As it has been shown before in multiple studies, data derived from these culture devices can directly be used for scale up to stirred tank reactors. [31-33]. After investigating the impact of the aforementioned cultivation parameters, FIBs were produced in a 2 L stirred tank reactor batch fermentation at increased carbon concentrations to determine process specific performance indicators like the final FIB titers and space-time-yield.

2 Materials and methods

2.1 Microorganisms and media

The gene fusions encoding the fusion protein TDoT-L-YFP and a soluble control construct lacking the TDoT coiled-coil domain (Fig. 1A, C) were produced in *E. coli* BL21(DE3) employing pET28a (Novagen, Darmstadt, Germany) as expression vector [27]. Microscopy images of the respective strains after production of the fusion protein are shown in Fig 1. The employed variant of the yellow fluorescent protein (YFP) is a monomeric version of enhanced YFP bearing the A206K mutation [34, 35] but lacking the Q69K mutation, which renders mYFP less pH-sensitive in the neutral pH range [36]. All cultivation media were supplemented with 0.05 g/L kanamycin for plasmid maintenance. For cultivations in complex media, lysogeny broth (LB) medium was applied as pre-culture (5 g/L yeast extract, 10 g/L tryptone, 10 g/L NaCl) and premixed terrific broth (TB) medium (12 g/L casein, 24 g/L yeast extract, 9.4 g/L K2HPO4, 2.2 g/L KH2PO4) supplemented with 5 g/L glycerol, 2 g/L lactose and 0.5 g/L glucose was used as main culture [15, 37]. Cultivations in minimal media were performed with modified Wilms-MOPS medium [38] according to Rahmen *et al*. [39] with a pH-value set to 7.5 with NaOH. Pre-cultures in modified Wilms-MOPS medium were supplemented with 5 g/L glucose. Main cultures were supplemented with 5 g/L glycerol, 2 g/L lactose and 0.5 g/L glucose if not stated otherwise. All medium solutions were sterilized separately by autoclaving or filtration before mixing.

2.2 Cultivation with online monitoring and offline sampling

The pre-cultures in LB medium were inoculated from a cyro culture (OD600 0.02), which was stored at -80 °C and cultivated according to Diener *et al*. [15] (25 mL filling volume in 250 mL shake flask; 130 rpm, 50 mm shaking diameter, 37 °C cultivation temperature). The main culture in TB autoinduction medium was inoculated with OD600 0.05. Unless stated otherwise, the cultivations were performed in 250 mL shake flasks with 25 mL filling volume at 90 rpm and 50 mm shaking diameter or in 48-deepwell MTPs (m2plabs, Baesweiler, Germany) with 2 mL filling volume at 600 rpm and 3 mm shaking diameter. Pre-cultures in minimal Wilms-MOPS medium were inoculated from a cyro culture (OD600 0.02) and incubated over-night. The pre-cultures were performed in 250 mL shake flasks with 10 mL filling volume at 350 rpm and 50 mm shaking diameter. Unless stated otherwise, the main cultivation in minimal Wilms-MOPS medium was performed in 48-deepwell MTPs (m2plabs, Baesweiler, Germany) with 2 mL filling volume at 600 rpm and 3 mm shaking diameter.

The oxygen transfer rate (OTR) in shake flasks was monitored by applying the Respiration Activity MOnitoring System (RAMOS) built in-house. Commercial versions of the device can be purchased from Kuhner AG, Switzerland or HiTec Zang GmbH, Germany [29, 40]. The oxygen transfer rate (OTR) in 48-deepwell MTPs was monitored by applying the micro Respiration

Activity MOnitoring System (µRAMOS) built in-house [41]. Online fluorescence (λex/λem 515/530 nm) and scattered light (λex/λem 620/620 nm) measurements were performed using in-house built BioLector devices [42, 43]. From all displayed online data (fluorescence and scattered light) the initial intensity is subtracted (I – I0). To reduce noise of raw online data from Fig. 2, a median filter with a window size of seven was applied.

2.3 Offline analysis

For offline sampling, the complete culture broth from single wells was taken out at different time points as indicated. After sampling, the used wells were not subjected to further online analysis.

2.3.1 Optical density

The optical density was determined with a spectrophotometer (Genesys 20, Thermo Fisher Scientific, USA) at a wavelength of 600 nm in 1 cm cuvettes. The sample was appropriately diluted to measure values below 0.4 using 0.9% NaCl (mineral medium) or TB medium (complex medium). NaCl and TB medium were used as blanks.

2.3.2 pH-value

The pH-value was determined with an InLab Easy pH electrode (Mettler Toledo, Germany) that was calibrated using the appropriate calibration buffers and a CyberScan pH 510 meter (Eutech Instruments, Thermo Scientific, Germany).

2.3.3 Cell lysis and isolation of soluble and insoluble cell fractions

In order to quantify the amount of FIBs formed during cultivation, the cells were lysed and the insoluble and soluble cell fractions were separated. Cell lysis was performed in 48-deepwell MTPs. First, the MTP was centrifuged for 3 minutes at 4000 rpm and 4 °C (Hettich Rotina 35R, Germany). The supernatant was discarded. The cell pellets were resuspended in 200 µL of a lysis mastermix (Bugbuster, Merck supplemented with 25 U Benzonase, Merck and 0.2 g/L lysozyme, Carl Roth) and incubated for 15 min at 700 rpm and room temperature. Then, 600 µL lysis buffer (35.6 g/L Na2HPO4 · 2 H2O, 27.6 g/L NaH2PO4, 5.8 g/L NaCl) were added to obtain the crude cell extract (CCE). Afterwards, the MTP was centrifuged for 3 minutes at 4000 rpm and 4 °C (Hettich Rotina 35R, Germany). The supernatant (soluble fraction) was carefully transferred into a new 48-deepwell MTP to measure the fraction of soluble YFP. The insoluble pellet (insoluble fraction) was washed with lysis buffer and then used for further analysis (fluorescence measurements, SDS-PAGE). Since even in diluted samples YFP is highly concentrated inside the inclusion bodies, inner filters effects occur that prevent quantification of the proportion of active to inactive YFP in inclusion bodies. Therefore, only relative values are given throughout this study [44]. Offline YFP fluorescence was measured by a BioLector prototype, which is controlled by a LabVIEW software developed by ZUMOLab, Wesseling Germany.

2.3.4 SDS-PAGE

Sodium dodecylsulfate polyacrylamide gel electrophoresis (SDS-PAGE) was performed to determine the protein distribution in the soluble and insoluble cell fraction. The samples were appropriately diluted with a defined sample/water ratio and mixed with four-fold concentrated NuPAGE® LDS Sample Buffer (Thermo Fisher Scientific, USA). The prepared samples were placed on a thermo shaker and incubated at 600 rpm and a temperature of 95 °C for 5 min. For protein separation, 17-well or 12-well NuPAGE® 4-12% Bis-Tris gradient gels were used (Thermo Fisher Scientific, USA) and 10 or 20 µL sample were loaded per gel lane, respectively. Electrophoresis was carried out using XCell SureLock™ Mini-Cell electrophoresis system (Invitrogen, Germany) set to 200 V, 0.25 W for 35-45 min. Afterwards, the gels were stained over night at room temperature in Roti®-Blue staining solution (Roth, Germany) and destained using deionized water. The gels were scanned using an Epson perfection V700 photo scanner (Epson, Japan).

2.3.5 HPLC measurement

The concentration of the different carbon sources and overflow metabolites (glycerol, lactose, glucose and acetate) was determined via ion-exclusion chromatography analysis. An organic acid resin column (250 x 8 mm, CS Chromatographie Services, Germany) was used for separation at a temperature of 80 °C and a flow rate of 0.8 mL/min. As a mobile phase 75 mM H_2SO_4 was used. For the determination of lactose in complex TB medium, anion exchange chromatography according to Anders *et al.* [45] was performed.

2.4 Down scale from 5 L shake flask

To enable online monitoring and a higher degree of parallelization a down scale from 5 L shake flask as used by Diener *et al.* (2016) to 250 mL shake flask was performed. Therefore, the maximum oxygen transfer capacity was calculated according to equation (1) from Meier *et al.* (2016)

$$OTR_{max} = 3.72 \cdot 10^{-7} \cdot Osmol^{0.05} \cdot n^{\left(1.18-\frac{Osmol}{10.1}\right)} \cdot V_L{}^{-0.74} \cdot {d_0}^{0.33} \cdot d^{1.88} \cdot p_R \cdot {y_{O_2}}^{*} \quad (1)$$

For the scale down, the osmolality of the medium (Osmol), the absolute pressure (p_R) and the oxygen concentration of the gas phase (y_{O2}^*) were constant for all scales. For the calculation of the maximum

oxygen transfer capacity of the 5 L shake flask, the shaking frequency (n = 130 rpm), filling volume (V_L = 500 mL), shaking diameter (d_0 = 50 mm) and the diameter of the flask (d = 216.4 mm) were set to values as described by Diener *et al*. (2016) For the scale down to 250 mL shake flask, the relative filling volume was kept constant at 10 % and the shaking frequency was calculated to retain the same maximum oxygen transfer capacity as for the 5 L shake flask.

2.5 Batch fermentation in stirred tank reactor

A Satorius BIOSTAT® Bplus fermenter (Sartorius, Göttingen Germany) with two six-blade Rushton turbines (5.3 cm diameter) were used. The working volume was 1.5 L. For aeration, a ring sparger with 0.5 vvm compressed air was used. The dissolved oxygen tension was controlled at 30 % air saturation by adjusting the stirring rate. The pH was controlled to pH 7 using a 25 % (w/v) ammonia solution. As ammonia was added due to pH control, the initial ammonium concentration was reduced to 10 %. The MOPS buffer was completely omitted from the mineral Wilms-MOPS medium. As the medium osmolality is thereby reduced, an additional amount of initial carbon was added to reach the same osmolality, compared to the cultivation in MTPs with the highest initial carbon concentration (Cx3 medium with 1.5 g/L glucose, 6 g/L lactose and 15 g/L glycerol shown in Supplementary Data 3). Thus, the batch fermentation medium was prepared with 4.9 g/L glucose, 19.7 g/L lactose and 49.2 g/L glycerol. To determine cell dry weight, 1.9 mL culture broth was centrifuged for 3 min at 14,000 rpm (1-15 Sigma Laborzentrifugen, Germany) in dried pre-weighed 2 mL tubes in duplicates. After the supernatant was discarded, cell pellets were dried overnight and weighed. FIBs were isolated as described above and centrifuged in dried pre-weighted tubes. The pelletized FIBs were then dried overnight and weighted to determine the FIB concentration.

3 Results

The expression of a fusion protein consisting of TDoT-L-YFP leads to the formation of fluorescent inclusion bodies (FIBs) that contain high amounts of functional yellow fluorescent proteins (YFP) [9, 27]. The cultivation protocol with terrific broth (TB) auto-induction medium for the production of TDoT-L-YFP FIBs can be divided into two phases. In the first phase, *E. coli* grows on glucose as the preferred carbon source at a cultivation temperature of 37 °C. In the second phase, TDoT-L-YFP expression is induced due to the parallel consumption of lactose and glycerol, and the temperature is reduced to 15 °C [15, 37]. The produced

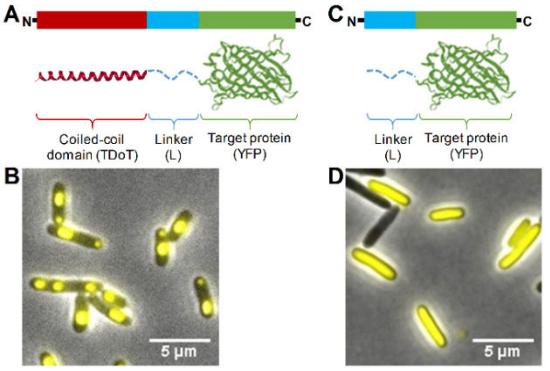


Fig. 1 Illustration of the fusion proteins and the resulting protein distribution within *E. coli* BL21 (DE3). (a) Schematic illustration of the fusion of the coiled-coil domain (TDoT, domain of the cell surface protein tetrabrachion of *Staphylothermus marinus,* PDB-ID: 1FE6) to a linker peptide consisting of a $(GGGS)_3$ motif and a cleavage site for the protease factor Xa and the target protein YFP (monomeric yellow fluorescent protein of *Aequorea victoria*, PDB-ID: 1YFP). (b) Microscopic image of *E. coli* BL21 (DE3) cells expressing TDoT-L-YFP show formation of fluorescent inclusion bodies. (c) Schematic illustration of the reference construct consisting of the linker peptide and the target protein (YFP). (d) Microscopic image of *E. coli* BL21 (DE3) expressing L-YFP with fluorescence equally distributed within cells.

FIBs are easily detectable by fluorescence microscopy and via the isolation of insoluble cell components after cell lysis. The YFP constructs and the intracellular distribution of YFP fluorescence are shown in Figure 1.

As a reference, a fusion protein consisting only of the linker peptide and YFP but lacking the TDoT coiled-coil domain was expressed under equivalent cultivation conditions to exclusively investigate the impact of the TDoT domain on the protein aggregation (Fig. 1C). The expression of this reference construct (L-YFP) leads to the formation of soluble YFP resulting in equally distributed fluorescence within the cell (Fig. 1D) [27].

3.1 Down scale from 5 L shake flask

The original cultivation process for the production of catalytically active inclusion bodies (CatIBs) published by Diener *et al*. [15] was performed in 5 L shake flasks. To characterize the cultivation process, a down-scaling from 5 L to 250 mL shake flasks and to 48-deepwell MTPs was conducted to enable online monitoring and a high degree of parallelization [29, 41, 42]. As down scaling criterion, the maximum oxygen transfer capacity was chosen. According to Meier *et al.* [46], the maximum oxygen transfer capacity in shake flasks can be calculated for known cultivation parameters. The osmolality of the medium is also an important parameter for the calculation of the maximum oxygen transfer capacity due to its strong effect on oxygen solubility and diffusivity in cultivation media [47, 48]. At first, the maximum oxygen transfer capacity was calculated using the cultivation parameters reported by Diener *et al*. [15] for the 5 L shake flask according to equation 1. For the 250 mL shake flask, the relative filling volume

was kept constant and the shaking frequency was calculated to retain the same maximum oxygen transfer capacity as for the 5 L shake flask. Since no correlation for MTPs is published that takes the osmolality of the medium into account, the µRAMOS technology was used to determine the downscaled cultivation parameters in MTPs (Supplementary Data 1) [41]. In summary, the shaking frequency for the 250 mL shake flask was set to 90 rpm with a filling volume of 25 mL and a shaking diameter of 50 mm. For 48-deepwell MTPs, the cultivation parameters were set to 600 rpm shaking frequency, 2 mL filling volume and 3 mm shaking diameter.

3.2 Characterization of the FIB production in complex TB autoinduction medium

Based on the downscaled cultivation parameters, the production of FIBs in complex TB autoinduction medium according to Diener *et al.* [15] was characterized with the RAMOS and BioLector technology (Fig. 2).

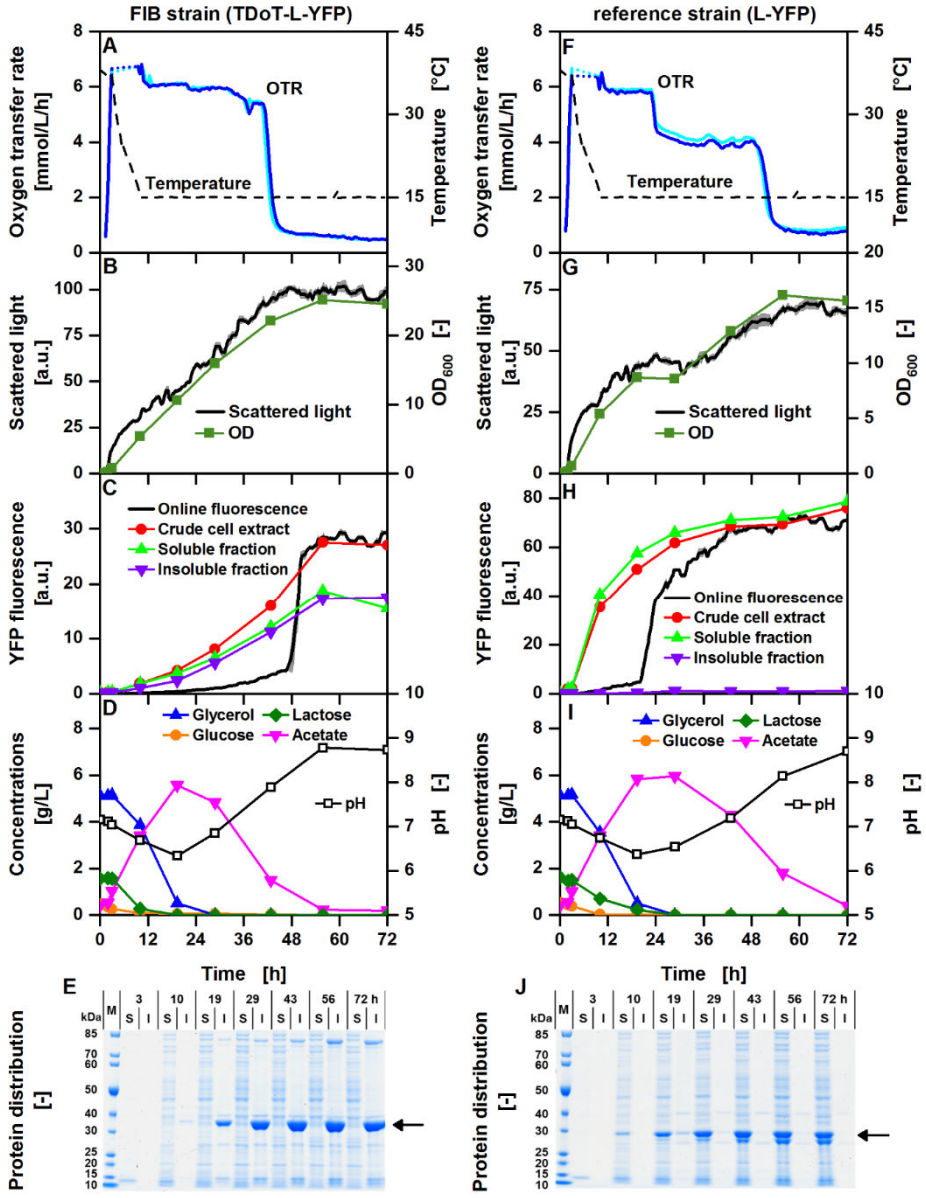


Fig. 2 Detailed characterization of the cultivation in complex TB autoinduction medium. Cultivation of *E. coli* BL21(DE3) TDoT-L-YFP (a-e) and L-YFP (f-j). (a+f) Oxygen transfer rate and temperature over time for *E. coli* BL21(DE3) expressing TDoT-L-YFP (insoluble) and L-YFP (soluble), respectively. For OTR, duplicates are displayed. Due to strong impact of the temperature shift on the oxygen sensor for OTR measurements, no OTR values are given in that period (dotted lines). (b+g) Scattered light intensity and offline OD_{600} as function of cultivation time. (c+h) Online YFP fluorescence and offline YFP fluorescence intensity of crude cell extract, soluble and washed insoluble fraction after cell disruption. For online fluorescence and scattered light, a median filter is applied and the mean of six wells with standard deviation is displayed. (d+i) Glucose, lactose, glycerol and acetate concentrations and pH. (e+j) SDS-PAGE analysis showing protein distribution per sample volume of soluble (S) and washed insoluble (I) fractions at 3, 10, 19, 29, 43, 56 and 72 h of cultivation. Arrows indicates size of target proteins (M = protein marker). Cultivation conditions (a, f): 250 mL RAMOS flask with 25 mL filling volume, 90 rpm shaking frequency, 50 mm shaking diameter. (b-e, g-j): 48-deepwell MTP with 2 mL filling volume, 600 rpm shaking frequency, 3 mm shaking diameter.

In addition to the *E. coli* strain (A-E) harboring the TDoT-L-YFP construct (hereafter referred to as FIB strain), the reference *E. coli* strain (F-J) harboring the L-YFP construct (hereafter referred to as reference strain) is cultured. After 3 hours at a cultivation temperature of 37 °C, a temperature shift to 15 °C is conducted. The oxygen transfer rate (OTR) increases exponentially indicating exponential biomass growth within the first 3 hours (Fig. 2A). During that period, HPLC analysis confirms the typical course of initial carbon sources in autoinduction media. Hence, glucose is consumed as preferred carbon source while lactose and glycerol concentrations remain constant (Fig. 2D) [37, 49]. Neither YFP fluorescence (Fig. 2C), nor a protein band on the SDS gel (Fig 2E) is detected after 3 h of cultivation, confirming non-inducing conditions due to catabolite repression. After 3 hours, an OTR plateau (6 mmol/L/h) is reached indicating oxygen limited conditions (Fig. 2A) [29]. The subsequent consumption of lactose and glycerol leads to the induction of YFP expression without interfering with the cultivation by the addition of an inducer (Fig. 2C, D, E). While lactose acts as the inducer of the *lac* operon, glycerol serves as an additional carbon and energy source [37, 39]. Lactose is depleted much earlier (10 h) than glycerol (19 h) (Fig. 2D). A reference cultivation in complex TB medium without the addition of lactose as inducer shows strong YFP fluorescence, which indicates a leaky expression system (Supplementary Data 2). In contrast, the cultivation in minimal Wilms-MOPS medium without addition of lactose shows no YFP fluorescence indicating a tightly regulated expression system. This difference between complex and minimal media has been reported before but is not fully understood yet [37, 50]. Due to the oxygen limitation, inhibiting amounts of acetate (5.6 g/L) are formed after 19 h of cultivation (Fig. 2A, D) [51]. Consequently, the pH changes strongly due to the production and subsequent consumption of acetate, the uptake of ammonia and the consumption of complex media components (Fig. 2D) [49, 52, 53].

A prominent feature of YFP (and all other GFP variants) is the oxygen dependent maturation accompanied by an equimolar generation of hydrogen peroxide after protein synthesis that is required for fluorescence to be measured [54, 55]. While this is commonly recognized as drawback of YFP as a reporter protein since the YFP fluorescence may not directly correlate with YFP synthesis, it can also be used as a tool to identify oxygen limited conditions during cultivation [56, 57]. Accordingly, during the oxygen limitation only a small increase of online YFP fluorescence is measured due to the oxygen dependent YFP maturation (Fig. 2C). Upon appearance of oxygen unlimited conditions (48 h), the online YFP fluorescence increases abruptly as shown by Ladner *et al.* [43] and Kunze *et al.* [58]. In comparison, the fluorescence intensity of the different fractions increases earlier indicating YFP maturation during sample preparation (Fig. 2C). Furthermore, the SDS gel analysis confirms that the online fluorescence does not depict the actual YFP synthesis rate (Fig. 2E). The SDS gel shows that TDoT-L-YFP (33 kDa) is mostly present within the insoluble fraction indicating the formation of inclusion bodies. However, the high YFP fluorescence in the soluble fraction shows that TDoT-L-YFP is partly also present in a soluble form. Remarkably, the measured fluorescence intensity is equally high in the soluble and insoluble fraction over the course of the cultivation. This effect might be attributed to the dense packing of YFP within FIBs that leads to lower fluorescence intensities and to an underestimation of active protein due to optical inner filter effects [44].

In contrast to the FIB strain (containing TDoT-L-YFP), the reference strain (containing L-YFP) shows no formation of FIBs indicated by the absence of fluorescence of the insoluble fraction (Fig. 2H) and the absence of a protein band (27.2 kDa) on the SDS gel in the insoluble fraction (Fig. 2J). The absence of FIBs is also indicated by much lower scattered light intensities of the reference strain compared to the FIB strain (Fig. 2B, G). Similar as conventional inactive IBs, FIBs also scatter light, and therefore, lead to increased scattered light intensities [59]. SDS-PAGE analysis of the cell lysate obtained from the reference strain (Fig. 2H) revealed two bands with a size of approximately 27 kDa and 26 kDa, respectively. This phenomenon was not further investigated but could originate from the cleavage of the linker (1 kDa) from soluble YFP. In the OTR, a strong decrease (24 h) is visible when glycerol and lactose are depleted. The metabolic switch to acetate as carbon source leads to a lower level of oxygen consumption (Fig. 2F, I). This is also visible in the scattered light and OD, which remain constant during that period (20 – 32 h) (Fig. 2G). At the end of oxygen limited conditions (24 h), the YFP online fluorescence intensity increases strongly due to oxygen dependent YFP maturation (Fig. 2F, H, J). The offline YFP fluorescence intensity increases earlier due to YFP maturation during sample preparation (Fig. 2H).

Despite strong oxygen limitation, high acetate formation and strong pH changes, high amounts of FIBs were produced by the FIB strain. However, these sub-optimal cultivation conditions and the leaky expression can be prevented by applying defined minimal media with increased buffer capacities. Furthermore, the carbon flux could be redirected from overflow metabolite formation to

FIB production by increasing the maximum oxygen transfer capacity.

3.3 Characterization of the FIB production on minimal Wilms-MOPS autoinduction medium

To investigate the impact of different cultivation parameters on FIB production, the complex TB medium was replaced by the minimal Wilms-MOPS medium. Thereby, the chemical medium composition is defined, and expression is more controlled (Fig. 3) [39, 50, 60]. Also, high batch-to-batch variations that are observed for complex substrates even if they are purchased from the same supplier are avoided [49]. Due to the omission of these considerable amounts of complex substrates (12 g/L casein, 24 g/L yeast extract) in minimal Wilms-MOPS autoinduction medium, lower FIB production is expected.

Fig. 3 shows the cultivation of the FIB strain and the reference strain on minimal Wilms-MOPS autoinduction medium. Again, in the first 3 h, an exponential growth on glucose occurs while lactose and glycerol concentrations remain constant (Fig. 3A, C). After 3 h, the temperature shift from 37 °C to 15 °C is conducted. From 3 – 20.5 h, lactose and glycerol are consumed in parallel and YFP expression is induced (Fig. 3C, D). As shown in Fig. 2, YFP fluorescence increases very slowly during oxygen limiting conditions. Upon depletion of all initial carbon sources (20.5 h), oxygen dependent YFP maturation takes place (Fig. 3B, C). At that time, only small amounts of acetate (0.5 g/L) have been formed compared to the cultivation in complex medium (Fig. 3C). The production of FIBs is confirmed by YFP fluorescence within the

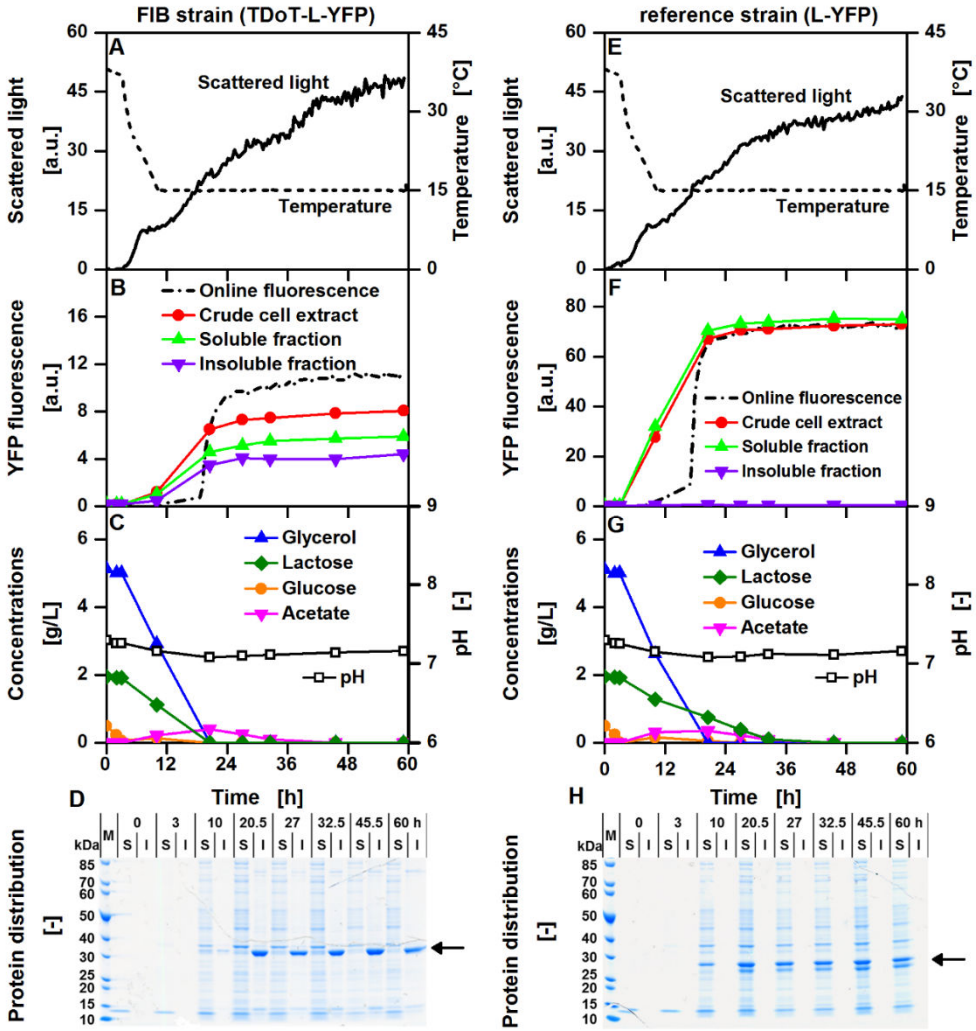


Fig. 3 Detailed characterization of the cultivation in minimal Wilms-MOPS autoinduction medium. Cultivation of *E. coli* BL21(DE3) TDoT-L-YFP (insoluble) (a-d) and L-YFP (soluble) (e-h). (a+e) Scattered light intensity and cultivation temperature as function of cultivation time for *E. coli* BL21(DE3) expressing TDoT-L-YFP (insoluble) and L-YFP (soluble). (b+f) Online YFP fluorescence and offline YFP fluorescence intensity of crude cell extract, soluble and washed insoluble fraction after cell disruption. (c+g) Glucose, lactose, glycerol and acetate concentrations and pH. (d+h) SDS-PAGE analysis showing protein content per sample volume of soluble (S) and washed insoluble (I) fractions at 3, 10, 21.5, 27, 32.5, 45.5 and 60 h of cultivation. Arrows indicates size of target proteins (M = protein marker). Cultivation conditions: 48-deepwell MTP with 2 mL filling volume, 600 rpm shaking frequency, 3 mm shaking diameter

insoluble fraction (Fig. 3B). Furthermore, the TDoT-L-YFP protein band (33 kDa) is mainly visible in the insoluble cell fraction (Fig. 3D). Remarkably, the YFP fluorescence distribution between the soluble and insoluble fractions remains constant after depletion of all carbon sources (32.5 – 59 h), even though the scattered light intensity increases (Fig. 3A, B). For the reference strain (L-YFP), no fluorescence is visible within the insoluble cell fraction (Fig. 3F). Additionally, no protein bands are detectable within the insoluble fraction by SDS-PAGE confirming the absence of IBs (Fig. 3H). The pH remains within a narrow range (7.1 – 7.2) over the course of cultivation for both strains (Fig. 3C, G).

As expected, lower amounts of FIBs are produced in minimal Wilms-MOPS autoinduction medium compared to the cultivation in TB autoinduction medium. This is also visible in the scattered light, which is only slightly higher for the FIB strain compared to the reference strain. This deviation is caused by the omission of large amounts of complex substrates (36 g/L complex substrates) compared to 7.5 g/L of sugars (Fig. 2C, 3B). These complex substrates (12 g/L casein, 24 g/L yeast extract) contain a mixture of carbohydrates, amino acids, peptides and trace elements [60]. The omission of these complex substrates leads to a lower overall carbon content, which decreases the amounts of produced FIBs. Additionally, the expression in TB autoinduction medium is amplified by leaky expression (Supplementary Data 2). By increasing the amount of glucose, lactose and glycerol, the amount of FIBs can easily be increased in minimal Wilms-MOPS autoinduction medium (Supplementary Data 3).

3.4 Cultivation at constant temperature

The strong effect of cultivation temperature on conventional IB formation has extensively been studied [61, 62]. To prevent IB formation, the cultivation temperature is often lowered to facilitate protein folding and to prevent protein aggregation. In case of FIB production, correct protein folding and protein aggregation is intended at the same time. Therefore, the impact of the temperature shift introduced by Diener *et al.* [15] was investigated in comparison to cultivations of the FIB strain and the reference strain at a constant cultivation temperature of 37 °C (Fig. 4).

Additional to the standard filling volume of 2 mL, lower filling volumes (1.5, 1.0, 0.6, 0.4 mL) were cultured to obtain increasing maximum oxygen transfer capacities. Within the first 3 h, the oxygen

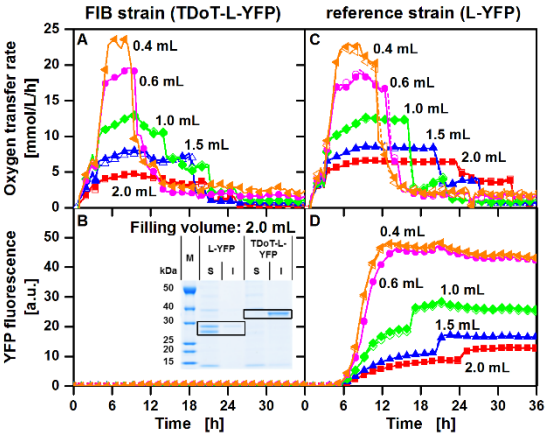


Fig. 4 Production of FIBs at a constant cultivation temperature of 37 °C. Cultivation of *E. coli* BL21(DE3) TDoT-L-YFP (a+b) and L-YFP (c+d) in Wilms-MOPS autoinduction medium (0.5 g/L glucose, 2 g/L lactose, 5 g/L glycerol). (a+c) Oxygen transfer rate as function of cultivation time. For clarity, a symbol for every 3rd data point is shown. (b+d) Online YFP fluorescence. For clarity, a symbol for every 8th data point is shown. (b insert) SDS-PAGE analysis showing protein content per sample volume of soluble (S) and washed insoluble (I) fractions at the end of cultivation. Boxes indicate target protein (M = protein marker). Duplicates are displayed in dashed lines and open symbols. Cultivation conditions: 48-deepwell MTP with 2 – 0.4 mL filling volume, 600 rpm shaking frequency, 3 mm shaking diameter, 37 °C cultivation temperature.

transfer rate of the FIB and the reference strain increases (Fig. 4A, C), while no YFP fluorescence intensity is detectable (Fig. 4A, C). Subsequently, the OTR drops shortly, which indicates the depletion of glucose [39]. Afterwards, the OTR increases while lactose and glycerol are consumed, indicated by the increasing YFP fluorescence intensity after 5 hours of cultivation of the reference strain (Fig. 4A, B, C). For lower filling volumes, higher OTRs are reached due to higher oxygen availabilities (Fig. 4A, C). At high filling volumes (2.0, 1.5 and 1.0 mL), OTR plateaus at different levels are reached indicating oxygen limiting conditions. For the reference strain and filling volumes of 1, 1.5 and 2 mL, YFP fluorescence increases abruptly upon oxygen unlimited conditions (16 h, 19 h, 24 h), which is indicated by the OTR drop at the of the OTR plateau. Cultures with 0.4 mL filling volume are not oxygen limited indicated by the absence of an OTR plateau and by the consistently increasing YFP fluorescence (Fig. 4C, D). Except for the cultures with high maximum oxygen transfer capacities (0.4 and 0.6 mL filling volume), lower maximum oxygen transfer capacities lead to lower final fluorescence intensities (Fig. 4C, D). While the reference strain shows high YFP fluorescence intensities, no fluorescence intensity is measured for the FIB strain (Fig. 4B). The SDS-PAGE analysis for the standard filling volume of 2 mL shows mainly soluble YFP for the reference strain and mainly insoluble YFP

for the FIB strain at the end of cultivation. Furthermore, the SDS gel shows a similar YFP amount for both strains. For the FIB strain, this indicates the formation of conventional IBs containing misfolded, aggregated, non-fluorescent YFP. Most likely, the protein folding of the entire monomeric fusion protein (TDoT-L-YFP) has first to be completed to be then incorporated in IBs in an active form. It has often been reported that lower cultivation temperatures lead to IBs with higher activity [18-21, 63]. However, in other studies, fusion proteins with aggregation-prone tags are produced that lead to the formation of active inclusion bodies even though the expression temperature is not lowered [13, 64-66]. Presumably, a higher aggregation tendency of the fusion tag and culture conditions that lead to high local protein concentrations require lower cultivation temperatures to obtain high amounts of actively folded proteins in IBs. In an upcoming publication, the impact of the cultivation temperature is studied in-depth using a MTP-based temperature profiling system established by Kunze *et al.* [67].

3.5 Cultivation with varying maximum oxygen transfer capacities

After the necessity of the temperature shift was confirmed, a cultivation with the standard temperature shift at different maximum oxygen transfer capacities was conducted to investigate the effect of oxygen limitation on the FIB production (Fig. 5).

The FIB strain is cultured in minimal Wilms-MOPS autoinduction medium with varying filling volumes (2.0, 1.6, 1.2, 0.6 mL). During the cultivation, a temperature shift after 3 h from 37 °C to 15 °C was conducted as previously described (Fig. 2, 3). Within the first 3 h of cultivation, the scattered light increases exponentially while no YFP fluorescence intensity is detected (Fig. 5A, B). Subsequently, the typical YFP fluorescence course is measured for the standard filling volume (2 mL). A slow linear increase is followed by an abrupt increase upon oxygen unlimited conditions (Fig. 5B) [43, 56, 57]. For lower filling volumes, this abrupt increase becomes less prominent due to higher maximum oxygen transfer capacities. At a filling volume of 0.6 mL no oxygen limitation occurs and the YFP fluorescence increases with a steady slope, depicting the actual production rate of TDoT-L-YFP. Eventually, the final YFP fluorescence intensities are similar for different filling volumes (Fig. 5B). Fig. 5c shows the final fluorescence intensities at the end of cultivation of the different

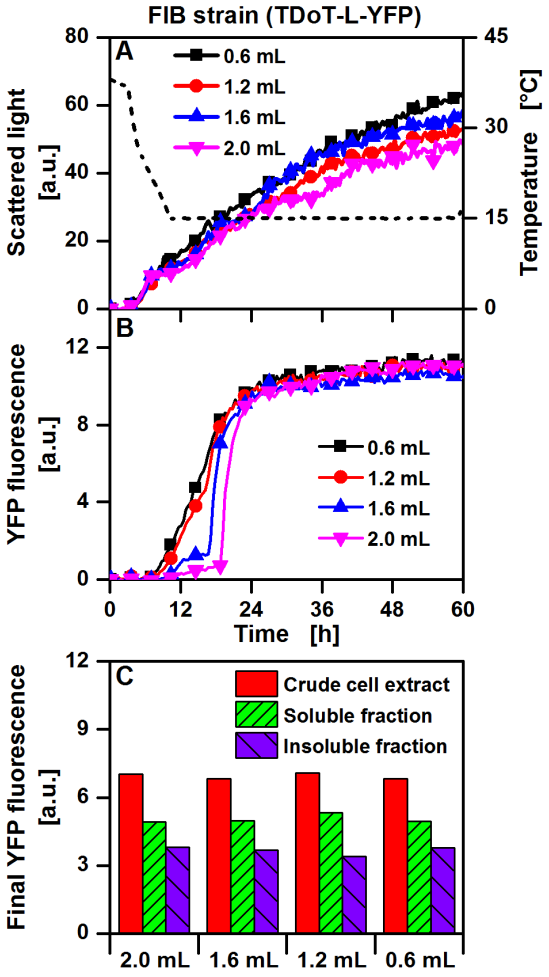


Fig. 5 Production of FIBs at increasing maximum oxygen transfer capacities. Cultivation of *E. coli* BL21(DE3) TDoT-L-YFP (a-c) in minimal Wilms-MOPS auto-induction medium (0.5 g/L glucose, 2 g/L lactose, 5 g/L glycerol) at different maximum oxygen transfer capacities, achieved by varying the filling volume (2.0 mL, 1.6 mL, 1.2 mL, 0.6 mL). (a) Scattered light intensity and cultivation temperature as function of cultivation time. (b) Online YFP fluorescence. For clarity, a symbol for every 10th data point is shown. (c) Final fluorescence intensity of crude cell extract, soluble and washed insoluble fraction at the end of cultivation. Cultivation conditions: 48-deepwell MTP with 2 – 0.6 mL filling volume, 600 rpm shaking frequency, 3 mm shaking diameter.

fractions. Slightly higher YFP fluorescence intensities are measured in the soluble than in the insoluble fraction as already shown in Fig. 3 (Fig. 5C). It is also obvious that the maximum oxygen transfer capacity has no impact on the final fluorescence intensity of FIBs. However, oxygen limiting conditions lead to several disadvantages like prolonged cultivation times and acidification of the culture broth due to acetate formation. Hence, oxygen limitation has to be avoided.

3.6 Impact of induction method and strength on FIB production

The induction method and strength is an important cultivation parameter for the production of

heterologous proteins as well as active IBs [16, 68]. Besides lactose, isopropyl β-D-1-thiogalactopyranoside (IPTG) at different concentrations is used to investigate the impact of induction strength on FIB production (Fig 6).

As the cultivation temperature is a crucial cultivation parameter to produce FIBs (Fig. 4), IPTG was added in different concentrations at the same time (after 4.5 h) to induce all cultures at the same temperature (Fig. 6B, black arrow). Within the first 4.5 h of cultivation, scattered light increases similarly for all cultivations. Subsequently, the slopes of scattered light curves are lower at increasing IPTG concentrations (Fig. 6A). For autoinduced cultures, scattered light increases similarly as in cultures with IPTG concentrations of 0.1-0.15 mM. Online YFP fluorescence increases after 4.5 h for all induced cultures (Fig. 6B). The final YFP fluorescence of autoinduced cultures is equal to cultures induced with 0.1 mM IPTG. The highest final YFP fluorescence is measured for cultures induced with 0.05 mM IPTG (Fig. 6B, C). For autoinduced cultures and cultures induced with IPTG concentrations of 0.15^{-1} mM, the final YFP fluorescence intensities of the crude cell extract and the insoluble fraction are similar. However, lower induction strengths (0.05 and 0.1 mM IPTG) lead to higher YFP fluorescence in the crude cell extract, and lower YFP fluorescence in the insoluble fraction. Thus, lower induction strengths shift the amount of YFP from FIBs to the soluble fraction. This was already observed in studies dealing with conventional, inactive IBs [22, 69]. Higher induction strengths lead to higher expression rates that reduce the production of native soluble protein, but increase the amount of active proteins in IBs [22]. Possibly, high local protein concentrations and misfolded proteins function as aggregation nucleus that capture additional native proteins. Thereby, the production of active IBs is increased even though the total amount (soluble and insoluble YFP) of active proteins is reduced. To produce active IBs, it is crucial to find the right balance between a high portion of active proteins and a high amount of proteins aggregated in IBs.

3.7 Batch fermentation in stirred tank reactor for the production of FIBs

To determine process specific performance indicators like the final FIB titer and space-time-yield and to obtain larger sample volumes, a 2 L batch fermentation with increased amount of carbon sources was performed (Fig. 7). The scalability of the obtained insights on FIB production from the MTP-scale is proven.

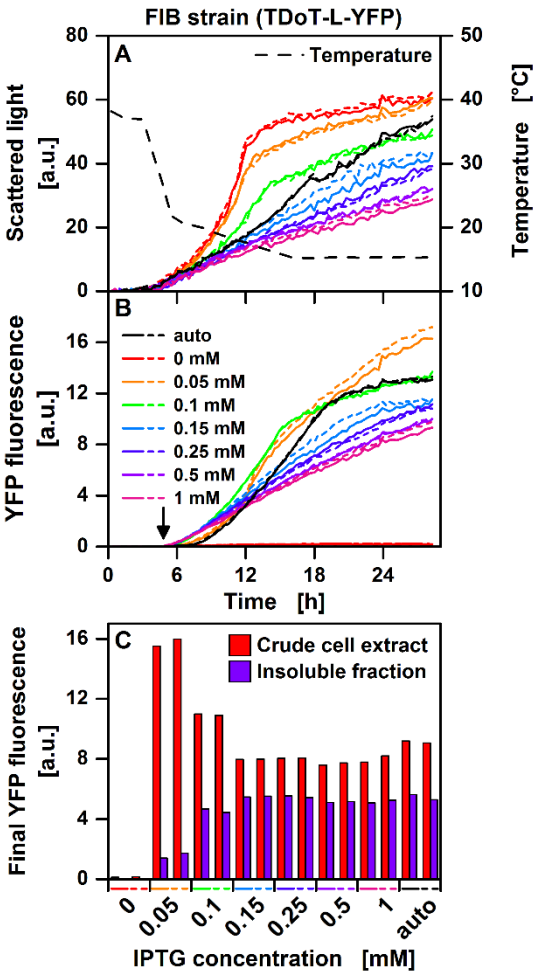


Fig. 6 Impact of autoinduction and different IPTG concentrations on FIB production. Cultivation of *E. coli* BL21(DE3) TDoT-L-YFP in minimal Wilms-MOPS medium. Cultures induced with IPTG were supplemented with 7.5 g/L glucose. IPTG (0 – 1 mM) was added after 4.5 h of cultivation (Arrow indicates time of IPTG addition.). Cultures with autoinduction medium contained the standard carbon concentrations (0.5 g/L glucose, 2 g/L lactose, 5 g/L glycerol). (a) Scattered light intensity and cultivation temperature as function of cultivation time. (b) Online YFP fluorescence. (c) Final YFP fluorescence intensity of crude cell extract and washed insoluble fraction after 36 h. Cultivation conditions: 48-deepwell MTP with 0.8 mL filling volume, 1000 rpm shaking frequency, 3 mm shaking diameter. Duplicates for all cultivation conditions are displayed.

As the importance of the temperature shift was demonstrated above, the temperature was reduced from 37 to 15 °C during cultivation (Fig. 7A). At 37 °C exponential growth on glucose takes place and no production of FIBs is observed (Fig. 7A, C, D). Due to the temperature shift and the depletion of glucose, the OTR drops after around 8 h of cultivation. Subsequently, the OTR increases until the end of fermentation up to 40 mmol/L/h, which is reflected in increasing glycerol and lactose consumption rates (Fig. 7A, D). Interestingly, the hydrolysis of lactose to galactose and glucose leads to the accumulation of up to 4 g/L glucose. Usually, glucose intracellularly produced by lactose

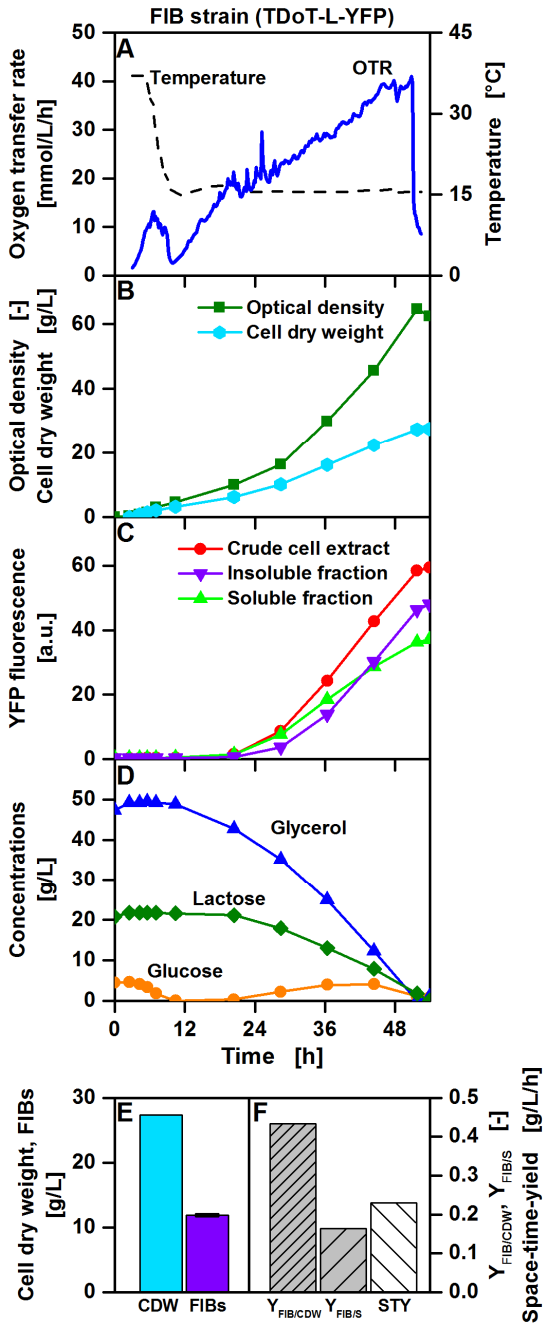


Fig. 7. Production of FIBs in 2 L stirred tank reactor batch fermentation. *E. coli* BL21(DE3) TDoT-L-YFP in minimal Wilms-MOPS autoinduction medium. Initial carbon concentrations were increased to 4.9 g/L glucose, 19.7 g/L lactose and 49.2 g/L glycerol. (A) Oxygen transfer rate and cultivation temperature as function of cultivation time. (B) Optical density and cell dry weight. For cell dry weight, the mean of duplicates is displayed (C) Offline YFP fluorescence of crude cell extract, soluble and washed insoluble fraction. (D) Glycerol, lactose and glucose concentration. (E) Final cell dry weight (mean of duplicates), FIB concentration (mean and standard deviation of triplicates displayed), yield coefficient of FIB concentration per cell dry weight, yield coefficient of FIB concentration per initial carbon concentrations (S) and space time yield (FIB production per liter and hour). Cultivation conditions: 1.5 L working volume, 0.5 vvm aeration, DOT controlled at 30 % air saturation, pH controlled at 7.

hydrolysis is phosphorylated and not secreted into the culture broth [70]. Potentially, the low cultivation temperature decelerated glucose phosphorylation, and thus, leads to glucose accumulation. The production of FIBs is confirmed by high YFP fluorescence in the insoluble fraction, which is approximately 10-fold increased compared to the standard cultivation in Wilms-MOPS medium (compare Fig. 7C and Fig. 3B). The production of IBs can also be indirectly inferred from the cell dry weight and optical density curves (Fig. 7B). During initial growth on glucose, the cell dry weight and optical density are similarly increasing. Subsequently, the optical density is increasing much stronger, compared to the cell dry weight, probably due to increased light scattering by the produced FIBs (Fig. 7B). After 53 h of cultivation, the final cell dry weight is 27.6 g/L and the FIB concentration is 11.9 g/L ± 0.15 g/L (Fig. 7E). Thus, a remarkably high biomass-specific FIB yield of 0.43 is achieved (Fig. 7F). The FIB yield per supplemented carbon source is 0.16. Overall, a space-time-yield of 0.23 g/L/h FIBs is reached (Fig. 7F).

4 Conclusion

To facilitate online monitoring and a higher degree of parallelization, a published cultivation protocol for the production of active IBs was scaled-down, based on the maximum oxygen transfer capacity. Subsequently, the production of FIBs in complex TB autoinduction medium was characterized and the impact of important cultivation parameters (cultivation medium, oxygen availability, cultivation temperature, and induction strength) on FIB production was systematically evaluated and compared with literature. The characterization of previously published cultivation protocol for FIB production in complex TB autoinduction medium showed strong oxygen limitation, high acetate formation, strong pH changes and leaky expression. By applying the defined mineral Wilms-MOPS autoinduction medium, tightly controlled expression was achieved, and strong acetate formation and pH shifts were avoided. It was shown that oxygen limiting conditions are not necessary and beneficial to produce FIBs. However, in order to prevent the production of conventional, inactive IBs, the temperature shift from 37 to 15 °C is crucial. Furthermore, a strong impact of the induction strength on FIB production was observed. Low induction strength lead to more active YFP, but lower amounts of active YFP in FIBs. For FIB production, it is therefore vital to find the right balance between a high induction strength to

effectively induce protein aggregation and a higher folding efficiency at lower induction strengths. These observations motivate further investigations regarding the structural differences between conventional inactive IBs and active IBs, as both kinds of IBs can be produced with the same target protein by simply altering the cultivation conditions. Finally, the general applicability and scalability of the gained insights were confirmed by experiments in a 2 L stirred tank reactor batch fermentation. Due to the increased amount of supplemented carbon sources, 11.9 g/L of highly active FIBs were produced that made up 43 % (w/w) of the total cell dry weight. In future, the insights on the production of FIBs have to be transferred to catalytically active inclusion bodies (CatIBs).

Acknowledgements

This study was funded by the Bioeconomy Science Center (BioSC), which is financially supported by the Ministry of Culture and Science of North-Rhine Westphalia within the framework of the NRW Strategieprojekt BioSC (Grant No. 313/32 3-400-002 13). BioSC is a research cluster consisting of the universities RWTH Aachen, Düsseldorf and Bonn, and the Forschungszentrum Jülich.

Compliance with ethical standards

Conflict of interest

The authors declare that they have no conflict of interest.

Ethical Approval

This article does not contain any studies with human participants or animals performed by any of the authors.

Funding

This study was funded by the Bioeconomy Science Center (BioSC), which is financially supported by the Ministry of Culture and Science of North-Rhine Westphalia within the framework of the NRW Strategieprojekt BioSC (Grant No. 313/32 3-400-002 13). BioSC is a research cluster consisting of the universities RWTH Aachen, Düsseldorf and Bonn, and the Forschungszentrum Jülich.

Nomenclature

d	Maximum shake flask diameter (mm)
d_0	Shaking diameter (cm)
n	Shaking frequency (rpm)
$Osmol$	Osmolality (Osmol kg^{-1})
OTR	Oxygen transfer rate (mol L^{-1} h^{-1})
OTR_{max}	Maximum oxygen transfer capacity (mol L^{-1} h^{-1})
p_R	Absolute pressure (bar)
V_L	Filling volume (mL)
Y_{O2}^*	Oxygen concentration of the gas phase (mol mol^{-1})

References

[1] R. Patel, R. Hanson, A. Goswami, V. Nanduri, A. Banerjee, M. J. Donovan, S. Goldberg, R. Johnston, D. Brzozowski, T. Tully, J. Howell, D. Cazzulino, R. Ko (2003) Enzymatic synthesis of chiral intermediates for pharmaceuticals. *J. Ind. Microbiol. Biotechnol.* 30: 252-259.

[2] B. M. Nestl, B. A. Nebel, B. Hauer (2011) Recent progress in industrial biocatalysis. *Curr. Opin. Chem. Biol.* 15: 187-193.

[3] G. R. Castro, T. Knubovets (2003) Homogeneous biocatalysis in organic solvents and water-organic mixtures. *Crit. Rev. Biotechnol.* 23: 195-231.

[4] V. M. Balcao, M. Vila (2015) Structural and functional stabilization of protein entities: state-of-the-art. *Adv. Drug Deliv. Rev.* 93: 25-41.

[5] A. Liese, L. Hilterhaus (2013) Evaluation of immobilized enzymes for industrial applications. *Chem. Soc. Rev.* 42: 6236-6249.

[6] J. M. Guisan (2013) *Immobilization of Enzymes and Cells*, pp. 1-13, Humana Press Inc, Totowa, NJ, USA.

[7] R. A. Sheldon (2011) Characteristic features and biotechnological applications of cross-linked enzyme aggregates (CLEAs). *Appl. Microbiol. Biotechnol.* 92: 467-477.

[8] P. Tielmann, H. Kierkels, A. Zonta, A. Ilie, M. T. Reetz (2014) Increasing the activity and enantioselectivity of lipases by sol-gel immobilization: further advancements of practical interest. *Nanoscale* 6: 6220-6228.

[9] U. Krauss, V. D. Jäger, M. Diener, M. Pohl, K. E. Jaeger (2017) Catalytically-active inclusion bodies-carrier-free protein immobilizates for application in biotechnology and biomedicine. *J. Biotechnol.* 258: 136-147.

[10] G. Georgiou, P. Valax (1996) Expression of correctly folded proteins in *Escherichia coli*. *Curr. Opin. Biotechnol.* 7: 190-197.

[11] A. Villaverde, M. M. Carrio (2003) Protein aggregation in recombinant bacteria: biological role of inclusion bodies. *Biotechnol. Lett* 25: 1385-1395.

[12] U. Rinas, E. Garcia-Fruitos, J. L. Corchero, E. Vazquez, J. Seras-Franzoso, A. Villaverde (2017) Bacterial Inclusion Bodies: Discovering Their Better Half. *Trends Biochem. Sci* 42: 726-737.

[13] E. Garcia-Fruitos, N. Gonzalez-Montalban, M. Morell, A. Vera, R. M. Ferraz, A. Aris, S. Ventura, A. Villaverde (2005) Aggregation as bacterial inclusion bodies does not imply inactivation of enzymes and fluorescent proteins. *Microb. Cell Fact.* 4: 27.

[14] J. Nahalka, B. Nidetzky (2007) Fusion to a pull-down domain: a novel approach of producing *Trigonopsis variabilis* D-amino acid oxidase as insoluble enzyme aggregates. *Biotechnol. Bioeng.* 97: 454-461.

[15] M. Diener, B. Kopka, M. Pohl, K.-E. Jaeger, U. Krauss (2016) Fusion of a coiled-coil domain facilitates the high-level production of catalytically active enzyme inclusion bodies. *ChemCatChem* 8: 142-152.

[16] A. de Marco, N. Ferrer-Miralles, E. Garcia-Fruitos, A. Mitraki, S. Peternel, U. Rinas, M. A. Trujillo-Roldan, N. A. Valdez-Cruz, E. Vazquez, A. Villaverde (2019) Bacterial inclusion bodies are industrially exploitable amyloids. *FEMS Microbiol Rev* 43: 53-72.

[17] J.-P. Arié, M. Miot, N. Sassoon, J.-M. Betton (2006) Formation of active inclusion bodies in the periplasm ofEscherichia coli. *Molecular Microbiology* 62: 427-437.

[18] N. S. de Groot, S. Ventura (2006) Effect of temperature on protein quality in bacterial inclusion bodies. *FEBS Lett.* 580: 6471-6476.

[19] S. M. Doglia, D. Ami, A. Natalello, P. Gatti-Lafranconi, M. Lotti (2008) Fourier transform infrared spectroscopy analysis of the conformational quality of recombinant proteins within inclusion bodies. *Biotechnol. J.* 3: 193-201.

[20] A. Vera, N. Gonzalez-Montalban, A. Aris, A. Villaverde (2007) The conformational quality of insoluble recombinant proteins is enhanced at low growth temperatures. *Biotech. Bioeng.* 96: 1101-1106.

[21] W. Wang, J. Sun, W. Xiao, L. Jiang, R. Wang, J. Fan (2017) Change of the N-terminal codon bias combined with tRNA supplementation outperforms the selected fusion tags for

production of human D-amino acid oxidase as active inclusion bodies. *Biotechnol. Lett* 39: 1733-1740.

[22] K. Jhamb, D. K. Sahoo (2012) Production of soluble recombinant proteins in Escherichia coli: effects of process conditions and chaperone co-expression on cell growth and production of xylanase. *Bioresour Technol* 123: 135-143.

[23] V. D. Jäger, R. Kloss, A. Grünberger, S. Seide, D. Hahn, T. Karmainski, M. Piqueray, J. Embruch, S. Longerich, U. Mackfeld, K.-E. Jaeger, W. Wiechert, M. Pohl, U. Krauss (2019) Tailoring the properties of (catalytically)-active inclusion bodies. *Microbial Cell Factories* 18: 33.

[24] V. D. Jäger, M. Piqueray, S. Seide, M. Pohl, W. Wiechert, K.-E. Jaeger, U. Krauss (2019) An Enzymatic 2 ‐ Step Cofactor and Co ‐ Product Recycling Cascade towards a Chiral 1,2 ‐ Diol. Part II: Catalytically Active Inclusion Bodies. *Adv Synth Catal*.

[25] R. Kloß, M. H. Limberg, U. Mackfeld, D. Hahn, A. Grunberger, V. D. Jager, U. Krauss, M. Oldiges, M. Pohl (2018) Catalytically active inclusion bodies of L-lysine decarboxylase from *E. coli* for 1,5-diaminopentane production. *Sci. Rep.* 8: 11.

[26] R. Kloß, T. Karmainski, V. D. Jager, D. Hahn, A. Grunberger, M. Baumgart, U. Krauss, K. E. Jaeger, W. Wiechert, M. Pohl (2018) Tailor-made catalytically active inclusion bodies for different applications in biocatalysis. *Catal. Sci. Technol.* 8: 5816-5826.

[27] V. D. Jäger, R. Lamm, R. Kloß, E. Kaganovitch, A. Grünberger, M. Pohl, J. Büchs, K. E. Jaeger, U. Krauss (2018) A synthetic reaction cascade implemented by colocalization of two proteins within catalytically active inclusion bodies. *ACS Synth Biol* 7: 2282-2295.

[28] C. Lattermann, J. Büchs (2015) Microscale and miniscale fermentation and screening. *Curr. Opin. Biotechnol.* 35: 1-6.

[29] T. Anderlei, J. Büchs (2001) Device for sterile online measurement of the oxygen transfer rate in shaking flasks. *Biochem. Eng. J.* 7: 157-162.

[30] M. Samorski, G. Muller-Newen, J. Büchs (2005) Quasi-continuous combined scattered light and fluorescence measurements: A novel measurement technique for shaken microtiter plates. *Biotech. Bioeng.* 92: 61-68.

[31] F. Kensy, C. Engelbrecht, J. Büchs (2009) Scale-up from microtiter plate to laboratory fermenter: evaluation by online monitoring techniques of growth and protein expression in *Escherichia coli* and *Hansenula polymorpha* fermentations. *Microb. Cell Fact.* 8.

[32] J. M. Seletzky, U. Noak, J. Fricke, E. Welk, W. Eberhard, C. Knocke, J. Büchs (2007) Scale-up from shake flasks to fermenters in batch and continuous mode with *Corynebacterium glutamicum* in lactic acid based on oxygen transfer and pH. *Biotech. Bioeng.* 98: 800-811.

[33] M. Funke, A. Buchenauer, W. Mokwa, S. Kluge, L. Hein, C. Muller, F. Kensy, J. Büchs (2010) Bioprocess control in microscale: scalable fermentations in disposable and user-friendly microfluidic systems. *Microb. Cell Fact.* 9: 13.

[34] D. A. Zacharias, J. D. Violin, A. C. Newton, R. Y. Tsien (2002) Partitioning of lipid-modified monomeric GFPs into membrane microdomains of live cells. *Science* 296: 913-916.

[35] R. M. Wachter, M. A. Elsliger, K. Kallio, G. T. Hanson, S. J. Remington (1998) Structural basis of spectral shifts in the yellow-emission variants of green fluorescent protein. *Structure* 6: 1267-1277.

[36] A. Miyawaki, O. Griesbeck, R. Heim, R. Y. Tsien (1999) Dynamic and quantitative Ca2+ measurements using improved cameleons. *Proc. Nat. Acad. Sci. U.S.A.* 96: 2135-2140.

[37] F. W. Studier (2005) Protein production by auto-induction in high-density shaking cultures. *Protein Expr. Purif.* 41: 207-234.

[38] B. Wilms, A. Hauck, M. Reuss, C. Syldatk, R. Mattes, M. Siemann, J. Altenbuchner (2001) High-cell-density fermentation for production of L-*N*-Carbamoylase using an expression system based on the *Escherichia coli rhaBAD p*romoter. *Biotechnol. Bioeng.* 73: 95-103.

[39] N. Rahmen, A. Fulton, N. Ihling, M. Magni, K. E. Jaeger, J. Büchs (2015) Exchange of single amino acids at different positions of a recombinant protein affects metabolic burden in *Escherichia coli*. *Microb. Cell Fact.* 14: 10.

[40] T. Anderlei, W. Zang, M. Papaspyrou, J. Büchs (2004) Online respiration activity measurement (OTR, CTR, RQ) in shake flasks. *Biochem. Eng. J.* 17: 187-194.

[41] D. Flitsch, S. Krabbe, T. Ladner, M. Beckers, J. Schilling, S. Mahr, U. Conrath, W. K. Schomburg, J. Büchs (2016) Respiration activity monitoring system for any individual well of a 48-well microtiter plate. *J. Biol. Eng.* 10: 14.

[42] T. Ladner, M. Beckers, B. Hitzmann, J. Büchs (2016) Parallel online multi-wavelength (2D) fluorescence spectroscopy in each well of a continuously shaken microtiter plate. *Biotechnol. J.* 11: 1605-1616.

[43] T. Ladner, M. Held, D. Flitsch, M. Beckers, J. Büchs (2016) Quasi-continuous parallel online scattered light, fluorescence and dissolved oxygen tension measurement combined with monitoring of the oxygen transfer rate in each well of a shaken microtiter plate. *Microb. Cell Fact.* 15.

[44] C. A. Parker, W. T. Rees (1962) Fluorescence spectrometry - a review. *Analyst* 87: 83-&.

[45] N. Anders, H. Humann, B. Langhans, A. C. Spiess (2015) Simultaneous determination of acid-soluble biomass-derived compounds using high performance anion exchange chromatography coupled with pulsed amperometric detection. *Anal. Methods* 7: 7866-7873.

[46] K. Meier, W. Klöckner, B. Bonhage, E. Antonov, L. Regestein, J. Büchs (2016) Correlation for the maximum oxygen transfer capacity in shake flasks for a wide range of operating conditions and for different culture media. *Biochem. Eng. J.* 109: 228-235.

[47] A. Schumpe (1993) The estimation of gas solubilities in salt-solutions. *Chem. Eng. Sci.* 48: 153-158.

[48] M. Popovic, H. Niebelschutz, M. Reuss (1979) Oxygen solubilities in fermentation fluids. *Eur. J. Appl. Microbiol. Biotechnol.* 8: 1-15.

[49] S. Diederichs, A. Korona, A. Staaden, W. Kroutil, K. Honda, H. Ohtake, J. Büchs (2014) Phenotyping the quality of complex medium components by simple online-monitored shake flask experiments. *Microb. Cell Fact.* 13: 149.

[50] T. H. Grossman, E. S. Kawasaki, S. R. Punreddy, M. S. Osburne (1998) Spontaneous cAMP-dependent derepression of gene expression in stationary phase plays a role in recombinant expression instability. *Gene* 209: 95-103.

[51] G. W. Luli, W. R. Strohl (1990) Compaorison of growth, actetate production, and acetate inhibition of Escherichia coli strains in batch and fed-batch fermentations. *Appl. Environ. Microbiol.* 56: 1004-1011.

[52] M. Losen, B. Frölich, M. Pohl, J. Büchs (2004) Effect of oxygen limitation and medium composition on *Escherichia coli* fermentation in shake-flask cultures. *Biotechnol. Prog.* 20: 1062-1068.

[53] M. L. Christensen, N. T. Eriksen (2002) Growth and proton exchange in recombinant *Escherichia coli* BL21. *Enzyme Microb. Technol.* 31: 566-574.

[54] C. W. Cody, D. C. Prasher, W. M. Westler, F. G. Prendergast, W. W. Ward (1993) Chemical-structure of the hexapeptide chromophore of the aequorea green-fluorescent protein. *Biochemistry* 32: 1212-1218.

[55] L. Zhang, H. N. Patel, J. W. Lappe, R. M. Wachter (2006) Reaction progress of chromophore biogenesis in green fluorescent protein. *J. Am. Chem. Soc.* 128: 4766-4772.

[56] T. Drepper, T. Eggert, F. Circolone, A. Heck, U. Krauss, J. K. Guterl, M. Wendorff, A. Losi, W. Gartner, K. E. Jaeger (2007) Reporter proteins for in vivo fluorescence without oxygen. *Nat. Biotechnol.* 25: 443-445.

[57] T. Drepper, R. Huber, A. Heck, F. Circolone, A. K. Hillmer, J. Büchs, K. E. Jaeger (2010) Flavin mononucleotide-based fluorescent reporter proteins outperform green fluorescent protein-like proteins as quantitative in vivo real-time reporters. *Appl. Environ. Microbiol.* 76: 5990-5994.

[58] M. Kunze, S. Roth, E. Gartz, J. Büchs (2014) Pitfalls in optical on-line monitoring for high-throughput screening of microbial systems. *Microb. Cell Fact.* 13: 53.

[59] C. Ude, N. Ben-Dov, A. Jochums, Z. P. Li, E. Segal, T. Scheper, S. Beutel (2016) Online analysis of protein inclusion bodies produced in E-coli by monitoring alterations in scattered and reflected light. *Appl. Microbiol. Biotechnol.* 100: 4147-4159.

[60] J. Y. Zhang, J. Reddy, B. Buckland, R. Greasham (2003) Toward consistent and productive complex media for industrial fermentations: Studies on yeast extract for a recombinant yeast fermentation process. *Biotechnol. Bioeng.* 82: 640-652.

[61] J. J. Chalmers, E. Kim, J. N. Telford, E. Y. Wong, W. C. Tacon, M. L. Shuler, D. B. Wilson (1990) Effects of the temperature on *Escherichia coli* overproducing beat-lactamase or human epidermal growth-factor. *Appl. Environ. Microbiol.* 56: 104-111.

[62] J. A. Vasina, F. Baneyx (1997) Expression of aggregation-prone recombinant proteins at low temperatures: A comparative study of the *Escherichia coli* cspA and tac promoter systems. *Protein Expr. Purif.* 9: 211-218.

[63] J. P. Arie, M. Miot, N. Sassoon, J. M. Betton (2006) Formation of active inclusion bodies in the periplasm of *Escherichia coli*. *Mol. Microbiol.* 62: 427-437.

[64] A. S. Korovashkina, A. N. Rymko, S. V. Kvach, A. I. Zinchenko (2013) Enzymatic synthesis of c-di-GMP using inclusion bodies of *Thermotoga maritima* full-length diguanylate cyclase. *J. Biotechnol.* 164: 276-280.

[65] M. Morell, R. Bravo, A. Espargaro, X. Sisquella, F. X. Aviles, X. Fernandez-Busquets, S. Ventura (2008) Inclusion bodies: specificity in their aggregation process and amyloid-like structure. *Biochim. Biophys. Acta* 1783: 1815-1825.

[66] W. S. Jong, D. Vikstrom, D. Houben, H. B. van den Berg van Saparoea, J. W. de Gier, J. Luirink (2017) Application of an *E. coli* signal sequence as a versatile inclusion body tag. *Microb. Cell Fact.* 16: 50.

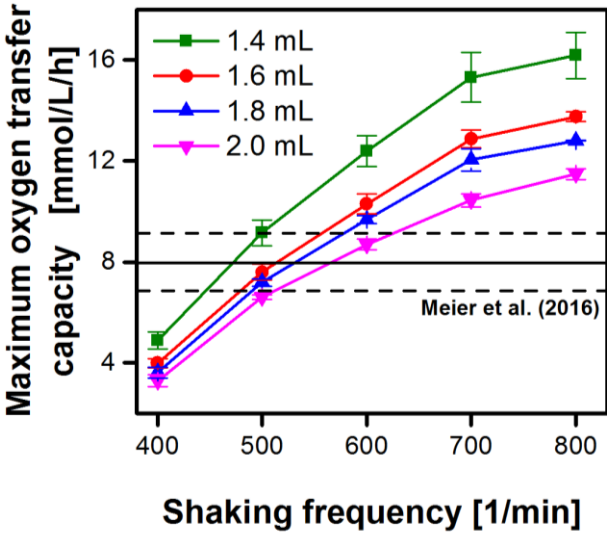
[67] M. Kunze, C. Lattermann, S. Diederichs, W. Kroutil, J. Büchs (2014) Minireactor-based high-throughput temperature profiling for the optimization of microbial and enzymatic processes. *J. Biol. Eng.* 8: 22.

[68] M. Mühlmann, E. Forsten, S. Noack, J. Büchs (2017) Optimizing recombinant protein expression via automated induction profiling in microtiter plates at different temperatures. *Microb. Cell Fact.* 16: 220.

[69] G. Margreiter, P. Messner, K. D. Caldwell, K. Bayer (2008) Size characterization of inclusion bodies by sedimentation field-flow fractionation. *J Biotechnol* 138: 67-73.

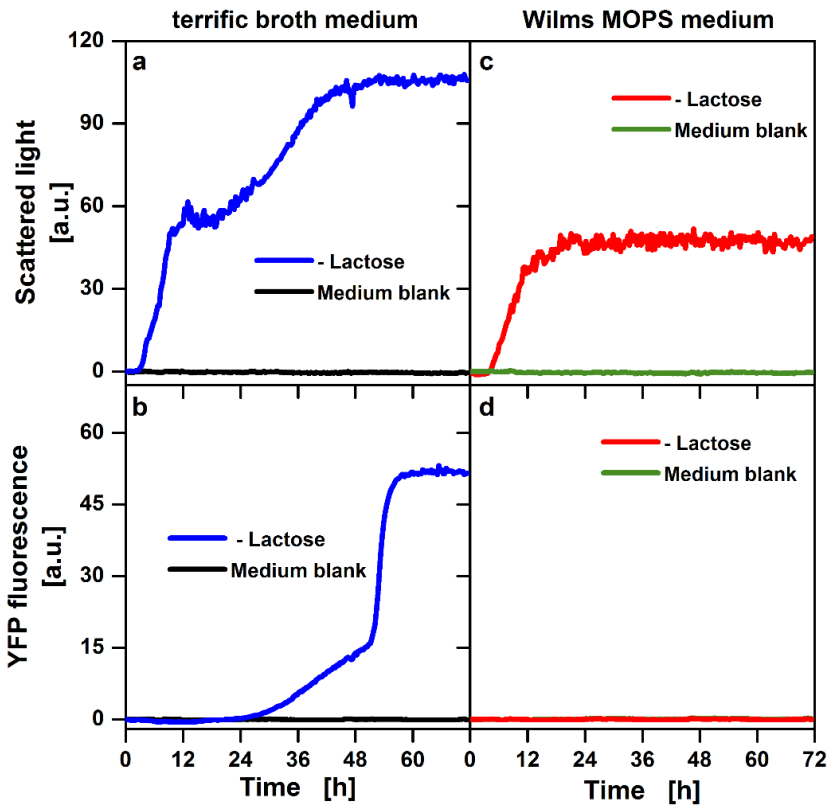
[70] K. Bettenbrock, S. Fischer, A. Kremling, K. Jahreis, T. Sauter, E. D. Gilles (2006) A quantitative approach to catabolite repression in *Escherichia coli*. *J Biol Chem* 281: 2578-2584.

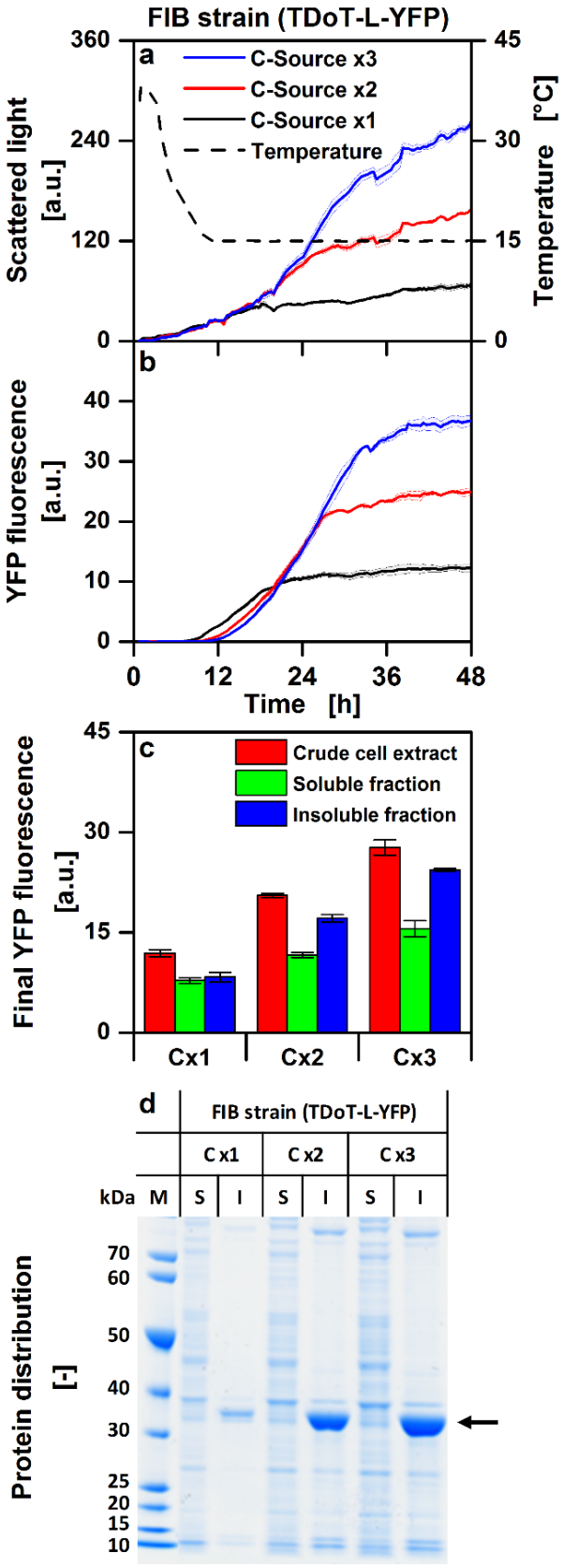
2.2.1 Publication II: Supporting Information



Supplementary Data 1 Maximum oxygen transfer capacity in 48-deepwell MTP in TB medium. *E. coli* BL21(DE3) cells where grown in complex TB medium supplemented with 10 g/L glucose under oxygen limitation at a shaking frequency of 800 rpm. Shaking frequency was stepwise decreased to obtain different levels of oxygen limitation. The presented data are averages of three parallel cultivations. Cultivation conditions: Shaking diameter d_0 = 3 mm, 37 °C. Black line indicates the calculated maximum oxygen transfer capacity of 5 L shake flask with 0.5 L filling volume, 130 rpm and 50 mm shaking frequency according to equation 1. Dashed lines depict 15 % standard error on calculated maximum oxygen transfer capacity.

Supplementary Data 2 Comparison of YFP expression in complex terrific broth and minimal Wilms MOPS medium under non-inducing conditions. Cultivation of *E. coli* BL21(DE3) L-YFP in complex terrific broth medium (A+B) and in minimal Wilms MOPS medium (C+D) both under non-inducing conditions supplemented with 7.5 g/L glucose. (A+C) Scattered light of cultivation of *E. coli* and non-inoculated medium as blank. (B+D) Online YFP fluorescence. Cultivation conditions: 48-deepwell microplate with 2 mL filling volume, 600 rpm shaking frequency, 3 mm shaking diameter.





Supplementary Data 3 Production of FIBs with increased carbon sources. Cultivation of *E. coli* BL21(DE3) TDoT-L-YFP in minimal Wilms-MOPS autoinduction medium with two (Cx2) and three (Cx3) times the amount of carbon sources compared to the standard (Cx1) concentrations (0.5 g/L glucose, 2 g/L lactose, 5 g/L glycerol). (A) Scattered light intensity and cultivation temperature as function of cultivation time. (B) Online YFP fluorescence. (C) Final fluorescence intensity of crude cell extract, soluble and washed insoluble fraction. The mean of three wells with standard deviation is displayed. (D) SDS-PAGE analysis showing protein content per sample volume of soluble (S) and washed insoluble (I) fractions. Arrow indicates size of target protein (M = protein marker). Cultivation conditions: 48-deepwell MTP with 0.8 mL filling volume, 1000 rpm shaking frequency, 3 mm shaking diameter

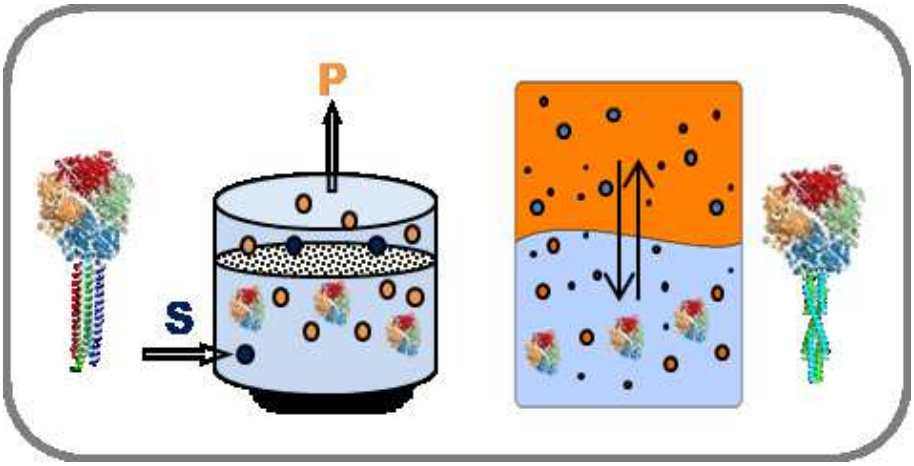
2.3 Publication III

Tailor-made catalytically active inclusion bodies for different applications in biocatalysis

Ramona Kloss, Tobias Karmainski, Vera D. Jäger, Doris Hahn, Alexander Grünberger, Meike Baumgart, Ulrich Krauss, Karl-Erich Jaeger, Wolfgang Wiechert, and Martina Pohl*

*corresponding author

Catalysis Science and Technology, 2018, 8(22): 5816-5826



Contributions:

VDJ, RK, and TK performed the construction of plasmids. VDJ, TK, DH, and RK performed production, purification, and characterization of the CatIBs. MB did the MALDI-TOF analysis with assistance of RK and VDJ. AG performed live-cell imaging with assistance of VDJ and RK. RK and MP wrote the manuscript with input from AG and MB. MP, UK, K-EJ, and WW planned the CatIB project and corrected the manuscript.

Copyright © 2018 The Royal Society of Chemistry. Reproduced by permission.

(https://pubs.rsc.org/en/content/articlelanding/2018/cy/c8cy01891j)

Published on 15 October 2018. Downloaded by Heinrich Heine University of Duesseldorf on 10/23/2018 7:27:03 PM.

Catalysis Science & Technology

PAPER

View Article Online
View Journal

Check for updates

Cite this: DOI: 10.1039/c8cy01891j

Tailor-made catalytically active inclusion bodies for different applications in biocatalysis†

Ramona Kloss, [ad] Tobias Karmainski, [a] Vera D. Jäger, [bd] Doris Hahn,[a] Alexander Grünberger, [ac] Meike Baumgart, [a] Ulrich Krauss, [bd] Karl-Erich Jaeger, [abd] Wolfgang Wiechert[ad] and Martina Pohl *[ad]

We have recently demonstrated that fusions of different target enzymes to the coiled-coil domain TDoT induced the formation of catalytically active inclusion bodies (CatIBs) in *E. coli* (doi:10.1016/j.jbiotec.2017.04.033). Here we show that the CatIB properties can be tailored to the requirements of different reaction systems using two different coiled-coil domains as fusion tags: TDoT and 3HAMP. As an example the benzaldehyde lyase from *Pseudomonas fluorescens* (*Pf*BAL) was chosen, which catalyzes the formation of 2-hydroxy ketones and benzoins from aromatic donor aldehydes and aromatic or aliphatic acceptor aldehydes. Using these fusion tags two different kinds of *Pf*BAL-CatIBs were successfully produced that differ in morphology, solubility during washing steps, initial rate activity, protein and lipid content. TDoT-*Pf*BAL and 3HAMP-*Pf*BAL CatIBs were studied relative to the soluble enzyme concerning their application in biocatalysis in continuous reaction mode and in batch using a mono- and biphasic solvent system. Both CatIBs outperformed the soluble enzyme with respect to stability under reaction conditions. In the buffer/DMSO system used for the continuous synthesis of (*R*)-2-hydroxy-1-phenylpropanone, TDoT-*Pf*BAL was superior to the soluble enzyme. Besides, 3HAMP-*Pf*BAL was more suitable in a biphasic reaction system for the synthesis of (*R*)-benzoins and revealed an up to 3-fold higher activity compared to the soluble enzyme.

Received 10th September 2018,
Accepted 12th October 2018

DOI: 10.1039/c8cy01891j

rsc.li/catalysis

1. Introduction

For the realization of cost-efficient and eco-efficient biocatalytic processes, high space–time yields and productivities are needed.[1,2a] To achieve this goal, biocatalysts should be easy to produce, should show a high stability specifically under technical reaction conditions and should be easily separable from the reaction mixture for recycling. All these properties can in principle be obtained with appropriate immobilization methods. Although immobilization goes often at the expense of activity, the gain in stability can compensate for this loss.

In this study, we have used a novel method for biocatalyst immobilization. We compare the properties of two different catalytically-active inclusion bodies (CatIBs) of benzaldehyde lyase from *Pseudomonas fluorescens* (*Pf*BAL). CatIBs represent a recently developed, cheap and simple alternative to generally applied immobilization methods, which comprise often time-consuming, laborious and expensive purification and immobilization steps.[2,3] CatIBs are a cell-free and carrier-free immobilizate which can easily be produced as insoluble protein fraction from *E. coli* cells,[4–7] and can directly be used as a cheap enzyme preparation for biotransformations, which is essential to operate biocatalytic steps economically.[2a,8] In the past, inclusion bodies were either regarded as waste or were produced prior to obtain the native target protein upon denaturation and refolding. However, recent studies showed that enzymes can retain some activity as inclusion bodies. Despite their accidental production,[7,9] active inclusion bodies can be produced by fusion of aggregation-inducing tags, such as cellulose binding domains,[10] natural and artificial peptides likes small surfactant-like peptides,[11] amphipathic[12a,b] and hydrophobic self-assembling peptides,[12c] and amyloidogenic peptides like Aβ.[13a] Further options are the fusion of aggregation-prone proteins and protein domains, amongst others, the viral capsid protein VP1 of the foot-and-mouth disease virus[13a] and a pyruvate oxidase.[13b] A detailed overview about the state of the art was recently published.[4]

[a] Forschungszentrum Jülich GmbH, IBG-1: Biotechnology, 52425 Jülich, Germany. E-mail: ma.pohl@fz-juelich.de
[b] Institut für Molekulare Enzymtechnologie, Heinrich-Heine-Universität Düsseldorf, Forschungszentrum Jülich, 52425 Jülich, Germany
[c] Multiscale Bioengineering, Bielefeld University, Universitätsstraße 25, 33615 Bielefeld, Germany
[d] Bioeconomy Science Center (BioSC), c/o, Forschungszentrum Jülich, 52425 Jülich, Germany

† Electronic supplementary information (ESI) available: Additional results, experimental and sequences. See DOI: 10.1039/c8cy01891j

Published on 15 October 2018. Downloaded by Heinrich Heine University of Duesseldorf on 10/23/2018 7:27:03 PM.

*Pf*BAL represents a promising enzyme for industrial application, since it catalyses the strictly (*R*)-selectively C–C-bond formation between an aromatic donor aldehyde and an aromatic or aliphatic acceptor aldehyde.[14–18] Additionally, *Pf*BAL catalyses also the reverse reaction, *i.e.* the cleavage of α-hydroxy ketones.[18–20] A well-studied reaction is the carboligation of benzaldehyde and acetaldehyde to (*R*)-2-hydroxy-1-phenylpropanone ((*R*)-HPP). Further biocatalytic reduction using appropriate alcohol dehydrogenases yields the important pharmaceutical building block (1*R*,2*R*)-1-phenylpropane-1,2-diol (PPD), *e.g.* for the calcium channel blocker diltiazem.[21] During this reaction in batch mode, (*R*)-benzoin occurs as an intermediate, especially at the beginning due to differences in reaction speed for the formation of (*R*)-benzoin and (*R*)-HPP, respectively.[22] In the presence of excess acetaldehyde, the reaction can be shifted to the preferred formation of (*R*)-HPP.[14,22–25]

The application of *Pf*BAL was broadly studied using aqueous,[18,26] monophasic[18,22–25,27–31] or biphasic[32–37] aqueous-organic solvents as well as micro-aqueous reaction systems[38,39] using the purified enzyme,[14,18,20,22,27,31,33,37] as whole cell biocatalyst,[36,38,39] and immobilized on or in different carriers.[23,24,29,30,32,34,35] Preferred water-miscible cosolvents for the enzyme are dimethyl sulfoxide (DMSO, 20–30 vol%),[18,20,22–25,27–30] methyl-*tert*-butyl ether (MTBE, 5 vol%),[26,28,33] and 2-methyltetrahydrofuran (5 vol%).[31] Different reactors were tested with *Pf*BAL. Besides batch[18,20,22,24,27–31,33,35,37] and fed-batch systems,[33,36,38,39] continuous reaction systems such as plug-flow reactors[23,34] and enzyme-membrane reactors were applied.[22,28] With whole cells also biphasic micro-aqueous as well as monophasic micro-aqueous reaction systems were successfully tested, which enable a significantly higher substrate concentration and thus a higher productivity.[36,38,39] Besides whole cells, which constitute the simplest way of immobilization, *Pf*BAL was entrapped in cryogel beads.[34,35] Further, immobilizations *via* the His-tag on a superparamagnetic solid support[29] as well as on the respective Sepharose® material were described.[23] Covalent binding was realized on chelate-epoxy modified magnetic nanoparticles[30] as well as on Sepharose® beads *via* the HaloTag® technology directly from crude cell extracts.[24] These carrier-based immobilization methods enabled efficient retention and recycling of the enzyme. However, there is only limited data available concerning potential stabilizing effects resulting from immobilization of this enzyme. This aspect is specifically relevant for *Pf*BAL, because the enzyme is known to be inactivated by aldehydes, which is only partly reversible.[40] Thus, soluble *Pf*BAL can usually not be reused. Using the HaloTag® technology, we could recently demonstrate that repetitive batch reactions were possible over seven cycles, most probably because the immobilizate was intensively washed in between the reaction steps.[24]

Here, we study the application of two different *Pf*BAL-CatIB constructs in batch and continuous reaction mode in a mono- and biphasic solvent system relative to the soluble enzyme using different carboligation reactions. CatIBs were obtained by fusion with two different coiled-coil domains. We previously evaluated the targeted production of CatIBs by fusion of the tetramerization domain of the cell-surface protein tetrabrachion (known as TDoT) from *Staphylothermus marinus* to different target enzymes as well as fluorescent proteins which resulted in the targeted formation of functional inclusion bodies.[4,41,42,55] Besides the TDoT-domain, the 3HAMP-domain was evaluated as an aggregation-inducing element. In its native context, the domain 3HAMP (Histidine kinases, Adenylyl cyclases, Methyl-accepting chemotaxis proteins (MCPs), and Phosphatases) is part of the soluble oxygen sensor Aer2 of *Pseudomonas aeruginosa*, which is an element of a prokaryotic signalling module.[43] Our results show that the kind of the fusion tag has a strong effect not only on the morphology but also on the stability and the activity of the resulting CatIBs. Depending on the reaction system, both evaluated *Pf*BAL-CatIBs exhibited properties superior to those of the soluble enzyme.

2. Results and discussion

2.1 Characteristics of two different kinds of CatIBs

Two different *Pf*BAL-CatIBs were generated by a genetic fusion of the genes encoding *Pf*BAL and the two different coiled-coil domains, 3HAMP and TDoT, yielding the respective N-terminal fusions of the coiled-coil domain to the *Pf*BAL.[41] The formation of inclusion bodies in *E. coli* cells was imaged using an inverted epifluorescence microscope.[44,45] As demonstrated in Fig. 1, the live cell images showed that the coiled-coil fusions determined the morphology of the inclusion bodies. While TDoT-*Pf*BAL forms typically dense and compact particles in *E. coli*,[46] 3HAMP-*Pf*BAL yields rather diffuse particles located at the cell poles, which are less clearly visible in unmodified phase-contrast images (Fig. 1B). The corresponding particles can however be clearly detected after local image equalization (see ESI,† Fig. S1). To distinguish between the different kinds of CatIBs, we called the TDoT-*Pf*BAL "compact CatIBs" and the 3HAMP-*Pf*BAL "diffuse CatIBs". To the best of our knowledge, such

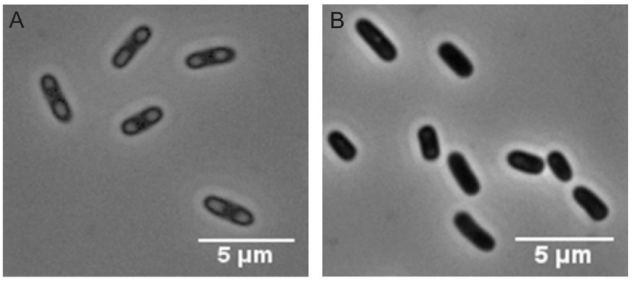


Fig. 1 Phase contrast microscopic images of *E. coli* BL21(DE3) cells containing *Pf*BAL-CatIBs. (A) TDoT-*Pf*BAL, (B) 3HAMP-*Pf*BAL. While TDoT-*Pf*BAL forms dense and compact particles in *E. coli*, 3HAMP-*Pf*BAL yields rather diffuse particles. Images were recorded by an inverted epifluorescence microscope in phase-contrast mode (see sect. 4.5). For a better visualization the pictures were modified by image equalization, as shown in the ESI,† Fig. S1.

This journal is © The Royal Society of Chemistry 2018

Published on 15 October 2018. Downloaded by Heinrich Heine University of Duesseldorf on 10/23/2018 7:27:03 PM.

morphology distinctions of inclusion bodies have not been described so far.

For a detailed comparative characterization, both CatIB types were extracted from the cells by cell disruption, followed by centrifugation and two washing steps using a previously developed standardised protocol.[41,42] Sodium dodecyl sulfate-polyacrylamide gel electrophoresis (SDS-PAGE) analysis of the purification steps demonstrated that TDoT-*Pf*BAL was only present in the insoluble cell fraction and was barely dissolved during the washing steps of the pellet, as expected (Fig. 2).[41]

In contrast, the diffuse 3HAMP-*Pf*BAL CatIBs are partially soluble, which results in progressive disintegration of the pellet during washing. As a consequence, the yield of lyophilised CatIBs obtained from 1 g of wet *E. coli* cells is about 4-fold higher for TDoT-*Pf*BAL (72 ± 8 mg) compared to 3HAMP-*Pf*BAL (18 ± 17 mg), whereas the yield of 3HAMP-*Pf*BAL could not be reproduced so well resulting in a high standard deviation (Table 1). Both CatIB variants differ enzymatic activity, protein content, and lipid content. TDoT-*Pf*BAL revealed a high protein content of 72 ± 5%, which is typical for inclusion bodies.[41,42] In contrast, 3HAMP-*Pf*BAL CatIBs contained only 34 ± 5% protein (Table 1). Inclusion bodies can contain phospholipids, membrane proteins and, depending on the purification procedure, also nucleic acids besides the target proteins.[47] A similar pattern of contaminating bands was observed for different TDoT-fusion-based CatIBs using SDS-PAGE.[41,42] Here, these accompanying proteins for TDoT-*Pf*BAL- (band #1) and 3HAMP-*Pf*BAL-CatIBs (band #2) were analysed by MALDI-TOF analysis. We identified the prominent additional bands as chaperones (IbpA and IbpB[48–50] at 15 kDa, band #4), membrane proteins (OmpA and OmpF[51] at 40 kDa, band #3), and murein lipoprotein (8 kDa, band #3). Remarkably, for 3HAMP-*Pf*BAL-CatIBs the band corresponding to OmpA and OmpF at about 40 kDa is as prominent as the target enzyme (Fig. 2). However, no proteins with reported enzymatic activity were identified, which could interfere with the reaction.

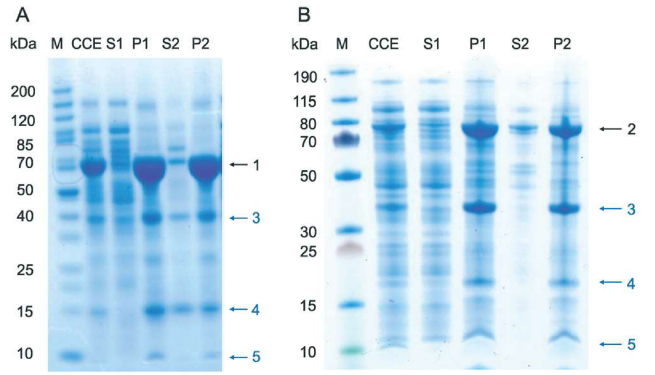


Fig. 2 SDS-PAGE analysis of the *Pf*BAL-CatIB preparations: TDoT-*Pf*BAL (A, band # 1), 3HAMP-*Pf*BAL (B, band # 2) (calculated molecular weight: 66.5 kDa and 79.3 kDa); CCE = crude cell extract, which was centrifuged for supernatant (S1) and pellet (P1) separation. P1 was washed once with MilliQ water by resuspension and subsequent centrifugation, which results in S2 and P2; the protein concentration in solution was measured using the Bradford assay (sect. 4.4). For SDS-PAGE (sect. 4.4) samples were diluted with water to obtain a protein concentration of 1 mg ml^{-1} (CCE, S1, P1, P2) except for S2, P2 of 3HAMP-*Pf*BAL (0.3 mg ml^{-1}) and S2 of TDoT-*Pf*BAL (0.4 mg ml^{-1}). By MALDI-TOF analysis the following accompanying proteins were identified: membrane proteins OmpA and OmpF (band # 3) at 40 kDa, chaperones IbpA and IbpB at 15 kDa (band # 4) and murein lipoprotein at 8 kDa (band # 5). M = marker (PageRuler Plus Unstained (A) or Prestained (B) Protein *ladder*, ThermoFisher Scientific).

Due to the co-purification of cellular proteins in the CatIB preparation, it was expected that membrane lipids such as phospholipids could also be associated with the CatIBs.[47] Therefore, the lipid content was determined gravimetrically upon extraction with methanol and chloroform (see sect. 4.6) and showed about double the amount for 3HAMP-*Pf*BAL (30%) compared to TDoT-*Pf*BAL-CatIBs (16%) based on the dry weight (Table 1). Finally, comparison of the initial rate activities revealed a 17-fold higher turnover number (k_{cat}) for 3HAMP-*Pf*BAL-CatIBs of 13.9 s^{-1} compared to 0.8 s^{-1} for TDoT-*Pf*BAL-CatIBs (Table 1). This is in line with the diffuse nature of the 3HAMP-*Pf*BAL-CatIBs. The less dense packing of the CatIB particles most probably results in smaller particles with a larger surface which enables better access of the substrate molecules and thus higher activity.

The protein yield obtained from 1 g of wet *E. coli* cells was comparable for the soluble *Pf*BAL, which was purified using metal ion affinity chromatography,[52,53] and 3HAMP-*Pf*BAL but four-times higher for TDoT-*Pf*BAL. Compared to the highly active soluble *Pf*BAL, TDoT-*Pf*BAL CatIBs reached approx. 1% and 3HAMP-*Pf*BAL-CatIBs 18% of its activity (k_{cat}) (Table 1). Generally, a reduction of activity relative to the soluble enzyme has been reported for several immobilised enzymes[54] due to lower flexibility, steric hindrance and diffusion limitations caused by the aggregation of the enzyme molecules.

In order to study the properties of the *Pf*BAL-CatIB variants under reaction conditions, they were analysed in buffer, in the absence and presence of DMSO as a cosolvent using an enzyme membrane reactor as well as in batch using a biphasic aqueous-organic solvent system.

2.2 Reactivity of *Pf*BAL-CatIBs and soluble enzyme in buffer in the absence and presence of DMSO

Stability in buffer. The stabilities of the two *Pf*BAL-CatIB variants were first measured in buffer relative to the soluble enzyme. For this purpose, the same protein concentration of each enzyme variant was incubated in triethanol amine (TEA)-buffer (50 mM, pH 7.5, supplemented with ThDP and magnesium sulfate) in polypropylene reaction tubes at 30 °C and 1000 rpm (see ESI,† sect. 2.11). These conditions resemble those chosen for subsequent biotransformations but did not contain any substrate or product. Residual activities were measured over 72 hours (see sect. 4.7). Half-lives decreased in the order TDoT-*Pf*BAL (57 h) > soluble *Pf*BAL (36 h) > 3HAMP-*Pf*BAL (23 h), which were estimated based on the course of the deactivation curve. This initial experiments showed different stabilities of the three *Pf*BAL variants

Published on 15 October 2018. Downloaded by Heinrich Heine University of Duesseldorf on 10/23/2018 7:27:03 PM.

Table 1 Characteristics of TDoT-*Pf*BAL and 3HAMP-*Pf*BAL-CatIBs compared to the soluble *Pf*BAL. The yield indicates the protein content in the lyophilisate obtained from 1 g wet cells after cell disruption and purification by washing and centrifugation steps (for CatIBs) or metal ion affinity chromatography (for soluble *Pf*BAL) (sect. 4.3). The protein content was determined by measuring the absorption at 280 nm after solubilization with guanidine hydrochloride (sect. 4.4). This value was calculated based on the weight of the dry CatIB lyophilisate (1–2 mg ml^{-1}). The lipid content was measured as described in sect. 4.6. The activity (k_{cat}) was determined for the carboligation of 3,5-dimethoxybenzaldehyde (DMBA) to (*R*)-(3,3′,5,5′)-tetramethoxybenzoin (TMBZ) (sect. 4.7). The employed protein concentration to determine k_{cat} was 0.12–0.30 mg ml^{-1} for TDoT-*Pf*BAL, 0.017–0.044 mg ml^{-1} for 3HAMP-*Pf*BAL, and 3–6 μg ml^{-1} for soluble *Pf*BAL. Errors correspond to the standard deviation of the mean obtained from a biological triplicate, except for lipid content and the data of soluble *Pf*BAL (n = 1, 3 technical replicates)

Variant	Yield [mg protein per g wet cells]	Protein content of the lyophilisate [%]	Lipid content [%]	k_{cat} [s^{-1}]	Residual activity^b [%]
Soluble *Pf*BAL	20 ± 14	74.9 ± 0.3^a	—	76.7 ± 2.3^a	100^a
TDoT-*Pf*BAL	72 ± 8	72 ± 5^a	16.4 ± 1.0	0.8 ± 0.1^a	1.0^a
3HAMP-*Pf*BAL	18 ± 17	34 ± 5	30.1 ± 4.7	13.9 ± 2.9	18.1

^{a} Data taken from ref. 55. ^{b} Compared to soluble enzyme.

already upon incubation in buffer, with TDoT-*Pf*BAL showing the highest stability.

Stability under continuous reaction conditions in buffer and buffer/DMSO. Subsequently, the stability under reaction conditions in the absence of DMSO was studied using a continuous enzyme membrane reactor (EMR).[56] The mixed carboligation of benzaldehyde and acetaldehyde towards (*R*)-2-hydroxy-1-phenylpropan-1-one ((*R*)-HPP) was chosen as a test reaction. The EMR was equipped with a membrane (cut-off 10 kDa) to retain the soluble enzyme with a size of 240 kDa. The results in Fig. 3A show that the presence of substrates and products in the absence of DMSO affected the enzyme stability. The highest stability was found for TDoT-*Pf*BAL (half-life 49 h), followed by 3HAMP-*Pf*BAL-CatIBs (half-life 10 h) and the soluble *Pf*BAL (half-life 7 h) (see ESI,† Table S4). TDoT-*Pf*BAL showed a 2–5-fold higher stability than 3HAMP-*Pf*BAL-CatIBs under these reaction conditions in the absence of DMSO.

The addition of DMSO (20–30 vol%) to the aqueous buffer is not only beneficial for the solubility of aromatic aldehydes and benzoins, it can also positively affect the stability of the soluble enzyme.[22,25] Therefore, the effect of 30 vol% DMSO on all *Pf*BAL-variants was tested under continuous reaction conditions. As demonstrated in Fig. 3B the stability of all variants was significantly increased in the presence of DMSO, with a 5.9-fold increase in half-life for 3HAMP-*Pf*BAL-CatIBs (59 h), a 2.7-fold increase for TDoT-*Pf*BAL (131 h), and even a 13-fold increase for the soluble *Pf*BAL (92 h) (see Fig. 3B and ESI,† Table S4).

Deactivation kinetics. In buffer and without substrates and products the soluble *Pf*BAL and the *Pf*BAL-CatIBs showed an unusual deactivation behaviour, which could not be described by a typical first-order deactivation (see ESI,† Fig. S2). Under continuous reaction conditions without DMSO, the course of deactivation of TDoT-*Pf*BAL follows a bi-phasic deactivation mechanism, with a slower initial part followed by a

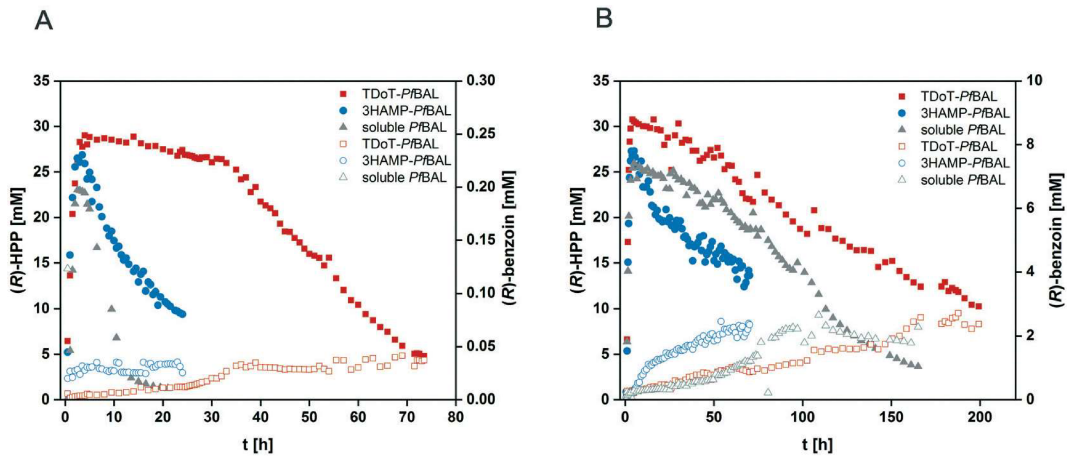


Fig. 3 Carboligation of benzaldehyde and acetaldehyde to (*R*)-HPP and (*R*)-benzoin by *Pf*BAL, TDoT-*Pf*BAL-, and 3HAMP-*Pf*BAL-CatIBs, respectively, in a continuous EMR in the absence (A) and presence (B) of 30 vol% DMSO. Filled symbols refer to (*R*)-HPP and empty symbols to the concentration of (*R*)-benzoin, which is formed as a by-product. Half-life was deduced from the point in time where 50% conversion to (*R*)-HPP (approx. 15 mM) was reached. Reaction conditions: 30 mM benzaldehyde, 90 mM acetaldehyde, TEA-buffer (50 mM, pH 7.5, 2.5 mM $MgSO_4$, 0.5 mM ThDP), 30 vol% DMSO (B); 28 U ml^{-1} protein concentrations of the enzymes: TDoT-*Pf*BAL (A: 50 mg ml^{-1}; B: 56.8 mg ml^{-1}), 3HAMP-*Pf*BAL (A: 3.8 mg ml^{-1}; B: 5.9 mg ml^{-1}), *Pf*BAL (0.94 mg ml^{-1}), 300 rpm, 30 °C, $V_{reactor}$ = 3 ml, residence time: 30 min, flow: 0.1 ml min^{-1}, PEEK (polyether ether ketone) – enzyme membrane reactor (EMR) with regenerated cellulose membrane (YM10 Milipore, 10 kDa cut-off), n = 1.

This journal is © The Royal Society of Chemistry 2018

Published on 15 October 2018. Downloaded by Heinrich Heine University of Duesseldorf on 10/23/2018 7:27:03 PM.

faster second part. The reason for the biphasic inactivation process is currently unclear. However, as the deactivation behaviour of the TDoT-*Pf*BAL-CatIBs in batch in the absence of substrates and products is similar (see ESI,† Fig. S2) to the deactivation in the EMR in the presence of these reaction components, effects caused by the reactor material, the membrane, substrates and products, as well as enzyme leakage from the EMR can be ruled out. The latter was additionally tested by SDS-PAGE analysis of the reactor efflux (data not shown). Besides, in the presence of 30 vol% DMSO the conversion curves of all three variants show the same form (Fig. 3B).

Accumulation of the reaction intermediate (*R*)-benzoin. In both reaction systems the concentration of (*R*)-benzoin in the efflux increased with progressive inactivation of the *Pf*BAL variants. Due to the presence of DMSO in the reaction buffer, the concentration of dissolved (*R*)-benzoin was higher compared to the experiments in the absence of DMSO (Fig. 3). In all cases, (*R*)-benzoin precipitated in the reaction chamber, which was observed when the reactor was opened at the end of the experiment and quantified in some cases (see ESI,† Table S4).

Absorption phenomena. The continuous reactions in the EMR revealed a maximum conversion of about 80% in the absence of DMSO and 90–95% with 30 vol% DMSO (Fig. 3). The reason, why full conversion could not be achieved was partially deduced to the absorption of benzaldehyde and (*R*)-HPP by the reactor material (polyether ether ketone = PEEK) (see ESI,† Fig. S3) and by the polypropylene (PP) reaction tubes (see ESI,† sect. 3.3.2 and Table S5), which were used for HPLC sample preparation. Furthermore, evaporation of benzaldehyde occurred from the open glass test tubes in the HPLC sampling device over longer storage time (see ESI,† Fig. S4). The evaporation of benzaldehyde and absorption of benzaldehyde and (*R*)-HPP resulted in an apparent lower conversion. Since the PEEK-reactor gave much better results compared to a stainless-steel reactor with respect to enzyme stability (data not shown), only the PP reaction tubes were exchanged by glass vials in the following experiments to minimize this error.

pH-effect. Besides DMSO as a cosolvent, the stability and activity of soluble *Pf*BAL is influenced by the pH of the aqueous reaction system. Based on earlier studies, the stability optimum is at pH 7, whereas the activity optimum was found between pH 8.5–9.5 in similar reaction systems.[22,25,27] However, these studies were not performed in an EMR and were carried out in the absence of substrates and products. To study the influence of the pH on the *Pf*BAL-CatIBs and the soluble enzyme under reaction conditions, respective experiments were additionally performed in the EMR at pH 9 as an option to increase the activity relative to the data obtained at pH 7.5 (Fig. 3). For this purpose, all parameters were kept constant and the pH of the TEA-buffer was adjusted after addition of DMSO and the aldehyde substrates. As demonstrated in Fig. S5 (ESI†), the stability decreased in all cases by a factor of 5 to 43 (compare ESI,† Table S4). Interestingly, at

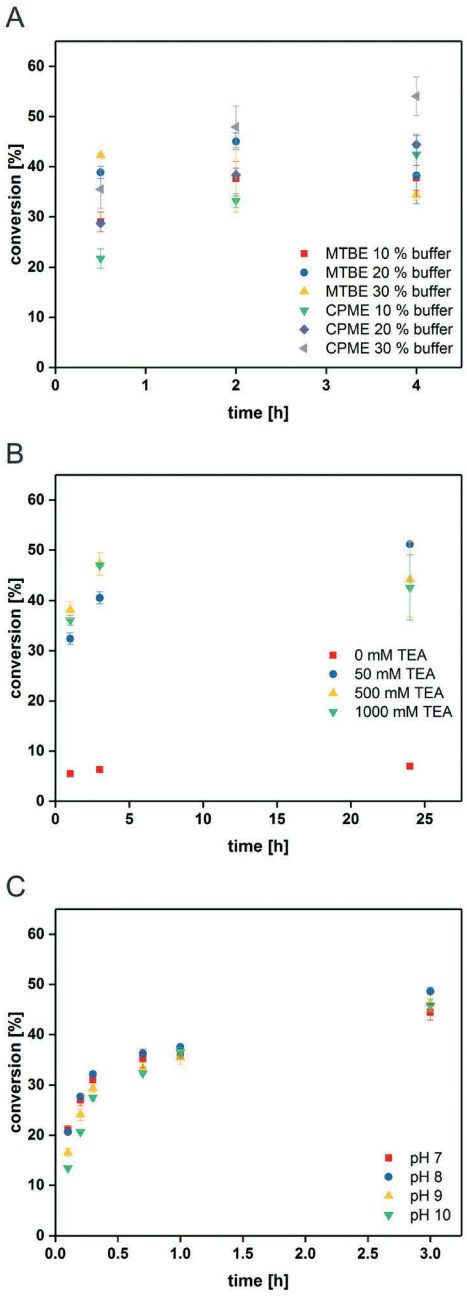


Fig. 4 Optimisation of (A) the buffer content, (B) the buffer salt concentration, and (C) the pH in an aqueous-organic two-phase system for the carboligation of DMBA to TMBZ, catalysed by 3HAMP-*Pf*BAL-CatIBs. (A) Reaction solutions contained a different buffer volume (10–30 vol% TEA-buffer, 1 M, pH 8, 2.5 mM $MgSO_4$, 0.1 mM ThDP) in CPME or MTBE, respectively, and 50 mM DMBA as the substrate. (B) Reaction solutions contained different buffer salt concentrations and were performed in CPME with 30 vol% TEA-buffer in different concentrations (0 mM, 50 mM, 500 mM or 1 M, pH 8, 2.5 mM $MgSO_4$, 0.1 mM ThDP) and 70 mM DMBA. (C) Reactions were performed in CPME with 30 vol% TEA-buffer with varying pH (50 mM, pH 7, 8, 9, or 10, 2.5 mM $MgSO_4$, 0.1 mM ThDP) and 85 mM DMBA as a substrate. All reactions were conducted with the following parameters: 6 U ml^{-1} 3HAMP-*Pf*BAL (1.1 mg ml^{-1} protein concentration) in 2 ml glass vials at 30 °C, 1400 rpm, V = 1 ml, in a thermomixer, n = 2. For experimental details see sect. 4.9.

Published on 15 October 2018. Downloaded by Heinrich Heine University of Duesseldorf on 10/23/2018 7:27:03 PM.

pH 9 the deactivation curves for all variants show a typical first order exponential decay.

The results demonstrated the very different impact of the reaction conditions on the *Pf*BAL-variants. Whereas the addition of 30 vol% DMSO increased the stability of all variants in a similar manner (Fig. 3B), the pH change altered the stabilities unpredictably. At pH 9, 3HAMP-*Pf*BAL showed a similar half-life to the soluble enzyme and TDoT-*Pf*BAL, which is most stable at pH 7.5, showed the lowest stability (Fig. S5, Table S4 in ESI†).

In summary, TDoT-*Pf*BAL-CatIBs showed the best performance in 30 vol% DMSO in TEA-buffer at pH 7.5 with a half-life of 131 h, which presents a clearly increased stability compared to the soluble enzyme (7 h).

2.3 3HAMP-*Pf*BAL-CatIBs can be used in a biphasic reaction system

Carboligations of aldehydes, which are less soluble than benzaldehyde and acetaldehyde in an aqueous reaction system, were carried out in a biphasic aqueous-organic system with more than 50 vol% organic solvent. As a model reaction, the carboligation of 3,5-dimethoxybenzaldehyde (DMBA) to (*R*)-(3,3′,5,5′)-tetramethoxy benzoin (TMBZ) was optimised regarding solvent, buffer content, buffer concentration, and pH. Preliminary studies revealed CPME (cyclopentyl methyl ether) and MTBE (methyl *tert*-butyl ether) as optimal organic solvents for the carboligation reaction with TDoT-*Pf*BAL-CatIBs (see ESI,† Fig. S6). Both solvents were first tested in the monophasic micro-aqueous mode. As the activity of the *Pf*BAL-CatIBs was too low under these conditions, the volume of the TEA-buffer (1 M, pH 8) was increased to 20 vol% (ESI,† Fig. S7). However, this study showed that TDoT-*Pf*BAL-CatIBs formed emulsions in the biphasic system upon shaking (ESI,† Fig. S8), which made the sample preparation and handling quite difficult. Since emulsion formation was less pronounced for 3HAMP-*Pf*BAL in MTBE resulting in a higher conversion of about 50% (Fig. 4A), these CatIBs were used for all subsequent experiments to optimise the reaction conditions.

A concentration of 3HAMP-*Pf*BAL corresponding to 6 U ml^{-1} was sufficient to increase the conversion of 50–85 mM DMBA up to 50%. In contrast to MTBE no emulsion formation was observed in CPME (ESI,† Fig. S9). Hence, this solvent was used in all subsequent experiments. Furthermore, CPME is regarded as a green solvent in contrast to MTBE.[57,58] The optimization experiments showed that 30 vol% of 50 mM TEA-buffer in CPME were optimal (Fig. 4A and B). Concerning the optimal pH range, 3HAMP-*Pf*BAL-CatIBs showed a very similar activity between pH 7–9 (Fig. 4C). However, in all cases the conversion did not exceed 50%, because the reaction equilibrium was reached (K_{eq} = 0.02 mM) (ESI,† Fig. S10 and Table S6). The higher substrate concentrations (50–85 mM DMBA), which could be applied in the biphasic system, yielded TMBZ concentrations much higher than K_M (5 mM)[40] which favours the *Pf*BAL-catalysed back reaction.

For the subsequent experiments 30 vol% buffer (50 mM TEA, pH 8) in CPME were chosen. Under these conditions, the carboligation reactions of DMBA to TMBZ (Fig. 5A) and of benzaldehyde to (*R*)-benzoin (Fig. 5B) were followed and compared using the soluble *Pf*BAL and the 3HAMP-*Pf*BAL-CatIBs, respectively. The formation of TMBZ catalysed by 3HAMP-*Pf*BAL is with 4.1 s^{-1} almost twice as fast as the formation of (*R*)-benzoin (2.6 s^{-1}). For the soluble *Pf*BAL, the formation of (*R*)-benzoin (2.0 s^{-1}) is slightly faster than the TMBZ formation (1.4 s^{-1}) (ESI,† Table S7). Thus, in the biphasic system the initial rate activity of 3HAMP-*Pf*BAL is up to 3-fold higher compared to the soluble enzyme. The latter

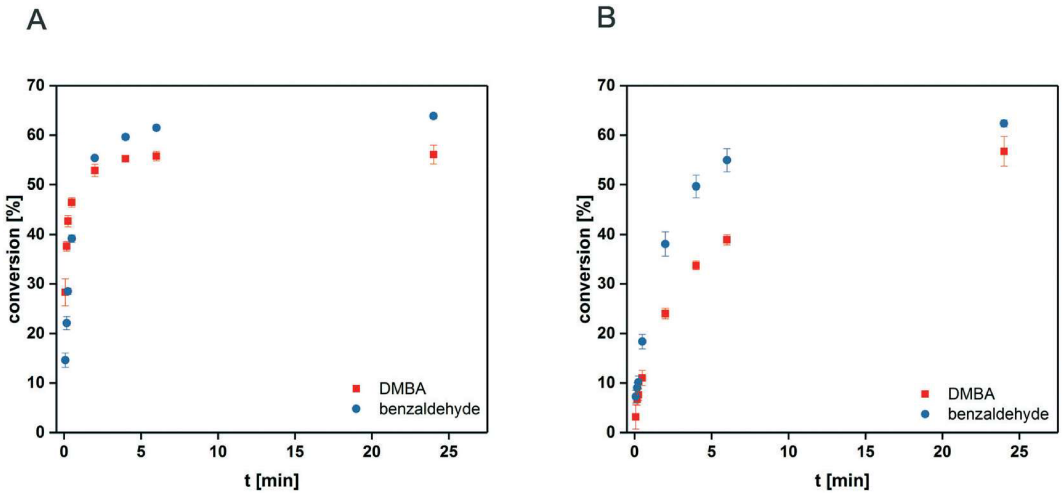


Fig. 5 Carboligation of benzaldehyde or DMBA (3,5-dimethoxybenzaldehyde) to the respective (*R*)-benzoin catalysed by (A) 3HAMP-*Pf*BAL or (B) soluble *Pf*BAL in the biphasic reaction system. Reaction conditions: 6 U ml^{-1} 3HAMP-*Pf*BAL (0.84 mg ml^{-1} protein concentration) and 2.6 U ml^{-1} *Pf*BAL (0.34 mg ml^{-1} protein concentration), 70 mM benzaldehyde or 70 mM DMBA in 1 ml reaction volume composed of 30 vol% TEA-buffer (50 mM, 2.5 mM $MgSO_4$, 0.5 mM ThDP, pH 7.5); 70 vol% CPME, 1400 rpm, 30 °C, *n* = 3. For experimental details see sect. 4.10.

This journal is © The Royal Society of Chemistry 2018

Published on 15 October 2018. Downloaded by Heinrich Heine University of Duesseldorf on 10/23/2018 7:27:03 PM.

will most probably be more affected by interphase inactivation as well as deactivation by the aldehyde substrates, which diminishes the stability of the soluble *Pf*BAL under these conditions.[32] Thus, 3HAMP-*Pf*BAL-CatIBs provide a viable alternative to the soluble *Pf*BAL in a biphasic system with CPME as an organic solvent.

3. Conclusions

In this study, we demonstrate that catalytically active inclusion bodies (CatIBs) represent an attractive immobilization strategy for benzaldehyde lyase from *Pseudomonas fluorescens* (*Pf*BAL). Two different kinds of CatIBs were produced by genetic fusion of *Pf*BAL with two different coiled-coil domains, namely TDoT and 3HAMP. The resulting TDoT-*Pf*BAL- and 3HAMP-*Pf*BAL-CatIBs differed in morphology, initial rate activity, protein and lipid content. TDoT-*Pf*BAL-CatIBs showed the typical characteristics of dense inclusion bodies, located at the cell poles in the *E. coli* production strain: a high protein (72%) and low lipid (16%) content, insolubility during the washing steps resulting in a high yield (72 mg dry TDoT-*Pf*BAL-CatIBs from 1 g wet cells), but a low initial rate activity (0.8 s^{-1}: approx. 1% residual activity compared to soluble *Pf*BAL). In contrast, 3HAMP-*Pf*BAL-CatIBs behaved completely different and formed diffuse particles in *E. coli*, which partially dissolved during the washing steps. This resulted in a lower yield (18 mg dry 3HAMP-*Pf*BAL-CatIBs from 1 g wet cells). Compared to the TDoT-CatIBs, the protein content was two-fold lower (34%) concomitant with two-fold higher lipid content (30%). Most probably as a result of the less dense packing of the particles, the activity of the 3HAMP-*Pf*BAL-CatIBs was 18-times higher than for TDoT-*Pf*BAL-CatIBs (18% relative to the soluble *Pf*BAL).

The application of both kinds of CatIBs was studied in a mono- and biphasic solvent system in comparison to the soluble *Pf*BAL in continuous reaction mode and in batch, respectively. Using the mono-phasic aqueous-organic solvent system, a continuous reaction mode for the carboligation of benzaldehyde and acetaldehyde towards (*R*)-HPP was realised using an EMR. This reactor enables constant reaction conditions for the enzyme and allows the direct determination of the inactivation processes from the conversion curve. For this reaction, TDoT-*Pf*BAL showed the highest stability in TEA-buffer at pH 7.5 with 30 vol% DMSO. The half-life was 1.4-fold higher compared to the soluble *Pf*BAL. Thus, the TDoT-*Pf*BAL represents a suitable alternative or the soluble enzyme in this monophasic continuous reaction mode.

In order to dissolve poorly water-soluble substrates, an aqueous-organic biphasic reaction system with CPME as an organic solvent was established. In this system, 3HAMP-*Pf*BAL CatIBs were more suitable than TDoT-*Pf*BAL CatIBs, since the latter formed emulsions, which impaired sample preparation and handling. The conversion of DMBA and benzaldehyde to the respective benzoins was followed under optimised reaction conditions (CPME with 30% TEA-buffer (pH 8, 50 mM)) and was compared to the soluble enzyme. 3HAMP-*Pf*BAL revealed a 3-fold higher activity than the soluble *Pf*BAL, indicating a higher stability in this biphasic reaction system, since high aldehyde concentrations as well as the interphase were reported to deactivate the soluble *Pf*BAL.[32] It can be concluded that 3HAMP-*Pf*BAL-CatIBs are a suitable alternative to the soluble enzyme in the biphasic reaction system.

In summary, we have demonstrated that different coiled-coil domains as aggregation-inducing tag significantly affect CatIB properties including enzymatic activity, stability, protein content, and emulsion-forming tendency. Our results thus suggest an experimental strategy to produce tailor-made CatIB immobilizates with activity under various reaction conditions prevailing in aqueous, micro aqueous, or biphasic systems.

4. Experimental

4.1 Materials

Chemicals were purchased from Sigma-Aldrich, Fluka, Roth, KMF, Biosolve, Alfa Aesar, AppliChem, and Merck. Enzymes for molecular biology were purchased from Thermo Scientific (Waltham, USA). Enantiopure (*R*)-2-hydroxy-1-phenylpropanone ((*R*)-HPP) for HPLC calibration was taken from a stock prepared as described elsewhere.[39]

4.2 Cloning

The fusion proteins TDoT-*Pf*BAL and 3HAMP-*Pf*BAL were constructed as recently described[41] by cloning of the *pf*bal gene into a modified pET28a vector already containing the 3HAMP- or TDoT-domain, so that the final vector consisted of the TDoT-domain or 3HAMP-domain, a linker containing a Factor Xa protease recognition site and 3xGGGS linker (L), and the *Pf*BAL enzyme (from N- to C-terminus). For a detailed description of the cloning strategy, the employed oligonucleotide primers, DNA- and protein sequences as well as used strains see ESI,† Table S1–S3 and section 2.1–2.10.

4.3 Enzyme production, cell disruption and protein purification

*Pf*BAL-CatIBs were produced in *E. coli* BL21(DE3). For cell disruption, cells were treated 3-times at 1000 bar using a high-pressure homogenizer (EmulsiFlex-C5, Avestin Europe GmbH, Mannheim, Germany). Subsequently, CatIBs were purified as recently described elsewhere.[41,42]

Soluble *Pf*BAL with a C-terminal hexahistidine tag, encoded on a pkk233_2 vector, was produced in *E. coli* SG 13009 according to protocol described elsewhere[18,40] in a 40 L Techfors fermenter (Infors AG, Swiss) at 30 °C in fed-batch mode.[59] The cell pellet was stored at −20 °C after harvesting and centrifugation. For purification, the cells were suspended in a 25% (w/v) of the equilibration buffer and disrupted on ice by sonication (UP200s, Hielscher Ultrasonics GmbH, Teltow, Germany) 10-times for 1 min at 70% amplitude and a cycle of 0.5, followed by a 1 min break. The soluble components containing the target enzyme were separated from the cell

Published on 15 October 2018. Downloaded by Heinrich Heine University of Duesseldorf on 10/23/2018 7:27:03 PM.

debris by centrifugation for 30 min (18 000 × *g*, 4 °C). The enzyme was purified as described earlier by metal ion affinity chromatography[52,53] using a Ni-NTA-sepharose column (Qiagen, Hilden, Germany) with the following buffers: equilibration buffer (50 mM TEA, pH 7.5, 2.5 mM $MgSO_4$, 0.5 mM ThDP, 300 mM NaCl), washing buffer (50 mM TEA, pH 7.5, 50 mM imidazole, 300 mM NaCl), elution buffer (50 mM TEA, pH 7.5, 250 mm imidazole, 300 mM NaCl); and for the final desalting step using a Sephadex-G25 (GE Healthcare, Little Chalfont, United Kingdom) column: 10 mM TEA buffer, pH 7.5, 2.5 mM $MgSO_4$, 0.1 mM ThDP. The TEA-HCl solution was adjusted by sodium hydroxide solution.

4.4 SDS-PAGE, MALDI-TOF analysis and protein assay

SDS-PAGE analysis of the purification steps was performed using the NuPAGE® Kit (ThermoFisher Scientific, Waltham, USA) by the protocol described recently.[42] For the preparation of SDS-PAGE samples, the protein concentration in the soluble fraction was determined *via* the Bradford assay.[60]

The protein content of the lyophilised CatIBs and soluble *Pf*BAL was determined at 280 nm after solubilisation with guanidine hydrochloride using a recently described protocol.[42] The protein content was estimated using the molar extinction coefficient (Table 2) which was calculated based on the amino acid composition by the ProtParam Tool (http://web.expasy.org/protparam).[61]

MALDI-TOF mass spectrometry was performed to identify the accompanying protein bands apparent on SDS-PAGE gel which had been stained with colloidal Coomassie.[62] The protein bands were excised and digested in-gel with trypsin as described previously.[63] Samples were analysed by mass spectrometry measurement as described earlier.[64]

4.5 Phase contrast image acquisition

Images were obtained as described recently by inverted epi-fluorescence microscope in phase-contrast.[42,44,45]

4.6 Lipid content determination

The gravimetric lipid determination was adapted from Morschett *et al.*[65] About 100 mg lyophilised CatIBs were weighed into a 50 ml falcon tube, mixed with 14 ml chloroform and 7 ml methanol and incubated for 2 h at 60 °C and 750 rpm in a thermomixer (Thermomixer comfort, Eppendorf, Hamburg, Germany). The mixture was transferred to a 50 ml separating funnel and washed with 5.6 ml NaCl solution (0.73% w/v). The lower organic phase containing the lipids was collected and the aqueous phase was extracted with 14 ml chloroform. The organic phases were pooled, dried over $MgSO_4$ and concentrated by a rotating evaporator (Rotavapor R-100, Büchi Labortechnik GmbH, Essen, Germany). The remaining liquid was transferred to a dry, pre-weighted glass vessel and dried first under the hood and then under high vacuum (0.2 mbar) over 24 h. The remaining lipid amount was determined gravimetrically and the lipid content was calculated based on the initial weight. All measurements were performed in triplicate for one batch of the respective CatIBs.

Table 2 Extinction coefficient of soluble *Pf*BAL, TDoT-*Pf*BAL and 3HAMP-*Pf*BAL calculated with ExPASy ProtParam Tool (http://expasy.org/tools/protparam)[61]

Protein	Molar extinction coefficient [L mol^{-1} cm^{-1}]
Soluble *Pf*BAL	52 160
TDoT-*Pf*BAL	55 140
3HAMP-*Pf*BAL	63 620

4.7 Activity assay

In order to determine the initial rate activity of soluble *Pf*BAL and *Pf*BAL-CatIBs, the carboligation of 3,5-dimethoxy benzaldehyde (DMBA) to (*R*)-(3,3′,5,5′)-tetramethoxy benzoin (TMBZ) was measured up to a conversion of 10% by a discontinuous HPLC assay (see sect. 4.13). The reaction was performed in a polypropylene reaction tube (1.5 ml safe-lock tube, Eppendorf, Germany) in 1 ml reaction volume containing 80 vol% TEA-buffer (50 mM, pH 7.5, 2.5 mM $MgSO_4$, 0.1 mM ThDP) and 20 vol% DMSO with 10 mM DMBA, which was incubated at 30 °C prior to reaction. The reaction was started by addition of the enzyme (protein concentration of approx. 0.12–0.30 mg ml^{-1} for TDoT-*Pf*BAL, 0.017–0.044 mg ml^{-1} for 3HAMP-*Pf*BAL, and 3–6 μg ml^{-1} for soluble *Pf*BAL) and was performed for 5 min at 30 °C and 1000 rpm in a thermomixer (Thermomixer comfort, Eppendorf, Germany). Sampling was performed every minute by taking 20 μl samples from the tubes, which were diluted (1:10) with 180 μl methanol (incl. 4.7 mM toluol or 0.1 vol‰ 4-methoxy benzaldehyde (4-MBA) as internal standard) to stop the reaction and to prepare the sample for HPLC analysis (see sect. 4.13). Activity was calculated as turnover number k_{cat} [s^{-1}] referring to the amount of enzyme (in μmol, calculated based on the protein content, and referring to one subunit) which catalyses the formation of 1 μmol TMBZ per second from the respective DMBA concentration under the applied reaction conditions. Activity was determined for three technical replicates of the respective biological triplicates.

4.8 Continuous reaction using an EMR

The EMR was developed in-house to realise a continuous reaction mode under constant reaction conditions and membrane-assisted enzyme retention. The EMR consists of PEEK (polyether ether ketone) with a 3 ml reaction chamber and a Teflon plate with integrated magnetic stirrer bar that fits right there. The EMR was equipped with a membrane with 10 kDa cut-off (regenerated cellulose, diameter = 44.5 mm, YM10 Millipore Amicon, Germany). Initial loading of the EMR was performed either by pumping a solution of the soluble enzyme (28.3 U ml, in TEA-buffer, 50 mM, pH 7.5 or 9.0, 2.5 mM $MgSO_4$, 0.5 mM ThDP) into the reactor using an Asia Syringe Pump (Syrris, Royston, United Kingdom) or by placing the lyophilised CatIBs directly into the reaction

This journal is © The Royal Society of Chemistry 2018

Published on 15 October 2018. Downloaded by Heinrich Heine University of Duesseldorf on 10/23/2018 7:27:03 PM.

chamber, which was then filled with buffer solution. Subsequently, the buffer system including substrates (30 mM distilled benzaldehyde and 90 mM acetaldehyde) required for the respective experiment was pumped through the reactor at 30 °C and 300 rpm. Prior, 30 vol% DMSO had been added to the buffer according to the required reaction conditions and the pH-value of the reaction solution was controlled and adjusted if necessary after the addition of the aldehydes and DMSO. The flow was adjusted to 100 μl min^{-1} which corresponds to a residence time of 30 min. A fraction collector (Pharmacia LKB Frac-100, Amersham Biosciences, United Kingdom) was applied to collect samples of 3 ml or 6 ml volume in open glass test tubes of 9.5 ml volume (3 cm filling height) or of 15 ml volume (3.8 cm filling height), respectively. The 20 μl sample was 1:20 diluted with acetonitrile (incl. 0.822 mM 4-methoxybenzaldehyde (4-MBA) as internal standard) and analysed by HPLC (see sect. 4.13). Continuous reactions were performed in single measurements. Half-lives were taken from the curve at 50% conversion in each case.

4.9 Optimization of the reaction conditions in the biphasic reaction system

In order to optimise the reaction conditions in the biphasic reaction system in batch, the buffer content, the buffer concentration and the pH were optimized for the carboligation reaction 3,5-dimethoxybenzaldehyde (DMBA) catalysed by 3HAMP-*Pf*BAL-CatIBs. The buffer content was optimised between 1–30 vol% TEA-buffer (1 M, pH 8, 2.5 mM $MgSO_4$, 0.1 mM ThDP) added to either MTBE or CPME and contained 50 mM DMBA. The buffer concentration was optimised between 0 mM and 1 M TEA-buffer (0 mM, 50 mM, 500 mM or1 M, pH 8, 2.5 mM $MgSO_4$, 0.1 mM ThDP). 30 vol% buffer were added to 70 vol% CPME and contained 70 mM DMBA. The pH optimum was measured between pH 7–10 in TEA-buffer (50 mM, pH 7, 8, 9, or 10, 2.5 mM $MgSO_4$, 0.1 mM ThDP). 30 vol% buffer were added to 70 vol% CPME and contained 85 mM DMBA. In each case 6 U ml^{-1} 3HAMP-*Pf*BAL (1.1 mg ml^{-1} protein concentration) were suspended in buffer and then the organic solvent containing the substrate was added. The reaction was performed in a volume of 1 ml in 2 ml glass reaction tubes (G1 clear, CS-Chromatographie Service GmbH, Germany) at 30 °C und 1400 rpm in a thermomixer (Thermomixer comfort, Eppendorf, Germany). Samples (20 μl) were taken from the organic phase after different points in time and were diluted 1 : 10 in 180 μl 2-methyltetrahydrofuran, thoroughly mixed and centrifuged at 15 800 × *g* for 1 min. Subsequently, a 20 μl sample from the supernatant was 1 : 10 diluted in 180 μl *n*-heptane (incl. 4.3 mM acetophenone as internal standard), which was analysed by HPLC (see sect. 4.13). These reactions were performed in duplicate.

4.10 Carboligation of benzaldehyde and DMBA in a biphasic reaction system

The carboligation reaction of 70 mM DMBA or 70 mM benzaldehyde to the respective benzoins was catalysed by 2.6 U ml^{-1} soluble *Pf*BAL (0.15 mg ml^{-1} protein concentration) or 6 U ml^{-1} 3HAMP-*Pf*BAL (0.83 mg ml^{-1} protein concentration), respectively. Therefore, biphasic reaction systems were prepared by mixing 30 vol% TEA-buffer (50 mM, pH 8, 2.5 mM $MgSO_4$, 0.1 mM ThDP) with 70 vol% CPME. First the CatIBs were suspended in buffer and then the organic solvent containing the substrate was added. The reaction was performed in 2 ml glass reaction tubes (G1 clear, CS-Chromatographie Service GmbH, Germany) in a total volume of 1 ml at 30 °C und 1400 rpm in a thermomixer (Thermomixer comfort, Eppendorf, Germany). Samples (20 μl) were taken from the organic phase after 5 min, 10 min, 15 min, 30 min, 2 h, 4 h, 6 h and 24 h, were prepared as described in sect. 4.9 and analysed by HPLC (see sect. 4.13). To analyse evaporation effects, control samples were prepared in the same manner without CatIBs. Each carboligation reaction was performed in technical triplicate.

4.11 Synthesis of TMBZ

TMBZ was synthesised by an enzymatic approach[40] and was used for HPLC calibration. *E. coli* whole cells containing *Pf*BAL (25 mg ml^{-1}) were transferred into 6 ml reaction solution consisting of MTBE, 150 μl TEA-buffer (1 M, pH 10, 0.5 mM $MgSO_4$, 0.1 mM ThDP), and 500 mM DMBA. The reaction was performed in an 8 ml glass vial and stirred at 1000 rpm and 30 °C overnight. The reaction was followed by thin-layer chromatography (TLC Plates Polygram® SIL G/UV_{254}, Macherey-Nagel, Düren, Germany). As full conversion of DMBA was not achieved, the reaction solution was chromatographically purified. For this purpose, the reaction solution was filtered and extracted two-times with MTBE. The MTBE phases were pooled, dried over $MgSO_4$, and concentrated by a rotating evaporator (Rotavapor R-100, Büchi Labortechnik GmbH, Essen, Germany). The TMBZ was separated from the DMBA by a chromatographic step with ethyl acetate and petroleum ether in a 4 : 6 mixture as the mobile phase and silica gel (0.04–0.063 mm (400–230 mesh), Roth, Karlsruhe, Germany) as the stationary phase. The TMBZ containing fractions were pooled and the solvent evaporated using a rotating evaporator (Rotavapor R-100, Büchi Labortechnik GmbH, Essen, Germany). After evaporation of residual organic solvents under high vacuum overnight, the purity of the product was determined by ^{1}H-NMR analysis (sect. 4.12). 292.5 mg of purified TMBZ was obtained with a purity of 80.8–82.0%. TMBZ was used for further calibration by HPLC (see sect. 4.13).

4.12 ^{1}H-NMR analysis

For ^{1}H-NMR analysis, 20 mg ml^{-1} TMBZ was dissolved in deuterated $CDCl_3$, which was supplemented with 0.03 vol% tetramethylsilane. The analysis was performed by a 600 MHz Avance DPX-600 (Bruker, Billerica, USA) spectrometer. The NMR-spectrum was analysed by MestReNova (Mestrelab Research, Santiago de Compostela, Spain) and was in-line with published data:[66,67] δ_H 7.06 (2 H, s,), 6.61 (1 H, s,), 6.47 (2 H,

Published on 15 October 2018. Downloaded by Heinrich Heine University of Duesseldorf on 10/23/2018 7:27:03 PM.

s,), 6.36 (1 H, s,), 5.79 (1 H, d, *J* 6.5), 4.46 (1 H, d, *J* 6.2), 3.78 (6 H, s), 3.75 (6 H, s) (compare ESI,† Fig. S11). Ethyl acetate (18.0–19.2 vol%) was included.

4.13 HPLC analysis

Prior to high performance liquid chromatography (HPLC) analysis, the samples were centrifuged at 15 800 × *g* for 1 min and the supernatant was transferred into HPLC vials with inlet. Subsequently, 10 μl of the prepared samples were analysed using either a Thermo Scientific Dionex Ultimate 3000 HPLC system containing a diode-array detector DAD-3000 (ThermoFisher Scientific, Waltham, MA, USA), or an HPLC system from Agilent Series 1100 (Agilent Technologies Santa Clara, USA) equipped with DAD. All samples were separated on a Chiralpak® IE column (4.6 μm × 250 mm, 5 μm particle size column, Daicel, Tokyo, Japan) combined with a pre-column (Chiralpak® IE 4 mm × 10 mm; Daicel, Tokyo, Japan), which was tempered to 20 °C. The HPLC conditions are given in Table S8 and S9 (ESI†) to quantify substances for the respective experiments. Calibration curves are given in Fig. S12–S14 in ESI.†

Conflicts of interest

There are no conflicts to declare.

Acknowledgements

The scientific activities of the Bioeconomy Science Center were financially supported by the Ministry of Innovation, Science and Research within the framework of the NRW Strategieprojekt BioSC (No. 313/323-400-002 13). BioSC is a research cluster of RWTH Aachen University, the universities of Düsseldorf and Bonn, and Forschungszentrum Jülich. The authors thank the Institute for Bioorganic Chemistry (HHU Düsseldorf and Forschungszentrum Jülich) for performing ^{1}H-NMR analysis.

References

1 R. Birner, in *Bioeconomy*, Springer International Publishing, Cham, 2018, pp. 17–38.
2 (*a*) A. Pellis, S. Cantone, C. Ebert and L. Gardossi, *New Biotechnol.*, 2018, **40**, 154–169; (*b*) R. A. Sheldon and J. M. Woodley, *Chem. Rev.*, 2018, **118**, 801–838.
3 J. M. Guisan, *Immobilization of Enzymes and Cells*, Humana Press, Totowa, NJ, 2nd edn, 2013, vol. 1051.
4 U. Krauss, V. D. Jäger, M. Diener, M. Pohl and K.-E. Jaeger, *J. Biotechnol.*, 2017, **258**, 136–147.
5 S. Li, K. Lin, H. Pang, Y. Wu and J. Xu, *Appl. Biochem. Biotechnol.*, 2013, **169**, 612–623.
6 J. Nahálka, *J. Ind. Microbiol. Biotechnol.*, 2008, **35**, 219–223.
7 D. M. Worrall and N. H. Goss, *Aust. J. Biotechnol.*, 1989, **3**, 28–32.
8 P. Tufvesson, J. Lima-Ramos, M. Nordblad and J. M. Woodley, *Org. Process Res. Dev.*, 2011, **15**, 266–274.
9 K. Tokatlidis, P. Dhurjati, J. Millet, P. Béguin and J.-P. Aubert, *FEBS Lett.*, 1991, **282**, 205–208.
10 (*a*) J. Nahálka and V. Pätoprstý, *Org. Biomol. Chem.*, 2009, **7**, 1778–1780; (*b*) S. L. Choi, S. J. Lee, J. S. Ha, J. J. Song, Y. H. Rhee and S. G. Lee, *Biotechnol. Bioprocess Eng.*, 2011, **16**, 1173–1179; (*c*) E. Hrabárová, L. Achbergerová and J. Nahálka, in *Insoluble Protein: Methods and protocols*, ed. E. García-Fruitós, Springer New York, 2015, vol. 1258, pp. 411–422.
11 B. Zhou, L. Xing, W. Wu, X. E. Zhang and Z. Lin, *Microb. Cell Fact.*, 2012, **11**, 10.
12 (*a*) Z. Lin, B. Zhou, W. Wu, L. Xing and Q. Zhao, *Faraday Discuss.*, 2013, **166**, 243–256; (*b*) W. Wu, L. Xing, B. Zhou and Z. Lin, *Microb. Cell Fact.*, 2011, **10**, 9; (*c*) X. Wang, B. Zhou, W. Hu, Q. Zhao and Z. Lin, *Microb. Cell Fact.*, 2015, **14**, 88.
13 (*a*) E. García-Fruitós, N. González-Montalbán, M. Morell, A. Vera, R. M. Ferraz, A. Arís, S. Ventura and A. Villaverde, *Microb. Cell Fact.*, 2005, **4**, 27; (*b*) S. Y. Park, S. H. Park and S. K. Choi, *Anal. Biochem.*, 2012, **426**, 63–65.
14 A. S. Demir, Ö. Şeşenoglu, E. Eren, B. Hosrik, M. Pohl, E. Janzen, D. Kolter, R. Feldmann, P. Dünkelmann and M. Müller, *Adv. Synth. Catal.*, 2002, **344**, 96–103.
15 A. S. Demir, O. Seşenoglu, P. Dünkelmann and M. Müller, *Org. Lett.*, 2003, **5**, 2047–2050.
16 P. Dünkelmann, D. Kolter-Jung, A. Nitsche, A. S. Demir, P. Siegert, B. Lingen, M. Baumann, M. Pohl and M. Müller, *J. Am. Chem. Soc.*, 2002, **124**, 12084–12085.
17 M. Sanchez-Gonzalez and J. P. N. Rosazza, *Adv. Synth. Catal.*, 2003, **345**, 819–824.
18 E. Janzen, M. Müller, D. Kolter-Jung, M. M. Kneen, M. J. McLeish and M. Pohl, *Bioorg. Chem.*, 2006, **34**, 345–361.
19 B. González and R. Vicuña, *J. Bacteriol.*, 1989, **171**, 2401–2405.
20 A. S. Demir, M. Pohl, E. Janzen and M. Müller, *J. Chem. Soc., Perkin Trans. 1*, 2001, 633–635.
21 B. M. Choudary, N. S. Chowdari, S. Madhi and M. L. Kantam, *J. Org. Chem.*, 2003, **68**, 1736–1746.
22 T. Stillger, M. Pohl, C. Wandrey and A. Liese, *Org. Process Res. Dev.*, 2006, **10**, 1172–1177.
23 N. Kurlemann and A. Liese, *Tetrahedron: Asymmetry*, 2004, **15**, 2955–2958.
24 J. Döbber and M. Pohl, *J. Biotechnol.*, 2017, **241**, 170–174.
25 P. Domínguez de María, T. Stillger, M. Pohl, S. Wallert, K. Drauz, H. Gröger, H. Trauthwein and A. Liese, *J. Mol. Catal. B: Enzym.*, 2006, **38**, 43–47.
26 T. Stillger, *doctoral thesis*, Rheinische Friedrich-Wilhelms-Universität Bonn, 2004.
27 T. Schmidt, M. Zavrel, A. Spiess and M. B. Ansorge-Schumacher, *Bioorg. Chem.*, 2009, **37**, 84–89.
28 F. Hildebrand, S. Kühl, M. Pohl, D. Vasic-Racki, M. Müller, C. Wandrey, S. Lütz, Đ. Vasić-Rački, M. Müller, C. Wandrey and S. Lütz, *Biotechnol. Bioeng.*, 2007, **96**, 835–843.
29 S. B. Sopaci, I. Simşek, B. Tural, M. Volkan and A. S. Demir, *Org. Biomol. Chem.*, 2009, **7**, 1658–1664.
30 B. Tural, S. Tural, E. Ertaş, İ. Yalınkılıç and A. S. Demir, *J. Mol. Catal. B: Enzym.*, 2013, **95**, 41–47.

This journal is © The Royal Society of Chemistry 2018

Published on 15 October 2018. Downloaded by Heinrich Heine University of Duesseldorf on 10/23/2018 7:27:03 PM.

31 S. Shanmuganathan, D. Natalia, A. van den Wittenboer, C. Kohlmann, L. Greiner and P. Domínguez de María, *Green Chem.*, 2010, **12**, 2240–2245.
32 A. van den Wittenboer, B. Niemeijer, S. K. Karmee and M. B. Ansorge-Schumacher, *J. Mol. Catal. B: Enzym.*, 2010, **67**, 208–213.
33 S. Kühl, D. Zehentgruber, M. Pohl, M. Müller and S. Lütz, *Chem. Eng. Sci.*, 2007, **62**, 5201–5205.
34 M. B. Ansorge-Schumacher, L. Greiner, F. Schroeper, S. Mirtschin and T. Hischer, *Biotechnol. J.*, 2006, **1**, 564–568.
35 T. Hischer, D. Gocke, M. Fernández, P. Hoyos, A. R. Alcántara, J. V. Sinisterra, W. Hartmeier and M. B. Ansorge-Schumacher, *Tetrahedron*, 2005, **61**, 7378–7383.
36 P. Domínguez de María, T. Stillger, M. Pohl, M. Kiesel, A. Liese, H. Gröger and H. Trauthwein, *Adv. Synth. Catal.*, 2008, **350**, 165–173.
37 A. van den Wittenboer, T. Schmidt, P. Müller, M. B. Ansorge-Schumacher and L. Greiner, *Biotechnol. J.*, 2009, **4**, 44–50.
38 J. Wachtmeister, A. Jakoblinnert, J. Kulig, H. Offermann and D. Rother, *ChemCatChem*, 2014, **6**, 1051–1058.
39 A. Jakoblinnert and D. Rother, *Green Chem.*, 2014, **16**, 3472.
40 M. Schwarz, *doctoral thesis*, Heinrich-Heine University Düsseldorf, 2010.
41 M. Diener, B. Kopka, M. Pohl, K.-E. Jaeger and U. Krauss, *ChemCatChem*, 2016, **8**, 142–152.
42 R. Kloss, M. H. Limberg, U. Mackfeld, D. Hahn, A. Grünberger, V. D. Jäger, U. Krauss, M. Oldiges and M. Pohl, *Sci. Rep.*, 2018, **8**, 5856.
43 M. V. Airola, K. J. Watts, A. M. Bilwes and B. R. Crane, *Structure*, 2010, **18**, 436–448.
44 A. Grünberger, C. Probst, S. Helfrich, A. Nanda, B. Stute, W. Wiechert, E. von Lieres, K. Nöh, J. Frunzke and D. Kohlheyer, *Cytometry, Part A*, 2015, **87**, 1101–1115.
45 A. Grünberger, C. Probst, A. Heyer, W. Wiechert, J. Frunzke and D. Kohlheyer, *J. Visualized Exp.*, 2013, 1–11.
46 A. Rokney, M. Shagan, M. Kessel, Y. Smith, I. Rosenshine and A. B. Oppenheim, *J. Mol. Biol.*, 2009, **392**, 589–601.
47 S. Ventura and A. Villaverde, *Trends Biotechnol.*, 2006, **24**, 179–185.
48 S. P. Allen, J. Polazzi, J. K. Gierse and A. M. Easton, *J. Bacteriol.*, 1992, **174**, 6938–6947.
49 M. M. Carrio and A. Villaverde, *J. Biotechnol.*, 2002, **96**, 3–12.
50 F. Hoffmann and U. Rinas, *Biotechnol. Prog.*, 2000, **16**, 1000–1007.
51 G. Georgiou and P. Valax, *Methods Enzymol.*, 1999, **309**, 48–58.
52 D. Gocke, L. Walter, E. Gauchenova, G. Kolter, M. Knoll, C. L. Berthold, G. Schneider, J. Pleiss, M. Müller and M. Pohl, *ChemBioChem*, 2008, **9**, 406–412.
53 M. Pohl, M. Müller and A. S. Demir, *US* 7045334B2, 2006.
54 C. Mateo, J. M. Palomo, L. M. van Langen, F. van Rantwijk and R. A. Sheldon, *Biotechnol. Bioeng.*, 2004, **86**, 273–276.
55 V. D. Jäger, R. Lamm, R. Kloß, E. Kaganovitch, A. Günberger, M. Pohl, J. Büchs, K.-E. Jaeger and U. Krauss, *ACS Synth. Biol.*, 2018, **7**, 2282–2295.
56 R. Wichmann, C. Wandrey, A. F. Buckmann and M. R. Kula, *Biotechnol. Bioeng.*, 1981, **23**, 2789–2802.
57 D. Prat, A. Wells, J. Hayler, H. Sneddon, C. R. Mcelroy, S. Abou-shehada and P. J. Dunn, *Green Chem.*, 2016, **18**, 288–296.
58 K. Watanabe, *Molecules*, 2013, **18**, 3183–3194.
59 D. J. Korz, U. Rinas, K. Hellmuth, E. A. Sanders and W.-D. Deckwer, *J. Biotechnol.*, 1995, **39**, 59–65.
60 M. M. Bradford, *Anal. Biochem.*, 1976, **72**, 248–254.
61 E. Gasteiger, C. Hoogland, A. Gattiker, S. Duvaud, M. R. Wilkins, R. D. Appel and A. Bairoch, in *The Proteomics Protocols Handbook*, ed. J. M. Walker, Humana Press, Totowa, NJ, 2005, vol. 31, pp. 571–607.
62 D. Kang, Y. S. Gho, M. Suh and C. Kang, *Bull. Korean Chem. Soc.*, 2002, **23**, 1511–1512.
63 S. Schaffer, B. Weil, V. D. Nguyen, G. Dongmann, K. Günther, M. Nickolaus, T. Hermann and M. Bott, *Electrophoresis*, 2001, **22**, 4404–4422.
64 A. Koch-Koerfges, A. Kabus, I. Ochrombel, K. Marin and M. Bott, *Biochim. Biophys. Acta, Bioenerg.*, 2012, **1817**, 370–380.
65 H. Morschett, W. Wiechert and M. Oldiges, *Microb. Cell Fact.*, 2016, **15**, 34.
66 J. E. T. Corrie and D. R. Trentham, *J. Chem. Soc., Perkin Trans. 1*, 1992, 2409–2417.
67 K. Arifin, L. J. Minggu, W. R. W. Daud, B. M. Yamin, R. Daik and M. B. Kassim, *Spectrochim. Acta, Part A*, 2014, **120**, 208–215.

2.3.1 Publication III: Supporting Information

The here presented Supporting Information of the Manuscript 'Tailor-made catalytically active inclusion bodies for different applications in biocatalysis' was shortened for clarity of the thesis. The original Supporting Information additionally contain DNA and amino acid sequences of the fusion constructs, figures of the expression vectors, as well as information about primer sequences, vectors, and expression hosts. This information can partially be found in the Supporting Information of the Manuscript 'Tailoring the properties of (catalytically)-active inclusion bodies' (2.1.1). The DNA and amino acid sequences can be found in the Appendix (5.2).

1 Experimental

1.1 Cloning & sequences

The gene encoding for *Pf*BAL was cloned into a pET28a vector containing the gene fragment encoding for the TDoT-domain, a linker region consisting of 3xGGGS linker and the Factor Xa protease recognition site (L), which was performed based on the earlier described cloning strategy.[1] In brief, the gene coding for *Pf*BAL was amplified by PCR using the below listed oligonucleotide primers, and subsequently inserted into the above described pET28a vector by restriction with *BamH*I and *Not*I and ligation, resulting in an N-terminal fusion of the target enzyme to linker and TDoT (pTDoT-Xa-L-*Pf*BAL). To insert the 3HAMP domain into the so generated vector (pTDoT-Xa-L-*Pf*BAL), the 3HAMP gene fragment was codon-optimized, synthesized by Eurofins Genomics (Ebersberg, Germany) and supplied on a plasmid (pEX-A-3HAMP-Linker). The DNA fragment coding for 3HAMP-Linker was subsequently cloned into the above described vector (pTDoT-Xa-L-*Pf*BAL) by restriction with endonucleases *Nde*I and *Spe*I and ligation to obtain a vector consisting of 3HAMP-domain, a linker region consisting of 3xGGGS linker and the Factor Xa protease recognition site (L) and the enzyme *Pf*BAL (p3HAMP-Xa-L-*Pf*BAL). All final constructs were verified by sequencing (LGC genomics, Berlin, Germany). Plasmid amplification was performed in *E. coli* DH5α.

1.2 Long-term stability measurement in buffer

Stability of the soluble *Pf*BAL and the CatIBs were analyzed after incubation in TEA-buffer (50 mM, pH 7.5, 2.5 mM $MgSO_4$, 0.5 mM ThDP) at 30°C and 1000 rpm. Therefor, 0.6 mg ml^{-1} protein (calculated based on the protein content) of each enzyme (weight: 14.47 mg *Pf*BAL, 9.92 mg TDoT-*Pf*BAL, 41.76 mg 3HAMP-*Pf*BAL) was incubated in 600 µl volume in polypropylene reaction tubes (1.5 ml safe-lock tube, Eppendorf, Germany) and sampled at different time points (0 h, 4 h, 24 h, 48 h, 72 h) to measure initial rate activity (see sect. 5.7 in the main paper). Therefor the enzyme solutions were respectively diluted. This stability assay was performed as single measurement.

1.3 Solvent selection for the micro-aqueous reaction system

To select an optimal organic solvent, the conversion of the carboligation reaction of 100 mM 3,5-dimethoxybenzaldehyde (DMBA) by 0.6 U ml^{-1} TDoT-*Pf*BAL was measured (2.89 mg ml^{-1} protein concentration). Therefor micro-aqueous systems were prepared by adding 5 vol% TEA-buffer (1 M, pH 8, 2.5 mM $MgSO_4$, 0.1 mM ThDP) to 5 different organic solvents (cyclopentyl methyl ether (CPME), methyl *tert*-butyl ether (MTBE), cyclohexanone, dimethyl carbonate, 2-methyltetrahydrofuran). First the CatIBs were suspended in buffer and then the organic solvent containing the substrate was added. The reaction was performed in a volume of 1 ml in 2 ml glass reaction tubes (G1 clear, CS-Chromatographie Service GmbH, Germany) at 30 °C und 1400 rpm in a thermomixer (Thermomixer comfort, Eppendorf, Germany). 20 µl samples were taken from the organic phase after 1 h and 17.5 h, and were diluted 1:10 in 180 µl 2-methyltetrahydrofuran, thoroughly mixed and centrifuged at 15800 x *g* for 1 min (Centrifuge 5424, Eppendorf, Germany). Subsequently, 20 µl sample from the supernatant was diluted 1:10 in 180 µl n-heptane (incl.4.3 mM acetophenone as internal standard), which was analyzed by HPLC (see sect. 5.13 in the main paper). To analyze evaporation effects, control samples were prepared in the same manner without CatIBs. Each solvent was tested once.

1.4 Optimization of the buffer content in the biphasic reaction system

The buffer content was optimized between 1 vol% - 20 vol% TEA-buffer (1 M, pH 8, 2.5 mM $MgSO_4$, 0.1 mM ThDP) added to either MTBE or CPME. The carboligation reaction of 50 mM DMBA was measured catalyzed by 0.6 U ml^{-1} TDoT-*Pf*BAL (2.9 mg ml^{-1} protein concentration). The reaction was performed as described in sect. 1.3. 20 µl samples taken at different points in time, were prepared as described in sect. 1.3, and analyzed by HPLC (see sect. 5.13 in the main paper). These reactions were performed in duplicate.

1.5 Determination of the reaction equilibrium in the biphasic reaction system

The reaction equilibrium was measured by the cleavage of 32 mM (*R*)-3,3´,5,5´-tetramethoxy benzoin (TMBZ) catalyzed by 6 U ml^{-1} 3HAMP-*Pf*BAL (1.1 mg ml^{-1} protein concentration) in 30 vol% TEA-buffer (50 mM, pH 8, 2.5 mM $MgSO_4$, 0.1 mM ThDP) in CPME. The reaction was performed as described in sect. 1.3. 20 µl samples taken after 1 h and, were prepared as described in sect. 1.3, and analyzed by HPLC (see sect. 5.13 in the main paper). These reactions were performed in as single measurement.

2 Results

2.1 Live cell images

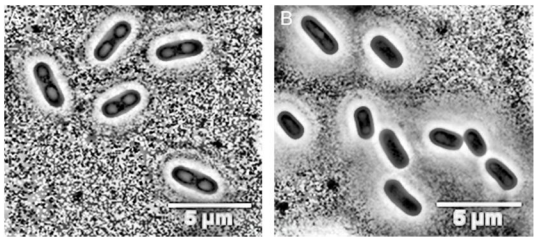


Fig S1 Live cell images of *E. coli* BL21(DE3) cells containing *Pf*BAL-CatIBs. A: TDoT-*Pf*BAL, B: 3HAMP-*Pf*BAL. Images were recorded using an inverted epifluorescence microscope in phase-contrast (see sect. 5.5 in the main paper) For better visualization the pictures were modified by image equalization with CorelDraw X6, version 16.0.0.707. 3HAMP-*Pf*BAL yielded rather diffuse particles at the cell poles, which are less clearly visible in unmodified phase-contrast images (main paper, Figure 1B). The corresponding particles can however be clearly detected after local image equalization (B), which involves increasing the contrast by resetting the darkest and lightest points and then evenly distributing the values across those two points.

2.2 Stability in buffer

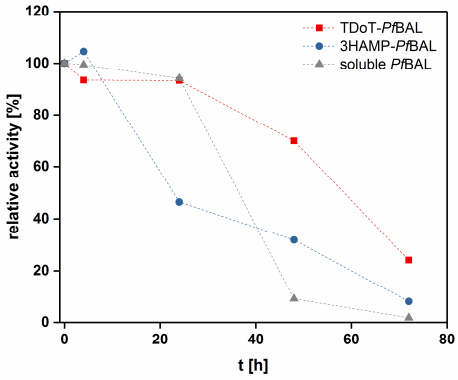


Fig S2 Stability of soluble *Pf*BAL, TDoT-*Pf*BAL and 3HAMP-*Pf*BAL incubated in 50 mM TEA-buffer (pH 7.5) at 30 °C and 1000 rpm. Incubation conditions: 50 mM TEA-buffer (pH 7.5, 2.5 mM $MgSO_4$, 0.5 mM ThDP), protein concentrations of the enzymes 0.6 mg ml^{-1}, 1000 rpm, T = 30 °C, V = 1 ml; n = 1. After distinct time points, the initial rate activity was measured. For experimental details see ESI sect. 1.2. The half-lives decreased in the order TDoT-*Pf*BAL (57 h) > soluble *Pf*BAL (36 h) > 3HAMP-*Pf*BAL (23 h) and were estimated based on the curve.

2.3 EMR experiments

2.3.1 Overview of results obtained in EMR experiments

Tab S1 Half-life and residual (*R*)-benzoin in the reaction chamber of *Pf*BAL, TDoT-*Pf*BAL, and 3HAMP-*Pf*BAL-CatIBs determined based on the experiments shown in Fig S5, Fig 3 in the main paper. Half-lives were taken from the curve at 50% conversion from benzaldehyde to (*R*)-HPP. For experimental details see sect. 5.8 in the main paper. The residual (*R*)-benzoin was determined by transferring the whole suspension from the reaction chamber into a glass vessel, where methyltetrahydrofuran (m-THF) was added to the water-phase. The water-phase was extracted by m-THF. The reaction chamber was washed with m-THF and pooled with the m-THF phase. Finally, the (*R*)-benzoin concentration in the m-THF phase was measured by HPLC and the amount of (*R*)-benzoin was calculated based on the measured concentration and the respective m-THF volume.

pH	reaction system	enzyme	half-life [h]	residual (*R*)-benzoin [mg]	(*R*)-benzoin conversion [%]
7.5	buffer	TDoT-*Pf*BAL	48	n.d.	n.d.
		3HAMP-*Pf*BAL	10	n.d.	n.d.
		*Pf*BAL	7	7.2	2.5
7.5	30 vol% DMSO in buffer	TDoT-*Pf*BAL	131	n.d.	n.d.
		3HAMP-*Pf*BAL	59	0.036	0.0054
		*Pf*BAL	92	114.3	7.2
9.0	30 vol% DMSO in buffer	TDoT-*Pf*BAL	3	157.3	57.1
		3HAMP-*Pf*BAL	13	n.d	n.d.
		*Pf*BAL	16	148.0	16.8

2.3.2 Absorption of benzaldehyde and (*R*)-HPP during the EMR experiments

Due to gaps in the mass balance and a maximum conversion of 80% (compare sect 3.2 in the main paper), the absorption of benzaldehyde and (*R*)-HPP by the PEEK-(polyether ether ketone)-reactor material was tested in the EMR under reaction conditions (30 °C and 300 rpm, 10 kDa membrane) in TEA-buffer or the buffer-DMSO system with 30 vol% DMSO. Therefore, either a benzaldehyde (30 mM) or (*R*)-HPP (30 mM) solution was pumped through the reactor under conditions given in sect. 5.8 in the main paper in the absence of enzyme. After pumping overnight, samples of the efflux (direct at the output, without storage) and the reaction chamber were taken (Fig S3) and analyzed by HPLC (see sect. 5.13 in the main paper). Furthermore, samples were collected in open glass test tubes by a fraction collector, which were stored for the given period under the hood for evaporation analysis (Fig S4). In Fig S3 the relative difference between the initial concentration in the substrate reservoir and in the efflux or reaction chamber are shown in a box plot to visualize the significance of the differences compared to 0 (no difference). The whiskers indicate the minimum and maximum of the data set and the upper and lower quartiles 25% and 75%. Furthermore, outliers, the median and mean are given, whereas the median refers to the middle value of the data set and the mean is calculated by summarizing all values divided by the number of values. If the box (upper and lower quartiles) is on the doted zero line, the difference can be considered as not significant, so that there is no significant absorption of benzaldehyde or (*R*)-HPP by the reactor material, as can be seen in all cases for the buffer-DMSO system. However, in the buffer system without DMSO, benzaldehyde and (*R*)-HPP were absorbed by the reactor material.

The open glass test tubes containing benzaldehyde or (*R*)-HPP solution were stored over different periods in time under the hood, which results in a more distinct evaporation of benzaldehyde in the buffer system without DMSO (A) than with 30 vol% DMSO (B) (Fig S4). The (*R*)-HPP concentration increased over a longer storage period due to evaporation of the solvent, which is more distinct for the buffer system without DMSO. (*R*)-HPP does not evaporate in both reaction systems.

Tab S2 shows the absorption of benzaldehyde by polypropylene (PP) reaction tubes over the time.

Tab S2 Absorption of benzaldehyde by polypropylene (PP) reaction tubes (1.5 ml safe-lock tube, Eppendorf, Germany) after different incubation times. Benzaldehyde (33.5 mM) was dissolved in TEA-buffer (50 mM, pH 7.5, 2.5 mM $MgSO_4$, 0.5 mM ThDP) in a glass flask and 500 µl were transferred into a PP reaction tube and incubated with closed lid at room temperature without shaking. Subsequently, the concentration of benzaldehyde in the PP tube was determined by HPLC (chapt. 5.13 in the main paper) after 2, 5 and 10 min.

time (min)	benzaldehyde (mM)	deviation (%)
0	33.5	
2	31.0	7.4
5	30.9	7.8
10	30.9	7.8

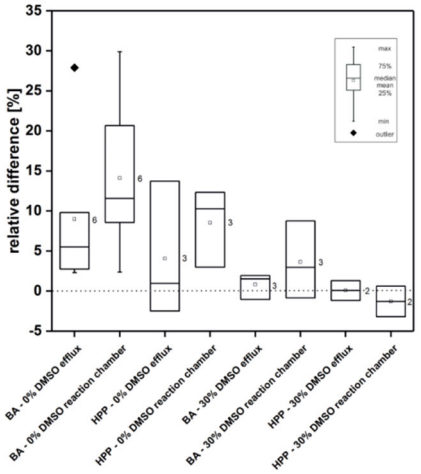
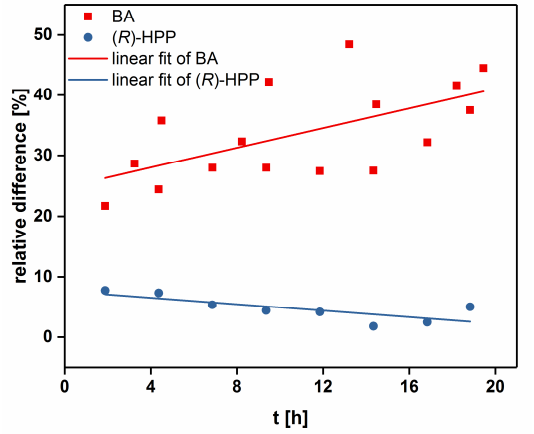


Fig S3 Absorption of benzaldehyde (BA) and (*R*)-2-hydroxy-1-phenylpropanone (HPP) by the PEEK (polyether ether ketone) material of the enzyme membrane reactor, Conditions: 30 mM benzaldehyde or 30 mM (*R*)-HPP in TEA-buffer (50 mM, pH 7.5, 2.5 mM $MgSO_4$, 0.5 mM ThDP), in the presence and absence of 30 vol% DMSO, 300 rpm, T = 30 °C , $V_{reactor}$ = 3 ml, residence time: 30 min, flow: 0.1 ml min^{-1},; membrane: regenerated cellulose membrane (YM10 Milipore, 10 kDa cut-off). Number of repetitions is given next to the box. For experimental details see chapter 5.8 in the main paper.

A



B

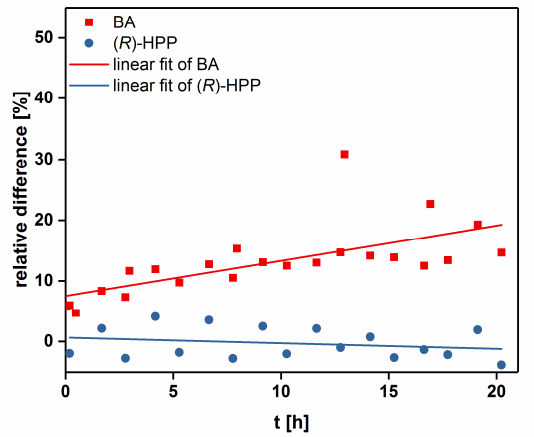


Fig S4 Evaporation of benzaldehyde (BA) and (*R*)-2-hydroxy-1-phenylpropanone (HPP) dissolved in TEA-buffer (A) without DMSO and (B) with 30 vol% DMSO after being pumped through the enzyme membrane reactor and stored in open glass test tubes over a time period. Conditions: 30 mM benzaldehyde or 30 mM HPP in TEA-buffer (50 mM, pH 7.5, 2.5 mM $MgSO_4$, 0.5 mM ThDP), in the presence and absence of 30 vol% DMSO, 300 rpm, T = 30 °C , $V_{reactor}$ = 3 ml, residence time: 30 min, flow: 0.1 ml min^{-1}, PEEK (polyether ether ketone) - enzyme membrane reactor (EMR) with regenerated cellulose membrane (YM10 Milipore, 10 kDa cut-off); n = 1-3. For experimental details see sect. 5.8 in the main paper.

2.3.3 EMR experiment in the buffer-DMSO system at pH 9

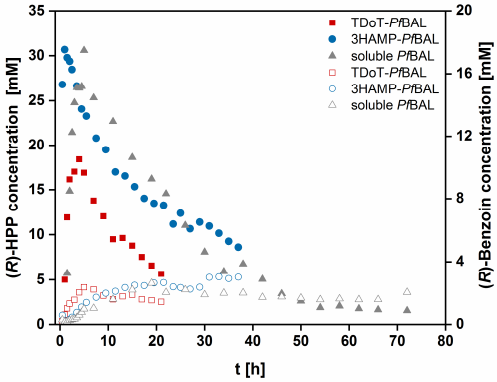


Fig S5 Carboligation of benzaldehyde and acetaldehyde to (*R*)-2-hydroxy-1-phenylpropanone (HPP) catalyzed by *Pf*BAL, TDoT-*Pf*BAL, and 3HAMP-*Pf*BAL-CatIBs, respectively, in an EMR. Filled symbols refer to (*R*)-HPP and empty symbols to (*R*)-benzoin concentration. Half-life was deduced from the point in time where 50 % conversion to (*R*)-HPP (approx. 15 mM) was reached. Reaction conditions: 30 mM benzaldehyde, 90 mM acetaldehyde, TEA-buffer (50 mM, pH 9, 2.5 mM $MgSO_4$, 0.5 mM ThDP), 30 vol% DMSO, 28 U ml^{-1} protein concentrations of the enzymes: TDoT-*Pf*BAL (56.8 mg ml^{-1}), 3HAMP-*Pf*BAL (5.9 mg ml^{-1}), *Pf*BAL (0.94 mg ml^{-1}), 300 rpm, T = 30 °C , $V_{reactor}$ = 3 ml, residence time: 30 min, flow: 0.1 ml min^{-1}, PEEK (polyether ether ketone) - enzyme membrane reactor (EMR) with regenerated cellulose membrane (YM10 Milipore, 10 kDa cut-off); n = 1. For experimental details see sect. 5.8 in the main paper. The halve-lives decreased in the order *Pf*BAL (16 h) >3HAMP-*Pf*BAL (13 h) > TDoT-*Pf*BAL (3 h) and were taken from at 50% conversion from benzaldehyde to (*R*)-HPP.

2.4 Results in the biphasic reaction system

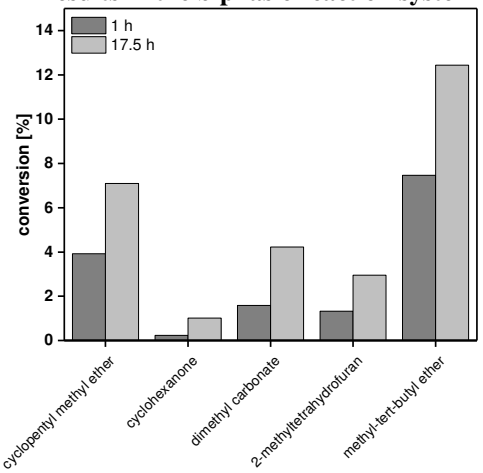


Fig S6 Solvent screening in the micro-aqueous reaction system for the carboligation of DMBA to TMBZ using TDot-*Pf*BAL-CatIBs. Reactions of DMBA to TMBZ were performed in the organic solvents (cyclopentyl methyl ether (CPME), cyclohexanone, dimethyl carbonate, 2-methyltetrahydrofuran, methyl *tert*-butyl ether (MTBE)) with 5 vol% TEA-buffer (1 M, pH 8, 2.5 mM $MgSO_4$, 0.1 mM ThDP), 100 mM DMBA, 0.6 U ml^{-1} TDoT-*Pf*BAL (2.9 mg ml^{-1} protein concentration) in 2 ml glass vials at T = 30°C, 1400 rpm, V = 1 ml, in a thermomixer, n = 1. For experimental details see sect. 1.3, n = 1. For MTBE and CPME the best results were obtained, so they were chosen for subsequent experiments.

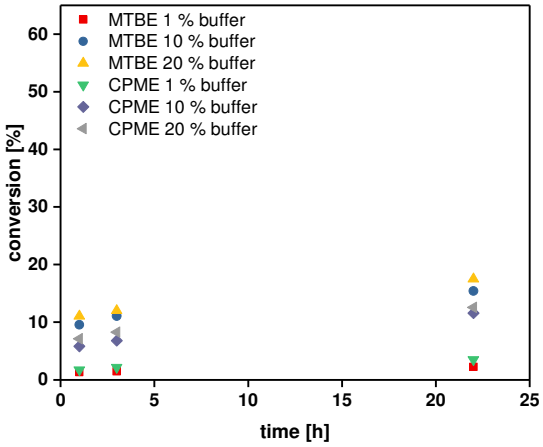


Fig S7 Optimization of the buffer content in MTBE/CPME in the aqueous-organic two-phase system for the carboligation of DMBA to TMBZ by using TDoT-*Pf*BAL-CatIBs. Reactions were performed in CPME or MTBE with 1-20 vol% TEA-buffer (1 M, pH 8, 2.5 mM $MgSO_4$, 0.1 mM ThDP), 100 mM DMBA, 0.6 U ml^{-1} TDoT-*Pf*BAL (2.9 mg ml^{-1} protein concentration) in 2 ml glass vials at T = 30°C, 1400 rpm, V = 1 ml, in a thermomixer, n = 1. For experimental details see sect. 1.4. A higher buffer content of 20 vol% is necessary to obtain a higher conversion. Reaction in MTBE with 20 vol% buffer revealed the best results.

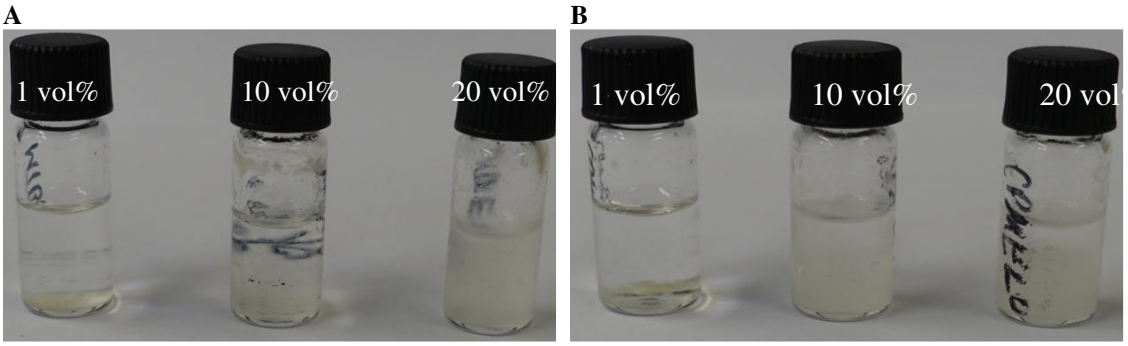


Fig S8 Emulsion formation of TDoT-*Pf*BAL-CatIBs in MTBE (A) or CPME (B) with 1 vol% 10 vol%, or 20 vol% buffer (from left to right) in the aqueous-organic two-phase system after carboligation of DMBA to TMBZ. Reactions were performed in CPME or MTBE with 1-20 vol% TEA-buffer (1 M, pH 8, 2.5 mM $MgSO_4$, 0.1 mM ThDP), 100 mM DMBA, 0.6 U ml^{-1} TDoT-*Pf*BAL (2.9 mg ml^{-1} protein concentration) in 2 ml glass vials at T = 30°C, 1400 rpm, V = 1 ml, in a thermomixer, n = 1. For experimental details see sect. 1.4.

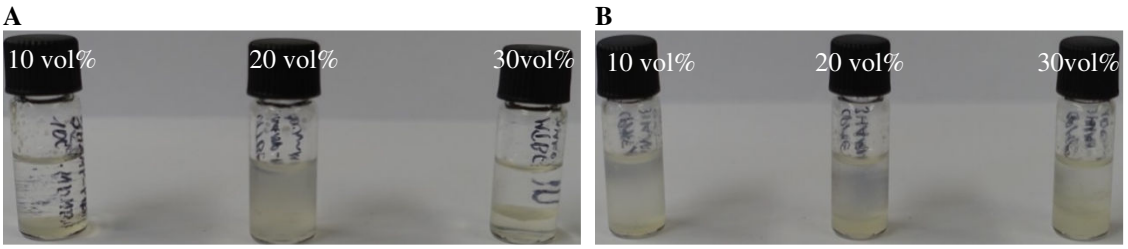


Fig S9 3HAMP-*Pf*BAL-CatIBs show emulsion formation in (A) MTBE and (B) CPME with 10 vol% 20 vol%, or 30 vol% buffer (from left to right). Carboligation reactions of DMBA to TMBZ were performed in MTBE with 10-30 vol% TEA-buffer (1 M, pH 8, 2.5 mM $MgSO_4$, 0.1 mM ThDP), 50 mM DMBA, 6 U ml^{-1} 3HAMP-*Pf*BAL (1.1 mg ml^{-1} protein concentration) in 2 ml glass vials at T = 30°C, 1400 rpm, V = 1 ml, in a thermomixer. Image was recorded 24 h after the last measuring point. In between they were stored at room temperature without shaking. At 30 vol% buffer, an emulsion was formed after 0.5 hours of reaction. Since the photo was taken 24 hours later, the 3HAMP-*Pf*BAL accumulated at the interface of the phases. n=1. For experimental details see sect. 1.4.

Tab S3: Equilibrium constant K_{eq} for the carboligation of DMBA to TMBZ by 3HAMP-*Pf*BAL-CatIBs in a biphasic system with different DMBA concentrations. Calculation based on the given Figures.

Figure no.	**DMBA**		**TMBZ**		
	start concentration [mM]	end concentration [mM]	start concentration [mM]	end concentration at [mM]	K_{eq} [mM^{-1}]
4A, main paper	50	25.0	0	12.5	0.02
4B, main paper	70	34.2	0	17.9	0.02
4C, main paper	85	46.8	0	19.1	0.01
S10, ESI	0	26.0	32	19.0	0.02

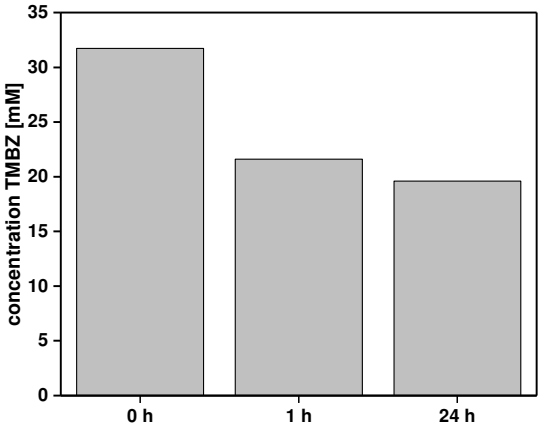


Fig S10 Analysis of the reaction equilibrium of TMBZ synthesis by 3HAMP-*Pf*BAL-CatIBs in the aqueous-organic two-phase system. Reaction equilibrium was measured by the conversion of 32 mM TMBZ to DMBA by 6 U ml^{-1} 3HAMP-*Pf*BAL (1.1 mg ml^{-1} protein concentration) in CPME with 30 vol% TEA-buffer (50 mM, pH 8, 2.5 mM $MgSO_4$, 0.1 mM ThDP), in 2 ml glass vial at T = 30°C, 1400 rpm, V = 1 ml, in a thermomixer, n = 1. For experimental details see sect. 1.5. It could be demonstrated that the reaction equilibrium is at about 50% conversion with a K_{eq} = 0.01 mM (compare Tab S3).

Tab S4 Initial rate actvitiy of the carboligation of benzaldehyde or DMBA to the respective benzoin catalyzed by 3HAMP-*Pf*BAL or soluble *Pf*BAL in biphasic reaction system. 6 U ml^{-1} 3HAMP-*Pf*BAL (0.84 mg ml^{-1} protein concentration), 2.6 U ml^{-1} *Pf*BAL (0.34 mg ml^{-1} protein concentration), 70 mM benzaldehyde or 70 mM DMBA in 1 ml reaction volume composed of 30 vol% TEA-buffer (50 mM, 2.5 mM $MgSO_4$, 0.5 mM ThDP, pH 7.5); 70 vol% CPME, 1400 rpm, 30 °C, n = 3. Calculations are based on Figure 5 in the main paper.

	3HAMP-*Pf*BAL		soluble *Pf*BAL	
	DMBA	benzaldehyde	DMBA	benzaldehyde
k_{cat} [s^{-1}]	4.1	2.6	1.4	2.0
SD	0.1	0.2	0.3	0.3

2.5 ^{1}H-NMR spectrum

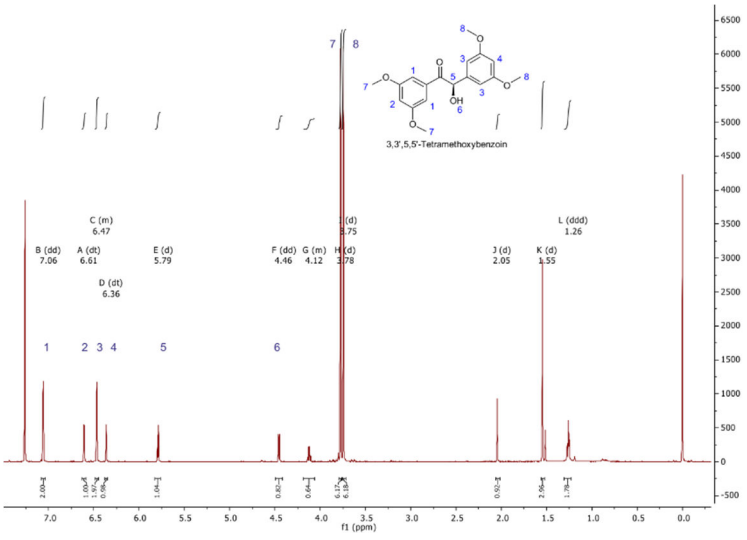


Fig S11 ^{1}H-NMR spectrum (600 MHz, $CDCl_3$) of (*R*)-3,3´,5,5´-tetramethoxy benzoin (TMBZ), which also includes 18.0-19.2 vol% ethyl acetate.

2.6 HPLC calibration curves and analysis

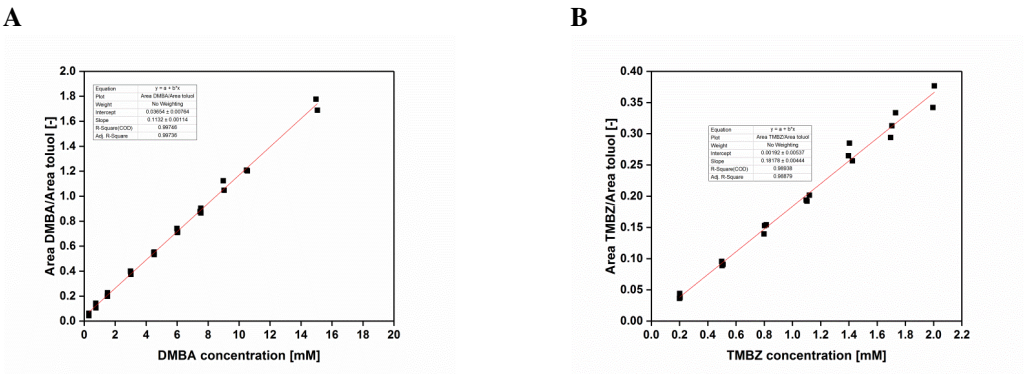


Fig S12 Calibration curve for (A) 3,5-dimethoxybenzaldehyde (DMBA) or (B) (*R*)-3,3‘,5,5‘-tetramethoxy benzoin (TMBZ) dissolved in 80 vol% TEA-buffer (50 mM, pH 7.5, 2.5 mM $MgSO_4$, 0.1 mM ThDP) and 20 vol% DMSO and was diluted 1:10 with 180 µl methanol (incl. 4.7 mM toluene as internal standard), HPLC analysis was performed with ACN/water as mobile phase (see sect. 5.13 in the main paper).

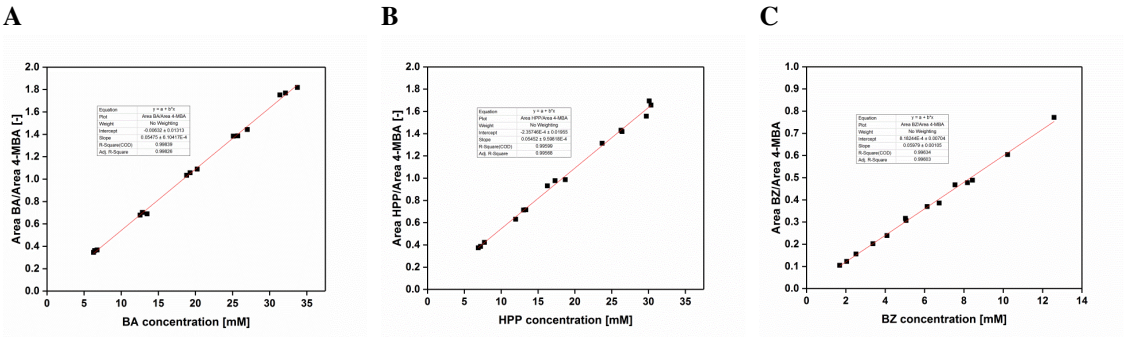


Fig S13 Calibration curve for (A) benzaldehyde (BA), (B) (*R*)-2-hydroxy-1-phenylpropanone (HPP), or (C) (*R*)-benzoin (BZ) dissolved in TEA-buffer (50 mM, pH 7.5, 2.5 mM $MgSO_4$, 0.1 mM ThDP) and was 1:20 diluted with acetonitrile (incl. 0.822 mM 4-methoxybenzaldehyde (4-MBA) as internal standard), HPLC analysis was performed with ACN/water as mobile phase (see sect. 5.13 in the main paper).

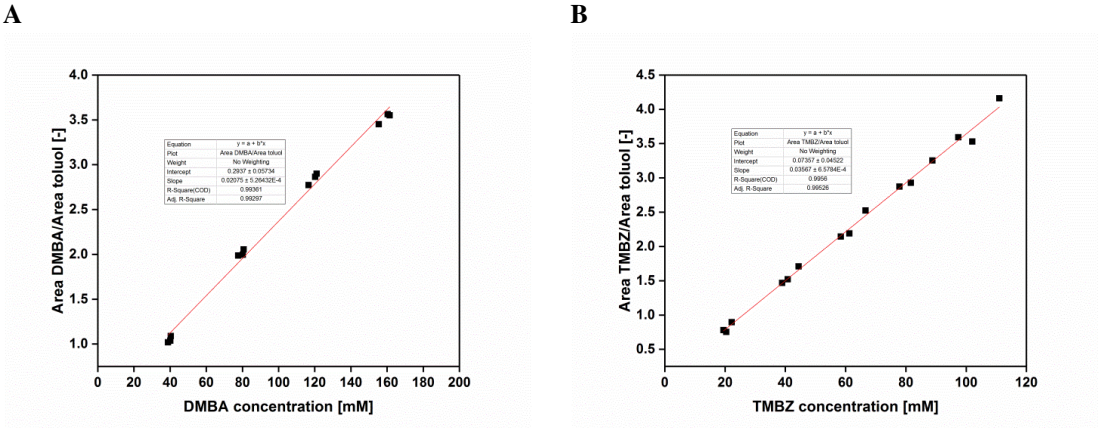


Fig S14 Calibration curve for (A) 3,5-dimethoxybenzaldehyde (DMBA) or B) (*R*)-(3,3‘,5,5‘)-tetramethoxy benzoin (TMBZ) dissolved in 2-methyltetrahydrofuran and 1:10 diluted in 2-methyltetrahydrofuran, and 1:10 diluted in 180 µl n-heptane (incl. 4.3 mM acetophenone as internal standard), HPLC analysis was performed with n-heptane/isopropanol as mobile phase (see sect. 5.13 in the main paper).

Tab S5 HPLC conditions to determine substrate and (side-) product concentrations from the specific reactions: 3,5-dimethoxybenzaldehyde (DMBA), (*R*)-(3,3′,5,5′)-tetramethoxy benzoin (TMBZ), (*R*)-2-hydroxy-1-phenylpropanone (HPP), benzaldehyde (BA) and (*R*)-benzoin (BZ) and the initial standards: toluene, 4-methoxybenzaldehyde (4-MBA), acetophenone. dd refers to double desalted and ACN to acetonitrile. For the gradient applied in the continuous reaction experiment see Tab S6. For HPLC analysis see sect. 5.13 in the main paper)

		initial rate activity determination	**continuous reaction in an EMR**	**reaction in biphasic system**
mobile phase	A	50 vol% (dd) H_2O	gradient of (dd) H_2O	70 vol% *n*-heptane
	B	50 vol% ACN	gradient of ACN	30 vol% 2-propanol
	flow (ml min^{-1})	1.0	0.9	1.5
retention times (min)	DMBA (215 nm)	7.6		4.2
	TMBZ (215 nm)	9.4		11.8
	HPP (245 nm)		7.9	
	BA (245 nm)		9.4	
	BZ (245 nm)		13.8	
	toluene (215 nm)	6.9		
	4-MBA (270 nm)	6.1	11.9	
	acetophenone (215 nm)			3.5

Tab S9 Gradient of the mobile phase for HPLC determination and separation of substrates/products during a continuous reaction in an EMR. A is double desalted (dd) H_2O and B acetonitrile (ACN). For HPLC analysis, see sect. 5.13 in the main paper)

time (min)	**B (%)**
0-7	35
7-8	35-60
8-14	60
14-15	60-35
15-20	35

3 References

1. Diener M, Kopka B, Pohl M, Jaeger K-E, Krauss U. Fusion of a coiled-coil domain facilitates the high-level production of catalytically active enzyme inclusion bodies. ChemCatChem. 2016;8(1):142–52.
2. Janzen E, Müller M, Kolter-Jung D, Kneen MM, McLeish MJ, Pohl M. Characterization of benzaldehyde lyase from *Pseudomonas fluorescens*: A versatile enzyme for asymmetric C–C bond formation. Bioorg Chem. 2006;34(6):345–61.
3. Studier FW, Moffatt BA. Use of bacteriophage T7 RNA polymerase to direct selective high-level expression of cloned genes. J Mol Biol. 1986;189(1):113–30.

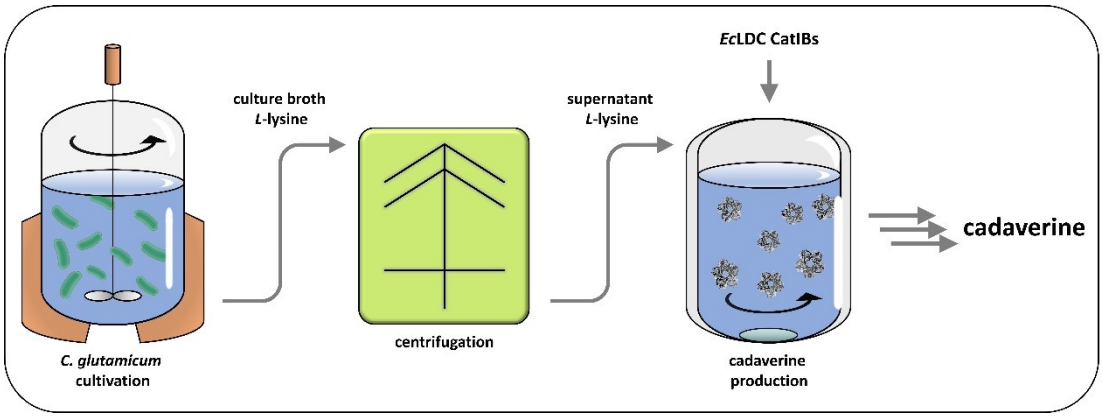
2.4 Publication IV

Catalytically active inclusion bodies of *L*-lysine decarboxylase from *E. coli* for 1,5-diaminopentane production

Ramona Kloss, Michael H. Limberg, Ursula Mackfeld, Doris Hahn, Alexander Grünberger, Vera D. Jäger, Ulrich Krauss, Marco Oldiges, and Martina Pohl*

*corresponding author

Scientific Reports, 2018, 8(1): 5856



Contributions:

DH performed the construction of plasmids supervised by RK and UK, who planned the genetic construct. VDJ and UK supported CatIB preparation. UM performed production, purification, and characterization of the CatIBs and analyzed the data with assistance of RK and MHL, under coordination and supervision of MP. AG performed live-cell imaging with the assistance of VDJ and RK. MHL and RK performed microbial *L*-lysine production under the coordination and supervision of MO. RK, MHL, and MP wrote the manuscript with input from AG, UK, VDJ, and MO.

Copyright © 2018 Nature Research. Reproduced by permission.

(https://www.nature.com/articles/s41598-018-24070-2)

SCIENTIFIC REPORTS

OPEN

Catalytically active inclusion bodies of L-lysine decarboxylase from *E. coli* for 1,5-diaminopentane production

Received: 22 November 2017
Accepted: 26 March 2018
Published online: 11 April 2018

Ramona Kloss[1,4], Michael H. Limberg[1], Ursula Mackfeld[1], Doris Hahn[1], Alexander Grünberger[1,5], Vera D. Jäger[2,4], Ulrich Krauss[2,4], Marco Oldiges[1,3] & Martina Pohl[1,4]

Sustainable and eco-efficient alternatives for the production of platform chemicals, fuels and chemical building blocks require the development of stable, reusable and recyclable biocatalysts. Here we present a novel concept for the biocatalytic production of 1,5-diaminopentane (DAP, trivial name: cadaverine) using catalytically active inclusion bodies (CatIBs) of the constitutive L-lysine decarboxylase from *E. coli* (*Ec*LDCc-CatIBs) to process L-lysine-containing culture supernatants from *Corynebacterium glutamicum*. *Ec*LDCc-CatIBs can easily be produced in *E. coli* followed by a simple purification protocol yielding up to 43% dry CatIBs per dry cell weight. The stability and recyclability of *Ec*LDCc-CatIBs was demonstrated in (repetitive) batch experiments starting from L-lysine concentrations of 0.1 M and 1 M. *Ec*LDC-CatIBs exhibited great stability under reaction conditions with an estimated half-life of about 54 h. High conversions to DAP of 87–100% were obtained in 30–60 ml batch reactions using approx. 180–300 mg *Ec*LDCc-CatIBs, respectively. This resulted in DAP titres of up to 88.4 g l^{-1} and space-time yields of up to 660 g_{DAP} l^{-1} d^{-1} per gram dry *Ec*LDCc-CatIBs. The new process for DAP production can therefore compete with the currently best fermentative process as described in the literature.

An interpolation from the current state of the petrochemical industry and fossil-based energy supply to the next century predicts the exhaustion of fossil carbon sources, which can be attributed to an alarmingly rapid exploitation of limited natural deposits[1]. In particular, this applies to crude oil, due to the steadily growing demand[2,3]. Consequently, society will face a notable future price increase for fossil resources, which has already focused public interest on sustainable and eco-efficient alternatives. This has thus encouraged the biotechnology industry to develop processes for the sustainable production of platform chemicals, biofuels[4–6], and in particular bio-based polymers[4,7]. Increasing knowledge about the prokaryotic metabolism and ongoing developments in systems engineering pave the way for the development of microbial hosts also enabling the economic production of intermediates and bulk chemicals. However, to meet economic demand, it is necessary to develop innovative concepts and improved bioprocesses.

Biotechnological workhorses such as *Escherichia coli*, *Saccharomyces cerevisiae* and *Corynebacterium glutamicum* have been engineered to produce ω-amino acids[8], aromatic monomers[9], diamines[10–12], dicarboxylic acids[13–15], diols[16] and hydroxy acids[17], respectively. From this broad spectrum of building blocks for biopolymer production, the linear aliphatic diamine 1,5-diaminopentane (DAP) is probably one of the most attractive options. One reason is its ability to produce fully bio-based polyamides, such as PA 5.4 and PA 5.10, based on DAP and dicarboxylic acids such as succinate[13,18] and sebacic acid[19], respectively. PA 5.10, in particular, exhibits material properties comparable or even superior to the widely used petroleum-based polyamide PA 6[20].

One option for the biotechnological production of DAP is the use of engineered, well-established L-lysine producers, especially *C. glutamicum*[10,21–24] and *E. coli*[12,25–30]. *C. glutamicum* DAP-producer strains are usually created

[1]Forschungszentrum Jülich GmbH, IBG-1: Biotechnology, 52425, Jülich, Germany. [2]Institute of Molecular Enzyme Technology, Heinrich-Heine-Universität Düsseldorf, Forschungszentrum Jülich, 52425, Jülich, Germany. [3]RWTH Aachen University, Institute of Biotechnology, 52074, Aachen, Germany. [4]Bioeconomy Science Center (BioSC), c/o, Forschungszentrum Jülich, 52425, Jülich, Germany. [5]Multiscale Bioengineering, Bielefeld University, Universitätsstraße 25, 33615, Bielefeld, Germany. Ramona Kloss and Michael H. Limberg contributed equally to this work. Correspondence and requests for materials should be addressed to M.P. (email: ma.pohl@fz-juelich.de)

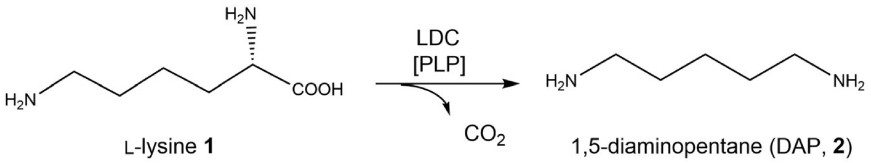


Figure 1. LDC-catalysed decarboxylation of L-lysine to DAP.

by the introduction of one of the L-lysine decarboxylase (LDC) genes from *E. coli* (*cadA*[21] or *ldcC*[10] encoding the acid-inducible enzyme CadA, and the constitutive LDCc, respectively), thus enabling the intracellular decarboxylation of the L-lysine (**1**) to DAP (**2**) (Fig. 1). Both enzymes are very similar (sequence similarity 84%)[31,32], require the cofactor pyridoxal-5′-phosphate (PLP), and appear as decamers composed of five dimers, as was deduced from cryo-electron microscopy[33] and X-ray crystallography[34].

Several constraints need to be tackled for fermentative microbial production, such as the tolerance of the microbial system with respect to DAP[35], the avoidance of by-products such as N-acetyl-1,5-diaminopentane[36] and the management of product export[37], which is no longer possible via the well-engineered lysine exporter LysE[38].

Another option for DAP production is the bioconversion of L-lysine by the addition of LDC to L-lysine containing culture supernatants. Here, immobilisation of the LDC enables easy separation from the reaction medium and recycling of the biocatalyst to decrease process costs. Different concepts have been employed for the immobilisation of LDC, e.g. using whole recombinant *E. coli* cells[25,27,29,39], immobilised recombinant *E. coli* cells in alginate beads[40,41], as well as immobilised LDC on poly(3-hydroxybutyrate) (P(3HB) biopolymer[42] or crosslinked enzyme aggregates (CLEAS) of LDC[43]. Generally, the bioconversions were performed in buffer and only in a few cases directly in culture supernatants of L-lysine producers[25,29].

Catalytically active inclusion bodies (CatIBs) represent biologically produced, cell-free and carrier-free immobilisates that can easily be produced in *E. coli* cells[44–47]. They are a simple and cheap alternative to common immobilisates, which require a case-to-case optimisation of several, often expensive and laborious, steps, including chromatographic purification of the enzyme followed by covalent or non-covalent immobilisation concepts in the presence or absence of carriers[48,49]. The production of immobilised enzymes directly *in vivo* could reduce the production costs of the biocatalyst to the level of crude cell extracts[50], since the insoluble cell fraction can be directly used for biotransformations. Furthermore, CatIB-based biotransformations are free of genetically modified organisms (GMO-free), since any remaining vital recombinant *E. coli* cells can be efficiently inactivated and separated during the production process[51].

Active inclusion bodies can be formed either naturally by self-aggregation of the enzyme[46,52] or by fusion to a tag containing an aggregation-prone part, e.g. cellulose binding domains[53–56], pyruvate oxidase (PoxB) of *Paenibacillus polymyxa*[57], the viral capsid protein VP1, the human Aβ-amyloid peptide[58] or various self-assembling peptides[59,60]. For a detailed overview of the state of the art in this field we refer to a recent review[47]. We previously evaluated the tetramerisation domain of the cell-surface protein tetrabrachion (known as TDoT) from *Staphylothermus marinus*[61] for its potential to induce CatIB formation. The TDoT domain has a rope-like structure forming a stable parallel tetrameric coiled coil[61]. Previous studies have demonstrated that the fusion of the TDoT domain to various enzymes of different complexity resulted in all cases in the formation of CatIBs, which implies that the TDoT-domain is a promising new fusion tag to induce the formation of active inclusion bodies[62].

We here report on an innovative immobilisation approach using CatIBs of the constitutive L-lysine decarboxylase (*Ec*LDCc) and the application of this GMO-free approach to produce DAP in L-lysine-containing culture supernatants. In this study, we demonstrate that this approach also works for the complex PLP-dependent decameric *Ec*LDCc. This enzyme was chosen instead of the frequently used CadA mainly because of the broader pH optimum of *Ec*LDCc (pH 6.2–8) compared to CadA (pH 5.7)[63]. This property makes *Ec*LDCc advantageous for application in L-lysine-containing culture supernatants of the respective *C. glutamicum* producer strains, which exhibit pH values in the range of 6 to 8.5[64,65].

The respective *Ec*LDCc-CatIBs were produced in *E. coli* and successfully applied in culture supernatants of a *C. glutamicum* lysine producer with lysine concentrations of up to 1 M to demonstrate the applicability of this approach on the preparative scale. Under optimised conditions, 74.7–88.4 $g\,l^{-1}$ DAP was produced with 10 $g\,l^{-1}$ dry *Ec*LDCc-CatIBs with a space-time yield of 296–660 $g_{DAP}\,l^{-1}\,d^{-1}$ per gram dry *Ec*LDC-CatIBs (see Table 1).

Results and Discussion

Production of *Ec*LDCc-CatIBs. The gene encoding the constitutive *Ec*LDCc was introduced into a pET28 vector already containing the gene sequences encoding the coiled-coil domain TDoT and an additional 3xGGGS linker region as described elsewhere[62]. Based on the quaternary structure of *Ec*LDCc, the TDoT domain was fused to the C-terminus, since the N-terminus is located within the protein structure[33].

*Ec*LDCc-CatIBs could be easily produced in *E. coli* BL21(DE3) using an auto-induction medium (see Sect. 5.3). The formation of *Ec*LDCc-CatIBs in the respective recombinant *E. coli* cells was demonstrated with inverted epifluorescence microscopy[66,67] showing the CatIBs as bright spots at the cell poles (Fig. 2), which is typical of the deposition of recombinant proteins as inclusion bodies in *E. coli*[68].

A previously developed protocol[62] was further optimised for the purification of *Ec*LDCc-CatIBs (see Fig. 3, left). After two washing steps with water followed by centrifugation, the pellet containing the CatIBs and some cell membrane fractions was lyophilised, yielding 130 ± 37 mg dry CatIBs per gram of wet cells (approx. 13% of

Reference	Present study				Ref[23]
Reaction mode	**repetitive batch**	**repetitive batch**	**batch conversion**		**batch cultivation**
Reaction volume [ml]	$9 \times 60 = 540$	60	30	30	300[2]
Total reaction time [h]	69	4	24	9	50
Temperature [°C]	30	30	30	30	30
PLP [M]	0.0001	0.0001	0.0001	0.0001	—
PLP [mol]	$5.4\ 10^{-5}$	$5.4\ 10^{-5}$	$0.3\ 10^{-5}$	$0.3\ 10^{-5}$	—
L-Lys [M]	0.1	0.1	1	1	—
Total L-Lys [mol]	0.054	0.006	0.03	0.03	—
Total L-Lys [g]	7.89	0.88	4.39	4.39	—
DAP [M]	0.083[1]	0.098	0.87	0.73	0.86
DAP [$g\ l^{-1}$]	8.47	9.99	88.4	74.7	88
Total DAP [g]	4.57[1]	0.599	2.65	2.24	n.d.[2]
Total DAP [mol]	0.0447	0.0059	0.026	0.0219	n.d.[2]
*Ec*LDCc-CatIB [mg ml^{-1}]	3	3	10	10	—
Total amount of dry biocatalyst [mg]	180 (CatIBs)	180 (CatIBs)	300 (CatIBs)	300 (CatIBs)	n.d.[2] (*C. glutamicum*)
Respective WCW of *E. coli* for biocatalyst production [g][3]	1.4	1.4	2.3	2.3	—
Enzymatic productivity $g_{DAP}/g_{biocatalyst}$	25	3.33	8.8	7.5	n.d.[2]
STY [$g\ l^{-1}\ d^{-1}$]	2.94	—	89	198	52.8
STY [$g\ l^{-1}\ d^{-1}$] per g dry CatIBs	16	—	296	660	—
STY [$g\ l^{-1}\ d^{-1}$] per $g_{E.\ coli(WCW)}$	2.1	—	38	86	—
TTN [$mol_{DAP}\ mol_{PLP}^{-1}$]	547–994	978	8,667	7,300	—

Table 1. Productivity measures for the production of DAP. [1]Calculated over all batches. [2]300 ml start volume (no i.nformation concerning final volume available). [3]Refers to previous line.

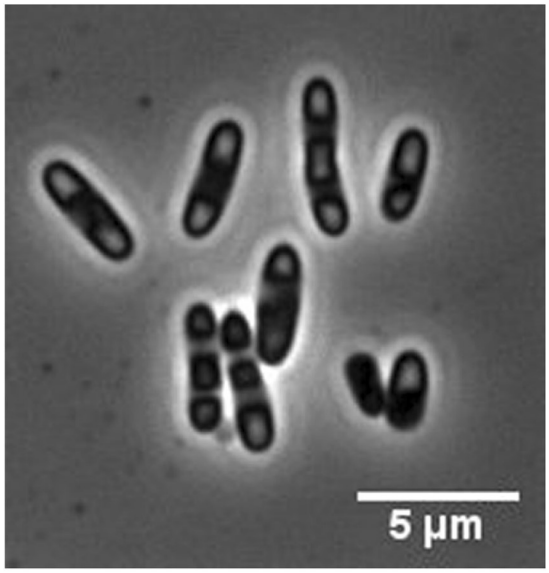


Figure 2. Live cell images of *E. coli* BL21(DE3) cells containing *Ec*LDCc-CatIBs. For details see Supplementary "Live cell imaging."

the wet cell weight, corresponding to 43% dry CatIBs based on dry cell weight). The protein content of the pellet was about 68%, which is comparable to previous results obtained with other CatIB enzymes[62]. The production process was monitored by sodium dodecyl sulfate-polyacrylamide gel electrophoresis (SDS-PAGE, Fig. 3, right) showing that the *Ec*LDCc-TDoT fusion is predominantly present in the pellet. Due to the simple purification protocol (see Methods), further cellular proteins co-purified with the CatIBs were expected, as was also reported for other inclusion body formulations[69].

The activity of the *Ec*LDCc-CatIBs was demonstrated in potassium phosphate buffer (KPi buffer) and cultivation medium (CGXII)[64] (Supplementary Fig. S2). Additionally, the CatIBs were compared to an *E. coli* whole cell biocatalyst containing the overproduced soluble LDCc. The results demonstrate that *Ec*LDCc-CatIBs can compete with the whole cell biocatalyst (for details see Supplementary Fig. S7a,b). Subsequently, the *Ec*LDCc-CatIBs

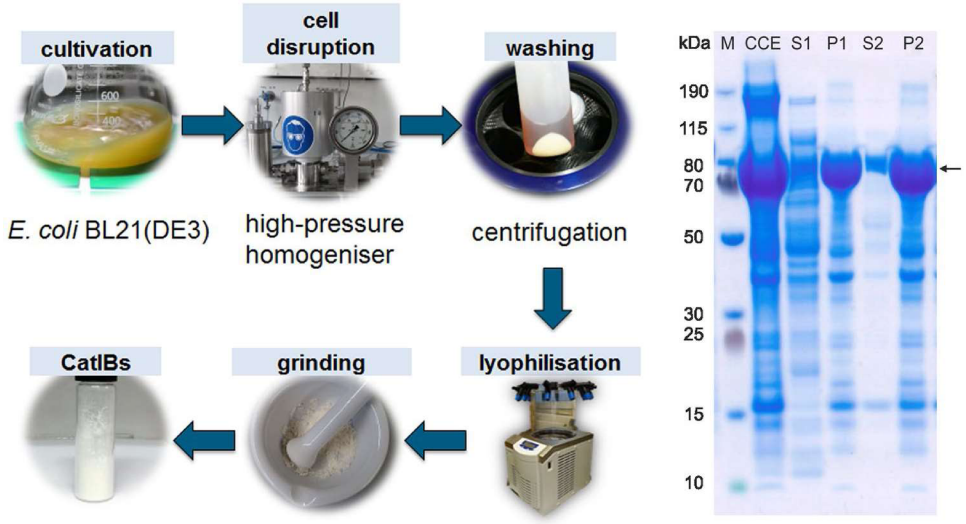


Figure 3. Left: Production and purification of *Ec*LDCc-CatIBs produced in *E. coli* BL21(DE3). Right: SDS-PAGE analysis of the *Ec*LDCc-CatIB preparation (calculated molecular weight: 87.8 kDa, arrow); CCE = crude cell extract, which was centrifuged to separate the supernatant (S1) from the pellet (P1). The pellet P1 was washed once with MilliQ water by resuspension and subsequent centrifugation, resulting in S2 and P2; the protein concentration was measured using the Bradford assay (see Methods). For SDS-PAGE, samples were diluted with water to a protein concentration of 1 mg ml^{-1} by the following dilution factors: 4 for CCE, 2 for S1 and P1, 4.5 for P2; 1 for S2; M = Marker. For details see Methods.

were characterised in CGXII medium and used for a case study under technical conditions in culture supernatants of a *C. glutamicum* L-lysine producer strain.

Characterisation of *Ec*LDCc-CatIBs. *Activity in phosphate buffer.* In a first step, the *Ec*LDCc-CatIBs were characterised in KPi buffer to determine the pH optimum in the pH range of 7–9 and the minimal requirement for PLP.

As already mentioned in the Introduction, the soluble wild-type *Ec*LDCc is active in a relatively broad pH range exhibiting maximal activity between pH 6.2 and pH 8, whereas at pH 8.8 the activity was shown to decrease to 30%[63]. As demonstrated in Fig. 4, *Ec*LDCc-CatIBs showed considerable activity between pH 7.5–9.0 with a clear activity maximum at pH 8. Furthermore, addition of the cofactor PLP was decisive in achieving optimal enzyme activity. Generally, the activity increased by 5–15% in the presence of the cofactor (Fig. 4). Strikingly, at pH 9 the positive PLP effect was approximately 35%. In additional studies, a PLP concentration of 0.05 mM was found to be sufficient for maximal activity of the *Ec*LDCc-CatIBs in buffer (see Supplementary Fig. S3). A similar positive effect of PLP on the LDC activity was recently reported for the second isoenzyme in *E. coli*, the acid-inducible CadA overproduced in recombinant *E. coli*, which was used as a whole-cell biocatalyst. In this case, full conversion of 1 M L-lysine to DAP was observed in the presence of 0.025 mM PLP, whereas without additional PLP only 20% conversion was achieved[29].

Activity in CGXII minimal medium. To verify the applicability of *Ec*LDCc-CatIBs at the preparative scale, DAP production was tested in CGXII cultivation medium providing an experimental setup close to requirements on the technical scale.

First, the optimal pH was determined between pH 7.0–9.0 in fresh CGXII medium with 0.1 mM PLP and 10 mM L-lysine. *Ec*LDCc-CatIBs revealed the highest conversion between pH 8–9, showing a maximum at 8.5 (see Supplementary Fig. S4), which closely corresponds to the pH optimum in KPi buffer (Fig. 4). To ensure comparability, all subsequent experiments were performed at pH 8 providing excellent conditions for *Ec*LDCc-CatIBs in CGXII medium as well as KPi buffer.

In technical processes, L-lysine concentrations of up to 120 g l^{-1} (820 mM) are expected[22]. Therefore, *Ec*LDCc-CatIBs were tested in (repetitive) batch reactions with substrate concentrations of up to 1 M L-lysine. In initial studies with 10–100 mM L-lysine, a concentration of 2 mg ml^{-1} *Ec*LDCc-CatIBs was shown to be sufficient to completely convert 100 mM L-lysine to DAP in 4 h (Fig. 5). Notably, the estimated activity increased from approx. 0.3 U mg^{-1} (10 mM L-lysine) to approx. 0.8 U mg^{-1} (100 mM L-lysine), giving rise to the conclusion that the maximum velocity (V_{max}) of the CatIBs requires a L-lysine concentration of 100 mM or higher. Under the applied conditions, *Ec*LDCc-CatIBs exhibited half-maximum activity at approx. 23 mM L-lysine. This value is much higher compared to the K_M value of 0.84 mM published for the soluble enzyme[70], which was determined under different reaction conditions (soluble *Ec*LDCc in 0.5 M sodium acetate buffer, pH 5.5), which makes a comparison of K_M values meaningless. However, the enormously increased K_M for the CatIBs could indicate a form of mass transport limitation of the substrate or product in the environment of the precipitated protein structure

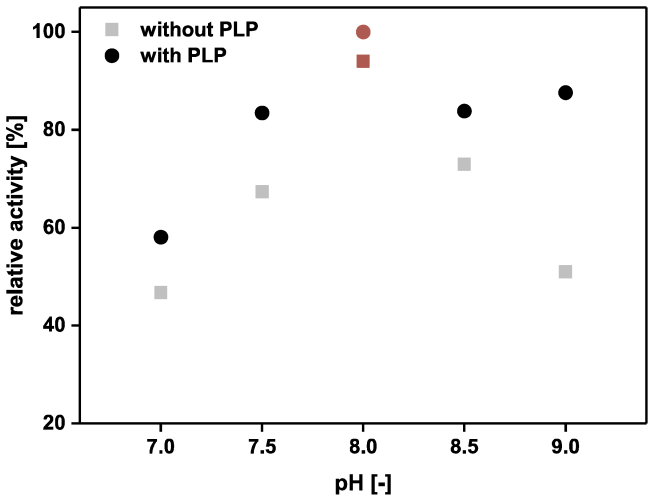


Figure 4. pH optimum of *Ec*LDCc-CatIBs for the decarboxylation of L-lysine in the presence (0.1 mM) and without additional PLP. For assay conditions see Methods. 100% relative activity refers to 0.34 U mg^{-1}_{CatIBs}, which corresponds to 0.52 U $mg^{-1}_{protein}$.

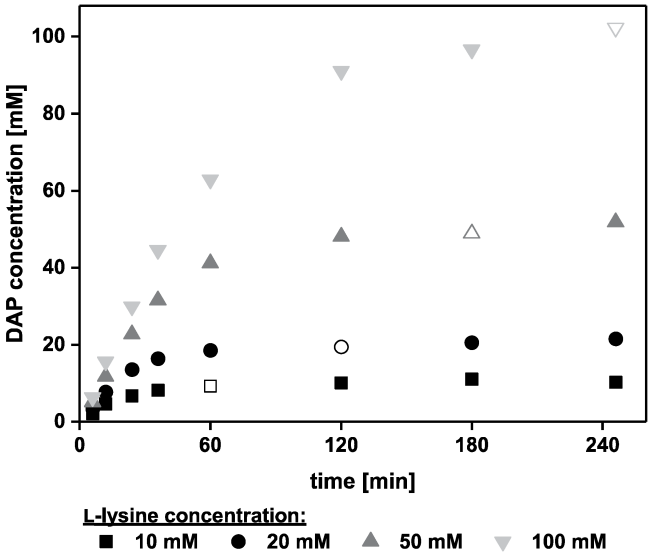


Figure 5. Conversion curves of the *Ec*LDCc-CatIB-catalysed decarboxylation of different L-lysine concentrations to DAP in CGXII medium. Empty symbols indicate the point in time at which full conversion was reached. 2 mg ml^{-1} lyophilised *Ec*LDCc-CatIBs. For details see Methods.

of the CatIBs. The highest enzymatic productivity of 4.9 $g_{DAP}\ g_{LDC\text{-}CatIBs}^{-1}$ (48 $mmol_{DAP}\ g_{LDC\text{-}CatIBs}^{-1}$) was achieved with 100 mM L-lysine in these first studies.

Application of EcLDC-CatIBs for the production of DAP. Subsequently, *Ec*LDC-CatIBs were characterised in CGXII medium containing L-lysine produced by a *C. glutamicum* DM1945 strain[71].

In the first trial, *Ec*LDCc-CatIBs were directly added to the cultivation medium to enable the simultaneous production of L-lysine followed by decarboxylation to DAP in one pot. Surprisingly, only low yields of DAP were obtained, although PLP was added to the cultivation medium. This result could be due to the degradation of PLP by photolysis or oxidation[72] or consumption of the cofactor by *C. glutamicum*, which was earlier reported by Kind *et al.*, who studied the positive effect of adding PLP to the cultivation broth of a *C. glutamicum* DAP producer strain[10]. A further reason could be the low apparent affinity of *Ec*LDCc-CatIBs to L-lysine (K_M approx. 23 mM) as discussed above, which results in low conversion rates at substrate concentrations <100 mM.

In order to circumvent this issue, the lysine-producing cultivation of *C. glutamicum* DM1945 was first completed in CGXII medium. The cell-free culture supernatant was further supplemented with L-lysine to 0.1 M and 0.1 mM PLP.

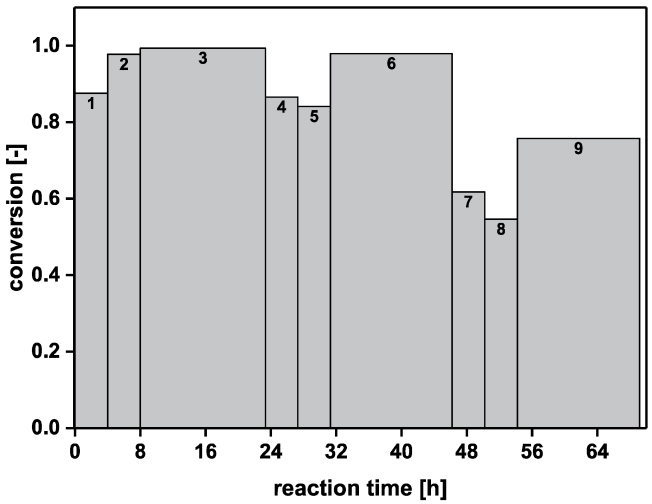


Figure 6. Repetitive batches for the production of DAP with *Ec*LDCc-CatIBs with pH-control. Experimental conditions: 3 mg ml^{-1} lyophilised *Ec*LDCc-CatIBs, 0.1 M L-lysine, 0.1 mM PLP in 60 ml cell-free culture supernatant (CGXII medium, pH 8). Two 4 h batches (batch 1, 2, 4, 5, 7, 8) were followed by 15 h overnight batches (3, 6, 9) on three subsequent days.

The initially performed determination of the stability of *Ec*LDC-CatIBs in this reaction system, as well as their continued application in repetitive batch mode, shows that *Ec*LDCc-CatIBs are fully stable for at least 24 h and can be recycled several times (for details see Supplementary Fig. S5). In repetitive batch mode, the CatIBs were reused after centrifugation and resuspension for five batch cycles, resulting in a productivity of 19.4 g_{DAP} $g_{LDC\text{-}CatIBs}^{-1}$ (190 $mmol_{DAP}$ $g_{LDC\text{-}CatIBs}^{-1}$), which is 4 times higher compared to a single batch (Fig. 5).

Based on these promising results, a repetitive batch on the 60 mL scale with 0.1 M L-lysine was set up in a pH-controlled environment, which was necessary since the reaction products CO_2 and DAP shift the pH. The nine-batch cycles took either 4 or 15 hours. The results of the repetitive batch experiment revealed a constant high conversion of 84–98% during the first 46 h (Fig. 6). The first two repetitive batches (each lasting 4 h) showed almost full conversions of 90–98%. Also the 3rd batch reaction (performed for 15 h) yielded full conversion. After 54 h reaction time (batch 8) the half-life of the *Ec*LDC-CatIBs has almost been achieved, since the conversion decreased to 54%. After 69 h reaction time, the 9th batch (lasting 15 h) only reached 76% conversion, demonstrating that 15 h reaction time was not sufficient to compensate the progressive inactivation. By means of the repetitive batch approach, the enzymatic productivity was increased to 25 $g_{DAP}/g_{LDC\text{-}CatIBs}$ (Table 1), which is 7.5 times higher compared to a single 60 ml batch reaction (e.g. 2nd batch: 3.33 g_{DAP} $g_{LDC\text{-}CatIBs}^{-1}$), yielding a final DAP concentration of 8.47 g l^{-1}, a specific space-time yield (STY) of 16 g_{DAP} l^{-1} d^{-1} per gram *Ec*LDCc-CatIBs, and a total turnover number (ttn) for PLP of up to 994. This experiment showed that the *Ec*LDCc-CatIBs could be reused for several cycles for at least 69 hours under the applied conditions.

To apply the *Ec*LDCc-CatIBs under the requirements on a technical scale, where L-lysine concentrations of up to 1 M are converted to DAP[22,29], the application was next tested in a batch reaction (30 ml) with 1 M L-lysine, which resulted in 87% conversion after approx. 24 h (Fig. 7). The specific activity of 0.75 U mg^{-1}, deduced from conversions $\leq$10%, was comparable to the reaction velocity observed with 100 mM L-lysine (see above), which indicates that there is no substrate inhibition for *Ec*LDCc-CatIBs up to 1 M L-lysine. Although the enzymatic productivity was reduced to 30% (8.8 g_{DAP} g^{-1}_{CatIBs}) compared to the previous repetitive batch experiments with 100 mM L-lysine, due to the higher concentration of CatIBs, the STY was increased 180-fold to 296 g_{DAP} l^{-1} d^{-1} per gram *Ec*LDC-CatIBs. As demonstrated in Fig. 7, the reaction slowed down after a process time of 9 h and between 9 h and 24 h conversion only increased by about 10%. The analysis of the reasons for the slowdown of the reaction requires further investigation. One possibility could be inactivation of the enzyme by negative effects caused by the pH-adjustment with NaOH and HCl or due to high concentrations of DAP, which could be targeted by reaction engineering. If the high DAP concentration is the reason for deactivation of the enzyme, stopping the reaction after 9 h would be a good option (Fig. 7). This would result in a more than twofold higher specific space-time yield of 660 g_{DAP} l^{-1} d^{-1} per gram *Ec*LDC-CatIBs. Accordingly, the ttn for the cofactor PLP was increased by a factor of 10 relative to the repetitive batch with 0.1 M L-lysine (see Table 1). Consequently, a 10 times higher product concentration was reached in one third of the time (24 h) needed for the repetitive batch mode using 0.1 M L-lysine.

Conclusions

The development of cheap, stable, reusable and recyclable biocatalysts is necessary for the prospective creation of competitive sustainable and eco-efficient production processes for platform chemicals, fuels, and polymer building blocks. One promising approach to fulfil industrial demands in terms of productivity, yield, and product titre is the application of whole-cell biotransformation[50] e.g. using resting or metabolically active microbial cells. However, the drawbacks of this approach are productivity issues, e.g. due to undesired side reactions, negative

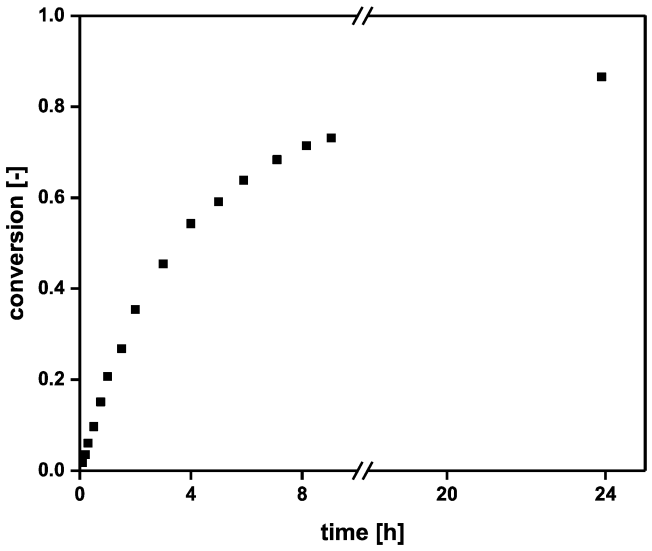


Figure 7. Conversion curve for the production of DAP with *Ec*LDCc-CatIBs in a 30 ml batch reactor with pH control. Experimental conditions: 10 mg ml^{-1} lyophilised *Ec*LDCc-CatIBs, 1 M L-lysine, 0.1 mM PLP, in 30 ml cell-free culture supernatant (CGXII medium, pH 8). For the dosage profile with NaOH and HCl, respectively, to keep the pH constant see Supplementary Fig. S6.

interactions of substrates and products with the microorganism as well as difficulties in downstream processing caused by lysed cells under process conditions. Furthermore, the application of genetically modified organisms (GMO) requires conformity with the respective safety standards. In contrast to whole cells, the preparation of catalytically active inclusion bodies (CatIBs) requires only a few additional steps (cell disruption, solid/liquid separation, washing with water) and thus represents a versatile and cheap GMO-free immobilisation method.

Here we demonstrate the application of CatIBs for the production of 1,5-diaminopentane (DAP) using the constitutive decameric and PLP-dependent lysine decarboxylase from *E. coli* (*Ec*LDCc). Currently, this represents the structurally most complex enzyme in our CatIB toolbox[62].

*Ec*LDCc-CatIBs can be produced with high yields (about 13% dry CatIBs based on the wet cell weight, equivalent to 43% dry CatIBs based on dry cell weight) at low cost comparable to crude cell extract[50]. A two-step process was applied whereby L-lysine is produced first through a *C. glutamicum* producer strain and the culture supernatant is subsequently treated with *Ec*LDCc-CatIBs to produce DAP. Maximal conversion rates were obtained with L-lysine concentrations of 0.1–1 M. As was found for soluble *Ec*LDCc[73] and whole cell catalysts[27,29], the addition of PLP was decisive for optimal CatIB activity. After optimisation of the reaction conditions, a study on a preparative scale demonstrated that *Ec*LDCc-CatIBs are recyclable and stable biocatalysts for DAP production directly applicable in L-lysine-containing culture supernatant. The *Ec*LDCc-CatIBs were successfully reused by simple centrifugation and resuspension steps. Starting from 1 M L-lysine, a maximal DAP concentration of 74.7–88.4 g l^{-1} and a specific STY of up to 296–660 g_{DAP} l^{-1} d^{-1} per gram *Ec*LDC-CatIBs were obtained (see Table 1). This result compares well with the currently best fermentative process using *C. glutamicum*, which also achieved a final titre of 88 g l^{-1} DAP after 50 hours of a combined batch/fed-batch fermentation, but a STY of only 52.8 g l^{-1} d^{-1} (2.2 g l^{-1} h^{-1})[23] (see Table 1). In order to fulfil the technically relevant demands, the usage of *Ec*LDCc CatIBs in batch mode at high substrate concentrations proved to be appropriate in order to obtain high STY.

Methods

Materials. All chemicals were purchased from Sigma-Aldrich, Roth, KMF and Merck. Enzymes for molecular biology were purchased from Thermo Scientific.

Cloning. See Supplementary "Cloning & sequences."

Protein production, cell disruption and protein purification. *Ec*LDCc-CatIBs were produced in *E. coli* BL21(DE3) as recently described elsewhere[62]. Here, a temperature of 15 °C during protein production was decisive for the formation of active *Ec*LDC-CatIBs. Cell disruption was performed with a high-pressure homogeniser (EmulsiFlex-C5, Avestin Europe GmbH, Mannheim, Germany) at 1000 bar using a cooled 10% (w/v) suspension of *E. coli* cells in cell lysis buffer (50 mM sodium phosphate, 100 mM NaCl, pH 8). To ensure thorough cell disruption, the suspension was passed three times through the high-pressure homogeniser under constant cooling. SDS-PAGE (see below) was used to analyse the distribution of the recombinant protein in the *E. coli* cells and during CatIB isolation. After cell disruption, the crude cell extract, and the soluble and insoluble protein fraction were separated by centrifugation at 15,000 × *g* for 30 min. The pellet was washed by suspension in MilliQ water in the initial volume followed by centrifugation. The obtained pellet was frozen overnight at −20 °C and a 10% (w/v) suspension in MilliQ water was prepared for lyophilisation (Christ ALPHA 1–3 LD Plus, Martin Christ Gefriertrocknungsanlagen GmbH, Osterode, Germany). In a mortar the dried pellet was ground to a fine powder, which was weighed and stored at −20 °C for further use.

SDS-PAGE and protein assay. SDS-PAGE analysis was performed using the NuPAGE® Kit (ThermoFisher Scientific), consisting of LDS Sample Buffer (4×) and NuPAGE® Reducing Agent (10×) with a final protein content of 1 mg ml^{-1}. Previously, the soluble protein concentration had been measured using the Bradford assay[74] and bovine serum albumin as a standard. Samples were applied to a NuPAGE™ 4–12% Bis-Tris protein gel, 1.0 mm, with 15 wells together with a protein marker (PageRuler Plus Prestained Protein *ladder*, ThermoFisher Scientific). Gel electrophoresis was performed in NuPAGE® MES SDS running buffer (1×) at 200 V, 100 mA and 15 W.

The protein content of the lyophilised CatIBs was determined by absorption at 280 nm. For this purpose, a defined amount (1–2 mg) of freeze-dried CatIBs was dissolved in 6 M aqueous guanidine hydrochloride solution (1 ml) and incubated at 30 °C for 30 min under constant shaking at 1000 rpm in a thermomixer (Thermomixer comfort, Eppendorf, Germany). The absorption of the protein solution was measured at 280 nm with a spectrophotometer (Shimadzu UV-1800/UV-1600). The protein content was estimated using the molar extinction coefficient (*Ec*LDCc-CatIBs: $\varepsilon = 109{,}210\,l\,mol^{-1}\,cm^{-1}$) as calculated based on the amino acid composition using the ProtParam Tool (http://web.expasy.org/protparam).

Live cell imaging. See Supplementary.

pH optimum of *Ec*LDC-CatIBs in KPi buffer and activity assay. In order to analyse the pH optimum, a reaction with 0.5 mg ml^{-1} lyophilised *Ec*LDCc-CatIBs in a reaction tube (2 ml safe-lock tube, Eppendorf, Germany) in 1 ml KPi buffer (50 mM, pH 7.0, 7.5, 8.0, 8.5, 9.0) containing 10 mM L-lysine, 0.1 mM PLP was performed for 20 min at 30 °C and 1000 rpm in a thermomixer (Thermomixer comfort, Eppendorf, Germany). After different time intervals (5, 10 and 20 min), 20 µl of the samples was taken from one vial. The reaction was stopped by incubation at 90 °C for 2 min and subsequent centrifugation for 2 min at 15,800 × *g*. The samples were then diluted to 1:50 in KPi buffer (50 mM, pH 7.0). The specific activity was calculated based on the DAP formed within the linear range, which was determined by HPLC analysis (see below).

One unit (U) of specific activity is defined as the amount of enzyme (in mg, calculated on the basis of protein content) which catalyses the formation of 1 µmol DAP per minute from the respective L-lysine concentration under the applied reaction conditions. The formation of DAP was monitored using HPLC as described below.

Characterisation of *Ec*LDCc-CatIBs in CGXII medium supplemented with different L-lysine concentrations. To characterise the performance of *Ec*LDCc-CatIBs for the transformation of different L-lysine concentrations from 10–100 mM, reactions of 2 mg ml^{-1} lyophilised *Ec*LDCc-CatIBs each were performed in reaction tubes (2 ml safe-lock tube, Eppendorf, Germany) in 1 ml CGXII medium[64] adjusted to pH 8.0 and containing 10, 20, 50, and 100 mM L-lysine and 0.1 mM PLP for 4 h at 30 °C and 1000 rpm in a thermomixer (Thermomixer comfort, Eppendorf, Germany). After different time intervals (6, 12, 24, 36, 60, 120, 180, and 246 min), 20 µl samples were taken and stopped by 1:5 dilution with methanol. The reaction mixture was then 1:10 diluted in KPi buffer (50 mM, pH 8.0) and subsequently centrifuged for 2 min at 15,800 × *g*. The samples thus obtained were diluted in an appropriate manner to obtain a final DAP concentration suitable for HPLC analysis (see below) between 10 and 100 µM. The specific activity was calculated as described above.

Bioreactor cultivation of *C. glutamicum*. See Supplementary.

Application of *Ec*LDCc-CatIBs in a (repetitive) batch. *Ec*LDCc-CatIBs were characterised in a cell-free culture supernatant (30 or 60 ml), with an adjusted pH of 8.0 and 0.1 mM PLP. Decarboxylation reactions of 100 mM and 1 M L-lysine were performed in repetetive batch and batch experiments, respectively. For the repetitive batch experiment, 3 mg ml^{-1} *Ec*LDCc-CatIBs were used in 60 ml reaction solution. For the single batch reaction, starting from 1 M L-lysine, 10 mg ml^{-1}*Ec*LDCc-CatIBs were added to 30 ml reaction solution. The experiments were performed under pH-control by dosing NaOH (2 M) and HCl (5%), respectively, using a 665 Dosimat, 632 pH meter equipped with a 614 Impulsomat from Metrohm, Germany. For the dosage profile of NaOH and HCl during the batch reaction starting from 1 M L-lysine see Supplementary Fig. S6. Reactions were performed in a doubled-walled 3-neck reactor vessel with two nozzles for the cooling supply to keep the temperature constant at 30 °C. The reaction mixture was stirred with a magnetic stirrer. For the repetitive batch approach, consecutive batch experiments were performed for either 4 h or 15 h. After a batch of 4 h or 15 h, the reaction mixture was transferred to a centrifugal beaker and centrifuged at 30,966 × *g* for 2 min. The pellet was suspended in the fresh reaction solution described above and transferred back into the doubled-walled flask reactor vessel. 20 µl samples were taken from the supernatant of the respective batch (60 ml approach) and the reaction was stopped by 1:5 dilution with methanol. The reaction mixture was then diluted 1:100 in KPi buffer (50 mM, pH 8.0). 5 µl samples were taken from the 30 ml batch experiment after different time intervals (6, 12, 18, 30, 45, 60, 90, 120, 180, 240, 300, 354, 426, 480, 543, and 1434 min) and the reaction was stopped by 1:20 dilution with methanol. The reaction mixture was then diluted (1:250) in KPi buffer (50 mM, pH 8.0). All samples were subsequently centrifuged for 2 min at 15,800 × *g*. The amount of DAP formed was determined by HPLC analysis (see below).The specific activity was calculated as described above.

Quantification of L-lysine and DAP by HPLC. To determine the DAP concentration in cell-free and CatIB-free reaction solutions, a HPLC-system (Agilent 1100 Infinity, Agilent Technologies, Santa Clara, USA) was used, equipped with a fluorescence detector (excitation: 230 nm; emission: 460 nm) and a C18 KinetexEvo column (Phenomenex, Torrence, USA). Prior to injection, samples were diluted 1:2 (v/v) with 100 µM α-aminobutyric acid as the internal standard (Sigma-Aldrich, St. Louis; USA). Analysis of DAP and L-lysine was performed by a method for amino acid quantification[71] including a pre-column derivatisation step at 18 °C using 5 µl *ortho*-phthaldialdehyde (OPA, Sigma-Aldrich) and 5 µl sample (6 mixing iterations). The mobile phase A was

composed of 7.12 g l^{-1} Na_2HPO_4, 6.24 g l^{-1} NaH_2PO_4 and 0.8% (v/v) THF in water, and the mobile phase B contained 50% (v/v) methanol, 45% (v/v) acetonitrile, and 5% (v/v) water. For chromatographic separation, a linear gradient was applied with a flow of 1 ml min^{-1} starting with 0% B, 0–2 min 0–38% B, 2–6 min 38–42% B, 6–7 min 42–70% B, 7–9 min 70–100% B, 9–13 min 100-0% B. Approximate retention times were 8 min for α-aminobutyric acid, 10 min for L-lysine, and 11 min for DAP. In order to correct for possible effects of the analytical matrix on derivatisation efficiency, α-aminobutyric acid (Sigma-Aldrich, St. Louis; USA) was used as an internal standard. The DAP concentration was derived from the linear calibration of five reference solutions (10 µM to 100 µM), included in each measurement run (for the calibration curve see Supplementary Fig. S8).

Data availability. The datasets generated during the current study are available from the corresponding author on reasonable request.

References

1. Kriegler, E. *et al.* Fossil-fueled development (SSP5): An energy and resource intensive scenario for the 21st century. *Glob. Environ. Chang.* **42**, 297–315 (2017).
2. U.S. Energy Information Administration. *International Energy Outlook 2016*. **0484**, (2016).
3. Magnusson, L. U., Gummesson, B., Joksimović, P., Farewell, A. & Nyström, T. Identical, independent, and opposing roles of ppGpp and DksA in *Escherichia coli*. *J. Bacteriol.* **189**, 5193–5202 (2007).
4. Chung, H. *et al.* Bio-based production of monomers and polymers by metabolically engineered microorganisms. *Curr. Opin. Biotechnol.* **36**, 73–84 (2015).
5. Kremer, F., Blank, L. M., Jones, P. R. & Akhtar, M. K. A comparison of the microbial production and combustion characteristics of three alcohol biofuels: Ethanol, 1-butanol, and 1-octanol. *Front. Bioeng. Biotechnol.* **3**, 112 (2015).
6. Wendisch, V. F. Microbial production of amino acids and derived chemicals: Synthetic biology approaches to strain development. *Curr. Opin. Biotechnol.* **30**, 51–58 (2014).
7. Erickson, B., Nelson & Winters, P. Perspective on opportunities in industrial biotechnology in renewable chemicals. *Biotechnol. J.* **7**, 176–185 (2012).
8. Park, S. J. *et al.* Synthesis of nylon 4 from gamma-aminobutyrate (GABA) produced by recombinant *Escherichia coli*. *Bioprocess Biosyst. Eng.* **36**, 885–892 (2013).
9. Meng, D. C. *et al.* Production of poly(3-hydroxypropionate) and poly(3-hydroxybutyrate-co-3-hydroxypropionate) from glucose by engineering *Escherichia coli*. *Metab. Eng.* **29**, 189–195 (2015).
10. Kind, S., Jeong, W. K., Schröder, H. & Wittmann, C. Systems-wide metabolic pathway engineering in *Corynebacterium glutamicum* for bio-based production of diaminopentane. *Metab. Eng.* **12**, 341–351 (2010).
11. Jiang, Y. *et al.* Microbial production of short chain diols. *Microb. Cell Fact.* **13**, 165 (2014).
12. Ma, W. *et al.* Advances in cadaverine bacterial production and its applications. *Engineering* **3**, 308–317 (2017).
13. Litsanov, B., Brocker, M. & Bott, M. Toward homosuccinate fermentation: Metabolic engineering of *Corynebacterium glutamicum* for anaerobic production of succinate from glucose and formate. *Appl. Environ. Microbiol.* **78**, 3325–3337 (2012).
14. Raab, A. M., Gebhardt, G., Bolotina, N., Weuster-Botz, D. & Lang, C. Metabolic engineering of *Saccharomyces cerevisiae* for the biotechnological production of succinic acid. *Metab. Eng.* **12**, 518–525 (2010).
15. Thakker, C., Martínez, I., San, K.-Y. & Bennett, G. N. Succinate production in *Escherichia coli*. *Biotechnol. J.* **7**, 213–24 (2012).
16. Tai, Y.-S. *et al.* Engineering nonphosphorylative metabolism to generate lignocellulose-derived products. *Nat. Chem. Biol.* **12**, 247–253 (2016).
17. Honjo, H., Tsuruno, K., Tatsuke, T., Sato, M. & Hanai, T. Dual synthetic pathway for 3-hydroxypropionic acid production in engineered *Escherichia coli*. *J. Biosci. Bioeng.* **120**, 199–204 (2015).
18. Okino, S. *et al.* An efficient succinic acid production process in a metabolically engineered *Corynebacterium glutamicum* strain. *Appl. Microbiol. Biotechnol.* **81**, 459–464 (2008).
19. Ogunniyi, D. S. Castor oil: A vital industrial raw material. *Bioresour. Technol.* **97**, 1086–1091 (2006).
20. Thielen, M. Bio-polyamides for automotive applications. *Bioplastics Mag.* **5**, 10–11 (2010).
21. Mimitsuka, T., Sawai, H., Hatsu, M. & Yamada, K. Metabolic engineering of *Corynebacterium glutamicum* for cadaverine fermentation. *Biosci. Biotechnol. Biochem.* **71**, 2130–2135 (2007).
22. Becker, J., Zelder, O., Häfner, S., Schröder, H. & Wittmann, C. From zero to hero—Design-based systems metabolic engineering of *Corynebacterium glutamicum* for L-lysine production. *Metab. Eng.* **13**, 159–168 (2011).
23. Kind, S. *et al.* From zero to hero - Production of bio-based nylon from renewable resources using engineered *Corynebacterium glutamicum*. *Metab. Eng.* **25**, 113–123 (2014).
24. Eggeling, L. & Bott, M. A giant market and a powerful metabolism: l-lysine provided by *Corynebacterium glutamicum*. *Appl. Microbiol. Biotechnol.* **99**, 3387–3394 (2015).
25. Oh, Y. H. *et al.* Development of engineered *Escherichia coli* whole-cell biocatalysts for high-level conversion of L-lysine into cadaverine. *J. Ind. Microbiol. Biotechnol.* **42**, 1481–1491 (2015).
26. Liu, P., Zhu, X., Tan, Z., Zhang, X. & Ma, Y. *in Advances in Biochemical Engineering/Biotechnology* **123**, 107–140 (2015).
27. Kim, J.-H. *et al.* Functional study of lysine decarboxylases from *Klebsiella pneumoniae* in *Escherichia coli* and application of whole cell bioconversion for cadaverine production. *J. Microbiol. Biotechnol.* **26**, 1586–1592 (2016).
28. Li, S., Xu, N., Liu, L. & Chen, J. Engineering of carboligase activity reaction in *Candida glabrata* for acetoin production. *Metab. Eng.* **22**, 32–9 (2014).
29. Kim, H. J. *et al.* Optimization of direct lysine decarboxylase biotransformation for cadaverine production with whole-cell biocatalysts at high lysine concentration. *J. Microbiol. Biotechnol.* **25**, 1108–1113 (2015).
30. Qian, Z. G., Xia, X. X. & Lee, S. Y. Metabolic engineering of *Escherichia coli* for the production of cadaverine: A five carbon diamine. *Biotechnol. Bioeng.* **108**, 93–103 (2011).
31. Yamamoto, Y., Miwa, Y., Miyoshi, K., Furuyama, J. & Ohmori, H. The *Escherichia coli* ldcC gene encodes another lysine decarboxylase, probably a constitutive enzyme. *Genes Genet. Syst.* **72**, 167–172 (1997).
32. Snider, J. *et al.* Formation of a distinctive complex between the inducible bacterial lysine decarboxylase and a novel AAA+ ATPase. *J. Biol. Chem.* **281**, 1532–1546 (2006).
33. Kandiah, E. *et al.* Structural insights into the *Escherichia coli* lysine decarboxylases and molecular determinants of interaction with the AAA+ ATPase RavA. *Sci. Rep.* **6**, 24601 (2016).
34. Kanjee, U. *et al.* Linkage between the bacterial acid stress and stringent responses: the structure of the inducible lysine decarboxylase. *EMBO J.* **30**, 931–944 (2011).
35. Ma, W. *et al.* Enhanced cadaverine production from L-lysine using recombinant *Escherichia coli* co-overexpressing CadA and CadB. *Biotechnol. Lett.* **37**, 799–806 (2015).

36. Kind, S., Jeong, W. K., Schröder, H., Zelder, O. & Wittmann, C. Identification and elimination of the competing N-acetyldiaminopentane pathway for improved production of diaminopentane by *Corynebacterium glutamicum*. *Appl. Environ. Microbiol.* **76**, 5175–80 (2010).
37. Li, M. *et al.* Improving the secretion of cadaverine in *Corynebacterium glutamicum* by cadaverine-lysine antiporter. *J. Ind. Microbiol. Biotechnol.* **41**, 701–9 (2014).
38. Vrljic, M., Sahm, H. & Eggeling, L. A new type of transporter with a new type of cellular function: L-lysine export from *Corynebacterium glutamicum*. *Mol. Microbiol.* **22**, 815–26 (1996).
39. Li, N., Chou, H., Yu, L. & Xu, Y. Cadaverine production by heterologous expression of *Klebsiella oxytoca* lysine decarboxylase. *Biotechnol. Bioprocess Eng.* **19**, 965–972 (2014).
40. Bhatia, S. K. *et al.* Biotransformation of lysine into cadaverine using barium alginate-immobilized *Escherichia coli* overexpressing CadA. *Bioprocess Biosyst. Eng.* **38**, 2315–2322 (2015).
41. Kim, J.-H. *et al.* Development of a continuous L-lysine bioconversion system for cadaverine production. *J. Ind. Eng. Chem.* **46**, 44–48 (2016).
42. Seo, H. M. *et al.* *In situ* immobilization of lysine decarboxylase on a biopolymer by fusion with phasin: Immobilization of CadA on intracellular PHA. *Process Biochem.* **51**, 1413–1419 (2016).
43. Park, S. H., Soetyono, F. & Kim, H. K. Cadaverine production by using cross-linked enzyme aggregate of *Escherichia coli* lysine decarboxylase. *J. Microbiol. Biotechnol.* **27**, 289–296 (2017).
44. Li, S., Lin, K., Pang, H., Wu, Y. & Xu, J. Production, characterization, and application of an organic solvent-tolerant lipase present in active inclusion bodies. *Appl. Biochem. Biotechnol.* **169**, 612–623 (2013).
45. Nahálka, J., Vikartovská, A. & Hrabárová, E. A crosslinked inclusion body process for sialic acid synthesis. *J. Biotechnol.* **134**, 146–153 (2008).
46. Worrall, D. M. & Goss, N. H. The formation of biologically active beta-galactosidase inclusion bodies in *Escherichia coli*. *Aust. J. Biotechnol.* **3**, 28–32 (1989).
47. Krauss, U., Jäger, V. D., Diener, M., Pohl, M. & Jaeger, K.-E. Catalytically-active inclusion bodies—Carrier-free protein immobilizates for application in biotechnology and biomedicine. *J. Biotechnol.* **258**, 136–147 (2017).
48. Sheldon, R. A. Enzyme Immobilization: The Quest for Optimum Performance. *Adv. Synth. Catal.* **349**, 1289–1307 (2007).
49. Barbosa, O. *et al.* Strategies for the one-step immobilization–purification of enzymes as industrial biocatalysts. *Biotechnol. Adv.* **33**, 435–456 (2015).
50. Tufvesson, P., Lima-Ramos, J., Nordblad, M. & Woodley, J. M. Guidelines and cost analysis for catalyst production in biocatalytic processes. *Org. Process Res. Dev.* **15**, 266–274 (2011).
51. Rodríguez-Carmona, E., Cano-Garrido, O., Seras-Franzoso, J., Villaverde, A. & García-Fruitós, E. Isolation of cell-free bacterial inclusion bodies. *Microb. Cell Fact.* **9**, 71 (2010).
52. Tokatlidis, K., Dhurjati, P., Millet, J., Béguin, P. & Aubert, J.-P. High activity of inclusion bodies formed in *Escherichia coli* overproducing *Clostridium thermocellum* endoglucanase D. *FEBS Lett.* **282**, 205–208 (1991).
53. Nahálka, J. & Pätoprstý, V. Enzymatic synthesis of sialylation substrates powered by a novel polyphosphate kinase (PPK3). *Org. Biomol. Chem.* **7**, 1778–1780 (2009).
54. Choi, S. L. *et al.* Generation of catalytic protein particles in *Escherichia coli* cells using the cellulose-binding domain from *Cellulomonas fimi* as a fusion partner. *Biotechnol. Bioprocess Eng.* **16**, 1173–1179 (2011).
55. Hrabárová, E., Achbergerová, L. & Nahálka, J. In *Insoluble Protein: Methods and protocols* (ed. García-Fruitós, E.) **1258**, 411–422 (Springer New York, 2015).
56. Nahálka, J., Mislovicová, D. & Kavcová, H. Targeting lectin activity into inclusion bodies for the characterisation of glycoproteins. *Mol. Biosyst.* **5**, 819–21 (2009).
57. Park, S. Y., Park, S. H. & Choi, S. K. Active inclusion body formation using *Paenibacillus polymyxa* PoxB as a fusion partner in *Escherichia coli*. *Anal. Biochem.* **426**, 63–65 (2012).
58. García-Fruitós, E. *et al.* Aggregation as bacterial inclusion bodies does not imply inactivation of enzymes and fluorescent proteins. *Microb. Cell Fact.* **4**, 27 (2005).
59. Wang, X., Zhou, B., Hu, W., Zhao, Q. & Lin, Z. Formation of active inclusion bodies induced by hydrophobic self-assembling peptide GFIL8. *Microb. Cell Fact.* **14**, 88 (2015).
60. Zhou, B., Xing, L., Wu, W., Zhang, X.-E. & Lin, Z. Small surfactant-like peptides can drive soluble proteins into active aggregates. *Microb. Cell Fact.* **11**, 10 (2012).
61. Peters, J. *et al.* Tetrabrachion: A filamentous archaebacterial surface protein assembly of unusual structure and extreme stability. *J. Mol. Biol.* **245**, 385–401 (1995).
62. Diener, M., Kopka, B., Pohl, M., Jaeger, K.-E. & Krauss, U. Fusion of a coiled-coil domain facilitates the high-level production of catalytically active enzyme inclusion bodies. *ChemCatChem* **8**, 142–152 (2016).
63. Kikuchi, Y., Kojima, H., Tanaka, T., Takatsuka, Y. & Kamio, Y. Characterization of a second lysine decarboxylase isolated from. *Escherichia coli*. *J. Bacteriol.* **179**, 4486–4492 (1997).
64. Keilhauer, C., Eggeling, L. & Sahm, H. Isoleucine synthesis in *Corynebacterium glutamicum*: molecular analysis of the ilvB-ilvN-ilvC operon. *J. Bacteriol.* **175**, 5595–603 (1993).
65. Follmann, M. *et al.* Functional genomics of pH homeostasis in *Corynebacterium glutamicum* revealed novel links between pH response, oxidative stress, iron homeostasis and methionine synthesis. *BMC Genomics* **10**, 621 (2009).
66. Grünberger, A. *et al.* Microfluidic picoliter bioreactor for microbial single-cell analysis: Fabrication, system setup, and operation. *J. Vis. Exp.* 1–11 https://doi.org/10.3791/50560 (2013).
67. Grünberger, A. *et al.* Spatiotemporal microbial single-cell analysis using a high-throughput microfluidics cultivation platform. *Cytom. Part A* **87**, 1101–1115 (2015).
68. Rokney, A. *et al. E. coli* transports aggregated proteins to the poles by a specific and energy-dependent process. *J. Mol. Biol.* **392**, 589–601 (2009).
69. Ventura, S. & Villaverde, A. Protein quality in bacterial inclusion bodies. *Trends Biotechnol.* **24**, 179–185 (2006).
70. Krithika, G., Arunachalam, J., Priyanka, H. & Indulekha, K. The two forms of lysine decarboxylase; Kinetics and effect of expression in relation to acid tolerance response in *E. coli*. *J. Exp. Sci.* **1**, 10–21 (2010).
71. Limberg, M. H. *et al.* Metabolic profile of 1,5-diaminopentane producing *Corynebacterium glutamicum* under scale-down conditions: Blueprint for robustness to bioreactor inhomogeneities. *Biotechnol. Bioeng.* **114**, 560–575 (2017).
72. Reiber, H. Photochemical reactions of vitamin B6 compounds, isolation and properties of products. *Biochem. Biophys. Acta* **279**, 310–315 (1972).
73. Holde, V., Sabo, D. L. & Fischer, E. H. Chemical properties of Escherichia coli lysine decarboxylase including a segment of its pyridoxal 5′-phosphate binding site. *Biochemistry* **13**, 670–676 (1974).
74. Bradford, M. M. A rapid and sensitive method for the quantitation of microgram quantities of protein utilizing the principle of protein-dye binding. *Anal. Biochem.* 248–254 (1976).

Acknowledgements

The scientific activities of the Bioeconomy Science Center were financially supported by the Ministry of Innovation, Science and Research within the framework of the NRW Strategieprojekt BioSC (No. 313/323-400-002 13). BioSC is a research cluster of RWTH Aachen University, the universities of Düsseldorf and Bonn, and Forschungszentrum Jülich. The authors thank the Federal German Ministry of Education and Science for providing funding for the cluster project "Systematic consideration of inhomogeneity at the large scale" (grant no. 031A220A), which is embedded in the ERA-IB framework.

Author Contributions

D.H. performed the construction of plasmids under the direction of R.K. and U.K., who performed structure-based planning of the genetic construct. V.D.J. and U.K. supported CatIB preparation. U.M. performed production, purification, and characterisation of the CatIBs and analysed the data with the assistance of R.K. and M.H.L., and the coordination and supervision of M.P. A.G. performed live-cell imaging with the assistance of V.D.J. and R.K. M.H.L. and R.K. performed microbial L-lysine production under the coordination and supervision of M.O. R.K., M.H.L. and M.P. wrote the manuscript with input from A.G., U.K. and M.O.

Additional Information

Supplementary information accompanies this paper at https://doi.org/10.1038/s41598-018-24070-2.

Competing Interests: The authors declare no competing interests.

Publisher's note: Springer Nature remains neutral with regard to jurisdictional claims in published maps and institutional affiliations.

Open Access This article is licensed under a Creative Commons Attribution 4.0 International License, which permits use, sharing, adaptation, distribution and reproduction in any medium or format, as long as you give appropriate credit to the original author(s) and the source, provide a link to the Creative Commons license, and indicate if changes were made. The images or other third party material in this article are included in the article's Creative Commons license, unless indicated otherwise in a credit line to the material. If material is not included in the article's Creative Commons license and your intended use is not permitted by statutory regulation or exceeds the permitted use, you will need to obtain permission directly from the copyright holder. To view a copy of this license, visit http://creativecommons.org/licenses/by/4.0/.

© The Author(s) 2018

2.4.1 Publication IV: Supporting Information

The here presented Supporting Information of the Manuscript 'Catalytically active inclusion bodies of L-lysine decarboxylase from *E. coli* for 1,5-diaminopentane production' was shortened for clarity of the thesis. The original Supporting Information additionally contain DNA and amino acid sequences of the fusion construct, figures of the expression vectors, as well as information about primer sequences. This information can partially be found in the Supporting Information of the Manuscript 'Tailoring the properties of (catalytically)-active inclusion bodies' (2.1.1). The DNA and amino acid sequences can be found in the Appendix (5.2).

1 Methods

Cloning

Based on the earlier described cloning strategy[1], the gene encoding *Ec*LDCc was cloned into a pET28a vector containing the gene fragment encoding for i) the TDoT-domain, ii) a 3xGGGS linker (L) and iii) the enzyme *Ec*LDCc. The *Ec*LDCc gen was cloned into the vector by restriction with NdeI and NheI cleavage sites and ligation to attain a construct encoding a C-terminal fusion of the target enzyme to linker and TDoT. The final plasmid was sequenced by LGC genomics (Berlin, Germany).

Live cell imaging

After cultivation of *E. coli* BL21(DE3) containing *Ec*LDCc-CatIBs, 1 ml of the cell suspension in stationary growth phase was harvested by centrifugation at 15,800 *g* for 2 min. The cell pellet was frozen at -80°C overnight and suspended in cell lysis buffer (50 mM sodium phosphate buffer, 100 mM NaCl, pH 8) to an OD_{600} of approx. 10. The cell suspension was transferred by a syringe to an in-house developed microfluidic chip, which was prepared for single-cell analysis and cultivation[2,3]. This device comprises hundreds of cultivation chambers for monolayer growth to enable imaging on a plane layer. Images were recorded with a phase contrast inverted epifluorescence microscope (TI-Eclipse, Nikon GmbH, Düsseldorf, Germany), additionally equipped with a CCD camera (Clara DR-3041, Andor Technology Plc., Belfast, UK), an LED light source (pE-100 white, CoolLed, Andover, UK), a Nikon Plan Apo 100 Ph3 DM Oil objective, and a Nikon Perfect Focus System for thermal drift compensation. Final images were processed by ImageJ (Wayne Rasband, USA).

Bioreactor cultivation of *C. glutamicum*

Bioreactor cultivations of the L-lysine producing *C. glutamicum* DM1945[4] were carried out in a 1 L scale using CGXII minimal medium[5]. For cultivation 1.5 L DASGIP vessels in a DASGIP Bioblock system (DASGIP GmbH, Jülich, Germany) were used as parallel cultivation system. Each bioreactor was equipped with an optical pO_2 sensor (Hamilton, Visiferm DO 225) and a pH electrode (Mettler-Toledo, 405-DPAS-SC-K8S/225/120). The Bioblock controlling platform (DASGIP, DGCS4) was equipped with a monitoring system for pH and pO_2 (DASGIP, PH4PO4), an exhaust gas analyzer (DASGIP, GA4), a pumping device for titration (DASGIP, MP8), a gassing system (DASGIP, MF4) and a system for temperature and agitation control (DASGIP, TC4SC4). During cultivation pO_2 was maintained to 30% by controlling the agitation rate (maximum 1200 min^{-1}) and a constant aeration rate of 1 volume air per volume fermentation broth per minute (vvm). The pH of the medium was maintained at pH = 7 by the addition of 30% v/v aqueous H_3PO_4 and 17.7% v/v aqueous NH_3 solution. The temperature during cultivation was set to 30 °C.

Cultivations were directly inoculated from cryo culture stocks to an initial $OD_{600\ nm} = 0.05$. Cryo culture stocks were prepared as described by Unthan *et al.* [6], except that culture medium CGXII containing 20% (v/v) glycerol was used for storage instead of 0.9% (w/v) NaCl. The cell suspension was harvested 6 h after the pO_2 returned to the initial value of 100% saturation. Subsequently, the cell fraction was separated from the liquid culture supernatant by centrifugation (20 min, 12,227 x*g*, 4 ºC) and then stored at -20 ºC.

2. Supplementary information concerning the optimisation of the reaction system of *Ec*LDCc-CatIBs for the production of DAP from L-lysine

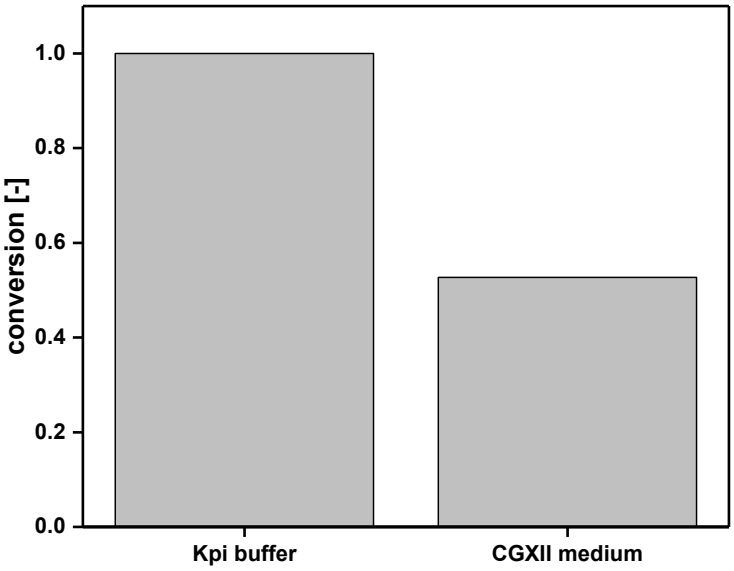


Figure S1: Decarboxylation reaction by 1 mg ml^{-1} *Ec*LDCc-CatIBs with assay conditions: 10 mM L-lysine, 0.1 mM PLP, KPi buffer (50 mM, pH 7.5) or CGXII medium (pH 7.5, 20 g l^{-1} Glucose, 5 g l^{-1} urea) for 1 h at 30°C and 1000 rpm; the reaction was stopped by heating at 90°C for 2 min and subsequent centrifugation; Analysis was performed by HPLC analysis after OPA derivatization (see section 3.1. in the main paper).

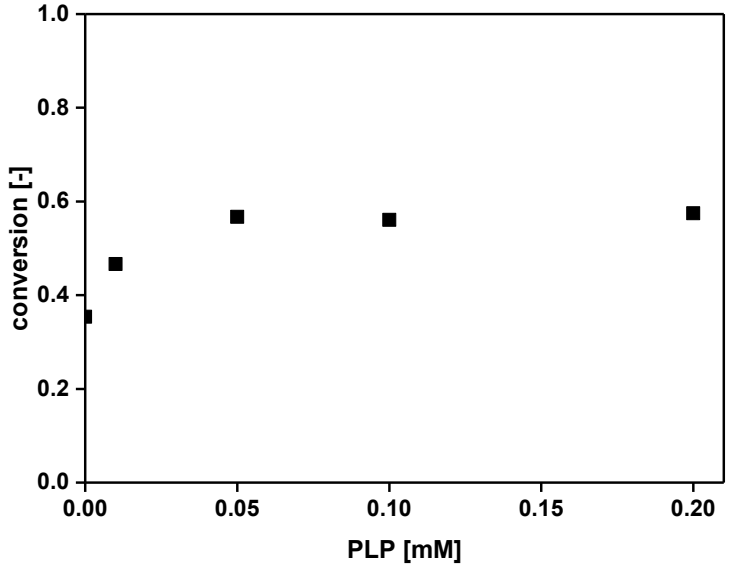


Figure S2: Effect of different PLP concentrations (0.0, 0.01, 0.05, 0.1 and 0.2 mM) on the conversion of L-lysine to DAP by 0.5 mg ml^{-1} *Ec*LDCc-CatIBs; experimental conditions: 10 mM L-lysine, KPi buffer (50 mM, pH 8, supplemented with PLP as indicated) for 30 min at 30°C and 1000 rpm; the reaction was stopped by heating at 90°C for 2 min and subsequent centrifugation; Analysis was performed by HPLC analysis after OPA derivatization (see section 3.2. in the main paper), n = 1

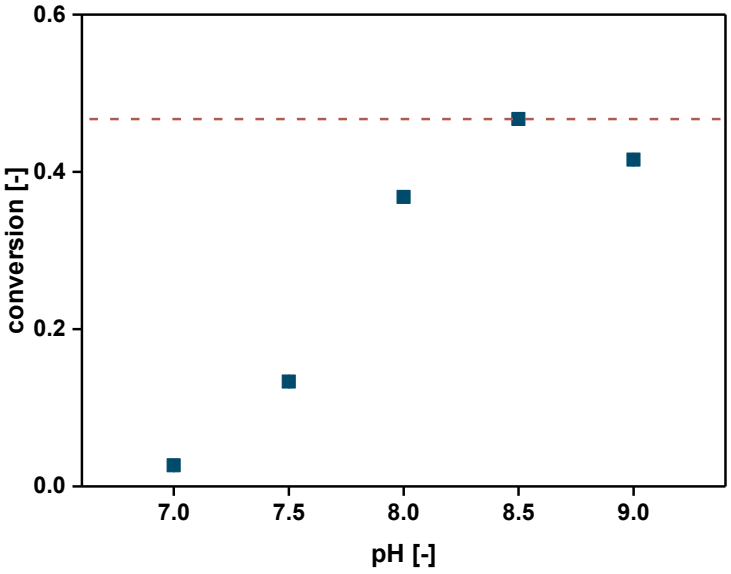


Figure S3: Determination of the optimal pH for the *Ec*LDCc-CatIB-catalysed decarboxylation of L-lysine. Experimental conditions: 0.5 mg ml^{-1} lyophilized *Ec*LDCc-CatIBs, 10 mM L-lysine, 0.1 mM PLP, CGXII medium (pH 7, 7.5, 8, 8.5, 9) for 30 min at 30°C and 1000 rpm; the reaction was stopped by 1:5 dilution with methanol and subsequent centrifugation; Analysis was performed by HPLC analysis after OPA derivatization (see section 3.2. in the main paper), n=3

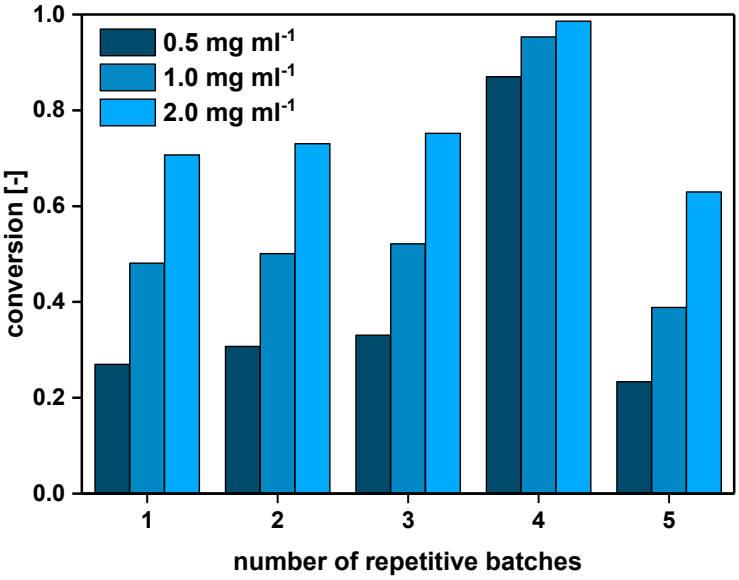


Figure S4: Repetitive batch reactions for DAP production catalysed by different concentrations of *Ec*LDCc-CatIBs (0.5, 1 or 2 mg ml^{-1}); Experimental conditions: total volume 1 ml, 100 mM L-lysine, 0.01 mM PLP in cell free culture supernatant (CGXII medium, pH 8) for 2 h at 30°C and 1000 rpm, except batch 4: 16 h overnight. The CatIBs used in the first batch were reused in the next batch after centrifugation and resuspension in a fresh reaction solution. The reaction was stopped by 1:5 dilution with methanol and subsequent centrifugation; HPLC analysis after OPA derivatization (see section 3.2. in the main paper).

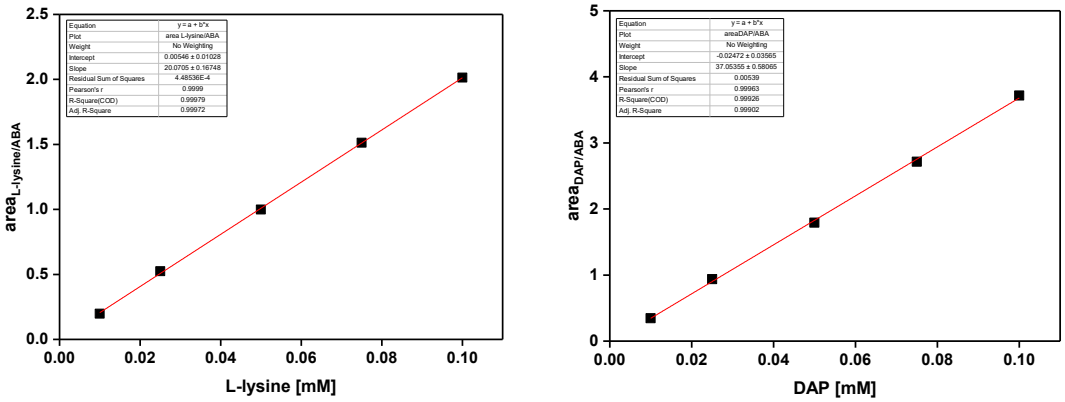


Figure S5 Calibration curve for DAP and L-lysine with the internal standard ABA (alpha-aminobutyric acid), HPLC analysis after OPA derivatization (section 5.10 in the main paper).

3. References

1. Diener, M., Kopka, B., Pohl, M., Jaeger, K.-E. & Krauss, U. Fusion of a coiled-coil domain facilitates the high-level production of catalytically active enzyme inclusion bodies. *ChemCatChem* **8,** 142–152 (2016).

2. Grünberger, A. *et al.* Microfluidic picoliter bioreactor for microbial single-cell analysis: Fabrication, system setup, and operation. *J. Vis. Exp.* 1–11 (2013). doi:10.3791/50560

3. Grünberger, A. *et al.* Spatiotemporal microbial single-cell analysis using a high-throughput microfluidics cultivation platform. *Cytom. Part A* **87,** 1101–1115 (2015).

4. Limberg, M. H. *et al.* Metabolic profile of 1,5-diaminopentane producing *Corynebacterium glutamicum* under scale-down conditions: Blueprint for robustness to bioreactor inhomogeneities. *Biotechnol. Bioeng.* **114,** 560–575 (2017).

5. Keilhauer, C., Eggeling, L. & Sahm, H. Isoleucine synthesis in *Corynebacterium glutamicum*: molecular analysis of the ilvB-ilvN-ilvC operon. *J. Bacteriol.* **175,** 5595–603 (1993).

6. Unthan, S. *et al.* Beyond growth rate 0.6: What drives *Corynebacterium glutamicum* to higher growth rates in defined medium. *Biotechnol. Bioeng.* **111,** 359–371 (2014).

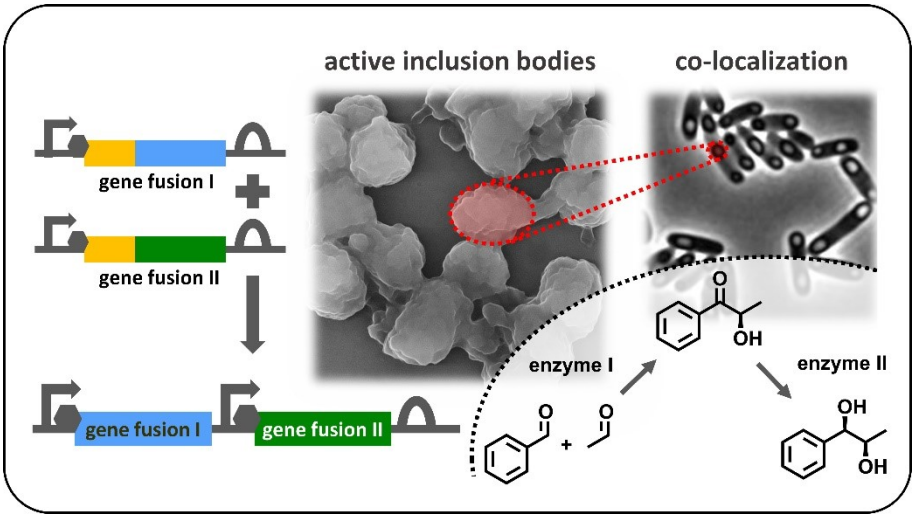
2.5 Publication V

A synthetic reaction cascade implemented by co-localization of two proteins within catalytically-active inclusion bodies

Vera D. Jäger, Robin Lamm, Ramona Kloss, Eugen Kaganovitch, Alexander Grünberger, Martina Pohl, Jochen Büchs, Karl-Erich Jaeger, and Ulrich Krauss*

*corresponding author

ASC Synthetic Biology, 2018, 7(9): 2282-2295



Contributions:

UK, MP, KEJ, and JB coordinated the project, VDJ designed and performed all experiments that are not otherwise mentioned, and analyzed the data, RL performed the online experiments using the BioLector device, EK and VDJ carried out microscopic analyses, AG and VDJ performed the microfluidic cultivations, RK provided reagents and constructs and contributed to assay development and HPLC analytics, UK and VDJ wrote the manuscript. All authors read and commented on the manuscript.

Copyright © 2018 American Chemical Society. Reproduced by permission.

(https://pubs.acs.org/doi/10.1021/acssynbio.8b00274)

ACS Synthetic Biology
Research Article
Cite This: ACS Synth. Biol. 2018, 7, 2282−2295
pubs.acs.org/synthbio

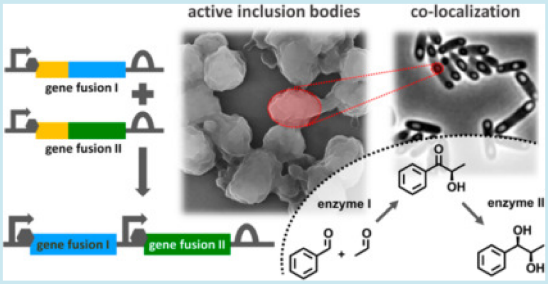
A Synthetic Reaction Cascade Implemented by Colocalization of Two Proteins within Catalytically Active Inclusion Bodies

Vera D. Jäger,[†,⊥] Robin Lamm,[‡,⊥] Ramona Kloß,[§,⊥] Eugen Kaganovitch,[§] Alexander Grünberger,[§,∥] Martina Pohl,[§,⊥] Jochen Büchs,[‡,⊥] Karl-Erich Jaeger,[†,§,⊥] and Ulrich Krauss*[,†,⊥]

[†]Institut für Molekulare Enzymtechnologie, Heinrich-Heine-Universität Düsseldorf, Forschungszentrum Jülich GmbH, D-52425 Jülich, Germany
[‡]AVT-Chair for Biochemical Engineering, RWTH Aachen University, D-52074 Aachen, Germany
[§]Institute of Bio- and Geosciences IBG-1: Biotechnology, Forschungszentrum Jülich GmbH, D-52425 Jülich, Germany
[∥]Multiscale Bioengineering group, Bielefeld University, D-33615 Bielefeld, Germany
[⊥]Bioeconomy Science Center (BioSc), Forschungszentrum Jülich, D-52425 Jülich, Germany

Supporting Information

ABSTRACT: In nature, enzymatic reaction cascades, *i.e.*, realized in metabolic networks, operate with unprecedented efficacy, with the reactions often being spatially and temporally orchestrated. The principle of "learning from nature" has in recent years inspired the setup of synthetic reaction cascades combining biocatalytic reaction steps to artificial cascades. Hereby, the spatial organization of multiple enzymes, *e.g.*, by coimmobilization, remains a challenging task, as currently no generic principles are available that work for every enzyme. We here present a tunable, genetically programmed coimmobilization strategy that relies on the fusion of a coiled-coil domain as aggregation inducing-tag, resulting in the formation of catalytically active inclusion body coimmobilizates (Co-CatIBs). Coexpression and coimmobilization was proven using two fluorescent proteins, and the strategy was subsequently extended to two enzymes, which enabled the realization of an integrated enzymatic two-step cascade for the production of (1*R*,2*R*)-1-phenylpropane-1,2-diol (PPD), a precursor of the calicum channel blocker diltiazem. In particular, the easy production and preparation of Co-CatIBs, readily yielding a biologically produced enzyme immobilizate renders the here presented strategy an interesting alternative to existing cascade immobilization techniques.



KEYWORDS: *inclusion bodies, enzyme immobilization, protein colocalization, biocatalysis, synthetic reaction cascades*

In nature, enzymatic reaction cascades as part of metabolic networks are operating within the cell to achieve the optimal physiologically relevant turnover and flux. Thereby, the cellular machinery is optimized to such an extent that a tremendous variety of simultaneous, often coupled, enzymatic reactions can occur at the same time. Thereby the accumulation of toxic intermediates is prevented by *e.g.*, a feedforward and feedback control.[1] Moreover, the reactions must be orchestrated to operate optimally under rapidly changing cellular and environmental conditions, while being dependent on the availability of various cofactors and substrates. Hereby, the spatial organization and temporal control of these cascades is instrumental for optimal function.[1] In particular, in biocatalysis and synthetic chemistry multienzyme reaction cascades or coupled chemoenzymatic reactions have in recent years been used extensively to broaden the available repertoire of chiral building blocks and commodity target molecules.[1] From an applied perspective, biocatalyst immobilization allows for stabilization, easy handling, and recycling, which facilitates higher space-time yields and thus renders the process more economic and sustainable.[2] Therefore, in the past, different immobilization methods were developed based on a variety of principles.[3−8] All of them, however, require case-to-case optimization as no common concepts are at present available that work for most enzymes. In the context of reaction cascades, the situation is even more challenging as multiple enzymes must be immobilized in/on carrier materials to realize the cascade in a stepwise manner, by mixing different independently prepared immobilizates, or by coimmobilization.[9] Alternatively, multiple enzymes can be coimmobilized in/on the same carrier.[10] Both of these approaches require case-to-case optimization, as not every immobilization strategy will necessarily work for each enzyme of the cascade or is compatible with the components of the reaction mixture. Thus, the spatial organization/immobilization of enzymes in reaction cascades remains an important issue that needs to be addressed for optimal economic cascade operation. This is particularly important for concurrent one-pot reactions, where coimmobilization might facilitate the immediate conversion of toxic or unstable intermediates, resulting in

Received: June 25, 2018
Published: July 27, 2018

ACS Publications © 2018 American Chemical Society

DOI: 10.1021/acssynbio.8b00274
ACS Synth. Biol. 2018, 7, 2282−2295

Downloaded via DUESSELDORF LIBRARIES on November 1, 2018 at 16:08:06 (UTC).
See https://pubs.acs.org/sharingguidelines for options on how to legitimately share published articles.

safer processes and preventing undesired side reactions.[11] Therefore, a variety of strategies have been implemented for enzyme coimmobilization, which often rely on principles found in nature.[10] Spatial organization/immobilization of multiple enzymes/proteins for the setup of *in vivo* and *in vitro* reaction cascades has been achieved by (i) direct fusion of enzymes,[12,13] (ii) coimmobilization on and in solid carrier materials,[14,15] (iii) scaffolding of enzymes by coupling to DNA,[16] RNA,[17] and proteins to control proximity,[18,19] and (iv) by encapsulation within vesicles,[20] protein containers,[21] and cellular compartments.[22] The latter approach utilizes biological, often naturally occurring, components such as liposomes,[20] membrane vesicles,[23] polymersomes, virus-like particles, protein shells, and bacterial microcompartments such as carboxysomes[24] and metabolosomes[22] for target protein encapsulation or binding.

An alternative protein-containing cellular structure, known to be present in both pro- and eukaryotes, are inclusion bodies (IBs) also called aggresomes in eukaryotes.[25] While IBs were traditionally regarded as intracellular waste reservoirs containing only unfolded and thus nonfunctional protein, our groups and others could recently show that enzymes and fluorescent proteins can retain some of their functionality when produced as IBs in *Escherichia coli*.[26−32] Among other approaches, the formation of such functional IBs (in case of enzymes called catalytically active IBs: CatIBs) can be induced by the molecular-biological fusion of the tetrameric coiled-coil domain of the cell-surface protein tetrabrachion (tetramerization domain of tetrabrachion, TDoT) of *Staphylothermus marinus*[33] to a target protein.[27] To the best of our knowledge, this strategy was so far only used for single fluorescent proteins and enzymes, whereas coexpression and colocalization of multiple proteins or enzymes to realize cascade reactions in CatIBs was not tested so far. This strategy has several advantages with regard to immobilization of different enzymes in a cascade. CatIBs are easy to produce in *E. coli*,[27] handling and storage is feasible as frozen suspension or in lyophilized form,[27] they often show increased stability compared to their soluble counterparts,[27] and they can easily be recycled to enable multiple reaction rounds due to their insolubility in both organic solvents and aqueous reaction systems.[27]

Given those advantages, we assessed the possibility to realize a synthetic reaction cascade by colocalization of two enzymes in CatIBs. We first evaluated the colocalization of two functional fluorescent proteins (FPs) within individual IB particles in an attempt to control the process by microscopy. When coproduced in *E. coli*, both FPs were colocalized forming functional fluorescent IBs (FIBs). Furthermore, the ratio of both FPs can be rationally tuned by the genetic design of the coexpression vector. Subsequently, this strategy was also tested with a two-step enzyme cascade for the production of (1*R*,2*R*)-1-phenylpropane-1,2-diol (PPD), a precursor of the calcium channel blocker diltiazem using colocalized CatIBs (Co-CatIBs) of the benzaldehyde lyase of *Pseudomonas fluorescens* (*Pf*BAL) and the alcohol dehydrogenase of *Ralstonia* sp. (RADH).

RESULTS AND DISCUSSION

Fusion of the TDoT Coiled-Coil Domain Allows the Production of Fluorescent Inclusion Bodies in *E. coli*. In order to test the colocalization of two functional proteins in IB particles (Co-IBs) we employed a monomeric version of the enhanced yellow fluorescent protein (eYFP, in the following designated as YFP) from *Aequorea victoria*[34,35] and the red-fluorescent protein mCherry from *Discosoma striata*,[36] as easy-to-detect model proteins with distinct spectral properties. In an initial set of experiments, the formation of fluorescent inclusion bodies (FIBs) of both target proteins by fusion of the aforementioned TDoT coiled-coil domain[33] was studied. Therefore, the TDoT domain, as IB-formation inducing element, was N-terminally fused to both FPs (Figure 1a). For

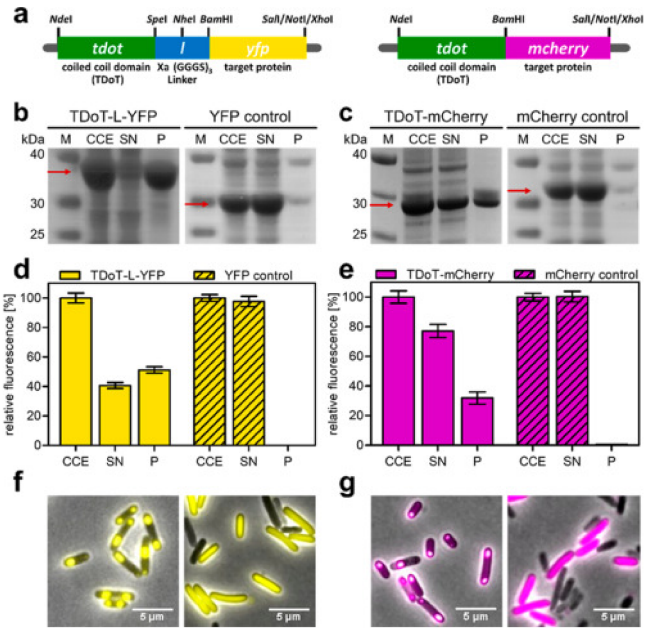


Figure 1. Formation of fluorescent IBs (FIBs) by applying the TDoT-fusion strategy. (a) Schematic illustration of the architecture of the constructed TDoT-L-YFP (left) and TDoT-mCherry (right) gene fusions. All expression vectors are modularly constructed, so that key elements, like the coiled-coil domain, the target gene, as well as the linker can easily be exchanged using the depicted restriction endonuclease recognition sites. The TDoT-L-YFP fusion additionally contained a linker polypeptide constituted by the cleavage site of the protease Factor Xa and a triple $(GGGS)_3$ motif. In TDoT-mCherry, the two protein modules are not fused *via* a longer linker but instead are only connected *via* two amino acids (glycine-serine) encoded by the *Bam*HI site employed for construction. (b,c) SDS-PAGE analysis illustrating the production of TDoT-FIBs (left) and the soluble controls (right) of (b) YFP and (c) mCherry. The red arrows mark the expected molecular mass of the respective (fusion) protein: TDoT-L-YFP: 34.6 kDa, TDoT-L-mCherry: 32.7 kDa, soluble YFP: 28.9 kDa, soluble mCherry: 28.6 kDa. After overexpression in *E. coli* BL21(DE3), cells were disrupted and the resulting crude cell extract (CCE) was separated into the soluble protein-containing supernatant (SN) and the IB-containing pellet (P) by centrifugation. (d,e) Fluorescence distribution in cellular fractions of *E. coli* cells producing TDoT FIBs (left) and the soluble controls (right) of (d) YFP and (e) mCherry. The fluorescence in the SN and P fraction is expressed relatively to the fluorescence of the CCE (set to 100%). (f,g) Microscopy images of TDoT-FIBs (left) and soluble controls (right) of (f) YFP- and (g) mCherry-producing *E. coli* BL21(DE3) cells. Images are shown as a composite of phase contrast and fluorescence. For experimental details, see the Methods section. Error bars correspond to the standard deviation of the mean derived from at least three biological replicates for FIBs and three technical replicates for the soluble controls.

amino acid sequences and DNA sequences of all constructs see Supporting Information (SI: Annex). Both gene fusions were cloned into pET28a and expressed from the P_{T7} promoter in *E. coli* BL21(DE3). After cell disruption, the crude cell extract,

DOI: 10.1021/acssynbio.8b00274
ACS Synth. Biol. 2018, 7, 2282−2295

the soluble protein-containing supernatant, and the inclusion-body-containing pellet were separated by centrifugation and analyzed by sodium dodecyl sulfate polyacrylamide gel electrophoresis (SDS-PAGE), fluorescence spectroscopy and microscopy (Figure 1b–g; left panels). A significant fraction of both fusion proteins was found in the insoluble, IB-containing, pellet fraction (Figure 1b and c; left panels each). About 51% (TDoT-L-YFP) and 32% (TDoT-mCherry) of the fluorescence detected in the crude cell extract was found in the corresponding pellet fractions (Figure 1d,e; left side of graph; see also Table S1). In contrast to previous studies, where TDoT was used as a CatIB-formation-inducing tag,[27] particularly TDoT-mCherry was also detected in significant amounts in the soluble fraction (Figure 1e; left side of graph), which most likely relates to the high solubility of this target protein. As soluble controls, gene fusions of both FPs without the TDoT-tag, were produced and analyzed under identical conditions (Figure 1b–g; right panels). Here, in contrast to TDoT-L-YFP and TDoT-mCherry, the majority of the fluorescence was found in the supernatant containing the soluble protein, with almost no detectable fluorescence in the pellet (Figure 1d,e; right panels). These results were further supported by SDS-PAGE analyses (Figure 1b,c; right panels). TDoT-L-YFP and TDoT-mCherry FIBs were visualized by fluorescence microscopy, with the corresponding images showing the formation of refractive, dense particles that accumulate preferentially at the cell poles in *E. coli* (Figure 1f,g; left panels), which is typical for intracellular IBs.[37] In contrast, the corresponding control strains producing soluble YFP and mCherry displayed an equal distribution of the fluorescence signal within the cytoplasm (Figure 1f,g; right panels). Hence, our analyses unequivocally prove that the previously described TDoT-fusion strategy to induce CatIB formation[26,27] can be transferred easily to fluorescent proteins to enable the formation of FIBs.

Two Fluorescent Proteins Can Be Colocalized in Inclusion Bodies. To allow easy verification of successful colocalization, the gene fusions encoding for TDoT-L-YFP and TDoT-mCherry were coexpressed in *E. coli* using four different coexpression constructs. The different coexpression constructs were designed to allow for the rational tuning of the YFP to mCherry ratio within IBs. Therefore, the number of P_{T7} promotors and the series of the genes were varied (see Figure 2a). To this end, we generated two coexpression vector sets (Figure 2a); one, where both gene fusions are under the control of two independent P_{T7} promoters (pDouble-A and pDouble-B, in the following designated as constructs A and B), and a second where both gene fusions are under the control of only one P_{T7} promoter, localized in front of the first gene fusion (pDouble-C and pDouble-D, in the following designated as constructs C and D). In the constructs A and C, the TDoT-L-YFP encoding gene fusion was localized at the 5′ end of the two-gene operon followed by the gene fusion encoding TDoT-mCherry. In constructs B and D, this order was reversed (see Figure 2a). All constructs contained a T_7-terminator sequence behind the second gene. Hence, in case of the constructs A and B two different transcripts are expected to be produced by the T_7 RNA polymerase: a long transcript that comprises both gene fusions on a single mRNA and one that comprises only the rear gene fusion. This should result in a ratio of 67 to 33% for the rear gene fusion over the gene fusion located at the 5′ end. For the constructs C and D, only one long transcript comprising both gene fusions should be generated, resulting in a 50 to 50% ratio (see also Figure 2a for details). In order to

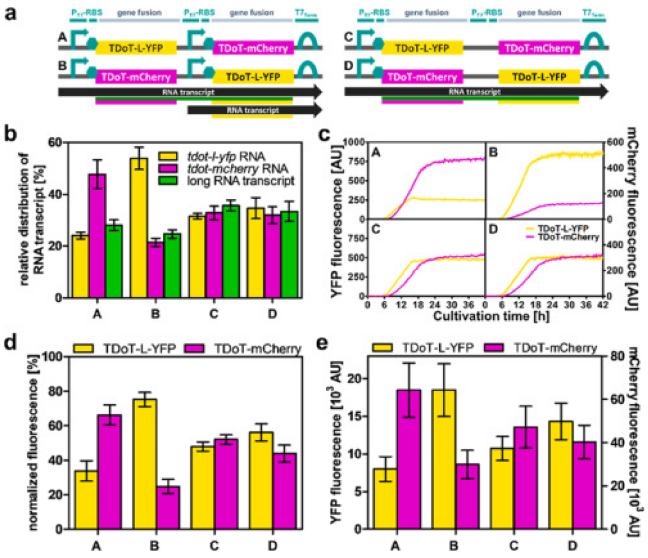


Figure 2. Evaluation of the coexpression strategy to produce Co-FIBs. (a) Schematic illustration of the architecture of the coexpression constructs A to D, with the gene fusions encoding for TDoT-L-YFP (yellow) and TDoT-mCherry (pink), along with the P_{T7} promoter elements (blue arrows), the ribosome binding site (blue hexagon) and the T_7 terminator (blue semicircle). Below the drawing, the theoretically possible transcripts for B and D are shown as black arrows. (b) Relative distribution of RNA transcripts of *tdot-l-yfp* (yellow), *tdot-mcherry* (pink), and the long RNA transcript of both genes (green). The amount of transcript was quantified using quantitative real-time PCR (qPCR) after standard expression in *E. coli* BL21(DE3) for 21 h at 15 °C. Error bars correspond to the standard deviation of the mean derived from three biological replicates. (c) Online fluorescence of YFP (yellow, left ordinate) and mCherry (pink, right ordinate) during cultivation of *E. coli* BL21(DE3) strains carrying the coexpression constructs A to D, using a BioLector prototype.[43] During cultivation, the temperature was reduced from 37 to 15 °C 3 h after inoculation. Results are given as mean of a biological triplicate with standard deviation. (d) Normalized fluorescence within the Co-FIBs A to D after standard expression in *E. coli* BL21(DE3) and cell disruption. The normalized YFP and mCherry fluorescence was calculated taking into account the different fluorescence quantum yields and extinction coefficients of the respective fluorescent reporter proteins.[36,38] The relative distribution of YFP and mCherry fluorescence in the crude cell extract, the soluble protein-containing fraction, and the insoluble IB-containing pellet fraction is shown in Figure S1d. Error bars correspond to the standard deviation of the mean derived from at least three biological replicates. (e) YFP and mCherry fluorescence of IB particles was detected using fluorescence microscopy. For each construct, over 3000 FIBs were analyzed using the Fiji software.[44,45] The error bars correspond to the standard deviation of the mean derived from three biological replicates, with at least 1000 FIBs analyzed per replicate.

test this assumption, the transcript levels of the TDoT-L-YFP and TDoT-mCherry encoding gene fusions were quantified for the constructs A to D using quantitative real-time PCR (qPCR) (Figure 2b). Primers for qPCR were designed to enable the detection of the individual TDoT-L-YFP (yellow bars in Figure 2b) and TDoT-mCherry (magenta bars in Figure 2b) transcripts as well as the long transcript comprising both gene fusions (green bars in Figure 2b). As theoretically expected, for construct A and B about twice the amount of transcript was detected for the corresponding rear gene fusion, while comparable transcript levels were observed for constructs C and D (Figure 2b). As expected, the amount of the long transcript

DOI: 10.1021/acssynbio.8b00274
ACS Synth. Biol. 2018, 7, 2282–2295

was in all cases similar to the amount of transcript of the gene fusion localized at the front (Figure 2b).

To evaluate whether the differences in transcript levels observed for the four different coexpression constructs are directly reflected at the protein level, YFP and mCherry fluorescence was measured online during *E. coli* cultivations using a BioLector device (see Methods for details) (Figure 2c). Due to the different quantum yields and extinction coefficients of YFP and mCherry, the levels of YFP[38] and mCherry[36] fluorescence can only be directly compared for the same FP between different constructs, but not between YFP and mCherry. For all constructs, YFP as well as mCherry fluorescence could be detected. For constructs C and D, the level of YFP and mCherry fluorescence was very similar. Compared to construct C and D, higher and lower mCherry levels were observed for construct A and B, respectively. For YFP, the exact opposite behavior was observed. Here, compared to construct C and D, lower (construct A) and higher (construct B) YFP fluorescence was detectable. Although a quantitative comparison between the YFP and mCherry levels of the different constructs was not possible due to the reasons mentioned above, we nevertheless observed the same overall trend as seen on the transcript level. The scattered light signal (corresponding to the optical density of the culture), did not reveal the typical exponential growth, which is probably due to the temperature shift from 37 to 15 °C, applied during cultivations, which slowed cell growths down (Figure S1a). Nevertheless, all tested strains showed a very similar growth behavior, ruling out that the differences in YFP and mCherry levels are due to different cell growth. Interestingly, we consistently observed the rise of mCherry fluorescence after YFP fluorescence, which is consistent with the longer maturation time reported for the mCherry fluorophore compared to the YFP fluorophore.[39−41]

In order to quantitatively compare the different constructs and validate whether FIBs with both YFP and mCherry fluorescence were formed, we prepared the corresponding Co-FIBs. Therefore, *E. coli* strains carrying the coexpression constructs A−D were grown under identical conditions as described for single YFP and mCherry FIBs. As demonstrated in the SI (Figure S1b), the corresponding production cultures showed different colors, indicating different YFP and mCherry levels. Subsequently, cells were disrupted to obtain a crude cell extract, and the soluble protein-containing fraction was separated from the insoluble IB-containing pellet fraction by centrifugation. As observed for single YFP and mCherry FIBs, large amounts of target protein were present in the insoluble IB-containing pellet fraction (Figure S1c). Please note that TDoT-L-YFP and TDoT-mCherry have similar molecular mass (34.6 and 32.7 kDa, respectively) and isoelectric points[42] (pI) (YFP: 5.32; mCherry: 5.24) so that they cannot be separated by SDS-PAGE, isoelectric focusing (IEF) gels or 2D-PAGE. Since both YFP and mCherry fluorescence could be detected in the insoluble IB-containing pellet fraction, the signals observed in the corresponding SDS-PAGE analyses were assumed to contain both target proteins (Figure S1c). In contrast to the corresponding single FIBs, where the majority of the fluorescence was detected in the insoluble IB-containing fraction (Figure 1d and e), larger proportions of the corresponding functional target proteins were observed in the soluble protein-containing supernatant of the Co-FIBs producing *E. coli* strains (Figure S1d and Table S1). This effect was more pronounced for YFP than for mCherry. Interestingly, while for the single FIBs about 50% of functional TDoT-L-YFP was found in the IB-containing pellet fraction, for the Co-FIBs the amount within the pellet drops to approximately 30%. Coincidently, the amount of functional TDoT-mCherry in the pellet was only about 30% for the single FIBs, but was increased to about 60% in the Co-FIBs (Figure S1d). This hints at stabilization of TDoT-mCherry in Co-FIBs in the presence of TDoT-L-YFP, *e.g.*, supported by intermolecular interactions of the two structurally similar target proteins.

To assess the relative content of functional TDoT-L-YFP and TDoT-mCherry in the corresponding Co-FIBs in a semi-quantitative manner, we normalized the measured fluorescence intensity of YFP and mCherry by the YFP and mCherry specific extinction coefficients and fluorescence quantum yields. This yielded normalized fluorescence values, which take the different fluorescence brightness of the two reporters into account[36,38] (Figure 2d) and hence provide a measure of their relative stoichiometry. Here, as in the corresponding qPCR analyses (Figure 2b) the observed ratios are close to the theoretically expected values. Thus, while for constructs A and B about 66% protein of the rear gene fusion (TDoT-mCherry in construct A, TDoT-L-YFP in construct B) is produced in functional form, the ratio of TDoT-L-YFP and TDoT-mCherry in constructs C and D is very similar (about 50% for both targets) (Figure 2d). Taken together, this proves that the trend observed in qPCR analyses also holds at the level of the functional target proteins.

The analyses presented so far, although being indicative of FIB formation, do not directly and unequivocally prove the formation of intracellular Co-FIBs. Therefore, to visualize Co-FIB formation *in vivo*, fluorescence microscopy images of *E. coli* cells carrying the four coexpression constructs were taken (Figure 3), with both phase contrast, as well as using specific excitation and emission filters for YFP and mCherry. To this end, *E. coli* BL21(DE3) cells, right before harvesting under standard growth conditions (see Methods section), were analyzed. The corresponding fluorescence images showed YFP and mCherry fluorescence in every single inclusion body. This unequivocally proves that the coexpression of two FIB-forming gene fusions in *E. coli* results in the coexpression and colocalization of the target protein in IBs (Co-FIBs). Furthermore, as expected for IB producing cells, the corresponding fluorescent particles are localized at the cell poles. This observation appears to be contradictory to the above presented fluorescence measurements, in which a significant amount of fluorescence was detected in the soluble protein-containing supernatant after cell disruption (Figure S1d). This suggests increased solubility of the respective fusions and/or that the target proteins are at least partially solubilized from the FIBs during cell disruption. To assess the differences between the four constructs, the fluorescence intensity of YFP and mCherry was quantified within individual FIBs using the Fiji software[44,45] (Figure 2e). As already mentioned for the above-described *in vivo* growth comparison (Figure 2c), and due to technical issues (different excitation and emission filter sets for the detection of YFP and mCherry), a direct comparison of the YFP and mCherry fluorescence levels within one Co-FIB is not possible. However, YFP and mCherry levels, compared between the four different coexpression constructs match the theoretical assumptions and are in line with all other analyses (Figure 2b-d). In addition, we also recorded videos of *E. coli* strains carrying the four different coexpression constructs to visualize the formation of Co-FIBs during microfluidic cultivation (see Figure S2 and Videos S1 and S2). Here, apart from the apparent colocalization, the time course of YFP and

DOI: 10.1021/acssynbio.8b00274
ACS Synth. Biol. 2018, 7, 2282−2295

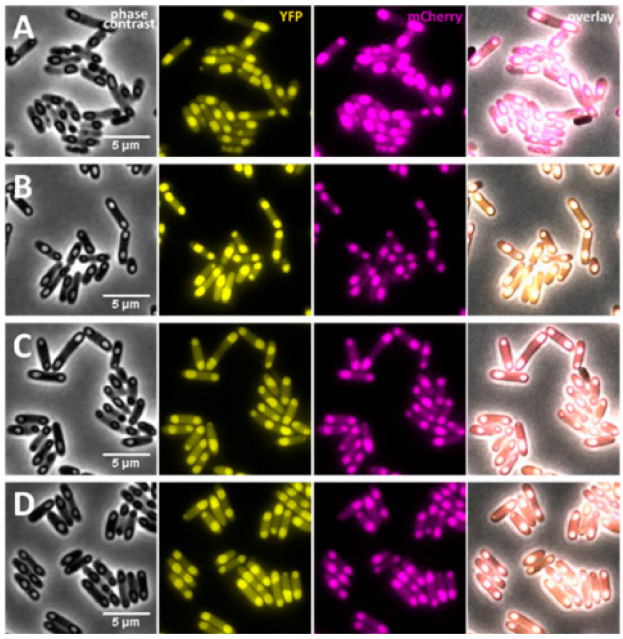


Figure 3. Coexpression and colocalization of TDoT-L-YFP and TDoT-mCherry in *E. coli*. Fluorescence microscopy images of *E. coli* BL21(DE3) cells carrying the four coexpression constructs A–D (construct identity given in the upper left corner of the phase contrast image), after standard cultivation. All strains were grown under standard growth conditions as described in the Methods section. Per row: from left to right: phase constrast, YFP-specific fluorescence, mCherry-specific fluorescence, and overlay image. Note here, that for better visualization the mCherry intensity of construct A, and the YFP intensity of construct B is reduced to 50% in the single fluorescence images. The overlay image is not modified. Experimental details are given in the Methods section.

mCherry maturation becomes visible, again revealing a longer maturation time of the mCherry fluorophore[39−41] (compare YFP and mCherry channels in Figure S2 and see Videos S1 and S2), as also discussed above (Figure 2c). As there was no detectable difference in morphology and growth behavior of the different *E. coli* strains (Figure S1a), an influence of the vector design on the life cycle of the bacterium can be excluded.

In conclusion, by using several complementary *in vivo* and *in vitro* experiments we could unequivocally demonstrate that two fluorescent reporter proteins colocalize in functional form within IB particles (Co-FIBs), thus allowing for *in vivo* coimmobilization. Moreover, the ratio of the two proteins within the particles can be adjusted by the vector design. Taken together, this highlights the general feasibility to realize a two-enzyme cascade in IBs by coimmobilization of two enzymes in IB particles, thereby enforcing spatial proximity, and enabling easy production as well as recycling of the resulting biocatalyst. A related, recently presented strategy employed leucine-zipper tags to target multiple soluble enzymes to the surface of bacterial IBs for the production of 1-butanol from glucose.[46] While such a strategy clearly has advantages, certain drawbacks have to be considered. (i) It is at present unclear, how stable the leucine-zipper (bait-prey) interaction is with regard to the choice of the reaction system (*i.e.*, in the presence of organic (co)-solvents), which could result in leaching of the enzyme from the IB-carrier. (ii) The stability of surface-immobilized soluble enzymes should be considerably lower compared to enzymes immobilized in IBs (CatIBs), *i.e.*, due to the direct exposure to the reaction medium. (iii) The relative enzyme load per IB particle is difficult to control by genetic means, as both gene expression levels as well as leucine-zipper bait-prey affinities will play a role. Here, our strategy, which relies on the colocalization of enzymes within IB particles appears advantageous, as CatIBs have earlier been shown to be stable in buffer-saturated organic solvents and not prone to leaching in aqueous reaction systems.[27] As demonstrated here with two fluorescent proteins, the relative ratio of two target proteins can easily be controlled by the design of the coexpression construct. Compared to other tuning strategies,[47,48] the here employed genetic design is rather simplistic and should be considered as a starting point for further improvement. In the future, *e.g.*, the use of different, tightly controlled, inducible promotors and differently strong ribosome binding sites (RBS) for coexpression could hereby provide the required fine-control, to optimize cascade performance. Due to the modular nature of our expression constructs, such modifications can easily be implemented.

Proof-of-Concept Realization of a Two-Enzyme Cascade. To realize a synthetic two-enzyme reaction cascade using the presented coimmobilization strategy, the results obtained for (Co)-FIBs have to be transferred to (Co)-CatIBs by utilizing suitable (co)-expressions constructs (Figure 4a). As target reaction we choose the two-enzyme one-pot synthesis of (1*R*,2*R*)-1-phenylpropane-1,2-diol (PPD) from benzaldehyde and acetaldehyde (Figure 4b). PPD is an important building block for the production of pharmaceuticals, such as the calicum channel blocker diltiazem, used as a vasodilative in angiology diseases.[49] The cascade reaction can be realized using two enzymes, namely the thiamine diphosphate-dependent benzaldehyde lyase from *Pseudomonas fluorescence* (*Pf*BAL),[50] which catalyzes the carboligation of benzaldehyde **1** and acetaldehyde **2** to (*R*)-2-hydroxy-1-phenylpropanone (HPP, **3**), and an alcohol dehydrogenase from *Ralstonia* sp. (RADH),[51,52] catalyzing the reduction of HPP **3** to PPD **4**. RADH requires the cofactor nicotinamide adenine dinucleotide phosphate (NADPH) which provides the redox equivalents for the reduction of the substrate. Since NADPH is consumed during the reaction, cofactor regeneration is crucial for economical performance of the cascade. In our setup, this is envisioned to be achieved by the RADH in a cosubstrate-coupled approach employing the oxidation of benzyl alcolhol **5** to benzaldehyde **1**, thereby regenerating the benzaldehyde substrate, which is used in the carboligation step.

PfBAL and RADH Can Be Produced as CatIBs and Co-CatIBs. CatIBs of both target enzymes constitute the prerequisite for the realization of the above-described cascade with colocalized catalytically active IBs (Co-CatIBs). So far, CatIB formation had been demonstrated neither for *Pf*BAL nor for RADH. Both soluble enzymes have earlier been extensively characterized, but might present a challenge for the CatIB strategy, since both are cofactor-dependent tetrameric enzymes. As inferred from the corresponding crystal structures (*Pf*BAL: PDB-ID: 2AG0,[53] RADH: PDB-ID: 4BMS[54]) the minimal functional units for *Pf*BAL and RADH are a dimer and monomer, respectively. While *Pf*BAL requires magnesium ions and thiamine diphosphate as cofactors, the RADH needs calcium ions[51] and NADPH. Together with a subunit size of 60.0 kDa for *Pf*BAL and 26.7 kDa for RADH, both targets appear challenging for the CatIB approach, as both enzymes need to be (at least partially) correctly folded within the IBs particles to achieve catalytic activity.

As a proof-of-concept for the feasibility of the CatIB strategy, both enzymes were fused to TDoT employing a flexible linker

DOI: 10.1021/acssynbio.8b00274
ACS Synth. Biol. 2018, 7, 2282−2295

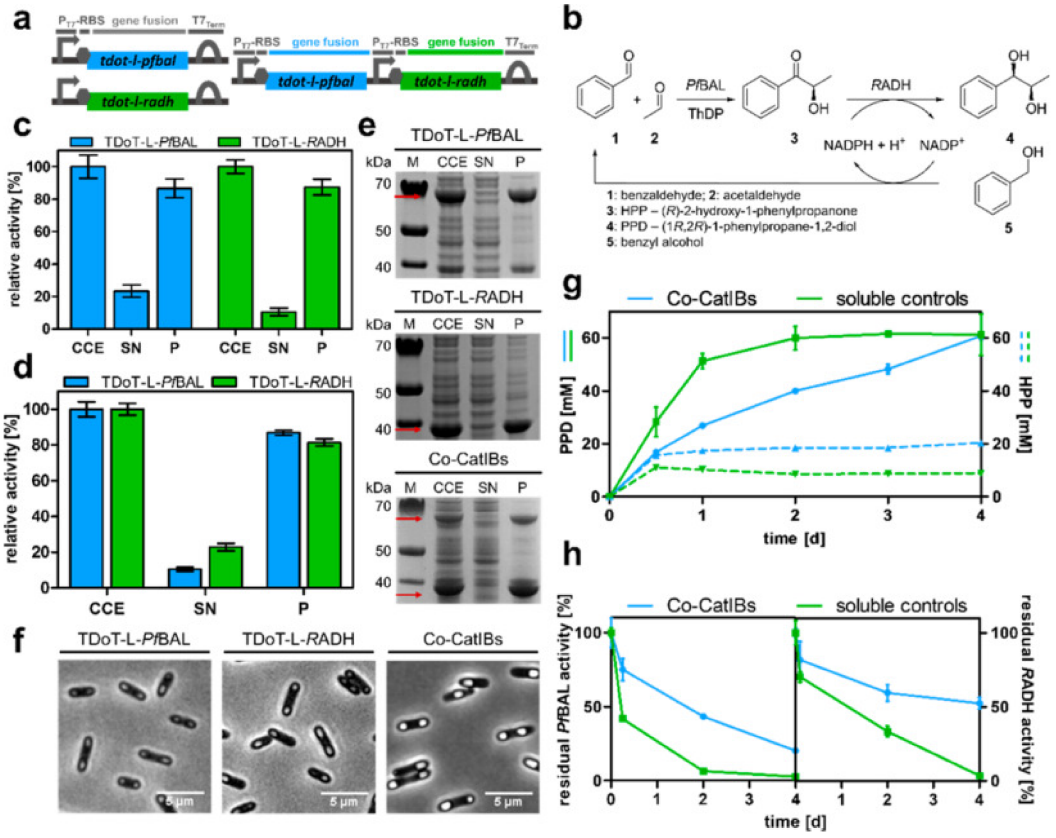


Figure 4. Evaluation of *Pf*BAL and *R*ADH in (Co-)CatIBs and proof-of-concept two-enzyme one-pot cascade reaction. (a) Schematic illustration of the architecture of the TDoT-L-*Pf*BAL and TDoT-L-*R*ADH gene fusion as single expression construct for CatIB formation (left) and as coexpression construct for the production of the corresponding Co-CatIBs (right). Displayed are the P_{T7} promoters (arrows), the ribosome binding sites (hexagons) and the T_7 terminator (semicircle). (b) Envisioned two-enzyme cascade reaction. In the first step, the *Pf*BAL was chosen for the carboligation of benzaldehyde 1 and acetaldehyde 2 to yield the intermediate (*R*)-2-hydroxy-1-phenylpropanone (HPP, 3). In the second step, HPP is reduced by *R*ADH to (1*R*,2*R*)-1-phenylpropane-1,2-diol (PPD, 4), requiring NADPH as a cofactor. Regeneration of the NADPH cofactor is achieved by oxidation of benzyl alcohol 5 as cosubstrate for the *R*ADH. The latter reaction also results in the regeneration of the benzaldehyde substrate 1 for the *Pf*BAL reaction.[65] (c,d) TDoT-L-*Pf*BAL and TDoT-L-*R*ADH activity distribution observed for single enzyme CatIBs (c) and the corresponding two-enzyme Co-CatIBs (d). After overexpression of the gene fusions in *E. coli* BL21(DE3), cells were disrupted and the resulting crude cell extract (CCE) was separated into the soluble protein-containing supernatant (SN) and the insoluble IB-containing pellet (P) fraction by centrifugation. The activity in SN and P fractions is given relative to the activity found in the CCE (set to 100%). Activities were determined as described in the Methods section. Error bars correspond to the standard deviation of the mean derived from three biological replicates. (e) SDS-PAGE analysis illustrating the production of TDoT-L-*Pf*BAL (66.5 kDa) and TDoT-L-*R*ADH (34.3 kDa), indicated by red arrows, in single CatIBs and Co-CatIBs. (f) Phase contrast microscopy images of TDoT-L-*Pf*BAL and TDoT-L-*R*ADH producing *E. coli* BL21(DE3) as single CatIBs and Co-CatIBs. (g) Production of (1*R*,2*R*)-1-phenylpropane-1,2-diol (PPD, 4, solid lines) and the intermediate (*R*)-2-hydroxy-1-phenylpropanone (HPP, 3, dotted lines) performed with TDoT-L-*Pf*BAL and TDoT-L-*R*ADH Co-CatIBs (blue) or with soluble controls (green) under the same conditions. For experimental details see Methods section. (h) Stability of *Pf*BAL (left) and *R*ADH (right) in Co-CatIBs (blue) and in the soluble control (green) under process conditions. Error bars in (g) and (h) correspond to the standard deviation of the mean derived from the three independently performed cascade reactions using the same CatIB/enzyme lyophilizate.

(Figure 4a, left side of panel) as described for the TDoT-L-YFP fusion. Both gene fusions were expressed as single CatIBs in *E. coli* BL21(DE3). As described for FIBs, cells were lysed and the crude cell extract (CCE) was separated into the soluble protein-containing supernatant (SN) and insoluble IB-containing pellet (P) by centrifugation. As before, the activity in SN and P fraction is given relative to the activity observed in the CCE. Both the TDoT-L-*Pf*BAL and TDoT-L-*R*ADH gene fusions are produced predominantly in CatIBs (Figure 4c and Figure 4e for the corresponding SDS-PAGE analyses). In both cases about 88% of the total TDoT-L-*Pf*BAL and TDoT-L-*R*ADH activity detected in the CCE was found in the insoluble IB-containing pellet fraction (see also Table S2). In contrast, the corresponding control constructs, lacking the TDoT domain and the linker region, were largely soluble (Figure S3). This suggests that the previously presented CatIB strategy is also applicable to complex cofactor-dependent enzymes, as was also demonstrated previously for the thiamine diphosphate-dependent enzyme MenD of *E. coli*.[27] For most enzymes, immobilization results in a certain loss of catalytic activity. To address this issue, we determined the catalytic constant (k_{cat}) of the single TDoT-L-*Pf*BAL and TDoT-L-*R*ADH CatIBs in comparison to the respective purified soluble enzymes (Table 1). Initial rate activities were determined using the assays shown in Figure S4. Additionally, we also measured the protein content of the CatIB lyophilizates and determined the yields for the produced CatIBs (Table 1).

Compared to purified soluble *Pf*BAL and *R*ADH, the corresponding CatIBs only retain about 1% and 2% activity, respectively. However, this low activity retention is at least partially compensated by a 5-fold higher catalyst yield for CatIBs

DOI: 10.1021/acssynbio.8b00274
ACS Synth. Biol. 2018, 7, 2282−2295

Table 1. Comparison of Activity, Protein Content and Catalyst Yield for (Co-)CatIBs and the Corresponding Purified Soluble Enzymes[a]

protein		activity [U mg^{-1}][b,d]	k_{cat} [s^{-1}][c,d]	residual activity [%][e]	protein content of lyophilizate [%]	yield [glycophillizate/100 g cells]
CatIBs	*Pf*BAL	0.50 ± 0.07	0.77 ± 0.12	1.0	71.9 ± 4.5	8.8 ± 1.0
	*R*ADH	0.08 ± 0.01	0.05 ± 0.01	2.0	84.6 ± 3.9	9.7 ± 1.7
Co-CatIBs	*Pf*BAL	0.61 ± 0.24	2.56 ± 0.52	3.3	77.5 ± 1.3	9.0 ± 0.4
	*R*ADH	0.04 ± 0.003	0.04 ± 0.003	1.4		
soluble	*Pf*BAL	58.18 ± 1.72[f]	76.65 ± 2.26[f]	100	74.9 ± 0.3[d]	1.7 ± 0.7
	*R*ADH	1.79 ± 0.02[e,f]	2.77 ± 0.04[f]	100	28.7 ± 0.1[d]	1.9 ± 1.1

[a]Parameters for the calculation of the protein content are listed in Table S4. For the Co-CatIBs a weighted molecular mass as well as a weighted extinction coefficient was calculated, based on the densitometric analysis of the corresponding SDS gels (Figure S5). [b]Per mg lyophilizate. [c]Taking into account the protein content of the lyophilizate, referring to 1 $\mu mol_{product}$ s^{-1} (per subunit). [d]*Pf*BAL activity determined for the carboligation of 3,5-dimethoxy benzaldehyde (DMBA) to (*R*)-(3,3′,5,5′)-tetramethoxy benzoin (TMBZ) (Figure S4a), *R*ADH activity determined for the reduction of cyclohexanone to cyclohexanol (Figure S4b). [e]Calculated on the basis of k_{cat}. [f]Derived from three technical replicates of one purified protein preparation.

compared to the purified enzymes. The CatIB lyophilizates consisted of 72 to 85% protein besides other cellular components like lipids, while the lyophilizates of the purified protein contained between 29% (*R*ADH) and 75% (*Pf*BAL) protein besides buffer salts, respectively (Table 1). Compared to the protein content of various commercial enzyme preparations, for example determined for various lipase preparations (0.5 to 30%),[55] the high protein content of CatIBs is clearly advantageous for application. With regard to morphology and properties, CatIBs are best compared to cross-linked enzyme aggregates (CLEAs), which are prepared by precipitation and cross-linking of (partially) purified proteins or crude cell extracts.[56] A brief, by no means comprehensive, review of the more recent CLEA literature revealed residual CLEA activities between 3.5% and 90% (Table S3).[55,57−61] It should however be noted that in those studies often the specific activity of the starting enzyme preparation (*e.g.*, cell extracts) is considered as a reference to calculate the residual activity of the CLEA preparation. Thus, if selective precipitation of the target enzyme results in CLEA formation, which is considered one of the advantages of CLEAs,[56] the resulting immobilizate will be purer than the starting preparation and hence the residual activities will likely be overestimated. For CatIBs, as intracellularly formed aggregates, such a comparison is not possible.

To enable the coimmobilization of *Pf*BAL and *R*ADH in CatIBs, both enzymes have to be produced by coexpression of the respective TDoT-gene fusions in *E. coli*. The higher activity of the soluble *Pf*BAL (k_{cat} = 335 s^{-1} for HPP formation[62]) compared to the soluble *R*ADH (k_{cat} = 160 s^{-1} for PPD formation[52]), suggests that it might be beneficial to generate Co-CatIBs containing excess *R*ADH to limit accumulation of the HPP intermediate. Please note that for optimal cascade set up, the kinetic parameters of the two enzymes would have to be considered.[63,64] Those, however, would ideally have to be determined under process conditions, *i.e.*, considering the presence of reaction intermediates and the cosubstrate used for cofactor regeneration, both of which continuously change during the cascade reaction. As we attempted here to demonstrate proof-of-concept, we deem such complex kinetic characterizations beyond the scope of the present contribution and therefore designed our Co-CatIB construct based on the above-described, admittedly simplistic, rate matching argument. We therefore generated a coexpression construct, analogous to construct A, which was previously used for the coexpression of YFP and mCherry as Co-FIBs (Figure 4a; right side of panel). This construct carried the gene fusions encoding for TDoT-L-*Pf*BAL and TDoT-L-*R*ADH under the control of two independent P_{T7} promoters with the TDoT-L-*R*ADH encoding gene fusion at the rear end with an expected 33% to 66% ratio of *Pf*BAL and *R*ADH. TDoT-L-*Pf*BAL/TDoT-L-*R*ADH Co-CatIBs were prepared in an identical manner as described for single TDoT-L-*Pf*BAL and TDoT-L-*R*ADH CatIBs and the activity for *Pf*BAL and *R*ADH was measured in crude cell extract, the soluble protein-containing supernatant, and the insoluble IB-containing pellet fraction (Figure 4d), with similar results as observed for the corresponding single CatIBs (Figure 4c). Both TDoT-L-*Pf*BAL and TDoT-L-*R*ADH were mainly produced in the insoluble IB-containing pellet fraction with activities amounting to 87 and 81% of the total activity of the crude cell extract, respectively (Figure 4d). Moreover, the corresponding SDS-PAGE revealed that, as expected from the employed vector design, more TDoT-L-*R*ADH accumulates than TDoT-L-*Pf*BAL (Figure 4e, lowest panel, marked by red arrows). To infer the relative distribution of *Pf*BAL and *R*ADH in Co-CatIBs, we analyzed SDS gels densitometrically (for an exemplary analysis see Figure S5). This yields a relative stoichiometry of 32 ± 1% (*Pf*BAL) to 68 ± 1% (*R*ADH), which is very close to the theoretically expected values. Based on this distribution we estimated the specific activity of both enzymes in the corresponding Co-CatIBs (Table 1). While, compared to purified soluble *Pf*BAL and *R*ADH, the two enzymes in the Co-CatIBs retained 3.3% (*Pf*BAL) and 1.4% (*R*ADH) activity, the corresponding single CatIBs retained about 1% (*Pf*BAL) and 2% (*R*ADH) activity (Table 1). Thus, *Pf*BAL appears to be a little more active in Co-CatIBs. In terms of protein content and catalyst yield the Co-CatIBs resemble the corresponding single CatIBs (Table 1). Microscopy images of the corresponding CatIB producing cells unequivocally proved the formation of intracellular IBs (Figure 4f), as for both single TDoT-L-*Pf*BAL and TDoT-L-*R*ADH CatIBs as well as for the corresponding Co-CatIBs intracellular IB particles could be detected as refractive, dense particles at the cell poles (Figure 4f).

We next tested whether a functional two-enzyme cascade can be realized using TDoT-L-*Pf*BAL/TDoT-L-*R*ADH Co-CatIBs. An initial experiment was conducted under nonoptimized conditions in which we simply used 6 mg mL^{-1} of the Co-CatIB catalyst (2.50 U *Pf*BAL, 165 mU *R*ADH) and monitored reaction progress in terms of (1*R*,2*R*)-1-phenylpropane-1,2-diol (PPD, **4**) product formation and accumulation of the (*R*)-2-hydroxy-1-phenylpropanone (HPP, **3**) intermediate. Cascade reactions were performed in an aqueous buffered reaction system containing the two substrates benzaldehyde **1** (15 mM) and

DOI: 10.1021/acssynbio.8b00274
ACS Synth. Biol. 2018, 7, 2282−2295

acetaldehyde **2** (150 mM) as well as benzyl alcohol **5** (120 mM) as a cosubstrate for NADPH regeneration. Oxidation of the latter will deliver additional benzaldehyde for the first step.[65] Benzaldehyde was initially kept at 15 mM to start the reaction. The cascade reaction, carried out over 9 days (Figure S6), yielded a final PPD concentration of about 25 mM, which corresponds to 18% of the theoretical possible yield, as calculated based on the initial concentrations of benzaldehyde (15 mM) and benzyl alcohol (120 mM). During the course of the reaction, we observed a rapid accumulation of the HPP intermediate, reaching a concentration of about 20 mM after 9 days of reaction time. This indicates that the *R*ADH reaction is the limiting step of the cascade. We therefore performed a second experiment in which the catalyst load was increased to 10.6 mg mL^{-1} (7.33 U *Pf*BAL and 500 mU *R*ADH) and the initial concentration of the benzaldehyde substrate was decreased to 10 mM. As reference, we carried out the same cascade reaction with equivalent amounts of soluble purified *Pf*BAL and *R*ADH (in terms of activity units). The formation of the HPP reaction intermediate and the final PPD product was followed over 4 days. Compared to the Co-CatIBs (Figure 4g, blue line), PPD formation was faster for the soluble control (Figure 4g, green line), reaching a plateau within 2 days of reaction time. In contrast, product formation by Co-CatIBs proceeded almost linearly over the reaction time, reaching very similar final product levels (Figure 4g, blue line) of about 60 mM, which corresponds to 47% of the theoretical possible yield, based on the initial concentrations of benzaldehyde (10 mM) and benzyl alcohol (120 mM). The slower reaction progress observed in Co-CatIBs might hereby hint at diffusional limitation for substrate transport into the CatIBs, as was also suggested to be the case for CatIBs of a hydroxynitrile lyase of *Arabidopsis thaliana*.[27] In both cases we observed the formation of the HPP intermediate which reaches its maximum after 1 day, after which the HPP levels remained constant, with the final values being slightly higher for the Co-CatIBs compared to the soluble control (Figure 4g, dashed blue and green lines). Additionally, we also determined the stability of *Pf*BAL (Figure 4h, left) and *R*ADH (Figure 4h, right) in Co-CatIBs (blue lines) and in the corresponding soluble control reactions (green lines) under process conditions. To this end, samples were withdrawn at day 0, 2, and 4 of the reaction and the residual *Pf*BAL and *R*ADH activity was measured using orthogonal assays. Here, *Pf*BAL and *R*ADH show clearly higher stability in Co-CatIBs than in soluble form, revealing about 7- (*Pf*BAL) and 15-fold (*R*ADH) higher residual activities after 4 days of reaction time (Figure 4h). The same cascade reaction has previously been realized using whole-cells in a microaqueous reaction system.[66,67] Compared to the presented Co-CatIB approach, the authors observed superior yields.[66,67] However, in these studies methyl *tert*-butyl ether was employed as reaction medium, which enables much higher substrate loads. Additionally, to increase the final product yield, a pulsed mode was used, where acetaldehyde was added to the reaction in defined intervals.[66,67] Due to the low stability of the isolated *R*ADH in organic solvents, and the decreased activity in the presence of cosolvents,[65] we did not use microaqueous solvents for the cascade using Co-CatIBs.

Although there is room for improvement, with the here presented proof-of-concept cascade our studies demonstrate that two-enzyme cascades can be realized using Co-CatIBs of the respective enzymes. Moreover, coproduction of both enzymes as Co-CatIBs simplifies catalyst production and immobilization, which in case of Co-CatIBs occurs simultaneously. This in turn contributes to the sustainable management of resources by reducing catalyst production costs, as, *i.e.*, once expression levels and cascade performance have been optimized for Co-CatIBs only the production of a single batch of cells is necessary for catalyst production. Optimization of this cascade is currently underway in our laboratory. Potential optimization parameters include reaction pH, addition of organic cosolvents, the use of microaqueous organic media, pulsed mode operation, and construct optimization.

CONCLUSIONS

In the present contribution, we aimed to demonstrate the setup of a synthetic two-enzyme cascade consisting of catalytically active inclusion bodies (CatIBs) employing two complex enzymes as target. The general strategy was initially evaluated using two easy-to-detect fluorescent reporter proteins, with various complementary methods unequivocally proving coexpression of the corresponding gene fusions and colocalization of the two target proteins in individual IB particles. On the basis of the employed coexpression vector design, the relative ratio of the two target proteins can be rationally tuned. The here presented proof-of-concept cascade reaction highlights the suitability of CatIBs/Co-CatIBs for the realization of synthetic *in vitro* reaction cascades. In particular, the easy production and preparation of CatIBs and Co-CatIBs, readily producing a biologically obtained, spatially defined, enzyme (co)immobilizate, renders our strategy an interesting alternative to existing and often complex cascade immobilization techniques that rely on the scaffolding or encapsulation of enzymes. The here presented coimmobilization strategy is simple, fast, and inexpensive. Furthermore, it will prove particularly advantageous for the realization of one-pot simultaneous cascades, where the spatial proximity of the enzymes in Co-CatIBs might facilitate an improved substrate conversion, *e.g.*, due to substrate-channeling effects.

METHODS

Bacterial Strains and Media. *E. coli* DH5*α* was used for all cloning purposes, and *E. coli* BL21(DE3) was employed for heterologous expression of recombinant gene fusions. For shake flasks experiments, all bacterial strains used in this study were either grown in Luria−Bertani (LB) broth[68] or in autoinduction (AI) media (adapted from[69]) for heterologous expression. In brief, LB media consisted of 10 g L^{-1} Tryptone, 5 g L^{-1} yeast extract, 10 g L^{-1} NaCl at pH 7.0, while AI media contained 12 g L^{-1} casein-hydrolysate, 24 g L^{-1} yeast extract, 2.2 g L^{-1} KH_2PO_4, 9.4 g L^{-1} K_2HPO_4, and 5 g L^{-1} glycerol at pH 7.2. The media were supplemented for induction with 0.5 g L^{-1} glucose and 2 g L^{-1} lactose. For BioLector growth experiments Wilms-MOPS autoinduction medium[70] was used as described before.[71] In brief, the medium contained a set of basic ingredients (6.98 g L^{-1} $(NH_4)_2SO_4$, 3 g L^{-1} K_2HPO_4, 2 g L^{-1} Na_2SO_4, and 41.85 g L^{-1} MOPS) together with 0.5 g L^{-1} $MgSO_4 \cdot 7H_2O$, 0.01 g L^{-1} Thiamin, and several trace elements (0.54 mg L^{-1} $ZnSO_4 \cdot 7H_2O$, 0.48 mg L^{-1} $CuSO_4 \cdot 5H_2O$, 0.3 mg L^{-1} $MnSO_4 \cdot H_2O$, 0.54 mg L^{-1} $CoCl_2 \cdot 6H_2O$, 41.76 mg L^{-1} $FeCl_3 \cdot 6H_2O$, 1.98 mg L^{-1} $CaCl_2 \cdot 2H_2O$, and 33.4 mg L^{-1} $Na_2EDTA \cdot 6H_2O$). Precultures were supplemented with 5 g L^{-1} glucose and main cultures were supplemented with 0.5 g L^{-1} glucose, 2 g L^{-1} lactose, and 5 g L^{-1} glycerol. Microfluidic cultivations were carried out in M9CA medium, containing 4 g L^{-1} Bacto casamino acids (BD Biosciences,

DOI: 10.1021/acssynbio.8b00274
ACS Synth. Biol. 2018, 7, 2282−2295

Franklin Lakes, NJ, USA), 6.8 g L^{-1} Na_2HPO_4, 3 g L^{-1} KH_2PO_4, 0.5 g L^{-1} NaCl, 1 g L^{-1} NH_4Cl, 0.24 g L^{-1} $MgSO_4$, and 5 g L^{-1} glycerol, adjusted to pH 6.8 at 25 °C) and sterile filtered before use. For plasmid maintenance kanamycin was added at a final concentration of 50 μg mL^{-1} to all media.

Construction of Expression Plasmids. The construction of the initial expression plasmid for the generation of CatIBs by fusion of the TDoT coiled-coil domain has been described before.[72] This construct (pTDoT-Linker-YFP), which was based on pET28a vector backbone (Merck, Darmstadt, Germany), contained an in-frame fusion of the TDoT-coiled-coil domain, a linker polypeptide, consisting of the cleavage site of the Factor Xa protease and a flexible triple $(GGGS)_3$ motif, as well as the gene coding for a monomeric version of the enhanced yellow fluorescent protein (eYFP) bearing the A206 K mutation.[35] In contrast to mYFP[73] this variant lacks the Q69K mutation, which renders mYFP less pH-sensitive in the neutral pH range.[74] At the 5′-end, the gene fusion contained the DNA sequence coding for an N-terminal hexa-histidine-tag (His_6-tag), which was already present on the pET28a vector. To simplify the starting construct, the His_6-tag was removed by digestion of pTDoT-Linker-YFP with *Xba*I and *Nde*I, resulting in the release of a DNA fragment containing the His_6-tag as well as the vector's own ribosome binding site (RBS). A double stranded DNA fragment containing only the ribosome binding site (RBS) as well as a short upstream DNA sequence was assembled from oligonucleotides, containing a 5′-*Xba*I and 3′-*Nde*I site which facilitated the cloning into similarly digested pTDoT-Linker-YFP. This resulted in the simplified TDoT-L-YFP containing construct used in this study (here denoted as pTDoT-L-YFP). The genes coding for mCherry, *Pf*BAL and *R*ADH were amplified by standard PCR utilizing oligonucleotide primers containing a 5′-*BamH*I and a 3′-*Sal*I (mCherry, *R*ADH) or *Not*I (*Pf*BAL) site. After digestion with respective restriction endonucleases, PCR products were ligated into the similarly hydrolyzed pTDoT-L-YFP vector. This resulted in the plasmids pTDoT-L-mCherry, pTDoT-L-*Pf*BAL and pTDoT-L-*R*ADH. For details see Table S5. For the generation of the TDoT-mCherry construct, which lacks the linker polypeptide, comprising the cleavage site of the Factor Xa protease and the triple $(GGGS)_3$ motif, the gene fragment encoding the isolated TDoT-domain was amplified by PCR using oligonucleotide primers containing a 5′-*Nde*I and 3′-*Bam*HI site. The initially constructed pTDoT-L-mCherry plasmid (with linker) was digested with *Bam*HI and *Nde*I to release the gene fragment encoding the TDoT-domain as well as the linker, and ligated with the similarly hydrolyzed PCR product, resulting in the plasmid pTDoT-mCherry. To verify that solely the fused TDoT domain is responsible for the production of fluorescent YFP and mCherry IBs, a set of control constructs were generated, which lacked only the TDoT domain, but still contained the corresponding linker and the Factor Xa cleavage site. To this end, pTDoT-L-YFP and pTDOT-L-mCherry were digested with *Nde*I and *Nhe*I to release the gene fragment encoding for the TDoT-domain as well as the Factor Xa protease cleave site, and ligated with a gene fragment assembled from two oligonucleotides (Control_fw, Control_rv; Table S6), which contained the Factor Xa protease site as well as 5′-*Nde*I and 3′-*Nhe*I overhangs.[72] To construct the TDoT-L-YFP/TDoT-mCherry coexpression plasmids (pDouble-A to pDouble-D), the gene fusions to be localized at the rear (5′-end) of the two-gene-fusion assembly were amplified including RBS by standard PCR using oligonucleotide primers containing a *Sal*I recognition site at the 5′- and 3′-end. For the construction of the coexpression plasmids containing two P_{T7} promotor regions (pDouble-A and pDouble-B), the respective forward oligonucleotide primers additionally contained the P_{T7} binding site. The PCR products were digested with *Sal*I, while the single expression plasmid containing the front (5′end) gene fusion, used as backbone, was digested with *Xho*I endonuclease. Exploiting *Sal*I/*Xho*I compatible ends, the hydrolyzed target plasmid and the respective hydrolyzed PCR product were ligated, resulting in the corresponding pDouble expression plasmids (pDouble-A to pDouble-D). Plasmids with the correct orientation of the inserted PCR product were selected by test digestion with *Bgl*II. The coexpression plasmid for the production of *Pf*BAL/RADH Co-CatIBs (pDouble-*Pf*BAL-*R*ADH) was constructed in an identical manner. All sequences were verified by sequencing (Seqlab GmbH, Göttingen, Germany). Information about all oligonucleotide primers and plasmids, used in this study, is given in Tables S5 and S6 of the SI.

Production and Purification of Inclusion Bodies (IBs) and Soluble *Pf*BAL and *R*ADH. All target gene fusions, either for the production of (colocalized) fluorescent IBs (FIBs and Co-FIBs) or (colocalized) catalytically active IBs (CatIBs and Co-CatIBs), were heterologously expressed in *E. coli* BL21(DE3) under identical conditions as described previously.[27] Cells were grown in autoinduction (AI) medium for 3 h at 37 °C and 130 rpm (shaking diameter 50 mm), after that the temperature was decreased to 15 °C and the cells were grown for additional 69 h under constant agitation at 130 rpm. For cultivation, shake flasks with a filling volume of 10% were used. After harvesting by centrifugation (30 min, 7500*g*, 4 °C), the cells were resuspended as a 10% (w/v) suspension in lysis buffer (50 mM sodium phosphate buffer, 100 mM NaCl, pH 8.0) and disrupted using an Emulsiflex-C5 high-pressure homogenizer (Avestin Europe GmbH, Mannheim, Germany) at 1000−1500 bar internal cell pressure in 3 cycles under constant cooling. For purification the crude cell extract (CCE) was separated into the soluble protein-containing supernatant (SN) and the IB-containing pellet (P) fraction by centrifugation for 30 min at 4 °C and 15 000*g*. Subsequently, the IB-containing pellet was washed once by suspension in ddH_2O. Soluble *R*ADH was heterologously produced in *E. coli* BL21(DE3) in the same manner as the CatIBs.[52] Soluble *Pf*BAL was encoded on a pkk233_2 vector including a C-terminal *His-Tag* and produced in *E. coli* SG 13009 at 30 °C in a 40 l Techfors fed-batch fermenter (Infors AG, Bottmingen, Switzerland)[75] as described elsewhere.[62,76] Cell disruption was performed from a 25% (w/v) suspension by sonication using a UP200 (Hielscher Ultrasonics GmbH, Teltow, Germany) cell disruptor (10 cycles for 1 min at a 70% amplitude and 1 cycle of 0.5, followed by a 1 min break). Cell debris was separated by centrifugation at 18 000*g* and 4 °C for 30 min. For the purification of soluble *R*ADH anion exchange chromatography was used as described elsewhere.[52] Briefly, the protein extract was desalted by gel filtration (Sephadex-G25 column, GE Healthcare, Little Chalfont, United Kingdom) in 10 mM TEA buffer (pH 7.5, with 0.8 mM $CaCl_2$), followed by chromatographic separation by an anion exchanger (Q-Sepharose Fast Flow column, GE Healthcare, Little Chalfont, United Kingdom) with a linear gradient of up to 200 mM NaCl (50 mM TEA, pH 7.5, 0.8 mM $CaCl_2$, 200 mM NaCl) at a flow of 1 mL min^{-1} for 2.5 h. Subsequently, a second desalting step was performed. The soluble *Pf*BAL was purified by a metal ion affinity chromatography as described before,[77,78] with a

DOI: 10.1021/acssynbio.8b00274
ACS Synth. Biol. 2018, 7, 2282−2295

Ni-NTA-sepharose column (Qiagen, Hilden, Germany); equilibration buffer: 50 mM TEA, pH 7.5, 2.5 mM $MgSO_4$, 0.5 mM ThDP, 300 mM NaCl; washing buffer: 50 mM TEA, pH 7.5, 50 mM imidazole, 300 mM NaCl; and elution buffer: 50 mM TEA, pH 7.5, 250 mM imidazole, 300 mM NaCl. Desalting was performed with a Sephadex-G25 column (GE Healthcare, Little Chalfont, United Kingdom) in 10 mM TEA buffer (pH 7.5, 2.5 mM $MgSO_4$, 0.1 mM ThDP).

The final pellet of the IB purification procedure, as well as the purified *Pf*BAL and *R*ADH enzyme solutions, were lyophilized for 72 h from a frozen (−80 °C) 10% (w/v) suspension in ddH_2O or the respective buffer in case of purified enzymes, using a Christ ALPHA 1−3 LD Plus (Martin Christ Gefriertrocknungsanlagen GmbH, Osterode, Germany). The resulting dried CatIBs were grounded and stored as a fine powder under argon atmosphere at −20 °C until further use.

Sodium Dodecyl Sulfate-Polyacrylamide Gel Electrophoresis (SDS-PAGE) and Protein Concentration Determination. The distribution of the recombinant fusion proteins in *E. coli* cell extract fractions (crude cell extract (CCE), soluble protein-containing supernatant (SN), and insoluble IB-containing pellet (P)) as well as the success of the IB-purification was analyzed by SDS-PAGE using precast NuPAGE 4−12% Bis-Tris Protein Gels with MES SDS running buffer (50 mM MES, 50 mM Tris, 0.1% SDS, 1 mM EDTA, pH 7.3). The total protein content in the SN fraction was determined, using Bradford assay[79] with bovine serum albumin (0.01−0.1 mg mL^{-1}) as standard. SDS-PAGE samples of the SN fraction were prepared to contain 10 μg protein. SDS-PAGE samples of the CCE and P fractions were prepared relatively to the SN fraction by using the same sample volume. Samples for SDS-PAGE were denatured by incubation at 99 °C for 15 min before loading. 7−10 μL of PageRuler Prestained Protein Ladder (ThermoFisher Nunc, Waltham, MA, USA) were used as size standard.

Cell Fractionation and Determination of the Fluorescence/Activity Distribution. The success of the inclusion body production was evaluated by determining the distribution of the functional recombinant fusion proteins in different *E. coli* cell extract fractions. Crude cell extracts (CCE) were prepared as described above, and the fluorescence (for (Co-)FIBs) or the activity (for (Co-)CatIBs) of the respective target proteins was measured using a suitable dilution of the CCE in lysis buffer (50 mM sodium phosphate buffer, 100 mM sodium chloride, pH 8.0). Subsequently, the diluted CCE sample was separated into the soluble protein-containing supernatant (SN) fraction and insoluble IB-containing pellet fraction (P) by centrifugation (2 min, 7697*g*, room temperature). The fluorescence/activity in the SN was measured as outlined below, and the P fraction was washed once with lysis buffer before resuspension in the initial volume of lysis buffer. Finally, the fluorescence/activity was determined for the washed P fraction. The fluorescence/activity in the P (IBs) and SN (soluble protein) was expressed relative to the activity of the crude cell extract (set to 100%).

Fluorescence Spectrophotometry, Fluorescence Distribution and Quantitative Comparison. The YFP/mCherry fluorescence distribution in the crude cell extract (CCE), the soluble protein-containing supernatant (SN), and the insoluble IB-containing pellet (P) fraction was determined using fluorescence spectroscopy, employing a TECAN infinite M1000 PRO fluorescence MTP reader (TECAN, Männedorf, Switzerland). All measurements were carried out at room temperature in black 96-well microtiter plates (MTP) (ThermoFisher Nunc, Waltham, MA, USA) containing 100 μL of sample per well. YFP was excitated at λ_{ex} 513 nm and fluorescence emission detected at λ_{em} 527 nm; mCherry was excited at λ_{ex} 587 nm and λ_{em} 610 nm (bandwidth 5 nm in both excitation and emission, z-position 18.909 μm, enhancement 120, flash number 25, flash frequency 400 Hz). The different cell fractions were prepared as described above. All measurements were performed at least as four technical replicates of biological triplicates.

To allow a quantitative comparison of the YFP and mCherry levels in Co-FIBs, the different fluorescence quantum yields (Φ_F: 0.61 for YFP[38] and 0.22 for mCherry[36]) and extinction coefficients ($\varepsilon_{514\ nm}$: 83 400 M^{-1} cm^{-1} for YFP[38] and $\varepsilon_{587\ nm}$: 72 000 M^{-1} cm^{-1} for mCherry[36]) have to be taken into account. To this end, the measured YFP and mCherry fluorescence values (in AU) were normalized by using the following formula:

$$\text{normalized fluorescence} = \frac{\text{measured fluorescence}}{\Phi F^{*}\varepsilon}$$

The normalized YFP and mCherry fluorescence in the pellet was expressed relative to the sum of the normalized YFP and mCherry fluorescence (set to 100%).

Online Analysis of YFP and mCherry Fluorescence during Microtiter Plate Cultivations. Cultivations were carried out in Wilms-MOPS autoinduction medium[70] as described before.[71] Precultures were grown overnight in a volume of 10 mL in 250 mL round flasks (starting OD_{600} of 0.02) at 37 °C and 350 rpm with a shaking diameter of 50 mm. Main cultures were grown in 48-deepwell microtiter plates (m2p-laboratories GmbH, Baesweiler, Germany), with a starting OD_{600} of 0.1 and a filling volume of 800 μL with a shaking diameter of 3 mm and a shaking frequency of 1000 rpm. Online fluorescence and scattered light measurements were performed in an in-house built BioLector prototype.[43] Fluorescence (mYFP: λ_{ex} 515 nm and λ_{em} 528 nm; mCherry: λ_{ex} 590 nm and λ_{em} 611 nm) and (back)-scattered light (λ_{ex} 650 nm, λ_{em} 650 nm) were measured in each well with the respective wavelengths in a continuously shaken microtiter plate. All experiments were performed as biological triplicates.

Quantitative Real-Time PCR (qPCR). YFP and mCherry transcript levels were determined using quantitative real-time PCR (qPCR). Here, *E. coli* BL21(DE3) strains carrying the coexpression constructs pDouble-A to pDouble-D were grown in shake flasks as described above. After 21 h at 15 °C, cell samples were harvested by centrifugation (2 min, 16 060*g*, room temperature) and stored as a cell pellet at −80 °C until further use. RNA was prepared using the NucloSpin RNA Kit (Macherey-Nagel, Düren, Germany), the RNase-Free DNase Set (Qiagen, Hilden, Germany), and the Ambion DNase I Kit (ThermoFisher Scientific, Waltham, MA, USA). The Maxima First Strand cDNA Synthesis Kit for RT-qPCR (ThermoFisher Scientific, Waltham, MA, USA) was used for cDNA synthesis employing 1000 ng of RNA. 50 ng cDNA was used per qPCR reaction (20 μL) using the Maxima SYBR/ROX qPCR Master Mix (ThermoFisher Scientific, Waltham, MA, USA). A 7900HT Fast Real-Time PCR System (Applied Biosystems, ThermoFisher, Waltham, MA, USA) was employed for qPCR. Negative controls with RNA and water were performed. All samples were measured as four technical replicates of biological triplicates. For absolute quantification of the YFP/mCherry transcript levels, the corresponding gene fragments were amplified by standard PCR using the coexpression plasmids (pDouble-A to pDouble-D)

DOI: 10.1021/acssynbio.8b00274
ACS Synth. Biol. 2018, 7, 2282−2295

as template and employing the same oligonucleotide primers as for qPCR (Table S6). Dilutions of 1×10^{-2} to 5×10^{-6} ng of the respective standard DNA were employed for absolute quantification.

Microscopy and Live Cell Imaging. Formation of inclusion bodies was detected by live cell imaging using an inverted Nikon Eclipse Ti microscope (Nicon GmbH, Düsseldorf, Germany) equipped with an Apo TIRF 100× Oil DIC N objective (ALA OBJ-Heater, Ala Scientific Instruments, USA), an ANDOR Zyla CMOS camera (Andor Technology plc., Belfast, UK), an Intensilight (Nicon GmbH, Düsseldorf, Germany) light source for fluorescence excitation, and fluorescence filters for YFP (excitation: 520/60 nm, dichroic mirror: 510 nm, emission: 540/40 nm) and mCherry (excitation: 575/15 nm, dichroic mirror: 593 nm, emission: 629/56 nm) (AHF Analysentechnik, Tübingen, Germany). The filter spectra are given in nm as peak/peak width. The dichroic mirror serves as long-pass filter for wavelengths larger than the given value. Fluorescence and camera exposure was 200 ms for both filters at 25 or 12.5% lamp intensity. Cells were grown for 69 h as described above. A volume of 1.5 μL with an OD_{600} of approximately 10 was applied on a microscope slide with a 1% (w/v) agarose base, covered with a coverslip and placed in the microscope setup for imaging. All samples were measured in three biological replicates. Analysis of cell images were performed with Fiji[44] and the plugin MicrobeJ,[45] in biological triplicate, with a statistical population of at least 1000 analyzed inclusion bodies each ($\sum \geq 3000$ for each construct).

Microfluidic Cultivation. The microfluidic system used in this study was described before.[80,81] Cell suspensions for chip perfusion were prepared by inoculating fresh cultures of *E. coli* BL21(DE3) in M9CA medium, transformed with the plasmids pDouble-A to pDouble-D (Table S5), from precultures in the mid logarithmic growth phase of *E. coli* to an OD_{600} of 0.1. These cell suspensions were infused in a polydimethylsiloxane (PDMS) microfluidic chip, containing several hundred monolayer growth chambers (dimensions: 1 μm × 40 μm × 40 μm) to inoculate single mother cells into the growth chambers. Cell growth was performed at 22 °C with a constant flow of 200 nl min^{-1} M9CA medium with 50 $\mu g\ mL^{-1}$ kanamycin using a Cetoni Nemesys syringe pump system (Cetoni, Korbußen, Germany) for continuous medium perfusion. After 5 h Co-FIB formation was induced with 0.5 mM IPTG. During cultivation, pictures of the growth chambers were taken at intervals of 15 min as described above. Analysis of time lapse images and videos was performed with Fiji.[44]

Photometric *Pf*BAL and *R*ADH Activity Assays for the Analysis of Cellular Fractions. All measurements were performed in 10 × 4 mm quartz-glass cuvettes with a volume of 1 mL (4 mm light path in excitation) using a Fluorolog3−22 spectrofluorimeter (Horiba Jobin Yvon, Bensheim, Germany). To minimize light scattering due to turbid CatIB suspensions, fluorescence emission was detected at a 22.5° front-face angle. *Pf*BAL activity was determined by following the decrease in fluorescence emission of the fluorescent substrate 3,5-dimethoxybenzaldehyde (DMBA), which is converted by *Pf*BAL to the product (*R*)-1,2-bis(3,5-dimethoxyphenyl)-2-hydroxyethanone (TMBZ) by carboligation of two substrate molecules[82] (Figure S4a). This results in a loss of the DMBA-specific fluorescence. DMBA consumption was monitored continuously for 90 s at 25 °C by excitation at λ_{ex} 350 nm and monitoring DMBA emission at λ_{em} 460 nm (bandwidth 1.3 nm in both excitation and emission). All reactions were performed at 25 °C using TEA buffer (50 mM TEA, 0.5 mM ThDP, 2.5 mM $MgSO_4$, pH 8.0) with 3 mM DMBA (in DMSO) and 200 μL sample suspension in suitable dilutions. The final concentration of DMSO was 20% (v/v). *R*ADH activity was followed by detecting the enzyme-catalyzed reduction of cyclohexanone to cyclohexanol (Figure S4b), whereby the consumption of the NADPH cofactor was monitored continuously for 90 s at 25 °C by excitation at λ_{ex} 350 nm while recording NADPH emission at λ_{em} 460 nm (bandwidth 1.4 nm in both excitation and emission).[51] Reactions were performed at 30 °C using TEA buffer (50 mM TEA, 0.8 mM $CaCl_2$, pH 7.5) with 100 mM cyclohexanone, 0.2 mM NADPH, and 200 μL sample suspension in suitable dilutions. All measurements were performed at least as four technical replicates of biological triplicates.

***Pf*BAL and *R*ADH Activity Assays for the Determination of Specific Activities.** The initial rate activities of *Pf*BAL-CatIBs and soluble *Pf*BAL, were determined by following the carboligation of 3,5-dimethoxy benzaldehyde (DMBA) to (*R*)-(3,3′,5,5′)-tetramethoxy benzoin (TMBZ) (Figure S4a) by using a discontinuous HPLC assay. For the reaction a volume of 1 mL containing 80% (v/v) TEA-buffer (50 mM, pH 7.5, 2.5 mM $MgSO_4$, 0.1 mM ThDP), 20% (v/v) DMSO and 10 mM DMBA was incubated for 2.5 min at 30 °C, before the reaction was started by the addition of about 0.5 mg mL^{-1} (Co-)CatIBs or about 10 $\mu g\ mL^{-1}$ soluble *Pf*BAL (initial sample weight). The reaction was performed for 5 min at 30 °C and 1000 rpm in a thermomixer (Thermomixer comfort, Eppendorf, Germany) under sampling (20 μL) every minute. Samples were stopped by 1:10 dilution with methanol (internal standard: 0.1‰ (v/v) *p*-methoxy benzaldehyde (*p*-MBA)) and analyzed by high performance liquid chromatography (HPLC).

*R*ADH initial rate activities of (Co-)CatIBs or the soluble control were measured by a discontinuous photometric assay following the enzyme-catalyzed reduction of cyclohexanone to cyclohexanol (Figure S4b). Thereby, the consumption of the NADPH cofactor was measured photometrically at 340 nm. For the quantification of NADPH a molar extinction coefficient of $\varepsilon_{340\ nm} = 1975\ mM^{-1}\ cm^{-1}$ determined under assay conditions was used. Reactions were set up in 2 mL Eppendorf tubes (reaction a volume of 1750 μL containing 0.4 mM NADPH, and 100 mM cyclohexanone in TEA-buffer (50 mM, pH 7.5, 0.8 mM $CaCl_2$)) and equilibrated for 2.5 min at 30 °C. The reaction was started by the addition of about 0.5 mg mL^{-1} (Co-)CatIBs or about 10 $\mu g\ mL^{-1}$ soluble *R*ADH (initial sample weight) and performed for 5 min at 30 °C and 1000 rpm in a thermomixer (Thermomixer comfort, Eppendorf, Germany) under sampling (250 μL) every minute. Samples were stopped by 1:3 dilution with 500 μL methanol, centrifuged for 5 min (7697*g*, room temperature) and measured in standard disposable half-micro cuvettes.

All measurements of the initial rate activities were performed at least as three technical replicates of the respective biological triplicates. The specific activity was calculated as U mg^{-1} (initial sample weight; 1 U referring to 1 $\mu mol_{product}\ min^{-1}$), and as turn over number k_{cat} [s^{-1}], referring to the amount of enzyme (in μmol, per subunit) which catalyzes the formation of 1 $\mu mol_{product}\ s^{-1}$, under the applied reaction conditions.

Determination of the Protein Concentration. The protein content of lyophilized (Co)-CatIBs or of lyophilized soluble enzymes was determined photometrically after denaturation in guanidine hydrochloride. Therefore, samples were dissolved in 6 M guanidine hydrochloride and incubated for 30 min at 30 °C and 1000 rpm (Thermomixer comfort,

DOI: 10.1021/acssynbio.8b00274
ACS Synth. Biol. 2018, 7, 2282−2295

Eppendorf, Germany), and subsequently centrifuged for 20 min at 4 °C and 16 060*g*. The absorption of the protein solution was measured at 280 nm. The protein content was estimated using the molar extinction coefficient as calculated based on the amino acid composition using the ExPaSy ProtParam Tool (http://web.expasy.org/protparam)[83] (Table S4). For the Co-CatIBs the molar extinction coefficient and the molecular mass was weighted based on densitometric analysis of the corespodning SDS gels (Figure S5).

Two-Enzyme Cascade Reaction. Initially, the one-pot synthesis of (1*R*,2*R*)-1-phenylpropane-1,2-diol (PPD **4**) was performed in an aqueous buffer system (50 mM TEA, 0.5 mM ThDP, 2.5 mM $MgSO_4$, 0.8 mM $CaCl_2$, pH 8.0) supplemented with 150 mM acetaldehyde, 120 mM benzyl alcohol, 15 mM benzaldehyde and 0.3 mM $NADP^+$, using 6 mg mL^{-1} Co-CatIBs (2.50 U *Pf*BAL, 165 mU *R*ADH). Reactions were started with the addition of the Co-CatIBs and incubated for 9 d at 30 °C and 1000 rpm. To avoid evaporation of the aldehyde substrates, sealed glas vials containing 1 mL aliquots were used. In a second experiment the catalyst load was increased to 10.6 mg mL^{-1} Co-CatIBs (7.33 U *Pf*BAL and 500 mU *R*ADH). As a control, equivalent amounts (in terms of activity units) of soluble *Pf*BAL (0.13 mg mL^{-1}) and *R*ADH (0.3 mg mL^{-1}) were used for the cascade reaction. In this second set of experiments the benzaldehyde concentration was reduced to 10 mM. To follow the reaction progress, 20 μL samples, drawn at specific time points, were mixed with 180 μL methanol (with 0.1‰ (v/v) *p*-methoxy benzaldehyde (*p*-MBA) as internal standard), vortexed and centrifuged to remove residual CatIBs/precipated enzyme. All samples were analyzed by high performance liquid chromatography (HPLC) as described below. At specific times (0, 2, and 4 days), the residual activity of *R*ADH and *Pf*BAL was measured using orthogonal assays. Therefore, (Co-)CatIBs were removed from the reaction medium by centrifugation (2 min, 7697*g*, room temperature) and resuspended in the respective assay buffer in suitable concentrations. Samples of the soluble control could not be centrifuged and were therefore just diluted in the respective buffers. Subsequently, activity assays were performed as described for the determination of specific activities. For quantification of stability, activities are given relative to the starting activity. All reactions were performed in triplicate using three separate CatIB samples of the same preparation.

High Performance Liquid Chromatography Analysis (HPLC). All cascade HPLC samples were analyzed using a Thermo Scientific Dionex Ultimate 3000 HPLC system, equipped with a Diode Array detector DAD-3000 (both: ThermoFisher Scientific, Waltham, MA, USA) and a Chiralpak IE column (4.6 μm × 250 mm, 5 μm particle; precolumn: Chiralpak IE; 4 mm × 10 mm; both Daicel, Tokyo, Japan). A binary mobile phase (A: ddH_2O and B: acetonitrile; flow rate 1 mL min^{-1}) was used. For separation a gradient program was used: 15% (v/v) B for 8 min, 35% (v/v) B for 3 min, 60% (v/v) B for 3 min, and 15% (v/v) B for 3 min. PPD (11.2 min) was detected at 210 nm, HPP (15.4 min) at 210 nm, and *p*-MBA (17.1 min) at 270 nm. Quantification of PPD and HPP was achieved by calibration with authentic PPD and HPP. For the determination of specific *Pf*BAL activities the conversion of DMBA to TMBZ was monitored by HPLC. The same HPLC system, column, flow rate, internal standard and binary mobile phase as desribed above for the cascade was used. Separation was achieved by isocratic elution using 50% (v/v) B for 20 min. DMBA (7.6 min) and TMBZ (9.4 min) were detected at 215 nm, *p*-MBA (6.1 min) at 270 nm. Quantification of substrate and product were achieved by calibration with authentic DMBA and TMBZ.

■ ASSOCIATED CONTENT

Supporting Information

The Supporting Information is available free of charge on the ACS Publications website at DOI: 10.1021/acssynbio.8b00274.

Tables S1−S6, Figures S1−S6, Annex (PDF)
Video S1 (AVI)
Video S2 (AVI)

■ AUTHOR INFORMATION

Corresponding Author

*E-mail: u.krauss@fz-juelich.de. Phone: +49 2461-61-2939.

ORCID

Karl-Erich Jaeger: 0000-0002-6036-0708
Ulrich Krauss: 0000-0003-2219-7388

Author Contributions

UK, MP, KEJ, and JB coordinated the project, VDJ designed and performed all experiments that are not otherwise mentioned, and analyzed the data, RL performed the online experiments using the BioLector device, EK and VDJ carried out microscopic analyses, AG and VDJ performed the microfluidic cultivations, RK provided reagents and constructs and contributed to assay development and HPLC analytics, UK and VDJ wrote the manuscript. All authors read and commented on the manuscript.

Notes

The authors declare no competing financial interest.

■ ACKNOWLEDGMENTS

We thank Michael Dietrich for the construction of the plasmids pDouble-A to pDouble-D, Stefanie Longerich for performing initial experiments with (Co-)CatIBs, and Maja Piqueray for technical assistance. This work was funded by the Bioeconomy Science Center (BioSC), which is financially supported by the Ministry of Culture and Science of North-Rhine Westphalia within the framework of the NRW Strategieprojekt BioSC (No. 313/32 3-400-002 13). BioSC is a research cluster consisting of the universities RWTH Aachen, Düsseldorf and Bonn, and the Forschungszentrum Jülich. Alexander Grünberger is financially supported by the Helmholtz Association (PD-311).

■ REFERENCES

(1) Quin, M. B., Wallin, K. K., Zhang, G., and Schmidt-Dannert, C. (2017) Spatial organization of multi-enzyme biocatalytic cascades. *Org. Biomol. Chem. 15*, 4260−4271.
(2) Hanefeld, U., Gardossi, L., and Magner, E. (2009) Understanding enzyme immobilisation. *Chem. Soc. Rev. 38*, 453−468.
(3) Rehm, F. B., Chen, S., and Rehm, B. H. (2016) Enzyme engineering for *in situ* immobilization. *Molecules 21*, 1370.
(4) Cao, L. (2005) *Carrier-Bound Immobilized Enzymes: Principles, Applications and Design*, pp 1−563, Wiley-VCH Verlag GmbH & Co. KGaA, Weinheim, Germany.
(5) Datta, S., Christena, L. R., and Rajaram, Y. R. S. (2013) Enzyme immobilization: an overview on techniques and support materials. *3 Biotech 3*, 1−9.
(6) Cao, L., van Rantwijk, F., and Sheldon, R. A. (2000) Cross-linked enzyme aggregates: a simple and effective method for the immobilization of penicillin acylase. *Org. Lett. 2*, 1361−1364.

(7) Guiseppi-Elie, A., Sheppard, N. F., Brahim, S., and Narinesingh, D. (2001) Enzyme microgels in packed-bed bioreactors with downstream amperometric detection using microfabricated interdigitated microsensor electrode arrays. *Biotechnol. Bioeng. 75*, 475−484.
(8) Jia, F., Mallapragada, S. K., and Narasimhan, B. (2015) Multienzyme immobilization and colocalization on nanoparticles enabled by DNA hybridization. *Ind. Eng. Chem. Res. 54*, 10212−10220.
(9) Ji, Q., Wang, B., Tan, J., Zhu, L., and Li, L. (2016) Immobilized multienzymatic systems for catalysis of cascade reactions. *Process Biochem. 51*, 1193−1203.
(10) Kazenwadel, F., Franzreb, M., and Rapp, B. E. (2015) Synthetic enzyme supercomplexes: co-immobilization of enzyme cascades. *Anal. Methods 7*, 4030−4037.
(11) García-Junceda, E., Lavandera, I., Rother, D., and Schrittwieser, J. H. (2015) (Chemo)enzymatic cascades - Nature's synthetic strategy transferred to the laboratory. *J. Mol. Catal. B: Enzym. 114*, 1−6.
(12) Aalbers, F. S., and Fraaije, M. W. (2017) Coupled reactions by coupled enzymes: alcohol to lactone cascade with alcohol dehydrogenase-cyclohexanone monooxygenase fusions. *Appl. Microbiol. Biotechnol. 101*, 7557−7565.
(13) Jeon, E.-Y., Baek, A.-H., Bornscheuer, U. T., and Park, J.-B. (2015) Enzyme fusion for whole-cell biotransformation of long-chain sec-alcohols into esters. *Appl. Microbiol. Biotechnol. 99*, 6267−6275.
(14) Krzek, M., van Beek, H. L., Permentier, H. P., Bischoff, R., and Fraaije, M. W. (2016) Covalent immobilization of a flavoprotein monooxygenase via its flavin cofactor. *Enzyme Microb. Technol. 82*, 138−143.
(15) Velasco-Lozano, S., Benitez-Mateos, A. I., and Lopez-Gallego, F. (2017) Co-immobilized phosphorylated cofactors and enzymes as self-sufficient heterogeneous biocatalysts for chemical processes. *Angew. Chem., Int. Ed. 56*, 771−775.
(16) Timm, C., and Niemeyer, C. M. (2015) Assembly and purification of enzyme-functionalized DNA origami structures. *Angew. Chem., Int. Ed. 54*, 6745−6750.
(17) Delebecque, C. J., Lindner, A. B., Silver, P. A., and Aldaye, F. A. (2011) Organization of intracellular reactions with rationally designed RNA assemblies. *Science 333*, 470−474.
(18) Visser, F., Müller, B., Rose, J., Prüfer, D., and Noll, G. A. (2016) Forizymes − functionalised artificial forisomes as a platform for the production and immobilisation of single enzymes and multi-enzyme complexes. *Sci. Rep.*, DOI: 10.1038/srep30839.
(19) Tan, C. Y., Hirakawa, H., and Nagamune, T. (2015) Supramolecular protein assembly supports immobilization of a cytochrome P450 monooxygenase system as water-insoluble gel. *Sci. Rep. 5*, 8648.
(20) Noireaux, V., and Libchaber, A. (2004) A vesicle bioreactor as a step toward an artificial cell assembly. *Proc. Natl. Acad. Sci. U. S. A. 101*, 17669−17674.
(21) Chowdhury, C., Sinha, S., Chun, S., Yeates, T. O., and Bobik, T. A. (2014) Diverse bacterial microcompartment organelles. *Microbiol. Mol. Biol. Rev. 78*, 438−468.
(22) Huber, I., Palmer, D. J., Ludwig, K. N., Brown, I. R., Warren, M. J., and Frunzke, J. (2017) Construction of recombinant Pdu metabolosome shells for small molecule production in *Corynebacterium glutamicum*. *ACS Synth. Biol. 6*, 2145−2156.
(23) Li, A., Ilie, A., Sun, Z., Lonsdale, R., Xu, J. H., and Reetz, M. T. (2016) Whole-cell-catalyzed multiple regio- and stereoselective functionalizations in cascade reactions enabled by directed evolution. *Angew. Chem., Int. Ed. 55*, 12026−12029.
(24) Menon, B. B., Dou, Z., Heinhorst, S., Shively, J. M., and Cannon, G. C. (2008) *Halothiobacillus neapolitanus* carboxysomes sequester heterologous and chimeric RubisCO species. *PLoS One 3*, e3570.
(25) Kopito, R. R. (2000) Aggresomes, inclusion bodies and protein aggregation. *Trends Cell Biol. 10*, 524−530.
(26) Krauss, U., Jäger, V. D., Diener, M., Pohl, M., and Jaeger, K. E. (2017) Catalytically-active inclusion bodies - Carrier-free protein immobilizates for application in biotechnology and biomedicine. *J. Biotechnol. 258*, 136−147.
(27) Diener, M., Kopka, B., Pohl, M., Jaeger, K. E., and Krauss, U. (2016) Fusion of a coiled-coil domain facilitates the high-level production of catalytically active enzyme inclusion bodies. *ChemCatChem 8*, 142−152.
(28) Wang, X., Zhou, B., Hu, W., Zhao, Q., and Lin, Z. (2015) Formation of active inclusion bodies induced by hydrophobic self-assembling peptide GFIL8. *Microb. Cell Fact. 14*, 88.
(29) Nahálka, J., and Nidetzky, B. (2007) Fusion to a pull-down domain: a novel approach of producing *Trigonopsis variabilis* D-amino acid oxidase as insoluble enzyme aggregates. *Biotechnol. Bioeng. 97*, 454−461.
(30) Choi, S. L., Lee, S. J., Yeom, S. J., Kim, H. J., Rhee, Y. H., Jung, H. C., and Lee, S. G. (2014) Controlled localization of functionally active proteins to inclusion bodies using leucine zippers. *PLoS One 9*, e97093.
(31) García-Fruitós, E., Arís, A., and Villaverde, A. (2007) Localization of functional polypeptides in bacterial inclusion bodies. *Appl. Environ. Microb. 73*, 289−294.
(32) Arie, J. P., Miot, M., Sassoon, N., and Betton, J. M. (2006) Formation of active inclusion bodies in the periplasm of *Escherichia coli*. *Mol. Microbiol. 62*, 427−437.
(33) Stetefeld, J., Jenny, M., Schulthess, T., Landwehr, R., Engel, J., and Kammerer, R. A. (2000) Crystal structure of a naturally occurring parallel right-handed coiled coil tetramer. *Nat. Struct. Biol. 7*, 772−776.
(34) Wachter, R. M., Elsliger, M. A., Kallio, K., Hanson, G. T., and Remington, S. J. (1998) Structural basis of spectral shifts in the yellow-emission variants of green fluorescent protein. *Structure 6*, 1267−1277.
(35) Zacharias, D. A., Violin, J. D., Newton, A. C., and Tsien, R. Y. (2002) Partitioning of lipid-modified monomeric GFPs into membrane microdomains of live cells. *Science 296*, 913−916.
(36) Shaner, N. C., Campbell, R. E., Steinbach, P. A., Giepmans, B. N., Palmer, A. E., and Tsien, R. Y. (2004) Improved monomeric red, orange and yellow fluorescent proteins derived from *Discosoma* sp. red fluorescent protein. *Nat. Biotechnol. 22*, 1567−1572.
(37) Lindner, A. B., Madden, R., Demarez, A., Stewart, E. J., and Taddei, F. (2008) Asymmetric segregation of protein aggregates is associated with cellular aging and rejuvenation. *Proc. Natl. Acad. Sci. U. S. A. 105*, 3076−3081.
(38) Tsien, R. Y. (1998) The Green Fluorescent Protein. *Annu. Rev. Biochem. 67*, 509−544.
(39) Iizuka, R., Yamagishi-Shirasaki, M., and Funatsu, T. (2011) Kinetic study of de novo chromophore maturation of fluorescent proteins. *Anal. Biochem. 414*, 173−178.
(40) Merzlyak, E. M., Goedhart, J., Shcherbo, D., Bulina, M. E., Shcheglov, A. S., Fradkov, A. F., Gaintzeva, A., Lukyanov, K. A., Lukyanov, S., Gadella, T. W. J., and Chudakov, D. M. (2007) Bright monomeric red fluorescent protein with an extended fluorescence lifetime. *Nat. Methods 4*, 555−557.
(41) Macdonald, P. J., Chen, Y., and Mueller, J. D. (2012) Chromophore maturation and fluorescence fluctuation spectroscopy of fluorescent proteins in a cell-free expression system. *Anal. Biochem. 421*, 291−298.
(42) Artimo, P., Jonnalagedda, M., Arnold, K., Baratin, D., Csardi, G., de Castro, E., Duvaud, S., Flegel, V., Fortier, A., Gasteiger, E., Grosdidier, A., Hernandez, C., Ioannidis, V., Kuznetsov, D., Liechti, R., Moretti, S., Mostaguir, K., Redaschi, N., Rossier, G., Xenarios, I., and Stockinger, H. (2012) ExPASy: SIB bioinformatics resource portal. *Nucleic Acids Res. 40*, W597−603.
(43) Ladner, T., Beckers, M., Hitzmann, B., and Büchs, J. (2016) Parallel online multi-wavelength (2D) fluorescence spectroscopy in each well of a continuously shaken microtiter plate. *Biotechnol. J. 11*, 1605−1616.
(44) Schneider, C. A., Rasband, W. S., and Eliceiri, K. W. (2012) NIH Image to ImageJ: 25 years of image analysis. *Nat. Methods 9*, 671−675.
(45) Ducret, A., Quardokus, E. M., and Brun, Y. V. (2016) MicrobeJ, a tool for high throughput bacterial cell detection and quantitative analysis. *Nat. Microbiol. 1*, 16077.

DOI: 10.1021/acssynbio.8b00274
ACS Synth. Biol. 2018, 7, 2282−2295

(46) Han, G. H., Seong, W., Fu, Y., Yoon, P. K., Kim, S. K., Yeom, S. J., Lee, D. H., and Lee, S. G. (2017) Leucine zipper-mediated targeting of multi-enzyme cascade reactions to inclusion bodies in *Escherichia coli* for enhanced production of 1-butanol. *Metab. Eng. 40*, 41−49.
(47) Engstrom, M. D., and Pfleger, B. F. (2017) Transcription control engineering and applications in synthetic biology. *Synth. Syst. Biotechnol. 2*, 176−191.
(48) Bittihn, P., Din, M. O., Tsimring, L. S., and Hasty, J. (2018) Rational engineering of synthetic microbial systems: from single cells to consortia. *Curr. Opin. Microbiol. 45*, 92−99.
(49) Choudary, B. M., Chowdari, N. S., Madhi, S., and Kantam, M. L. (2003) A trifunctional catalyst for one-pot synthesis of chiral diols via Heck coupling-N-oxidation-asymmetric dihydroxylation: application for the synthesis of diltiazem and taxol side chain. *J. Org. Chem. 68*, 1736−1746.
(50) Gonzalez, B., and Vicuna, R. (1989) Benzaldehyde lyase, a novel thiamine PPi-requiring enzyme, from *Pseudomonas fluorescens* biovar I. *J. Bacteriol. 171*, 2401−2405.
(51) Kulig, J., Frese, A., Kroutil, W., Pohl, M., and Rother, D. (2013) Biochemical characterization of an alcohol dehydrogenase from *Ralstonia* sp. *Biotechnol. Bioeng. 110*, 1838−1848.
(52) Kulig, J., Simon, R. C., Rose, C. A., Husain, S. M., Hackh, M., Ludeke, S., Zeitler, K., Kroutil, W., Pohl, M., and Rother, D. (2012) Stereoselective synthesis of bulky 1,2-diols with alcohol dehydrogenases. *Catal. Sci. Technol. 2*, 1580−1589.
(53) Mosbacher, T. G., Mueller, M., and Schulz, G. E. (2005) Structure and mechanism of the ThDP-dependent benzaldehyde lyase from *Pseudomonas fluorescens*. *FEBS J. 272*, 6067−6076.
(54) Man, H., Kędziora, K., Kulig, J., Frank, A., Lavandera, I., Gotor-Fernández, V., Rother, D., Hart, S., Turkenburg, J. P., and Grogan, G. (2014) Structures of alcohol dehydrogenases from *Ralstonia* and *Sphingobium* spp. reveal the molecular basis for their recognition of 'bulky−bulky' ketones. *Top. Catal. 57*, 356−365.
(55) Guauque Torres Mdel, P., Foresti, M. L., and Ferreira, M. L. (2013) Cross-linked enzyme aggregates (CLEAs) of selected lipases: a procedure for the proper calculation of their recovered activity. *AMB Express 3*, 25.
(56) Sheldon, R. A., and van Pelt, S. (2013) Enzyme immobilisation in biocatalysis: why, what and how. *Chem. Soc. Rev. 42*, 6223−6235.
(57) Mateo, C., Palomo, J. M., van Langen, L. M., van Rantwijk, F., and Sheldon, R. A. (2004) A new, mild cross-linking methodology to prepare cross-linked enzyme aggregates. *Biotechnol. Bioeng. 86*, 273−276.
(58) Cui, J. D., Sun, L. M., and Li, L. L. (2013) A simple technique of preparing stable CLEAs of phenylalanine ammonia lyase using co-aggregation with starch and bovine serum albumin. *Appl. Biochem. Biotechnol. 170*, 1827−1837.
(59) Chmura, A., van der Kraan, G. M., Kielar, F., van Langen, L. M., van Rantwijk, F., and Sheldon, R. A. (2006) Cross-linked aggregates of the hydroxynitrile lyase from *Manihot esculenta*: Highly active and robust biocatalysts. *Adv. Synth. Catal. 348*, 1655−1661.
(60) Park, S. H., Soetyono, F., and Kim, H. K. (2017) Cadaverine production by using cross-linked enzyme aggregate of *Escherichia coli* lysine decarboxylase. *J. Microbiol. Biotechnol. 27*, 289−296.
(61) Easa, M. N., Yusof, F., and Abd. Halim, A. (2017) Kinetic performance of Cross-Linked Enzyme Aggregates (CLEA)-amylase from *Zophobas morio*. *Int. Food Res. J. 24*, S335−S339.
(62) Janzen, E., Muller, M., Kolter-Jung, D., Kneen, M. M., McLeish, M. J., and Pohl, M. (2006) Characterization of benzaldehyde lyase from *Pseudomonas fluorescens*: A versatile enzyme for asymmetric C-C bond formation. *Bioorg. Chem. 34*, 345−361.
(63) Zhang, Y., Tsitkov, S., and Hess, H. (2016) Proximity does not contribute to activity enhancement in the glucose oxidase−horseradish peroxidase cascade. *Nat. Commun. 7*, 13982.
(64) Zhang, Y., Ge, J., and Liu, Z. (2015) Enhanced Activity of Immobilized or Chemically Modified Enzymes. *ACS Catal. 5*, 4503−4513.
(65) Kulig, J. K. (2013) *Stereoselective Synthesis of Vicinal Diols with Enzymatic Cascade Reactions*, Doctoral thesis, Heinrich-Heine Universität Düsseldorf, https://docserv.uni-duesseldorf.de/servlets/DocumentServlet?id=27545.
(66) Jakoblinnert, A., and Rother, D. (2014) A two-step biocatalytic cascade in micro-aqueous medium: using whole cells to obtain high concentrations of a vicinal diol. *Green Chem. 16*, 3472−3482.
(67) Wachtmeister, J., Jakoblinnert, A., Kulig, J., Offermann, H., and Rother, D. (2014) Whole-Cell teabag catalysis for the modularisation of synthetic enzyme cascades in micro-aqueous systems. *ChemCatChem 6*, 1051−1058.
(68) Sambrook, J., Fritsch, E. F., and Maniatis, T. (1998) *Molecular Cloning: A Laboratory Manual*, 2nd ed., Cold Spring Harbor Laboratory Press, Cold Spring Harbor, NY.
(69) Studier, F. W. (2005) Protein production by auto-induction in high density shaking cultures. *Protein Expression Purif. 41*, 207−234.
(70) Wilms, B., Hauck, A., Reuss, M., Syldatk, C., Mattes, R., Siemann, M., and Altenbuchner, J. (2001) High-cell-density fermentation for production of L-N-carbamoylase using an expression system based on the *Escherichia coli* rhaBAD promoter. *Biotechnol. Bioeng. 73*, 95−103.
(71) Rahmen, N., Fulton, A., Ihling, N., Magni, M., Jaeger, K. E., and Büchs, J. (2015) Exchange of single amino acids at different positions of a recombinant protein affects metabolic burden in *Escherichia coli*. *Microb. Cell Fact. 14*, 10.
(72) Diener, M. (2014) *Von gezielter Oligomerisierung zu katalytisch aktiven inclusion bodies—Eine alternative Strategie zur Stabilisierung und Immobilisierung von Biokatalysatoren*, Doctoral thesis, Heinrich-Heine University Düsseldorf, https://docserv.uni-duesseldorf.de/servlets/DocumentServlet?id=34230.
(73) Shaner, N. C., Steinbach, P. A., and Tsien, R. Y. (2005) A guide to choosing fluorescent proteins. *Nat. Methods 2*, 905−909.
(74) Miyawaki, A., Griesbeck, O., Heim, R., and Tsien, R. Y. (1999) Dynamic and quantitative Ca^{2+} measurements using improved cameleons. *Proc. Natl. Acad. Sci. U. S. A. 96*, 2135−2140.
(75) Korz, D. J., Rinas, U., Hellmuth, K., Sanders, E. A., and Deckwer, W. D. (1995) Simple fed-batch technique for high cell density cultivation of *Escherichia coli*. *J. Biotechnol. 39*, 59−65.
(76) Schwarz, M. (2010) *Einflussfaktoren auf die Stabilität und Aktivität der Benzaldehydlyase aus Pseudomonas fluorescens in Carboligasereaktionen mit aromatischen Aldehyden*, Forschungszentrum Jülich GmbH.
(77) Gocke, D., Walter, L., Gauchenova, E., Kolter, G., Knoll, M., Berthold, C. L., Schneider, G., Pleiss, J., Muller, M., and Pohl, M. (2008) Rational protein design of ThDP-dependent enzymes-engineering stereoselectivity. *ChemBioChem 9*, 406−412.
(78) Pohl, M., Müller, M., and Demir, A. S. (2006) Nucleotide sequence encoding a benzaldehyde lyase, and process for stereoselectively synthesizing 2-hydroxyketones, US7045334B2.
(79) Bradford, M. M. (1976) A rapid and sensitive method for the quantitation of microgram quantities of protein utilizing the principle of protein-dye binding. *Anal. Biochem. 72*, 248−254.
(80) Grünberger, A., Probst, C., Helfrich, S., Nanda, A., Stute, B., Wiechert, W., von Lieres, E., Noh, K., Frunzke, J., and Kohlheyer, D. (2015) Spatiotemporal microbial single-cell analysis using a high-throughput microfluidics cultivation platform. *Cytometry, Part A 87*, 1101−1115.
(81) Probst, C., Grünberger, A., Braun, N., Helfrich, S., Noh, K., Wiechert, W., and Kohlheyer, D. (2015) Rapid inoculation of single bacteria into parallel picoliter fermentation chambers. *Anal. Methods 7*, 91−98.
(82) Zavrel, M., Schmidt, T., Michalik, C., Ansorge-Schumacher, M., Marquardt, W., Buchs, J., and Spiess, A. C. (2008) Mechanistic kinetic model for symmetric carboligations using benzaldehyde lyase. *Biotechnol. Bioeng. 101*, 27−38.
(83) Gasteiger, E., Hoogland, C., Gattiker, A., Duvaud, S. E., Wilkins, M. R., Appel, R. D., and Bairoch, A. (2005) Protein identification and analysis tools on the ExPASy server, In *The Proteomics Protocols Handbook* (Walker, J. M., Ed.), pp 571−607, Humana Press, Totowa, NJ.

DOI: 10.1021/acssynbio.8b00274
ACS Synth. Biol. 2018, 7, 2282−2295

2.5.1 Publication V: Supporting Information

The here presented Supporting Information of the Manuscript 'A synthetic reaction cascade implemented by co-localization of two proteins within catalytically-active inclusion bodies' was shortened for clarity of the thesis. The original Supporting Information additionally contain DNA and amino acid sequences of the fusion constructs, as well as information of all expression vectors and primer sequences. This information can partially be found in the Supporting Information of the Manuscript 'Tailoring the properties of (catalytically)-active inclusion bodies' (2.1.1). The DNA and amino acid sequences can be found in the Appendix (5.2).

(Co-)FIBs	fluorescence distribution [%][a]			
	TDoT-L-YFP		TDoT-mCherry	
	SN	P	SN	P
Co-FIBs A	73.3 ± 2.4	17.8 ± 7.5	66.9 ± 4.7	38.3 ± 3.0
Co-FIBs B	53.5 ± 2.3	31.1 ± 5.0	49.3 ± 2.3	56.7 ± 6.3
Co-FIBs C	61.0 ± 3.2	29.4 ± 9.0	49.6 ± 6.2	54.8 ± 2.9
Co-FIBs D	56.2 ± 7.2	30.7 ± 3.4	48.2 ± 8.1	59.8 ± 3.3
TDoT-L-YFP	40.6 ± 4.5	51.1 ± 4.9	n.a.	n.a.
TDoT-mCherry	n.a.	n.a.	77.1 ± 8.9	31.8 ± 8.2

Table S1. Distribution of YFP and mCherry fluorescence in different (Co-)FIBs after cell disruption.

[a:] YFP and mCherry fluorescence of the soluble-protein-containing supernatant (SN) and the insoluble, IB-containing pellet (P) relative to the fluorescence of the crude cell extract (set to 100%). n.a. not applicable

(Co-) CatIBs	activity distribution [%][a]			
	TDoT-L-*Pf*BAL		TDoT-L-*R*ADH	
	SN	P	SN	P
TDoT-L-*Pf*BAL	23.4 ± 6.5	86.7 ± 9.9	n.a.	n.a.
TDoT-L-*R*ADH	n.a.	n.a.	10.5 ± 4.6	87.5 ± 9.7
Co-CatIBs	10.5 ± 1.9	86.8 ± 2.5	22.9 ± 3.7	81.4 ± 3.5

Table S2. Distribution of *Pf*BAL and *R*ADH activity in different (Co-)CatIBs after cell disruption.

[a:] *Pf*BAL and *R*ADH activity of the soluble-protein-containing supernatant (SN) and the insoluble, IB-containing pellet (P), relative to the activity of the crude cell extract (set to 100%). n.a. not applicable

(Co-)CatIBs	molecular mass [kDa]	molar extinction coefficient (ε) [M^{-1} cm^{-1}]
TDoT-L-*Pf*BAL	66.5	55 140
TDoT-L-*R*ADH	34.3	17 420
Co-CatIBs	44.5	29 431

Table S4. Molecular mass and molar extinction coefficients (ε) of different (Co-)CatIB fusions, as determined with the ExPaSy Protparam Tool (http://expasy.org/tools/protparam).[7] For the Co-CatIBs a weighted molecular mass as well as a weighted extinction coefficient was calculated, based on densitometric analysis of the pellet (Co-CatIB) fraction as shown in Figure S5.

Table S3. Residual activities of exemplary cross-linked enzyme aggregate (CLEA) immobilizates as inferred from literature.

enzyme	origin	Residual acivity [%]	starting preparation	comments	ref
lipozyme TTL	*Thermomyces lanuginosa*	4-11	Novozymes commercial preparation	residual activity relative to starting prepartion per mg precipatable protein	1
oxynitrilase	*Prunus amydalus*	10	Jülich Fine Chemicals	glutaraldehyde, presence of dextran polyaldehyde, residual activity relative to activity of starting solution, purity of starting preparation unclear	2
nitrilase	*Pseudomonas fluorescens*	0-50	cell free extract		
nitrilase 1004	*BioCatalytics 1004*	0-60	commercial preparation, BioCatalytics		
ADH	*Lactococcus brevis*	0-10	Jülich Fine Chemicals		
penicillin G acylase	*Escherichia coli*	48-90	commercial preparation, Sigma		
phenylalanine ammonia lyase	*Rhodotorula glutinis*	8-36	partially purified protein	prepared with different additives BSA, starch, residual activity relative to activity of starting solution, purity of starting preparation unclear	3
amylase	*Zophobas morio*	27	*Z. morio* extract	crosslinking in presence of BSA, residual activity relative to activity of extract, purity of starting preparation unclear	4
hydroxynitrile lyase	*Manihot esculenta*	11-35 (cleavage) 6-93 (synthesis)	partially purified MeHNL, Jülich Fine Chemicals	relative to starting activity, purity of starting preparation unclear	5
leucine decarboxylase	*Escherichia coli*	8	prepared from crude cell extract	relative to starting activity, purity of starting preparation unclear	6

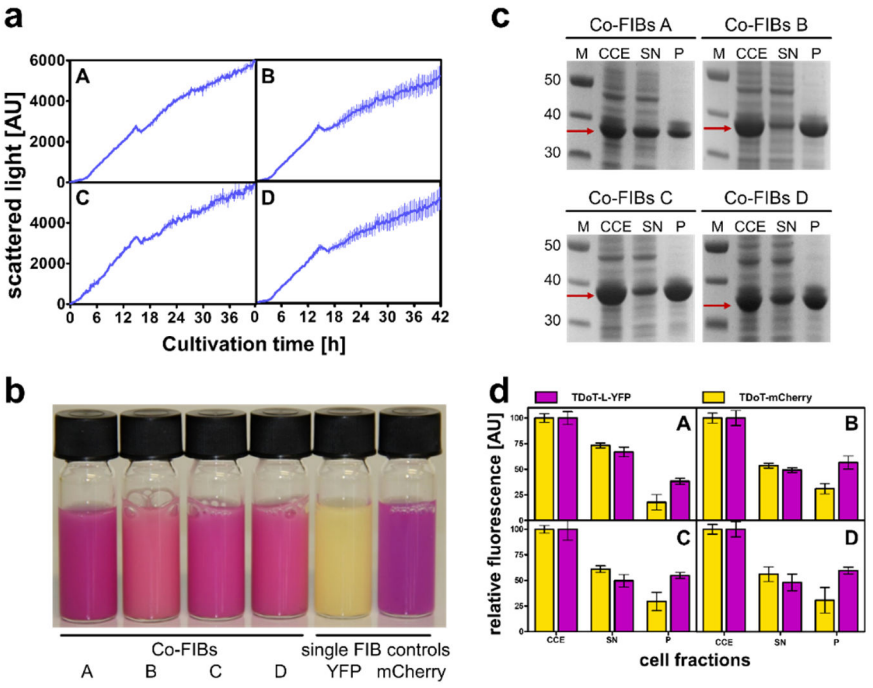


Figure S1. Evaluation of the co-expression strategy to produce co-localized fluorescent IBs (CoFIBs). (a) Backscattered light at 650 nm of *E. coli* BL21(DE3) cultures expressing the four constructs A to D (see Figure 2c in the main manuscript), using a BioLector prototype.[10] The temperature was reduced after 3 h from 37 to 15 °C. Results are given as mean of a triplicate with standard deviation. (b) *E. coli* BL21(DE3) cells after standard expression of Co-FIBs A to D and single FIB controls. Cells were harvested and resuspended in lysis buffer (50 mM sodium phosphate buffer, 100 mM sodium chloride, pH 8.0). (c) SDS-PAGE analyses illustrating the production of TDoT-L-YFP and TDoT-mCherry by *E. coli* BL21(DE3) cells carrying the four different co-expression constructs pDoubleA to D. Please note, that due to the very similar molecular mass (TDoT-L-YFP: 34.6 kDa and TDoT-mCherry: 32.7 kDa) the two fusion proteins cannot be separated by SDS-PAGE. The band potentially containing both fusion proteins is marked by red arrows. After overexpression in *E. coli* BL21(DE3), cells were disrupted and the resulting crude cell extract (CCE) was separated into the soluble-protein-containing supernatant (SN) and the IB-containing pellet (P) fraction by centrifugation. (d) Distribution of YFP and mCherry fluorescence within the Co-FIBs A to D. The fluorescence in the supernatant (SN) and pellet (P) is given relatively to the crude cell extract (CCE, set to 100%). Error bars correspond to the standard deviation of the mean derived from three biological replicates.

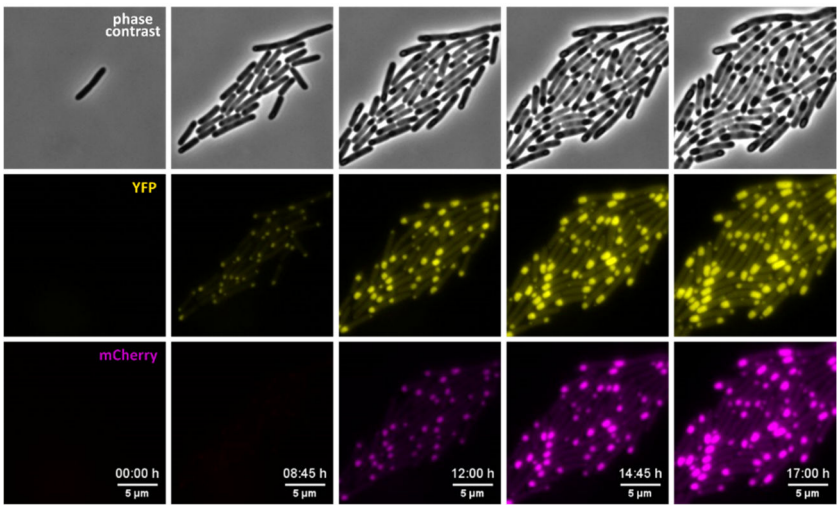


Figure S2. Co-expression and co-localization of TDoT-L-YFP and TDoT-mCherry in *E. coli*. Exemplary microscopy images of a microfluidic cultivation of *E. coli* BL21(DE3) carrying the co-expression constructs pDouble-D taken at different time points during the cultivation. The different panels show phase contrast (top), YFP (middle), and mCherry (bottom) fluorescence images at the indicated times. Videos of the respective microfluodic cultivations of *E. coli* BL21(DE3), carrying the co-expression constructs pDouble-A to pDouble-D, which illustrate the co-expression and co-localization of TDoT-L-YFP and TDoT-mCherry, are provided as separate files as part of the Supporting Information.

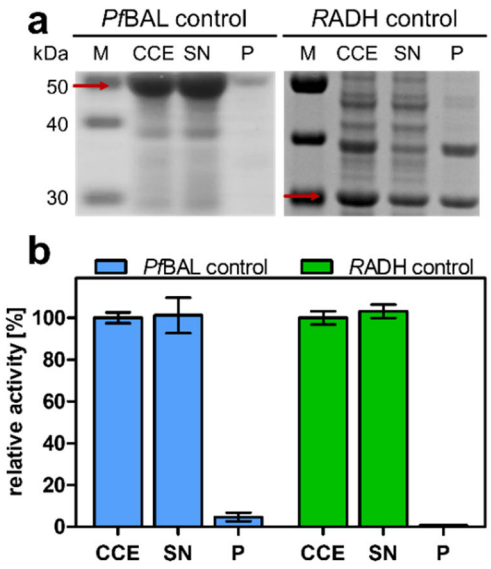


Figure S3. Control experiments for the evaluation of the TDoT-fusion strategy to induce the formation of active IBs. For *Pf*BAL and *R*ADH control experiments, pET-vectors containing only the corresponding gene instead of a gene fusion were used. (a) SDS-PAGE analyses illustrating the production of the soluble controls *Pf*BAL (left) and *R*ADH (right). The expected molecular mass of the target proteins are marked by red arrows (*Pf*BAL: 60.0 kDa and *R*ADH: 26.7 kDa). After overexpression in *E. coli* BL21(DE3), the cells were disrupted and the resulting crude cell extract (CCE) was separated into the soluble-protein-containing supernatant (SN) and the insoluble IB-containing pellet (P) fraction by centrifugation. (b) Activity distribution of cells producing soluble *Pf*BAL and *R*ADH. The activity in the CCE was set to 100%, and the values for SN and P are given relatively to the CCE. Error bars correspond to the standard deviation of the mean derived from four technical replicates.

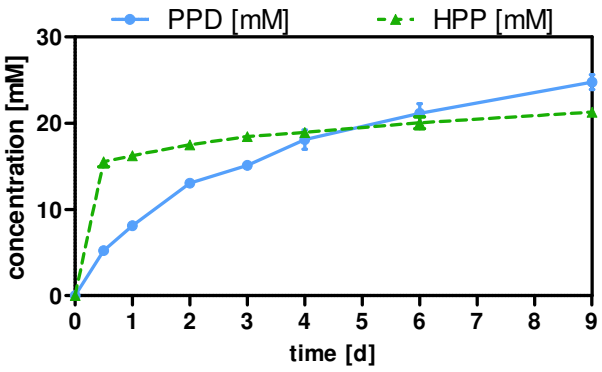


Figure S4. Initial experiments for the production of (1*R*,2*R*)-1-phenylpropane-1,2-diol (PPD, **4**, solid blue) and the intermediate (*R*)-2-hydroxy-1-phenylpropanone (HPP, **3**, dotted green) performed with Co-CatIBs. 6 mg ml^{-1} of Co-CatIBs were used in 50 mM TEA, pH 8.0, supplemented with 0.5 mM ThDP, 2.5 mM $MgSO_4$, and 0.8 mM $CaCl_2$. The reaction mixture further contained 15 mM benzaldehyde **1**, 150 mM acetaldehyde **2**, 120 mM benzyl alcohol **5**, and 0.3 mM $NADP^+$. The reaction was performed at 30 °C and 1000 rpm. Error bars correspond to the standard deviation of the mean derived from three technical replicates.

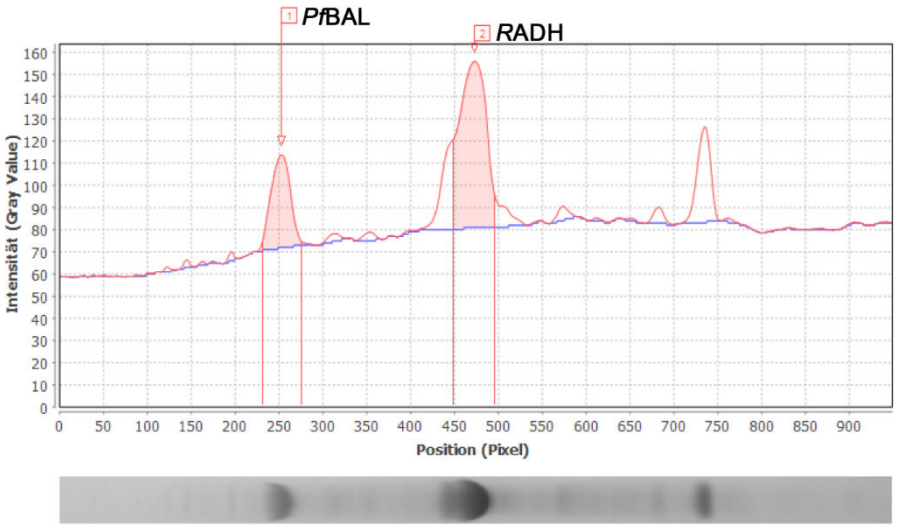


Figure S6. Exemplary densitometric analysis of the *Pf*BAL/*R*ADH distribution in Co-CatIBs. SDS-Gels were analysed using the LabImage 1D Software (Kapelan BioImaging solutions, Leipzig, Germany). The upper part of the figure shows the profile (in red) derived from the SDS-PAGE lane shown below. The baseline is shown in blue. Analysed peaks are highlighted. Densitometric analysis of this SDS gel yields a relative stoichiometry of 29% (*Pf*BAL) to 71% (*R*ADH). The final values of 32 ± 1% (*Pf*BAL) to 68 ± 1% (*R*ADH) presented in the main manuscript derive from densitometric evaluation of two SDS gels.

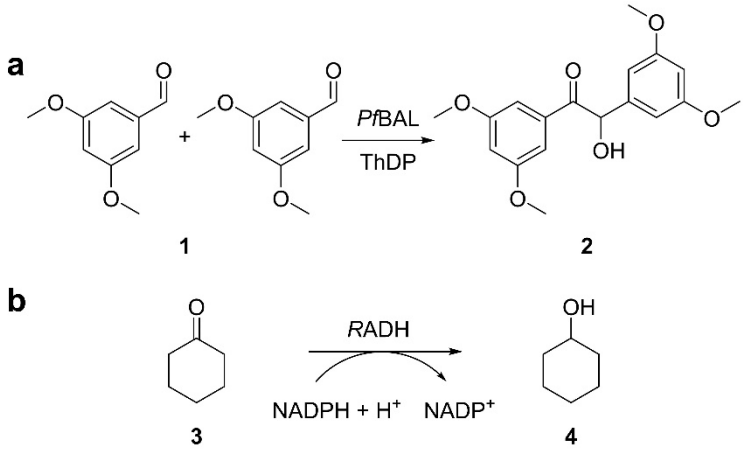


Figure S5. Principle of the spectrofluorimetric *Pf*BAL (a) and *R*ADH (b) activity assay. (a) The activity of *Pf*BAL was determined by following the carboligation of two 3,5-dimethoxybenzaldehyde (DMBA) molecules **1** to yield (*R*)-1,2-bis(3,5-dimethoxyphenyl)-2-hydroxyethanone (TMBZ) **2**. The consumption of DMBA can be detected fluorometrically (excitation: λ_{ex} 350 nm and emission: λ_{em} 460 nm) or by HPLC. (b) The activity of *R*ADH was determined by following NADPH-dependent reduction of cyclohexanone **3** to cyclohexanol **4**, whereby the oxidation of NADPH can be detected photometrically (at 340 nm) or fluorometrically (excitation: λ_{ex} 350 nm and emission: λ_{em} 460 nm).

Supporting References

(1) Guauque Torres Mdel, P., Foresti, M. L., and Ferreira, M. L. (2013) Cross-linked enzyme aggregates (CLEAs) of selected lipases: a procedure for the proper calculation of their recovered activity. *AMB Express 3*, 25.

(2) Mateo, C., Palomo, J. M., van Langen, L. M., van Rantwijk, F., and Sheldon, R. A. (2004) A new, mild cross-linking methodology to prepare cross-linked enzyme aggregates. *Biotechnol. Bioeng. 86*, 273-276.

(3) Cui, J. D., Sun, L. M., and Li, L. L. (2013) A simple technique of preparing stable CLEAs of phenylalanine ammonia lyase using co-aggregation with starch and bovine serum albumin. *Appl. Biochem. Biotech. 170*, 1827-1837.

(4) Easa M.N., Yusof, F., and Abd. Halim, A. (2017) Kinetic performance of Cross-Linked Enzyme Aggregates (CLEA)-amylase from *Zophobas morio*. *Int. Food Res. J. 24*, S335-S339.

(5) Chmura, A., van der Kraan, G. M., Kielar, F., van Langen, L. M., van Rantwijk, F., and Sheldon, R. A. (2006) Cross-linked aggregates of the hydroxynitrile lyase from *Manihot esculenta*: Highly active and robust biocatalysts. *Adv. Synth. Catal. 348*, 1655-1661.

(6) Park, S. H., Soetyono, F., and Kim, H. K. (2017) Cadaverine production by using cross-linked enzyme aggregate of *Escherichia coli* lysine decarboxylase. *J. Microbiol. Biotechn. 27*, 289-296.

(7) Gasteiger, E., Hoogland, C., Gattiker, A., Duvaud, S. e., Wilkins, M. R., Appel, R. D., and Bairoch, A. (2005) Protein identification and analysis tools on the ExPASy server. In *The Proteomics Protocols Handbook* (Walker, J. M., Ed.), pp 571-607, Humana Press, Totowa, NJ.

(8) Diener, M. (2014) Von gezielter Oligomerisierung zu katalytisch aktiven *inclusion bodies* – Eine alternative Strategie zur Stabilisierung und Immobilisierung von Biokatalysatoren. Doctoral thesis. *Heinrich-Heine University Düsseldorf.* https://docserv.uni-duesseldorf.de/servlets/DocumentServlet?id=34230

(9) Janzen, E., Muller, M., Kolter-Jung, D., Kneen, M. M., McLeish, M. J., and Pohl, M. (2006) Characterization of benzaldehyde lyase from *Pseudomonas fluorescens*: A versatile enzyme for asymmetric C-C bond formation. *Bioorg. Chem. 34*, 345-361.

(10) Rahmen, N., Fulton, A., Ihling, N., Magni, M., Jaeger, K. E., and Büchs, J. (2015) Exchange of single amino acids at different positions of a recombinant protein affects metabolic burden in *Escherichia coli*. *Microb. Cell Fact. 14*, 10.

(11) Shaner, N. C., Steinbach, P. A., and Tsien, R. Y. (2005) A guide to choosing fluorescent proteins. *Nat. Methods 2*, 905-909.

(12) Miyawaki, A., Griesbeck, O., Heim, R., and Tsien, R. Y. (1999) Dynamic and quantitative Ca^{2+} measurements using improved cameleons. *P. Natl. Acad. Sci. U.S.A. 96*, 2135-2140.

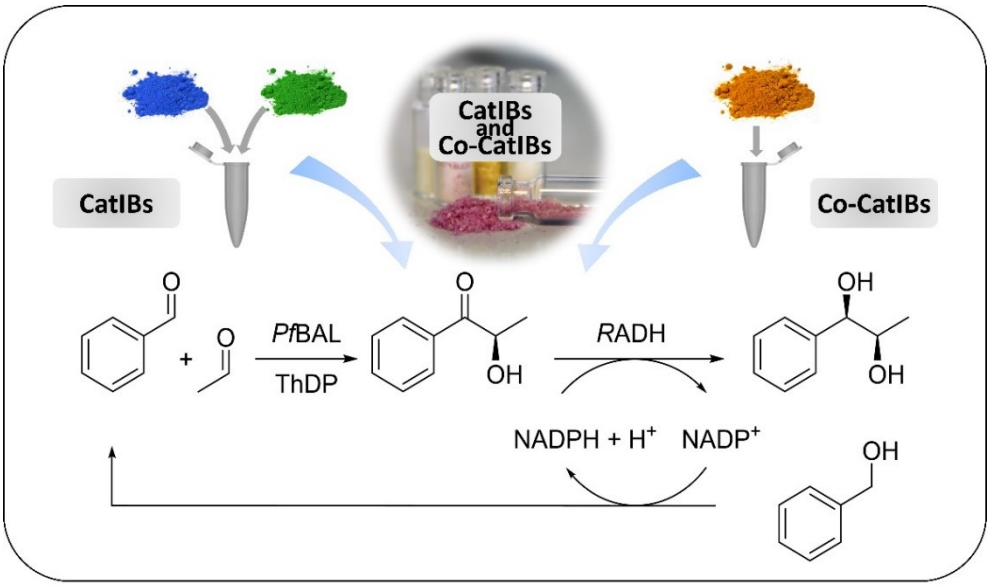
2.6 Publication VI

An Enzymatic 2-Step Cofactor and Co-Product Recycling Cascade towards a Chiral 1,2-Diol. Part II: Catalytically Active Inclusion Bodies

Vera D. Jäger, Maja Piquaray, Selina Seide, Martina Pohl, Wolfgang Wiechert, Karl-Erich Jaeger, Ulrich Krauss*

*corresponding author

Advanced Synthesis and Catalysis, 2019, 361(11).



Contributions:

VDJ, UK, and MPohl designed the study. VDJ performed the experiments with the help of MPiquaray. VDJ, UK, and MPohl interpreted the data and wrote the manuscript. UK, MPohl, KEJ, and WW initiated and coordinated this study. All authors read, commented, and approved the final manuscript.

© 2019 Wiley-VCH Verlag GmbH & Co. KGaA, Weinheim. Reproduced by permission.

(https://onlinelibrary.wiley.com/doi/full/10.1002/adsc.201900189)

DOI: 10.1002/adsc.201900189
Advanced Synthesis & Catalysis

An Enzymatic 2-Step Cofactor and Co-Product Recycling Cascade towards a Chiral 1,2-Diol. Part II: Catalytically Active Inclusion Bodies

Vera D. Jäger,[a, c] Maja Piqueray,[a] Selina Seide,[b, c] Martina Pohl,[b, c] Wolfgang Wiechert,[b, c] Karl-Erich Jaeger,[a, b, c] and Ulrich Krauss[a, c,*]

[a] Institut für Molekulare Enzymtechnologie, Heinrich-Heine-Universität Düsseldorf, Forschungszentrum Jülich, 52425 Jülich, Germany
Phone: +49-2461-61-2939
Fax: +49-2461-61-2490
E-mail: u.krauss@fz-juelich.de
[b] Forschungszentrum Jülich GmbH, IBG-1: Biotechnology, 52425 Jülich, Germany
[c] Bioeconomy Science Center (BioSC), c/o, Forschungszentrum Jülich, 52425 Jülich, Germany

Manuscript received: February 8, 2019; Revised manuscript received: April 8, 2019;
Version of record online: May 3, 2019

Supporting information for this article is available on the WWW under https://doi.org/10.1002/adsc.201900189

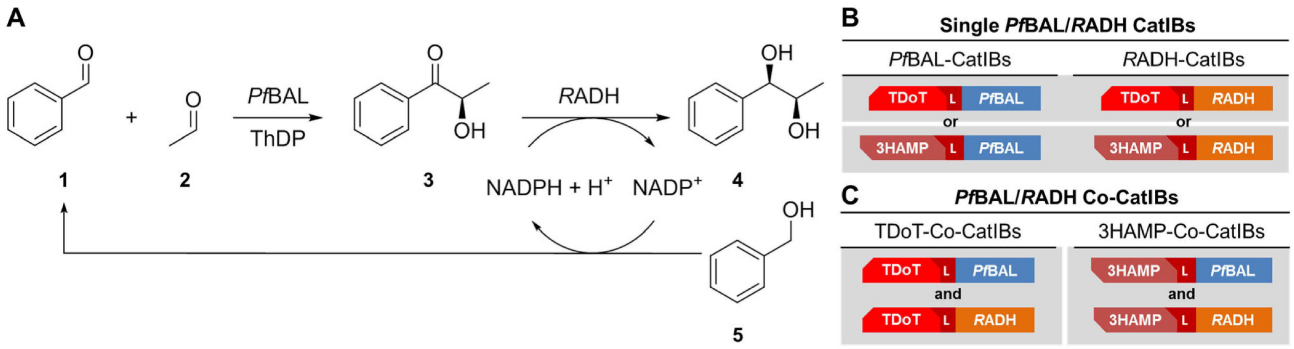
Abstract: Optimal performance of multi-step enzymatic one-pot cascades requires a facile balance between enzymatic activity and stability of multiple enzymes under the employed reaction conditions. We here describe the optimization of an exemplary two-step one-pot recycling cascade utilizing the thiamine diphosphate (ThDP)-dependent benzaldehyde lyase from *Pseudomonas fluorescens* (*Pf*BAL) and the alcohol dehydrogenase from *Ralstonia sp.* (*R*ADH) for the production of the vicinal 1,2-diol (1*R*,2*R*)-1-phenylpropane-1,2-diol (PPD) using both enzymes as catalytically active inclusion bodies (CatIBs). *Pf*BAL is hereby used to convert benzaldehyde and acetaldehyde to (*R*)-2-hydroxy-1-phenylpropanone (HPP), which is subsequently converted to PPD. For recycling of the nicotinamide cofactor of the *R*ADH, benzyl alcohol is employed as co-substrate, which is oxidized by *R*ADH to benzaldehyde, establishing a recycling cascade. In particular the application of the *R*ADH, required for both the reduction of HPP and the oxidation of benzyl alcohol in the recycling cascade is challenging, since the enzyme shows deviating pH optima for reduction (pH 6–10) and oxidation (pH 10.5), while both enzymes show only low stability at pH > 8. This inherent stability problem hampers the application of soluble enzymes and was here successfully addressed by employing CatIBs of *Pf*BAL and *R*ADH, either as single, independently mixed CatIBs, or as co-immobilizates (Co-CatIBs). Single CatIBs, as well as the Co-CatIBs showed improved stability compared to the soluble, purified enzymes. After optimization of the reaction pH, the *R*ADH/*Pf*BAL ratio and the co-solvent content, we could demonstrate that almost full conversion (> 90%) was possible with CatIBs, while under the same conditions the soluble enzymes yielded at most > 50% conversion. Our study thus provides convincing evidence that (Co-)CatIB-immobilizates can be used efficiently for the realization of cascade reactions, i.e. under conditions where enzyme stability is a limiting issue.

Keywords: inclusion bodies; enzyme immobilization; protein co-localization; biocatalysis; synthetic reaction cascades

Introduction

Optically pure 1,2-diols represent valuable building blocks for the production of pharmaceuticals, chemical catalysts, and agrochemicals.[1] Apart from using chemical methods,[2] they can be obtained biocatalytically from either prochiral α-hydroxy ketones, by NAD(P)H-dependent alcohol dehydrogenases (ADHs),[3] or by combining the carboligation of aldehydes by thiamine diphosphate (ThDP)-dependent enzymes with ADHs in a cascade reaction.[4] For example, by combining a set of different ThDP-dependent enzymes with different ADHs all four stereoisomers of 1-phenyl-1,2-propanediol have been

© 2019 Wiley-VCH Verlag GmbH & Co. KGaA, Weinheim



Scheme 1. Two-enzyme one-pot cascade for the synthesis of (1*R*,2*R*)-1-phenylpropane-1,2-diol (A). In the first step, *Pf*BAL catalyzes the carboligation of benzaldehyde **1** and acetaldehyde **2** to yield the intermediate (*R*)-2-hydroxy-1-phenylpropanone (HPP, **3**). In the second step, HPP is reduced by *R*ADH to yield (1*R*,2*R*)-1-phenylpropane-1,2-diol (PPD, **4**). *R*ADH requires NADPH as a cofactor, which is regenerated in a co-substrate driven approach utilizing the oxidation of benzyl alcohol **5** to yield the benzaldehyde substrate **1** for the *Pf*BAL reaction. Schematic illustration of the fusion constructs used in this study for the generation single *Pf*BAL/*R*ADH CatIBs (B) and the corresponding Co-CatIBs (C). (Co-)CatIB formation is achieved by molecular biological fusion of two different coiled-coil domains (TDoT and 3HAMP; dark and light red) to *Pf*BAL (blue) and *R*ADH (orange) via a linker polypeptide (L; dark red) constituted by 3-fold GlyGlyGlySer repeat and a Factor Xa protease cleavage site. For the generation of Co-CatIBs both gene fusions were co-expressed in *E. coli*, which results in the co-immobilization of the two enzymes within inclusion body (IB) particles. CatIBs that were used together in cascade reactions are marked by grey boxes.

obtained,[4a] and the production of the vicinal 1,2-diol (1*R*,2*R*)-1-phenylpropane-1,2-diol (PPD), a precursor of the calcium channel blocker diltiazem[5] was optimized, by employing either purified, isolated enzymes in aqueous media[6] or by using whole cells in microaqueous organic solvent.[4a,b] Here, a two-step one-pot reaction cascade for the synthesis of (PPD, **4**) was realized using the benzaldehyde lyase of *Pseudomonas fluorescens* (*Pf*BAL) and the alcohol dehydrogenase from *Ralstonia sp.* (*R*ADH) starting from benzaldehyde **1** and acetaldehyde **2** yielding (*R*)-2-hydroxy-1-phenylpropanone (HPP, **3**) as an intermediate. The use of benzyl alcohol **5** as a co-substrate for the substrate-coupled regeneration of the nicotinamide cofactor (NADPH) results in recycling of benzaldehyde **1**, which can then by reused in the carboligation reaction of the first step (Scheme 1, A). The general functionality of such a recycling cascade has been shown in part I of this paper by employing soluble, purified *Pf*BAL and *R*ADH.[6] However, only suboptimal conversions were observed, which we speculate is most probably due to stability issues of the two soluble enzymes in the cascade. Several stability studies of *Pf*BAL have been performed in the past, indicating that specifically the contact with the aldehyde substrates like benzaldehyde and acetaldehyde causes fast inactivation in batch processes.[7] Further, using *R*ADH for both the reduction of HPP and the oxidation of benzyl alcohol in the recycling cascade is challenging, since the enzyme shows deviating pH optima for reduction (pH 6–10) and oxidation (pH 10.5), but only low stability at pH > 8.[8]

To address those stability issues, we have recently developed a simple and efficient strategy to immobilize enzymes in catalytically active inclusion bodies (CatIBs) directly in the *E. coli* production cell. Thereby, CatIB formation is induced by aggregation-inducing tags such as the tetrameric coiled-coil domain of the cell surface protein Tetrabrachion (tetramerization domain of tetrabrachion; TDoT) from the from *Staphylothermus marinus*[9] or the dimeric 3HAMP coiled-coil domain (belonging to the family of signaling domains found in histidine kinases, adenylyl cyclases, methyl-accepting chemotaxis proteins, and phosphatases), derived from the soluble oxygen sensor Aer2 from *Pseudomonas aeruginosa*.[10] Both have previously been employed to induce CatIB formation for a variety of enzymes and fluorescent proteins,[11] among those also *Pf*BAL and *R*ADH.[11a,b] As demonstrated earlier, fusion of TDoT and 3HAMP to these enzymes, yielding the fusion proteins TdoT-L-*Pf*BAL, 3HAMP-L-*Pf*BAL, TdoT-L-*R*ADH, and 3HAMP-L-*R*ADH (L denoting the presence of an interdomain linker polypeptide consisting of a 3-fold GlyGlyGlySer repeat and a Factor Xa protease cleavage site) (Scheme 1, B), resulted in all cases in the formation of CatIBs.[11c] We also demonstrated recently that both enzymes can be jointly produced in TDoT-based Co-CatIBs (Scheme 1, C, left), although the activity specifically of the *R*ADH in these Co-CatIBs was not yet optimal.[11b] As we could demonstrate that 3HAMP-based CatIBs are generally much more active compared to TDoT-based CatIBs,[11a,c] we here evaluate 3HAMP-based Co-CatIBs as well as the single CatIBs of both enzymes as an alternative to the cascade with soluble enzymes for the synthesis of the chiral 1,2-diol PPD **4** (Scheme 1, A). The stability of all enzyme preparations was additionally studied relative to the soluble enzymes

© 2019 Wiley-VCH Verlag GmbH & Co. KGaA, Weinheim

under reaction conditions to delineate potential stabilizing effects caused by immobilization in (Co-)CatIBs. We demonstrate that due to the higher stability of *Pf*BAL and *R*ADH in CatIBs the conversion of the cascade in batch could be optimized to reach >90% conversion, while accumulating only marginal amounts of the HPP by-product, which can be attributed to the higher stability of the CatIBs making reactions at 30 °C possible (compared to 20 °C chosen in part I of this paper[6]).

Results and Discussion

Modulation of the (Co-)CatIB Properties by Different Coiled-Coil Domains

As a first step to improve cascade performance, we compared a set of different single CatIBs of *Pf*BAL and *R*ADH (Scheme 1, B) as well as different Co-CatIBs (Scheme 1, C), the latter containing both enzymes in a fixed ratio.

As previously shown for TDoT Co-CatIBs[11b] (data also shown for comparison in Figure 1, B), co-expression of the 3HAMP-L-*Pf*BAL and 3HAMP-L-*R*ADH encoding gene fusions resulted in the formation of Co-CatIBs, as can be deduced from the high respective enzymatic activities in the insoluble IB-containing cellular fraction (I) (Figure 1, B; for SDS-PAGE analysis see ESI, Figure S5). The observed CatIB-formation efficiency, defined as the activity of the respective enzyme in the insoluble inclusion body (IB)-containing fraction relative to the activity of the crude cell extract (set to 100%), was very similar for all analyzed fusion enzymes (in all cases >70% of the activity was found in the insoluble IB-containing fraction), but huge differences were observed with regard to the specific activities of the (Co-)CatIBs. Whereas all TDoT-derived (Co-)CatIBs showed low residual activities (1.0% and 3.3%) compared to the corresponding purified soluble enzymes, the 3HAMP-derived (Co-)CatIBs retained much higher residual activities (8.6% and 18.1%) (Figure 1, C and ESI Table S1). Overall, the residual activity of both *Pf*BAL and *R*ADH appears to be lower in the 3HAMP Co-CatIBs relative to the corresponding single 3HAMP CatIBs (Figure 1, C and Table S1). In conclusion, the higher activity observed for the 3HAMP (Co-)CatIBs compared to the TDoT (Co-)CatIBs highlights the possibility to tailor the properties of CatIBs by fusion of different coiled-coil domains. This was also recently demonstrated for 3HAMP-CatIBs of *Pf*BAL, which were shown to be more suitable for the synthesis of (*R*)-benzoins in a biphasic system, than the corresponding TDoT-*Pf*BAL CatIBs, even outperforming the soluble, purified enzyme.[11a]

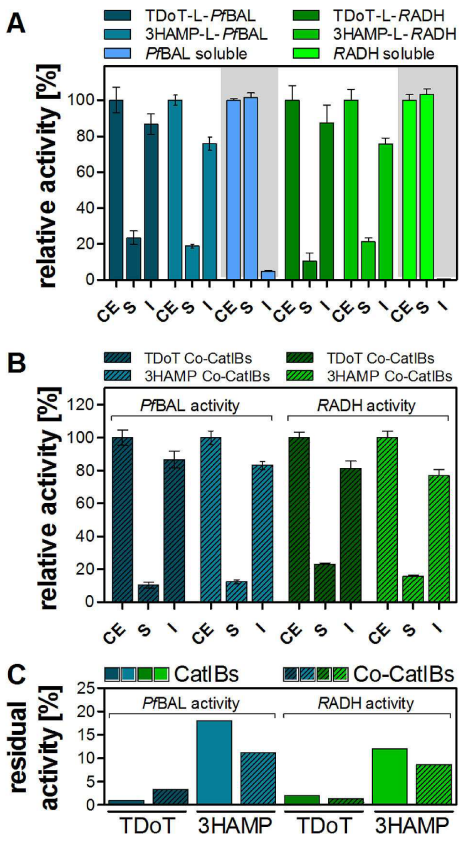


Figure 1. Distribution of *Pf*BAL and *R*ADH activity in cellular fractions after cell lysis of *E. coli* BL21(DE3) producing (A) single *Pf*PBAL- and *R*ADH-CatIBs as well as (B) the corresponding Co-CatIBs. CE: crude cell extract, S: soluble protein-containing fraction, I: insoluble inclusion bodies (IBs) containing fraction. The SDS-PAGE analysis illustrating the 3HAMP Co-CatIBs purification procedure is shown in ESI Figure S5. (C) Residual activity of the TDoT- and 3HAMP-(Co-) CatIBs. Residual activity was determined based on k_{cat}; relative to the activity of the corresponding soluble purified enzyme (see ESI, Table S1). For details see Experimental Section. Error bars correspond to the standard deviation of the mean derived from at least three technical relicates of three independent biological triplicates. Except the data for the 3HAMP Co-CatIBs, the depicted data has been presented previously.[11a–c]

Single CatIBs of *Pf*BAL and *R*ADH Outperform the Corresponding Co-CatIBs in Cascade Reactions Yielding PPD

Prompted by the above presented promising results, all of the generated (Co-)CatIBs were tested concerning their performance in the synthesis of PPD using the two-enzyme one-pot recycling cascade set up (Scheme 1, A). To directly compare cascade performance using single CatIBs of *Pf*BAL and *R*ADH, respectively, *Pf*BAL/*R*ADH Co-CatIBs, and the corresponding soluble enzyme controls, all enzyme variants were supplied in equivalent activity concentration, as determined for the *Pf*BAL/*R*ADH Co-CatIBs, with a

© 2019 Wiley-VCH Verlag GmbH & Co. KGaA, Weinheim

Table 1. Comparison of all cascade reactions performed in this study. PPD formation, overall conversion (in %) as determined relative to the sum of the employed aromatic substrates (benzaldehyde: 10 mM, benzyl alcohol: 120 mM) and HPP formation using TDoT- and 3HAMP (Co-)CatIBs, single CatIBs and the corresponding soluble enzymes determined after 4 d (8 d). Reactions were performed as described in the Experimental Section. Errors correspond to the standard deviation of the mean derived from 3 independent cascade reactions. [a:] activity concentration determined by taking the protein content and the active fraction of the corresponding enzyme/(Co-)CatIB lyophilisate into account (see Table S2).

entry	reaction conditions	*Pf*BAL [μM][a]	*R*ADH [μM][a]	*R*ADH/*Pf*BAL	PPD [mM]	conv. [%]	HPP [mM]
	pH 8.0						
1	TDoT-CatIBs	1.5	3.0	2	68.3 ± 4.1	52.4 ± 3.2	10.9 ± 0.4
2	TDoT-Co-CatIBs	1.6	3.0	2	60.8 ± 1.4	46.8 ± 1.1	20.4 ± 0.3
3	soluble control	1.4	3.0	2	61.3 ± 7.8	47.1 ± 6.0	8.9 ± 0.1
4	3HAMP-CatIBs	0.8	3.0	4	83.1 ± 0.4	63.9 ± 0.3	19.8 ± 0.1
5	3HAMP-Co-CatIBs	0.8	3.0	4	68.2 ± 0.9	52.2 ± 0.7	31.0 ± 1.9
6	soluble enzyme control	0.7	3.0	4	67.7	52.1	9.2
	pH 7.5						
7	TDoT-CatIBs	0.6	3.0	5	64.5 ± 0.9	37.9 ± 3.5	10.0 ± 0.1
8	3HAMP-CatIBs	0.6	3.0	5	49.3 ± 4.5	49.6 ± 0.7	14.0 ± 0.3
9	soluble enzyme control	0.5	3.0	6	52.7	40.6	9.5
	pH 9.0						
10	TDoT-CatIBs	0.6	3.0	5	99.0 ± 1.3	76.2 ± 1.0	1.9 ± 0.3
11	3HAMP-CatIBs	0.6	3.0	5	90.7 ± 1.5	69.8 ± 1.2	2.1 ± 0.2
12	soluble enzyme control	0.5	3.0	6	92.6 ± 1.5	71.2 ± 1.2	3.6 ± 0.2
	pH 9.0/2.5% (v/v) DMSO				PPD [mM] 4 d (8 d)	conv. [%] 4 d (8 d)	HPP [mM] 4 d (8 d)
13	TDoT-CatIBs	0.5	3.0	6	117.6 ± 1.9 (121.2 ± 8.2)	90.5 ± 1.4 (93.2 ± 6.3)	3.4 ± 0.3 (0.6 ± 0.1)
14	3HAMP-CatIBs	0.5	3.0	6	108.4 ± 5.2 (112.4 ± 4.7)	83.4 ± 4.0 (86.5 ± 3.6)	1.6 ± 0.2 (1.3 ± 0.5)
15	TDoT-Co-CatIBs	1.6	3.0	6	89.7 ± 4.0 (102.2 ± 2.5)	69.0 ± 3.1 (78.7 ± 1.9)	13.7 ± 0.5 (12.0 ± 1.2)
16	3HAMP-Co-CatIBs	0.9	3.0	2	113.5 ± 2.6 (115.9 ± 1.3)	87.3 ± 2.0 (89.1 ± 1.0)	5.9 ± 0.3 (5.1 ± 0.2)
17	soluble enzyme control	0.5	3.0	3	70.2 ± 2.0 (74.4 ± 4.6)	54.0 ± 1.5 (57.2 ± 3.5)	8.0 ± 0.8 (7.1 ± 1.0)

fixed *Pf*BAL/*R*ADH ratio (see Table 1). The activity concentration (in μM; per subunit) per cascade reaction was determined by taking the protein content of the respective enzyme preparations (lyophilizates of soluble enzymes or (Co-)CatIBs)) into account as well as the residual activity of the (Co-)CatIBs relative to the activity of the soluble enzymes (set to 100%) (see Table S2). In an initial experimental set up, the single CatIBs (TDoT and 3HAMP) and the corresponding TDoT and 3HAMP Co-CatIBs were used under identical conditions at pH 8.0 as described recently for the use of the TDoT-derived *Pf*BAL/*R*ADH Co-CatIBs.[11b]

Under these conditions, we previously observed suboptimal conversion and the accumulation of the intermediate HPP, derived from the carboligation of benzaldehyde and acetaldehyde by *Pf*BAL (Scheme 1, A). Figure 2 displays the results obtained with all (Co-) CatIBs and the conversion curves following the intermediate HPP and the chiral target product PPD (diastereomeric excess (*de*) for 1*R*,2*R*-PPD in all cases >99%; data not shown). The overall conversion based on the total amount of benzaldehyde (10 mM) and benzyl alcohol (120 mM) is summarized in Table 1. In all cases, the use of single CatIBs (Figure 2, A and C; solid blue lines), even though supplied in equivalent activity concentrations as in the corresponding Co-CatIBs, resulted in higher overall conversions compared to all tested Co-CatIBs (Figure 2, A and C; solid green lines). After 4 days of reaction time about 68 mM and 83 mM PPD, respectively, were produced by the single TDoT- and 3HAMP-CatIBs, which corresponds to overall conversions of about 52% and 64%, respectively (Table 1, entries 1 and 4). During the same reaction

 © 2019 Wiley-VCH Verlag GmbH & Co. KGaA, Weinheim

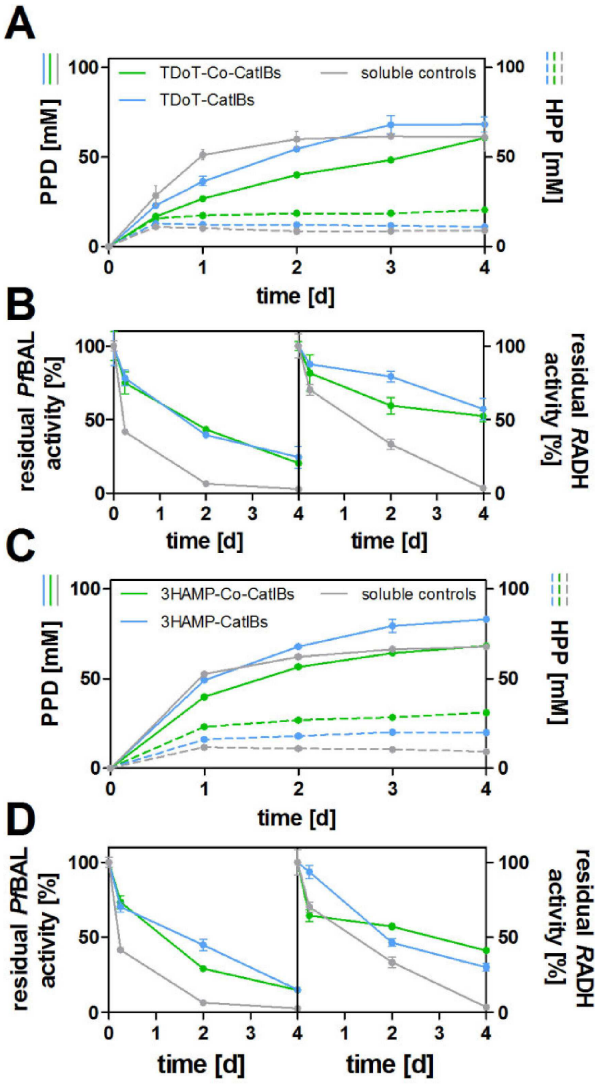


Figure 2. Two-enzyme one-pot recycling cascade for the production of PPD (solid lines in A and C) performed at pH 8.0 using TDoT-(Co-)CatIBs (A) and 3HAMP-(Co-)CatIBs (C). For reaction conditions see Experimental Section. In addition to the product PPD, also the intermediate HPP (dashed lines in A and C) was quantified. For quantification of benzaldehyde and benzoin see ESI Figure S1. Stability of *Pf*BAL (left) and *R*ADH (right) in (B) TDoT-(Co-)CatIBs and (D) 3HAMP-(Co-)CatIBs. The residual activies under reaction conditions and the activity at a given time point were measured with orthogonal assays and expressed relative to the activity of the respective enzyme preparation before starting the cascade reaction (see Experimental Section). All panels also contain data for the corresponding soluble control set-up (grey, solid and dashed lines), using *Pf*BAL and *R*ADH in an equivalent activity concentration. For comparison, the previously obtained results with TDoT Co-CatIBs are included in panel A (green solid and dashed line; see also Figure 4, g in[11b]). The employed catalyst concentrations are given in Table 1 and Table S2, entries 1–6. Error bars correspond to the standard deviation of the mean of three independent reactions. For details see the Experimental Section.

time, only about 61 mM and 68 mM PPD, corresponding to overall conversions of 47% and 52%, respectively, were obtained by using TDoT and 3HAMP Co-CatIBs. Moreover, in all cases the 3HAMP (Co-)CatIBs outperformed the TDoT (Co-)CatIBs with regard to overall PPD yield (Figure 2, Table 1, entries 2 and 5). The control reactions, containing equivalent amounts of purified, soluble *Pf*BAL and *R*ADH gave similar conversions to PPD like the Co-CatIBs, corresponding to only 81–90% of the conversion yields obtained with the single CatIBs (Table 1, entries 1–6). As demonstrated in Figure 2 the reaction with the soluble enzymes initially proceeded faster until a plateau was reached after 2 days, after which no significant further formation of PPD was observed (Figure 2 B,C). The somewhat slower conversion observed for both CatIBs and Co-CatIBs might be related to diffusional/mass transfer limitation which is known for enzyme immobilizates in general[12] and for CatIBs in particular.[11f] In all cases tested with this intial setup significant amounts of the cascade intermediate HPP accumulated during the course of the reaction (Figure 2, A and C; dashed lines; Table 1, entries 1–6). A further by-product was benzoin, formed by *Pf*BAL catalysis from two molecules of benzaldehyde.[7c,13] Benzoin accumulated to 0.015 mM in cascades employing 3HAMP-Co-CatIBs, but was not observed with the other enzyme preparations (ESI, Figure S1). The formation of side products is an undesired effect as the atom efficiency of the cascade is decreased and the workup of the final product is complicated. In the present case the formation of benzoin suggests that both enzymes are most probably inactivated under the reaction conditions, since the theoretically possible conversion could not be achieved. Benzoin is a known intermediate of the *Pf*BAL reaction during the formation of HPP and usually disappears during the course of the reaction with excess acetaldehyde.[14] This was also observed here directly under cascade reaction conditions where soluble *Pf*BAL and *R*ADH were completely inactivated after 2 or 4 days, respectively (Figure 2, B, D; grey line). In contrast, under the same conditions all (Co-)CatIBs showed increased stability (Figure 2, B, D; green and blue lines). The accumulation of the intermediate HPP, moreover, suggests that the *R*ADH-catalyzed part of the cascade is specifically limiting under the employed reaction conditions. This can be improved by altering the *Pf*BAL/*R*ADH ratio. This, however, is not feasible for Co-CatIBs, as the *Pf*BAL/*R*ADH ratio is determined by the relative expression yields and fixed by the co-expression strategy.[11b] Therefore, in the following experiments, only single *Pf*BAL and *R*ADH CatIBs were employed, where the *R*ADH/*Pf*BAL ratio was increased by keeping the *R*ADH concentration constant, while reducing the amount of *Pf*BAL (Table 1, entries 7–12).

 © 2019 Wiley-VCH Verlag GmbH & Co. KGaA, Weinheim

pH Optimization of the Cascade

For the here presented two-enzyme one-pot recycling cascade, in particular the pH value is critical, since for both enzymes the pH-optima of initial rate activities differ from the stability optima. The pH-optimum of *Pf*BAL has been investigated for both benzoin cleavage (lyase reaction) in the presence of acetaldehyde resulting in the formation of HPP as well as benzoin formation (ligase reaction) from benzaldehyde.[13] In both cases, *Pf*BAL showed an activity optimum at pH 8.0, with rapidly decreasing activities at more acidic pH values. At pH 9.0 the enzyme still retains about 80% of the maximum activity.[13] Regarding stability, soluble *Pf*BAL was shown to be stable between pH 6.0 and pH 8.0, but rather instable at pH 9.0 (10% residual activity after 27 h).[13] Soluble *R*ADH exhibits different pH-optima for reductive and oxidative reactions.[8] Kulig *et al.* found a broad pH optimum between pH 6 and 9.5 for the reduction of benzaldehyde, whereas a sharp pH optimum around pH 10.5 was found for the oxidation of cyclohexanol.[8] At pH 9.0 the enzyme showed a half-life of 20 h whereas at pH 9.5 *R*ADH was rapidly inactivated.[8] The low stability of the soluble enzyme at alkaline pH collides with the necessity of *R*ADH to catalyze both the reduction of HPP and the oxidation of benzyl alcohol efficiently in the 2-step cascade (Scheme 1, A), which requires a pH around 9 to enable both *R*ADH-catalyzed reactions (part I of the paper).[6] It must be mentioned that the reported stabilities were measured just in buffer and the presence of aldehydes most probably will further decrease the enzyme stability.

Therefore, to optimize cascade performance and to elucidate the pH-dependent stability of *Pf*BAL and *R*ADH under reaction conditions, the cascade was performed at different pH values (7.5 and 9.0), while, as before, the stabilities of all enzyme preparations were analyzed concomitantly. At pH 7.5 and pH 8.0 (see above) *Pf*BAL and *R*ADH in single CatIBs and Co-CatIBs clearly showed increased stability compared to the soluble enzymes, in most cases retaining up to or more than 50% residual activity after two days of reaction time (Figure 2 and ESI, Figure S2, B and D; ESI Table S3). At pH 9 the differences in stability converge, specifically for the *Pf*BAL variants, whereas both single *R*ADH CatIBs show similar but higher stability than the soluble enzyme (ESI, Figure S2, B and D).

At all tested pH-values, the *Pf*BAL preparations were less stable compared to *R*ADH under the tested conditions. The rapid inactivation of *Pf*BAL can be explained by the inactivation of the free enzyme by the employed aldehyde substrates.[7d] This explains the decelerated conversion after 2 days, which was only observed for the cascades performed with the soluble enzymes (Figure 2, Figure 4, ESI Figure S2, B and D, respectively).

The reaction rates and total conversions of the cascade increased from pH 7.5 to pH 9.0 (Figure 2 and ESI, Figure S2, B and D, Table 1) and thus show the inverse pattern observed for the stability of both enzymes. Maximal conversion (76%) was achieved at pH 9.0 using TDoT-CatIBs (ESI, Figure S2, C; Table 1, entry 10). Concomittantly, the accumulation of HPP was reduced to 2–3.6 mM after 4 days of reaction time (ESI, Figure S2, C; dashed lines), which is significantly lower than observed at pH 7.5 and pH 8.0 (Figure 2, ESI, Figure S2, Table 1). Again the formation of benzoin was neglegtable and only observed with the 3HAMP-(Co-)CatIBs at pH 9.0 (ESI, Figure S3). Although *Pf*BAL and *R*ADH show the lowest stability at pH 9.0, the better performance of the cascade at this pH is most probably due to the higher activity of *R*ADH specifically with respect to the oxidation of benzyl alcohol. Unfortunately, CatIB formation did not significantly increase the stability of the enzymes at pH 9.0, whereas pronounced stabilization was observed at pH 7.5 and pH 8.0 (Figure 2, B and D, ESI, Figure S2, B).

Addition of 2.5 vol% DMSO Improved *R*ADH Stability and Cascade Performance

It is known that for many enzymes, the addition of organic co-solvents can influence activity and stability.[15] As shown earlier, 20–30 vol% dimethyl sulfoxide (DMSO) in the aqueous buffer showed significant stabilizing and activity enhancing effects on soluble *Pf*BAL.[7c,13]

However, under these conditions *R*ADH is not active and already 5 vol% DMSO diminished the activity to about 43% of the activity observed in buffer.[4c] To further optimize the *R*ADH part of the two-enzyme cascade, we therefore tested the influence of small amounts (2.5 vol%) of DMSO and methyl *tert*-butyl ether (MTBE) and comparatively analyzed the formation of PPD from HPP catalyzed by *R*ADH (Figure 3, for half-lives under cascade reaction conditions see SI Table S3). All tests were performed at pH 7.5, 8.0, and 9.0. Interestingly, for soluble *R*ADH, addition of DMSO had no significant effect on the *R*ADH-catalyzed conversion of HPP, while addition of MTBE even resulted in about 40% lower conversions relative to TEA-buffer without organic co-solvent. The effects observed for the *R*ADH-CatIBs were more variable. For both the TDoT- and the 3HAMP-derived *R*ADH-CatIBs, addition of MTBE yielded lower conversion at all tested pH values compared to the buffer control. Also, addition of DMSO resulted only in a marginal increase in conversion at pH 7.5 and 8.0. However, at pH 9.0, where the cascade in buffer yielded already the best results but *R*ADH also showed

© 2019 Wiley-VCH Verlag GmbH & Co. KGaA, Weinheim

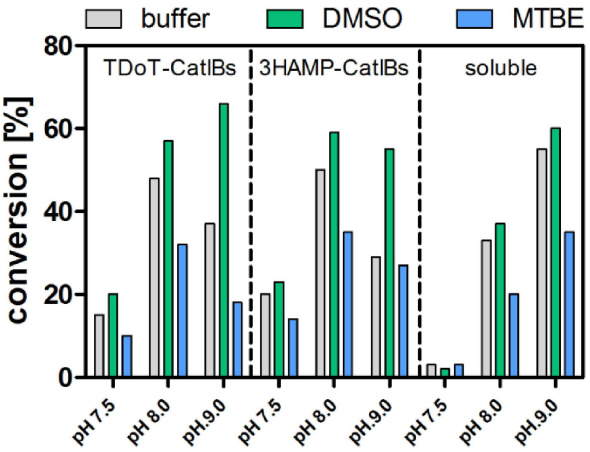


Figure 3. Evaluation of the *R*ADH-catalyzed reduction of HPP to PPD in 50 mM TEA buffer (grey bars), in the presence of 2.5 vol% DMSO (green bars) and 2.5 vol% MTBE (blue bars). Reactions were performed at pH 7.5, pH 8.0, and pH 9.0 as indicated. Details can be found in the Experimental Section.

the lowest stability, addition of DMSO was surprisingly beneficial, resulting in about 2-fold higher conversion compared to the reaction in TEA-buffer.

In conclusion, for the *R*ADH-part of the cascade, and most importantly for the *R*ADH CatIBs, addition of 2.5 vol% DMSO at pH 9.0 appears to be beneficial. Therefore, a final experiment was performed in which all CatIBs and Co-CatIBs were compared under these optimized reaction conditions (Figure 4). All reactions were performed at pH 9.0 in the presence of 2.5 vol% DMSO, and the reaction time was increased to 8 days to allow for maximal conversion of the substrates. Single CatIBs of *Pf*BAL and *R*ADH were supplied in amounts similar to the experiment performed in the absence of DMSO (ESI, Figure S2, C; see also Table 1, Table S2). Co-CatIBs were supplied at a fixed activity concentration of *R*ADH of 3 μM, which unavoidably results in an increased *Pf*BAL supply as compared to the single CatIBs, where the relative amount of *Pf*BAL is adjustable (Table 1, entries 15 and 16). Under these optimized reaction conditions the TDoT-derived single CatIBs gave the best conversion of 90.5–93% (after 4–8 days; Figure 4, A; Table 1 entry 13), resulting in a PPD yield of 121 mM after 8 days.

Similar results were obtained for the 3HAMP-derived (Co-)CatIBs, albeit with slightly lower overall PPD yields (112–115 mM PPD, 86.5–89% conversion) (Figure 4, A, Table 1 entries 14 and 16). Application of the 3HAMP Co-CatIBs yielded higher conversions as the corresponding TDoT-derived Co-CatIBs (Figure 4, C, Table 1 entry 15 and 16). However, compared to the cascade reaction performed with single CatIBs (Table 1, entries 13, 14) clearly increased amounts of HPP accumulated during the reactions catalyzed by the Co-CatIBs (Table 1, entries 15 and 16). This can be

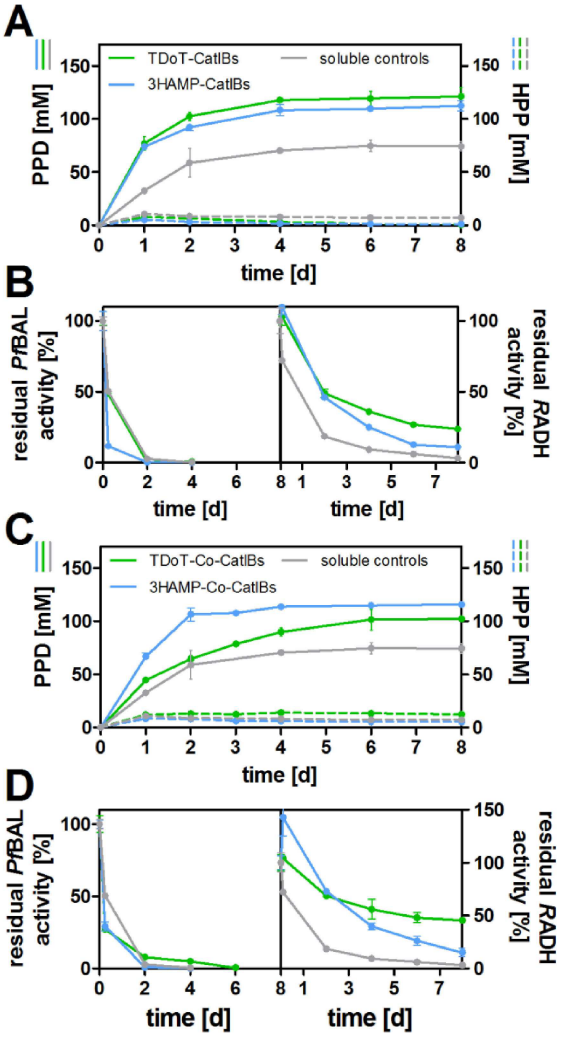


Figure 4. Optimized two-enzyme one-pot recycling cascade reaction for the production of PPD (solid lines in A and C) performed at pH 9.0 in the presence of 2.5 vol% DMSO using (A) TDoT- and 3HAMP-CatIBs as well as the corresponding (C) Co-CatIBs. For reaction conditions see Experimental Section. In addition to the PPD product, also the cascade intermediate HPP (dashed lines in A and C) was quantified. For quantification of benzaldehyde and benzoin see ESI Figure S4. Stability of *Pf*BAL (left) and *R*ADH (right) in TDoT-(Co-) CatIBs (B) and 3HAMP-(Co-)CatIBs (D). All panels also contain data for the corresponding soluble control set-up (grey, solid, and dashed lines), using equivalent activity concentrations of *Pf*BAL and *R*ADH. The employed catalyst concentrations are given in Table 1 and Table S2 entries 13–17. Error bars correspond to the standard deviation of the mean of three independent reactions.

explained by the higher activity of *Pf*BAL relative to *R*ADH within those Co-CatIBs. Hereby, it is obvious that the highest HPP concentration (13.7 mM) was formed with TDoT-Co-CatIBs, containing the highest *Pf*BAL activity concentration in the tested series (Table 1, entry 15). Under these optimized conditions

© 2019 Wiley-VCH Verlag GmbH & Co. KGaA, Weinheim

all CatIBs clearly outperformed the soluble enzymes, which, when applied in equivalent activity concentration, yielded only about 70 mM PPD (57% conversion) within 8 days, thereby accumulating approx. 7 mM HPP (Table 1, entry 17). The increased conversions, which were observed for all (Co-)CatIB preparations hereby appear to be related to an increase in stability specifically of the *R*ADH in (Co-)CatIBs in the presence of 2.5 vol% DMSO (Figure 4, B and D; compared to ESI, Figure S2, B and D for the reactions without DMSO; for half-lives see Table S3). Using the best setup (TDoT single CatIBs, pH 9.0, 2.5 vol% DMSO); PPD was prepared and isolated at a larger scale (see ESI, Supporting Methods). Product identity and purity was verified by ^{1}H- and ^{13}C-NMR and chiral GC (ESI, Figure S7/S8).

Conclusion

In the present contribution, a two-enzyme one-pot recycling cascade for the production of the vicinal 1,2-diol (1*R*,2*R*)-1-phenylpropane-1,2-diol (PPD) was optimized. As for most one-pot cascade reactions a facile balance between enzyme activity and enzyme stability proved instrumental for optimal cascade performance, where, in the present case, optimal conversion was limited by deviating pH optima and stabilities of the two employed enzymes. The problem was here mainly caused by the application of *R*ADH to catalyze the main reaction (reduction of HPP to PPD) and also cofactor regeneration through oxidation of benzylalcohol. As a consequence of the diverging pH optima for reduction and oxidation, pH 9 represents a compromise to enable both reactions with sufficient activity. However, concomitantly this results in reduced stability of both enzymes. Stabilization of *Pf*BAL can be achieved by addition of organic co-solvents, as was deduced from previous studies.[7c,13] Soluble *Pf*BAL hereby requires 20–30 vol% of DMSO for stabilization, which, however, is by far too much for *R*ADH to remain active.[4c]

The inherent stability problem was therefore here addressed by employing catalytically active inclusion bodies (CatIBs) of *Pf*BAL and *R*ADH, which, compared to the soluble, purified enzymes, show improved stability.[11b] After optimization of the reaction pH, the *R*ADH/*Pf*BAL ratio and the co-solvent content, we could demonstrate that almost full conversion (>90%), corresponding to the theoretically possible conversion calculated in part I of this paper,[6] was possible with both TDoT- and 3HAMP-CatIBs operating in the presence of low DMSO concentrations (2.5 vol%) at 30 °C. Specifically the stability of *R*ADH-CatIBs benefits from the added DMSO at pH 9 (Figure 3 and 4). Besides *Pf*BAL-CatIBs were not stabilized under these condition. However, it can be assumed that due to the high activity of this enzyme,[16] even immobilized in CatIBs, the conversion is still faster than the inactivation rate. At the end of the reaction with TDoT-CatIBs the *R*ADH CatIBs still showed 50% residual activity and could principally be reused (see SI, Table S2). The instability of *Pf*BAL under optimized conditions now limits the cascade with regard to improved space-time yields and at present prohibits the recycling of the catalyst in batch. Further experiments would be needed to optimize the stability of the *Pf*BAL-CatIBs, which could be achieved e.g. by cross-linking[17] or magnetization.[18]

Experimental Section

Materials

Chemicals and enzymes were purchased from Sigma-Aldrich, Fluka, Roth, Biosolve, Alfa Aesar, AppliChem, Merck, and Thermo Scientific (Waltham, MA, USA). Enantiopure (*R*)-(3,3′,5,5′)-tetramethoxy benzoin (TMBZ) was taken from a stock prepared as described elsewhere.[11a] Enantiopure (*R*)-2-hydroxy-1-phenylpropane-1-one (HPP) and (1*R*,2*R*)-1-phenylpropane-1,2-diol (PPD) was synthesized as described before (HPP;[4b] PPD[19]).

Construction of Expression Plasmids and Production of (Co-)CatIBs and Soluble Control Proteins

The construction of the different (co-)expression plasmids,[11a–c,f] the production of (Co-)CatIBs as well as of the corresponding soluble control proteins in *E. coli* and their subsequent purification[11a,b, f] was described before. Details can be found in the ESI, Supporting Methods section.

Cell Fractionation and Determination of (Co-)CatIB Formation Efficiency

The efficiency of (Co-)CatIB formation was evaluated by quantifying *R*ADH- or *Pf*BAL-activity in the different *E. coli* cell extract fractions after cell disruption as described before.[11b] In brief, the crude cell extract (CE), obtained by cell lysis, was separated in the soluble-protein containing supernatant fraction (S) and the insoluble, IB-containing pellet fraction by centrifugation (2 min, 7,697 *xg*, room temperature) employing suitable CE dilutions in lysis buffer (50 mM Na_2PO_4, 100 mM NaCl, pH 8.0). The resulting pellet was washed once with lysis buffer, centrifuged (2 min, 7,697 *xg*, room temperature) and resuspended in the initial volume of lysis buffer, resulting in the final insoluble IB-containing pellet fraction (I), for which activities were measured. The activities in the S and I fractions were expressed relative to the activity of the CE fraction (set to 100%). *R*ADH and *Pf*BAL activity was determined in 4× 10 mm quartz-glass fluorescence cuvettes using a continuous fluorometric activity assay by employing a Fluorolog3-22 spectrofluorometer (Horiba Jobin Yvon, Bensheim, Germany) at front-face angle geometry as described before.[7d,11b] *R*ADH activity was measured by following the reduction of cyclohexanone to cyclohexanol (ESI, Scheme S1, A) by monitoring the consumption of the cofactor NADPH recorded for 90 s at

© 2019 Wiley-VCH Verlag GmbH & Co. KGaA, Weinheim

30 °C by excitation at λ_{ex} = 350 nm and emission at λ_{em} = 460 nm (bandwidth 1.4 nm in excitation and emission). Reactions contained 100 mM cyclohexanone, 0.2 mM NADPH, and 200 µl sample in TEA-buffer (50 mM TEA, 0.8 mM $CaCl_2$, pH 7.5) in a volume of 1 ml. For measuring the *Pf*BAL activity the carboligation of 3,5-dimethoxybenzaldehyde (DMBA) to (*R*)-1,2-bis(3,5-dimethoxyphenyl)-2-hydroxyethanone (TMBZ) (ESI, Scheme S1, B) was monitored for 90 s at 25 °C by excitation at λ_{ex} = 350 nm and emission at λ_{em} = 460 nm (bandwidth 1.3 nm in excitation and emission) with 3 mM DMBA (in DMSO, final concentration 20% (v/v)) and 200 µl sample in TEA-buffer (50 mM TEA, 0.5 mM ThDP, 2.5 mM $MgSO_4$, pH 8.0) in a volume of 1 ml. All measurements were performed at least as four technical replicates of biological triplicates.

Determination of Specific Enzyme Activities and Stability Investigations

*R*ADH and *Pf*BAL-activity assays were used to determine the residual activity of the different (Co-)CatIB preparations relative to the respective soluble, purified enzyme. Likewise, those assays were employed for stability investigations, performed during the cascade reactions, to determine the stability of the respective enzyme preparation under varying reaction conditions. The employed assays have been described before.[11b]

In brief, initial *R*ADH rate activities were measured by a discontinuous photometric assay following the reduction of cyclohexanone to cyclohexanol, whereby the consumption of the NADPH-cofactor was measured photometrically at 340 nm (ESI, Scheme S1, A). The molecular extinction coefficient of NADPH was determined under assay conditions ($\varepsilon_{340\,nm}$ = 1975 $mM^{-1}\,cm^{-1}$). The assay (volume 1400 µl) contained 0.4 mM NADPH and 100 mM cyclohexanol, in TEA-buffer (50 mM, 0.8 mM $CaCl_2$, pH 7.5), pre-tempered to 30 °C. Reactions were started by addition of 350 µl pre-tempered enzyme sample ((Co-)CatIBs, or soluble *R*ADH) in suitable dilutions. Reactions were incubated for 5 min at 30 °C and 1000 rpm (Thermomixer comfort, Eppendorf, Germany), under sampling (250 µl) every minute. To stop the reaction, samples were diluted 1:3 with 500 µl methanol, centrifuged (5 min, 7697 *xg*, room temperature), and the NADPH-specific absorption was measured in standard disposable half-micro cuvettes. Initial *Pf*BAL rate activities were determined by following the carboligation of 3,5-dimethoxy benzaldehyde (DMBA) to (*R*)-(3,3‘,5,5‘)-tetramethoxy benzoin (TMBZ) (ESI, Scheme S1, B) by using a discontinuous HPLC assay.[7d] The assay solutions (volume 800 µl), contained 80% (v/v) TEA-buffer (50 mM, 2.5 mM $MgSO_4$, 0.1 mM ThDP, pH 7.5), 20% (v/v) DMSO, and 10 mM DMBA, pre-tempered at 30 °C. The reactions were started by adding 200 µl pre-tempered enzyme sample ((Co-)CatIBs, or soluble *Pf*BAL) in suitable dilutions. Reactions were incubated for 5 min at 30 °C and 1000 rpm (Thermomixer comfort, Eppendorf, Germany) under sampling (20 µl) every minute. Reactions were stopped by 1:10 dilution with methanol (including 0.1‰ (v/v) *p*-methoxy benzaldehyde (*p*-MBA) as internal standard) and analysed by high performance liquid chromatography (HPLC, see Experimental Section: *HPLC analysis*). For calibration data see ESI Figure S5.

The stability of different enzyme preparations ((Co-)CatIBs, or soluble enzyme) during the cascade reaction was determined using those assays and calculated as residual activity relative to the starting activity, as described previously.[11b] In brief, (Co-)CatIBs were removed from the cascade reaction medium by centrifugation (2 min, 7697 *xg*, room temperature) and resuspended in the fresh assay buffer in suitable concentrations. Samples of the soluble control were directly diluted in the respective buffers. For quantification of the stability, activities are given relative to the starting activity of the enzymes (before addition of the cascade reactions substrates). All reactions were performed in triplicate using three separate samples of the same preparation.

*R*ADH-Catalyzed Reactions in Presence of DMSO and MTBE

To evaluate the influence of organic co-solvents such as dimethyl sulfoxide (DMSO) and methyl *tert*-butyl ether (MTBE) on the efficacy of the *R*ADH-catalyzed reaction step (HPP to PPD) as well as on the cofactor regeneration reaction, we directly determined PPD formation from HPP (Scheme 1, A). All experiments were carried out under conditions similar to the corresponding cascade reactions at pH 7.5, 8.0, and 9.0. The reactions (volume 1 ml) were carried out in the respective assay buffer (see Experimental Section: *Cascade reaction optimization*), supplemented with 10 mM HPP, 120 mM benzyl alcohol, and 0.2 mM $NADP^+$. The influence of organic co-solvents was tested by addition of 2.5 vol% DMSO and MTBE, respectively. In order to quantitatively compare the conversion by the soluble purified *R*ADH to the conversion catalyzed by the corresponding CatIBs, 0.05 U ml^{-1} *R*ADH was used. This corresponds to: 0.73 mg ml^{-1} TDoT-*R*ADH, 0.26 mg ml^{-1} 3HAMP-*R*ADH, and 0.03 mg ml^{-1} soluble *R*ADH. Reactions were carried out as described for the cascade reactions (see Experimental Section: *Cascade reaction optimization*) at 30 °C and 1000 rpm for 1 d. Samples were prepared and analysed by HPLC as described below.

Cascade Reaction Optimization

General Reaction Setup

The general reaction setup for the synthesis of PPD from benzaldehyde and acetaldehyde using co-immobilized CatIBs (Co-CatIBs) of *Pf*BAL and *R*ADH has been described before.[11b] In brief, all reactions have been performed in 50 mM TEA buffer at different pH values (pH 7.5, pH 8.0, or pH 9.0) supplemented with 0.5 mM ThDP, 2.5 mM $MgSO_4$, and 0.8 mM $CaCl_2$. Acetaldehyde (150 mM) and benzaldehyde (10 mM) were added as substrates as well as benzyl alcohol (120 mM) as a co-substrate. Oxidation of benzyl alcohol delivers redox equivalents for the substrate-coupled cofactor regeneration catalyzed by *R*ADH, thereby generating benzaldehyde as a substrate for the *Pf*BAL-catalyzed first reaction step. All reactions were set up in sealed glass vials, to avoid evaporation of aldehyde substrates, containing a total volume of 1 ml. Reactions were incubated at 30 °C and 1000 rpm over a period of up to 8 days (Thermomixer comfort, Eppendorf, Germany). All reactions contained 0.5 U ml^{-1} *R*ADH, corresponding to an *R*ADH activity concentration of 3 µM, but

 © 2019 Wiley-VCH Verlag GmbH & Co. KGaA, Weinheim

variable amounts of *Pf*BAL (see Table 1/Table S2) (activity measured with the orthogonal assays, see Experimental Section: *Determination of specific enzyme activities and stability investigations*). Reactions were started by addition of the enzymes.

To follow the reaction progress, 20 µl samples, drawn at specific time points from freshly opened and afterwards discarded aliquots, were mixed with 180 µl methanol (including 0.1‰ (v/v) *p*-methoxy benzaldehyde (*p*-MBA) as internal standard). Samples were then vortexed and centrifuged to remove residual aggregates, and analysed by high performance liquid chromatography (HPLC). To analyse the stability of the corresponding enzyme preparations ((Co-)CatIBs or soluble *Pf*BAL/RADH) under cascade reaction conditions, the residual activity of the employed enzyme preparation (relative to the starting activity) was determined at specific time points using orthogonal assays. All cascade reactions using (Co-)CatIBs were performed in triplicate using three separate CatIB samples of the same preparation.

To optimize conversion and reduce formation of the HPP intermediate, the cascade operating conditions were optimized with regard to the employed (Co)-CatIB construct, $NADP^+$ concentration, volumetric activity of the employed enzyme preparations, reaction pH and addition of co-solvents:

a) Initial Experiments at pH 8

Initially, to compare different *Pf*BAL/*R*ADH (Co)-CatIB preparations, cascade reactions were performed in an identical manner as described by Jäger *et al.*,[11b] using 50 mM TEA buffer pH 8.0 supplemented with ThDP, $MgSO_4$, and $CaCl_2$ as described above. $NADP^+$ was provided at a concentration of 0.3 mM. In all cases *R*ADH was employed at a fixed volumetric activity of 0.5 U ml^{-1}, corresponding to 3 µM active *R*ADH (Table1/Table S2).

To directly compare cascade performance between reactions carried out using single CatIBs, Co-CatIBs, and the corresponding soluble controls, soluble *Pf*BAL, and single *Pf*BAL-CatIBs were supplied in amounts to yield the same volumetric activity (and therefore the same activity concentration) as the Co-CatIBs, where the *Pf*BAL/*R*ADH ratio cannot be adjusted. The employed catalyst concentrations are listed in Table 1/Table S2.

b) pH Optimization

To evaluate the influence of the buffer pH on cascade performance and enzyme stability, the reactions were additionally carried out at pH 7.5 and pH 9.0. For the reactions at pH 7.5 Tris buffer (50 mM) was used, while the reactions at pH 9.0 were carried out in TEA buffer (50 mM). Both buffers were supplemented with ThDP, $MgSO_4$ and $CaCl_2$ as described above. $NADP^+$ was supplied at a concentration of 0.8 mM. In both cases 0.5 U ml^{-1} *R*ADH (3 µM active enzyme) and 2.8 U ml^{-1} *Pf*BAL (~0.6 µM active enzyme) were employed (Table 1/Table S2).

c) Optimized Reaction Cascade at pH 9.0 with DMSO as a Co-Solvent

A final set of experiments was carried out to compare the CatIBs and Co-CatIBs cascade performance under optimized conditions. Reactions were performed in 50 mM TEA buffer supplemented with ThDP, $MgSO_4$, and $CaCl_2$ as described above. $NADP^+$ was provided at a final concentration of 0.8 mM as described above. Reactions were carried out in the presence of 2.5 vol% DMSO. As before a fixed *R*ADH volumetric activity of 0.5 U ml^{-1} (3 µM active enzyme) was used (Table 1/Table S2), while different volumetric *Pf*BAL activities were employed (2.5 U ml^{-1} for single TDoT- and 3HAMP-CatIBs (0.5 µM active enzyme); and variable U ml^{-1} for the corresponding Co-CatIBs; see Table 1/Table S2).

HPLC Analysis

All HPLC samples were analyzed using a Thermo Scientific Dionex Ultimate 3000 HPLC system, equipped with a Diode Array detector DAD-3000 (both: ThermoFisher Scientific, Waltham, MA, USA) and a Chiralpak® IE column (4,6 µm × 250 mm, 5 µm particle; pre-column: Chiralpak® IE; 4 mm × 10 mm; both Daicel, Tokyo, Japan). A binary mobile phase (A: dd H_2O and B: acetonitrile; flow rate 1 ml min^{-1}) was used for separation, employing two different protocols as described before.[11b]

For samples originating from cascade reactions, the following gradient was used: 15 vol% B for 8 min, 35 vol% B for 3 min, 60 vol% B for 3 min, and 15 vol% B for 3 min. Retention times: PPD: 210 nm, R_t = 11.2 min; HPP: 245 nm, R_t = 15.4 min; benzaldehyde: 245 nm, R_t = 16.2 min; benzyl alcohol: 210 nm, R_t = 10.2 min; benzoin: 210 nm, R_t = 18.5 min; *p*-MBA (internal standard): 270 nm, R_t = 17.1 min.

For HPLC samples originating from *Pf*BAL activity assays, DMBA and TMBZ were separated by isocratic elution (50 vol % B for 20 min). DMBA (R_t = 7.6 min) and TMBZ (R_t = 9.4 min) were detected at 215 nm, *p*-MBA (internal standard, R_t = 6.1 min) was detected at 270 nm. Quantification of all substrates and products was achieved by calibration using respective reference compounds (see ESI Figure S5).

Acknowledgements

We thank Stefanie Longerich (Heinrich-Heine-Universität Düsseldorf) for her help during the initial phases of the study, Ramona Kloß for the set-up of the HPLC analysis, and Prof. Wolfgang Kroutil (University of Graz, Austria) for providing the radh gene. Furthermore, we thank Ursula Mackfeld (Forschungszentrum Jülich GmbH, IBG-1) for her excellent help with the work-up of PPD as well as GC and NMR analyses. This work was funded by the Bioeconomy Science Center (BioSC), which is financially supported by the Ministry of Culture and Science of North-Rhine Westphalia within the framework of the NRW Strategieprojekt BioSC (No. 313/32 3-400-002 13). BioSC is a research cluster consisting of the universities RWTH Aachen, Düsseldorf, and Bonn, and the Forschungszentrum Jülich.

 © 2019 Wiley-VCH Verlag GmbH & Co. KGaA, Weinheim

References

[1] M. Kurina-Sanz, F. R. Bisogno, I. Lavandera, A. A. Orden, V. Gotor, *Adv. Synth. Catal.* **2009**, *351*, 1842–1848.

[2] a) T. H. Johnson, K. C. Klein, *J. Org. Chem.* **1979**, *44*, 461–462; b) R. Noyori, I. Tomino, Y. Tanimoto, *J. Am. Chem. Soc.* **1979**, *101*, 3129–3131; c) Z. Wang, Y. T. Cui, Z. B. Xu, J. Qu, *J. Org. Chem.* **2008**, *73*, 2270–2274; d) M. Tokunaga, J. F. Larrow, F. Kakiuchi, E. N. Jacobsen, *Science* **1997**, *277*, 936–938; e) W. Notz, B. List, *J. Am. Chem. Soc.* **2000**, *122*, 7386–7387.

[3] a) D. Kihumbu, T. Stillger, W. Hummel, A. Liese, *Tetrahedron: Asymmetry* **2002**, *13*, 1069–1072; b) J. Kulig, R. C. Simon, C. A. Rose, S. M. Husain, M. Hackh, S. Ludeke, K. Zeitler, W. Kroutil, M. Pohl, D. Rother, *Catal. Sci. Technol.* **2012**, *2*, 1580–1589; c) S. M. Husain, T. Stillger, P. Dünkelmann, M. Lodige, L. Walter, E. Breitling, M. Pohl, M. Burchner, I. Krossing, M. Müller, D. Romano, F. Molinari, *Adv. Synth. Catal.* **2011**, *353*, 2359–2362.

[4] a) J. Wachtmeister, A. Jakoblinnert, D. Rother, *Org. Process Res. Dev.* **2016**, *20*, 1744–1753; b) A. Jakoblinnert, D. Rother, *Green Chem.* **2014**, *16*, 3472–3482; c) J. K. Kulig, Dissertation thesis, Heinrich-Heine Universität Düsseldorf 2013.

[5] B. M. Choudary, N. S. Chowdari, S. Madhi, M. L. Kantam, *J. Org. Chem.* **2003**, *68*, 1736–1746.

[6] J. Kulig, T. Sehl, U. Mackfeld, W. Wiechert, M. Pohl, D. Rother, *Adv. Synth. Catal.* **2019**, *361*, DOI: 10.1002/adsc.201900187.

[7] a) F. Hildebrand, S. Kuhl, M. Pohl, D. Vasic-Racki, M. Müller, C. Wandrey, S. Lutz, *Biotechnol. Bioeng.* **2007**, *96*, 835–843; b) T. Stillger, Dissertation thesis, University Bonn 2004; c) P. Domínguez de María, T. Stillger, M. Pohl, S. Wallert, K. Drauz, H. Gröger, H. Trauthwein, A. Liese, *J. Mol. Catal. B* **2006**, *38*, 43–47; d) M. Schwarz, Dissertation thesis, Heinrich-Heine University Düsseldorf 2010.

[8] J. Kulig, A. Frese, W. Kroutil, M. Pohl, D. Rother, *Biotechnol. Bioeng.* **2013**, *110*, 1838–1848.

[9] J. Stetefeld, M. Jenny, T. Schulthess, R. Landwehr, J. Engel, R. A. Kammerer, *Nat. Struct. Biol.* **2000**, *7*, 772–776.

[10] M. V. Airola, K. J. Watts, A. M. Bilwes, B. R. Crane, *Structure* **2010**, *18*, 436–448.

[11] a) R. Kloss, T. Karmainski, V. D. Jäger, D. Hahn, A. Grünberger, M. Baumgart, U. Krauss, K.-E. Jaeger, W. Wiechert, M. Pohl, *Catal. Sci. Technol.* **2018**, *8*, 5816–5826; b) V. D. Jäger, R. Lamm, R. Kloß, E. Kaganovitch, A. Grünberger, M. Pohl, J. Büchs, K.-E. Jaeger, U. Krauss, *ACS Synth. Biol.* **2018**, *7*, 2282–2295; c) V. D. Jäger, R. Kloss, A. Grünberger, S. Seide, D. Hahn, T. Karmainski, M. Piqueray, J. Embruch, S. Longerich, U. Mackfeld, K.-E. Jaeger, W. Wiechert, M. Pohl, U. Krauss, *Microb. Cell Fact.* **2019**, *18:33*; d) R. Kloss, M. H. Limberg, U. Mackfeld, D. Hahn, A. Grünberger, V. D. Jäger, U. Krauss, M. Oldiges, M. Pohl, *Sci. Rep.* **2018**, *8*, 5856; e) U. Krauss, V. D. Jäger, M. Diener, M. Pohl, K.-E. Jaeger, *J. Biotechnol.* **2017**, *258*, 136–147; f) M. Diener, B. Kopka, M. Pohl, K. E. Jaeger, U. Krauss, *ChemCatChem* **2016**, *8*, 142–152.

[12] a) B. Schmieg, J. Döbber, F. Kirschhofer, M. Pohl, M. Franzreb, *Front. Bioeng. Biotechnol.* **2019**, *6*, 211; b) R. A. Sheldon, J. M. Woodley, *Chem. Rev.* **2018**, *118*, 801–838.

[13] E. Janzen, M. Müller, D. Kolter-Jung, M. M. Kneen, M. J. McLeish, M. Pohl, *Bioorg. Chem.* **2006**, *34*, 345–361.

[14] A. S. Demir, M. Pohl, E. Janzen, M. Müller, *J. Chem. Soc. Perkin Trans. 1* **2001**, 633–635.

[15] M. T. Reetz, *J. Am. Chem. Soc.* **2013**, *135*, 12480–12496.

[16] T. Stillger, M. Pohl, C. Wandrey, A. Liese, *Org. Process Res. Dev.* **2006**, *10*, 1172–1177.

[17] J. Nahalka, A. Vikartovska, E. Hrabarova, *J. Biotechnol.* **2008**, *134*, 146–153.

[18] R. Koszagova, T. Krajcovic, K. Palencarova-Talafova, V. Patoprsty, A. Vikartovska, K. Pospiskova, I. Safarik, J. Nahalka, *Microb. Cell Fact.* **2018**, *17*.

[19] J. Kulig, R. C. Simon, C. A. Rose, S. M. Husain, M. Häckh, S. Lüdeke, K. Zeitler, W. Kroutil, M. Pohl, D. Rother, *Catal. Sci. Technol.* **2012**, *2*, 1580–1589.

 © 2019 Wiley-VCH Verlag GmbH & Co. KGaA, Weinheim

2.6.1 Publication VI: Supporting Information

Supporting Methods

Construction of expression plasmids

All constructs for the production of (Co-)CatIBs were generated using pET28a vector (Merck, Darmstadt, Germany) as backbone. The general design framework for generation of the fusion proteins TDoT-L-*Pf*BAL and TDoT-L-*R*ADH, as well as 3HAMP-L-*Pf*BAL and 3HAMP-L-*R*ADH has been described recently.[1] The resulting CatIB expression vectors (pTDoT-L-*Pf*BAL, pTDoT-L-*R*ADH, p3HAMP-L-*Pf*BAL, and p3HAMP-L-*R*ADH) are described in Kloss *et al.* (see also ESI, Table S4 for details).[1c] In all cases the target enzymes are genetically fused to the coiled-coil domains by a flexible linker, consisting of a factor Xa recognition site and a $(GGGS)_3$ motif. The strategy for the generation of the corresponding TDoT-*Pf*BAL/TDoT-*R*ADH co-expression plasmids, has been described recently (Co-CatIBs; see also ESI, Table S4 for details). Here, the gene fusion coding for TDoT-L-*Pf*BAL was located at the 5'-end and the gene fusion coding for TDoT-L-*R*ADH was located at the 3'-end of an artificial two-gene operon. Each gene fusion carried its own P_{T7} promotor and ribosome binding site (RBS) upstream of the start codon, and the expression plasmids contained a T_7 terminator sequence downstream of the second gene of the two-gene operon. The co-expression plasmid containing the gene fusions coding for the 3HAMP-L-*Pf*BAL and 3HAMP-L-*R*ADH were constructed in an identical manner. In brief, the gene fusion *3hamp-l-radh* including the upstream sequence containing the P_{T7} promotor and an RBS was amplified by PCR using oligonucleotide primers (ESI, Table S5) containing *Sal*I recognition sites at 5'- as well as 3'-end. The PCR product was digested with *Sal*I, while a p3HAMP-L-*Pf*BAL vector (see [1c]; see ESI Table S4) was digested with *Xho*I. Exploiting *Sal*I/*Xho*I compatible ends, the hydrolysed target plasmid and the PCR product were ligated, resulting in the corresponding pDouble-3HAMP-*Pf*BAL-*R*ADH expression plasmid. All (co-)expression plasmids were sequenced before use (Seqlab GmbH, Göttingen, Germany).

Production and purification of (Co-)CatIBs and soluble control proteins

All gene fusions for the production of (Co-) CatIBs were heterologously expressed in *E. coli* BL21(DE3) cells using autoinduction medium[2] for 3 h at 37 °C and 69 h at 15 °C and 130 rpm as described before.[1a, 1b] After harvesting (centrifugation for 30 min at 4 °C and 7500 *xg*), cells were disrupted from a 10% (w/v) suspension in lysis buffer (50 mM sodium phosphate buffer, 100 mM NaCl, pH 8.0) using an Emulsiflex-C5 high-pressure homogenizer (Avestin Europe GmbH, Mannheim, Germany).[1b, 1c] For purification, the IB-containing pellet was separated from the soluble supernatant by centrifugation (30 min at 4 °C and 15 000 *xg*), washed once with the initial volume of MilliQ water, and again centrifuged. Pellets were lyophilized from a frozen (-80 °C) 10% (w/v) suspension in dd H_2O using a Christ ALPHA 1-3 LD Plus freeze dryer (Martin Christ Gefriertrocknungsanlagen GmbH, Osterode, Germany) and stored as a fine powder at -20 C under argon atmosphere until further use.[1b, 1c]

For expression and purification of soluble *R*ADH, an *R*ADH encoding pET22b construct,[3] was used. The soluble *R*ADH was produced in *E. coli* BL21(DE3) according to the same protocol as used for the (Co-)CatIBs. For expression and purification of soluble *Pf*BAL, the pkk233_2 vector was used, which carried a C-terminally hexahistidine (His_6)-tagged version of the *Pf*BAL encoding gene.[4] His_6-tagged *Pf*BAL was produced in *E coli* SG 13009 using a 40 L Techfors fermenter (Infors AG, Bottmingen, Swiss) at 30 °C in fed-batch mode as described elsewhere.[4-5] Cells were harvested by centrifugation and disrupted from 25% (w/v) cell suspensions in equilibration buffer (*R*ADH: 50 mM TEA, pH 7.5, 0.8 mM $CaCl_2$, and *Pf*BAL: 50 mM TEA, pH 7.5, 2.5 mM $MgSO_4$, 0.5 mM ThDP) by sonication using a UP200 (Hielscher Ultrasonics GmbH, Teltow, Germany) cell disruptor as described before.[1b] Soluble enzymes were separated from cell debris by centrifugation of the crude cell extract for 30 min (18 000 *xg*, 4 °C). Soluble *R*ADH was purified by anion exchange chromatography as described before,[1b, 1d, 3] soluble *Pf*BAL was purified, using metal ion affinity chromatograph as described earlier.[1b, 1d] Purified enzymes were lyophilized as described above from a frozen (-80 °C) 10% (w/v) suspension in the respective equilibration buffer and stored in the same manner as the (Co-)CatIBs.

Determination of protein concentration in (Co-) CatIBs, SDS-PAGE, and densitometry

The protein content of lyophilized (Co-)CatIBs or enzyme powders was determined photometrically by measuring the absorption at 280 nm of the corresponding protein solutions obtained by solubilization in 6 M guanidine hydrochloride, as described before.[1b, 1d] The protein content was calculated using theoretical molar extinction coefficients, determined based on the amino acid composition derived using the ExPaSy ProtParam Tool (http://web.expasy.org/protparam,[6] ESI Table S6). For the composition of the Co-CatIBs the molar extinction coefficient and the molecular mass was weighted based on densiometric analysis of the corresponding SDS-PAGE gels as described in Jäger *et al.*[1b] An exemplary densitometric analysis along with an example calculation is shown in the ESI Figure S5. For SDS-PAGE analysis the distribution of the recombinant fusion proteins in *E. coli* cell extract fractions (crude cell extract (CE), soluble supernatant (S), and insoluble IB-containing pellet (I)) was analyzed using pre-cast NuPAGE™ 4-12% Bis-Tris Protein Gels (ThermoFisher Nunc, Waltham, MA, USA) with MES SDS running buffer (50 mM MES, 50 mM Tris, 0.1% SDS, 1 mM EDTA, pH 7.3) as described before[1b]. The respective data, with the exception of the SDS-PAGE analysis of the 3HAMP-Co-CatIBs has already been presented elsewhere [1b-d] and are therefore not depicted here.

Chiral analysis by gas chromatography (GC)

Final concentrations of the cascade product PPD stereoisomers (underivatised stereoisomers of 1-phenyl-propane-1,2-diol) were determined by GC-analysis using a chiral-phase CP-Chirasil-DEX CB column (25 m x 0.25 mm x 0.25 mm Varian, Palo Alto, USA) with a flame ionisation detector (FID) and hydrogen as carrier gas. Samples were extracted with ethyl acetate supplemented with 1-dodecanol as internal standard. Separation was achieved as described before.[7] In brief: injection temperature: 140 °C, isothermal run for 30 min. Retention times of the different PPD stereoisomers: $R_{t,(1S,2S)}$ = 24.1 min, $R_{t,(1R,2R)}$ = 25.9 min, $R_{t,(1S,2R)}$ = 27.4 min, $R_{t,(1R,2S)}$ = 28.3 min. The synthesis of the respective reference compounds and the assignment of the absolute configuration assignment was described elsewhere.[3]

Cascade reaction at preparative scale and product isolation

To verify product quality after isolation, the cascade reaction was performed at preparative scale (25 ml), under the reaction conditions that yielded the highest PPD amounts (50 mM TEA buffer, pH 9, supplemented with 0.5 mM ThDP, 2.5 mM $MgSO_4$, and 0.8 mM $CaCl_2$; 0.8 mM $NADP^+$; 2.5 vol% DMSO; 0.5 U ml^{-1} (3 µM active enzyme) of TDoT-*R*ADH CatIBs; 2.5 U ml^{-1} (0.5 µM active enzyme) TDoT-*Pf*BAL CatIBs. The reaction was performed in glass vials (1 ml each) as described in the main part of the manuscript for 4 d at 30°C and 1000 rpm (Thermomixer comfort, Eppendorf, Germany). Subsequently, the samples were pooled and CatIBs were removed by centrifugation and filtration using an Amicon® cell with an YM-10 membrane (10 kDa cut-off, Merck, Darmstadt, Germany). Substrates and products were extracted with ethyl acetate (3x20 ml). The organic fractions were pooled, dried with $MgSO_4$, and the ethyl acetate was evaporated applying reduced pressure. Chromatographic separation of PPD was achieved by using a silica gel column (3.5 x 3.8 cm, 8 g silica gel) with a solvent phase consisting of different ratios of petrol ether (PE) and ethyl acetate (EA) (60 ml PE:EA 3:1, 40 ml PE:EA 1:1, 40 ml EA). Fractions (3 ml) containing PPD were identified by GC and pooled. The solvent was removed using reduced pressure. In total 39.3 mg of white crystals, corresponding to a yield of 12.8%, was obtained. Please note that, preparative scale synthesis was only performed to proof product quality after isolation. Therefore, neither cascade operation at preparative scale nor product workup was optimized.

Product identification and determination of purity

The product was analyzed by chiral GC (see above, and Figure S8) and nuclear magnetic resonance (NMR) spectroscopy, using $CDCl_3$ (d=7.26 ppm) with TMS (d=0.00 ppm) as internal standard (see Figure S7).

Identification by NMR

^{1}H-NMR (600 MHz, $CDCl_3$). 1.04 (d, $^{3}J_{1,2}$ = 6.3 Hz, 3H, CH_3), 2.74 (brs, 1H, OH); 2.94 (brs, 1H, OH); 3.84 (dq, 1H, $^{3}J_{2,1}$ = 6.3 Hz, $^{3}J_{2,3}$ = 7.4 Hz, C2H), 4.34 (d, ^{3}J3,2 = 7.4 Hz, 1H, C3H), 7.27-7.41 (m, 5H, arom.-H); solvent signal at 7.26

^{13}C-NMR (600 MHz, $CDCl_3$). 18.8 (C-3), 72.2 (C2), 79.5 (C1), 126.9 (arom-CH), 128.2 (arom-CH), 128.5 (arom-CH), 141.1 (arom-CH); three solvent signals at 76.9, 77.1, 77.3

The spectra match the results for previously published data for (1*R*,2*R*)-1-phenylpropane-1,2-diol.[8] Thus, the product was identified as 1-phenylpropane-1,2-diol by NMR. ^{1}H- and ^{13}C-NMR spectra can be found in Figure S7.

Table S1. Comparison of different (Co-)CatIBs and the corresponding soluble enzymes with regard to activity, protein content, and catalyst yield. Activities were measured using discontinuous assays following the reduction of cyclohexanone to cyclohexanol for *R*ADH and the carboligation of DMBA to TMBZ for *Pf*BAL as described in Experimental Section of the main paper. For the calculation of the protein content of Co-CatIB lyophilizates a weighted molecular mass and a weighted extinction coefficient, determined from densitometric analysis of the corresponding SDS gels ([1b] and Figure S4), was used. [a] Coiled-coil domain used to induce CatIB formation; [b] k_{cat} ($\mu mol_{Product}\ s^{-1}$, per subunit) calculated from the initial rate activity (U mg^{-1}; based on the protein content of the lyophilizate); [c] determined based on k_{cat}; [d] protein content calculated using the parameters given in Table S5.

CC-domain[a]	type of CatIBs	enzyme	k_{cat} [s^{-1}][b]	residual activity [%][c]	protein content of lyophilizate [%][d]	yield [$\frac{g\ lyophillizate}{100\ g\ cells}$]	Ref.
TDoT	CatIBs	*Pf*BAL	0.77 ± 0.12	1.0	71.9 ± 4.5	8.8 ± 1.0	[1b]
		*R*ADH	0.05 ± 0.01	2.0	84.6 ± 3.9	9.7 ± 1.7	[1b]
	Co-CatIBs	*Pf*BAL	2.56 ± 0.52	3.3	24.6 ± 0.4	9.0 ± 0.4	[1b]
		*R*ADH	0.04 ± 0.003	1.4	52.8 ± 0.9		
3HAMP	CatIBs	*Pf*BAL	13.9 ± 2.9	18.1	33.8 ± 5.2	3.3 ± 0.5	[1c, 1d]
		*R*ADH	0.33 ± 0.02	12.0	50.9 ± 7.6	3.8 ± 0.5	[1d]
	Co-CatIBs	*Pf*BAL	8.6 ± 2.2	11.2	13.8 ± 5.6	3.0 ± 0.6	this work
		*R*ADH	0.24 ± 0.04	8.6	33.6 ± 4.0		
	soluble	*Pf*BAL	76.65 ± 2.26	100	74.9 ± 0.3[c]	1.7 ± 0.7	[1b]
		*R*ADH	2.77 ± 0.04[c]	100	28.7 ± 0.1[c]	1.9 ± 1.1	[1b]

Table S3. Half-lives [h] of all enzyme preparations. Reaction conditions: 50 mM TEA buffer at different pH values (pH 7.5, 8.0, or 9.0) supplemented with 0.5 mM ThDP, 2.5 mM $MgSO_4$, and 0.8 mM $CaCl_2$. Acetaldehyde (150 mM) and benzaldehyde (10 mM) were added as substrates as well as benzyl alcohol (120 mM) as a cosubstrate, corresponding to cascade A in the first part of this paper.[9] *Pf*BAL and *R*ADH were added in varying concentrations and different preparations. Values were estimated based on the stability measurements of *Pf*BAL and *R*ADH (in the main paper).

Preparation			pH 7.5	pH 8.0	pH 9.0	pH 9.0 + 2.5 vol% DMSO
CatIBs	TDoT	*Pf*BAL	38	36	0-6	6
		*R*ADH	>96	>96	0-6	48
	3HAMP	*Pf*BAL	10	38	0-6	4
		*R*ADH	72	46	0-6	46
Co-CatIBs	TDoT	*Pf*BAL	n.d.	38	n.d.	5
		*R*ADH	n.d.	>96	n.d.	132
	3HAMP	*Pf*BAL	n.d.	29	n.d.	5
		*R*ADH	n.d.	70	n.d.	82
soluble		*Pf*BAL	5	5	0-6	6
		*R*ADH	62	26	0-6	20

Table S2. Enzyme preparations (soluble enzymes/(Co-)CatIBs) employed for the setup of the cascade reactions. Calculation of concentration of active protein used for each cascade. The entry numbers correspond to the cascade reactions depicted in Table 1 of the main paper.

entry	reaction conditions	lyophilisate amount [mg/ml]		protein content [%][a, b]		residual activity (%)[b]		active protein [mg/ml]		molecular weight per subunit [Da]		activity concentration [µM]		*R*ADH/*Pf*BAL ratio
		*Pf*BAL	*R*ADH	*Pf*BAL	*R*ADH	*Pf*BAL	*R*ADH	*Pf*BAL	*R*ADH	*Pf*BAL	*R*ADH	*Pf*BAL	*R*ADH	
							pH 8.0							
1	TDoT-CatIBs	2.66	7.28	91.7	87.6	4.0	1.6	0.097	0.103	66503	34314	1.5	3.0	2
2	TDoT-Co-CatIBs	10.59		23.1	49.6	4.3	2.0	0.106	0.103	66503	34314	1.6	3.0	2
3	soluble control	0.13	0.28	68.7	28.7	100	100	0.087	0.080	59985	26730	1.4	3.0	2
4	3HAMP-CatIBs	1.46	2.56	22.6	61.1	18.6	9.1	0.062	0.142	79300	47111	0.8	3.0	4
5	3HAMP-Co-CatIBs	3.90		15.0	36.5	10.5	9.9	0.062	0.142	79300	47111	0.8	3.0	4
6	soluble enzyme	0.06	0.28	68.7	28.7	100	100	0.042	0.080	59985	26730	0.7	3.0	4
							pH 7.5							
7	TDoT-CatIBs	5.75	7.28	70.0	87.6	1.0	1.6	0.040	0.103	66503	34314	0.6	3.0	5
8	3HAMP- CatIBs	1.01	2.83	31.6	47.2	14.8	10.6	0.047	0.142	79300	47111	0.6	3.0	5
9	soluble enzyme	0.05	0.28	68.7	28.7	100	100	0.032	0.080	59985	26730	0.5	3.0	6
							pH 9.0							
10	TDoT-CatIBs	6.22	7,28	75.5	87.6	0.8	1.6	0.040	0.103	66503	34314	0.6	3.0	5
11	3HAMP-CatIBs	1.01	2.83	31.6	47.3	14.8	10.6	0.047	0.142	79300	47111	0.6	3.0	5
12	soluble enzyme	0.05	0.28	68.7	28.7	100	100	0.032	0.080	59985	26730	0.5	3.0	6
							pH 9.0 / 2.5 vol% DMSO							
13	TDoT-CatIBs	5.66	7.28	75.5	87.6	0.8	1.6	0.036	0.103	66503	34314	0.5	3.0	6
14	3HAMP- CatIBs	0.92	2.83	31.6	47.3	14.8	10.6	0.043	0.142	79300	47111	0.5	3.0	6
15	TDoT-Co-CatIBs	10.59		23.1	49.6	4.3	2.0	0.106	0.103	66503	34314	1.6	3.0	6
16	3HAMP-Co-CatIBs	5.12		12.7	31.0	11.5	8.9	0.075	0.142	79300	47111	0.9	3.0	2
17	soluble enzyme	0.04	0.28	68.7	28.7	100	100	0.030	0.080	59985	26730	0.5	3.0	3

[a:] relative *Pf*BAL and *R*ADH content determined from densitometric analysis of SDS gels; [b:] Please note that the values given here for protein content and residual activity of the specific protein preparation that was used for the cascade can vary from the mean values shown in Table S1, which were derived from three independent preparations.

Table S4. Plasmids used in this study.

Vector	Genotyp	Description
pTDoT-*Pf*BAL	pET-28a, P_{T7}, gene fusion [*tdot*-factor Xa recognition site-*(GGGS)$_3$ linker- pfbal*]	pTDoT-YFP derivative, insertion of 1699 bp PCR-amplified *Bam*HI/*Not*I *pfbal* fragment in pTDoT-YFP; without the 739 bp fragment containing *yfp*[1b]
p3HAMP-*Pf*BAL	pET-28a, P_{T7}, gene fusion [*3hamp*-factor Xa recognition site-*(GGGS)$_3$ linker- pfbal*]	pTDoT-*Pf*BAL derivative, insertion of a 518 bp *Nde*I/*Spe*I *3hamp*-containing fragment in pTDoT-*Pf*BAL; without the 155 bp fragment containing *tdot*
pKK233_2-*Pf*BAL-*His*	pKK233_2 P_{trc}, *pfbal* gene, *His-tag*	Control vector for the production of soluble *Pf*BAL[10]
pTDoT-*R*ADH	pET-28a, P_{T7}, gene fusion [*tdot*-factor Xa recognition site-*(GGGS)$_3$ linker-radh*]	pTDoT-YFP derivative, insertion of 756 bp PCR-amplified *Bam*HI/*Sal*I *radh* fragment in pTDoT-L-YFP; without the 726 bp fragment containing *yfp*[1b]
p3HAMP-*R*ADH	pET-28a, P_{T7}, gene fusion [*3hamp*- factor Xa recognition site-*(GGGS)$_3$ linker-radh*]	pTDoT-*R*ADH derivative, insertion of a 518 bp *Nde*I/*Spe*I *3hamp*-containing fragment in pTDoT-*Pf*BAL; without the 155 bp fragment containing *tdot*
pET22b *R*ADH	pET-22b, P_{T7}, *radh* gene	Control vector for the production of soluble *R*ADH[3]
pDouble-TDoT-*Pf*BAL-*R*ADH	pET-28a, P_{T7}, gene fusion [TDoT-*Pf*BAL], P_{T7}, gene fusion [TDoT-*R*ADH]	pTDoT-*Pf*BAL derivative, insertion of 1102 bp PCR-amplified *Sal*I/*Sal*I P_{T7}-*RBS-tdot-l-radh* containing fragment in *Xho*I-digested pTDoT-*Pf*BAL
pDouble-3HAMP-*Pf*BAL-*R*ADH	pET-28a, P_{T7}, gene fusion [TDoT-*Pf*BAL], P_{T7}, gene fusion [TDoT-*R*ADH]	p3HAMP-*Pf*BAL derivative, insertion of 1465 bp PCR-amplified *Sal*I/*Sal*I P_{T7}-*RBS-3hapm-l-radh* containing fragment in *Xho*I-digested p3HAMP-*Pf*BAL

Table S5. Primers used in this study.

Name	Sequence (5' - 3')	Application
*Bam*HI_*Pf*BAL_fw	ATATATGGATCCATGGCGATGATTACAGGCGGCGAAC	PCR amplification of *pfbal*
*Pf*BAL_*Not*I_rv	ATATATGCGGCCGCTTATGCGAAGGGTCCATG	
*Bam*HI_*R*ADH_fw	ATATATGGATCCATGTATCGTCTGCTGAATAAAACCGC	PCR amplification of *radh*
*R*ADH_*Sal*I_rv	ATATATGTCGACTTAAACCTGGGTCAGACCACCATC	
*Sal*I_Double_T_7_fw	TATATAGTCGACCGGCGTAGAGGATCGAGATCTC	Construction of double expression vectors

Table S6. Molecular mass and molar extinction coefficients (ε) of soluble enzymes and different (Co-)CatIB fusions, as determined with the ExPaSy Protparam Tool (http://expasy.org/tools/protparam).[6] For the Co-CatIBs a weighted molecular mass as well as a weighted extinction coefficient was calculated, based on densitometric analysis of the pellet fraction as shown exemplary in Figure S4.

enzymes	molecular mass [kDa]	molar extinction coefficient (ε) [M^{-1} cm^{-1}]
TDoT-L-*Pf*BAL	66.5	55 140
3HAMP-L-*Pf*BAL	79.3	63 620
soluble *Pf*BAL	60.0	52 160
TDoT-L-*R*ADH	34.3	17 420
3HAMP-L-*R*ADH	47.1	25 900
soluble *R*ADH	26.7	14 440
TDoT-Co-CatIBs	44.5	29 431
3HAMP-Co-CatIBs	56.5	36 882

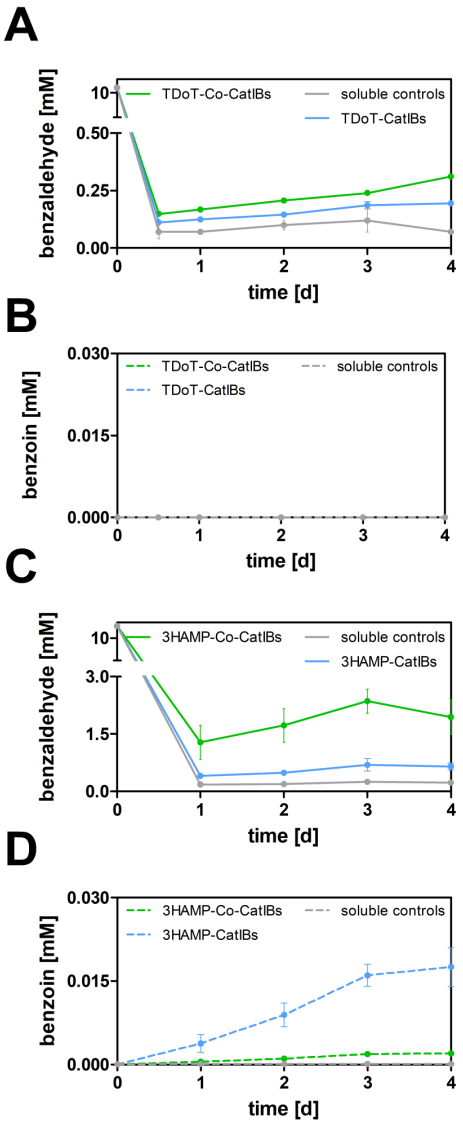


Figure S1. Conversion of benzaldehyde (A and C) and production of the side-product benzoin (B and D) for the two-enzyme one-pot cascade reaction performed at **pH 8.0**, complementary to the data shown in Figure 2 of the main paper, performed with TDoT-(Co-)CatIBs (A and B) or 3HAMP-(Co-)CatIBs (C and D). All panels also contain data for the corresponding soluble controls (grey, solid and dashed lines), set up using equivalent volumetric activities of PfBAL and RADH. The employed catalyst concentrations are given in Table 1. For reaction conditions see Experimental Section in the main manuscript. Error bars correspond to the standard deviation of the mean of at least three independent reactions.

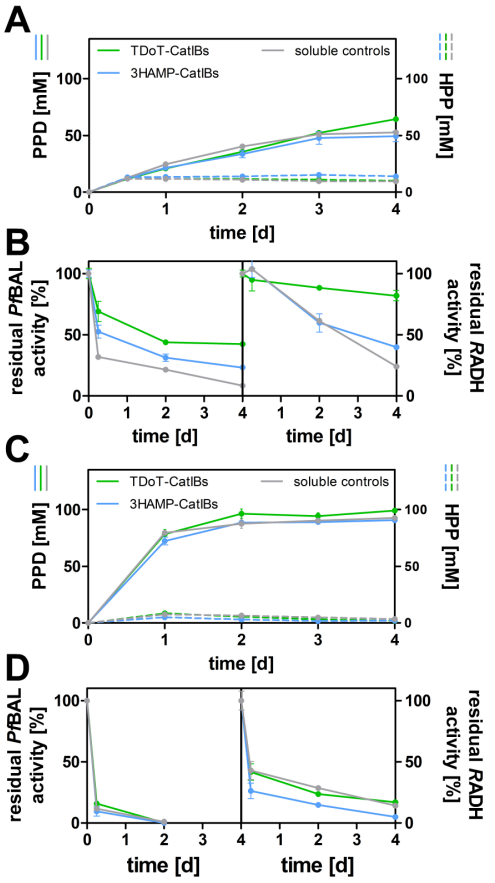


Figure S2. Two-enzyme one-pot recycling cascade for the production of PPD (solid lines in A and C) performed using TDoT-CatIBs and 3HAMP-CatIBs at **pH 7.5** (A) and **pH 9.0** (C). For reaction conditions see Experimental Section. In addition to the PPD product, also the cascade intermediate HPP (dashed lines in A and C) was quantified. For quantification of benzaldehyde and benzoin see ESI Figure S3. Stability of *Pf*BAL (left) and *R*ADH (right) in TDoT-CatIBs (B) and 3HAMP-CatIBs (D) was measured as described in Experimental section. All panels also contain data for the corresponding soluble control set-up (grey, solid and dashed lines), using soluble *Pf*BAL and *R*ADH in equivalent activity concentrations. The employed catalyst concentrations are given in Table 1 and Table S2, entries 13-17. Error bars correspond to the standard deviation of the mean of three independent reactions.

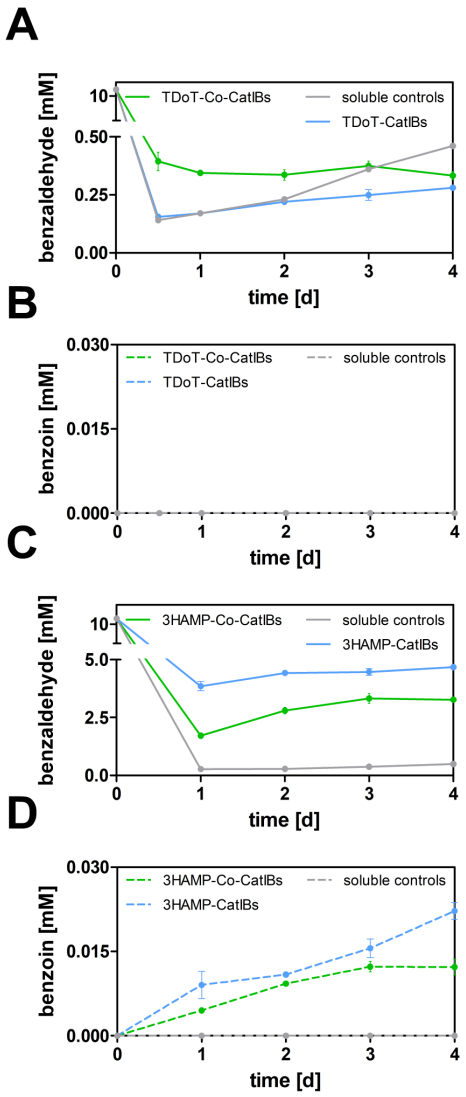


Figure S3. Conversion of benzaldehyde (A and C) and production of benzoin (B and D) for the two-enzyme one-pot cascade reaction performed with TDoT- and 3HAMP-CatIBs at **pH 7.5** (A and B) or **pH 9.0** (D and C) as seen in Figure S2. All panels also contain data for the corresponding soluble controls (grey, solid and dashed lines), set up using equivalent amounts of *Pf*BAL and *R*ADH. The employed catalyst concentrations are given in Table 1. For reaction conditions see Experimental Section in the main manuscript. Error bars correspond to the standard deviation of the mean of at least three independent reactions.

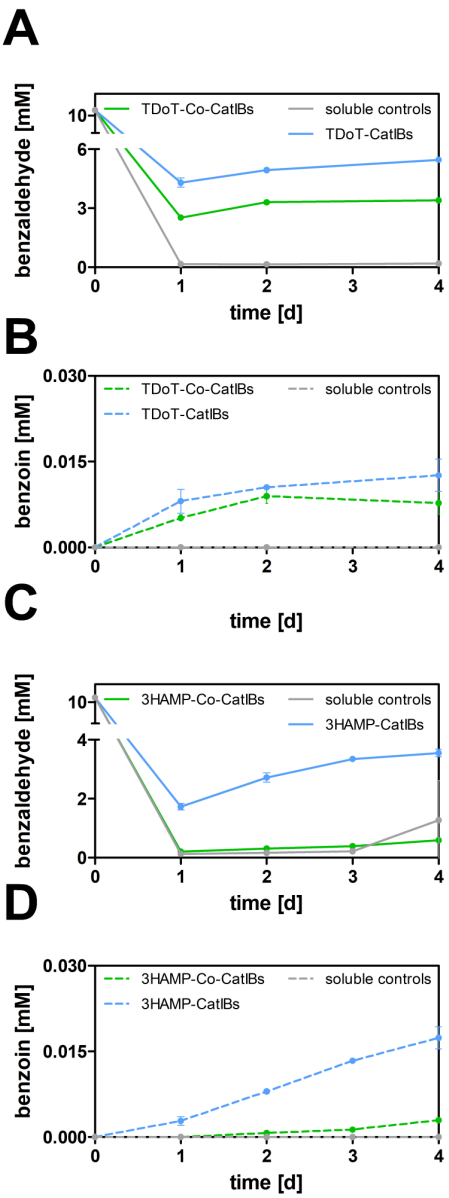
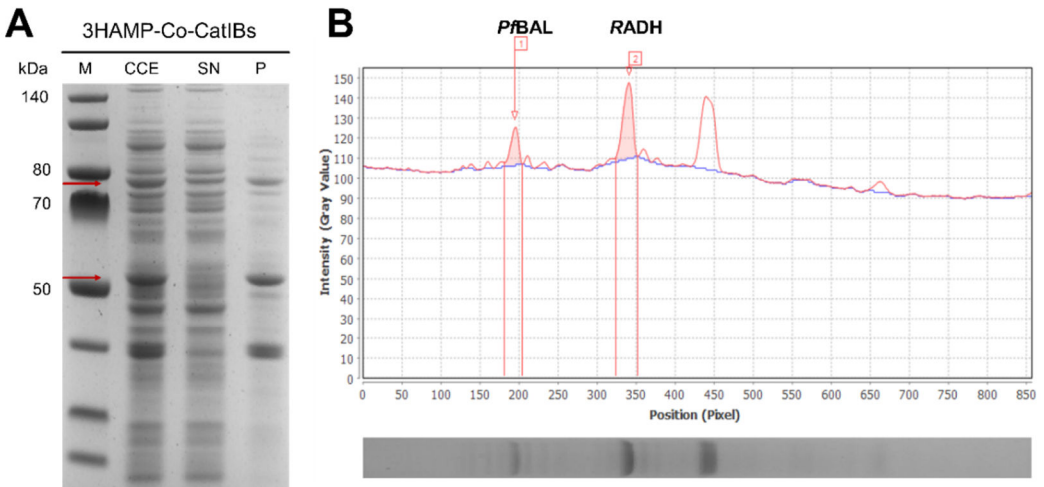


Figure S4. Conversion of benzaldehyde (A and C) and production of benzoin (B and D) for the two-enzyme one-pot cascade reaction performed at **pH 9.0 with 2.5 vol% DMSO** as seen in Figure 4 of the main paper, performed with (A and B) TDoT-(Co-)CatIBs or (C and D) 3HAMP-(Co-)CatIBs. All panels also contain data for the corresponding soluble controls (grey, solid and dashed lines), set up using equivalent amounts of *Pf*BAL and *R*ADH. The employed catalyst concentrations are given in Table 1. For reaction conditions see Experimental Section in the main manuscript. Error bars correspond to the standard deviation of the mean of at least three independent reactions.



C

protein		ratio of enzymes [%]	protein content of lyophilizate [%]	protein content of enzymes [%]
3HAMP-CoCatIBs	*Pf*BAL	29.1 ± 1.8	47.4 ± 5.6	13.8 ± 1.6
	*R*ADH	70.9 ± 4.3		33.6 ± 4.0

Figure S5. Exemplary densiometric analysis of *Pf*BAL/*R*ADH distribution in 3HAMP-Co-CatIBs. (A) SDS-PAGE analysis illustrating the production of 3HAMP-*Pf*BAL (66.5 kDa) and 3HAMP-*R*ADH (34.3 kDa), indicated by red arrows, in Co-CatIBs. (B) SDS-Gels were analysed using the LabImage 1D Software (Kapelan BioImaging solutions, Leipzig, Germany). The graph shows the profile (red) derived from the SDS-PAGE lane (below the graph). The baseline is given in blue. Analyzed peaks are highlighted. (C) Stoichiometry of the enzymes *Pf*BAL and *R*ADH in 3HAMP-CoCatIBs. All data derived from at least three replicates. The data of the other (Co-)CatIBs have been already published before.[1b, 1d]

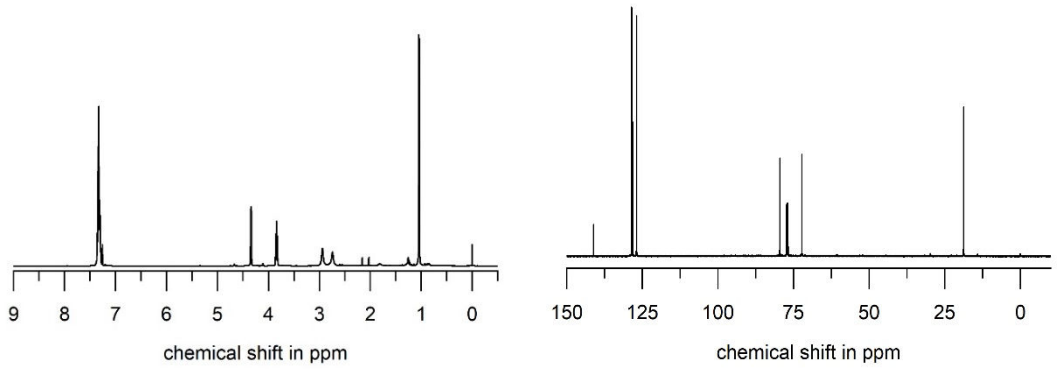


Figure S6. ^{1}H-NMR (left) and ^{13}C-NMR (right) spectra of the isolated product (see above).

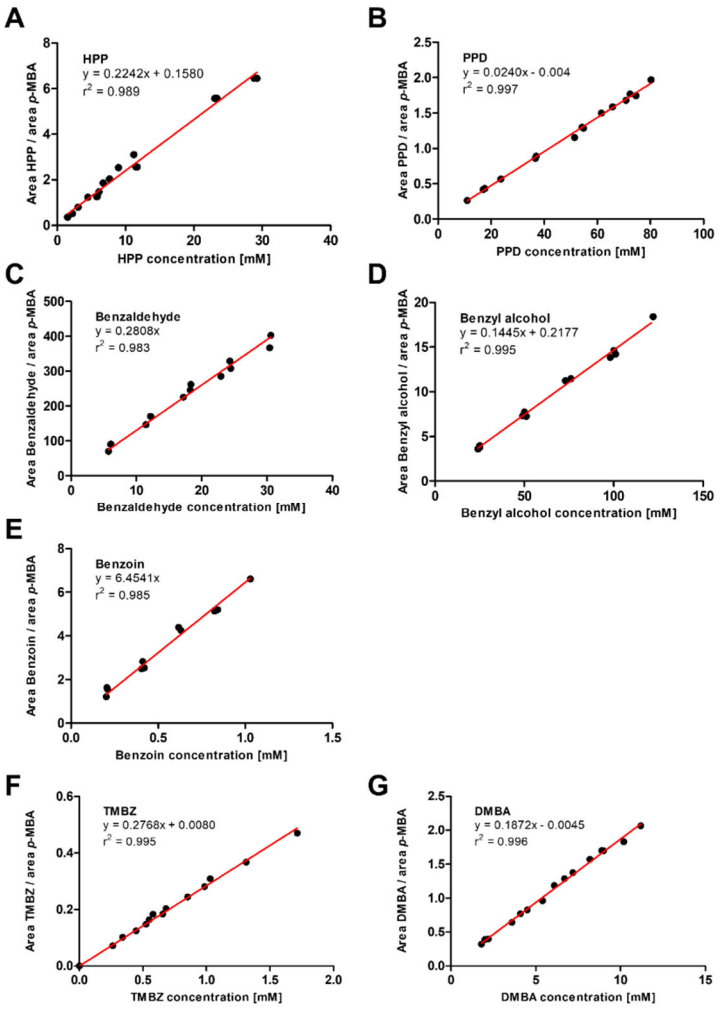
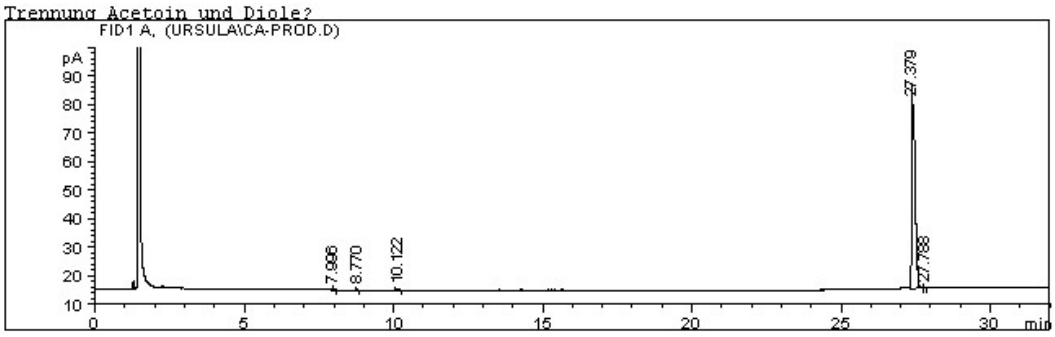
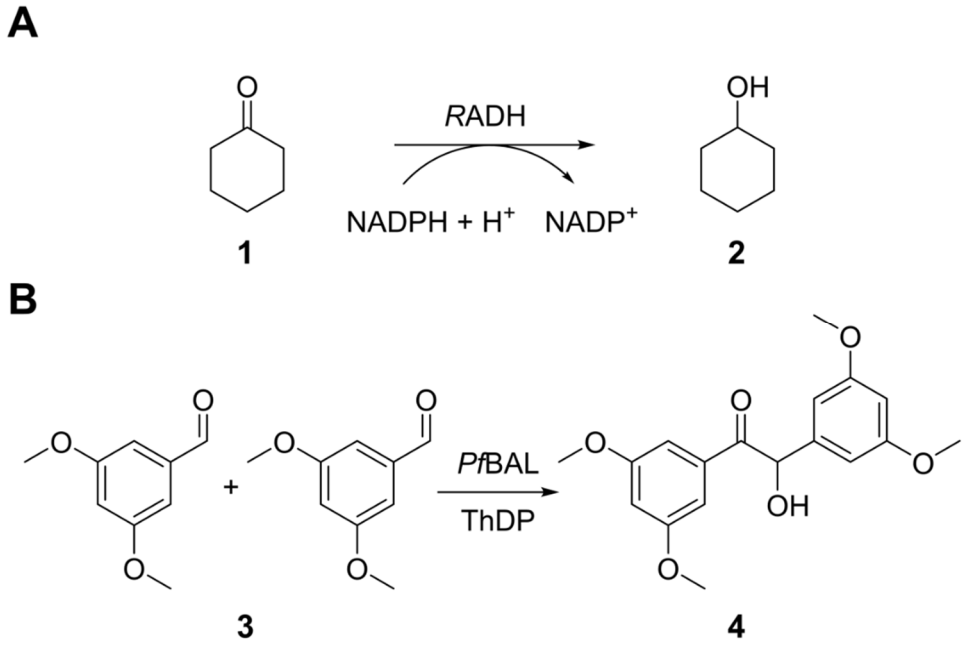


Figure S7. Calibration curves of all quantified substrates and products. (A) (*R*)-2-hydroxy-1-phenylpropanone (HPP), (B) (1*R*,2*R*)-1-phenylpropane-1,2-diol (PPD), (C) benzaldehyde, (D) benzyl alcohol, (E) benzoin, (F) (*R*)-(3,3‘,5,5‘)-tetramethoxy benzoin (TMBZ), and (G) 3,5-dimethoxybenzaldehyde (DMBA). Conditions: All HPLC samples were analyzed using a Thermo Scientific Dionex Ultimate 3000 HPLC system, equipped with a Diode Array detector DAD-3000 (both: ThermoFisher Scientific, Waltham, MA, USA) and Chiralpak® IE column (4,6 µm x 250 mm, 5 µm particle; pre-column: Chiralpak® IE; 4 mm x 10 mm; both Daicel, Tokyo, Japan). A binary mobile phase (A: dd H_2O and B: acetonitrile; flow rate 1 ml min^{-1}) was used for separation, employing two different protocols as described before.[1b]



	benzaldehyde	not identified	benzyl alcohol	1*R*,2*R* PPD	1*S*,2*R* PPD
min	7.996	8.770	10.122	27.379	27.788
area	0.39	0.35	1.77	556.19	0.88

Figure S8. GC spectrum of the isolated product (see above). A purity of 99.43 and a diastereomeric excess (*de*) of > 99% was achieved.



Scheme S1. Principle of the spectrofluorometric continuous activity assays used for (a) *R*ADH and (b) *Pf*BAL. (a) The activity of *R*ADH was determined by following NADPH-dependent reduction of cyclohexanone 1 to cyclohexanol 2, whereby the oxidation of NADPH can be detected photometrically (at 340 nm) or fluorometrically (excitation: λ_{ex} 350 nm and emission: λ_{em} 460 nm). (b) The activity of *Pf*BAL was determined by following the carboligation of two 3,5-dimethoxybenzaldehyde (DMBA) molecules 3 to the product (*R*)-1,2-bis(3,5-dimethoxyphenyl)-2-hydroxy-ethanone (TMBZ) 4. The consumption of DMBA is detected fluorometrically (excitation: λ_{ex} 350 nm and emission: λ_{em} 460 nm) or by HPLC.

3 Chapter 3
General Discussion

In this thesis a ‘toolbox’ of fusion proteins consisting of ten different target enzymes and proteins, as well as two coiled-coil domains, as aggregation-inducing tag, was established. In all cases, catalytically-active inclusion bodies (CatIBs; for catalytically-active targets such as enzymes) or functional inclusion bodies (FIBs; for not catalytically-active targets such as fluorescent proteins) could be obtained. Gene fusions were designed to investigate the potential for optimization of the CatIB-formation process and to systematically address the biotechnological relevant properties of CatIBs (2.1). Furthermore, structure-function relations were studied to address the predictability of the CatIB/FIB strategy (2.1). The influence of the expression conditions on CatIB production was studied (2.2). The application of CatIBs and their stability and activity under different reaction conditions was explored (2.3) and the biotechnological application of CatIBs for the production of 1,5-diaminopentane, an important precursor for the production of bio-based polyamides, was demonstrated (2.4). Further, the CatIB strategy was expanded to the co-immobilization of multiple proteins and enzymes to create Co-FIBs and Co-CatIBs (2.5), and finally a two-enzyme, one-pot cascade for the production of (1*R*,2*R*)-1-phenylpropane-1,2-diol, an important precursor for the calcium channel blocker diltiazem, was realized with (Co-)CatIBs (2.6).

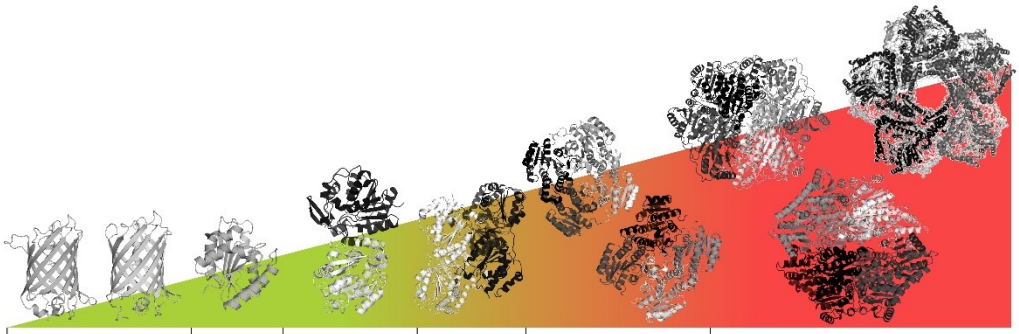
In the following, I will discuss optimization strategies for the production of CatIBs (3.1), outline the present knowledge about the formation of CatIBs and conventional IBs in light of the findings presented in this thesis (3.2), present and discuss different biotechnological applications that were realized with CatIBs, develop an overview about the advantages and disadvantages of the CatIB strategy in relation to already established immobilization methods (3.3 and 3.4), and finally conclude the discussion with a brief outlook chapter (3.5 and 3.6).

3.1 General set-up of a 'CatIB toolbox'

As outlined in the introduction (1.1.2), the production of enzymes for biotechnical application needs to be achieved by using economical, fast, and generic methods, ideally avoiding time consuming and costly chromatographic purification and immobilization steps. In this regard, CatIBs as easy to produce, cheap, and stable enzyme immobilizates, represent a promising enzyme preparation that fulfils those requirements. To study the broad applicability of the CatIB approach, initially a 'CatIB toolbox' was established, which covers ten different target enzymes and proteins of different complexity (Figure 3-1). Three of them, the *B. subtilis* lipase A (*Bs*LA), the *Arabidopsis thaliana* hydroxynitrile lyase (*At*HNL), and the *E. coli* enzyme 2-succinyl-5-enol-pyruvyl-6-hydroxy-3-cyclohexene-1-carboxylate synthase (*Ec*MenD), were already tested in a previous doctoral thesis on CatIBs by Martin Diener [22, 107]. For comparison they are included here, although no further experiments were performed. Additionally, two fluorescent proteins (FPs) were included as easy detectable model proteins. All utilized enzymes and FPs were briefly described in the introduction (1.4). The target proteins were selected to address critical issues that might complicate the formation of CatIBs or FIBs, such as folding, quaternary structure, cofactor dependence.

The simplest targets for the study of CatIBs, or in this case FIBs, are FPs, since they can easily be detected by fluorescence spectroscopy without the need for an enzyme assay (1.4.1). The formation and maturation of the fluorescent chromophore of GFP-related FPs is an autocatalytic process that, apart from a correctly folded FP monomer, requires only atmospheric oxygen. Thus, in contrast to enzyme CatIBs, substrate availability and diffusional limitation is not an issue for FP-containing FIBs. However, analogously, quenching or inner filter effects can occur that might falsify the outcome. FIBs are therefore ideal model proteins for initial proof-of-principle experiments whose results can then, under ideal conditions, be transferred to CatIBs. In this thesis, a monomeric version of the yellow fluorescent protein (YFP) (1.4.1.1) and the monomeric red-fluorescent protein mCherry (1.4.1.2) were used as target FPs.

In contrast to simple FPs, a number of additional issues might complicate the formation and application of the here established enzyme CatIBs. For the enzymes to show activity in CatIBs, they have to be folded correctly and in case of enzymes forming functional multimers, the subunits have to assemble to the correct quaternary structure. Additionally, eventually required cofactors must be able to bind to the enzyme in CatIBs and complexes of functional cofactor containing oligomers must form correctly. Last but not least, substrates as well as products must be able to diffuse in and out of the CatIBs, which might represent a critical issue, if the CatIBs are packed too tight. On the other hand, for recycling and easy downstream processing, e.g. for the separation of products, CatIBs must be stable and should not disintegrate and leak soluble enzyme.



	YFP	mCherry	*Bs*LA	*At*HNL	*Ec*MenD	*R*ADH	*Lb*ADH	*Pf*BAL	*Pp*BFD	*Ec*LDC
EC class	proteins		3.1.1.3	4.1.2.10	2.2.1.9	1.1.1.1.		4.1.2.38	4.1.1.7	4.1.1.18
structural comlpexity	monomer		monomer	dimer	dimer	tetramer		tetramer	tetramer	decamer
functional complexity	monomer		monomer	monomer	dimer	dimer		monomer	monomer	dimer
size per subunit [kDa]	27.0	26.7	19.4	29.2	61.4	26.7	26.8	58.9	56.6	80.6
co-factor	-	-	-	-	ThDP, Mg^{2+}	NADPH	NADPH	ThDP, Mg^{2+}	ThDP, Mg^{2+}	PLP
pdb number	1YFP	2H5Q	1ISP	3DQZ	2JLC	4BMN	1ZK4	2UZ1	5DEI	5FKZ

Figure 3-1 Target proteins used to set-up the 'CatIB toolbox', shown in order of increasing complexity. The monomer subunits of the proteins are colored in different shades of grey. The first four (YFP, mCherry, *Bs*LA and *At*HNL) are cofactor independent. *Ec*MenD, *Pf*BAL, and *Pp*BFD require both thiamine diphosphate (ThDP) as well as magnesium ions. Both *R*ADH and *Lb*ADH are nicotinamide adenine dinucleotide phosphate (NADPH) dependent enzymes, while *Ec*LDC requires pyridoxal-5'-phosphate (PLP). A more detailed description of the target proteins is given in the introduction section (1.4).

Of the enzymes tested in CatIBs, only *Bs*LA, is a monomer in its native form [22]. All other target enzymes form structural or functional multimeric complexes. In terms of complexity, this extends from dimers (*Ec*MenD and *At*HNL) to structural tetramers (*R*ADH, *Lb*ADH, *Pf*BAL, and *Pp*BFD) up to a structural decamer in case of the *Ec*LDC (1.4.4). Here, problems may arise especially for *Ec*MenD [22] and *Ec*LDC (1.4.4), since for their activity these enzymes must form at least a functional dimer, with the active sites being localized at the dimer interface.

In conclusion, the 'CatIB toolbox' was set up to cover a broad range of different enzymes and proteins ranging from simple monomeric FPs to complex multimeric, cofactor-dependent enzymes. Therefore, successful CatIB formation for the covered range of enzymes is indicative for the broad applicability of the approach.

3.1.1 Strategies for CatIB optimization

When the CatIB strategy was first established by Martin Diener, CatIB formation was only shown for three enzymes (*Bs*LA, *At*HNL, and *Ec*MenD) and one FP (YFP), with the fusion of the TDoT coiled-coil domain in all cases leading to CatIB-formation efficiencies above 70% [22, 107]. CatIB/FIB-formation efficiency (in %) is hereby defined as the activity or fluorescence of the insoluble IB-containing protein fraction relative to the activity or fluorescence of the corresponding crude cell extract (set to 100%) (2.1). In contrast, the here tested FP mCherry, although structurally very similar to YFP, for which

robust FIB formation is observed, showed a considerably lower FIB-formation efficiency of only 4%. Likewise, the two new target enzymes *Lb*ADH and *Pp*BFD only showed low CatIB-formation efficiencies of 5 and 1%, respectively. As a consequence, several strategies were tested to enhance CatIB/FIB formation (2.1).

CatIB-formation is induced by molecular biological fusion of a coiled-coil domain (TDoT in the original study, [107]) to a given target protein *via* a flexible linker polypeptide. The resulting gene fusion was cloned into an expression vector, which facilitates the expression of the gene fusion under the control of the strong P_{T7} promotor. In the initial construct generated by Martin Diener [22, 107], the coding sequence for the TDoT coiled-coil domain was fused to the N-terminus of the target protein and the gene fusion was constructed in a modular manner, so that every part could easily be exchanged or deleted (Figure 3-2). This modular design was here utilized to realize different optimization strategies by fusion-protein redesign (2.1). In particular, the effect of deleting the linker region, exchanging the coiled-coil domain, and the effect of fusing the coiled-coil domain to the C-terminus instead of the N-terminus was tested.

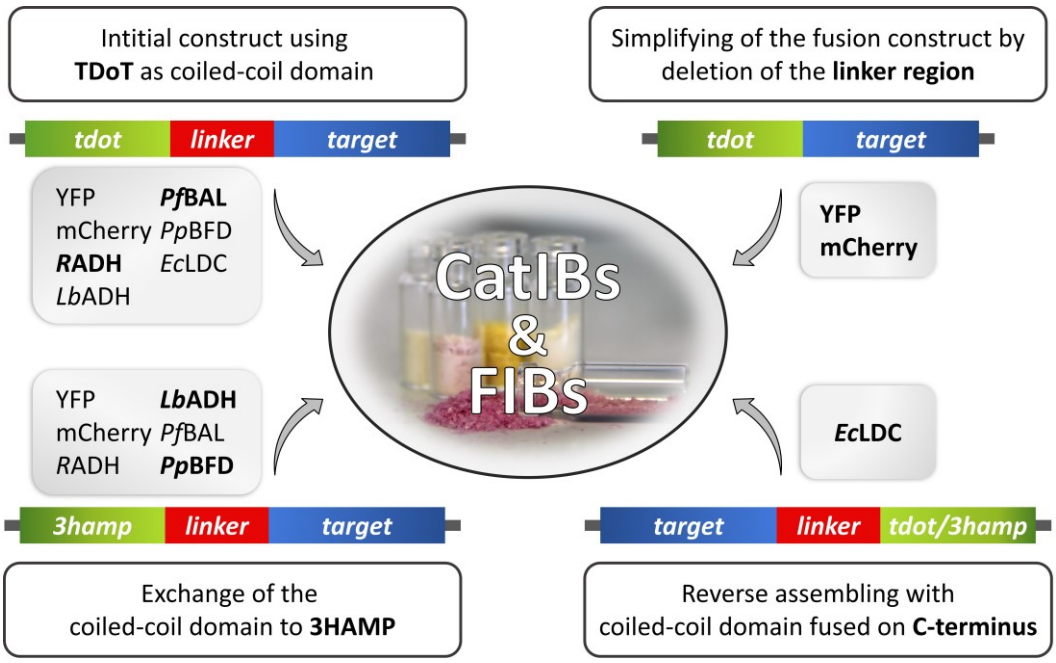


Figure 3-2 Strategies for the optimization of CatIB-formation. The original N-terminal gene fusion (upper left) was designed in a modular manner so that every part could be exchanged or deleted easily. Based on this, alternative gene fusions were created, by deletion of the linker (upper right), exchanging the coiled-coil domain to 3HAMP (lower left), or interchange between N- and C-terminal TDoT/3HAMP fusion (lower right). Not every target was tested with all four strategies. For every target the best results with regard to CatIBs/FIBs formation efficiencies are shown in bold within grey boxes.

Gene fusions were redesigned and tested, until satisfying results were obtained with regard to CatIB or FIB-formation efficiency. Therefore, not all design strategies were tested for every target. For example, the deletion of the linker was only tested for the FPs YFP and mCherry. From previous studies, it is known from previous studies that the

linker employed in a gene fusion can have a huge impact on the functionality of the resulting fusion proteins [219, 220]. In our case, the deletion of the linker resulted in an increase in FIB-formation efficiency. This was especially pronounced for mCherry, where linker deletion increased the FIB-formation efficiency almost 10-fold. But also, for YFP a 10% increase was observed. Since the employed linker consists of a $(GGGS)_3$ sequence (and a cleavage site for the Factor Xa protease), it is of a flexible nature. Therefore, its deletion might result in increased rigidity of the fusion protein, facilitating more efficient FIB-formation.

Another important issue, for the design of fusion proteins, are steric constrains imposed by the quaternary structure of the target, like the localization of the termini. The analysis of the structures of our multimeric target proteins revealed that the N-terminus of *Ec*LDC is buried within the decamer, while in all other cases it is localized at the protein surface. Therefore, it seems reasonable to assume that N-terminal fusion of TDoT could impair the proper assembly of the *Ec*LDC multimer in CatIBs. In fact, when the N-terminal TDoT-*Ec*LDC fusion protein was produced in *E. coli*, we obtained large amounts of IBs, which however did show only marginal activity. To address this issue, a gene fusion was constructed in which the coiled-coil domain was placed at the C-terminus of *Ec*LDC. The resulting *Ec*LDC CatIBs showed a residual activity that was increased by more than six magnitudes compared to the IBs obtained by N-terminal fusion (2.1).

In order to study the influence of the coiled-coil domain on the resulting CatIBs and FIBs, the 3HAMP coiled-coil domain of the oxygen sensor Aer2 [161] was employed as an alternative aggregation-inducing tag (1.3.5.2). The use of the much longer 3HAMP domain as fusion partner for different targets had variable effects on CatIB formation. While for *Lb*ADH and *Pp*BFD CatIB-formation efficiency could be dramatically increased, it was slightly reduced for *R*ADH and *Pf*BAL. In contrast, the FIB-formation efficiency for both FPs was severely reduced to only about 5%. So, while the use of a longer coiled-coil domain enhances CatIB formation for the larger multimeric enzymes, it appears to impair FIB-formation for the monomeric FPs. This phenomenon was further explored in Chapter 2.1 and is discussed in detail in Chapter 3.2.

In conclusion, several optimization strategies were here identified, which can be used to enhance CatIB or FIB formation, e.g. for targets for which our initial fusion strategy appears to fail.

3.1.2 Optimizing the expression conditions for CatIBs and FIBs

For the heterologous production of proteins, it is known that the expression system (e.g. pro- *vs.* eukaryotic, promotor and RBS strength, plasmid copy number), the expression conditions (temperature, shaking frequency, oxygenation), as well as the employed cultivation medium (rich or defined minimal media) play an important role [91, 221]. It is therefore reasonable to assume that also the expression conditions play a vital

role for the production of CatIBs. Thus, the influence of the expression conditions on the formation of CatIBs and FIBs was analyzed in cooperation with Robin Lamm (AVT - Aachener Verfahrenstechnik, Biochemical Engineering, RWTH Aachen University). As a model system, the influence of the expression conditions on the production of TDoT-YFP FIBs and soluble YFP was studied comparatively. Initially, the expression conditions established for shake flasks (0.1 to 1 l scale) were down-scaled to 48-deepwell microtiter plates (MTP). This allowed the application of high-throughput (HTP) online monitoring technologies, which, when combined with offline sampling, enable the HTP evaluation of expression conditions (2.2).

The standard protocol for CatIB/FIB production was established by Martin Diener [22] and is based on a cultivation in TB-autoinduction medium [222]. Initially, cells are cultivated at 37 °C, utilizing glucose as carbon source. This prevents the metabolization of lactose by a combination of catabolite repression and inducer exclusion [223]. After 3 h the cultures are shifted from 37 to 15 °C. Gene expression is induced after the depletion of glucose and the transition to the less favoured lactose as carbon source. During the latter phase glycerol is used as additional carbon source. Hitherto, the time point of the onset of FIB production during cultivation on TB-autoinduction medium was unclear. Online monitoring of all growth parameters revealed that functional FIB formation indeed did not occur during the initial 3 h cultivation period, but as expected, coincides with mid-logarithmic growth.

Further, it could be shown that until the early mid-exponential growth phase the pH drops from 7.0 to 6.2, and subsequently increases up to a pH of approx. 9 at the end of the cultivation. This entails not only a problem for potential pH-sensitive targets, but also for the *E. coli* culture, since maintenance of intracellular pH increases the energy demand and can inhibit cell growth and protein production [224]. The initial pH drop is caused first by the formation of acetate due to a limitation in oxygen and the subsequent pH increase likely relates to the consumption of acetate, after lactose and glucose are depleted. This effect was much less severe when using Wilms-MOPS minimal medium [225] for CatIB/FIB production. Therefore, for a more detailed characterization of the expression conditions and the FIB formation process Wilms-MOPS minimal medium was employed.

From those detailed studies, along with the initial growth experiments performed with TB-autoinduction medium, the following conclusions can be drawn: First, the FIB-formation efficiency remains constant during cultivation, regardless of oxygen availability and medium pH, which is important since it allows the robust production of FIBs even under changing cultivation conditions. However, improved pH control for the cultivation in full media would be desirable. Secondly, it was shown that the production of FIBs ceases after about 48 h, so the cultivation time commonly used for the lab-scale production of CatIBs/FIBs could easily be reduced from three to two days.

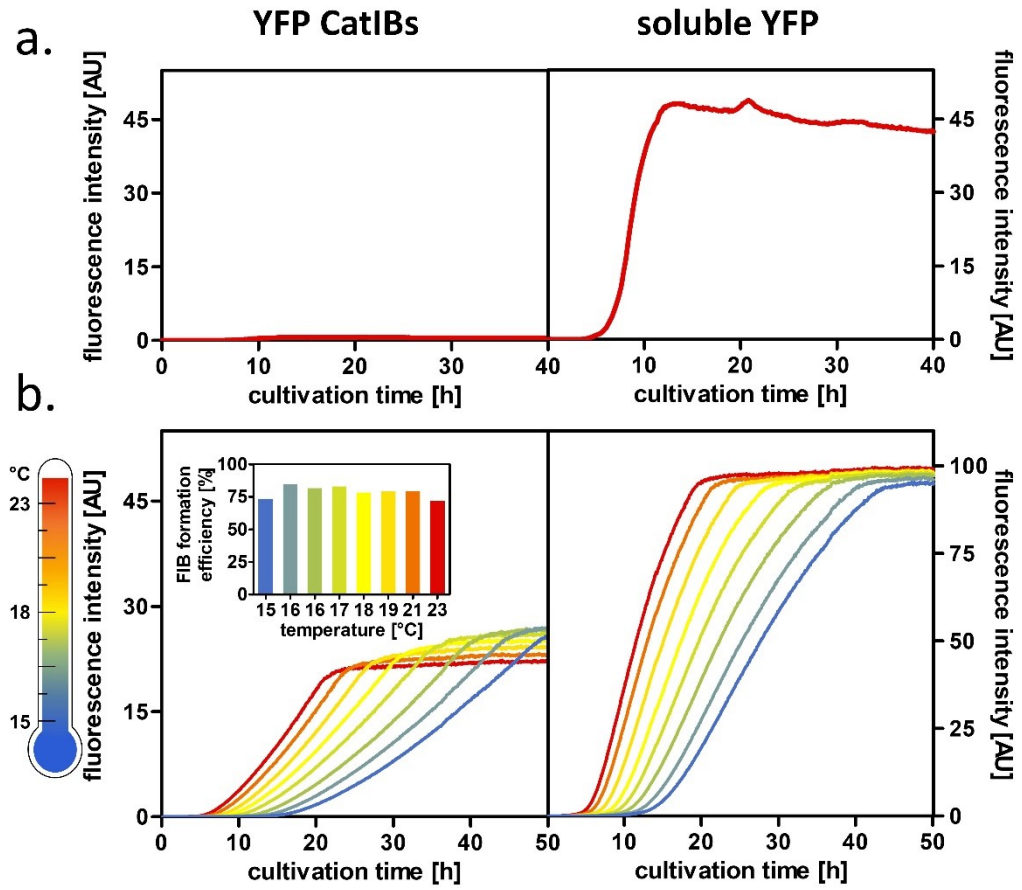


Figure 3-3 Cultivation of *E. coli* BL21(DE3) producing TDoT-YFP FIBs (left) or soluble YFP (right) at different temperatures. (a): Cultivation at 37 °C without temperature change. (b): The temperature was initially kept at 37 °C for 3 h and was subsequently reduced to establish a gradient along the MTP ranging from 15 to 23 °C. The inset (left) depicts the FIB-formation efficiency determined offline after cell disruption at the end of each cultivation. Cells were cultivated for 60 h in Wilms-MOPS auto-induction medium (0.5 g l^{-1} glucose, 2 g l^{-1} lactose, 5 g l^{-1} glycerol) with continuous measurement of YFP fluorescence. Cultivation conditions: 48-deepwell MTP with 800 µl filling volume, 1000 rpm shaking frequency, 3 mm shaking diameter. For a more detailed procedure, see Chapter 2.2. All data was taken with permission from the doctoral thesis of Robin Lamm (AVT - Aachener Verfahrenstechnik, Biochemical Engineering, RWTH Aachen University).

Most importantly, the performed online monitoring experiments demonstrated that the temperature shift from 37 to 15 °C is absolutely essential for the formation of functional FIBs. Cultivation at a constant temperature of 37 °C led to the formation of inactive IBs of the fusion protein (Figure 3-3a). Remarkably, such a temperature-shift strategy is commonly reported in literature to avoid formation of IBs in the first place [89, 91, 226, 227]. In additional tests, Robin Lamm could show that the production of functional fluorescent protein in FIBs is increased with decreasing cultivation temperatures (Figure 3-3b), while at the same time the FIB-formation efficiency (i.e. the relative amount of functional protein in FIBs, relative to the crude-cell extract) remained constant within a temperature range of 15 to 23 °C (Figure 3-3, inset) (unpublished, personal communication). This suggests that at lower temperatures higher amounts of functional fluorescent fusion protein accumulates in both the soluble fraction as well as in FIBs. The same observation has been reported before [89, 226, 228], while in other studies no temperature-shift was needed for the formation of CatIBs [119, 120, 122, 229]. These

conflicting results highlight the notion that the formation of CatIB/FIBs or IBs in general is a much more complex process as initially thought. More systematic studies are therefore needed to understand the mechanistic basis of the CatIB/FIB formation process.

In conclusion, the formation of CatIBs and FIBs not only depends on the aggregation-inducing tag and the gene fusion design, but also on the employed expression conditions. CatIBs/FIBs and conventional, inactive IBs of the same construct can be obtained, by simply changing the expression temperature. This observation might in the future help to delineate the structural differences between CatIBs/FIBs and conventional, inactive IBs.

Thus, while certain optimization strategies could be identified within this thesis, the most important open issue here remains the direct comparison of the performance of CatIBs, produced by TDoT and 3HAMP fusion, relative to other known aggregation-inducing tags (1.3.3).

3.2 Understanding IB formation - lessons learned from CatIBs and FIBs

Until today, it is not completely clear, how the formation of CatIBs/FIBs and even more generally the formation of IBs takes place. In particular it is unknown, what structures the IB-constituting proteins adopt. The observation of functional and catalytically-active IBs, hereby stresses the notion, that at least some of the IB-constituting target protein should be correctly folded [97, 119, 120, 125]. The here presented studies, using a toolbox of differently complex targets, including cofactor dependent multimeric enzymes, further suggest that to a certain degree the native quaternary structure of the target should be retained when incorporated into CatIBs or FIBs. Additionally, the structural basis as to why certain targets form CatIBs/FIBs, while others do not, remains largely elusive. Hereby, the observation that for different targets different CatIB/FIB-formation efficiencies are observed, raises the question whether CatIB/FIB formation can be predicted based on sequence or structure-based bioinformatic analyses [97, 99].

Nowadays, two theories accounting for the formation of IBs have been presented (1.3.1). The classical theory assumes that IBs are formed from misfolded polypeptides as a giant amorphous aggregate, starting from only a limited number of nucleation sites [88, 98]. In contrast, a more recent theory favours the formation of several proto-aggregates, that converge into an ‘aggregate-of-aggregates’ [88, 91].

In the following, the findings of the within this thesis presented studies in relation to both theories will be discussed. Thereby the focus lies on the comparative characterization of the different CatIBs/FIBs of the ‘CatIB toolbox’ (2.1) and by further analyzing some of the results obtained for the co-immobilization of two proteins within CatIBs and FIBs (2.5).

3.2.1 Morphologically-distinct CatIBs/FIBs are formed depending on the fused aggregation-inducing tag

The structural and morphological character of CatIBs and FIBs was studied both *in vivo* by fluorescence microscopy of CatIB/FIB formation within *E. coli* as well as *in vitro* by scanning electron microscopy (SEM) of CatIBs/FIBs preparations after purification and lyophilization (2.1). The fluorescence microscopy analysis was performed in cooperation with Alexander Grünberger and Eugen Kaganovitch (IBG-1, Forschungszentrum Jülich), while the SEM images where taken together with Steffen Köhler of the Center for Advanced Imaging (Heinrich-Heine University Düsseldorf).

From the presented microscopy images (Figure 3-4a) it is directly apparent that TDoT- and 3HAMP-FIBs of the same target accumulate as morphologically distinct aggregates in *E. coli*. This was also observed, with a few exceptions, for 3HAMP and TDoT enzyme CatIBs (2.1). Hereby, TDoT FIBs of YFP and mCherry appear to form compact IBs, i.e. refractile, dense particles, at the cell poles, which is a typical feature reported for IB formation in *E. coli* [126, 160, 230, 231]. In contrast, 3HAMP-FIBs seem to be of a much more 'diffuse' nature. The fusion proteins appear to be more evenly distributed throughout the cytoplasm and a certain fraction seems to associate with the cytoplasmic membrane. These kinds of inclusion bodies are also described in literature for the overexpression of membrane proteins in *E. coli* [232, 233]. It is remarkable that often a sort of proto-IB can be identified at the end of the cell poles in the fluorescence images. Interestingly, in the corresponding phase contrast images, such particles are not visible, which hints at a much more diffuse nature compared to TDoT FIBs or conventional IBs. The potential association of certain 3HAMP constructs to the lipid bilayer of the cell membrane is further corroborated by a higher lipid content of the corresponding 3HAMP CatIBs/FIBs compared to TDoT CatIBs/FIBs (2.1).

A similar morphological distinction was also described for FIBs derived from the aggregation-inducing tag 18aWT, a short apolipoprotein possessing an amphipathic helical structure with lipid binding ability [234]. For different variants of the 18aWT tag, different lipid 'binding' affinities were detected. The resulting GFP fusions thus showed variable membrane associations ranging from 'compact', TDoT-like to 'diffuse', 3HAMP-like FIBs [126]. Interestingly, for both kinds of morphologically different CatIBs exceptions could be found (Appendix, Figure 4-1). While most TDoT CatIBs/FIBs could be classified as 'compact', TDoT-*Pp*BFD and TDoT-*Lb*ADH did not show compact CatIBs within *E. coli*. Likewise, *Ec*LDC-3HAMP forms compact CatIBs, even though all other 3HAMP fusions form 'diffuse' CatIBs/FIBs.

Further structural analyses of selected lyophilized CatIB and FIB preparations by SEM revealed that TDoT fusions formed classical IBs with a round or barrel-like shape. On the other hand most of the corresponding 3HAMP fusions appear less well ordered, with the smallest observable particles having flake-like shapes with rather rough, less well defined

edges (Figure 3-4b). This would corroborate their more diffuse nature as already suggested by conventional (fluorescence) microscopy.

Therefore, depending on the employed aggregation-inducing tag, morphologically distinct CatIBs/FIBs can be obtained. This feature, as well as the observed exceptions, are further discussed in the following chapters (3.2.2 and 3.2.6). In conclusion, although no clear CatIB formation was detected for certain 3HAMP constructs, the CatIB preparation strategy, nevertheless, yielded functional particulate immobilizates. They could also be employed as biocatalysts, as demonstrated for the application of 3HAMP and TDoT *Pf*BAL-CatIBs in different reaction systems (2.3).

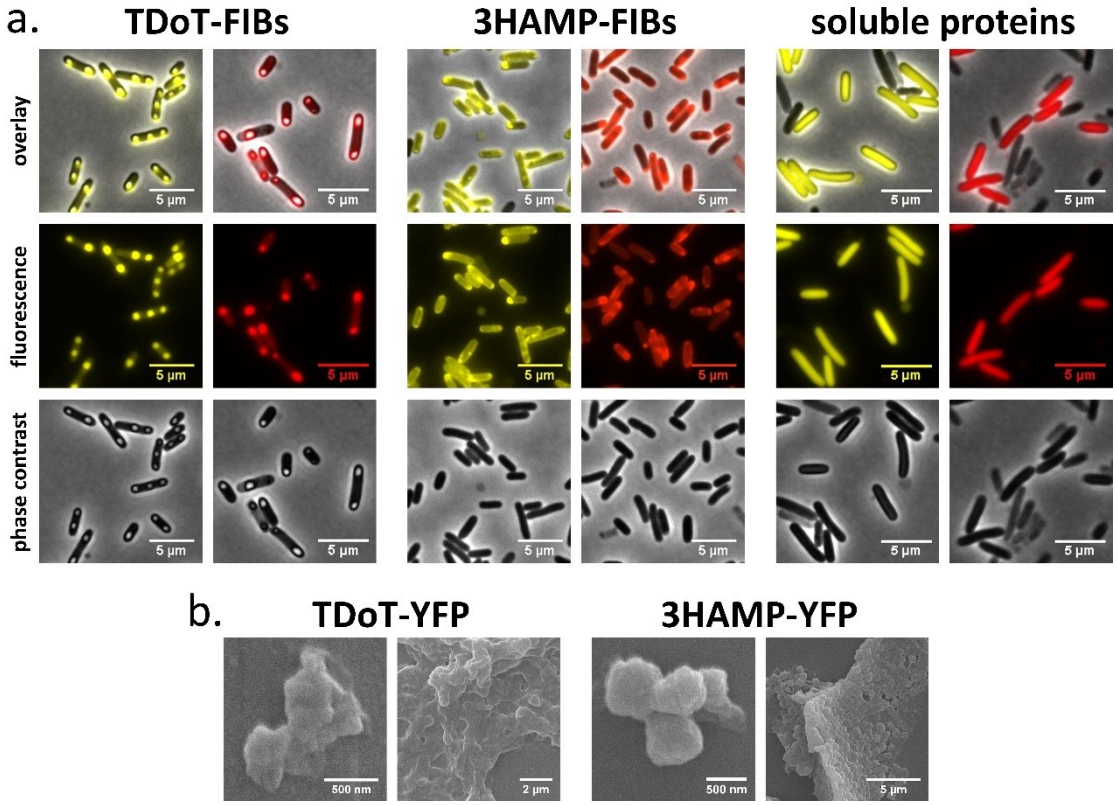


Figure 3-4 (Fluorescence) Microscopy (a) and SEM (b) images illustrating the formation of FIBS. (a): Intracellular formation of YFP (yellow) and mCherry FIBs (red) within *E. coli* cells. FIB formation was induced by TDoT (left) or 3HAMP (right) fusion. Each case shows from top to bottom: overlay, fluorescence image, and phase contrast image. (b): SEM images of YFP FIBs after cell disruption, IB purification, and lyophilization. For experimental details, see Chapter 2.1.

3.2.2 3HAMP and TDoT CatIBs possess distinct functional properties

As outlined above, most 3HAMP fusions do not seem to form classical IBs within the cells (Figure 3-5a). Nevertheless, the resulting CatIB/FIB particles can mostly be processed just like classical TDoT CatIBs/FIBs with high CatIB/FIB-formation efficiencies (Figure 3-5b). However, in terms of handling, 3HAMP CatIBs appear to dissolve more easily during preparation, i.e. as a result of several washing steps, which are commonly employed for CatIB preparation (Figure 3-5c). Likewise, when used as

biocatalyst, 3HAMP CatIBs are less stable than the corresponding TDoT-CatIBs. This effect was observed both in single-enzyme reactions using an enzyme membrane reactor (3.3.1), as well as in a two-enzyme, one-pot cascade reaction (3.3.3).

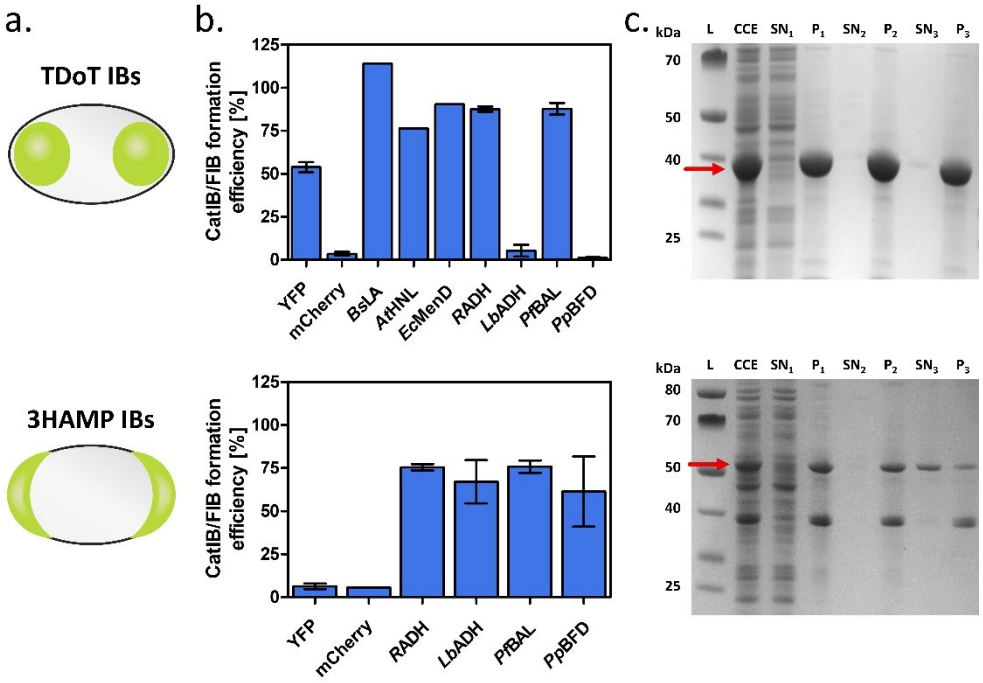


Figure 3-5 Comparison of TDoT (top) and 3HAMP (bottom) fusions with regard to CatIB/FIB-formation efficiency. (a): Fusion of TDoT to different targets result mostly in compact IBs within *E. coli*, while 3HAMP fusions seem mostly to accumulate as more diffuse IBs. (b): CatIB/FIB-formation efficiencies of TDoT and 3HAMP fusions. The target enzymes tested by Martin Diener were only fused to TDoT (*Bs*LA, *At*HNL, *Ec*MenD) [22]. (c): SDS-PAGE analysis of samples withdrawn during the preparation of TDoT-*R*ADH and 3HAMP-*R*ADH CatIBs. After cell disruption the crude cell extract (CCE) was separated into supernatant (SN_1) and IB-containing pellet (P_1) by centrifugation. P_1 was washed twice with water and again centrifuged, which resulted in SN_{2-3} and P_{2-3}. Sample volumes, corresponding to 10 mg ml^{-1} of SN_1, were applied per gel lane. The molecular mass of the fusion proteins TDoT-*R*ADH (34 kDa) and 3HAMP-*R*ADH (47 kDa) are indicated by red arrows. For further details, see Chapter 2.1.

Further, SDS-PAGE analyses indicated, that the expression of gene fusions with TDoT yielded much higher amounts of the recombinant protein than the corresponding fusions with 3HAMP (Figure 3-5c). The same was also observed when comparing the yield of the final CatIB/FIB lyophilizate per 100 g cells, which was generally much higher for TDoT CatIBs, than for the corresponding 3HAMP CatIBs. This effect was additionally reinforced, since most of the 3HAMP CatIBs also possessed a much lower protein content of about 30 to 50% compared to TDoT CatIBs with about 70 to 90% (2.1). These findings thus corroborate the more diffuse and more fragile nature of 3HAMP CatIBs compared to the TDoT CatIBs. Most interestingly, it appears that the discussed morphological distinctions between TDoT and 3HAMP CatIBs are directly correlated to their functionality, as all 3HAMP CatIB preparations generally showed a much higher catalytic activity compared to their TDoT counterparts (2.1). A more diffuse nature of the corresponding 3HAMP CatIBs would hereby facilitate better substrate availability, manifested in reduced diffusional limitation (3.1).

3.2.3 CatIB-formation results in activation of the protein quality control machinery

The formation of insoluble protein aggregates is often the inevitable consequence of heterologous protein production. In unstressed cells it is assumed that the formation of IBs, as a final state of protein aggregation, is prevented by the cellular protein quality control machinery. This involves a number of different chaperones, which have been categorized in 'folding chaperones', as DnaK/DnaJ and GroEL/GroES, and 'holding chaperones', like the IB-associated proteins IbpA/IbpB [89].

The small heat shock proteins (sHsps) IbpA/IbpB, which have been identified previously as IB-associating proteins [89, 235, 236], could also be identified as one of the protein contaminations within CatIBs (Figure 3-6), together with two other unspecific proteins (2.3). Thereby the percentage of IbpA/IbpB as contaminant of the respective CatIB preparations was much higher for TDoT than for 3HAMP CatIBs. The other proteins that could be identified here as CatIB contaminants, are an outer membrane protein (OmpA/OmpB) and a murein lipoprotein, indicating the presence of residual membrane components, that are also present in *E. coli* cells producing soluble enzyme and are therefore probably not involved in IB formation.

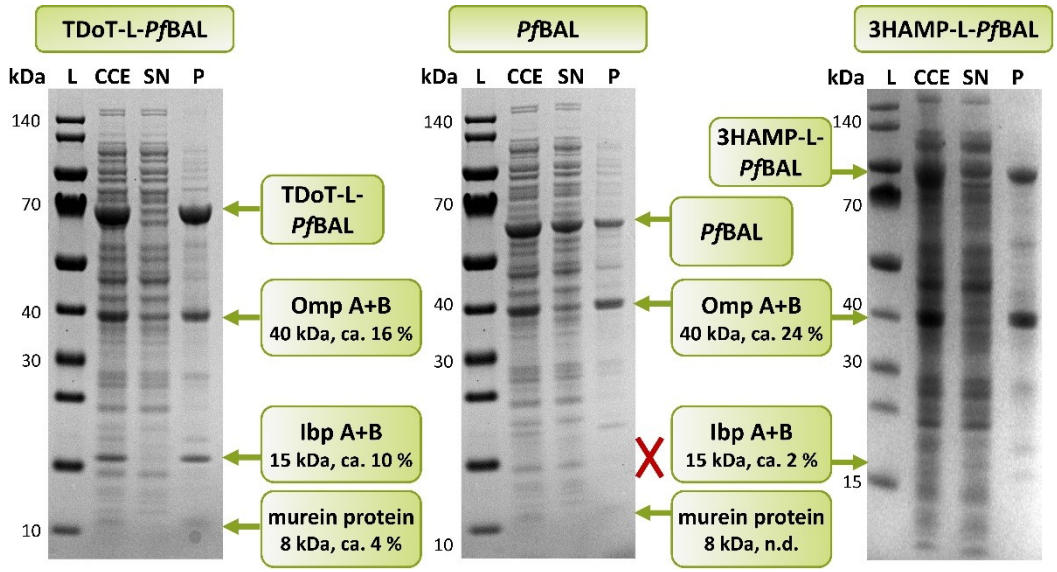


Figure 3-6 SDS-PAGE analysis of contaminant bands in TDoT-*Pf*BAL CatIB (left), soluble *Pf*BAL (right), and TDoT-*Pf*BAL CatIBs preparations. CCE: crude cell extract, SN: soluble protein containing supernatant fraction, P: insoluble IB-containing pellet fraction. The three dominant CatIB-contaminating proteins OmpA+B, IbpA+B, and a murein lipoprotein were identified by MALDI-TOF analysis in cooperation with Meike Baumgart (IBG-1, Forschungszentrum Jülich). The relative proportions were calculated with LabImage1D (Kapelan BioImaging solutions, Leipzig, Germany). For experimental details, see Chapter 2.1 and 2.3.

Until today the role of sHsps within the chaperone network is poorly understood. Their function as 'holding chaperones' most likely arises from their frequent tendency to be associated with insoluble protein. A functional triade of IbpA/B together with DnaK and ClpB was suggested, where sHsps function indirectly by facilitating the extraction of unfolded proteins form aggregates [236]. The fact, that they were identified in CatIBs

represents unequivocal evidence that the heat shock response in *E. coli* is activated and that the protein quality control machinery is actively working against IB formation.

3.2.4 Two proteins can be co-localized within the same IB particles

In an effort to further evaluate CatIB/FIB formation and broaden the application range of the CatIB approach, I went a step further and tested whether two proteins can be co-immobilized within IB particles (2.5). To the best of our knowledge, this idea has not been tested before. Hereby, the co-immobilization of two enzymes within CatIB particles would be especially beneficial for the realization of enzyme cascades, as close spatial proximity of the two enzymes, e.g. enforced by co-immobilization within CatIB particles, could enhance substrate channelling effects [237, 238]. In the context of two-enzyme cascades, substrate channelling would hereby be defined as the direct transfer of a reaction intermediate between two enzymes that catalyze sequential reactions. Spatial proximity of the two enzymes in turn could enhance the reaction velocity, by decreasing the transit time and by preventing diffusional loss of the intermediate. Further it can minimize the generation of by-products and reduce intermediate or product inhibition [237]. Likewise, these analyses could help elucidating the deposition process of proteins within IBs, thereby contributing to our understanding of the IB formation process.

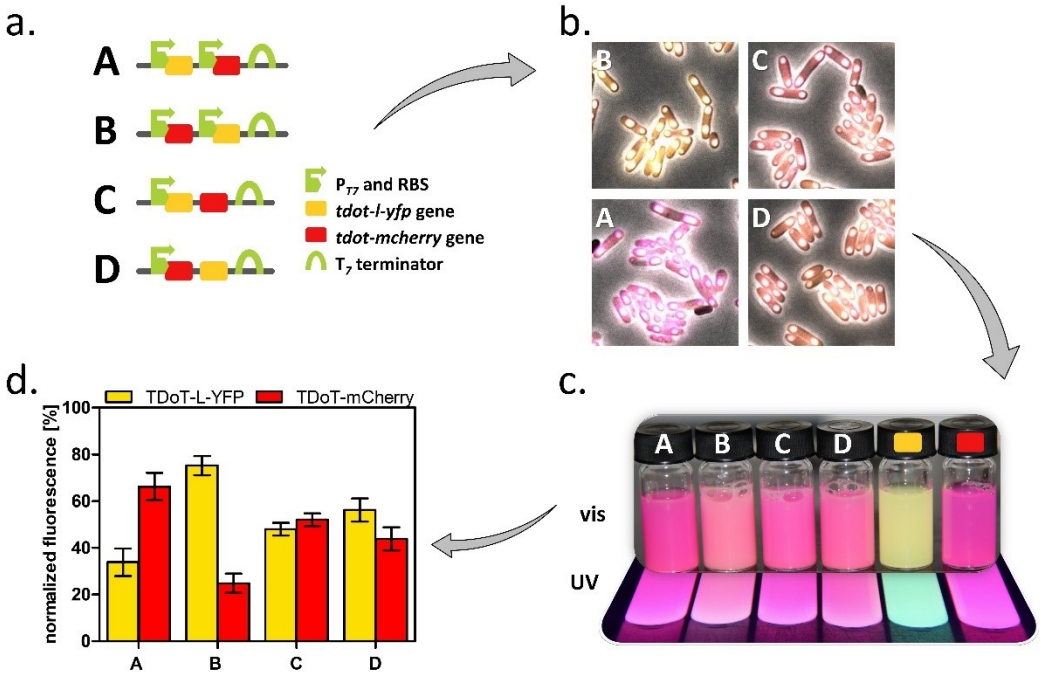


Figure 3-7 Co-localization of TDoT-YFP and TDoT-mCherry in FIBs. (a): Four different co-expression constructs were generated: A+B with two independent P_{T7} promotors upstream of each gene fusion, C+D with only one P_{T7} promotor upstream of an artificial operon constituted by the TDoT-L-YFP and TDoT-mCherry encoding gene fusions. In A/C and C/D the order of the two gene fusions was reversed (b): Microscopy images of *E. coli* cells carrying the four co-expression plasmids as a composite of fluorescence (YFP and mCherry channel) and phase contrast images. (c): Pellet fractions of the Co-FIBs as well as single YFP and mCherry FIBs, suspended in buffer under visible and UV-light (shown as mirrored image below the vials). (d): Normalized fluorescence within the Co-FIBs A to D. The normalized fluorescence was calculated taking into account the different fluorescence quantum yields and extinction coefficients of the respective fluorescent reporter proteins (for experimental details, see Chapter 2.5).

As target proteins to generate co-immobilized functional inclusion bodies (Co-FIBs), we initially selected the two fluorescent proteins YFP and mCherry, as their fluorescence can be independently determined. Moreover, for both targets FIB formation by fusion of TDoT had already been established (see 1.4.1 and 3.1.1).

To address, whether the composition of the Co-FIBs can be influenced by tuning the expression of the two co-expressed gene fusions, four different expression plasmids were constructed (co-constructs A to D, Figure 3-7a). In one set both gene fusions were placed under the control of two independent P_{T7} promoters (constructs A and B) and in a second set both gene fusions were expressed from only one P_{T7} promoter, localized upstream of the artificial operon (constructs C and D). Each set further consisted of two constructs, where only the order of the two gene fusions was reversed, with either TDoT-L-YFP being localized upstream of TDoT-mCherry (A and C) or *vice versa* (B and D).

The relative ratios of YFP and mCherry in the resulting Co-FIBs were intensively studied at the RNA-level as well as *in vivo* (Figure 3-7b) and *in vitro* (Figure 3-7c), revealing that indeed the relative ratios of the fusion proteins within Co-FIBs can be tuned rationally (Figure 3-7d) by selecting an appropriate vector design (see 2.5 for a detailed discussion). Interestingly, microscopic analyses revealed that all IBs showed both YFP and mCherry fluorescence (Figure 3-7b; see also 2.5), thus providing clear evidence for co-immobilization irrespective of the effective YFP to mCherry ratio. Further noteworthy is that the FIB-formation efficiency of TDoT-mCherry within Co-FIBs is strongly increased compared to single TDoT-mCherry (Appendix, Figure 4-2). Concomitantly, the FIB-formation efficiency of TDoT-L-YFP decreases by about the same amount, meaning that while TDoT-mCherry is stabilized within Co-FIBs, TDoT-L-YFP is destabilized.

Table 3-1 Comparison of activity, yield, and composition of different Co-CatIBs. 1: Ratio was calculated based upon densitometric analysis of the corresponding SDS gels. 2: Taking into account the protein content of the lyophilizate, referring to 1 $\mu mol_{product}\ s^{-1}$. 3: Compared to soluble purified enzyme. For experimental details see Chapter 2.5 and 2.6.

protein		protein content of lyophilizate [%]	ratio of *Pf*BAL to *R*ADH[1]	activity (k_{cat})[2] [s^{-1}]	residual activity[3] [%]	yield [g lyophilizate per 100 g cells]
TDoT Co-CatIBs	*Pf*BAL	77.5 ± 1.3	1 : 2.1	2.56 ± 0.52	3.3	9.0 ± 0.4
	*R*ADH			0.04 ± 0.003	1.4	
3HAMP Co-CatIBs	*Pf*BAL	47.4 ± 5.6	1 : 2.4	8.60 ± 2.15	11.2	3.0 ± 0.6
	*R*ADH			0.24 ± 0.04	8.6	
single TDoT CatIBs	*Pf*BAL	71.9 ± 4.5	-	0.77 ± 0.12	1.0	8.8 ± 1.0
	*R*ADH	84.6 ± 3.9		0.05 ± 0.01	2.0	9.7 ± 1.7
single 3HAMP CatIBs	*Pf*BAL	33.8 ± 5.2	-	13.86 ± 2.87	18	3.1 ± 0.5
	*R*ADH	51.0 ± 7.8		0.33 ± 0.02	12	3.9 ± 0.5

The presented co-immobilization approach, established for two FPs, was subsequently transferred to two enzymes, namely *Pf*BAL and *R*ADH (2.5 and 2.6). The resulting Co-CatIBs were later on used to realize a two-enzyme, one-pot cascade for the synthesis of (1*R*,2*R*)-1-phenylpropane-1,2-diol (PPD, see 3.3.3) and are here used only to discuss

certain issues related to (Co-)CatIB formation. Fusions with TDoT and 3HAMP were generated for both enzymes, named here TDoT Co-CatIBs and 3HAMP Co-CatIBs. The *Pf*BAL/*R*ADH Co-CatIBs were generated employing the vector architecture established for the Co-FIB producing construct A, where both gene fusions are under the control of two independent P_{T7} promotors with the *Pf*BAL containing gene fusion upstream of the *R*ADH-containing gene fusion. This should always result in a hypothetical ratio of *Pf*BAL to *R*ADH within the Co-CatIBs of 1:3. In praxis, the amount of *R*ADH was always lower than expected (Table 3-1). Interestingly, the residual activity of *Pf*BAL in TDoT Co-CatIBs was much higher than the corresponding single *Pf*BAL CatIBs, while the activity of *R*ADH in Co-CatIBs slightly decreased compared to single CatIBs. This could indicate that the Co-CatIBs contain a higher amount of correctly folded *Pf*BAL than *R*ADH.

In conclusion, the co-localization and thereby the direct intracellular co-immobilization of two proteins within CatIBs/FIBs is possible. The presence of a second protein apparently can influence the deposition of active protein within IBs, as for certain targets higher residual activity and/or increased CatIB/FIB-formation efficiencies were observed for a given enzyme/protein in Co-CatIBs/Co-FIBs compared to the corresponding single CatIBs/FIBs.

3.2.5 Influence of the surface hydrophobicity of the target on (Cat)IB formation

The observation, that for different targets different CatIB/FIB-formation efficiencies (2.1) as well as stabilities (2.3 and 2.6) are observed, stresses the notation that certain target protein properties also influence the formation and stability of the resulting CatIBs/FIBs. Based thereon, we tried to infer, if there is a correlation between IB formation, composition, and structural properties of the target proteins. Recent studies have indicated that the tendency for IB formation is linked to the presence of certain aggregation-prone stretches of amino acids [97], depending on physicochemical properties like hydrophobicity or charge of the polypeptide chain [239]. Therefore, the amino acid sequences of the targets were analyzed using sequence-based aggregation predictions by employing the AGGRESCAN tool [240]. This software calculates a normalized, average aggregation tendency of an amino acid sequence, based on various parameters. For all TDoT fusions, there seems to be a weak linear relationship between CatIB/FIB-formation efficiencies and aggregation tendency, although here, *Lb*ADH and *Pp*BFD appear to be outliers (Figure 3-8a). 3HAMP fusions display a slightly better correlation, when excluding YFP, but considering the high standard deviations and the small number of analyzed constructs, the trend remains to be verified (Figure 3-8b).

Consequentially, simple sequence-based predictions can be used as a first approximation to predict aggregation tendencies for a given target. The fact that catalytic activity is observed in IBs for all of our tested target proteins, suggests that aggregation does not

solely occur from the unfolded state, as the above simplistic sequence-based prediction assumes. Therefore, it seems reasonable that also structural features of the correctly-folded target protein should play a role in CatIB/FIB formation.

One driving force for the accumulation of correctly-folded protein within IBs might be found in the presence of large hydrophobic surface patches. Therefore, we analyzed the available target protein structures for such patches by utilizing the hpatch tool of the Rosetta protein design software [241-243]. This software infers the presence of continuous patches of surface exposed hydrophobic atoms, which in turn allows the calculation of the percentage of the hydrophobic patch area relative to the overall solvent accessible surface area (SASA) of a given protein target.

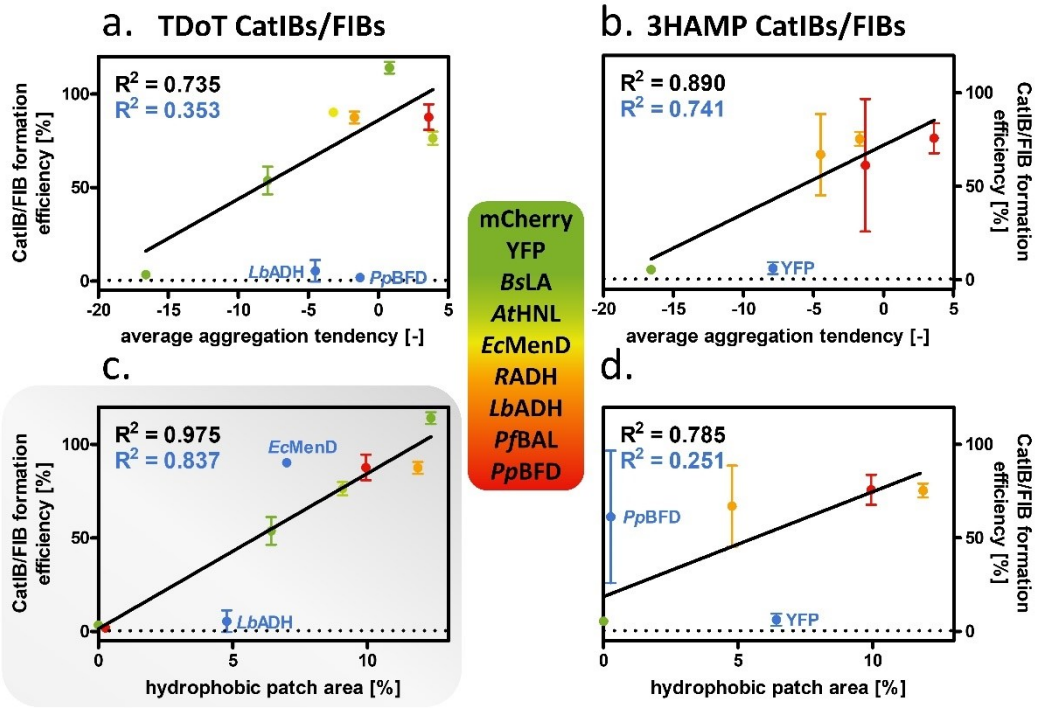


Figure 3-8 Computational analysis of (a, b) target protein amino acid sequences and (c, d) structural determinants of CatIB/FIB formation. Analyzations are based on the (a, c) TDoT and (b, d) 3HAMP dataset. Target proteins are colored, according to their size and multimer complexity, estimated in Figure 3-1. Coefficient of determination values (R^2) are given excluding (black) and including (blue) the blue-highlighted outliers. (a, b): Normalized average sequence-based aggregation propensities were inferred using the AGGRESCAN webserver [240]. (c, d): The area of hydrophobic surface patches for target protein structures was quantified using the hpatch tool, implemented in Rosetta [241-243]. Surface areas were quantified using Pymol 1.7.0.0 (Schrödinger, LCC, New York, NY, USA). The best correlation (c) is highlighted in grey. All calculations were performed by Ulrich Krauss. For a more detailed description, please see Chapter 2.1.

For most TDoT fusion targets this yielded a very good linear correlation, which could be even further improved when alternative oligomeric assemblies were considered, as inferred by the PISA webserver (Figure 3-8c) [244]. The latter, structure-based method thereby yields a good correlation for 7 out of 9 target proteins. Apart from the target proteins, hydrophobic patches are also found on the surface of the both coiled-coil domains (Appendix, Figure 4-3). However, since the relation between surface hydrophobicity of the tag and the target is unclear, they were not considered explicitly for

these calculations.

It appears that the presence of large hydrophobic patches on the surface of the target proteins clearly correlates with a tendency for CatIB formation. This provides a structural explanation, why highly soluble proteins, like mCherry, show low CatIB/FIB-formation efficiencies or form only intercellular FIBs that mostly disintegrate during cell lysis. For the 3HAMP fusions a much weaker correlation between CatIB/FIB-formation efficiency and the relative hydrophobic patch area was observed. Even excluding *Pp*BFD and YFP, the remaining four data sets do not really seem to correlate, especially when considering the high standard deviations of the experimentally derived CatIB/FIB-formation efficiencies (Figure 3-8d). In conclusion, both sequence and structure-based calculations can be used to a certain degree to predict the CatIB/FIB-formation tendency of a given target protein. This not only might allow the prediction whether or not CatIB-based immobilization of a target seems feasible, it also contributes to our understanding of IB formation process in general.

3.2.6 A unified model for IB and CatIB formation?

As outlined in the beginning of Chapter 3.2, two predominant theories exist that could account for the formation of IBs (Figure 3-9a, see also 1.3.1). The classic picture explains IB formation as the aggregation of mis- or unfolded polypeptide chains starting from only a single or a limited number of nucleation sites to a form giant amorphous IB aggregate [88, 98]. A more recent theory, that also accounts for CatIBs as IB-aggregates with catalytic activity, describes IBs as an aggregate formed from a number of 'soluble' proto-aggregates, which can contain correctly folded (active) protein alongside with misfolded (inactive) and fibrillar and amyloid-like (inactive) protein material [88, 91].

All results discussed in the previous chapters would clearly favour the second theory, altogether indicating that the formation of CatIBs/FIBs in *E. coli* is a complex process depending on a variety of different factors. This includes the general architecture of the aggregating target fusion (presence of linkers, N- *vs.* C-terminal fusion, 3.1.1), the employed aggregation-inducing tag (3.1.1 and 3.2.2), the expression temperature (3.1.2), the presence of other co-aggregating fusion proteins (3.2.3), as well as the structural properties (oligomerization, surface hydrophobicity, 3.2.5) of the target protein.

One model that would accommodate the functional and morphological differences observed for diffuse and compact CatIBs, as described in Chapter 3.2.1 and 3.2.2, assumes that the diffuse aggregates observed in the respective fluorescent microscopic images (Figure 3-4a) represent a kind of incompletely formed IB proto-aggregates. These further aggregate after cell disruption (as already discussed in Chapter 3.2.2), thereby encapsulating soluble, active/functional protein (Figure 3-9b, left). A similar phenomenon, known as 'native-like aggregation', was observed for the acylphosphatase from *Sulfolobus solfataricus* [245].

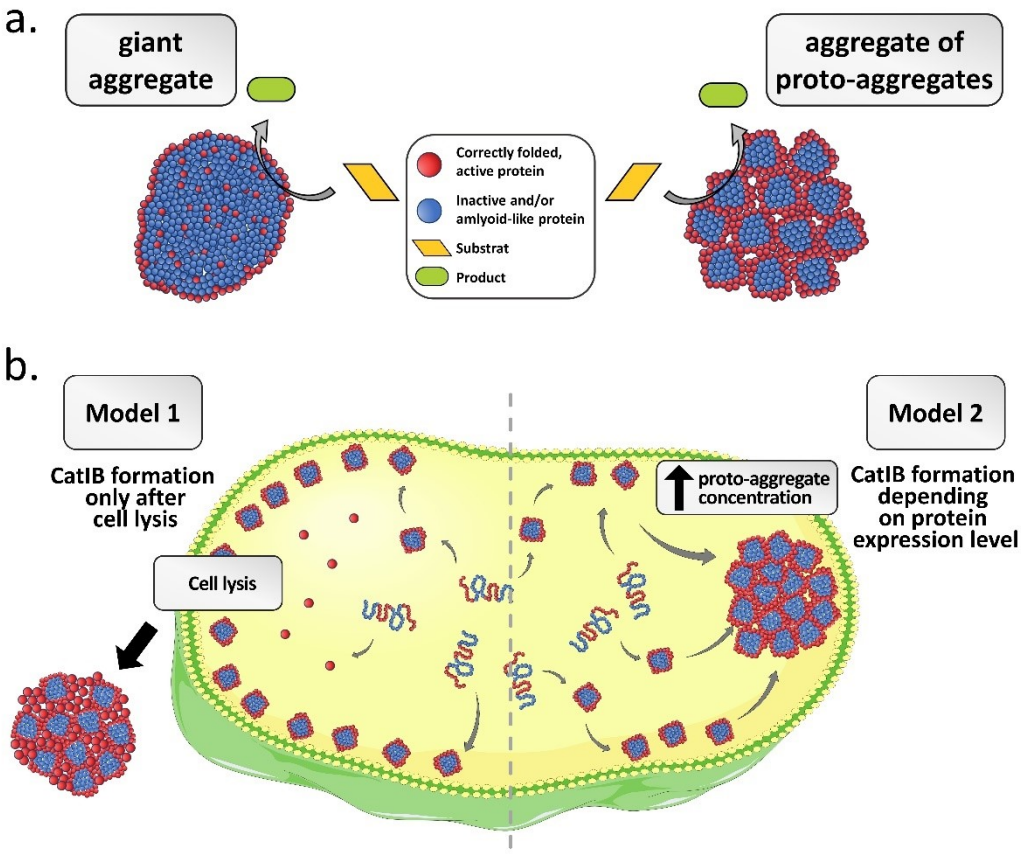


Figure 3-9 Different theories about CatIB formation. (a): The classic model is that of a giant aggregate (left) starting of a limited number of aggregation sites. The more recent model (right) starting with small proto-aggregates that form an 'aggregate-of-aggregates' also accounts for the formation of CatIBs. The two models were originally adapted by [88]. (b): Differences in diffuse and compact CatIBs can be explained by two different models. Model 1 (left) states formation of diffuse CatIBs solely after cell lysis and incorporation of soluble protein. Model 2 (right) predicates formation of diffuse *vs.* compact CatIBs depending on the protein expression, and thus proto-aggregate, level.

Another related model which is supported by our data assumes that diffuse CatIBs, formed due to 3HAMP fusion, somehow represent an intermediate step towards the formation of more compact classical IBs. Under this assumption, the diffuse, membrane-associated spots seen in the corresponding fluorescence images (3.2.1Figure 3-4) could represent 'soluble' proto-aggregates [88, 91, 235], too small to be discernible as particles by conventional fluorescence microscopy (Figure 3-9b, right). This would likewise account for their higher fluorescence, due to a better volume-to-surface ratio. An increased surface hydrophobicity of such 'soluble' proto-aggregates, for example due to exposed unfolded polypeptides, could hereby account for their membrane association. In turn, the diffuse cell-pole localized aggregates observed in some cells would represent the growing 'aggregate-of-aggregates' that eventually might yield classic compact CatIBs. If true, it still remains unclear, which factors determine the formation of diffuse *vs.* compact CatIBs, or following the just presented hypothesis, determine the development of classical compact CatIBs from diffuse proto-aggregates. One factor that immediately comes to mind is the intracellular concentration of the fusion protein. Here, for most 3HAMP fusions lower expression levels were observed in SDS-PAGE analyses,

as compared to the corresponding TDoT fusions (see 3.2.2). Intriguingly, the only 3HAMP fusion protein (*Ec*LDC-L-3HAMP; see 2.1), which apparently forms compact CatIBs (Appendix, Figure 4-1), is also produced at higher levels (see Figure S6, Chapter 2.1.1). Evidence against this hypothesis was found in our microfluidic cultivation experiments, were TDoT-YFP FIBs formed more or less instantaneously after induction without any observable diffuse intermediate (Appendix, Figure 4-4).

Moreover, from a structural perspective, it remains totally unclear why the fusion of coiled-coil domains, other short polypeptide tags [123-126, 129], or even whole proteins [120, 121, 127, 128, 133, 134], induces the formation of CatIBs (see 1.3.3). There is no unifying structural feature that would be common in all of the known aggregation-inducing tags. Interestingly, it was recently described for the acylphosphatase from *Sulfolobus solfataricus* that *in vivo* and *in vitro* aggregation [245] proceeds from native-like folded active protein, *via* the spontaneous rearrangement into inactive, amyloid-like structures, eventually yielding IBs *in vivo* [246]. Moreover, the aggregation process was enhanced in the presence of an unfolded N-terminal region [246]. In light of the observation that the fusion of various structurally dissimilar aggregation-inducing tags can induce the formation of CatIBs, it appears tempting to speculate that the fused tags remain unfolded, while the functional target protein core folds properly. The unfolded N- or C-terminal tag would then mediate the aggregation into IBs. In such a model, the structure of the tag would not play a role for the aggregation process, while its length and composition should still have an influence.

The often low residual activities observed for CatIBs further suggest that at least a certain fraction of the produced fusion protein should be unfolded or present as inactive, amyloid-like material, rich in cross β-sheet structures. The latter feature has in recent years been shown for many IBs and CatIBs alike [99, 106, 119, 120, 125]. For the here described CatIBs the presence of cross β-sheet rich amyloid-like structures was demonstrated exemplary for TDoT-*At*HNL and TDoT-*Ec*MenD [97], albeit only for the final CatIB preparation and not during cultivation. The here presented on-line cultivation data, recorded in cooperation with Robin Lamm (AVT - Aachener Verfahrenstechnik, Biochemical Engineering, RWTH Aachen University) do not show a decrease in fluorescence under any conditions, that would indicate rearrangement within IBs from active to amyloid-like structures (2.2). However, this does not exclude the possibility that a certain fraction of the produced fusion protein aggregates into inactive, amyloid-like material, without first folding into the native state.

The most likely model that would accommodate all of our findings, would suggest that CatIBs, in similarity to classical inactive IBs, consist of a certain fraction of mis- or unfolded protein, along with amyloid-like material, which form the matrix wherein active, correctly folded protein is incorporated. This model is in full agreement with the above described ‘aggregate of proto-aggregates’ hypothesis (Figure 3-9b, right). The degree of

incorporation might hereby depend on both the employed aggregation-inducing tag and the hydrophobic surface area of the target (3.2.5). This model might also include further aggregation occurring after cell lysis (see above).

Based on our data the following questions remain:

i) Does the aggregation-inducing tag need to be folded to mediate aggregation?
ii) What is the localization of the active protein within CatIBs, i.e. is the active protein only found at the CatIB surface or is it evenly distributed throughout the particle?
iii) How do diffuse CatIBs form within the cell and does aggregation after cell disruption really play a role for the CatIB formation process?
iv) What role does diffusional limitation play, i.e. with regard to the low residual activities observed for CatIBs?
v) What structure does the active protein adopt within CatIBs?
vi) Do all IBs, under the right conditions, contain active/functional protein?

In conclusion, while certain questions regarding the formation, structure, and function of CatIBs could be answered within this thesis, we are still far away from a unified model for IB and CatIB formation.

3.3 Biotechnological application of CatIBs

In the following chapters, several, within this thesis realized, biotechnological applications of CatIBs will be presented and the obtained results will be discussed with regard to the competitiveness of the CatIB-immobilization method compared to other well-established immobilization approaches.

3.3.1 Stability of *Pf*BAL CatIBs in different reaction systems

CatIBs of the benzaldehyde lyase from *Pseudomonas fluorescens* (*Pf*BAL, see 1.4.3.1), as one of the more complex target enzymes of the 'CatIB toolbox', were characterized intensively within this thesis (2.3). The purified soluble enzyme is rather instable, with a half-life of only 8 h at pH 8.0 or 16 h at pH 6.5 in aqueous buffered solution [247, 248]. As described above, TDoT-L-*Pf*BAL and 3HAMP-L-*Pf*BAL form two different kinds of CatIBs, the first being of compact, the latter of diffuse morphology (3.2.1). The overall protein yield determined for 3HAMP-*Pf*BAL CatIBs per gram cells was about the same as for purified soluble *Pf*BAL, while for the TDoT-*Pf*BAL CatIBs the yield was approximately four-times higher (2.3). At the same time the residual activity of the TDoT-*Pf*BAL CatIBs was only 1%, while 3HAMP-*Pf*BAL CatIBs possessed a residual activity of 18% compared to the purified soluble enzyme.

Soluble *Pf*BAL tolerates the addition of organic solvents, like 5% methyl *tert*-butyl

ether (MTBE) or 20 to 30% dimethyl sulfoxide (DMSO). Moreover, addition of these organic-solvents enormously enhances the half-life of the enzyme by a factor of 75 and 150, respectively [247, 249]. Based on these data, the influence of different organic solvents was tested in cooperation with Ramona Kloss and Tobias Karmainski (IBG-1, Forschungszentrum Jülich). In these experiments an enzyme membrane reactor (EMR) [250] was utilized to evaluate the performance of CatIBs in a continuous process. The chosen reaction comprised the well-studied carboligation of benzaldehyde and acetaldehyde to (*R*)-2-hydroxy-1-phenylpropanone (HPP). At pH 7.5 a half-life for purified soluble *Pf*BAL of about 7 h and of 10 and 49 h for 3HAMP and TDoT CatIBs was estimated, respectively. Especially for purified soluble *Pf*BAL, the half-life was much lower as compared to the half-life of the enzyme in buffer (Table 3-2), likely caused by presence of aldehydes. As demonstrated before, even small amounts of aldehydes were shown to rapidly inactivate soluble *Pf*BAL [251]. Similar to published data, the addition of 30% DMSO enhanced the half-lives of all tested *Pf*BAL preparations. However, this effect was much more pronounced for the purified soluble enzyme than for the corresponding CatIBs.

Table 3-2 Half-lives [h] of *Pf*BAL CatIBs and purified soluble *Pf*BAL determined under different conditions. Incubation conditions: 30°C, 1000 rpm shaking. The stability in buffer was measured at different time points during incubation by following the carboligation of DMBA to TMBZ in a discontinuous assay. Half-lives were taken from the stability curves at 50% residual activity. EMR conditions: 30 °C, 300 rpm, reactor volume: 3 ml, residence time: 0.5 h, flow: 0.1 ml min^{-1}. Reaction: 30 mM benzaldehyde and 90 mM acetaldehyde for the carboligation to HPP. Buffer conditions: 50 mM TEA, 2.5 mM $MgSO_4$, 0.5 mM ThDP. Half-lives were taken from the reaction curves at 50% conversion. For experimental details, please see Chapter 2.3.

reaction system	TDoT-*Pf*BAL	3HAMP-*Pf*BAL	soluble *Pf*BAL
Incubation: buffer, pH 7.5	57	23	36
EMR: buffer, pH 7.5	48	10	7
EMR: buffer, pH 7.5, 30% (v/v) DMSO	131	59	92

In a further experiment CatIBs were tested in a mono- and biphasic reaction system with different organic (co-)solvents. MTBE and cyclopentyl methyl ether (CPME) were identified as the best solvents for the carboligation of 3,5-dimethoxybenzaldehyde (DMBA) to (*R*)-(3,3',5,5')-tetramethoxy benzoin (TMBZ) in a micro-aqueous buffer system. Increasing the buffer content to yield a biphasic system resulted in emulsion formation, thus hampering sample handling and recycling. This effect was least pronounced for the 3HAMP CatIBs in CPME. Therefore, CPME seems superior to MTBE for the use with 3HAMP CatIBs in biphasic reaction systems, especially since in contrast to MTBE it is considered a green solvent. Interestingly, a further increase of the buffer content resulted in reduced emulsion formation, so that the best results could be achieved with a biphasic system containing 30% buffer (pH 8.0) and CPME as second phase. Under these conditions, 3HAMP CatIBs clearly outperformed even purified soluble *Pf*BAL in the carboligation of both DMBA and benzaldehyde, respectively. In contrast, in a monophasic buffer/DMSO system used for the continuous synthesis of HPP,

TDoT-*Pf*BAL CatIBs were superior to the soluble enzyme.

Furthermore, in a third approach the recyclability of *Pf*BAL CatIBs was tested in batch mode using a buffered system at pH 7.5 with 20vol% DMSO as a co-solvent [252]. Both types of CatIBs could easily be recycled nine times in batches of 1 h each. After the last reaction round TDoT-*Pf*BAL CatIBs still showed 45% residual activity, while the 3HAMP-*Pf*BAL CatIBs even retained 77% of their initial activity (Table 3-3).

Table 3-3 Comparison of *Pf*BAL CatIBs to different *Pf*BAL immobilizates from literature. n.i.: No information provided
*: Data estimated from published values. $: activity after last reaction round

***Pf*BAL immobilizate**	**half-life [h]**	**recycling [no x reaction duration]**	**residual recycling activity$**	**activity compared to soluble *Pf*BAL**	**Ref.**
TDoT CatIBs	131	9 x 1 h	77	1%	our work, [252]
3HAMP CatIBs	59	9 x 1 h	45	18%	
whole-cell biocatalysts	n.i.	n.i.	n.i.	about 4.5-times higher initial rate activity compared to CCE*	[253]
covalent binding of *Pf*BAL to a HaloTag®	n.i.	7 x 40–250 min	10	30%	[254]
covalent binding to magnetic nanoparticles	n.i.	5 x 110 min	100	approx. equal	[255]
*Pf*BAL-$(His)_6$ chelated with superparamagnetic nanoparticles	n.i.	5 x 40 min	87	approx. equal	[256]
*Pf*BAL-$(His)_6$ chelated with sepharose	n.i.	2 x n.i.	70*	approx. equal	[257]
hydrogel beads of PVA	103	recycling only mentioned, but no data given		n.i.	[258, 259]
Pickering-emulsion of *Pf*BAL encapsulated in SiO_2 nanoparticles	n.i.	recycling not performed		8-times higher than in biphasic system*	[260]
Pickering-emulsion of *Pf*BAL encapsulated in PEG	n.i.	recycling not performed		225-times higher than in biphasic system	[261]
Pickering-emulsion of pNIPAM-*Pf*BAL	n.i.	recycling not performed		275-times higher than in biphasic system	[262]

In literature numerous immobilization approaches have been described for *Pf*BAL, ranging from the use of whole-cell biocatalysts, utilization of carrier-based immobilizates obtained by covalent- and affinity-binding, to the use of encapsulated enzymes (Table 3-3). A comparison however proofs difficult, since not much information about stabilizing effects is given. CatIBs can best be compared to a preparation where *Pf*BAL, genetically fused to the commercially available HaloTag®, was bound covalently to a sepharose-based HaloLink® resin (1.2.1) [254]. There, the enzyme could be immobilized directly from crude-cell extract with a residual activity of 30% compared to the soluble purified enzyme. Further, the immobilizate could be recycled for seven rounds, although the activity decreased much faster, than in case of CatIBs, already dropping to 60% after one round [254]. Just recently, very high *Pf*BAL activities could be achieved by using Pickering-emulsions [260-262], which are emulsions stabilized by addition of solid particles, that are adsorbed to the interface between two phases [263]. *Pf*BAL, when encapsulated within a polyethylene glycol (PEG) block copolymer or grafted onto

poly(*N*-isopropylacrylamide) (pNIPAM) polymers showed an impressively improved catalytic performance in an emulsified biphasic system, yielding 225- and 275-times higher activity compared to the traditional (non-emulsified) biphasic system, respectively [261, 262]. Unfortunately, although mentioned to be possible, recycling of the immobilizate was not tested in any of these cases.

In conclusion, *Pf*BAL CatIBs, regardless of the coiled-coil domain, are stabilized compared to the soluble enzyme in aqueous buffer. Addition of 30% DMSO as co-solvent resulted in further stabilization. In terms of application, the 3HAMP-*Pf*BAL CatIBs appear to be better suited for the use in biphasic reaction systems, e.g. with CPME as second phase, while the TDoT-*Pf*BAL CatIBs are better suited for the use in monophasic buffer/DMSO mixtures. Thus, depending on the target reaction system, it might be possible to specifically tailor CatIB-properties, e.g. by the choice of the aggregation-inducing tag.

3.3.2 *Ec*LDC CatIBs allow the competitive production of 1,5-diamino-pentane

CatIBs of the lysine decarboxylase from *E. coli* (*Ec*LDC) were used to demonstrate the applicability of CatIBs under technical conditions (2.4). In cooperation with Ramona Kloss and Michael H. Limberg (IBG-1, Forschungszentrum Jülich), *Ec*LDC-TDoT CatIBs produced from the C-terminal *Ec*LDC-L-TDoT fusion protein were used for the decarboxylation of L-lysine to 1,5-diaminopentane (DAP, trivial name: cadaverine). This reaction is of particular interest, since DAP is an important precursor for the production of fully bio-based polyamides, such as PA5.4 or PA5.10, and thus can contribute to the sustainable management of fossil resources (1.4.4) [264-266].

Of the two LDC enzymes present in *E. coli* (LDCc and CadA), the constitutive LDCc was used here, since it has a broader pH optimum (pH 6.5 to 8.0) [212, 217]. In fact, initial experiments demonstrated that *Ec*LDC-TDoT CatIBs displayed a slightly more alkaline optimal pH range of pH 7.5 to 9.0 in KPi buffer and even pH 8.0 to 9.0 in CGXII, the medium used for the production of L-lysine by fermentation of *Corynebacterium glutamicum* [267]. A broader pH range is advantageous since the reaction products DAP and CO_2 shift the pH, which was already observed previously [266, 268].

The industrial process imitated here, not only comprises the production of DAP by *Ec*LDC CatIBs, but also of the substrate L-lysine by *C. glutamicum*, to reduce process costs. Thereby, apparently, it was absolutely essential, to first remove the *C. glutamicum cells* from the L-lysine containing culture broth before addition of CatIBs, since otherwise only very low amounts of DAP were obtained. This was interpreted to be likely caused by the degradation of pyridoxal-5'-phosphate (PLP), the cofactor of *Ec*LDC, either by photolysis, oxidation [269], or consumption by *C. glutamicum* [270].

Table 3-4 Comparison of 1,5-diaminopentane production by CatIBs and other approaches from literature. n.i.: No information provided. *: Data estimated from given parameters 1: L-lysine was produced and directly converted by *C. glutamicum*.

immobilization of LDC	process	reaction time [h]	L-lysine [M]	DAP [g l^{-1}]	conversion [%]	catalyst amount	STY [g l^{-1} d^{-1}]	Ref.
CatIBs of LDCc-TDoT	batch	24	1	88	87	3 mg l^{-1}	89	this work
	repetitive batch, 9 cycles	6 x 4 3 x 15 = 69	0.1	8.5	100 (2^{nd} cycle) 54 (8^{th} cycle)	10 mg l^{-1}	3	
CLEAs of CadA	repetitive batch, 10 cycles	10 x 2 = 20	0.1	n.i.	100 (1^{st} cycle) 53 (last cycle)	65 mg l^{-1}*	n.i.	[266]
CadA-P(3HB)	repetitive batch, 5 cycles	5 x 1 = 5	0.1	38-41	75-80 for each cycle	n.i.	approx. 190-197*	[271]
E. coli whole-cells with LDCc	batch	120	1.37	134	96	OD_{600} of 50	30*	[268]
C. glutamicum whole-cells with LDCc[1]	fermentation	50	n.i.	88	n.i.	up to OD_{600} of 120	42*	[265]
E. coli whole-cells with CadA and CadB	fed-batch	16	1.9*	221	92	8 g_{DCW} l^{-1}	332*	[272]
E. coli whole-cells with CadA	batch	2	1.75	143*	80	61 units	1716*	[273]
E. coli whole-cells with CadA in barium alginate	batch	4	1	76	84	45 units	456*	[274]
E. coli whole-cells with CadA in alginate	continuous	123	1*	85*	82*	n.i.	17*	[275]

Overall two different set-ups were used, a repetitive batch for nine cycles over 69 h that yielded a space time yield (STY) of 3 g l^{-1} d^{-1} and an experiment in batch mode, employing a 10-fold higher substrate concentration (1 M) for 24 h that yielded a STY of 89 g l^{-1} d^{-1}.

Cadaverine production has already been demonstrated using a variety of different immobilizates, such as whole cells [265, 268, 272, 273], alginate beads [274, 275], cross-linked enzyme aggregates (CLEAs, 1.2.3) [266], or biopolymers like poly(3-hydroxybutyrate) (P(3HB)) [271], albeit most biotransformations were performed with whole cells that were either directly applied or further immobilized in alginate beads for long-term stabilization (Table 3-4). This renders a direct comparison to the here described CatIB-based process difficult, since the STY is calculated based on non-comparable catalyst amounts. Nevertheless, the use of *Ec*LDC CatIBs in batch mode yielded a conversion and a STY competitive with other whole-cell conversions. Of special interest here is the whole-cell production utilizing *C. glutamicum*, where not only the L-lysine but also DAP was produced in the same host [265]. This approach further reduces the production costs, although only a rather low STY of 42 g l^{-1} d^{-1} could be achieved. In a down-stream process DAP was extracted from the fermentation broth and further co-polymerised to PA5.10 with sebacic acid. Incidentally, this was also the only case, where the production was not performed in *E. coli*.

CatIBs, as a form of immobilizate, can best be compared to other carrier-free immobilizates like CLEAs or to biopolymers like P(3HB)-based immobilizates, which were also used for the production of DAP. The parameters used for CadA-CLEAs were serendipitously very similar to our repetitive batch [266]. Both utilized 100 mM L-lysine and yielded a conversion of 100% during the first batches and about 50% during the last cycles. Unfortunately, the batch times differed in our case from 4 to 15 h, so it remains unclear, at which point the activity of the CatIBs dropped. Here, the shorter batch time of 2 h for CadA-CLEAs seems favourable. However, it goes along with a 6-fold higher catalyst load compared to the CatIB approach. Alas no final DAP concentration was given for the CadA-CLEAs, so no STY could be estimated.

In another study, CadA was immobilized on P(3HB) (Figure 1-6a) [271]. In a repetitive batch the P(3HB)-immobilizates yielded a STY of approximately 190 g l^{-1} d^{-1}, which is much higher than in the CatIBs-based repetitive batch (3 g l^{-1} d^{-1}). But here, the shorter batch time of only 1 h for only 5 cycles has to be considered. Furthermore, no information about the catalyst load was given for CadA-P(3HB).

In conclusion, while the direct comparison to other DAP production approaches is difficult, DAP production by CatIBs appears competitive compared to the best processes described in literature.

3.3.3 Realization of a two-enzyme cascade reaction with CatIBs and Co-CatIBs

*Pf*BAL and *R*ADH, which were studied here extensively as CatIBs (2.1 and 2.3) can be used to set up a two-enzyme reaction cascade for the production of (1*R*,2*R*)-1-phenylpropane-1,2-diol (PPD) [276-278], an important precursor for the calcium channel blocker diltiazem, used as a treatment for hypertension or angina pectoris [279]. This reaction serves as a model reaction for synthesis of vicinal diols (1,2-diols), as important chiral building blocks for various pharmaceuticals or agrochemicals [181]. Hitherto, *syn*-vicinal diols are often chemically synthesized by asymmetrical dihydroxylation of alkenes *via* a [3+2] cycloaddition of an osmium tetroxide-ligand complex [280]. For the synthesis of *trans*-vicinal diols, alkenes need to be epoxidized first, followed by epoxide hydroxylation [181]. Other reactions are the Woodward reaction and the Prévost hydroxylation for *syn*- and *anti*-vicinal diols, respectively, which use iodine and silver acetate [65, 281]. However, these reactions all face the drawback of low stereoselectivity. The production of vicinal diols thus clearly would benefit from the use to stereospecific enzymes.

Therefore, and as an extension of the existing CatIB strategy, we employed the already established TDoT CatIBs as well as 3HAMP CatIBs of *Pf*BAL and *R*ADH for this cascade reaction and compared the performance of single CatIBs and Co-CatIBs, as well as of TDoT to 3HAMP CatIBs (2.5 and 2.6). Properties, like yield, activity, and protein

content of those (Co-)CatIB immobilizates have already been discussed above (see 3.2.2 and 3.2.4). The envisioned cascade reaction is shown schematically in Figure 3-10. Here, the *Pf*BAL-catalyzed carboligation of benzaldehyde and acetaldehyde to yield (*R*)-2-hydroxy-1-phenylpropanone (HPP) is combined with the reduction of HPP by *R*ADH to yield the final product PPD. The regeneration of the nicotinamide cofactor NADPH of the *R*ADH is achieved by oxidation of the co-substrate benzyl alcohol, simultaneously regenerating benzaldehyde, which is then used again as substrate for *Pf*BAL, thereby generating a self-sufficient cascade.

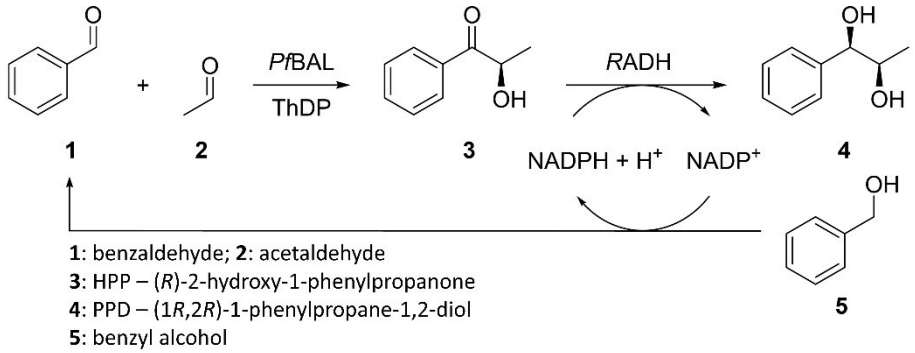


Figure 3-10 Two-enzyme, one-pot cascade reaction. In the first step, *Pf*BAL catalyzes the carboligation of benzaldehyde **1** and acetaldehyde **2** to yield the intermediate (*R*)-2-hydroxy-1-phenylpropanone (HPP, **3**). In a second step, HPP **3** is reduced to (1*R*,2*R*)-1-phenylpropane-1,2-diol (PPD, **4**) by *R*ADH. This reaction requires NADPH as cofactor, which is regenerated by a co-substrate coupled approach that simultaneously regenerates the substrate benzaldehyde **1** from benzyl alcohol ***5***.

Hereby, the one-pot approach has several benefits over sequential cascades, such as the need for fewer process steps, lower reaction volumes, higher volumetric and space-time yields, production of less waste, and the avoidance of unfavourable equilibria of intermediates [238]. Due to these benefits, enzymatic cascades comply with the *12 Principles of Green Chemistry* [34] and the *Principles of Green Engineering* [35, 36] (see 1.1.2, Figure 1-2). However, for the set-up of an efficient one-pot enzymatic cascade, several obstacles have to be overcome. Most importantly, finding conditions under which two or more enzymes work optimally, can be challenging. This renders the optimization of these cascades an important but often tedious issue.

In this regard, the here realized cascade is no exception, as for example for *Pf*BAL, stability and activity optima are found at opposing pH values: while pH stability is optimal at pH 7.0, the activity is maximal at pH 8.0 to 9.0 [208, 249]. On the other hand, *R*ADH has a broad stability optimum from pH 5.5 to 8.0, but while the optimum for reduction is at neutral pH (7.0 to 8.0) the cofactor recycling works better at alkaline pH (10.0 to 11.0) [193]. In the here presented specific case, further challenges derive from the employed aldehyde substrates, which are known to rapidly inactivate enzymes such as *Pf*BAL [251]. Thus, optimal cascade performance in the presented case is clearly limited by opposing pH-optima and general stability issues, both with regard to reaction pH, but also due to inactivation by the employed aldehyde substrates.

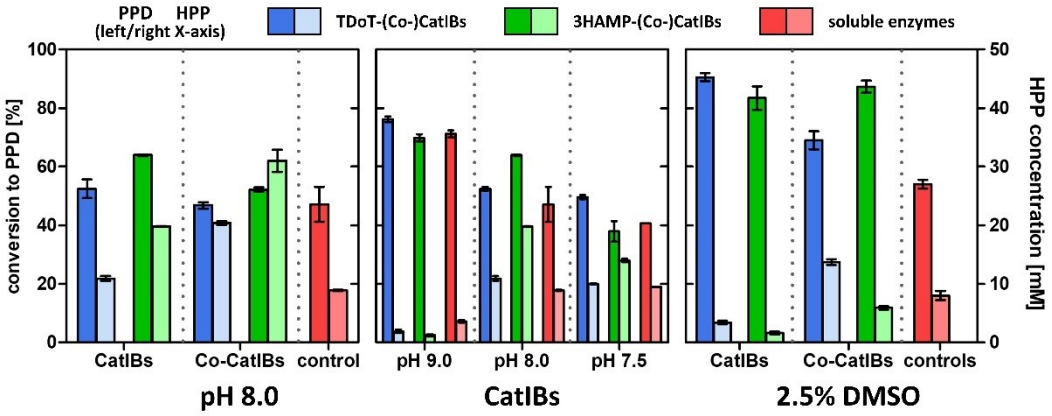


Figure 3-11 PPD production observed in the two-enzyme, one-pot cascade reactions. The cascade was performed for 4 d utilizing single CatIBs, Co-CatIBs, or the purified soluble protein as control. Left: Initial set-up at pH 8.0. Middle: Conversion with CatIBs at different pH values. Right: Conversion under optimal conditions (pH 9.0, 2.5% (v/v) DMSO). TDoT (Co-)CatIBs are colored in blue, 3HAMP (Co-)CatIBs in green, and soluble controls in red. For each preparation/ condition the final amount of the HPP intermediate is shown as bar in lighter colors next to the bar for the final PPD amount. Further information can be found in the Chapters 2.5 and 2.6.

As mentioned above, we compared three different set-ups: one in which the enzymes where applied as single CatIBs and another one, where Co-CatIBs of *R*ADH and *Pf*BAL were used (3.2.4). A third reference reaction set-up, employing the purified soluble enzymes at equivalent volumetric activity, was always used as control. Further we compared TDoT and 3HAMP (Co-)CatIBs. To identify optimal conditions, the reaction pH was varied from pH 7.5 to pH 9.0 and the effect of the addition of co-solvents such as DMSO and MTBE was analyzed (2.6). From initial experiments, presented as a proof-of-concept in Chapter 2.5, total PPD production and minimal accumulation of the HPP intermediate were identified as cascade optimization parameters.

In conclusion, TDoT CatIBs clearly outperformed 3HAMP CatIBs and single CatIBs performed better than Co-CatIBs, i.e. in terms of final conversion and minimal accumulation of the HPP intermediate. The reduced yield observed for Co-CatIBs compared to single CatIBs, however, can at least partially be compensated by their more cost-efficient preparation. The controls with soluble enzyme displayed similar conversions as 3HAMP CatIBs. This is probably due to a higher stability of the TDoT over the 3HAMP CatIBs under these harsh conditions. The PPD yield increased when raising the pH from 7.5 to 9.0 (Figure 3-11) even though at the same time the stability of *Pf*BAL decreased rapidly (Table 3-5).

Under optimal conditions, that is at pH 9.0 with 2.5% (v/v) DMSO as co-solvent, almost full conversion was be observed in the best case (single TDoT CatIBs). 3HAMP Co-CatIBs yielded similar conversions but increased amounts of HPP accumulated during the reaction, which would be problematic for easy product work-up. Overall, from our data we can conclude that the cofactor recycling step, catalyzed by *R*ADH, clearly represents the limiting step of the whole cascade. Thus operating the cascade at pH 9.0, where the cofactor recycling steps works optimally, and further imposing conditions that

stabilize *R*ADH CatIBs (2.5% (v/v) DMSO) [282], clearly result in optimal performance (Figure 3-11).

Table 3-5 Half-lives [h] of different *Pf*BAL/*R*ADH (Co-)CatIBs and of the corresponding purified soluble enzymes within the two enzyme, one-pot cascade reactions under various conditions. Values were estimated based on stability measurements of *Pf*BAL and *R*ADH. n.d.: Not determined. For further details, see Chapter 2.6.

preparation			pH 7.5	pH 8.0	pH 9.0	pH 9.0 + 2.5% (v/v) DMSO
CatIBs	TDoT	*Pf*BAL	38	36	0-6	6
		*R*ADH	>96	>96	0-6	48
	3HAMP	*Pf*BAL	10	38	0-6	4
		*R*ADH	72	46	0-6	46
Co-CatIBs	TDoT	*Pf*BAL	n.d.	5	n.d.	5
		*R*ADH	n.d.	132	n.d.	132
	3HAMP	*Pf*BAL	n.d.	5	n.d.	5
		*R*ADH	n.d.	82	n.d.	82
soluble		*Pf*BAL	5	5	0-6	6
		*R*ADH	62	26	0-6	20

The same cascade reaction has so far only been tested in initial studies with purified soluble enzyme in an aqueous system [278]. The optimal conditions ascertained from this approach served as orientation for our cascade studies, therefore it is not surprising that the maximum yield of this approach was achieved with similar conditions as found in our study, e.g. regarding substrate and cofactor concentrations, pH value of the buffer, and reaction temperature. However, a higher catalyst load of *R*ADH was used [278].

In another study the same two-enzyme, one-pot cascade was carried out with whole cells, immobilized in fluoroplastic 'teabags', using a micro-aqueous reaction system with MTBE as solvent [276, 277]. Comparison to our CatIB cascade is complicated, due to divergent reaction conditions. The use of organic solvents enables much higher substrate concentrations (500 mM benzaldehyde *versus* 130 mM substrates (benzaldehyde and benzyl alcohol) in the aqueous cascade), thus resulting a much higher STY. With whole cells, within 11 h a space-time yield (STY) of 78 g l^{-1} d^{-1} [277] was reached, while our reaction yielded 12 g l^{-1} d^{-1} at best (TDoT CatIBs, pH 9.0, with DMSO, calculated after 1 day). This calculation could only be performed assuming the catalyst load reported in [276] (g whole cells *vs*. g CatIB lyophilizate). It is however impossible to directly compare CatIBs to whole cells, since no information about the specific activity of the whole cells was given in [276]. On the other hand, the aqueous CatIB cascade yields almost full conversion, with only 2.6% of the HPP intermediate (3.4 mM) formed, while the whole-cell cascade only yielded about 60 to 70% conversion with 11% HPP (45 mM) [276]. Thus, product work-up would clearly be easier in case of the aqueous CatIB-based cascade.

In conclusion, the use of CatIBs and Co-CatIBs for the realization of enzyme cascades can be beneficial in particular under conditions where enzyme stability is a limiting issue.

While single CatIBs clearly outperformed the Co-CatIBs in the presented case, optimization of the *Pf*BAL/*R*ADH ratio in Co-CatIBs by using genetic means, as for example employing independently controllable promotors, could facilitate the generation of Co-CatIB immobilizates that perform equally well, while reducing the production costs by 50%, since only one Co-CatIB-batch would have to be produced.

3.4 CatIBs in comparison to other immobilization strategies

In the following chapters the CatIB-immobilization strategy will be compared to similar carrier-free and related carrier-based immobilization strategies. Additionally, alternative methods for the co-immobilization of protein, i.e. for the realization of reaction cascades, will be presented and compared to the above described Co-CatIB-strategy.

3.4.1 CatIBs produced by fusion of small, artificial peptides or aggregation-prone proteins

The comparison of CatIBs-immobilizates to preparations obtained by other immobilization methods proofs difficult, since the preparation methods and available characteristics often differ greatly. With regard to other fusion-tag induced CatIBs, like artificial peptides or aggregation-prone protein domains (Table 3-6), coiled-coil CatIBs yield at least as much insoluble protein (IB formation efficiency). Alas, they often show lower residual activities compared to the respective purified soluble target as for example CatIBs obtained by fusion of small artificial peptides [123-126, 129]. One possible reason could be, that with the rather small artificial peptides (8 to 18 amino acids), a higher level of correctly folded protein can be maintained within the respective CatIBs. However, the target enzymes tested with other aggregation-inducing tags, such as the monomeric enzymes lipase A from *B. subtilis* [283] or amadoriase II from *A. fumigatus* [284], were certainly less complex then the here tested cofactor-dependent multimeric enzymes. Additionally, in those studies mostly morphological aspects were investigated without providing direct evidence for any biotechnological application, i.e. those CatIB-immobilizates were seldom tested for recycling and stability. Furthermore, residual activities are often given compared to cell lysates containing the soluble counterpart instead of comparing with the purified soluble enzymes [120, 123-127, 130]. At present, no direct one-to-one comparison between the here presented TDoT- and 3HAMP-based CatIB strategy and the use of other aggregation-inducing tags has been presented. Therefore, the relative performance of the here described CatIBs, obtained by TDoT- and 3HAMP fusion, remains to be thoroughly investigated.

Table 3-6 Comparison of residual activities of CatIBs obtained by fusion of different CatIB-formation inducing tags. More details about the fusion tags can be found in Table 1-1. 1: Soluble enzyme was purchased from Sigma and further purified.

CatIB-inducing tag	target enzyme	target origin	reference for residual activity	residual activity [%]	Ref.
I. Coiled-coil induced CatIBs					
TDoT	lyase	*A. thaliana*	purified	11	[107]
	alcohol dehydrogenase	*Ralstonia* sp.	purified	2	this work
		L. brevis		6	
	lyase	*P. fluorescens*		1	
	decarboxylase	*P. putida*		4	
3HAMP	alcohol dehydrogenase	*Ralstonia* sp.	purified	12	this work
		L. brevis		1	
	lyase	*P. fluorescens*		18	
	decarboxylase	*P. putida*		10	
II. Small, artificial peptides					
L6KD	lipase A	*B. subtilis*	cell lysate	30	[123]
	amadoriase II	*A. fumigatus*		93	
	xylosidase	*B. pumilus*		26	
GFIL8	lipase A	*B. subtilis*	cell lysate	43	[124]
	amadoriase II	*A. fumigatus*		54	
	Ulp1 protease	*S. cerevisiae*	purified	40	[129]
ELK16	amadoriase II	*A. fumigatus*	cell lysate	88	[125]
	xylosidase	*B. pumilus*		77	
18A	lipase A	*B. subtilis*	cell lysate	150	[126]
III. Aggregation-prone proteins and protein domains					
CBDclos	D-amino acid oxidase	*T. variabilis*	cell lysate	42	[127]
	sialic acid aldolase	*E. coli* K12		100	[130]
CBDcell	β-glucuronidase	*E. coli* MG1665	purified[1]	19	[133]
VP1	β-galactosidas	*E. coli*	cell lysate	166	[120]
Cry3Aa	lipase A	*B. subtilis*	purified	221	[134]
	esterase	*B. subtilis*		101	
	deformylase	*B. burgdorferi*		48	

3.4.2 CatIBs, CLEAs, and HaloTag®-immobilizates: similarities and differences

With regard to preparation and morphology, the here presented CatIB immobilizates can best be compared to CLEAs (1.2.3) or to immobilizates obtained by using the commercially available HaloTag® system (1.2.1), since all these methods mostly forego enzyme purification. The CLEA technology has become popular in the 1990s and is now a well-established method for enzyme immobilization that circumvents the use of expensive carrier materials. CLEAs are prepared from mildly-precipitated enzymes, covalently linked by a cross-linker, usually glutaraldehyde. The immobilization of enzymes by utilizing HaloTag® fusion proteins bound to suitable carrier materials, on the other hand, is a very new strategy. Albeit HaloTag® protein purification systems are commercially available from Promega (Madison, USA) or ChromoTek GmbH (Martinsried, Germany), they have up to now mostly been used for biomedical applications [285] or the purification of proteins [286]. A brief, but by far not comprehensive, overview is given in Table 3-7.

Table 3-7 Comparison of selected CLEA and HaloTag® immobilized enzymes in comparison to CatIBs. CLEA preparations are highlighted in blue, HaloTag® immobilizates in red, and CatIB preparations in green. 1: For CLEAs: recovered activity compared to the initial activity of the starting enzyme preparation before immobilization; For HaloTag® immobilizates and CatIBs: residual activity compared to purified soluble target enzymes. GLA: glutaraldehyde, DPA: dextran polyaldehyde, EG-NHS: ethylene glycol-bis [succinic acid N-hydroxy succinimide]. n.i.: No information given. Table columns ordered according to the enzyme class (EC) of the target.

EC	enzyme	origin	activity[1] [%]	starting preparation	comments	Ref.
1	ADH	*Ralstonia* sp. *Lactobacillus brevis*	2 and 12 1 and 6	*in vivo* immobilization	CatIBs with TDoT and 3HAMP	this work
1	ADH	*Lactobacillus brevis*	35	crude cell extract	HaloTag®-enzyme	[287]
1	ADH	*Lactococcus brevis*	0 or 10	Jülich Fine Chemicals	cross-linker: GLA or DPA	[84]
1	laccase	*Tinea versicolor*	32	commercial preparation, Sigma	magnetic CLEAs with GTA	[288]
1	tyrosinase	mushroom	100	commercial preparation, Sigma	cross-linker: GLA	[289]
1	peroxidase	*Armoracia rusticana*	83	commercial preparation, Fluka	cross-linker: GLA	[290]
3	lipase	*Pencilluim notatum*	24 and 52 (hydrolysis) 35 and 64 (esterification)	n.i.	cross-linker: GLA and EG-NHS	[291]
3	α-L-rhamnosidase	*Brevundimonas* sp.	82	partially purified cell extract	cross-linker: GLA	[292]
3	α-amylase	*Bacillus* sp.	100 and 45	commercial preparation, Sigma	magnetic and classical CLEAs with GTA	[293]
3	penicillin G acylase	*Escherichia coli*	48 or 90	commercial preparation, Sigma	cross-linker: GLA or DPA	[84]
4	benzoylformate decarboxylase	*Pseudomonas putida*	4 and 10	*in vivo* immobilization	CatIBs with TDoT and 3HAMP	this work
4	benzoylformate decarboxylase	*Pseudomonas putida*	65	crude cell extract	HaloTag®-enzyme	[287]
4	benzaldehyde lyase	*Pseudomonas fluorescens*	1 and 18	*in vivo* immobilization	CatIBs with TDoT and 3HAMP	this work
4	benzaldehyde lyase	*Pseudomonas fluorescens*	60	crude cell extract	HaloTag®-enzyme	[254]
4	hydroxynitrile lyase	*Arabidopsis thaliana*	11	*in vivo* immobilization	CatIBs with TDoT	[107]
4	hydroxynitrile lyase	*Prunus amydalus*	10	Jülich Fine Chemicals	cross-linker: GLA or DPA	[84]
4	nitrilase	*Pseudomonas fluorescens*	0 or 50	cell-free extract	cross-linker: GLA or DPA	[84]
4	phenylalanine ammonia lyase	*Rhodotorula glutinis*	8 to 36	partially purified protein	cross-linker: GLA with different precipitants	[294]
4	lysine decarboxylase	*Escherichia coli*	8	crude cell extract	cross-linker: GLA	[266]
4	nitrile hydratase	*Haloalkaliphilic actinobacterium*	23	cell-free extract	cross-linker: GLA	[295]

The activity of CLEAs is commonly given as residual activity after immobilization relative to the activity of the starting enzyme preparation before immobilization, usually crude cell-free extracts. This somewhat hampers a direct comparison to the residual activity of our CatIB immobilizates, for which the activity of the purified soluble target protein is commonly used as a reference. In general, as can be seen from Table 3-7, the

activity of CLEAs varies widely (from 0 to 100%), sometimes even within the same study, which is mostly related to the use of different cross-linking agents or precipitants. For example, a nitrilase from *Pseudomonas fluorescens*, while not showing any activity when cross-linked with glutaraldehyde, retains 50% activity when cross-linked with dextran polyaldehyde [84]. Based on this data, it becomes clear that the CLEA strategy requires case-to-case optimization and can thus hardly be considered as generically applicable. The HaloTag® strategy was serendipitously used for the same enzymes, which are also available as CatIBs. Compared to the corresponding CatIBs they show higher residual activities. For example, *Pp*BFD immobilized *via* HaloTag® showed a 6.5-times higher activity than the corresponding 3HAMP-*Pp*BFD CatIBs. Even the highest residual activity observed for CatIBs (3HAMP-*Pf*BAL CatIBs) was still more than 3-times lower compared to the corresponding HaloTag®-immobilized *Pf*BAL preparation.

In conclusion, while CLEAs and HaloTag® immobilizates apparently retain higher residual activities than CatIBs, both methods either include additional immobilization steps (e.g. cross-linking; CLEAs) or require the use of expensive carrier materials (HaloLink® resin; HaloTag® immobilizates). Thus, under economical aspects, they are still more expensive and less straightforward to produce than CatIBs.

3.4.3 Immobilization of multiple enzymes for cascades

The co-immobilization of enzymes for cascade operation, resulting in enhanced performance due to substrate channeling, is often discussed as a big advantage [238]. Enzymes are either co-immobilized undirected, yielding a statistical distribution, or they are immobilized in a directed manner, often by differential methods allowing for a controlled spatial orientation and distribution [238]. The latter approach, while facilitating high control over localization and exploitation of substrate channeling, nevertheless needs tedious and time-consuming fine-tuning and is therefore not well suited for a comparison to the generic Co-CatIBs-based method.

Undirected co-immobilization has been realized by several different methods, e.g. by direct fusion of enzymes for the use in whole cells [296], co-immobilization as combi-CLEAs (1.2.3) [297-300], or by co-immobilization on solid carrier materials [301], scaffolding of enzymes by coupling to DNA [302] and proteins [143], or by different IB-based methods (1.3.4) [30, 142, 303]. A brief, by no means comprehensive overview of different co-immobilized enzymes is given in Table 3-8.

The comparison of Co-CatIBs to other immobilization techniques is even more complicated than for single CatIBs (3.4.2), since most methods have usually been tested only in proof-of-concept experiments. This is for example reflected by the fact that residual activities of each of the co-immobilized enzymes, compared to its purified soluble counterpart are given even more rarely, than for single immobilized enzymes. In cases where activity values were provided, they are often given as ‘recovered activity’

instead of 'residual activity', meaning the activity of the co-immobilized enzyme in relation to the activity of the starting preparation used for immobilization. Depending on the starting preparation (e.g. crude cell-free extracts), those values can be quite different from the activity of the purified soluble enzyme, which renders a direct comparison useless. The only case where 'real' residual activities were published was a study with combi-CLEAs of two aminopeptidases (PepX and PepN) that were applied for the hydrolysis of casein [297]. Under the best conditions this co-immobilizate yielded 9 and 18% residual activity for the two enzymes, respectively, which is equivalent to the residual activities determined for 3HAMP Co-CatIBs of *R*ADH (9%) and *Pf*BAL (11%). Additionally, in many cases the alleged co-immobilizates are not used for the realization of a 'true' cascade reaction, but instead the second enzyme is often just used to regenerate the cofactor of the first enzyme [301, 302].

Even though the direct comparison to Co-CatIBs proves difficult, the co-immobilization strategies found in literature are nevertheless, fascinating. The immobilization of enzymes within forisomes (plant-derived mechanoproteins, 1.3.4) resulting in immobilizates called forizymes, for example, is not that different from our CatIB strategy [143]. Similar to CatIBs, immobilization is achieved by a genetic fusion, and just like CatIBs they can be obtained in single or co-immobilized form. However, a brief search did not yield other publications on the biotechnological use of forizymes.

Another interesting aspect is the number of different enzymes that can be co-immobilized. The most impressive example here is certainly the *in vivo* immobilization of multiple enzymes on the surface of cellulose-binding domain IBs by means of a 'bait and prey' leucine zipper (1.3.4 and Figure 1-6b), where four different enzymes could be co-immobilized, forming an artificial metabolon in *E. coli*, which was used for the production of 1-butanol from glucose [137]. Admittedly, the immobilization of those enzymes after cell disruption yielded much better results than the *in vi*vo immobilization and batch fermentation with living cells, probably due to an overload of enzymes on the IB and a hitherto relating metabolic malfunction in *E. coli*. Apart from this exotic example, however, at most two enzymes have been co-immobilized.

In conclusion, the immobilization of multiple enzymes for the realization of enzymatic cascades is still in its infancy. In this regard, our Co-CatIB strategy certainly represents one of the easier, more generically applicable methods. For efficient operation, however a number of questions still need to be addressed. This includes for example: (i) Can the relative ratio of two or multiple enzymes with in CatIBs be tuned rationally, e.g. by using different independently controlled inducible promotors? and (ii) How many TDoT or 3HAMP gene fusions can be co-expressed in *E. coli* and thus how many proteins can be co-immobilized effectively within Co-CatIBs, without overstressing the cells to a degree that prevents cell growth and heterologous gene expression?

Table 3-8 Examples of different strategies to co-immobilize enzymes in comparison to Co-CatIBs. *: values are not residual but recovered activity, meaning the activity in relation to the solution that was subjected to immobilization. HCoA: Hydroxybutyryl-CoA. BCoA: Burtyryl-CoA. CBD: cellulose binding domain. n.i.: No information provided.

approach and number of enzymes		enzymes	origins	residual activity [%]	starting preparation	comment	Ref.
Co-CatIBs	2	BAL	*Pseudomonas fluorescens*	3 or 11	*in vivo* immobilization	Co-CatIBs with TDoT or 3HAMP as coiled-coil domain	this work
		ADH	*Ralstonia* sp	1 or 9			
combi-CLEAs	2	aminopeptidase PepX	*Lactobacillus helveticus*	18	purified enzymes	used for casein hydrolysis	[297]
		aminopeptidase PepN		9			
combi-CLEAs	2	lipase	*Ictalurus punctatus*	95*	crude cell extract	production in channel catfish; used for food stain removal	[298]
		protease		58*			
direct fusion	2	ADH	*Micrococcus luteus*	about 140%	whole cells	direct recycling of NAPH due to reaction design	[296]
		Baeyer-Villiger monooxygenase	*Pseudomonas putida*				
direct fusion and co-immobilization on agarose	2	phenylacetone monooxygenase	*Thermobifida fusca*	similar to soluble fusion	purified enzyme fusion	immobilization *via* covalently bound cofactor (FAD); phosphite dehydrogenase only for cofactor recycling	[301]
		phosphite dehydrogenase	n.i.				
immobilization of on DNA scaffold	2	oxidoreductase	*Saccharomyces cerevisiae*	n.i.	purified enzymes	enzymes linked by different tags; reductase domain only for cofactor recycling	[302]
		BMR	*Bacillus megaterium*				
immobilization on PhaC IBs by coiled-coil fusion system	2	ADH	*Rhodococcus erythropolis*	n.i.	*in vitro* immobilization from crude cell extract	formate dehydrogenase only for cofactor recycling	[303]
		formate dehydrogenase	*Candida boidinii*				
immobilized in forizymes	2	glucose-6-phosphate dehydrogenasee	*Saccharomyces cerevisiae*	n.i.	*in vivo* immobilization in *Saccharomyces cerevisiae*	enzymes genetically fused to a forizyme (MtSEO-F1) of *Medicago truncatula* in single and co-immobilized form	[143]
		hexokinase 2					
combi-CLEAs	3	pectinase	*Aspergillus niger*	approx. 100*	commercial preparation, Novozymes (Copenhagen, Denmark)	from the same preparation, displaying all three enzyme activities not intended for cascade reaction but as multipurpose biocatalyst	[299]
		xylanase					
		cellulase					
immobilization on magnetic nanoparticles	3	endoglucanase	*Clostridium thermocellum*	n.i.	*in vivo* immobilization, purification from lysate by a magnetic field	enzymes fused to magnetosome anchor in series; CBD only for binding of crystalline cellulose; hydrolysis of insoluble cellulose possible	[142]
		β-glucanase					
		CBD					
combi-CLEAs	3	α-amylase	LARASE® L-40 000	n.i.	commercial preparation, Riddhi Siddhi Gluco Biols Ltd. (Gokak, India)	recycling demonstrated	[300]
		glucoamylase	OPTIDEX® L-300				
		pullulanase	OPTIMAX® L-300				
immobilization on CBD inclusion bodies by leucine zipper-mediated capture	4	HCoA dehydrogenase	*Clostridium acetobutylicum*	64*	*in vivo,* with whole cells or *in vitro*, starting from cell-free extract	artificial metabolon in *E. coli* for 1-butanol production from glucose cells with artificial metabolon performed approx. 50% better than metabolon free cells	[137]
		HCoA dehydratase		82*			
		ADH		75*			
		BCoA dehydratase	*Treponema denticola*	51*			

3.5 Conclusions: CatIBs as a new method for enzyme immobilization

The here presented CatIB-strategy, as a generic, solely biological method for enzyme immobilization poses several advantages. The biggest certainly is their easy production: they can be directly produced in *E. coli* yielding natural, and thus biodegradable, carrier-free immobilizates. Therefore, no tedious and expensive chromatographic purification steps are needed for the preparation. The general principle used for the preparation of CatIBs is illustrated in Figure 3-12. Following this protocol only a few contaminations, such as lipids and membrane proteins are commonly present in the CatIB preparation (Figure 3-6). To the best of our knowledge, these however do not exhibit any catalytic activity or interfere with the target enzymes.

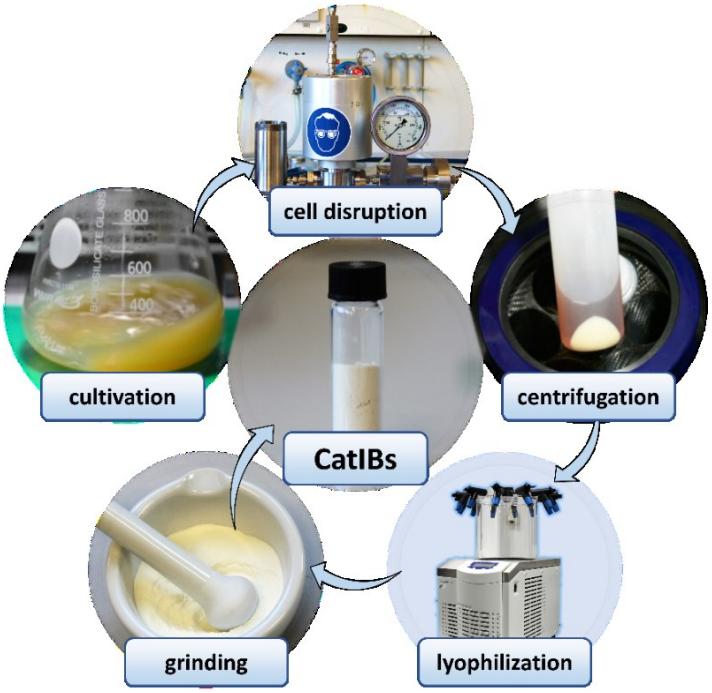


Figure 3-12 Production of CatIBs by a simple standardized protocol. CatIBs are produced by expression of TDoT or 3HAMP gene fusions in *E. coli* BL21(DE3), cells are disrupted by ultra-homogenizer and subsequently the CatIB-containing pellet is separated from the soluble protein-containing fraction by centrifugation and washed once with water. Lyophilization and grinding, yields the final CatIB preparation.

Furthermore, an enhanced stability of CatIBs compared to purified soluble target enzyme could be demonstrated here for different enzymes in multiple applications (2.3 to 2.6). For *Pf*BAL and *Ec*LDC, also the recycling was tested in CatIBs, resulting in excellent stabilities over several batches (2.3 and 2.4).

Notwithstanding these advantages, CatIBs also possess certain disadvantages. The biggest drawback is certainly their comparatively low activity, with regard to the respective purified soluble enzyme. However, loss of activity due to immobilization is a feature observed for most immobilizates, which is also observed for other immobilization methods like CLEAs or immobilization *via* the HaloTag® system. Nevertheless, their

generic production and applicability as well as easy and cost-efficient production, render CatIBs a promising new enzyme preparation for application in synthetic chemistry and biocatalysis.

3.5.1 Evaluation of CatIBs under economical aspects

From an industrial perspective, the final decisive parameter that decides for or against the application of a given enzyme preparation in a process, are the costs associated with its production. Therefore, a final calculation should be done to see, whether CatIBs can be applied cost-efficiently in biotechnology. Most importantly, the question needs to be addressed, whether the often-observed low residual activities of CatIBs can be compensated by lower production costs and longer life time.

Of course, such calculations include several assumptions, so that process costs can only be estimated. The results presented here, must therefore be handled with care. Furthermore, the results obtained as part of this thesis, e.g. yields and activities, are derived in an academic setting and hence will differ, when the preparation is performed at larger, i.e. industrial scale.

A very good cost estimation for biotechnological processes was presented by Tufvesson *et al*. in 2011 [44]. The authors derived individual cost factors for the different process steps needed for enzyme preparation, which include the preparation of crude cell extracts, purified enzyme, or immobilization relative to the production of whole cells. The costs associated with the production of whole cells was set to 1, while for crude cell extracts (obtained by cell lysis) a cost factor of 2 and for the purification of the enzyme a cost factor of 10 was assumed. The production costs for CatIBs are likely much closer to the costs assumed for the preparation of crude cell extracts as only a separation (e.g. by centrifugation) and washing steps are needed for their preparation. Therefore, a cost factor of 3 was here estimated for the production of CatIBs. This calculation neglects the lyophilisation step, used here for drying of the CatIBs before application, since this step, in principle, can also be omitted. Using the cost factors provided by Tufvesson *et al*. a cost calculation for the production of TDoT and 3HAMP CatIBs of *Pf*BAL and *R*ADH was performed (Table 3-9). For comparison, the production costs were also calculated for the respective purified soluble enzymes (Table 3-9). An example calculation can be found in the Appendix (see Table 4-1).

With regard to the isolated production costs, the production of *Pf*BAL CatIBs (in terms of costs per Unit of activity) is still more expensive than the production of the corresponding purified soluble enzyme. Cost differences hereby amount to factors of four and 10 for 3HAMP and TDoT CatIBs, respectively. In contrast, the production of both types of *R*ADH CatIBs are by a factor of 2 cheaper than the production of purified soluble *R*ADH. This calculation even neglects that for the production of *R*ADH two chromatographic steps are needed, which would further raise the costs.

Table 3-9 Calculation of activity yield and production costs for *Pf*BAL and *R*ADH when produced as TDoT and 3HAMP CatIBs or as soluble enzyme. Values for yield, activity, and specific activity were taken from Chapter 2.1. Cost factors for production and immobilization were taken from [44], apart from *, which was estimated as described above. Values for half-life are taken from Chapter 2.6 (cascade reaction at pH 8). The results are highlighted in green, yellow, and red according to their value. An example calculation can be seen in Table 4-1.

preparation	*Pf*BAL			*R*ADH		
	CatIBs		soluble	CatIBs		soluble
	TDoT	3HAMP		TDoT	3HAMP	
protein yield per $g_{wet\ cells}$ [mg]	63	11	20	82	19	2
relative [%]	315	55	-	4100	950	-
specific activity [s^{-1}]	0.77	13.9	76.7	0.05	0.33	2.77
relative [%]	1.0	18.1	-	2.0	12.0	-
activity [U mg^{-1}]	0.69	10.5	76.7	0.10	0.42	6.21
total activity yield [U]	43.5	115.5	1533.5	7.95	8.02	12.43
relative [%]	2.8	7.5	-	64.0	64.5	-
relative production cost factor [-]	3*	3*	10	3*	3*	10
production costs [U^{-1}]	$69 \cdot 10^{-3}$	$26 \cdot 10^{-3}$	$7 \cdot 10^{-3}$	0.38	0.37	0.81
relative [%]	985.7	371.4	-	46.8	46.5	-
relative immobilization cost factor [-]	1	1	4	1	1	4
final costs [U^{-1}]	$69 \cdot 10^{-3}$	$26 \cdot 10^{-3}$	$28 \cdot 10^{-3}$	0.38	0.37	3.22
relative [%]	246.4	92.9	-	11.7	11.6	-
stability (half-life) [h]	36	38	5	96	46	26
usability [h U]	522	1462	714	183	123	8
relative [%]	73.1	204.8	-	2287.5	1537.5	-

Further including the immobilization costs in the calculation for the soluble enzyme, which are not required for CatIBs, the relation changes, so that the costs for the production of 3HAMP-*Pf*BAL CatIBs are almost equal to immobilized *Pf*BAL. Alas, the TDoT-*Pf*BAL CatIBs, due to their low activity yield, are still about 2.5-times more expensive. Immobilization of soluble *R*ADH further increases the production costs, so that the costs for immobilized *R*ADH is about a magnitude higher than for CatIBs.

As a last factor the stability of CatIBs and immobilized control enzymes was included, calculating a usability of the different preparations. Due to the higher stability of *Pf*BAL CatIBs compared to soluble enzyme, TDoT-*Pf*BAL shows a usability slightly below the level of immobilized *Pf*BAL, while the usability of 3HAMP-*Pf*BAL outranks that of immobilized *Pf*BAL by a factor of 2. In case of *R*ADH, the higher stabilities of CatIBs lead to usabilities of TDoT- and 3HAMP-*R*ADH by a factor of 23 and 15 higher compared to immobilized *R*ADH. However, it has to be mentioned that these calculations neglect the probability that soluble enzymes are also stabilized due to immobilization, which would lead to higher usabilities for the reference enzymes.

When performing such estimations of production costs and usability for Co-CatIBs, compared to single, individually prepared *Pf*BAL and *R*ADH CatIBs, an additional cost advantage is provided by the simultaneous production of both enzyme immobilizates, which further reduces the production cost factor from 3 to 1.5. In comparison to soluble

purified and subsequently immobilized enzymes, this further increases the cost benefit, which clearly outperforms the slightly lower specific activities as discussed above (see 3.2.4, Table 3-1).

In conclusion, even though CatIBs often possess low residual activity, their low productions costs, mainly resulting from the elimination of tedious, time consuming, and thus expensive chromatographic purification steps, and direct *in situ* immobilization, can overcompensate their low activity. This is especially pronounced when the costs for CatIB production are compared to the production costs for enzyme immobilizates prepared from purified enzyme.

3.6 The future of CatIBs

In this thesis a 'toolbox' of fusion proteins consisting of ten different enzymes and proteins, as well as two coiled-coil domains was established. In all cases, after optimization by fusion protein redesign (2.1; discussed in 3.1.1) CatIBs or FIBs could be produced successfully. This impressively illustrates the generic applicability of the CatIB-immobilization strategy. Even though the expression conditions could be optimized with regard to duration and cultivation medium pH stability (2.2; discussed in 3.1.2), all here described CatIBs were produced using essentially the same simple cultivation protocol. This further highlights the robustness of the method. The computational studies presented as part of Chapter 2.1 (discussed in 3.2.5) provide evidence that the feasibility of the general approach might be predicted based on sequence or structural features of the target enzyme.

The presented application studies (2.3, 2.4, and 2.6; discussed in 3.3) suggest that CatIBs can be used under a variety of different reaction conditions, ranging from aqueous media with or without co-solvent, to biphasic and micro-aqueous organic solvent-based reaction systems [22, 107]. They can either be employed as single CatIBs or Co-CatIBs, both allowing for the realization of enzymatic reaction cascades. In all cases, their improved stability compared to the purified soluble enzymes, proved beneficial for application (2.3, 2.4, and 2.6; discussed in 3.3). Last but not least, production cost estimations revealed that CatIBs can be produced at competitive costs, especially when stability issues and immobilization is taken into account.

While this thesis nicely illustrates the broad applicability of the CatIB strategy, nevertheless, a lot of questions, raised throughout the discussion section, still remain. These predominantly concern the formation and morphology of CatIBs with regard to conventional, non-active IBs. Albeit different theories about CatIB formation have been put forward based on the outcome of this thesis (3.2.6), nevertheless no unified model about formation and morphology can yet be presented. In particular structural studies, e.g. by Fourier-transform infrared spectroscopy (FTIR) [89, 120], circular dichroism

(CD) spectroscopy [304], or solid-state nuclear magnetic resonance (NMR) [305], could be used to comparatively characterize CatIBs and conventional, inactive IBs. Additionally, the comparison of compact and diffuse CatIBs (3.2.1), by using those methods, could help to elucidate structural differences. The observation that depending on the cultivation temperature, either CatIBs/FIBs or conventional, inactive IBs are produced (3.1.2), could be utilized to obtain active and inactive IBs of the same construct for comparative characterization. Likewise, microfluidic growth studies in conjunction with real-time fluorescence microscopy could be used to monitor the formation of diffuse FIBs, much like it has been done for compact FIBs (3.2.4, Appendix, Figure 4-4). Amyloid-specific dyes such as Thioflavin-T (Th-T) [97] or Congo-Red (CR) [304] could be employed to monitor the amyloid content of the different CatIBs/FIBs and conventional, inactive IBs, i.e. also with regard to different expression conditions. Further, comparative 'omic' analyses of CatIB/FIB or conventional, inactive IBs producing cells could be performed to gain a better insight into the *E. coli* quality control machinery, or the cellular responses during CatIB formation [88, 236].

The other issue of the current CatIB strategy are the comparatively low residual activities that are observed for certain CatIBs. In view of the significant differences observed for TDoT and 3HAMP CatIBs, the use of alternative coiled-coil domains, e.g. with differing sizes or subunits (identified in the coiled coil database CC+ [306]), could be beneficial. Alternatively, small artificial peptides, like GFL8 or 18A, could be used as aggregation-inducing tag, facilitating the direct comparison to the TDoT/3HAMP system. Additionally, from the application perspective, recycling aspects should gain more attention, since this is one of the big advantages of immobilizations.

The performance of Co-CatIBs could be improved by better controlling the ratio of the two target enzymes within the Co-CatIBs by genetic means, e.g. employing independently controllable promotors. Along the same lines, the question arises how many proteins can be effectively co-immobilized within Co-CatIBs, before overstressing *E. coli* to a degree that prevents the formation of CatIBs or negatively affecting *E. coli* growth.

4 Chapter 4
References

1. **Ulber R and Soyez K.** 5000 Jahre Biotechnologie: Vom Wein zum Penicillin. *Chemie in unserer Zeit.* 2004. 38(3): 172-180.
2. **Lindström B and Pettersson LJ.** A Brief History of Catalysis. *CATTECH.* 2003. 7(4): 130-138.
3. **Berzelius JJ.** Årsberättelsen om framsteg i fysik och kemi. *Royal Swedish Academy of Sciences.* 1835.
4. **Pasteur L.** Mémoire sur la fermentation appelée lactique, ed. Pasteur V-R. Masson, Paris. *Œuvres de Pasteur*. 1922
5. **Kühne W.** Ueber das Trypsin (Enzym des Pankreas). *FEBS Letters.* 1976. 62(S1): E8-E12.
6. **Buchner E.** Alkoholische Gärung ohne Hefezellen. *Berichte der deutschen chemischen Gesellschaft.* 1897. 30(1): 1110-1113.
7. **Bornscheuer UT, Huisman GW, Kazlauskas RJ, Lutz S, Moore JC, and Robins K.** Engineering the third wave of biocatalysis. *Nature.* 2012. 485(7397): 185-194.
8. **Faber K.** Biotransformations in Organic Chemistry - A Textbook. Cham, Switzerland. *Springer International Publishing*. 2018. Vol. 7.
9. **Grand View Research Inc.** Catalyst Market Analysis by Raw Material, Chemical Compounds, by Product, Application, Petrochemicals & Polymers, Environmental and Segment Forecasts to 2024. San Francisco, USA. *Grand View Research*. 2017. Vol. ID: 4396403.
10. **Watson JD and Crick FHC.** Molecular Structure of Nucleic Acids: A Structure for Deoxyribose Nucleic Acid. *Nature.* 1953. 171: 737-738.
11. **Cohen SN, Chang AC, Boyer HW, and Helling RB.** Construction of biologically functional bacterial plasmids *in vitro*. *Proceedings of the National Academy of Sciences.* 1973. 70(11): 3240-3244.
12. **Schmid A, Dordick JS, Hauer B, Kiener A, Wubbolts M, and Witholt B.** Industrial biocatalysis today and tomorrow. *Nature.* 2001. 409(6817): 258-268.
13. **Liese A, Seelbach K, and Wandrey C.** Industrial Biotransformations. 2nd ed. Weinheim, Germany. *Wiley-VCH*. 2006
14. **Libavius A.** Alchemia. Frankfurt, Germany. *Johannes Sautrius*. 1597
15. **Grünewald H.** Nobel Lectures Chemistry 1901–1921 und 1922–1941. *Angewandte Chemie.* 1968. 80(1): 52-52.
16. **Rosenthaler L.** Durch Enzyme bewirkte asymmetrische Synthesen. *Biochemische Zeitschrift.* 1908. 14: 238–253.
17. **Trommsdorff E.** Dr. Otto Röhm - Chemiker und Unternehmer. Düsseldorf, Germany. *Econ Verlag* 1976
18. **Sumner JB.** The Isolation and Crystallization of the Enzyme Urease. *Journal of Biological Chemistry.* 1926. 69(2): 435-441.
19. **Sanger F, Nicklen S, and Coulson AR.** DNA sequencing with chain-terminating inhibitors. *Proceedings of the National Academy of Sciences.* 1977. 74(12): 5463-5467.
20. **Rabinow P.** Making PCR: A Story Of Biotechnology. Chicago, USA. *University of Chicago Press*. 1996
21. **Nobel Media AB.** The Nobel Prize in Chemistry 2018. *Nobelprize.org*. Accessed: 29th, November, 2018. Available from: www.nobelprize.org/prizes/chemistry/2018/prize-announcement.
22. **Diener M.** Von gezielter Oligomerisierung zu katalytisch aktiven *inclusion bodies* – Eine alternative Strategie zur Stabilisierung und Immobilisierung von Biokatalysatoren. *Heinrich-Heine University Düsseldorf.* 2014
23. **Wetterstrand KA.** DNA Sequencing Costs: Data from the NHGRI Genome Sequencing Program (GSP). Accessed: 28th, November 2018. Available from: www.genome.gov/sequencingcostsdata.
24. **Fowler DM, Araya CL, Fleishman SJ, Kellogg EH, Stephany JJ, Baker D, and Fields S.** High Resolution Mapping of Protein Sequence – Function Relationships. *Nature Methods.* 2010. 7(9): 741-746.
25. **Altschul SF, Gish W, Miller W, Myers EW, and Lipman DJ.** Basic local alignment search tool. *Journal of Molecular Biology.* 1990. 215(3): 403-410. Available from: https://blast.ncbi.nlm.nih.gov/Blast.cgi.
26. **Benson DA, Cavanaugh M, Clark K, Karsch-Mizrachi I, Lipman DJ, Ostell J, and Sayers EW.** GenBank. *Nucleic Acids Research.* 2013. 41(Database issue): D36-42. Available from: www.ncbi.nlm.nih.gov/genbank.

27. **The UniProt Consortium.** UniProt: the universal protein knowledgebase. *Nucleic Acids Research.* 2017. 45(Database Issue): D158-D169. Available from: www.uniprot.org.
28. **Berman HM, Westbrook J, Feng Z, Gilliland G, Bhat TN, Weissig H, Shindyalov IN, and Bourne PE.** The Protein Data Bank. *Nucleic Acids Research.* 2000. 28(1): 235-242. Available from: www.rcsb.org/pdb.
29. **Kan SBJ, Lewis RD, Chen K, and Arnold FH.** Directed evolution of cytochrome c for carbon–silicon bond formation: Bringing silicon to life. *Science.* 2016. 354(6315): 1048-1051.
30. **Bornscheuer UT.** The fourth wave of biocatalysis is approaching. *Philosophical transactions. Series A, Mathematical, physical, and engineering sciences.* 2018. 376(2110): 1-7.
31. **Straathof AJJ, Panke S, and Schmid A.** The production of fine chemicals by biotransformations. *Current Opinion in Biotechnology.* 2002. 13(6): 548-556.
32. **Wegman MA, Janssen MHA, van Rantwijk F, and Sheldon RA.** Towards Biocatalytic Synthesis of β-Lactam Antibiotics. *Advanced Synthesis and Catalysis.* 2001. 343(6-7): 559-576.
33. **Sheldon RA.** Green solvents for sustainable organic synthesis: state of the art. *Green Chemistry.* 2005. 7(5): 267-278.
34. **Anastas P and Warner J.** Green Chemistry: Theory and Practice. Oxford, United Kingdom. *Oxford University Press*. 1998
35. **Tang SY, Bourne RA, Smith RL, and Poliakoff M.** The 24 Principles of Green Engineering and Green Chemistry: "IMPROVEMENTS PRODUCTIVELY". *Green Chemistry.* 2008. 10(3): 268-269.
36. **Tang SLY, Smith RL, and Poliakoff M.** Principles of green chemistry: PRODUCTIVELY. *Green Chemistry.* 2005. 7(11): 761-762.
37. **Constable DJC, Curzons AD, and Cunningham VL.** Metrics to 'green' chemistry-which are the best? *Green Chemistry.* 2002. 4(6): 521-527.
38. **Erbeldinger M, Mesiano AJ, and Russell AJ.** Enzymatic Catalysis of Formation of Z-Aspartame in Ionic lLquid - An Alternative to Enzymatic Catalysis in Organic Solvents. *Biotechnology Progress.* 2000. 16(6): 1129-1131.
39. **Nagayama K, Spieß AC, and Büchs J.** Enhanced catalytic performance of immobilized *Parvibaculum lavamentivorans* alcohol dehydrogenase in a gas phase bioreactor using glycerol as an additive. *Chemical Engineering Journal.* 2012. 207-208: 342-348.
40. **Doukyu N and Ogino H.** Organic solvent-tolerant enzymes. *Biochemical Engineering Journal.* 2010. 48(3): 270-282.
41. **Patel RN.** Enzymatic synthesis of chiral intermediates for drug development. *Advanced Synthesis and Catalysis.* 2001. 343(6-7): 527-546.
42. **Kazuoka T, Oikawa T, Muraoka I, Kuroda S, and Soda K.** A cold-active and thermostable alcohol dehydrogenase of a psychrotorelant from Antarctic seawater, *Flavobacterium frigidimaris* KUC-1. *Extremophiles.* 2007. 11(2): 257-267.
43. **Schomburg I, Jeske L, Ulbrich M, Placzek S, Chang A, and Schomburg D.** The BRENDA enzyme information system – From a database to an expert system. *Journal of Biotechnology.* 2017. 261: 194-206. Available from: www.brenda-enzymes.org.
44. **Tufvesson P, Lima-Ramos J, Nordblad M, and Woodley JM.** Guidelines and cost analysis for catalyst production in biocatalytic processes. *Organic Process Research and Development.* 2011. 15(1): 266-274.
45. **Hanefeld U, Gardossi L, and Magner E.** Understanding enzyme immobilisation. *Chemical Society Reviews.* 2009. 38(2): 453-468.
46. **Paul CE and Hollmann F.** A survey of synthetic nicotinamide cofactors in enzymatic processes. *Applied Microbiology and Biotechnology.* 2016. 100(11): 4773-4778.
47. **Nelson JM and Griffin EG.** Adsorption of Invertase. *Journal of the American Chemical Society.* 1916. 38(5): 1109-1115.
48. **Homaei AA, Sariri R, Vianello F, and Stevanato R.** Enzyme immobilization: an update. *Journal of Chemical Biology.* 2013. 6(4): 185-205.
49. **Sheldon RA and van Pelt S.** Enzyme immobilisation in biocatalysis: why, what and how. *Chemical Society Reviews.* 2013. 42(15): 6223-6235.
50. **Barbosa O, Ortiz C, Berenguer-Murcia A, Torres R, Rodrigues RC, and Fernandez-Lafuente R.** Strategies for the one-step immobilization-purification of enzymes as industrial biocatalysts. *Biotechnology Advances.* 2015. 33(5): 435-456.
51. **Kopka B, Diener M, Wirtz A, Pohl M, Jaeger KE, and Krauss U.** Purification and simultaneous immobilization of *Arabidopsis thaliana* hydroxynitrile lyase using a family 2 carbohydrate-binding module. *Biotechnology Journal.* 2015. 10(5): 811-819.
52. **Lauer SA and Nolan JP.** Development and characterization of Ni-NTA-bearing microspheres. *Cytometry.* 2002. 48(3): 136-145.
53. **Batista CM, Saad F, Ceccoti SPC, Eger I, and Soares MJ.** Subcellular localisation of FLAG tagged enzymes of the dynamic protein *S*-palmitoylation cycle of *Trypanosoma cruzi* epimastigotes. *Memórias do Instituto Oswaldo Cruz.* 2018. 113(8): e180086.
54. **Malhotra A.** Chapter 16: Tagging for Protein Expression. in: Methods in Enzymology, Editors: Burgess RR and Deutscher MP. 2009, *Academic Press*.
55. **Encell LP, Friedman Ohana R, Zimmerman K, Otto P, Vidugiris G, Wood MG, Los GV, McDougall MG, *et al.*** Development of a dehalogenase-based protein fusion tag capable of rapid, selective and covalent attachment to customizable ligands. *Current Chemical Genomics and Translational Medicine.* 2012. 6: 55-71.
56. **Krajewska B.** Application of chitin- and chitosan-based materials for enzyme immobilizations: a review. *Enzyme and Microbial Technology.* 2004. 35(2): 126-139.
57. **Tosa T, Mori T, Fuse N, and Chibata I.** Studies on continuous enzyme reactions. I. Screening of carriers for preparation of water-insoluble aminoacylase. *Enzymologia.* 1966. 31(4): 214-224.

58. **Wiemann LO, Weisshaupt P, Nieguth R, Thum O, and Ansorge-Schumacher MB.** Enzyme stabilization by deposition of silicone coatings. *Organic Process Research and Development.* 2009. 13(3): 617-620.
59. **Katchalski-Katzir E and Kraemer DM.** Eupergit® C, a carrier for immobilization of enzymes of industrial potential. *Journal of Molecular Catalysis B: Enzymatic.* 2000. 10(1): 157-176.
60. **Petkar M, Lali A, Caimi P, and Daminati M.** Immobilization of lipases for non-aqueous synthesis. *Journal of Molecular Catalysis B: Enzymatic.* 2006. 39(1): 83-90.
61. **Sakaguchi K, Matsui M, and Mizukami F.** Applications of zeolite inorganic composites in biotechnology: current state and perspectives. *Applied Microbiology and Biotechnology.* 2005. 67(3): 306-311.
62. **Deere J, Magner E, Wall JG, and Hodnett BK.** Mechanistic and structural features of protein adsorption onto mesoporous slicates. *The Journal of Physical Chemistry B.* 2002. 106(29): 7340-7347.
63. **Hartmann M and Kostrov X.** Immobilization of enzymes on porous silicas - benefits and challenges. *Chemical Society Reviews.* 2013. 42(15): 6277-6289.
64. **Kreiner M and Parker M-C.** Protein-coated microcrystals for use in organic solvents: application to oxidoreductases. *Biotechnology Letters.* 2005. 27(20): 1571-1577.
65. **López C, Cruz-Izquierdo A, Picó EA, García-Bárcena T, Villarroel N, Llama MJ, and Serra JL.** Magnetic biocatalysts and their uses to obtain biodiesel and biosurfactants. *Frontiers in Chemistry.* 2014. 2: 72.
66. **Daniel M-C and Astruc D.** Gold nanoparticles: assembly, supramolecular chemistry, quantum-size-related properties, and applications toward biology, catalysis, and nanotechnology. *Chemical Reviews.* 2004. 104(1): 293-346.
67. **Galaev I and Mattiasson B.** Smart Polymers for Bioseparation and Bioprocessing. 1st ed. London, United Kingdom. *CRC Press*. 2001
68. **Ivanov AE, Edink E, Kumar A, Galaev IY, Arendsen AF, Bruggink A, and Mattiasson B.** Conjugation of penicillin acylase with the reactive copolymer of *N*-isopropylacrylamide: a step toward a thermosensitive industrial biocatalyst. *Biotechnology Progress.* 2003. 19(4): 1167-1175.
69. **Brady D and Jordaan J.** Advances in enzyme immobilisation. *Biotechnology Letters.* 2009. 31(11): 1639-1650.
70. **Rehm FB, Chen S, and Rehm BH.** Enzyme engineering for *in situ* immobilization. *Molecules.* 2016. 21(10).
71. **Krasňan V, Stloukal R, Rosenberg M, and Rebroš M.** Immobilization of cells and enzymes to LentiKats®. *Applied Microbiology and Biotechnology.* 2016. 100(6): 2535-2553.
72. **Gröger H, Capan E, Barthuber A, and Vorlop KD.** Asymmetric synthesis of an (*R*)-cyanohydrin using enzymes entrapped in lens-shaped gels. *Organic Letters.* 2001. 3(13): 1969-1972.
73. **Monteiro N, Martins A, Reis RL, and Neves NM.** Liposomes in tissue engineering and regenerative medicine. *Journal of the Royal Society Interface.* 2014. 11(101): 1-24.
74. **Nieh M-P, Dolinar P, Kučerka N, Kline SR, Debeer-Schmitt LM, Littrell KC, and Katsaras J.** Formation of kinetically trapped nanoscopic unilamellar vesicles from metastable nanodiscs. *Langmuir.* 2011. 27(23): 14308-14316.
75. **Bremond N, Santanach-Carreras E, Chu L-Y, and Bibette J.** Formation of liquid-core capsules having a thin hydrogel membrane: liquid pearls. *Soft Matter.* 2010. 6(11): 2484-2488.
76. **Xiong XY, Li QH, Li YP, Guo L, Li ZL, and Gong YC.** Pluronic P85/poly(lactic acid) vesicles as novel carrier for oral insulin delivery. *Colloids and Surfaces B: Biointerfaces.* 2013. 111: 282-288.
77. **Yiamsawas D, Baier G, Thines E, Landfester K, and Wurm FR.** Biodegradable lignin nanocontainers. *RSC Advances.* 2014. 4(23): 11661-11663.
78. **Schneider JL, Dingman RK, and Balu-Iyer SV.** Lipidic nanoparticles comprising phosphatidylinositol mitigate immunogenicity and improve efficacy of recombinant humanacid α-glucosidase in a murine model of pompe disease. *Journal of Pharmaceutical Sciences.* 2018. 107(3): 831-837.
79. **Lin C, Guo Y, Zhao M, Sun M, Luo F, Guo L, Qiu B, Lin Z, *et al.*** Highly sensitive colorimetric immunosensor for influenza virus H5N1 based on enzyme-encapsulated liposome. *Analytica Chimica Acta.* 2017. 963: 112-118.
80. **Taylor TM, Davidson PM, Bruce BD, and Weiss J.** Liposomal nanocapsules in food science and agriculture. *Critical Reviews in Food Science and Nutrition.* 2005. 45(7-8): 587-605.
81. **Sheldon RA.** Characteristic features and biotechnological applications of cross-linked enzyme aggregates (CLEAs). *Applied Microbiology and Biotechnology.* 2011. 92(3): 467-477.
82. **Quiocho FA and Richards FM.** Intermolecular cross linking of a protein in the crystalline state: carboxypeptidase-A. *Proceedings of the National Academy of Sciences.* 1964. 52: 833-839.
83. **Margolin AL and Navia MA.** Protein crystals as novel catalytic materials. *Angewandte Chemie International Edition.* 2001. 40(12): 2204-2222.
84. **Mateo C, Palomo JM, van Langen LM, van Rantwijk F, and Sheldon RA.** A new, mild cross-linking methodology to prepare cross-linked enzyme aggregates. *Biotechnology and Bioengineering.* 2004. 86(3): 273-276.
85. **Nuijens T, Cusan C, van Dooren TJGM, Moody HM, Merkx R, Kruijtzer JAW, Rijkers DTS, Liskamp RMJ, *et al.*** Fully enzymatic peptide synthesis using C-terminal *tert*-butyl ester interconversion. *Advanced Synthesis and Catalysis.* 2010. 352(14-15): 2399-2404.
86. **Hickey AM, Marle L, McCreedy T, Watts P, Greenway GM, and Littlechild JA.** Immobilization of thermophilic enzymes in miniaturized flow reactors. *Biochemical Society Transactions.* 2007. 35(Pt 6): 1621-1623.
87. **Cao L, van Rantwijk F, and Sheldon RA.** Cross-linked enzyme aggregates: A smple and effective

method for the immobilization of penicillin acylase. *Organic Letters.* 2000. 2(10): 1361-1364.

88. **Kopito RR.** Aggresomes, inclusion bodies and protein aggregation. *Trends in Cell Biology.* 2000. 10(12): 524-530.
89. **Doglia SM, Ami D, Natalello A, Gatti-Lafranconi P, and Lotti M.** Fourier transform infrared spectroscopy analysis of the conformational quality of recombinant proteins within inclusion bodies. *Biotechnology Journal.* 2008. 3(2): 193-201.
90. **Worrall DM and Goss NH.** The formation of biologically active β-galactosidase inclusion bodies in *Escherichia coli. Australian Journal of Biotechnology.* 1989. 3(1): 28-32.
91. **Peternel S and Komel R.** Active protein aggregates produced in *Escherichia coli. International Journal of Molecular Sciences.* 2011. 12(11): 8275-8287.
92. **Billman-Jacobe H, Wang L, Kortt A, Stewart D, and Radford A.** Expression and secretion of heterologous proteases by *Corynebacterium glutamicum. Applied and Environmental Microbiology.* 1995. 61(4): 1610-1613.
93. **Lu W, Kong J, and Kong W.** Construction and application of food-grade expression system for *Lactococcus lactis. Molecular Biotechnology.* 2013. 54(2): 170-176.
94. **Welsch N, Homuth G, and Schweder T.** Stepwise optimization of a low-temperature *Bacillus subtilis* expression system for 'difficult to express' proteins. *Applied Microbiology and Biotechnology.* 2015. 99(15): 6363-6376.
95. **Matsuyama A, Arai R, Yashiroda Y, Shirai A, Kamata A, Sekido S, Kobayashi Y, Hashimoto A, *et al.*** ORFeome cloning and global analysis of protein localization in the fission yeast *Schizosaccharomyces pombe. Nature Biotechnology.* 2006. 24: 841-847.
96. **Cohen A, Ross L, Nachman I, and Bar-Nun S.** Aggregation of PolyQ proteins is increased upon yeast aging and affected by Sir2 and Hsf1: Novel quantitative biochemical and microscopic assays. *PLOS ONE.* 2012. 7(9): e44785.
97. **Krauss U, Jäger VD, Diener M, Pohl M, and Jaeger K-E.** Catalytically-active inclusion bodies - Carrier-free protein immobilizates for application in biotechnology and biomedicine. *Journal of Biotechnology.* 2017. 258: 136-147.
98. **Speed MA, Wang DI, and King J.** Specific aggregation of partially folded polypeptide chains: the molecular basis of inclusion body composition. *Nature Biotechnology.* 1996. 14(10): 1283-1287.
99. **Rinas U, Garcia-Fruitós E, Corchero JL, Vázquez E, Seras-Franzoso J, and Villaverde A.** Bacterial inclusion bodies: discovering their better half. *Trends in Biochemical Sciences.* 2017. 42(9): 726-737.
100. **Cano-Garrido O, Rodríguez-Carmona E, Díez-Gil C, Vázquez E, Elizondo E, Cubarsi R, Seras-Franzoso J, Corchero JL, *et al.*** Supramolecular organization of protein-releasing functional amyloids solved in bacterial inclusion bodies. *Acta Biomaterialia.* 2013. 9(4): 6134-6142.
101. **Hunke S and Betton J-M.** Temperature effect on inclusion body formation and stress response in the periplasm of *Escherichia coli. Molecular Microbiology.* 2003. 50(5): 1579-1589.
102. **Laloux G and Jacobs-Wagner C.** How do bacteria localize proteins to the cell pole? *Journal of Cell Science.* 2014. 127(1): 11-19.
103. **Winkler J, Seybert A, König L, Pruggnaller S, Haselmann U, Sourjik V, Weiss M, Frangakis AS, *et al.*** Quantitative and spatio-temporal features of protein aggregation in *Escherichia coli* and consequences on protein quality control and cellular ageing. *The EMBO Journal.* 2010. 29(5): 910-923.
104. **Amen T and Kaganovich D.** Dynamic droplets: the role of cytoplasmic inclusions in stress, function, and disease. *Cellular and Molecular Life Sciences.* 2015. 72(3): 401-415.
105. **García-Fruítos E, Vázquez E, Díez-Gil C, Corchero JL, Seras-Franzoso J, Ratera I, Veciana J, and Villaverde A.** Bacterial inclusion bodies: making gold from waste. *Trends in Biotechnology.* 2012. 30(2): 65-70.
106. **Singh A, Upadhyay V, Upadhyay AK, Singh SM, and Panda AK.** Protein recovery from inclusion bodies of *Escherichia coli* using mild solubilization process. *Microbial Cell Factories.* 2015. 14(41): 1-10.
107. **Diener M, Kopka B, Pohl M, Jaeger KE, and Krauss U.** Fusion of a coiled-coil domain facilitates the high-level production of catalytically active enzyme inclusion bodies. *ChemCatChem.* 2016. 8(1): 142-152.
108. **Rueda F, Gasser B, Sánchez-Chardi A, Roldán M, Villegas S, Puxbaum V, Ferrer-Miralles N, Unzueta U, *et al.*** Functional inclusion bodies produced in the yeast *Pichia pastoris. Microbial Cell Factories.* 2016. 15(166): 1-12.
109. **Rodríguez-Carmona E, Cano-Garrido O, Seras-Franzoso J, Villaverde A, and García-Fruitós E.** Isolation of cell-free bacterial inclusion bodies. *Microbial Cell Factories.* 2010. 9(71): 1-9.
110. **Yang X, Pistolozzi M, and Lin Z.** New trends in aggregating tags for therapeutic protein purification. *Biotechnology Letters.* 2018. 40(5): 745-753.
111. **Torrealba D, Seras-Franzoso J, Mamat U, Wilke K, Villaverde A, Roher N, and García-Fruitós E.** Complex particulate biomaterials as immunostimulant-delivery platforms. *PLOS ONE.* 2016. 11(10): e0164073.
112. **García-Fruitós E, Rodríguez-Carmona E, Díez-Gil C, Ferraz RM, Vázquez E, Corchero JL, Cano-Sarabia M, Ratera I, *et al.*** Surface cell growth engineering assisted by a novel bacterial nanomaterial. *Advanced Materials.* 2009. 21(42): 4249-4253.
113. **Seras-Franzoso J, Sánchez-Chardi A, García-Fruitós E, Vázquez E, and Villaverde A.** Cellular uptake and intracellular fate of protein releasing bacterial amyloids in mammalian cells. *Soft Matter.* 2016. 12(14): 3451-3460.
114. **Vázquez E, Corchero JL, Burgueño JF, Seras-Franzoso J, Kosoy A, Bosser R, Mendoza R, Martínez-Láinez JM, *et al.*** Functional inclusion bodies produced in bacteria as naturally occurring nanopills for advanced cell therapies. *Advanced Materials.* 2012. 24(13): 1742-1747.

115. **Liovic M, Ozir M, Zavec AB, Peternel S, Komel R, and Zupancic T.** Inclusion bodies as potential vehicles for recombinant protein delivery into epithelial cells. *Microbial Cell Factories.* 2012. 11(67): 1-5.
116. **Espargaró A, Villar-Piqué A, Sabaté R, and Ventura S.** Yeast prions form infectious amyloid inclusion bodies in bacteria. *Microbial Cell Factories.* 2012. 11(89): 1-12.
117. **Dong Q, Yan X, Zheng M, and Yang Z.** Characterization of an extremely thermostable but cold-adaptive β-galactosidase from the hyperthermophilic archaeon *Pyrococcus furiosus* for use as a recombinant aggregation for batch lactose degradation at high temperature. *Journal of Bioscience and Bioengineering.* 2014. 117(6): 706-710.
118. **Tokatlidis K, Dhurjati P, Millet J, Béguin P, and Aubert J-P.** High activity of inclusion bodies formed in *Escherichia coli* overproducing *Clostridium thermocellum* endoglucanase D. *FEBS Letters.* 1991. 282(1): 205-208.
119. **Li S, Lin K, Pang H, Wu Y, and Xu J.** Production, characterization, and application of an organic solvent-tolerant lipase present in active inclusion bodies. *Applied Biochemistry and Biotechnology.* 2013. 169(2): 612-623.
120. **García-Fruitós E, González-Montalbán N, Morell M, Vera A, Ferraz RM, Arís A, Ventura S, and Villaverde A.** Aggregation as bacterial inclusion bodies does not imply inactivation of enzymes and fluorescent proteins. *Microbial Cell Factories.* 2005. 4(27): 1-6.
121. **Park S-Y, Park S-H, and Choi S-K.** Active inclusion body formation using *Paenibacillus polymyxa* PoxB as a fusion partner in *Escherichia coli*. *Analytical Biochemistry.* 2012. 426(1): 63-65.
122. **Korovashkina AS, Rymko AN, Kvach SV, and Zinchenko AI.** Enzymatic synthesis of c-di-GMP using inclusion bodies of *Thermotoga maritima* full-length diguanylate cyclase. *Journal of Biotechnology.* 2013. 164(2): 276-280.
123. **Zhou B, Xing L, Wu W, Zhang X-E, and Lin Z.** Small surfactant-like peptides can drive soluble proteins into active aggregates. *Microbial Cell Factories.* 2012. 11(10): 1-8.
124. **Wang X, Zhou B, Hu W, Zhao Q, and Lin Z.** Formation of active inclusion bodies induced by hydrophobic self-assembling peptide GFIL8. *Microbial Cell Factories.* 2015. 14(88): 1-8.
125. **Wu W, Xing L, Zhou B, and Lin Z.** Active protein aggregates induced by terminally attached self-assembling peptide ELK16 in *Escherichia coli*. *Microbial Cell Factories.* 2011. 10(9): 1-8.
126. **Lin Z, Zhou B, Wu W, Xing L, and Zhao Q.** Self-assembling amphipathic α-helical peptides induce the formation of active protein aggregates *in vivo*. *Faraday Discussions.* 2013. 166(0): 243-256.
127. **Nahálka J and Nidetzky B.** Fusion to a pull-down domain: a novel approach of producing *Trigonopsis variabilis* D-amino acid oxidase as insoluble enzyme aggregates. *Biotechnology and Bioengineering.* 2007. 97(3): 454-461.
128. **Arié J-P, Miot M, Sassoon N, and Betton J-M.** Formation of active inclusion bodies in the periplasm of *Escherichia coli*. *Molecular Microbiology.* 2006. 62(2): 427-437.
129. **Jiang L, Xiao W, Zhou X, Wang W, and Fan J.** Comparative study of the insoluble and soluble Ulp1 protease constructs as carrier free and dependent protein immobilizates. *Journal of Bioscience and Bioengineering.* 2018. 127(1): 23-29.
130. **Nahálka J, Vikartovská A, and Hrabárová E.** A crosslinked inclusion body process for sialic acid synthesis. *Journal of Biotechnology.* 2008. 134(1-2): 146-153.
131. **Nahálka J.** Physiological aggregation of maltodextrin phosphorylase from *Pyrococcus furiosus* and its application in a process of batch starch degradation to α-D-glucose-1-phosphate. *Journal of Industrial Microbiology and Biotechnology.* 2008. 35(4): 219-23.
132. **Nahálka J and Pätoprstý V.** Enzymatic synthesis of sialylation substrates powered by a novel polyphosphate kinase (PPK3). *Organic and Biomolecular Chemistry.* 2009. 7(9): 1778-1780.
133. **Choi S-L, Lee SJ, Ha J-S, Song JJ, Rhee YH, and Lee S-G.** Generation of catalytic protein particles in *Escherichia coli* cells using the cellulose-binding domain from *Cellulomonas fimi* as a fusion partner. *Biotechnology and Bioprocess Engineering.* 2011. 16(6): 1173-1179.
134. **Heater BS, Lee MM, and Chan MK.** Direct production of a genetically-encoded immobilized biodiesel catalyst. *Scientific Reports.* 2018. 8(1): 12783.
135. **Jendrossek D.** Polyhydroxyalkanoate granules are complex subcellular organelles (carbonosomes). *Journal of Bacteriology.* 2009. 191(10): 3195-3202.
136. **Jahns AC, Maspolim Y, Chen S, Guthrie JM, Blackwell LF, and Rehm BH.** *In vivo* self-assembly of fluorescent protein microparticles displaying specific binding domains. *Bioconjugate Chemistry.* 2013. 24(8): 1314-1323.
137. **Han GH, Seong W, Fu Y, Yoon PK, Kim SK, Yeom SJ, Lee DH, and Lee SG.** Leucine zipper-mediated targeting of multi-enzyme cascade reactions to inclusion bodies in *Escherichia coli* for enhanced production of 1-butanol. *Metabolic Engineering.* 2017. 40: 41-49.
138. **Steinmann B, Christmann A, Heiseler T, Fritz J, and Kolmar H.** *In vivo* enzyme immobilization by inclusion body display. *Applied and Environmental Microbiology.* 2010. 76(16): 5563-5569.
139. **Ginet N, Pardoux R, Adryanczyk G, Garcia D, Brutesco C, and Pignol D.** Single-step production of a recyclable nanobiocatalyst for organophosphate pesticides biodegradation using functionalized bacterial magnetosomes. *PLOS ONE.* 2011. 6(6): e21442.
140. **Sührer I, Langemann T, Lubitz W, Weuster-Botz D, and Castiglione K.** A novel one-step expression and immobilization method for the production of biocatalytic preparations. *Microbial Cell Factories.* 2015. 14(180): 1-9.
141. **Bazylinski DA and Frankel RB.** Magnetosome formation in prokaryotes. *Nature Reviews Microbiology.* 2004. 2: 217-230.
142. **Honda T, Tanaka T, and Yoshino T.** Stoichiometrically controlled immobilization of

multiple enzymes on magnetic nanoparticles by the magnetosome display system for efficient cellulose hydrolysis. *Biomacromolecules.* 2015. 16(12): 3863-3868.

143. **Visser F, Müller B, Rose J, Prüfer D, and Noll GA.** Forizymes - functionalised artificial forisomes as a platform for the production and immobilisation of single enzymes and multi-enzyme complexes. *Scientific Reports.* 2016. 6(1): 30839.
144. **Scholz KE, Kopka B, Wirtz A, Pohl M, Jaeger KE, and Krauss U.** Fusion of a flavin-based fluorescent protein to hydroxynitrile lyase from *Arabidopsis thaliana* improves enzyme stability. *Applied and Environmental Microbiology.* 2013. 79(15): 4727-4733.
145. **Lupas AN and Gruber M.** The structure of α-helical coiled coils. *Advances in Protein Chemistry.* 2005. 70: 37-78.
146. **Woolfson DN, Bartlett GJ, Bruning M, and Thomson AR.** New currency for old rope: from coiled-coil assemblies to α-helical barrels. *Current Opinion in Structural Biology.* 2012. 22(4): 432-441.
147. **Robson Marsden H and Kros A.** Self-assembly of coiled coils in synthetic biology: inspiration and progress. *Angewandte Chemie International Edition.* 2010. 49(17): 2988-3005.
148. **Mason JM and Arndt KM.** Coiled-coil domains: stability, specificity, and biological implications. *ChemBioChem.* 2004. 5(2): 170-176.
149. **Crick FHC.** Is α-keratin a coiled coil? *Nature.* 1952. 170(4334): 882883.
150. **Pauling L and Corey RB.** Compound helical configurations of polypeptide chains: structure of proteins of the α-keratin type. *Nature.* 1953. 171(4341): 59-61.
151. **Ausmees N, Kuhn JR, and Jacobs-Wagner C.** The Bacterial Cytoskeleton. *Cell.* 2003. 115(6): 705-713.
152. **Hartmann MD.** Functional and structural roles of coiled coils. in: Fibrous Proteins: Structures and Mechanisms, Editors: Parry DAD and Squire JM. 2017, *Springer International Publishing*. Cham, Switzerland.
153. **Miller M.** The importance of being flexible: the case of basic region leucine zipper transcriptional regulators. *Current Protein and Peptide Science.* 2009. 10(3): 244-269.
154. **Schwaiger I, Sattler C, Hostetter DR, and Rief M.** The myosin coiled-coil is a truly elastic protein structure. *Nature Materials.* 2002. 1(4): 232-235.
155. **Diensthuber RP, Bommer M, Gleichmann T, and Möglich A.** Full-length structure of a sensor histidine kinase pinpoints coaxial coiled coils as signal transducers and modulators. *Structure.* 2013. 21(7): 1127-1136.
156. **Stetefeld J, Jenny M, Schulthess T, Landwehr R, Engel J, and Kammerer RA.** Crystal structure of a naturally occurring parallel right-handed coiled-coil tetramer. *Nature Structural and Molecular Biology.* 2000. 7(9): 772-776.
157. **Peters J, Baumeister W, and Lupas A.** Hyperthermostable surfce layer protein tetrabrachion from the Archaebacterium *Staphylothermus marinus*: Evidence for the presence of a right-handed coiled coil derived from the primary structure. *Journal of Molecular Biology.* 1996. 257(5): 1031-1041.
158. **Fiala G, Stetter KO, Jannasch HW, Langworthy TA, and Madon J.** *Staphylothermus marinus* sp. nov. represents a novel genus of extremely thermophilic submarine heterotrophic Archaebacteria growing up to 98°C. *Systematic and Applied Microbiology.* 1986. 8(1): 106-113.
159. **Anderson IJ, Dharmarajan L, Rodriguez J, Hooper S, Porat I, Ulrich LE, Elkins JG, Mavromatis K, *et al.*** The complete genome sequence of *Staphylothermus marinus* reveals differences in sulfur metabolism among heterotrophic Crenarchaeota. *BMC Genomics.* 2009. 10: 145-145.
160. **Diener M, Pohl M, Jaeger KE, and Krauss U.** Catalytically active protein aggregates and methods for producing the same. 2017.
161. **Airola MV, Watts KJ, Bilwes AM, and Crane BR.** Structure of concatenated HAMP domains provides a mechanism for signal transduction. *Structure.* 2010. 18(4): 436-448.
162. **Aravind L and Ponting CP.** The cytoplasmic helical linker domain of receptor histidine kinase and methyl-accepting proteins is common to many prokaryotic signalling proteins. *FEMS Microbiology Letters.* 1999. 176(1): 111-116.
163. **Tsien RY.** The Green Fluorescent Protein. *Annual Review of Biochemistry.* 1998. 67(1): 509-544.
164. **Morise H, Shimomura O, Johnson FH, and Winant J.** Intermolecular energy transfer in the bioluminescent system of *Aequorea. Biochemistry.* 1974. 13(12): 2656-2662.
165. **Day RN and Davidson MW.** The fluorescent protein palette: tools for cellular imaging. *Chemical Society Reviews.* 2009. 38(10): 2887-2921.
166. **Prasher DC, Eckenrode VK, Ward WW, Prendergast FG, and Cormier MJ.** Primary structure of the *Aequorea victoria* green-fluorescent protein. *Gene.* 1992. 111(2): 229-233.
167. **Yang F, Moss LG, and Phillips GN.** The molecular structure of green fluorescent protein. *Nature Biotechnology.* 1996. 14(10): 1246-1251.
168. **Ormö M, Cubitt AB, Kallio K, Gross LA, Tsien RY, and Remington SJ.** Crystal structure of the *Aequorea victoria* green fluorescent protein. *Science.* 1996. 273(5280): 1392-1395.
169. **Wang L, Jackson WC, Steinbach PA, and Tsien RY.** Evolution of new nonantibody proteins via iterative somatic hypermutation. *Proceedings of the National Academy of Sciences.* 2004. 101(48): 16745-16749.
170. **Chica RA, Moore MM, Allen BD, and Mayo SL.** Generation of longer emission wavelength red fluorescent proteins using computationally designed libraries. *Proceedings of the National Academy of Sciences.* 2010. 107(47): 20257-20262.
171. **Mena MA, Treynor TP, Mayo SL, and Daugherty PS.** Blue fluorescent proteins with enhanced brightness and photostability from a structurally targeted library. *Nature Biotechnology.* 2006. 24(12): 1569-1571.
172. **Piatkevich KD, Malashkevich VN, Morozova KS, Nemkovich NA, Almo SC, and Verkhusha VV.** Extended Stokes shift in fluorescent proteins: chromophore-protein interactions in a near-infrared

TagRFP675 variant. *Scientific Reports.* 2013. 3: 1847.
173. **Förster T.** Zwischenmolekulare Energiewanderung und Fluoreszenz. *Annalen der Physik.* 1948. 437(1-2): 55-75.
174. **Moussa R, Baierl A, Steffen V, Kubitzki T, Wiechert W, and Pohl M.** An evaluation of genetically encoded FRET-based biosensors for quantitative metabolite analyses *in vivo*. *Journal of Biotechnology.* 2014. 191: 250-259.
175. **Kim J, Li X, Kang M-S, Im K-B, Genovesio A, and Grailhe R.** Quantification of protein interaction in living cells by two-photon spectral imaging with fluorescent protein fluorescence resonance energy transfer pair devoid of acceptor bleed-through. *Cytometry Part A.* 2012. 81(2): 112-119.
176. **Shaner NC, Patterson GH, and Davidson MW.** Advances in fluorescent protein technology. *Journal of Cell Science.* 2007. 120(24): 4247-4260.
177. **Zacharias DA, Violin JD, Newton AC, and Tsien RY.** Partitioning of lipid-modified monomeric GFPs into membrane microdomains of live cells. *Science.* 2002. 296(5569): 913-916.
178. **Matz MV, Fradkov AF, Labas YA, Savitsky AP, Zaraisky AG, Markelov ML, and Lukyanov SA.** Fluorescent proteins from nonbioluminescent Anthozoa species. *Nature Biotechnology.* 1999. 17(10): 969-973.
179. **Campbell RE, Tour O, Palmer AE, Steinbach PA, Baird GS, Zacharias DA, and Tsien RY.** A monomeric red fluorescent protein. *Proceedings of the National Academy of Sciences.* 2002. 99(12): 7877-7882.
180. **Shaner NC, Campbell RE, Steinbach PA, Giepmans BNG, Palmer AE, and Tsien RY.** Improved monomeric red, orange and yellow fluorescent proteins derived from *Discosoma* sp. red fluorescent protein. *Nature Biotechnology.* 2004. 22(12): 1567-1572.
181. **Patel RN.** Stereoselective biocatalysis. New York. *Marcel Dekker Inc.* 2000
182. **You K-S and Oppenheimer NJ.** Stereospecificity for nicotinamide nucleotides in enzymatic and chemical hydride transfer reaction. *Critical Reviews in Biochemistry.* 1985. 17(4): 313-451.
183. **Rossmann MG, Moras D, and Olsen KW.** Chemical and biological evolution of a nucleotide-binding protein. *Nature.* 1974. 250: 194-199.
184. **Carugo O and Argos P.** NADP-Dependent enzymes. I: Conserved stereochemistry of cofactor binding. *Proteins: Structure, Function, and Bioinformatics.* 1997. 28(1): 10-28.
185. **Wichmann R and Vasic-Racki D.** Cofactor regeneration at the lab scale. *Advances in Biochemical Engineering / Biotechnology.* 2005. 92: 225-260.
186. **Wong CH, Drueckhammer DG, and Sweers HM.** Enzymatic *vs.* fermentative synthesis - Thermostable glucose dehydrogenase catalyzed regeneration of NAD(P)H for use in enzymatic synthesis. *Journal of the American Chemical Society.* 1985. 107(13): 4028-4031.
187. **Müller U, Willnow P, Ruschig U, and Höpner T.** Formate Dehydrogenase from *Pseudomonas oxalaticus*. *European Journal of Biochemistry.* 1978. 83(2): 485-498.
188. **Kara S, Spickermann D, Schrittwieser JH, Leggewie C, van Berkel WJH, Arends IWCE, and Hollmann F.** More efficient redox biocatalysis by utilising 1,4-butanediol as a 'smart cosubstrate'. *Green Chemistry.* 2013. 15(2): 330-335.
189. **Lavandera I, Kern A, Ferreira-Silva B, Glieder A, de Wildeman S, and Kroutil W.** Stereoselective bioreduction of bulky-bulky ketones by a novel ADH from *Ralstonia* sp. *Journal of Organic Chemistry.* 2008. 73(15): 6003-6005.
190. **Filling C, Berndt KD, Benach J, Knapp S, Prozorovski T, Nordling E, Ladenstein R, Jörnvall H, *et al.*** Critical residues for structure and catalysis in short-chain dehydrogenases/reductases. *Journal of Biological Chemistry.* 2002. 277(28): 25677-25684.
191. **Man H, Kędziora K, Kulig J, Frank A, Lavandera I, Gotor-Fernández V, Rother D, Hart S, *et al.*** Structures of alcohol dehydrogenases from *Ralstonia* and *Sphingobium* spp. reveal the molecular basis for their recognition of 'bulky–bulky' ketones. *Topics in Catalysis.* 2014. 57(5): 356-365.
192. **Prelog V.** Specification of the stereospecificity of some oxido-reductases by diamond lattice sections. *Pure and Applied Chemistry.* 1964. 9(1): 119-130.
193. **Kulig J, Frese A, Kroutil W, Pohl M, and Rother D.** Biochemical characterization of an alcohol dehydrogenase from *Ralstonia* sp. *Biotechnology and Bioengineering.* 2013. 110(7): 1838-1848.
194. **Schlieben NH, Niefind K, Müller J, Riebel B, Hummel W, and Schomburg D.** Atomic resolution structures of *R*-specific alcohol dehydrogenase from *Lactobacillus brevis* provide the structural bases of its substrate and cosubstrate specificity. *Journal of Molecular Biology.* 2005. 349(4): 801-813.
195. **Niefind K, Müller J, Riebel B, Hummel W, and Schomburg D.** The crystal structure of *R*-specific alcohol dehydrogenase from *Lactobacillus brevis* suggests the structural basis of its metal dependency. *Journal of Molecular Biology.* 2003. 327(2): 317-328.
196. **Liang P, Qin B, Mu M, Zhang X, Jia X, and You S.** Prelog and anti-Prelog stereoselectivity of two ketoreductases from *Candida glabrata*. *Biotechnology Letters.* 2013. 35(9): 1469-1473.
197. **Widmann M, Radloff R, and Pleiss J.** The Thiamine diphosphate dependent Enzyme Engineering Database: A tool for the systematic analysis of sequence and structure relations. *BMC Biochemistry.* 2010. 11(1): 1-6. Available from: https://teed.biocatnet.de/.
198. **Vogel C and Pleiss J.** The modular structure of ThDP-dependent enzymes. *Proteins: Structure, Function, and Bioinformatics.* 2014. 82(10): 2523-2537.
199. **Müller M, Sprenger GA, and Pohl M.** C-C bond formation using ThDP-dependent lyases. *Current Opinion in Chemical Biology.* 2013. 17(2): 261-270.
200. **Andrews FH and McLeish MJ.** Substrate specificity in thiamin diphosphate-dependent decarboxylases. *Bioorganic Chemistry.* 2012. 43: 26-36.

201. **Muller YA, Lindqvist Y, Furey W, Schulz GE, Jordan F, and Schneider G.** A thiamin diphosphate binding fold revealed by comparison of the crystal structures of transketolase, pyruvate oxidase and pyruvate decarboxylase. *Structure.* 1993. 1(2): 95-103.
202. **Shaanan B and Chipman DM.** Reaction mechanisms of thiamin diphosphate enzymes: new insights into the role of a conserved glutamate residue. *FEBS Journal.* 2009. 276(9): 2447-2453.
203. **Frank RAW, Leeper FJ, and Luisi BF.** Structure, mechanism and catalytic duality of thiamine-dependent enzymes. *Cellular and Molecular Life Sciences.* 2007. 64(7): 892-905.
204. **Brovetto M, Gamenara D, Saenz Méndez P, and Seoane GA.** C−C bond-forming lyases in organic synthesis. *Chemical Reviews.* 2011. 111(7): 4346-4403.
205. **González B and Vicuña R.** Benzaldehyde lyase, a novel thiamine PPi-requiring enzyme, from *Pseudomonas fluorescens* biovar I. *Journal of Bacteriology.* 1989. 171(5): 2401-2405.
206. **Knoll M, Müller M, Pleiss J, and Pohl M.** Factors mediating activity, selectivity, and substrate specificity for the thiamin diphosphate-dependent enzymes benzaldehyde lyase and benzoylformate decarboxylase. *ChemBioChem.* 2006. 7(12): 1928-1934.
207. **Mosbacher TG, Mueller M, and Schulz GE.** Structure and mechanism of the ThDP-dependent benzaldehyde lyase from *Pseudomonas fluorescens*. *FEBS Journal.* 2005. 272(23): 6067-6076.
208. **Janzen E, Müller M, Kolter-Jung D, Kneen MM, McLeish MJ, and Pohl M.** Characterization of benzaldehyde lyase from *Pseudomonas fluorescens*: A versatile enzyme for asymmetric C–C bond formation. *Bioorganic Chemistry.* 2006. 34(6): 345-361.
209. **Hasson MS, Muscate A, McLeish MJ, Polovnikova LS, Gerlt JA, Kenyon GL, Petsko GA, and Ringe D.** The crystal structure of benzoylformate decarboxylase at 1.6 Å resolution: Diversity of catalytic residues in thiamin diphosphate-dependent enzymes. *Biochemistry.* 1998. 37(28): 9918-9930.
210. **Hegeman GD.** Synthesis of the enzymes of the mandelate pathway by *Pseudomonas putida*- I. Synthesis of enzymes by the wild type. *Journal of Bacteriology.* 1966. 91(3): 1140-1154.
211. **Iding H, Dünnwald T, Greiner L, Liese A, Müller M, Siegert P, Grötzinger J, Demir AS, *et al.*** Benzoylformate decarboxylase from *Pseudomonas putida* as stable catalyst for the synthesis of chiral 2-Hydroxy ketones. *Chemistry – A European Journal.* 2000. 6(8): 1483-1495.
212. **Yamamoto Y, Miwa Y, Miyoshi K, Furuyama J, and Ohmori H.** The *Escherichia coli ldcC* gene encodes another lysine decarboxylase, probably a constitutive enzyme. *Genes and Genetic Systems.* 1997. 72(3): 167-172.
213. **Kanjee U, Gutsche I, Alexopoulos E, Zhao B, El Bakkouri M, Thibault G, Liu K, Ramachandran S, *et al.*** Linkage between the bacterial acid stress and stringent responses: the structure of the inducible lysine decarboxylase. *The EMBO Journal.* 2011. 30(5): 931-944.
214. **Kandiah E, Carriel D, Perard J, Malet H, Bacia M, Liu K, Chan SW, Houry WA, *et al.*** Structural insights into the *Escherichia coli* lysine decarboxylases and molecular determinants of interaction with the AAA+ ATPase RavA. *Scientific Reports.* 2016. 6: 24601.
215. **Kanjee U and Houry WA.** Mechanisms of acid resistance in *Escherichia coli*. *Annual Review of Microbiology.* 2013. 67: 65-81.
216. **Tabor CW and Tabor H.** Polyamines. *Annual Review of Biochemistry.* 1984. 53: 749-790.
217. **Kikuchi Y, Kojima H, Tanaka T, Takatsuka Y, and Kamio Y.** Characterization of a second lysine decarboxylase isolated from *Escherichia coli*. *Journal of Bacteriology.* 1997. 179(14): 4486-4492.
218. **Jordan F and Patel H.** Catalysis in enzymatic decarboxylations: comparison of selected cofactor-dependent and cofactor-independent examples. *ACS Catalysis.* 2013. 3(7): 1601-1617.
219. **Arai R, Ueda H, Kitayama A, Kamiya N, and Nagamune T.** Design of the linkers which effectively separate domains of a bifunctional fusion protein. *Protein Engineering.* 2001. 14(8): 529-532.
220. **Chen X, Zaro JL, and Shen WC.** Fusion protein linkers: property, design and functionality. *Advanced Drug Delivery Reviews.* 2013. 65(10): 1357-1369.
221. **Rosano GL and Ceccarelli EA.** Recombinant protein expression in *Escherichia coli*: advances and challenges. *Frontiers in Microbiology.* 2014. 5(172): 1-17.
222. **Studier FW.** Protein production by auto-induction in high density shaking cultures. *Protein Expression and Purification.* 2005. 41(1): 207-234.
223. **Fox BG and Blommel PG.** Autoinduction of protein expression. *Current Protocols in Protein Science.* 2009. Chapter 5(1-25): Unit-.
224. **Luli GW and Strohl WR.** Comparison of growth, acetate production, and acetate inhibition of *Escherichia coli* strains in batch and fed-batch fermentations. *Applied and Environmental Microbiology.* 1990. 56(4): 1004-1011.
225. **Wilms B, Hauck A, Reuss M, Syldatk C, Mattes R, Siemann M, and Altenbuchner J.** High-cell-density fermentation for production of L-*N*-carbamoylase using an expression system based on the *Escherichia coli rhaBAD* promoter. *Biotechnology and Bioengineering.* 2001. 73(2): 95-103.
226. **Vera A, González-Montalbán N, Arís A, and Villaverde A.** The conformational quality of insoluble recombinant proteins is enhanced at low growth temperatures. *Biotechnology and Bioengineering.* 2007. 96(6): 1101-1106.
227. **Vasina JA and Baneyx F.** Expression of aggregation-prone recombinant proteins at low temperatures: a comparative study of the *Escherichia coli cspA* and *tac* promoter systems. *Protein Expression and Purification.* 1997. 9(2): 211-218.
228. **Wang W, Sun J, Xiao W, Jiang L, Wang R, and Fan J.** Change of the N-terminal codon bias combined with tRNA supplementation outperforms

the selected fusion tags for production of human D-amino acid oxidase as active inclusion bodies. *Biotechnology Letters.* 2017. 39(11): 1733-1740.

229. **Morell M, Bravo R, Espargaró A, Sisquella X, Avilés FX, Fernàndez-Busquets X, and Ventura S.** Inclusion bodies: Specificity in their aggregation process and amyloid-like structure. *Molecular Cell Research.* 2008. 1783(10): 1815-1825.
230. **Lee KK, Jang CS, Yoon JY, Kim SY, Kim TH, Ryu KH, and Kim W.** Abnormal cell division caused by inclusion bodies in *E. coli*; increased resistance against external stress. *Microbiological Research.* 2008. 163(4): 394-402.
231. **Raghunathan G, Munussami G, Moon H, Paik H-j, An SSA, Kim Y-S, Kang S, and Lee S-G.** A variant of green fluorescent protein exclusively deposited to active intracellular inclusion bodies. *Microbial Cell Factories.* 2014. 13: 68-68.
232. **Peschke M, Le Goff M, Koningstein GM, Karyolaimos A, de Gier J-W, van Ulsen P, and Luirink J.** SRP, FtsY, DnaK and YidC Are Required for the Biogenesis of the *E. coli* Tail-Anchored Membrane Proteins DjlC and Flk. *Journal of Molecular Biology.* 2018. 430(3): 389-403.
233. **Wagner S, Baars L, Ytterberg AJ, Klussmeier A, Wagner CS, Nord O, Nygren PA, van Wijk KJ, *et al.*** Consequences of membrane protein overexpression in *Escherichia coli*. *Molecular and Cellular Proteomics.* 2007. 6(9): 1527-1550.
234. **Mishra VK, Palgunachari MN, Segrest JP, and Anantharamaiah GM.** Interactions of synthetic peptide analogs of the class A amphipathic helix with lipids. Evidence for the snorkel hypothesis. *Journal of Biological Chemistry.* 1994. 269(10): 7185-7191.
235. **Schrödel A and de Marco A.** Characterization of the aggregates formed during recombinant protein expression in bacteria. *BMC Biochemistry.* 2005. 6(10): 1-11.
236. **Mogk A, Deuerling E, Vorderwülbecke S, Vierling E, and Bukau B.** Small heat shock proteins, ClpB and the DnaK system form a functional triade in reversing protein aggregation. *Molecular Microbiology.* 2003. 50(2): 585-595.
237. **Miles EW, Rhee S, and Davies DR.** The molecular basis of substrate channeling. *Journal of Biological Chemistry.* 1999. 274(18): 12193-12196.
238. **Kazenwadel F, Franzreb M, and Rapp BE.** Synthetic enzyme supercomplexes: co-immobilization of enzyme cascades. *Analytical Methods.* 2015. 7(10): 4030-4037.
239. **Chiti F, Stefani M, Taddei N, Ramponi G, and Dobson CM.** Rationalization of the effects of mutations on peptide and protein aggregation rates. *Nature.* 2003. 424(6950): 805-808.
240. **Conchillo-Solé O, de Groot NS, Avilés FX, Vendrell J, Daura X, and Ventura S.** AGGRESCAN: a server for the prediction and evaluation of "hot spots" of aggregation in polypeptides. *BMC Bioinformatics.* 2007. 8(65): 1-17.
241. **Rohl CA, Strauss CE, Misura KM, and Baker D.** Protein structure prediction using Rosetta. *Methods in Enzymology.* 2004. 383: 66-93.
242. **Kuhlman B and Baker D.** Native protein sequences are close to optimal for their structures. *Proceedings of the National Academy of Sciences.* 2000. 97(19): 10383-10388.
243. **Jacak R, Leaver-Fay A, and Kuhlman B.** Computational protein design with explicit consideration of surface hydrophobic patches. *Proteins.* 2012. 80(3): 825-838.
244. **Krissinel E and Henrick K.** Inference of macromolecular assemblies from crystalline state. *Journal of Molecular Biology.* 2007. 372(3): 774-797.
245. **Bemporad F and Chiti F.** "Native-like aggregation" of the acylphosphatase from *Sulfolobus solfataricus* and its biological implications. *FEBS Letters.* 2009. 583(16): 2630-2638.
246. **Elia F, Cantini F, Chiti F, Dobson CM, and Bemporad F.** Direct conversion of an enzyme from native-like to amyloid-like aggregates within inclusion bodies. *Biophysical Journal.* 2017. 112(12): 2540-2551.
247. **Domínguez de María P, Stillger T, Pohl M, Wallert S, Drauz K, Gröger H, Trauthwein H, and Liese A.** Preparative enantioselective synthesis of benzoins and (*R*)-2-hydroxy-1-phenylpropanone using benzaldehyde lyase. *Journal of Molecular Catalysis B: Enzymatic.* 2006. 38(1): 43-47.
248. **Mikolajek RJ, Spiess AC, Pohl M, and Büchs J.** Propioin synthesis using thiamine diphosphate-dependent enzymes. *Biotechnology Progress.* 2009. 25(1): 132-138.
249. **Stillger T.** Enantioselektive C-C-Knüpfung mit Enzymen : Charakterisierung und reaktionstechnische Bearbeitung der Benzaldehydlyase aus *Pseudomonas fluorescens* Biovar I. *University Bonn.* 2004
250. **Wichmann R, Wandrey C, Bückmann AF, and Kula M-R.** Continuous enzymatic transformation in an enzyme membrane reactor with simultaneous NAD(H) regeneration. *Biotechnology and Bioengineering.* 1981. 23(12): 2789-2802.
251. **Schwarz M.** Einflussfaktoren auf die Stabilität und Aktivität der Benzaldehydlyase aus *Pseudomonas fluorescens* in Carboligasereaktionen mit aromatischen Aldehyden. *Heinrich-Heine University Düsseldorf.* 2010
252. **Karmainski T.** Charakterisierung katalytisch aktiver *inclusion bodies* am Beispiel der Benzaldehydlyase aus *Pseudomonas fluorescens*. *Fachhochschule Aachen, Campus Jülich.* 2017
253. **Domínguez de María P, Stillger T, Pohl M, Kiesel M, Liese A, Gröger H, and Trauthwein H.** Enantioselective C-C bond ligation using recombinant *Escherichia coli*-whole-cell biocatalysts. *Advanced Synthesis and Catalysis.* 2008. 350(1): 165-173.
254. **Döbber J and Pohl M.** HaloTag™: Evaluation of a covalent one-step immobilization for biocatalysis. *Journal of Biotechnology.* 2017. 241: 170-174.
255. **Tural B, Tural S, Ertaş E, Yalınkılıç İ, and Demir AS.** Purification and covalent immobilization of benzaldehyde lyase with heterofunctional chelate-epoxy modified magnetic nanoparticles and its carboligation reactivity. *Journal of Molecular Catalysis B: Enzymatic.* 2013. 95: 41-47.

256. **Sopaci ŞB, Şimşek İ, Tural B, Volkan M, and Demir AS.** Carboligation reactions with benzaldehyde lyase immobilized on superparamagnetic solid support. *Organic and Biomolecular Chemistry.* 2009. 7(8): 1658-1664.
257. **Kurlemann N and Liese A.** Immobilization of benzaldehyde lyase and its application as a heterogeneous catalyst in the continuous synthesis of a chiral 2-hydroxy ketone. *Tetrahedron: Asymmetry.* 2004. 15(18): 2955-2958.
258. **Hischer T, Gocke D, Fernández M, Hoyos P, Alcántara AR, Sinisterra JV, Hartmeier W, and Ansorge-Schumacher MB.** Stereoselective synthesis of novel benzoins catalysed by benzaldehyde lyase in a gel-stabilised two-phase system. *Tetrahedron.* 2005. 61(31): 7378-7383.
259. **Ansorge-Schumacher MB, Greiner L, Schroeper F, Mirtschin S, and Hischer T.** Operational concept for the improved synthesis of (*R*)-3,3'-furoin and related hydrophobic compounds with benzaldehyde lyase. *Biotechnology Journal.* 2006. 1(5): 564-568.
260. **Wu C, Bai S, Ansorge-Schumacher MB, and Wang D.** Nanoparticle cages for enzyme catalysis in organic media. *Advanced Materials.* 2011. 23(47): 5694-5699.
261. **Zhao Q, Ansorge-Schumacher MB, Haag R, and Wu C.** Compartmentalized aqueous–organic emulsion for efficient biocatalysis. *Chemistry – A European Journal.* 2018. 24(43): 10966-10970.
262. **Sun Z, Glebe U, Charan H, Boker A, and Wu C.** Enzyme-polymer conjugates as robust Pickering interfacial biocatalysts for efficient biotransformations and one-pot cascade reactions. *Angewandte Chemie.* 2018. 57(42): 13810-13814.
263. **Binks BP.** Particles as surfactants - similarities and differences. *Current Opinion in Colloid and Interface Science.* 2002. 7(1): 21-41.
264. **Thielen M.** Bio-polyamides for automotive applications. *Bioplastics Magazine.* 2010. 5: 10-11.
265. **Kind S, Neubauer S, Becker J, Yamamoto M, Völkert M, Abendroth Gv, Zelder O, and Wittmann C.** From zero to hero – Production of bio-based nylon from renewable resources using engineered *Corynebacterium glutamicum. Metabolic Engineering.* 2014. 25: 113-123.
266. **Park SH, Soetyono F, and Kim HK.** Cadaverine production by using cross-linked enzyme aggregate of *Escherichia coli* lysine decarboxylase. *Journal of Microbiology and Biotechnology.* 2017. 27(2): 289-296.
267. **Keilhauer C, Eggeling L, and Sahm H.** Isoleucine synthesis in *Corynebacterium glutamicum*: molecular analysis of the *ilvB-ilvN-ilvC* operon. *Journal of Bacteriology.* 1993. 175(17): 5595-5603.
268. **Oh YH, Kang KH, Kwon MJ, Choi JW, Joo JC, Lee SH, Yang YH, Song BK, *et al.*** Development of engineered *Escherichia coli* whole-cell biocatalysts for high-level conversion of L-lysine into cadaverine. *Journal of Industrial Microbiology and Biotechnology.* 2015. 42(11): 1481-1491.
269. **Reiber H.** Photochemical reactions of vitamin B_6 compounds, isolation and properties of products. *Biochimica et Biophysica Acta.* 1972. 279(2): 310-315.
270. **Kind S, Jeong WK, Schröder H, and Wittmann C.** Systems-wide metabolic pathway engineering in *Corynebacterium glutamicum* for bio-based production of diaminopentane. *Metabolic Engineering.* 2010. 12(4): 341-351.
271. **Seo H-M, Kim J-H, Jeon J-M, Song H-S, Bhatia SK, Sathiyanarayanan G, Park K, Kim KJ, *et al.*** *In situ* immobilization of lysine decarboxylase on a biopolymer by fusion with phasin: Immobilization of CadA on intracellular PHA. *Process Biochemistry.* 2016. 51(10): 1413-1419.
272. **Ma W, Cao W, Zhang H, Chen K, Li Y, and Ouyang P.** Enhanced cadaverine production from L-lysine using recombinant *Escherichia coli* co-overexpressing CadA and CadB. *Biotechnology Letters.* 2015. 37(4): 799-806.
273. **Kim HJ, Kim YH, Shin JH, Bhatia SK, Sathiyanarayanan G, Seo HM, Choi KY, Yang YH, *et al.*** Optimization of direct lysine decarboxylase biotransformation for cadaverine production with whole-cell biocatalysts at high lysine concentration. *Journal of Microbiology and Biotechnology.* 2015. 25(7): 1108-1113.
274. **Bhatia SK, Kim YH, Kim HJ, Seo HM, Kim JH, Song HS, Sathiyanarayanan G, Park SH, *et al.*** Biotransformation of lysine into cadaverine using barium alginate-immobilized *Escherichia coli* overexpressing CadA. *Bioprocess and Biosystems Engineering.* 2015. 38(12): 2315-2322.
275. **Kim J-H, Seo H-M, Sathiyanarayanan G, Bhatia SK, Song H-S, Kim J, Jeon J-M, Yoon J-J, *et al.*** Development of a continuous l-lysine bioconversion system for cadaverine production. *Journal of Industrial and Engineering Chemistry.* 2017. 46: 44-48.
276. **Jakoblinnert A and Rother D.** A two-step biocatalytic cascade in micro-aqueous medium: using whole cells to obtain high concentrations of a vicinal diol. *Green Chemistry.* 2014. 16(7): 3472-3482.
277. **Wachtmeister J, Jakoblinnert A, Kulig J, Offermann H, and Rother D.** Whole-cell teabag catalysis for the modularisation of synthetic enzyme cascades in micro-aqueous systems. *ChemCatChem.* 2014. 6(4): 1051-1058.
278. **Kulig JK.** Stereoselective synthesis of vicinal diols with enzymatic cascade reactions. *Heinrich-Heine Universität Düsseldorf.* 2013
279. **O'Connor SE, Grosset A, and Janiak P.** The pharmacological basis and pathophysiological significance of the heart rate-lowering property of diltiazem. *Fundamental and Clinical Pharmacology.* 1999. 13(2): 145-153.
280. **Kolb HC, VanNieuwenhze MS, and Sharpless KB.** Catalytic Asymmetric Dihydroxylation. *Chemical Reviews.* 1994. 94(8): 2483-2547.
281. **Woodward RB and Brutcher FV.** *cis*-Hydroxylation of a synthetic steroid intermediate with iodine, silver acetate and wet acetic acid. *Journal of the American Chemical Society.* 1958. 80(1): 209-211.
282. **Seide S.** Characterization of catalytically active *Ralstonia* sp. alcohol dehydrogenase inclusion bodies. *FH Aachen.* 2018
283. **van Pouderoyen G, Eggert T, Jaeger K-E, and Dijkstra BW.** The crystal structure of *Bacillus*

subtilis lipase: a minimal α/β hydrolase fold enzyme. *Journal of Molecular Biology.* 2001. 309(1): 215-226.

284. **Collard F, Zhang J, Nemet I, Qanungo KR, Monnier VM, and Yee VC.** Crystal structure of the deglycating enzyme fructosamine oxidase (amadoriase II). *The Journal of Biological Chemistry.* 2008. 283(40): 27007-27016.
285. **Los GV, Encell LP, McDougall MG, Hartzell DD, Karassina N, Zimprich C, Wood MG, Learish R, *et al.*** HaloTag: a novel protein labeling technology for cell imaging and protein analysis. *ACS Chemical Biology.* 2008. 3(6): 373-382.
286. **Ohana RF, Hurst R, Vidugiriene J, Slater MR, Wood KV, and Urh M.** HaloTag-based purification of functional human kinases from mammalian cells. *Protein Expression and Purification.* 2011. 76(2): 154-164.
287. **Döbber J, Gerlach T, Offermann H, Rother D, and Pohl M.** Closing the gap for efficient immobilization of biocatalysts in continuous processes: HaloTag™ fusion enzymes for a continuous enzymatic cascade towards a vicinal chiral diol. *Green Chemistry.* 2018. 20(2): 544-552.
288. **Kumar VV, Sivanesan S, and Cabana H.** Magnetic cross-linked laccase aggregates - bioremediation tool for decolorization of distinct classes of recalcitrant dyes. *Science of the Total Environment.* 2014. 487: 830-839.
289. **Aytar BS and Bakir U.** Preparation of cross-linked tyrosinase aggregates. *Process Biochemistry.* 2008. 43(2): 125-131.
290. **Šulek F, Fernández DP, Knez Ž, Habulin M, and Sheldon RA.** Immobilization of horseradish peroxidase as crosslinked enzyme aggregates (CLEAs). *Process Biochemistry.* 2011. 46(3): 765-769.
291. **Rehman S, Bhatti HN, Bilal M, and Asgher M.** Cross-linked enzyme aggregates (CLEAs) of *Pencilluim notatum* lipase enzyme with improved activity, stability and reusability characteristics. *International Journal of Biological Macromolecules.* 2016. 91: 1161-1169.
292. **Alvarenga AE, Amoroso MJ, Illanes A, and Castro GR.** Cross-linked α-L-rhamnosidase aggregates with potential application in food industry. *European Food Research and Technology.* 2014. 238(5): 797-801.
293. **Talekar S, Ghodake V, Ghotage T, Rathod P, Deshmukh P, Nadar S, Mulla M, and Ladole M.** Novel magnetic cross-linked enzyme aggregates (magnetic CLEAs) of α-amylase. *Bioresource Technology.* 2012. 123: 542-547.
294. **Cui JD, Sun LM, and Li LL.** A simple technique of preparing stable CLEAs of phenylalanine ammonia lyase using co-aggregation with starch and bovine serum albumin. *Applied Biochemistry and Biotechnology.* 2013. 170(8): 1827-1837.
295. **van Pelt S, Quignard S, Kubáč D, Sorokin DY, van Rantwijk F, and Sheldon RA.** Nitrile hydratase CLEAs: The immobilization and stabilization of an industrially important enzyme. *Green Chemistry.* 2008. 10(4): 395-400.
296. **Jeon EY, Baek AH, Bornscheuer UT, and Park JB.** Enzyme fusion for whole-cell biotransformation of long-chain *sec*-alcohols into esters. *Applied Microbiology and Biotechnology.* 2015. 99(15): 6267-6275.
297. **Stressler T, Ewert J, Eisele T, and Fischer L.** Cross-linked enzyme aggregates (CLEAs) of PepX and PepN – production, partial characterization and application of combi-CLEAs for milk protein hydrolysis. *Biocatalysis and Agricultural Biotechnology.* 2015. 4(4): 752-760.
298. **Mahmod SS, Yusof F, Jami MS, Khanahmadi S, and Shah H.** Development of an immobilized biocatalyst with lipase and protease activities as a multipurpose cross-linked enzyme aggregate (multi-CLEA). *Process Biochemistry.* 2015. 50(12): 2144-2157.
299. **Dalal S, Sharma A, and Gupta MN.** A multipurpose immobilized biocatalyst with pectinase, xylanase and cellulase activities. *Chemistry Central Journal.* 2007. 1(16): 1-6.
300. **Talekar S, Pandharbale A, Ladole M, Nadar S, Mulla M, Japhalekar K, Pattankude K, and Arage D.** Carrier free co-immobilization of α-amylase, glucoamylase and pullulanase as combined cross-linked enzyme aggregates (combi-CLEAs): a tri-enzyme biocatalyst with one pot starch hydrolytic activity. *Bioresource Technology.* 2013. 147: 269-275.
301. **Krzek M, van Beek HL, Permentier HP, Bischoff R, and Fraaije MW.** Covalent immobilization of a flavoprotein monooxygenase via its flavin cofactor. *Enzyme and Microbial Technology.* 2016. 82: 138-143.
302. **Timm C and Niemeyer CM.** Assembly and purification of enzyme-functionalized DNA origami structures. *Angewandte Chemie.* 2015. 54(23): 6745-6750.
303. **Spieler V, Valldorf B, Maaß F, Kleinschek A, Hüttenhain SH, and Kolmar H.** Coupled reactions on bioparticles: Stereoselective reduction with cofactor regeneration on PhaC inclusion bodies. *Biotechnology Journal.* 2016. 11(7): 890-898.
304. **Carrió M, González-Montalbán N, Vera A, Villaverde A, and Ventura S.** Amyloid-like properties of bacterial inclusion bodies. *Journal of Molecular Biology.* 2005. 347(5): 1025-1037.
305. **Curtis-Fisk J, Spencer RM, and Weliky DP.** Native conformation at specific residues in recombinant inclusion body protein in whole cells determined with solid-state NMR spectroscopy. *Journal of the American Chemical Society.* 2008. 130(38): 12568-12569.
306. **Wolf E, Kim PS, and Berger B.** MultiCoil: a program for predicting two- and three-stranded coiled coils. *Protein Science.* 1997. 6(6): 1179-1189.

5 Chapter 5 Appendix

5.1 Additional information to support the General Discussion

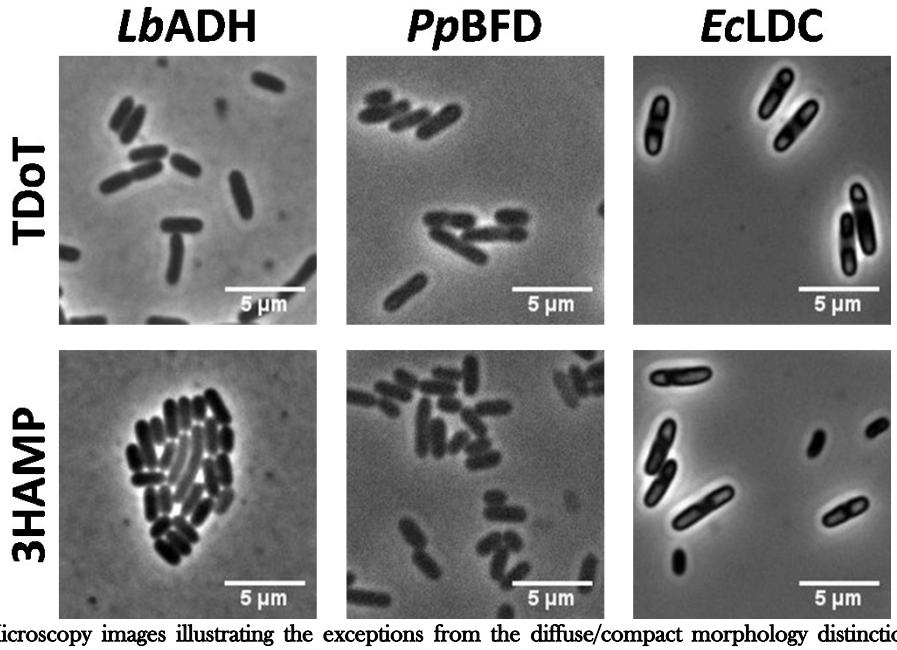


Figure 4-1 Microscopy images illustrating the exceptions from the diffuse/compact morphology distinction between 3HAMP and TDoT CatIBs. TDoT CatIBs of *Lb*ADH and *Pp*BFD do not form compact CatIBs like all other TDoT-fusions and look similar to the 3HAMP CatIBs. Likewise, *Ec*LDC-L-3HAMP forms compact CatIBs like *Ec*LDC-L-TDoT, even though all other 3HAMP-fusions form only diffuse CatIBs/FIBs. For experimental details, see Chapter 2.1.

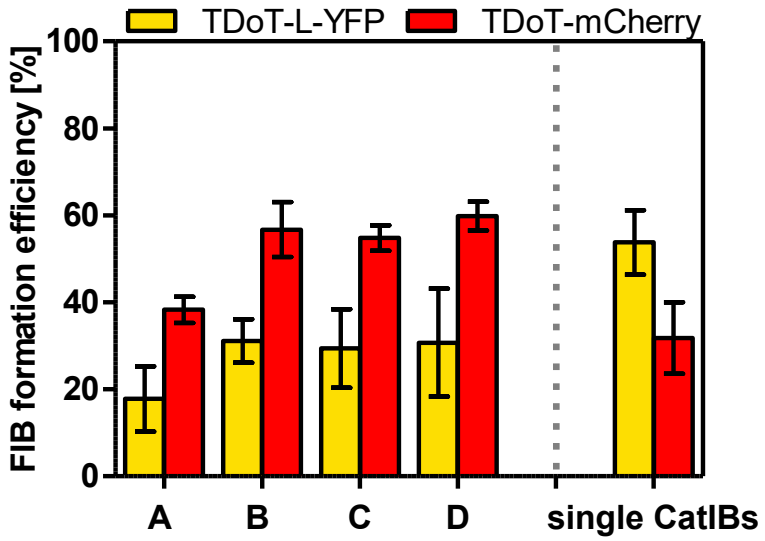


Figure 4-2 FIB-formation efficiency of Co-FIBs A-D and the single TDoT FIBs of YFP and mCherry. The fluorescence in the pellet (P) is given relatively to the crude cell extract (CCE, set to 100%, not shown). Error bars correspond to the standard deviation of the mean derived from three biological replicates. For further details, please see Chapter 2.5.



Figure 4-3 Hydrophobic patch analysis of TDoT (left, PDB: 1FE6) and 3HAMP (right PDB: 3LN3). Structures are shown in cartoon representation, subunits are highlighted in different shades of grey. The Rosetta-identified hydrophobic surface patches are shown in blue [241-243]. For further details, please see Chapter 2.1.

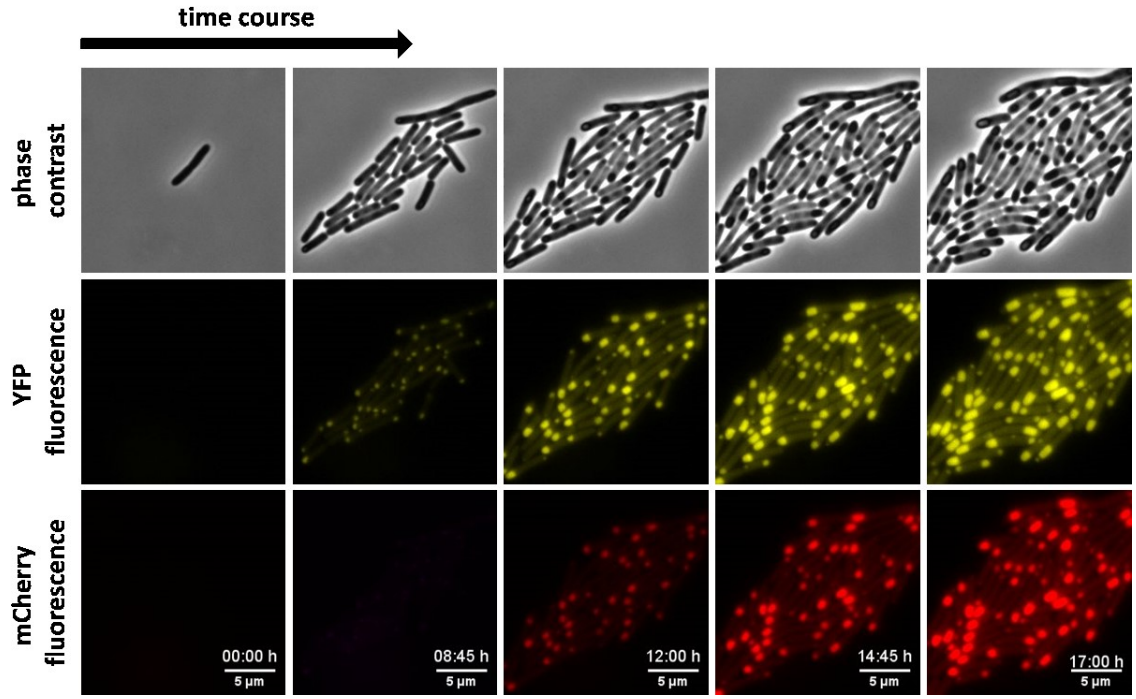


Figure 4-4 Time course of co-expression and co-localization of TDoT-YFP and TDoT-mCherry in *E. coli*. Exemplary microscopy images at different time points of a microfluidic cultivation of *E. coli* BL21(DE3) producing Co-FIBs C in phase contrast (top), YFP (middle), and mCherry (bottom) fluorescence images. For further details, please see Chapter 2.5.

Table 4-1 Example calculation of activity yield and production costs. Example calculations are shown for TDoT-*Pf*BAL CatIBs and purified soluble *Pf*BAL also shown in Table 3-9 . Values for yield, activity, and specific activity were taken from Chapter 2.1. Cost factors for production and immobilization were taken from [122], apart from *, which was estimated as described in Chapter 3.5.1. Values for half-life are taken from Chapter 2.6 (cascade reaction at pH 8). The respective best results are highlighted in grey.

Calculation	TDoT-*Pf*BAL CatIBs	purified soluble *Pf*BAL
yield per $g_{wet\ cells}$ [$mg_{protein}$]	63	20
relative [%] $= \frac{yield_{CatIBs}}{yield_{soluble}} \cdot 100$	$\frac{63}{20} \cdot 100 = 315$	-
specific activity [s^{-1}]	0.77	76.7
relative [%] $= \frac{sp.activity_{CatIBs}}{sp.activity_{soluble}} \cdot 100$	$\frac{0.77}{76.7} \cdot 100 = 1.0$	-
activity [U mg^{-1}]	0.69	76.7
total activity yield [U] $= activity \cdot yield$	$0.69 \cdot 63 = 43.5$	$76.7 \cdot 20 = 1533.5$
relative [%] $= \frac{total\ activity\ yield_{CatIBs}}{total\ activity\ yield_{soluble}} \cdot 100$	$\frac{43.5}{1533.5} \cdot 100 = 2.8$	-
relative production cost factor [-]	3*	10
production costs [U^{-1}] $= \frac{production\ costs}{activity\ yield}$	$\frac{3}{43.5} = 69 \cdot 10^{-3}$	$\frac{10}{1533.5} = 7 \cdot 10^{-3}$
relative [%] $= \frac{production\ per\ activity\ yield_{CatIBs}}{production\ per\ activity\ yield_{soluble}} \cdot 100$	$\frac{69 \cdot 10^{-3}}{7 \cdot 10^{-3}} = 9.86$	-
relative immobilization cost factor [-]	1	4
final costs [U^{-1}] $= production\ per\ activity\ yield \cdot immobilization$	$69 \cdot 10^{-3} \cdot 1 = 69 \cdot 10^{-3}$	$7 \cdot 10^{-3} \cdot 4 = 28 \cdot 10^{-3}$
relative [%] $= \frac{final\ costs_{CatIBs}}{final\ costs_{soluble}} \cdot 100$	$\frac{69 \cdot 10^{-3}}{28 \cdot 10^{-3}} = 2.46$	-
stability (half-life) [h]	36	5
usability [h U] $= \frac{stability}{final\ costs}$	$\frac{36}{69 \cdot 10^{-3}} = 522$	$\frac{5}{7 \cdot 10^{-3}} = 714$
relative [%] $= \frac{usability_{CatIBs}}{usability_{soluble}} \cdot 100$	$\frac{522}{714} = 0.73$	-

5.2 DNA and amino acid sequence of all fusion constructs

All DNA and amino acid sequences are presented in the following, with the coiled-coil domains in blue, the Xa recognition site in yellow, the $(GGGS)_3$ linker in red, the target enzyme or protein in green, and the betimes occurring His-Tags in violet. Endonuclease recognition sites are underlined.

TDoT-L-YFP

```
   M  I  I  N  E  T  A  D  D  I  V  Y  R  L  T  V  I  I  D  D  R  Y  E  S  L  K  N  L  I
CATATGATCATTAACGAAACTGCCGATGACATCGTTTATCGCCTGACAGTCATTATCGATGATCGCTACGAATCGCTGAAAAACCTGATT
NdeI          TDoT
T  L  R  A  D  R  L  E  M  I  I  N  D  N  V  S  T  I  L  A  S  I  T  S  I  E  G  R  A  S
ACCTTACGTGCAGATCGCTTGGAGATGATCATCAATGACAATGTGTCCACCATTCTCGCGAGCATTACTAGTATTGAAGGCCGTGCTAGC
                                                                  SpeI     Xa          NheI
G  G  G  S  G  G  G  S  G  G  G  S  G  S  M  V  S  K  G  E  E  L  F  T  G  V  V  P  I  L
GGCGGTGGGTCTGGAGGCGGCTCAGGTGGTGGGTCGGGATCCATGGTGAGCAAGGGCGAGGAGCTGTTCACCGGGGTGGTGCCCATCCTG
3xGGGS-Linker                        BamHI          YFP
V  E  L  D  G  D  V  N  G  H  K  F  S  V  S  G  E  G  E  G  D  A  T  Y  G  K  L  T  L  K
GTCGAGCTGGACGGCGACGTAAACGGCCACAAGTTCAGCGTGTCCGGCGAGGGCGAGGGCGATGCCACCTACGGCAAGCTGACCCTGAAG
F  I  C  T  T  G  K  L  P  V  P  W  P  T  L  V  T  T  F  G  Y  G  L  Q  C  F  A  R  Y  P
TTCATCTGCACCACCGGCAAGCTGCCCGTGCCCTGGCCCACCCTCGTGACCACCTTCGGCTACGGCCTGCAGTGCTTCGCCCGCTACCCC
D  H  M  K  Q  H  D  F  F  K  S  A  M  P  E  G  Y  V  Q  E  R  T  I  F  F  K  D  D  G  N
GACCACATGAAGCAGCACGACTTCTTCAAGTCCGCCATGCCCGAAGGCTACGTCCAGGAGCGCACCATCTTCTTCAAGGACGACGGCAAC
Y  K  T  R  A  E  V  K  F  E  G  D  T  L  V  N  R  I  E  L  K  G  I  D  F  K  E  D  G  N
TACAAGACCCGCGCCGAGGTGAAGTTCGAGGGCGACACCCTGGTGAACCGCATCGAGCTGAAGGGCATCGACTTCAAGGAGGACGGCAAC
I  L  G  H  K  L  E  Y  N  Y  N  S  H  N  V  Y  I  M  A  D  K  Q  K  N  G  I  K  V  N  F
ATCCTGGGGCACAAGCTGGAGTACAACTACAACAGCCACAACGTCTATATCATGGCCGACAAGCAGAAGAACGGCATCAAGGTGAACTTC
K  I  R  H  N  I  E  D  G  S  V  Q  L  A  D  H  Y  Q  Q  N  T  P  I  G  D  G  P  V  L  L
AAGATCCGCCACAACATCGAGGACGGCAGCGTGCAGCTCGCCGACCACTACCAGCAGAACACCCCCATCGGCGACGGCCCCGTGCTGCTG
P  D  N  H  Y  L  S  Y  Q  S  K  L  S  K  D  P  N  E  K  R  D  H  M  V  L  L  E  F  V  T
CCCGACAACCACTACCTGAGCTACCAGTCCAAACTGAGCAAAGACCCCAACGAGAAGCGCGATCACATGGTCCTGCTGGAGTTCGTGACC
A  A  G  I  T  L  G  M  D  E  L  Y  K  *
GCCGCCGGGATCACTCTCGGCATGGACGAGCTGTACAAGTAAGTCGACAAGCTTGCGGCCGCACTCGAG
                                        SalI          NotI     XhoI
```

TDoT-YFP

```
   M  I  I  N  E  T  A  D  D  I  V  Y  R  L  T  V  I  I  D  D  R  Y  E  S  L  K  N  L  I
CATATGATCATTAACGAAACTGCCGATGACATCGTTTATCGCCTGACAGTCATTATCGATGATCGCTACGAATCGCTGAAAAACCTGATT
NdeI          TDoT
T  L  R  A  D  R  L  E  M  I  I  N  D  N  V  S  T  I  L  A  S  I  G  S  M  V  S  K  G  E
ACCTTACGTGCAGATCGCTTGGAGATGATCATCAATGACAATGTGTCCACCATTCTCGCGAGCATTGGATCCATGGTGAGCAAGGGCGAG
                                                                  BamHI      YFP
E  L  F  T  G  V  V  P  I  L  V  E  L  D  G  D  V  N  G  H  K  F  S  V  S  G  E  G  E  G
GAGCTGTTCACCGGGGTGGTGCCCATCCTGGTCGAGCTGGACGGCGACGTAAACGGCCACAAGTTCAGCGTGTCCGGCGAGGGCGAGGGC
D  A  T  Y  G  K  L  T  L  K  F  I  C  T  T  G  K  L  P  V  P  W  P  T  L  V  T  T  F  G
GATGCCACCTACGGCAAGCTGACCCTGAAGTTCATCTGCACCACCGGCAAGCTGCCCGTGCCCTGGCCCACCCTCGTGACCACCTTCGGC
Y  G  L  Q  C  F  A  R  Y  P  D  H  M  K  Q  H  D  F  F  K  S  A  M  P  E  G  Y  V  Q  E
TACGGCCTGCAGTGCTTCGCCCGCTACCCCGACCACATGAAGCAGCACGACTTCTTCAAGTCCGCCATGCCCGAAGGCTACGTCCAGGAG
R  T  I  F  F  K  D  D  G  N  Y  K  T  R  A  E  V  K  F  E  G  D  T  L  V  N  R  I  E  L
CGCACCATCTTCTTCAAGGACGACGGCAACTACAAGACCCGCGCCGAGGTGAAGTTCGAGGGCGACACCCTGGTGAACCGCATCGAGCTG
K  G  I  D  F  K  E  D  G  N  I  L  G  H  K  L  E  Y  N  Y  N  S  H  N  V  Y  I  M  A  D
AAGGGCATCGACTTCAAGGAGGACGGCAACATCCTGGGGCACAAGCTGGAGTACAACTACAACAGCCACAACGTCTATATCATGGCCGAC
K  Q  K  N  G  I  K  V  N  F  K  I  R  H  N  I  E  D  G  S  V  Q  L  A  D  H  Y  Q  Q  N
AAGCAGAAGAACGGCATCAAGGTGAACTTCAAGATCCGCCACAACATCGAGGACGGCAGCGTGCAGCTCGCCGACCACTACCAGCAGAAC
T  P  I  G  D  G  P  V  L  L  P  D  N  H  Y  L  S  Y  Q  S  K  L  S  K  D  P  N  E  K  R
ACCCCCATCGGCGACGGCCCCGTGCTGCTGCCCGACAACCACTACCTGAGCTACCAGTCCAAACTGAGCAAAGACCCCAACGAGAAGCGC
D  H  M  V  L  L  E  F  V  T  A  A  G  I  T  L  G  M  D  E  L  Y  K  *
GATCACATGGTCCTGCTGGAGTTCGTGACCGCCGCCGGGATCACTCTCGGCATGGACGAGCTGTACAAGTAAGTCGACAAGCTTGCGGCC
GCACTCGAG                                                                 SalI          NotI
    XhoI
```

3HAMP-L-YFP

```
   M  G  L  F  N  A  H  A  V  A  Q  Q  R  A  D  R  I  A  T  L  L  Q  S  F  A  D  G  Q  L
CATATGGGCCTGTTTAACGCCCATGCAGTTGCGCAGCAACGCGCGGATCGCATTGCGACTCTCCTGCAGTCCTTTGCGGATGGTCAGTTG
NdeI          3HAMP
D  T  A  V  G  E  A  P  A  P  G  Y  E  R  L  Y  D  S  L  R  A  L  Q  R  Q  L  R  E  Q  R
GACACCGCCGTGGGTGAAGCGCCAGCACCTGGTTACGAACGCCTGTATGACTCGCTTCGCGCCCTTCAGCGCCAACTGCGCGAACAACGT
A  E  L  Q  Q  V  E  S  L  E  A  G  L  A  E  M  S  R  Q  H  E  A  G  W  I  D  Q  T  I  P
GCGGAGTTACAACAGGTTGAGAGCCTGGAAGCAGGCTTGGCTGAAATGAGTCGGCAGCATGAAGCAGGGTGGATTGACCAGACGATTCCG
A  E  R  L  E  G  R  A  A  R  I  A  K  G  V  N  E  L  V  A  A  H  I  A  V  K  M  K  V  V
```

```
GCTGAACGGTTAGAGGGCCGTGCAGCACGTATCGCCAAAGGCGTGAATGAGCTGGTTGCTGCGCACATTGCGGTGAAAATGAAAGTCGTG
S  V  V  T  A  Y  G  Q  G  N  F  E  P  L  M  D  R  L  P  G  K  K  A  Q  I  T  E  A  I  D
AGCGTAGTCACCGCGTATGGCCAAGGGAACTTCGAACCGCTCATGGATCGCCTGCCGGGTAAGAAAGCCCAGATCACGGAGGCCATTGAT
G  V  R  E  R  L  R  G  A  A  E  A  T  S  A  Q  L  A  T  A  A  Y  N  T  S  I  E  G  R  A
GGCGTACGTGAACGCCTGCGTGGAGCTGCTGAAGCGACCTCTGCGCAGCTGGCCACAGCCGCCTACAATACTAGTATTGAAGGCCGTGCT
                                                                        SpeI      Xa       NheI
S  G  G  G  S  G  G  G  S  G  G  G  S  G  S  M  V  S  K  G  E  E  L  F  T  G  V  V  P  I
AGCGGCGGTGGGTCTGGAGGCGGCTCAGGTGGTGGGTCGGGATCCATGGTGAGCAAGGGCGAGGAGCTGTTCACCGGGGTGGTGCCCATC
          3xGGGS-Linker                    BamHI          YFP
L  V  E  L  D  G  D  V  N  G  H  K  F  S  V  S  G  E  G  E  G  D  A  T  Y  G  K  L  T  L
CTGGTCGAGCTGGACGGCGACGTAAACGGCCACAAGTTCAGCGTGTCCGGCGAGGGCGAGGGCGATGCCACCTACGGCAAGCTGACCCTG
K  F  I  C  T  T  G  K  L  P  V  P  W  P  T  L  V  T  T  F  G  Y  G  L  Q  C  F  A  R  Y
AAGTTCATCTGCACCACCGGCAAGCTGCCCGTGCCCTGGCCCACCCTCGTGACCACCTTCGGCTACGGCCTGCAGTGCTTCGCCCGCTAC
P  D  H  M  K  Q  H  D  F  F  K  S  A  M  P  E  G  Y  V  Q  E  R  T  I  F  F  K  D  D  G
CCCGACCACATGAAGCAGCACGACTTCTTCAAGTCCGCCATGCCCGAAGGCTACGTCCAGGAGCGCACCATCTTCTTCAAGGACGACGGC
N  Y  K  T  R  A  E  V  K  F  E  G  D  T  L  V  N  R  I  E  L  K  G  I  D  F  K  E  D  G
AACTACAAGACCCGCGCCGAGGTGAAGTTCGAGGGCGACACCCTGGTGAACCGCATCGAGCTGAAGGGCATCGACTTCAAGGAGGACGGC
N  I  L  G  H  K  L  E  Y  N  Y  N  S  H  N  V  Y  I  M  A  D  K  Q  K  N  G  I  K  V  N
AACATCCTGGGGCACAAGCTGGAGTACAACTACAACAGCCACAACGTCTATATCATGGCCGACAAGCAGAAGAACGGCATCAAGGTGAAC
F  K  I  R  H  N  I  E  D  G  S  V  Q  L  A  D  H  Y  Q  Q  N  T  P  I  G  D  G  P  V  L
TTCAAGATCCGCCACAACATCGAGGACGGCAGCGTGCAGCTCGCCGACCACTACCAGCAGAACACCCCCATCGGCGACGGCCCCGTGCTG
L  P  D  N  H  Y  L  S  Y  Q  S  K  L  S  K  D  P  N  E  K  R  D  H  M  V  L  L  E  F  V
CTGCCCGACAACCACTACCTGAGCTACCAGTCCAAACTGAGCAAAGACCCCAACGAGAAGCGCGATCACATGGTCCTGCTGGAGTTCGTG
T  A  A  G  I  T  L  G  M  D  E  L  Y  K  *
ACCGCCGCCGGGATCACTCTCGGCATGGACGAGCTGTACAAGTAAGTCGACAAGCTTGCGGCCGCACTCGAG
                                              SalI        NotI     XhoI
```

Xa-L-YFP

```
   M  T  S  I  E  G  R  A  S  G  G  G  S  G  G  G  S  G  G  G  S  G  S  M  V  S  K  G  E
CATATGACTAGTATTGAAGGCCGTGCTAGCGGCGGTGGGTCTGGAGGCGGCTCAGGTGGTGGGTCGGGATCCATGGTGAGCAAGGGCGAG
NdeI   SpeI      Xa       NheI  3xGGGS-Linker                          BamHI          YFP
E  L  F  T  G  V  V  P  I  L  V  E  L  D  G  D  V  N  G  H  K  F  S  V  S  G  E  G  E  G
GAGCTGTTCACCGGGGTGGTGCCCATCCTGGTCGAGCTGGACGGCGACGTAAACGGCCACAAGTTCAGCGTGTCCGGCGAGGGCGAGGGC
D  A  T  Y  G  K  L  T  L  K  F  I  C  T  T  G  K  L  P  V  P  W  P  T  L  V  T  T  F  G
GATGCCACCTACGGCAAGCTGACCCTGAAGTTCATCTGCACCACCGGCAAGCTGCCCGTGCCCTGGCCCACCCTCGTGACCACCTTCGGC
Y  G  L  Q  C  F  A  R  Y  P  D  H  M  K  Q  H  D  F  F  K  S  A  M  P  E  G  Y  V  Q  E
TACGGCCTGCAGTGCTTCGCCCGCTACCCCGACCACATGAAGCAGCACGACTTCTTCAAGTCCGCCATGCCCGAAGGCTACGTCCAGGAG
R  T  I  F  F  K  D  D  G  N  Y  K  T  R  A  E  V  K  F  E  G  D  T  L  V  N  R  I  E  L
CGCACCATCTTCTTCAAGGACGACGGCAACTACAAGACCCGCGCCGAGGTGAAGTTCGAGGGCGACACCCTGGTGAACCGCATCGAGCTG
K  G  I  D  F  K  E  D  G  N  I  L  G  H  K  L  E  Y  N  Y  N  S  H  N  V  Y  I  M  A  D
AAGGGCATCGACTTCAAGGAGGACGGCAACATCCTGGGGCACAAGCTGGAGTACAACTACAACAGCCACAACGTCTATATCATGGCCGAC
K  Q  K  N  G  I  K  V  N  F  K  I  R  H  N  I  E  D  G  S  V  Q  L  A  D  H  Y  Q  Q  N
AAGCAGAAGAACGGCATCAAGGTGAACTTCAAGATCCGCCACAACATCGAGGACGGCAGCGTGCAGCTCGCCGACCACTACCAGCAGAAC
T  P  I  G  D  G  P  V  L  L  P  D  N  H  Y  L  S  Y  Q  S  K  L  S  K  D  P  N  E  K  R
ACCCCCATCGGCGACGGCCCCGTGCTGCTGCCCGACAACCACTACCTGAGCTACCAGTCCAAACTGAGCAAAGACCCCAACGAGAAGCGC
D  H  M  V  L  L  E  F  V  T  A  A  G  I  T  L  G  M  D  E  L  Y  K  *
GATCACATGGTCCTGCTGGAGTTCGTGACCGCCGCCGGGATCACTCTCGGCATGGACGAGCTGTACAAGTAAGTCGACAAGCTTGCGGCC
GCACTCGAG                                                              SalI        NotI
   XhoI
```

TDoT-L-mCherry

```
   M  I  I  N  E  T  A  D  D  I  V  Y  R  L  T  V  I  I  D  D  R  Y  E  S  L  K  N  L  I
CATATGATCATTAACGAAACTGCCGATGACATCGTTTATCGCCTGACAGTCATTATCGATGATCGCTACGAATCGCTGAAAAACCTGATT
NdeI       TDoT
T  L  R  A  D  R  L  E  M  I  I  N  D  N  V  S  T  I  L  A  S  I  T  S  I  E  G  R  A  S
ACCTTACGTGCAGATCGCTTGGAGATGATCATCAATGACAATGTGTCCACCATTCTCGCGAGCATTACTAGTATTGAAGGCCGTGCTAGC
                                                                  SpeI      Xa       NheI
G  G  G  S  G  G  G  S  G  G  G  S  G  S  M  V  S  K  G  E  E  D  N  M  A  I  I  K  E  F
GGCGGTGGGTCTGGAGGCGGCTCAGGTGGTGGGTCGGGATCCATGGTGAGCAAGGGCGAGGAGGATAACATGGCCATCATCAAGGAGTTC
3xGGGS-Linker                          BamHI          mCherry
M  R  F  K  V  H  M  E  G  S  V  N  G  H  E  F  E  I  E  G  E  G  E  G  R  P  Y  E  G  T
ATGCGCTTCAAGGTGCACATGGAGGGCTCCGTGAACGGCCACGAGTTCGAGATCGAGGGCGAGGGCGAGGGCCGCCCCTACGAGGGCACC
Q  T  A  K  L  K  V  T  K  G  G  P  L  P  F  A  W  D  I  L  S  P  Q  F  M  Y  G  S  K  A
CAGACCGCCAAGCTGAAGGTGACCAAGGGTGGCCCCCTGCCCTTCGCCTGGGACATCCTGTCCCCTCAGTTCATGTACGGCTCCAAGGCC
Y  V  K  H  P  A  D  I  P  D  Y  L  K  L  S  F  P  E  G  F  K  W  E  R  V  M  N  F  E  D
TACGTGAAGCACCCCGCCGACATCCCCGACTACTTGAAGCTGTCCTTCCCCGAGGGCTTCAAGTGGGAGCGCGTGATGAACTTCGAGGAC
G  G  V  V  T  V  T  Q  D  S  S  L  Q  D  G  E  F  I  Y  K  V  K  L  R  G  T  N  F  P  S
GGCGGCGTGGTGACCGTGACCCAGGACTCCTCCTTGCAGGACGGCGAGTTCATCTACAAGGTGAAGCTGCGCGGCACCAACTTCCCCTCC
D  G  P  V  M  Q  K  K  T  M  G  W  E  A  S  S  E  R  M  Y  P  E  D  G  A  L  K  G  E  I
GACGGCCCCGTAATGCAGAAGAAGACCATGGGCTGGGAGGCCTCCTCCGAGCGGATGTACCCCGAGGACGGCGCCCTGAAGGGCGAGATC
K  Q  R  L  K  L  K  D  G  G  H  Y  D  A  E  V  K  T  T  Y  K  A  K  K  P  V  Q  L  P  G
AAGCAGAGGCTGAAGCTGAAGGACGGCGGCCACTACGACGCTGAGGTCAAGACCACCTACAAGGCCAAGAAGCCCGTGCAGCTGCCCGGC
A  Y  N  V  N  I  K  L  D  I  T  S  H  N  E  D  Y  T  I  V  E  Q  Y  E  R  A  E  G  R  H
GCCTACAACGTCAACATCAAGTTGGACATCACCTCCCACAACGAGGACTACACCATCGTGGAACAGTACGAACGCGCCGAGGGCCGCCAC
S  T  G  G  M  D  E  L  Y  K  *
TCCACCGGCGGCATGGACGAGCTGTACAAGTAAGTCGACAAGCTTGCGGCCGCACTCGAG
                                  SalI        NotI     XhoI
```

TDoT-mCherry

```
   M  I  I  N  E  T  A  D  D  I  V  Y  R  L  T  V  I  I  D  D  R  Y  E  S  L  K  N  L  I
CATATGATCATTAACGAAACTGCCGATGACATCGTTTATCGCCTGACAGTCATTATCGATGATCGCTACGAATCGCTGAAAAACCTGATT
NdeI          TDoT
T  L  R  A  D  R  L  E  M  I  I  N  D  N  V  S  T  I  L  A  S  I  G  S  M  V  S  K  G  E
ACCTTACGTGCAGATCGCTTGGAGATGATCATCAATGACAATGTGTCCACCATTCTCGCGAGCATTGGATCCATGGTGAGCAAGGGCGAG
                                                                  BamHI        mCherry
E  D  N  M  A  I  I  K  E  F  M  R  F  K  V  H  M  E  G  S  V  N  G  H  E  F  E  I  E  G
GAGGATAACATGGCCATCATCAAGGAGTTCATGCGCTTCAAGGTGCACATGGAGGGCTCCGTGAACGGCCACGAGTTCGAGATCGAGGGC
E  G  E  G  R  P  Y  E  G  T  Q  T  A  K  L  K  V  T  K  G  G  P  L  P  F  A  W  D  I  L
GAGGGCGAGGGCCGCCCCTACGAGGGCACCCAGACCGCCAAGCTGAAGGTGACCAAGGGTGGCCCCCTGCCCTTCGCCTGGGACATCCTG
S  P  Q  F  M  Y  G  S  K  A  Y  V  K  H  P  A  D  I  P  D  Y  L  K  L  S  F  P  E  G  F
TCCCCTCAGTTCATGTACGGCTCCAAGGCCTACGTGAAGCACCCCGCCGACATCCCCGACTACTTGAAGCTGTCCTTCCCCGAGGGCTTC
K  W  E  R  V  M  N  F  E  D  G  G  V  V  T  V  T  Q  D  S  S  L  Q  D  G  E  F  I  Y  K
AAGTGGGAGCGCGTGATGAACTTCGAGGACGGCGGCGTGGTGACCGTGACCCAGGACTCCTCCTTCGCAGGACGGCGAGTTCATCTACAAG
V  K  L  R  G  T  N  F  P  S  D  G  P  V  M  Q  K  K  T  M  G  W  E  A  S  S  E  R  M  Y
GTGAAGCTGCGCGGCACCAACTTCCCCTCCGACGGCCCCGTAATGCAGAAGAAGACCATGGGCTGGGAGGCCTCCTCCGAGCGGATGTAC
P  E  D  G  A  L  K  G  E  I  K  Q  R  L  K  L  K  D  G  G  H  Y  D  A  E  V  K  T  T  Y
CCCGAGGACGGCGCCCTGAAGGGCGAGATCAAGCAGAGGCTGAAGCTGAAGGACGGCGGCCACTACGACGCTGAGGTCAAGACCACCTAC
K  A  K  K  P  V  Q  L  P  G  A  Y  N  V  N  I  K  L  D  I  T  S  H  N  E  D  Y  T  I  V
AAGGCCAAGAAGCCCGTGCAGCTGCCCGGCGCCTACAACGTCAACATCAAGTTGGACATCACCTCCCACAACGAGGACTACACCATCGTG
E  Q  Y  E  R  A  E  G  R  H  S  T  G  G  M  D  E  L  Y  K  *
GAACAGTACGAACGCGCCGAGGGCCGCCACTCCACCGGCGGCATGGACGAGCTGTACAAGTAAGTCGACAAGCTTGCGGCCGCACTCGAG
                                                              SalI        NotI        XhoI
```

3HAMP-L-mCherry

```
   M  G  L  F  N  A  H  A  V  A  Q  Q  R  A  D  R  I  A  T  L  L  Q  S  F  A  D  G  Q  L
CATATGGGCCTGTTTAACGCCCATGCAGTTGCGCAGCAACGCGCGGATCGCATTGCGACTCTCCTGCAGTCCTTTGCGGATGGTCAGTTG
NdeI          3HAMP
D  T  A  V  G  E  A  P  A  P  G  Y  E  R  L  Y  D  S  L  R  A  L  Q  R  Q  L  R  E  Q  R
GACACCGCCGTGGGTGAAGCGCCAGCACCTGGTTACGAACGCCTGTATGACTCGCTTCGCGCCCTTCAGCGCCAACTGCGCGAACAACGT
A  E  L  Q  Q  V  E  S  L  E  A  G  L  A  E  M  S  R  Q  H  E  A  G  W  I  D  Q  T  I  P
GCGGAGTTACAACAGGTTGAGAGCCTGGAAGCAGGCTTGGCTGAAATGAGTCGGCAGCATGAAGCAGGGTGGATTGACCAGACGATTCCG
A  E  R  L  E  G  R  A  A  R  I  A  K  G  V  N  E  L  V  A  A  H  I  A  V  K  M  K  V  V
GCTGAACGGTTAGAGGGCCGTGCAGCACGTATCGCCAAAGGCGTGAATGAGCTGGTTGCTGCGCACATTGCGGTGAAAATGAAAGTCGTG
S  V  V  T  A  Y  G  Q  G  N  F  E  P  L  M  D  R  L  P  G  K  K  A  Q  I  T  E  A  I  D
AGCGTAGTCACCGCGTATGGCCAAGGGAACTTCGAACCGCTCATGGATCGCCTGCCGGGTAAGAAAGCCCAGATCACGGAGGCCATTGAT
G  V  R  E  R  L  R  G  A  A  E  A  T  S  A  Q  L  A  T  A  A  Y  N  T  S  I  E  G  R  A
GGCGTACGTGAACGCCTGCGTGGAGCTGCTGAAGCGACCTCTGCGCAGCTGGCCACAGCCGCCTACAATACTAGTATTGAAGGCCGTGCT
                                                          SpeI      Xa        NheI
S  G  G  G  S  G  G  G  S  G  G  G  S  G  S  M  V  S  K  G  E  E  D  N  M  A  I  I  K  E
AGCGGCGGTGGGTCTGGAGGCGGCTCAGGTGGTGGGTCGGGATCCATGGTGAGCAAGGGCGAGGAGGATAACATGGCCATCATCAAGGAG
   3xGGGS-Linker                    BamHI              mCherry
F  M  R  F  K  V  H  M  E  G  S  V  N  G  H  E  F  E  I  E  G  E  G  E  G  R  P  Y  E  G
TTCATGCGCTTCAAGGTGCACATGGAGGGCTCCGTGAACGGCCACGAGTTCGAGATCGAGGGCGAGGGCGAGGGCCGCCCCTACGAGGGC
T  Q  T  A  K  L  K  V  T  K  G  G  P  L  P  F  A  W  D  I  L  S  P  Q  F  M  Y  G  S  K
ACCCAGACCGCCAAGCTGAAGGTGACCAAGGGTGGCCCCCTGCCCTTCGCCTGGGACATCCTGTCCCCTCAGTTCATGTACGGCTCCAAG
A  Y  V  K  H  P  A  D  I  P  D  Y  L  K  L  S  F  P  E  G  F  K  W  E  R  V  M  N  F  E
GCCTACGTGAAGCACCCCGCCGACATCCCCGACTACTTGAAGCTGTCCTTCCCCGAGGGCTTCAAGTGGGAGCGCGTGATGAACTTCGAG
D  G  G  V  V  T  V  T  Q  D  S  S  L  Q  D  G  E  F  I  Y  K  V  K  L  R  G  T  N  F  P
GACGGCGGCGTGGTGACCGTGACCCAGGACTCCTCCTTGCAGGACGGCGAGTTCATCTACAAGGTGAAGCTGCGCGGCACCAACTTCCCC
S  D  G  P  V  M  Q  K  T  M  G  W  E  A  S  S  E  R  M  Y  P  E  D  G  A  L  K  G  E
TCCGACGGCCCCGTAATGCAGAAGAAGACCATGGGCTGGGAGGCCTCCTCCGAGCGGATGTACCCCGAGGACGGCGCCCTGAAGGGCGAG
I  K  Q  R  L  K  L  K  D  G  G  H  Y  D  A  E  V  K  T  T  Y  K  A  K  K  P  V  Q  L  P
ATCAAGCAGAGGCTGAAGCTGAAGGACGGCGGCCACTACGACGCTGAGGTCAAGACCACCTACAAGGCCAAGAAGCCCGTGCAGCTGCCC
G  A  Y  N  V  N  I  K  L  D  I  T  S  H  N  E  D  Y  T  I  V  E  Q  Y  E  R  A  E  G  R
GGCGCCTACAACGTCAACATCAAGTTGGACATCACCTCCCACAACGAGGACTACACCATCGTGGAACAGTACGAACGCGCCGAGGGCCGC
H  S  T  G  G  M  D  E  L  Y  K  *
CACTCCACCGGCGGCATGGACGAGCTGTACAAGTAAGTCGACAAGCTTGCGGCCGCACTCGAG
                                  SalI        NotI        XhoI
```

Xa-L-mCherry

```
   M  T  S  I  E  G  R  A  S  G  G  G  S  G  G  G  S  G  G  G  S  G  S  M  V  S  K  G  E
CATATGACTAGTATTGAAGGCCGTGCTAGCGGCGGTGGGTCTGGAGGCGGCTCAGGTGGTGGGTCGGGATCCATGGTGAGCAAGGGCGAG
NdeI  SpeI     Xa        NheI   3xGGGS-Linker                    BamHI        mCherry
E  D  N  M  A  I  I  K  E  F  M  R  F  K  V  H  M  E  G  S  V  N  G  H  E  F  E  I  E  G
GAGGATAACATGGCCATCATCAAGGAGTTCATGCGCTTCAAGGTGCACATGGAGGGCTCCGTGAACGGCCACGAGTTCGAGATCGAGGGC
E  G  E  G  R  P  Y  E  G  T  Q  T  A  K  L  K  V  T  K  G  G  P  L  P  F  A  W  D  I  L
GAGGGCGAGGGCCGCCCCTACGAGGGCACCCAGACCGCCAAGCTGAAGGTGACCAAGGGTGGCCCCCTGCCCTTCGCCTGGGACATCCTG
S  P  Q  F  M  Y  G  S  K  A  Y  V  K  H  P  A  D  I  P  D  Y  L  K  L  S  F  P  E  G  F
TCCCCTCAGTTCATGTACGGCTCCAAGGCCTACGTGAAGCACCCCGCCGACATCCCCGACTACTTGAAGCTGTCCTTCCCCGAGGGCTTC
K  W  E  R  V  M  N  F  E  D  G  G  V  V  T  V  T  Q  D  S  S  L  Q  D  G  E  F  I  Y  K
AAGTGGGAGCGCGTGATGAACTTCGAGGACGGCGGCGTGGTGACCGTGACCCAGGACTCCTCCTTCGCAGGACGGCGAGTTCATCTACAAG
V  K  L  R  G  T  N  F  P  S  D  G  P  V  M  Q  K  K  T  M  G  W  E  A  S  S  E  R  M  Y
GTGAAGCTGCGCGGCACCAACTTCCCCTCCGACGGCCCCGTAATGCAGAAGAAGACCATGGGCTGGGAGGCCTCCTCCGAGCGGATGTAC
P  E  D  G  A  L  K  G  E  I  K  Q  R  L  K  L  K  D  G  G  H  Y  D  A  E  V  K  T  T  Y
CCCGAGGACGGCGCCCTGAAGGGCGAGATCAAGCAGAGGCTGAAGCTGAAGGACGGCGGCCACTACGACGCTGAGGTCAAGACCACCTAC
K  A  K  K  P  V  Q  L  P  G  A  Y  N  V  N  I  K  L  D  I  T  S  H  N  E  D  Y  T  I  V
AAGGCCAAGAAGCCCGTGCAGCTGCCCGGCGCCTACAACGTCAACATCAAGTTGGACATCACCTCCCACAACGAGGACTACACCATCGTG
```

```
E  Q  Y  E  R  A  E  G  R  H  S  T  G  G  M  D  E  L  Y  K  *
GAACAGTACGAACGCGCCGAGGGCCGCCACTCCACCGGCGGCATGGACGAGCTGTACAAGTAAGTCGACAAGCTTGCGGCCGCACTCGAG
                                                              SalI          NotI     XhoI
```

TDoT-L-*R*ADH

```
   M  I  I  N  E  T  A  D  D  I  V  Y  R  L  T  V  I  I  D  D  R  Y  E  S  L  K  N  L  I
CATATGATCATTAACGAAACTGCCGATGACATCGTTTATCGCCTGACAGTCATTATCGATGATCGCTACGAATCGCTGAAAAACCTGATT
NdeI          TDoT
T  L  R  A  D  R  L  E  M  I  I  N  D  N  V  S  T  I  L  A  S  I  T  S  I  E  G  R  A  S
ACCTTACGTGCAGATCGCTTGGAGATGATCATCAATGACAATGTGTCCACCATTCTCGCGAGCATTACTAGTATTGAAGGCCGTGCTAGC
                                                                  SpeI     Xa       NheI
G  G  G  S  G  G  G  S  G  G  G  S  G  S  M  Y  R  L  L  N  K  T  A  V  I  T  G  G  N  S
GGCGGTGGGTCTGGAGGCGGCTCAGGTGGTGGGTCGGGATCCATGTATCGTCTGCTGAATAAAACCGCAGTTATTACCGGTGGTAATAGC
   3xGGGS-Linker                      BamHI          RADH
G  I  G  L  A  T  A  K  R  F  V  A  E  G  A  Y  V  F  I  V  G  R  R  R  K  E  L  E  Q  A
GGTATTGGTCTGGCAACCGCAAAACGTTTTGTTGCCGAAGGTGCCTATGTTTTTATTGTTGGTCGTCGTCGTAAAGAACTGGAACAGGCA
A  A  E  I  G  R  N  V  T  A  V  K  A  D  V  T  K  L  E  D  L  D  R  L  Y  A  I  V  R  E
GCAGCAGAAATTGGTCGTAATGTTACCGCAGTTAAAGCCGATGTTACCAAACTGGAAGATCTGGATCGTCTGTATGCAATTGTTCGTGAA
Q  R  G  S  I  D  V  L  F  A  N  S  G  A  I  E  Q  K  T  L  E  E  I  T  P  E  H  Y  D  R
CAGCGTGGTAGCATTGATGTTCTGTTTGCAAATAGCGGTGCCATTGAACAGAAAACCCTGGAAGAAATTACACCGGAACATTATGATCGC
T  F  D  V  N  V  R  G  L  I  F  T  V  Q  K  A  L  P  L  L  R  D  G  G  S  V  I  L  T  S
ACCTTTGATGTTAATGTGCGTGGTCTGATTTTTACCGTTCAGAAAGCACTGCCGCTGCTGCGTGATGGTGGTAGCGTTATTCTGACCAGC
S  V  A  G  V  L  G  L  Q  A  H  D  T  Y  S  A  A  K  A  A  V  R  S  L  A  R  T  W  T  T
AGCGTTGCCGGTGTTCTGGGTCTGCAGGCACATGATACCTATAGCGCAGCAAAAGCAGCAGTTCGTAGCCTGGCACGTACCTGGACCACC
E  L  K  G  R  S  I  R  V  N  A  V  S  P  G  A  I  D  T  P  I  I  E  N  Q  V  S  T  Q  E
GAACTGAAAGGTCGTAGCATTCGTGTTAATGCAGTTAGTCCGGGTGCAATTGATACCCCGATTATTGAAAATCAGGTTAGCACCCAGGAA
E  A  D  E  L  R  A  K  F  A  A  A  T  P  L  G  R  V  G  R  P  E  E  L  A  A  A  V  L  F
GAAGCAGACGAACTGCGCGCAAAATTTGCAGCAGCAACACCGCTGGGTCGTGTTGGTCGTCCGGAAGAACTGGCAGCAGCCGTTCTGTTT
L  A  S  D  D  S  S  Y  V  A  G  I  E  L  F  V  D  G  G  L  T  Q  V  *
CTGGCAAGTGATGATAGCAGCTATGTTGCAGGTATTGAACTGTTTGTTGATGGTGGTCTGACCCAGGTTTAAGTCGACAAGCTTGCGGCC
GCACTCGAG                                                                SalI          NotI
   XhoI
```

3HAMP-L-*R*ADH

```
   M  G  L  F  N  A  H  A  V  A  Q  Q  R  A  D  R  I  A  T  L  L  Q  S  F  A  D  G  Q  L
CATATGGGCCTGTTTAACGCCCATGCAGTTGCGCAGCAACGCGCGGATCGCATTGCGACTCTCCTGCAGTCCTTTGCGGATGGTCAGTTG
NdeI          3HAMP
D  T  A  V  G  E  A  P  A  P  G  Y  E  R  L  Y  D  S  L  R  A  L  Q  R  Q  L  R  E  Q  R
GACACCGCCGTGGGTGAAGCGCCAGCACCTGGTTACGAACGCCTGTATGACTCGCTTCGCGCCCTTCAGCGCCAACTGCGCGAACAACGT
A  E  L  Q  Q  V  E  S  L  E  A  G  L  A  E  M  S  R  Q  H  E  A  G  W  I  D  Q  T  I  P
GCGGAGTTACAACAGGTTGAGAGCCTGGAAGCAGGCTTGGCTGAAATGAGTCGGCAGCATGAAGCAGGGTGGATTGACCAGACGATTCCG
A  E  R  L  E  G  R  A  A  R  I  A  K  G  V  N  E  L  V  A  A  H  I  A  V  K  M  K  V  V
GCTGAACGGTTAGAGGGCCGTGCAGCACGTATCGCCAAAGGCGTGAATGAGCTGGTTGCTGCGCACATTGCGGTGAAAATGAAAGTCGTG
S  V  V  T  A  Y  G  Q  G  N  F  E  P  L  M  D  R  L  P  G  K  K  A  Q  I  T  E  A  I  D
AGCGTAGTCACCGCGTATGGCCAAGGGAACTTCGAACCGCTCATGGATCGCCTGCCGGGTAAGAAAGCCCAGATCACGGAGGCCATTGAT
G  V  R  E  R  L  R  G  A  A  E  A  T  S  A  Q  L  A  T  A  A  Y  N  T  S  I  E  G  R  A
GGCGTACGTGAACGCCTGCGTGGAGCTGCTGAAGCGACCTCTGCGCAGCTGGCCACAGCCGCCTACAATACTAGTATTGAAGGCCGTGCT
                                                                  SpeI     Xa       NheI
S  G  G  G  S  G  G  G  S  G  G  G  S  G  S  M  Y  R  L  L  N  K  T  A  V  I  T  G  G  N
AGCGGCGGTGGGTCTGGAGGCGGCTCAGGTGGTGGGTCGGGATCCATGTATCGTCTGCTGAATAAAACCGCAGTTATTACCGGTGGTAAT
   3xGGGS-Linker                      BamHI          RADH
S  G  I  G  L  A  T  A  K  R  F  V  A  E  G  A  Y  V  F  I  V  G  R  R  R  K  E  L  E  Q
AGCGGTATTGGTCTGGCAACCGCAAAACGTTTTGTTGCCGAAGGTGCCTATGTTTTTATTGTTGGTCGTCGTCGTAAAGAACTGGAACAG
A  A  A  E  I  G  R  N  V  T  A  V  K  A  D  V  T  K  L  E  D  L  D  R  L  Y  A  I  V  R
GCAGCAGCAGAAATTGGTCGTAATGTTACCGCAGTTAAAGCCGATGTTACCAAACTGGAAGATCTGGATCGTCTGTATGCAATTGTTCGT
E  Q  R  G  S  I  D  V  L  F  A  N  S  G  A  I  E  Q  K  T  L  E  E  I  T  P  E  H  Y  D
GAACAGCGTGGTAGCATTGATGTTCTGTTTGCAAATAGCGGTGCCATTGAACAGAAAACCCTGGAAGAAATTACACCGGAACATTATGAT
R  T  F  D  V  N  V  R  G  L  I  F  T  V  Q  K  A  L  P  L  L  R  D  G  G  S  V  I  L  T
CGCACCTTTGATGTTAATGTGCGTGGTCTGATTTTTACCGTTCAGAAAGCACTGCCGCTGCTGCGTGATGGTGGTAGCGTTATTCTGACC
S  S  V  A  G  V  L  G  L  Q  A  H  D  T  Y  S  A  A  K  A  A  V  R  S  L  A  R  T  W  T
AGCAGCGTTGCCGGTGTTCTGGGTCTGCAGGCACATGATACCTATAGCGCAGCAAAAGCAGCAGTTCGTAGCCTGGCACGTACCTGGACC
T  E  L  K  G  R  S  I  R  V  N  A  V  S  P  G  A  I  D  T  P  I  I  E  N  Q  V  S  T  Q
ACCGAACTGAAAGGTCGTAGCATTCGTGTTAATGCAGTTAGTCCGGGTGCAATTGATACCCCGATTATTGAAAATCAGGTTAGCACCCAG
E  E  A  D  E  L  R  A  K  F  A  A  A  T  P  L  G  R  V  G  R  P  E  E  L  A  A  A  V  L
GAAGAAGCAGACGAACTGCGCGCAAAATTTGCAGCAGCAACACCGCTGGGTCGTGTTGGTCGTCCGGAAGAACTGGCAGCAGCCGTTCTG
F  L  A  S  D  D  S  S  Y  V  A  G  I  E  L  F  V  D  G  G  L  T  Q  V  *
TTTCTGGCAAGTGATGATAGCAGCTATGTTGCAGGTATTGAACTGTTTGTTGATGGTGGTCTGACCCAGGTTTAAGTCGACAAGCTTGCG
GCCGCACTCGAG                                                             SalI          NotI
      XhoI
```

*R*ADH

```
   M  Y  R  L  L  N  K  T  A  V  I  T  G  G  N  S  G  I  G  L  A  T  A  K  R  F  V  A  E
CATATGTATCGTCTGCTGAATAAAACCGCAGTTATTACCGGTGGTAATAGCGGTATTGGTCTGGCAACCGCAAAACGTTTTGTTGCCGAA
NdeI      RADH
G  A  Y  V  F  I  V  G  R  R  R  K  E  L  E  Q  A  A  A  E  I  G  R  N  V  T  A  V  K  A
GGTGCCTATGTTTTTATTGTTGGTCGTCGTCGTAAAGAACTGGAACAGGCAGCAGCAGAAATTGGTCGTAATGTTACCGCAGTTAAAGCC
D  V  T  K  L  E  D  L  D  R  L  Y  A  I  V  R  E  Q  R  G  S  I  D  V  L  F  A  N  S  G
GATGTTACCAAACTGGAAGATCTGGATCGTCTGTATGCAATTGTTCGTGAACAGCGTGGTAGCATTGATGTTCTGTTTGCAAATAGCGGT
A  I  E  Q  K  T  L  E  E  I  T  P  E  H  Y  D  R  T  F  D  V  N  V  R  G  L  I  F  T  V
```

```
GCCATTGAACAGAAAACCCTGGAAGAAATTACACCGGAACATTATGATCGCACCTTTGATGTTAATGTGCGTGGTCTGATTTTTACCGTT
Q  K  A  L  P  L  L  R  D  G  G  S  V  I  L  T  S  S  V  A  G  V  L  G  L  Q  A  H  D  T
CAGAAAGCACTGCCGCTGCTGCGTGATGGTGGTAGCGTTATTCTGACCAGCAGCGTTGCCGGTGTTCTGGGTCTGCAGGCACATGATACC
Y  S  A  A  K  A  A  V  R  S  L  A  R  T  W  T  T  E  L  K  G  R  S  I  R  V  N  A  V  S
TATAGCGCAGCAAAAGCAGCAGTTCGTAGCCTGGCACGTACCTGGACCACCGAACTGAAAGGTCGTAGCATTCGTGTTAATGCAGTTAGT
P  G  A  I  D  T  P  I  I  E  N  Q  V  S  T  Q  E  E  A  D  E  L  R  A  K  F  A  A  A  T
CCGGGTGCAATTGATACCCCGATTATTGAAAATCAGGTTAGCACCCAGGAAGAAGCAGACGAACTGCGCGCAAAATTTGCAGCAGCAACA
P  L  G  R  V  G  G  R  P  E  E  L  A  A  A  A  V  L  F  L  A  S  D  D  S  S  Y  V  A  G  I  E
CCGCTGGGTCGTGTTGGTCGTCCGGAAGAACTGGCAGCAGCCGTTCTGTTTCTGGCAAGTGATGATAGCAGCTATGTTGCAGGTATTGAA
L  F  V  D  G  G  L  T  Q  V  *  *
CTGTTTGTTGATGGTGGTCTGACCCAGGTTTAATAACTCGAG
                                    XhoI
```

TDoT-L-*Lb*ADH

```
   M  I  I  N  E  T  A  D  D  I  V  Y  R  L  T  V  I  I  D  D  R  Y  E  S  L  K  N  L  I
CATATGATCATTAACGAAACTGCCGATGACATCGTTTATCGCCTGACAGTCATTATCGATGATCGCTACGAATCGCTGAAAAACCTGATT
NdeI          TDoT
T  L  R  A  D  R  L  E  M  I  I  N  D  N  V  S  T  I  L  A  S  I  T  S  I  E  G  R  A  S
ACCTTACGTGCAGATCGCTTGGAGATGATCATCAATGACAATGTGTCCACCATTCTCGCGAGCATTACTAGTATTGAAGGCCGTGCTAGC
                                                                  SpeI     Xa       NheI
G  G  G  S  G  G  G  S  G  G  G  S  G  S  M  S  N  R  L  D  G  K  V  A  I  I  T  G  G  T
GGCGGTGGGTCTGGAGGCGGCTCAGGTGGTGGGTCGGGATCCATGTCTAACCGTTTGGATGGTAAGGTAGCAATCATTACAGGTGGTACG
   3xGGGS-Linker                      BamHI                  LbADH
L  G  I  G  L  A  I  A  T  K  F  V  E  E  G  A  K  V  M  I  T  G  R  H  S  D  V  G  E  K
TTGGGTATCGGTTTAGCTATCGCCACGAAGTTCGTTGAAGAAGGGGCTAAGGTCATGATTACCGGCCGGCACAGCGATGTTGGTGAAAAA
A  A  K  S  V  G  T  P  D  Q  I  Q  F  F  Q  H  D  S  S  D  E  D  G  W  T  K  L  F  D  A
GCAGCTAAGAGTGTCGGCACTCCTGATCAGATTCAATTTTTCCAACATGATTCTTCCGATGAAGACGGCTGGACGAAATTATTCGATGCA
T  E  K  A  F  G  P  V  S  T  L  V  N  N  A  G  I  A  V  N  K  S  V  E  E  T  T  T  A  E
ACGGAAAAAGCCTTTGGCCCAGTTTCTACATTAGTTAATAACGCTGGGATCGCGGTTAACAAGAGTGTCGAAGAAACCACGACTGCTGAA
W  R  K  L  L  A  V  N  L  D  G  V  F  F  G  T  R  L  G  I  Q  R  M  K  N  K  G  L  G  A
TGGCGTAAATTATTAGCCGTCAACCTTGATGGTGTCTTCTTCGGTACCCGATTAGGGATTCAACGGATGAAGAACAAAGGCTTAGGGGCT
S  I  I  N  M  S  S  I  E  G  F  V  G  D  P  S  L  G  A  Y  N  A  S  K  G  A  V  R  I  M
TCCATCATCAACATGTCTTCGATCGAAGGCTTTGTGGGTGATCCTAGCTTAGGGGCTTACAACGCATCTAAAGGGGCCGTACGGATTATG
S  K  S  A  A  L  D  C  A  L  K  D  Y  D  V  R  V  N  T  V  H  P  G  Y  I  K  T  P  L  V
TCCAAGTCAGCTGCCTTAGATTGTGCCCTAAAGGACTACGATGTTCGGGTAAACACTGTTCACCCTGGCTACATCAAGACACCATTGGTT
D  D  L  P  G  A  E  E  A  M  S  Q  R  T  K  T  P  M  G  H  I  G  E  P  N  D  I  A  Y  I
GATGACCTACCAGGGGCCGAAGAAGCGATGTCACAACGGACCAAGACGCCAATGGGCCATATCGGTGAACCTAACGATATTGCCTACATC
C  V  Y  L  A  S  N  E  S  K  F  A  T  G  S  E  F  V  V  D  G  G  Y  T  A  Q  *
TGTGTTTACTTGGCTTCTAACGAATCTAAATTTGCAACGGGTTCTGAATTCGTAGTTGACGGTGGCTACACTGCTCAATAGAGTCGACAA
GCTTGCGGCCGCACTCGAG                                                                SalI
   NotI     XhoI
```

3HAMP-L-*Lb*ADH

```
   M  G  L  F  N  A  H  A  V  A  Q  Q  R  A  D  R  I  A  T  L  L  Q  S  F  A  D  G  Q  L
CATATGGGCCTGTTTAACGCCCATGCAGTTGCGCAGCAACGCGCGGATCGCATTGCGACTCTCCTGCAGTCCTTTGCGGATGGTCAGTTG
NdeI          TDoT
D  T  A  V  G  E  A  P  A  P  G  Y  E  R  L  Y  D  S  L  R  A  L  Q  R  Q  L  R  E  Q  R
GACACCGCCGTGGGTGAAGCGCCAGCACCTGGTTACGAACGCCTGTATGACTCGCTTCGCGCCCTTCAGCGCCAACTGCGCGAACAACGT
A  E  L  Q  Q  V  E  S  L  E  A  G  L  A  E  M  S  R  Q  H  E  A  G  W  I  D  Q  T  I  P
GCGGAGTTACAACAGGTTGAGAGCCTGGAAGCAGGCTTGGCTGAAATGAGTCGGCAGCATGAAGCAGGGTGGATTGACCAGACGATTCCG
A  E  R  L  E  G  R  A  A  R  I  A  K  G  V  N  E  L  V  A  A  H  I  A  V  K  M  K  V  V
GCTGAACGGTTAGAGGGCCGTGCAGCACGTATCGCCAAAGGCGTGAATGAGCTGGTTGCTGCGCACATTGCGGTGAAAATGAAAGTCGTG
S  V  V  T  A  Y  G  Q  G  N  F  E  P  L  M  D  R  L  P  G  K  K  A  Q  I  T  E  A  I  D
AGCGTAGTCACCGCGTATGGCCAAGGGAACTTCGAACCGCTCATGGATCGCCTGCCGGGTAAGAAAGCCCAGATCACGGAGGCCATTGAT
G  V  R  E  R  L  R  G  A  A  E  A  T  S  A  Q  L  A  T  A  A  Y  N  T  S  I  E  G  R  A
GGCGTACGTGAACGCCTGCGTGGAGCTGCTGAAGCGACCTCTGCGCAGCTGGCCACAGCCGCCTACAATACTAGTATTGAAGGCCGTGCT
                                                                  SpeI     Xa       NheI
S  G  G  G  S  G  G  G  S  G  G  G  S  G  S  M  S  N  R  L  D  G  K  V  A  I  I  T  G  G
AGCGGCGGTGGGTCTGGAGGCGGCTCAGGTGGTGGGTCGGGATCCATGTCTAACCGTTTGGATGGTAAGGTAGCAATCATTACAGGTGGT
   3xGGGS-Linker                      BamHI                  LbADH
T  L  G  I  G  L  A  I  A  T  K  F  V  E  E  G  A  K  V  M  I  T  G  R  H  S  D  V  G  E
ACGTTGGGTATCGGTTTAGCTATCGCCACGAAGTTCGTTGAAGAAGGGGCTAAGGTCATGATTACCGGCCGGCACAGCGATGTTGGTGAA
K  A  A  K  S  V  G  T  P  D  Q  I  Q  F  F  Q  H  D  S  S  D  E  D  G  W  T  K  L  F  D
AAAGCAGCTAAGAGTGTCGGCACTCCTGATCAGATTCAATTTTTCCAACATGATTCTTCCGATGAAGACGGCTGGACGAAATTATTCGAT
A  T  E  K  A  F  G  P  V  S  T  L  V  N  N  A  G  I  A  V  N  K  S  V  E  E  T  T  T  A
GCAACGGAAAAAGCCTTTGGCCCAGTTTCTACATTAGTTAATAACGCTGGGATCGCGGTTAACAAGAGTGTCGAAGAAACCACGACTGCT
E  W  R  K  L  L  A  V  N  L  D  G  V  F  F  G  T  R  L  G  I  Q  R  M  K  N  K  G  L  G
GAATGGCGTAAATTATTAGCCGTCAACCTTGATGGTGTCTTCTTCGGTACCCGATTAGGGATTCAACGGATGAAGAACAAAGGCTTAGGG
A  S  I  I  N  M  S  S  I  E  G  F  V  G  D  P  S  L  G  A  Y  N  A  S  K  G  A  V  R  I
GCTTCCATCATCAACATGTCTTCGATCGAAGGCTTTGTGGGTGATCCTAGCTTAGGGGCTTACAACGCATCTAAAGGGGCCGTACGGATT
M  S  K  S  A  A  L  D  C  A  L  K  D  Y  D  V  R  V  N  T  V  H  P  G  Y  I  K  T  P  L
ATGTCCAAGTCAGCTGCCTTAGATTGTGCCCTAAAGGACTACGATGTTCGGGTAAACACTGTTCACCCTGGCTACATCAAGACACCATTG
V  D  D  L  P  G  A  E  E  A  M  S  Q  R  T  K  T  P  M  G  H  I  G  E  P  N  D  I  A  Y
GTTGATGACCTACCAGGGGCCGAAGAAGCGATGTCACAACGGACCAAGACGCCAATGGGCCATATCGGTGAACCTAACGATATTGCCTAC
I  C  V  Y  L  A  S  N  E  S  K  F  A  T  G  S  E  F  V  V  D  G  G  Y  T  A  Q  *
ATCTGTGTTTACTTGGCTTCTAACGAATCTAAATTTGCAACGGGTTCTGAATTCGTAGTTGACGGTGGCTACACTGCTCAATAGAGTCGA
CAAGCTTGCGGCCGCACTCGAG                                                             SalI
      NotI     XhoI
```

*Lb*ADH

```
   M  S  N  R  L  D  G  K  V  A  I  I  T  G  G  T  L  G  I  G  L  A  I  A  T  K  F  V  E
CATATGTCTAACCGTTTGGATGGTAAGGTAGCAATCATTACAGGTGGTACGTTGGGTATCGGTTTAGCTATCGCCACGAAGTTCGTTGAA
NdeI          LbADH
E  G  A  K  V  M  I  T  G  R  H  S  D  V  G  E  K  A  A  K  S  V  G  T  P  D  Q  I  Q  F
GAAGGGGCTAAGGTCATGATTACCGGCCGGCACAGCGATGTTGGTGAAAAAGCAGCTAAGAGTGTCGGCACTCCTGATCAGATTCAATTT
F  Q  H  D  S  S  D  E  D  G  W  T  K  L  F  D  A  T  E  K  A  F  G  P  V  S  T  L  V  N
TTCCAACATGATTCTTCCGATGAAGACGGCTGGACGAAATTATTCGATGCAACGGAAAAAGCCTTTGGCCCAGTTTCTACATTAGTTAAT
N  A  G  I  A  V  N  K  S  V  E  E  T  T  T  A  E  W  R  K  L  L  A  V  N  L  D  G  V  F
AACGCTGGGATCGCGGTTAACAAGAGTGTCGAAGAAACCACGACTGCTGAATGGCGTAAATTATTAGCCGTCAACCTTGATGGTGTCTTC
F  G  T  R  L  G  I  Q  R  M  K  N  K  G  L  G  A  S  I  I  N  M  S  S  I  E  G  F  V  G
TTCGGTACCCGATTAGGGATTCAACGGATGAAGAACAAAGGCTTAGGGGCTTCCATCATCAACATGTCTTCGATCGAAGGCTTTGTGGGT
D  P  S  L  G  A  Y  N  A  S  K  G  A  V  R  I  M  S  K  S  A  A  L  D  C  A  L  K  D  Y
GATCCTAGCTTAGGGGCTTACAACGCATCTAAAGGGGCCGTACGGATTATGTCCAAGTCAGCTGCCTTAGATTGTGCCCTAAAGGACTAC
D  V  R  V  N  T  V  H  P  G  Y  I  K  T  P  L  V  D  D  L  P  G  A  E  E  A  M  S  Q  R
GATGTTCGGGTAAACACTGTTCACCCTGGCTACATCAAGACACCATTGGTTGATGACCTACCAGGGGCCGAAGAAGCGATGTCACAACGG
T  K  T  P  M  G  H  I  G  E  P  N  D  I  A  Y  I  C  V  Y  L  A  S  N  E  S  K  F  A  T
ACCAAGACGCCAATGGGCCATATCGGTGAACCTAACGATATTGCCTACATCTGTGTTTACTTGGCTTCTAACGAATCTAAATTTGCAACG
G  S  E  F  V  V  D  G  G  Y  T  A  Q  *  *
GGTTCTGAATTCGTAGTTGACGGTGGCTACACTGCTCAATAGTAGCGCGGATCCGAATTCGAGCTCCGTCGACAAGCTTGCGGCCGC
                                          BamHI          SalI      NotI
```

TDoT-L-*Pf*BAL

```
   M  I  I  N  E  T  A  D  D  I  V  Y  R  L  T  V  I  I  D  D  R  Y  E  S  L  K  N  L  I
CATATGATCATTAACGAAACTGCCGATGACATCGTTTATCGCCTGACAGTCATTATCGATGATCGCTACGAATCGCTGAAAAACCTGATT
NdeI          TDoT
T  L  R  A  D  R  L  E  M  I  I  N  D  N  V  S  T  I  L  A  S  I  T  S  I  E  G  R  A  S
ACCTTACGTGCAGATCGCTTGGAGATGATCATCAATGACAATGTGTCCACCATTCTCGCGAGCATTACTAGTATTGAAGGCCGTGCTAGC
                                                                  SpeI      Xa        NheI
G  G  G  S  G  G  G  S  G  G  G  S  G  S  M  A  M  I  T  G  G  E  L  V  V  R  T  L  I  K
GGCGGTGGGTCTGGAGGCGGCTCAGGTGGTGGGTCGGGATCCATGGCGATGATTACAGGCGGCGAACTGGTTGTTCGCACCCTAATAAAG
   3xGGGS-Linker                      BamHI          PfBAL
A  G  V  E  H  L  F  G  L  H  G  A  H  I  D  T  I  F  Q  A  C  L  D  H  D  V  P  I  I  D
GCTGGGGTCGAACATCTGTTCGGCCTGCACGGCGCGCATATCGATACGATTTTTCAAGCCTGTCTCGATCATGATGTGCCGATCATCGAC
T  R  H  E  A  A  A  G  H  A  A  E  G  Y  A  R  A  G  A  K  L  G  V  A  L  V  T  A  G  G
ACCCGCCATGAGGCCGCCGCAGGGCATGCGGCCGAGGGCTATGCCCGCGCTGGCGCCAAGCTGGGCGTGGCGCTGGTCACGGCGGGCGGG
G  F  T  N  A  V  T  P  I  A  N  A  W  L  D  R  T  P  V  L  F  L  T  G  S  G  A  L  R  D
GGATTTACCAATGCGGTCACGCCCATTGCCAACGCTTGGCTGGATCGCACGCCGGTGCTCTTCCTCACCGGATCGGGCGCGCTGCGTGAT
D  E  T  N  T  L  Q  A  G  I  D  Q  V  A  M  A  A  P  I  T  K  W  A  H  R  V  M  A  T  E
GATGAAACCAACACGTTGCAGGCGGGGATTGATCAGGTCGCCATGGCGGCGCCCATTACCAAATGGGCGCATCGGGTGATGGCAACCGAG
H  I  P  R  L  V  M  Q  A  I  R  A  A  L  S  A  P  R  G  P  V  L  L  D  L  P  W  D  I  L
CATATCCCACGGCTGGTGATGCAGGCGATCCGCGCCGCGTTGAGCGCGCCACGCGGGCCGGTGTTGCTGGATCTGCCGTGGGATATTCTG
M  N  Q  I  D  E  D  S  V  I  I  P  D  L  V  L  S  A  H  G  A  R  P  D  P  A  D  L  D  Q
ATGAACCAGATTGATGAGGATAGCGTCATTATCCCCGATCTGGTCTTGTCCGCACATGGGGCCAGACCCGACCCTGCCGATCTGGATCAG
A  L  A  L  L  R  K  A  E  R  P  V  I  V  L  G  S  E  A  S  R  T  A  R  K  T  A  L  S  A
GCTCTCGCGCTTTTGCGCAAGGCGGAGCGGCCGGTCATCGTGCTCGGCTCAGAAGCCTCGCGGACAGCGCGCAAGACGGCGCTTAGCGCA
F  V  A  A  T  G  V  P  V  F  A  D  Y  E  G  L  S  M  L  S  G  L  P  D  A  M  R  G  G  L
TTCGTGGCGGCGACTGGCGTGCCGGTGTTTGCCGATTATGAAGGGCTAAGCATGCTCTCGGGGCTGCCCGATGCTATGCGGGGCGGGCTG
V  Q  N  L  Y  S  F  A  K  A  D  A  A  P  D  L  V  L  M  L  G  A  R  F  G  L  N  T  G  H
GTGCAAAACCTCTATTCTTTTGCCAAAGCCGATGCCGCGCCAGATCTCGTGCTGATGCTGGGGGCGCGCTTTGGCCTTAACACCGGGCAT
G  S  G  Q  L  I  P  H  S  A  Q  V  I  Q  V  D  P  D  A  C  E  L  G  R  L  Q  G  I  A  L
GGATCTGGGCAGTTGATCCCCCATAGCGCGCAGGTCATTCAGGTCGACCCTGATGCCTGCGAGCTGGGACGCCTGCAGGGCATCGCTCTG
G  I  V  A  D  V  G  G  T  I  E  A  L  A  Q  A  T  A  Q  D  A  A  W  P  D  R  G  D  W  C
GGCATTGTGGCCGATGTGGGTGGGACCATCGAGGCTTTGGCGCAGGCCACCGCGCAAGATGCGGCTTGGCCGGATCGCGGCGACTGGTGC
A  K  V  T  D  L  A  Q  E  R  Y  A  S  I  A  A  K  S  S  S  E  H  A  L  H  P  F  H  A  S
GCCAAAGTGACGGATCTGGCGCAAGAGCGCTATGCCAGCATCGCTGCGAAATCGAGCAGCGAGCATGCGCTCCACCCCTTTCACGCCTCG
Q  V  I  A  K  H  V  D  A  G  V  T  V  V  A  D  G  A  L  T  Y  L  W  L  S  E  V  M  S  R
CAGGTCATTGCCAAACACGTCGATGCAGGGGTGACGGTGGTAGCGGATGGTGCGCTGACCTATCTCTGGCTGTCCGAAGTGATGAGCCGC
V  K  P  G  G  F  L  C  H  G  Y  L  G  S  M  G  V  G  F  G  T  A  L  G  A  Q  V  A  D  L
GTGAAACCCGGCGGTTTTCTCTGCCACGGCTATCTAGGCTCGATGGGCGTGGGCTTCGGCACGGCGCTGGGCGCGCAAGTGGCCGATCTT
E  A  G  R  R  T  I  L  V  T  G  D  G  S  V  G  Y  S  I  G  E  F  D  T  L  V  R  K  Q  L
GAAGCAGGCCGCCGCACGATCCTTGTGACCGGCGATGGCTCGGTGGGCTATAGCATCGGTGAATTTGATACGCTGGTGCGCAAACAATTG
P  L  I  V  I  I  M  N  N  Q  S  W  G  A  T  L  H  F  Q  Q  L  A  V  G  P  N  R  V  T  G
CCGCTGATCGTCATCATCATGAACAACCAAAGCTGGGGGGCGACATTGCATTTCCAGCAATTGGCCGTCGGCCCCAATCGCGTGACGGGC
T  R  L  E  N  G  S  Y  H  G  V  A  A  A  F  G  A  D  G  Y  H  V  D  S  V  E  S  F  S  A
ACCCGTTTGGAAAATGGCTCCTATCACGGGGTGGCCGCCGCCTTTGGCGCGGATGGCTATCATGTCGACAGTGTGGAGAGCTTTTCTGCG
A  L  A  Q  A  L  A  H  N  R  P  A  C  I  N  V  A  V  A  L  D  P  I  P  P  E  E  L  I  L
GCTCTGGCCCAAGCGCTCGCCCATAATCGCCCCGCCTGCATCAATGTCGCGGTCGCGCTCGATCCGATCCCGCCCGAAGAACTCATTCTG
I  G  M  D  P  F  A  *
ATCGGCATGGACCCCTTCGCATAAGCGGCCGCACTCGAG
                         NotI     XhoI
```

3HAMP-L-*Pf*BAL

```
   M  G  L  F  N  A  H  A  V  A  Q  Q  R  A  D  R  I  A  T  L  L  Q  S  F  A  D  G  Q  L
CATATGGGCCTGTTTAACGCCCATGCAGTTGCGCAGCAACGCGCGGATCGCATTGCGACTCTCCTGCAGTCCTTTGCGGATGGTCAGTTG
NdeI          3HAMP
D  T  A  V  G  E  A  P  A  P  G  Y  E  R  L  Y  D  S  L  R  A  L  Q  R  Q  L  R  E  Q  R
GACACCGCCGTGGGTGAAGCGCCAGCACCTGGTTACGAACGCCTGTATGACTCGCTTCGCGCCCTTCAGCGCCAACTGCGCGAACAACGT
A  E  L  Q  Q  V  E  S  L  E  A  G  L  A  E  M  S  R  Q  H  E  A  G  W  I  D  Q  T  I  P
```

```
GCGGAGTTACAACAGGTTGAGAGCCTGGAAGCAGGCTTGGCTGAAATGAGTCGGCAGCATGAAGCAGGGTGGATTGACCAGACGATTCCG
A  E  R  L  E  G  R  A  A  R  I  A  K  G  V  N  E  L  V  A  A  H  I  A  V  K  M  K  V  V
GCTGAACGGTTAGAGGGCCGTGCAGCACGTATCGCCAAAGGCGTGAATGAGCTGGTTGCTGCGCACATTGCGGTGAAAATGAAAGTCGTG
S  V  V  T  A  Y  G  Q  G  N  F  E  P  L  M  D  R  L  P  G  K  K  A  Q  I  T  E  A  I  D
AGCGTAGTCACCGCGTATGGCCAAGGGAACTTCGAACCGCTCATGGATCGCCTGCCGGGTAAGAAAGCCCAGATCACGGAGGCCATTGAT
G  V  R  E  R  L  R  G  A  A  E  A  T  S  A  Q  L  A  T  A  A  A  Y  N  T  S  I  E  G  R  A
GGCGTACGTGAACGCCTGCGTGGAGCTGCTGAAGCGACCTCTGCGCAGCTGGCCACAGCCGCCTACAATACTAGTATTGAAGGCCGTGCT
                                                                        SpeI      Xa      NheI
S  G  G  G  S  G  G  G  S  G  G  G  S  G  S  M  A  M  I  T  G  G  E  L  V  V  R  T  L  I
AGCGGCGGTGGGTCTGGAGGCGGCTCAGGTGGTGGGTCGGGATCCATGGCGATGATTACAGGCGGCGAACTGGTTGTTCGCACCCTAATA
     3xGGGS-Linker                          BamHI                PfBAL
K  A  G  V  E  H  L  F  G  L  H  G  A  H  I  D  T  I  F  Q  A  C  L  D  H  D  V  P  I  I
AAGGCTGGGGTCGAACATCTGTTCGGCCTGCACGGCGCGCATATCGATACGATTTTTCAAGCCTGTCTCGATCATGATGTGCCGATCATC
D  T  R  H  E  A  A  A  G  H  A  A  E  G  Y  A  R  A  G  A  K  L  G  V  A  L  V  T  A  G
GACACCCGCCATGAGGCCGCCGCAGGGCATGCGGCCGAGGGCTATGCCCGCGCTGGCGCCAAGCTGGGCGTGGCGCTGGTCACGGCGGGC
G  G  F  T  N  A  V  T  P  I  A  N  A  W  L  D  R  T  P  V  L  F  L  T  G  S  G  A  L  R
GGGGGATTTACCAATGCGGTCACGCCCATTGCCAACGCTTGGCTGGATCGCACGCCGGTGCTCTTCCTCACCGGATCGGGCGCGCTGCGT
D  D  E  T  N  T  L  Q  A  G  I  D  Q  V  A  M  A  A  P  I  T  K  W  A  H  R  V  M  A  T
GATGATGAAACCAACACGTTGCAGGCGGGGATTGATCAGGTCGCCATGGCGGCGCCCATTACCAAATGGGCGCATCGGGTGATGGCAACC
E  H  I  P  R  L  V  M  Q  A  I  R  A  A  L  S  A  P  R  G  P  V  L  L  D  L  P  W  D  I
GAGCATATCCCACGGCTGGTGATGCAGGCGATCCGCGCCGCGTTGAGCGCGCCACGCGGGCCGGTGTTGCTGGATCTGCCGTGGGATATT
L  M  N  Q  I  D  E  D  S  V  I  I  P  D  L  V  L  S  A  H  G  A  R  P  D  P  A  D  L  D
CTGATGAACCAGATTGATGAGGATAGCGTCATTATCCCCGATCTGGTCTTGTCCGCACATGGGGCCAGACCCGACCCTGCCGATCTGGAT
Q  A  L  A  L  L  R  K  A  E  R  P  V  I  V  L  G  S  E  A  S  R  T  A  R  K  T  A  L  S
CAGGCTCTCGCGCTTTTGCGCAAGGCGGAGCGGCCGGTCATCGTGCTCGGCTCAGAAGCCTCGCGGACAGCGCGCAAGACGGCGCTTAGC
A  F  V  A  A  T  G  V  P  V  F  A  D  Y  E  G  L  S  M  L  S  G  L  P  D  A  M  R  G  G
GCATTCGTGGCGGCGACTGGCGTGCCGGTGTTTGCCGATTATGAAGGGCTAAGCATGCTCTCGGGGCTGCCCGATGCTATGCGGGGCGGG
L  V  Q  N  L  Y  S  F  A  K  A  D  A  A  P  D  L  V  L  M  L  G  A  R  F  G  L  N  T  G
CTGGTGCAAAACCTCTATTCTTTTGCCAAAGCCGATGCCGCGCCAGATCTCGTGCTGATGCTGGGGGCGCGCTTTGGCCTTAACACCGGG
H  G  S  G  Q  L  I  P  H  S  A  Q  V  I  Q  V  D  P  D  A  C  E  L  G  R  L  Q  G  I  A
CATGGATCTGGGCAGTTGATCCCCCATAGCGCGCAGGTCATTCAGGTCGACCCTGATGCCTGCGAGCTGGGACGCCTGCAGGGCATCGCT
L  G  I  V  A  D  V  G  G  T  I  E  A  L  A  Q  A  T  A  Q  D  A  A  W  P  D  R  G  D  W
CTGGGCATTGTGGCCGATGTGGGTGGGACCATCGAGGCTTTGGCGCAGGCCACCGCGCAAGATGCGGCTTGGCCGGATCGCGGCGACTGG
C  A  K  V  T  D  L  A  Q  E  R  Y  A  S  I  A  A  K  S  S  S  E  H  A  L  H  P  F  H  A
TGCGCCAAAGTGACGGATCTGGCGCAAGAGCGCTATGCCAGCATCGCTGCGAAATCGAGCAGCGAGCATGCGCTCCACCCCTTTCACGCC
S  Q  V  I  A  K  H  V  D  A  G  V  T  V  V  A  D  G  A  L  T  Y  L  W  L  S  E  V  M  S
TCGCAGGTCATTGCCAAACACGTCGATGCAGGGGTGACGGTGGTAGCGGATGGTGCGCTGACCTATCTCTGGCTGTCCGAAGTGATGAGC
R  V  K  P  G  G  F  L  C  H  G  Y  L  G  S  M  G  V  G  F  G  T  A  L  G  A  Q  V  A  D
CGCGTGAAACCCGGCGGTTTTCTCTGCCACGGCTATCTAGGCTCGATGGGCGTGGGCTTCGGCACGGCGCTGGGCGCGCAAGTGGCCGAT
L  E  A  G  R  R  T  I  L  V  T  G  D  G  S  V  G  Y  S  I  G  E  F  D  T  L  V  R  K  Q
CTTGAAGCAGGCCGCCGCACGATCCTTGTGACCGGCGATGGCTCGGTGGGCTATAGCATCGGTGAATTTGATACGCTGGTGCGCAAACAA
L  P  L  I  V  I  I  M  N  N  Q  S  W  G  A  T  L  H  F  Q  Q  L  A  V  G  P  N  R  V  T
TTGCCGCTGATCGTCATCATCATGAACAACCAAAGCTGGGGGGCGACATTGCATTTCCAGCAATTGGCCGTCGGCCCCAATCGCGTGACG
G  T  R  L  E  N  G  S  Y  H  G  V  A  A  A  F  G  A  D  G  Y  H  V  D  S  V  E  S  F  S
GGCACCCGTTTGGAAAATGGCTCCTATCACGGGGTGGCCGCCGCCTTTGGCGCGGATGGCTATCATGTCGACAGTGTGGAGAGCTTTTCT
A  A  L  A  Q  A  L  A  H  N  R  P  A  C  I  N  V  A  V  A  L  D  P  I  P  P  E  E  L  I
GCGGCTCTGGCCCAAGCGCTCGCCCATAATCGCCCCGCCTGCATCAATGTCGCGGTCGCGCTCGATCCGATCCCGCCCGAAGAACTCATT
L  I  G  M  D  P  F  A  *
CTGATCGGCATGGACCCCTTCGCATAAGCGGCCGCACTCGAG
                            NotI     XhoI
```

*Pf*BAL

```
   M  A  M  I  T  G  G  E  L  V  V  R  T  L  I  K  A  G  V  E  H  L  F  G  L  H  G  A  H
ACCATGGCGATGATTACAGGCGGCGAACTGGTTGTTCGCACCCTAATAAAGGCTGGGGTCGAACATCTGTTCGGCCTGCACGGCGCGCAT
  NcoI          PfBAL
I  D  T  I  F  Q  A  C  L  D  H  D  V  P  I  I  D  T  R  H  E  A  A  A  G  H  A  A  E  G
ATCGATACGATTTTTCAAGCCTGTCTCGATCATGATGTGCCGATCATCGACACCCGCCATGAGGCCGCCGCAGGGCATGCGGCCGAGGGC
Y  A  R  A  G  A  K  L  G  V  A  L  V  T  A  G  G  G  F  T  N  A  V  T  P  I  A  N  A  W
TATGCCCGCGCTGGCGCCAAGCTGGGCGTGGCGCTGGTCACGGCGGGCGGGGGGATTTACCAATGCGGTCACGCCCATTGCCAACGCTTGG
L  D  R  T  P  V  L  F  L  T  G  S  G  A  L  R  D  D  E  T  N  T  L  Q  A  G  I  D  Q  V
CTGGATCGCACGCCGGTGCTCTTCCTCACCGGATCGGGCGCGCTGCGTGATGATGAAACCAACACGTTGCAGGCGGGGATTGATCAGGTC
A  M  A  A  P  I  T  K  W  A  H  R  V  M  A  T  E  H  I  P  R  L  V  M  Q  A  I  R  A  A
GCGATGGCGGCGCCCATTACCAAATGGGCGCATCGGGTGATGGCAACCGAGCATATCCCACGGCTGGTGATGCAGGCGATCCGCGCCGCG
L  S  A  P  R  G  P  V  L  L  D  L  P  W  D  I  L  M  N  Q  I  D  E  D  S  V  I  I  P  D
TTGAGCGCGCCACGCGGGCCGGTGTTGCTGGATCTGCCGTGGGATATTCTGATGAACCAGATTGATGAGGATAGCGTCATTATCCCCGAT
L  V  L  S  A  H  G  A  R  P  D  P  A  D  L  D  Q  A  L  A  L  L  R  K  A  E  R  P  V  I
CTGGTCTTGTCCGCGCATGGGGCCAGACCCGACCCTGCCGATCTGGATCAGGCTCTCGCGCTTTTGCGCAAGGCGGAGCGGCCGGTCATC
V  L  G  S  E  A  S  R  T  A  R  K  T  A  L  S  A  F  V  A  A  T  G  V  P  V  F  A  D  Y
GTGCTCGGCTCAGAAGCCTCGCGGACAGCGCGCAAGACGGCGCTTAGCGCCTTCGTGGCGGCGACTGGCGTGCCGGTGTTTGCCGATTAT
E  G  L  S  M  L  S  G  L  P  D  A  M  R  G  G  L  V  Q  N  L  Y  S  F  A  K  A  D  A  A
GAAGGGCTAAGCATGCTCTCGGGGCTGCCCGATGCTATGCGGGGCGGGCTGGTGCAAAACCTCTATTCTTTTGCCAAAGCCGATGCCGCG
P  D  L  V  L  M  L  G  A  R  F  G  L  N  T  G  H  G  S  G  Q  L  I  P  H  S  A  Q  V  I
CCAGATCTCGTGCTGATGCTGGGGGCGCGCTTTGGCCTTAACACCGGGCATGGATCTGGGCAGTTGATCCCCCATAGCGCGCAGGTCATT
Q  V  D  P  D  A  C  E  L  G  R  L  Q  G  I  A  L  G  I  V  A  D  V  G  G  T  I  E  A  L
CAGGTCGACCCTGATGCCTGCGAGCTGGGACGCCTGCAGGGCATCGCTCTGGGCATTGTGGCCGATGTGGGTGGGACCATCGAGGCTTTG
A  Q  A  T  A  Q  D  A  A  W  P  D  R  G  D  W  C  A  K  V  T  D  L  A  Q  E  R  Y  A  S
GCGCAGGCCACCGCGCAAGATGCGGCTTGGCCGGATCGCGGCGACTGGTGCGCCAAAGTGACGGATCTGGCGCAAGAGCGCTATGCCAGC
I  A  A  K  S  S  S  E  H  A  L  H  P  F  H  A  S  Q  V  I  A  K  H  V  D  A  G  V  T  V
ATCGCTGCGAAATCGAGCAGCGAGCATGCGCTCCACCCCTTTCACGCCTCGCAGGTCATTGCCAAACACGTCGATGCAGGGGTGACGGTG
V  A  D  G  A  L  T  Y  L  W  L  S  E  V  M  S  R  V  K  P  G  G  F  L  C  H  G  Y  L  G
```

```
GTAGCGGATGGTGCGCTGACCTATCTCTGGCTGTCCGAAGTGATGAGCCGCGTGAAACCCGGCGGTTTTCTCTGCCACGGCTATCTAGGC
S  M  G  V  G  F  G  T  A  L  G  A  Q  V  A  D  L  E  A  G  R  R  T  I  L  V  T  G  D  G
TCGATGGGCGTGGGCTTCGGCACGGCGCTGGGCGCGCAAGTGGCCGATCTTGAAGCAGGCCGCCGCACGATCCTTGTGACCGGCGATGGC
S  V  G  Y  S  I  G  E  F  D  T  L  V  R  K  Q  L  P  L  I  V  I  I  M  N  N  Q  S  W  G
TCGGTGGGCTATAGCATCGGTGAATTTGATACGCTGGTGCGCAAACAATTGCCGCTGATCGTCATCATCATGAACAACCAAAGCTGGGGG
A  T  L  H  F  Q  Q  L  A  V  G  P  N  R  V  T  G  T  R  L  E  N  G  S  Y  H  G  V  A  A
GCGACATTGCATTTCCAGCAATTGGCCGTCGGCCCCAATCGCGTGACGGGCACCCGTTTGGAAAATGGCTCCTATCACGGGGTGGCCGCC
A  F  G  A  D  G  Y  H  V  D  S  V  E  S  F  S  A  A  L  A  Q  A  L  A  H  N  R  P  A  C
GCCTTTGGCGCGGATGGCTATCATGTCGACAGTGTGGAGAGCTTTTCTGCGGCTCTGGCCCAAGCGCTCGCCCATAATCGCCCCGCCTGC
I  N  V  A  V  A  L  D  P  I  P  P  E  E  L  I  L  I  G  M  D  P  F  G  S  H  H  H  H  H
ATCAATGTCGCGGTCGCGCTCGATCCGATCCCGCCCGAAGAACTCATTCTGATCGGCATGGACCCCTTCGATCTCATCACCATCACCATC
H  *                                                                                His-Tag
ACTAAGCTTCT
      HindIII
```

TDoT-L-*Pp*BFD

```
   M  I  I  N  E  T  A  D  D  I  V  Y  R  L  T  V  I  I  D  D  R  Y  E  S  L  K  N  L  I
CATATGATCATTAACGAAACTGCCGATGACATCGTTTATCGCCTGACAGTCATTATCGATGATCGCTACGAATCGCTGAAAAACCTGATT
NdeI           TDoT
T  L  R  A  D  R  L  E  M  I  I  N  D  N  V  S  T  I  L  A  S  I  T  S  I  E  G  R  A  S
ACCTTACGTGCAGATCGCTTGGAGATGATCATCAATGACAATGTGTCCACCATTCTCGCGAGCATTACTAGTATTGAAGGCCGTGCTAGC
                                                                  SpeI     Xa       NheI
G  G  G  S  G  G  G  S  G  G  G  S  G  S  M  A  S  V  H  G  T  T  Y  E  L  L  R  R  Q  G
GGCGGTGGGTCTGGAGGCGGCTCAGGTGGTGGGTCGGGATCCATGGCTTCGGTACACGGCACCACATACGAACTCTTGCGACGTCAAGGC
3xGGGS-Linker                        BamHI          PpBFD
I  D  T  V  F  G  N  P  G  S  N  E  L  P  F  L  K  D  F  P  E  D  F  R  Y  I  L  A  L  Q
ATCGATACGGTCTTCGGCAATCCTGGCTCGAACGAGCTCCCGTTTTTGAAGGACTTTCCAGAGGACTTTCGATACATCCTGGCTTTGCAG
E  A  C  V  V  G  I  A  D  G  Y  A  Q  A  S  R  K  P  A  F  I  N  L  H  S  A  A  G  T  G
GAAGCGTGTGTGGTGGGCATTGCAGACGGCTATGCGCAAGCCAGTCGGAAGCCGGCTTTCATTAACCTGCATTCTGCTGCTGGTACCGGC
N  A  M  G  A  L  S  N  A  W  N  S  H  S  P  L  I  V  T  A  G  Q  Q  T  R  A  M  I  G  V
AATGCTATGGGTGCACTCAGTAACGCCTGGAACTCACATTCCCCGCTGATCGTCACTGCCGGCCAGCAGACCAGGGCGATGATTGGCGTT
E  A  L  L  T  N  V  D  A  A  N  L  P  R  P  L  V  K  W  S  Y  E  P  A  S  A  A  E  V  P
GAAGCTCTGCTGACCAACGTCGATGCCGCCAACCTGCCACGACCACTTGTCAAATGGAGCTACGAGCCCGCAAGCGCAGCAGAAGTCCCT
H  A  M  S  R  A  I  H  M  A  S  M  A  P  Q  G  P  V  Y  L  S  V  P  Y  D  D  W  D  K  D
CATGCGATGAGCAGGGCTATCCATATGGCAAGCATGGCGCCACAAGGCCCTGTCTATCTTTCGGTGCCATATGACGATTGGGATAAGGAT
A  D  P  Q  S  H  H  L  F  D  R  H  V  S  S  S  V  R  L  N  D  Q  D  L  D  I  L  V  K  A
GCTGATCCTCAGTCCCACCACCTTTTTGATCGCCATGTCAGTTCATCAGTACGCCTGAACGACCAGGATCTCGATATTCTGGTGAAAGCT
L  N  S  A  S  N  P  A  I  V  L  G  P  D  V  D  A  A  N  A  N  A  D  C  V  M  L  A  E  R
CTCAACAGCGCATCCAACCCGGCGATCGTCCTGGGCCCGGACGTCGACGCAGCAAATGCGAACGCAGACTGCGTCATGTTGGCCGAACGC
L  K  A  P  V  W  V  A  P  S  A  P  R  C  P  F  P  T  R  H  P  C  F  R  G  L  M  P  A  G
CTCAAAGCTCCGGTTTGGGTTGCGCCATCCGCTCCACGCTGCCCATTCCCTACCCGTCATCCTTGCTTCCGTGGATTGATGCCAGCTGGC
I  A  A  I  S  Q  L  L  E  G  H  D  V  V  L  V  I  G  A  P  V  F  R  Y  H  Q  Y  D  P  G
ATCGCAGCGATTTCTCAGCTGCTCGAAGGTCACGATGTGGTTTTGGTAATCGGCGCTCCAGTGTTCCGTTACCACCAATACGACCCAGGT
Q  Y  L  K  P  G  T  R  L  I  S  V  T  C  D  P  L  E  A  A  R  A  P  M  G  D  A  I  V  A
CAATATCTCAAACCTGGCACGCGATTGATTTCGGTGACCTGCGACCCGCTCGAAGCTGCACGCGCGCCAATGGGCGATGCGATCGTGGCA
D  I  G  A  M  A  S  A  L  A  N  L  V  E  E  S  S  R  Q  L  P  T  A  A  P  E  P  A  K  V
GACATTGGTGCGATGGCTAGCGCTCTTGCCAACTTGGTTGAAGAGAGCAGCCGCCAGCTCCCAACTGCAGCTCCGGAACCCGCGAAGGTT
D  Q  D  A  G  R  L  H  P  E  T  V  F  D  T  L  N  D  M  A  P  E  N  A  I  Y  L  N  E  S
GACCAAGACGCTGGCCGACTTCACCCAGAGACAGTGTTCGACACACTGAACGACATGGCCCCGGAGAATGCGATTTACCTGAACGAGTCG
T  S  T  T  A  Q  M  W  Q  R  L  N  M  R  N  P  G  S  Y  Y  F  C  A  A  G  G  L  G  F  A
ACTTCAACGACCGCCCAAATGTGGCAGCGCCTGAACATGCGCAACCCTGGTAGCTACTACTTCTGTGCAGCTGGCGGACTGGGCTTCGCC
L  P  A  A  I  G  V  Q  L  A  E  P  E  R  Q  V  I  A  V  I  G  D  G  S  A  N  Y  S  I  S
CTGCCTGCAGCAATTGGCGTTCAACTCGCAGAACCCGAGCGACAAGTCATCGCCGTCATTGGCGACGGATCGGCGAACTACAGCATTAGT
A  L  W  T  A  A  Q  Y  N  I  P  T  I  F  V  I  M  N  N  G  T  Y  G  A  L  R  W  F  A  G
GCGTTGTGGACTGCAGCTCAGTACAACATCCCCACTATCTTCGTGATCATGAACAACGGCACCTACGGTGCGTTGCGATGGTTTGCCGGC
V  L  E  A  E  N  V  P  G  Q  D  V  P  G  I  D  F  R  A  L  A  K  G  Y  G  V  Q  A  L  K
GTTCTCGAAGCAGAAAACGTTCCTGGGCAGGATGTGCCAGGGATCGACTTCCGCGCACTCGCCAAGGGCTATGGGGTCCAAGCGCTGAAA
A  D  N  L  E  Q  L  K  G  S  L  Q  E  A  L  S  A  K  G  P  V  L  I  E  V  S  T  V  S  P
GCCGACAACCTTGAGCAGCTCAAGGGTTCGCTACAAGAAGCGCTTTCTGCCAAAGGCCCGGTACTTATCGAAGTAAGCACCGTAAGCCCG
V  K  R  S  *
GTGAAGAGATCTTAAGCGGCCGCACTCGAG
          NotI     XhoI
```

3HAMP-L-*Pp*BFD

```
   M  G  L  F  N  A  H  A  V  A  Q  Q  R  A  D  R  I  A  T  L  L  Q  S  F  A  D  G  Q  L
CATATGGGCCTGTTTAACGCCCATGCAGTTGCGCAGCAACGCGCGGATCGCATTGCGACTCTCCTGCAGTCCTTTGCGGATGGTCAGTTG
NdeI           TDoT
D  T  A  V  G  E  A  P  A  P  G  Y  E  R  L  Y  D  S  L  R  A  L  Q  R  Q  L  R  E  Q  R
GACACCGCCGTGGGTGAAGCGCCAGCACCTGGTTACGAACGCCTGTATGACTCGCTTCGCGCCCTTCAGCGCCAACTGCGCGAACAACGT
A  E  L  Q  Q  V  E  S  L  E  A  G  L  A  E  M  S  R  Q  H  E  A  G  W  I  D  Q  T  I  P
GCGGAGTTACAACAGGTTGAGAGCCTGGAAGCAGGCTTGGCTGAAATGAGTCGGCAGCATGAAGCAGGGTGGATTGACCAGACGATTCCG
A  E  R  L  E  G  R  A  A  R  I  A  K  G  V  N  E  L  V  A  A  H  I  A  V  K  M  K  V  V
GCTGAACGGTTAGAGGGCCGTGCAGCACGTATCGCCAAAGGCGTGAATGAGCTGGTTGCTGCGCACATTGCGGTGAAAATGAAAGTCGTG
S  V  V  T  A  Y  G  Q  G  N  F  E  P  L  M  D  R  L  P  G  K  K  A  Q  I  T  E  A  I  D
AGCGTAGTCACCGCGTATGGCCAAGGGAACTTCGAACCGCTCATGGATCGCCTGCCGGGTAAGAAAGCCCAGATCACGGAGGCCATTGAT
G  V  R  E  R  L  R  G  A  A  E  A  T  S  A  Q  L  A  T  A  A  Y  N  T  S  I  E  G  R  A
GGCGTACGTGAACGCCTGCGTGGAGCTGCTGAAGCGACCTCTGCGCAGCTGGCCACAGCCGCCTACAATACTAGTATTGAAGGCCGTGCT
                                                                  SpeI     Xa       NheI
S  G  G  G  S  G  G  G  S  G  G  G  S  G  S  M  A  S  V  H  G  T  T  Y  E  L  L  R  R  Q
```

```
AGCGGCGGTGGGTCTGGAGGCGGCTCAGGTGGTGGGTCGGGATCCATGGCTTCGGTACACGGCACCACATACGAACTCTTGCGACGTCAA
        3xGGGS-Linker                    BamHI          PpBFD
G  I  D  T  V  F  G  N  P  G  S  N  E  L  P  F  L  K  D  F  P  E  D  F  R  Y  I  L  A  L
GGCATCGATACGGTCTTCGGCAATCCTGGCTCGAACGAGCTCCCGTTTTTGAAGGACTTTCCAGAGGACTTTCGATACATCCTGGCTTTG
Q  E  A  C  V  V  G  I  A  D  G  Y  A  Q  A  S  R  K  P  A  F  I  N  L  H  S  A  A  G  T
CAGGAAGCGTGTGTGGTGGGCATTGCAGACGGCTATGCGCAAGCCAGTCGGAAGCCGGCTTTCATTAACCTGCATTCTGCTGCTGGTACC
G  N  A  M  G  A  L  S  N  A  W  N  S  H  S  P  L  I  V  T  A  G  Q  Q  T  R  A  M  I  G
GGCAATGCTATGGGTGCACTCAGTAACGCCTGGAACTCACATTCCCCGCTGATCGTCACTGCCGGCCAGCAGACCAGGGCGATGATTGGC
V  E  A  L  L  T  N  V  D  A  A  N  L  P  R  P  L  V  K  W  S  Y  E  P  A  S  A  A  E  V
GTTGAAGCTCTGCTGACCAACGTCGATGCCGCCAACCTGCCACGACCACTTGTCAAATGGAGCTACGAGCCCGCAAGCGCAGCAGAAGTC
P  H  A  M  S  R  A  I  H  M  A  S  M  A  P  Q  G  P  V  Y  L  S  V  P  Y  D  D  W  D  K
CCTCATGCGATGAGCAGGGCTATCCATATGGCAAGCATGGCGCCACAAGGCCCTGTCTATCTTTCGGTGCCATATGACGATTGGGATAAG
D  A  D  P  Q  S  H  H  L  F  D  R  H  V  S  S  S  V  R  L  N  D  Q  D  L  D  I  L  V  K
GATGCTGATCCTCAGTCCCACCACCTTTTTGATCGCCATGTCAGTTCATCAGTACGCCTGAACGACCAGGATCTCGATATTCTGGTGAAA
A  L  N  S  A  S  N  P  A  I  V  L  G  P  D  V  D  A  A  N  A  N  A  D  C  V  M  L  A  E
GCTCTCAACAGCGCATCCAACCCGGCGATCGTCCTGGGCCCGGACGTCGACGCAGCAAATGCGAACGCAGACTGCGTCATGTTGGCCGAA
R  L  K  A  P  V  W  V  A  P  S  A  P  R  C  P  F  P  T  R  H  P  C  F  R  G  L  M  P  A
CGCCTCAAAGCTCCGGTTTGGGTTGCGCCATCCGCTCCACGCTGCCCATTCCCTACCCGTCATCCTTGCTTCCGTGGATTGATGCCAGCT
G  I  A  A  I  S  Q  L  L  E  G  H  D  V  V  L  V  I  G  A  P  V  F  R  Y  H  Q  Y  D  P
GGCATCGCAGCGATTTCTCAGCTGCTCGAAGGTCACGATGTGGTTTTGGTAATCGGCGCTCCAGTGTTCCGTTACCACCAATACGACCCA
G  Q  Y  L  K  P  G  T  R  L  I  S  V  T  C  D  P  L  E  A  A  R  A  P  M  G  D  A  I  V
GGTCAATATCTCAAACCTGGCACGCGATTGATTTCGGTGACCTGCGACCCGCTCGAAGCTGCACGCGCGCCAATGGGCGATGCGATCGTG
A  D  I  G  A  M  A  S  A  L  A  N  L  V  E  E  S  S  R  Q  L  P  T  A  A  P  E  P  A  K
GCAGACATTGGTGCGATGGCTAGCGCTCTTGCCAACTTGGTTGAAGAGAGCAGCCGCCAGCTCCCAACTGCAGCTCCGGAACCCGCGAAG
V  D  Q  D  A  G  R  L  H  P  E  T  V  F  D  T  L  N  D  M  A  P  E  N  A  I  Y  L  N  E
GTTGACCAAGACGCTGGCCGACTTCACCCAGAGACAGTGTTCGACACACTGAACGACATGGCCCCGGAGAATGCGATTTACCTGAACGAG
S  T  S  T  T  A  Q  M  W  Q  R  L  N  M  R  N  P  G  S  Y  Y  F  C  A  A  G  G  L  G  F
TCGACTTCAACGACCGCCCAAATGTGGCAGCGCCTGAACATGCGCAACCCTGGTAGCTACTACTTCTGTGCAGCTGGCGGACTGGGCTTC
A  L  P  A  A  I  G  V  Q  L  A  E  P  E  R  Q  V  I  A  V  I  G  D  G  S  A  N  Y  S  I
GCCCTGCCTGCAGCAATTGGCGTTCAACTCGCAGAACCCGAGCGACAAGTCATCGCCGTCATTGGCGACGGATCGGCGAACTACAGCATT
S  A  L  W  T  A  A  Q  Y  N  I  P  T  I  F  V  I  M  N  N  G  T  Y  G  A  L  R  W  F  A
AGTGCGTTGTGGACTGCAGCTCAGTACAACATCCCCACTATCTTCGTGATCATGAACAACGGCACCTACGGTGCGTTGCGATGGTTTGCC
G  V  L  E  A  E  N  V  P  G  Q  D  V  P  G  I  D  F  R  A  L  A  K  G  Y  G  V  Q  A  L
GGCGTTCTCGAAGCAGAAAACGTTCCTGGGCAGGATGTGCCAGGGATCGACTTCCGCGCACTCGCCAAGGGCTATGGGGTCCAAGCGCTG
K  A  D  N  L  E  Q  L  K  G  S  L  Q  E  A  L  S  A  K  G  P  V  L  I  E  V  S  T  V  S
AAAGCCGACAACCTTGAGCAGCTCAAGGGTTCGCTACAAGAAGCGCTTTCTGCCAAAGGCCCGGTACTTATCGAAGTAAGCACCGTAAGC
P  V  K  R  S  *
CCGGTGAAGAGATCTTAAGCGGCCGCACTCGAG
                   NotI    XhoI
```

*Pp*BFD

```
M  A  S  V  H  G  T  T  Y  E  L  L  R  R  Q  G  I  D  T  V  F  G  N  P  G  S  N  E  L  P
ATGGCTTCGGTACACGGCACCACATACGAACTCTTGCGACGTCAAGGCATCGATACGGTCTTCGGCAATCCTGGCTCGAACGAGCTCCCG
   PpBFD
F  L  K  D  F  P  E  D  F  R  Y  I  L  A  L  Q  E  A  C  V  V  G  I  A  D  G  Y  A  Q  A
TTTTTGAAGGACTTTCCAGAGGACTTTCGATACATCCTGGCTTTGCAGGAAGCGTGTGTGGTGGGCATTGCAGACGGCTATGCGCAAGCC
S  R  K  P  A  F  I  N  L  H  S  A  A  G  T  G  N  A  M  G  A  L  S  N  A  W  N  S  H  S
AGTCGGAAGCCGGCTTTCATTAACCTGCATTCTGCTGCTGGTACCGGCAATGCTATGGGTGCACTCAGTAACGCCTGGAACTCACATTCC
P  L  I  V  T  A  G  Q  Q  T  R  A  M  I  G  V  E  A  L  L  T  N  V  D  A  A  N  L  P  R
CCGCTGATCGTCACTGCCGGCCAGCAGACCAGGGCGATGATTGGCGTTGAAGCTCTGCTGACCAACGTCGATGCCGCCAACCTGCCACGA
P  L  V  K  W  S  Y  E  P  A  S  A  A  E  V  P  H  A  M  S  R  A  I  H  M  A  S  M  A  P
CCACTTGTCAAATGGAGCTACGAGCCCGCAAGCGCAGCAGAAGTCCCTCATGCGATGAGCAGGGCTATCCATATGGCAAGCATGGCGCCA
Q  G  P  V  Y  L  S  V  P  Y  D  D  W  D  K  D  A  D  P  Q  S  H  H  L  F  D  R  H  V  S
CAAGGCCCTGTCTATCTTTCGGTGCCATATGACGATTGGGATAAGGATGCTGATCCTCAGTCCCACCACCTTTTTGATCGCCATGTCAGT
S  S  V  R  L  N  D  Q  D  L  D  I  L  V  K  A  L  N  S  A  S  N  P  A  I  V  L  G  P  D
TCATCAGTACGCCTGAACGACCAGGATCTCGATATTCTGGTGAAAGCTCTCAACAGCGCATCCAACCCGGCGATCGTCCTGGGCCCGGAC
V  D  A  A  N  A  N  A  D  C  V  M  L  A  E  R  L  K  A  P  V  W  V  A  P  S  A  P  R  C
GTCGACGCAGCAAATGCGAACGCAGACTGCGTCATGTTGGCCGAACGCCTCAAAGCTCCGGTTTGGGTTGCGCCATCCGCTCCACGCTGC
P  F  P  T  R  H  P  C  F  R  G  L  M  P  A  G  I  A  A  I  S  Q  L  L  E  G  H  D  V  V
CCATTCCCTACCCGTCATCCTTGCTTCCGTGGATTGATGCCAGCTGGCATCGCAGCGATTTCTCAGCTGCTCGAAGGTCACGATGTGGTT
L  V  I  G  A  P  V  F  R  Y  H  Q  Y  D  P  G  Q  Y  L  K  P  G  T  R  L  I  S  V  T  C
TTGGTAATCGGCGCTCCAGTGTTCCGTTACCACCAATACGACCCAGGTCAATATCTCAAACCTGGCACGCGATTGATTTCGGTGACCTGC
D  P  L  E  A  A  R  A  P  M  G  D  A  I  V  A  D  I  G  A  M  A  S  A  L  A  N  L  V  E
GACCCGCTCGAAGCTGCACGCGCGCCAATGGGCGATGCGATCGTGGCAGACATTGGTGCGATGGCTAGCGCTCTTGCCAACTTGGTTGAA
E  S  S  R  Q  L  P  T  A  A  P  E  P  A  K  V  D  Q  D  A  G  R  L  H  P  E  T  V  F  D
GAGAGCAGCCGCCAGCTCCCAACTGCAGCTCCGGAACCCGCGAAGGTTGACCAAGACGCTGGCCGACTTCACCCAGAGACAGTGTTCGAC
T  L  N  D  M  A  P  E  N  A  I  Y  L  N  E  S  T  S  T  T  A  Q  M  W  Q  R  L  N  M  R
ACACTGAACGACATGGCCCCGGAGAATGCGATTTACCTGAACGAGTCGACTTCAACGACCGCCCAAATGTGGCAGCGCCTGAACATGCGC
N  P  G  S  Y  Y  F  C  A  A  G  G  L  G  F  A  L  P  A  A  I  G  V  Q  L  A  E  P  E  R
AACCCTGGTAGCTACTACTTCTGTGCAGCTGGCGGACTGGGCTTCGCCCTGCCTGCAGCAATTGGCGTTCAACTCGCAGAACCCGAGCGA
Q  V  I  A  V  I  G  D  G  S  A  N  Y  S  I  S  A  L  W  T  A  A  Q  Y  N  I  P  T  I  F
CAAGTCATCGCCGTCATTGGCGACGGATCGGCGAACTACAGCATTAGTGCGTTGTGGACTGCAGCTCAGTACAACATCCCCACTATCTTC
V  I  M  N  N  G  T  Y  G  A  L  R  W  F  A  G  V  L  E  A  E  N  V  P  G  Q  D  V  P  G
GTGATCATGAACAACGGCACCTACGGTGCGTTGCGATGGTTTGCCGGCGTTCTCGAAGCAGAAAACGTTCCTGGGCAGGATGTGCCAGGG
I  D  F  R  A  L  A  K  G  Y  G  V  Q  A  L  K  A  D  N  L  E  Q  L  K  G  S  L  Q  E  A
ATCGACTTCCGCGCACTCGCCAAGGGCTATGGGGTCCAAGCGCTGAAAGCCGACAACCTTGAGCAGCTCAAGGGTTCGCTACAAGAAGCG
L  S  A  K  G  P  V  L  I  E  V  S  T  V  S  P  V  K  R  S  H  H  H  H  H  H  *
CTTTCTGCCAAAGGCCCGGTACTTATCGAAGTAAGCACCGTAAGCCCGGTGAAGAGATCTCATCACCATCACCATCACTAAGCTTCTAGA
                                                              His-Tag          HindIII
```

TDoT-L-*Ec*LDC

```
   M  I  I  N  E  T  A  D  D  I  V  Y  R  L  T  V  I  I  D  D  R  Y  E  S  L  K  N  L  I
CATATGATCATTAACGAAACTGCCGATGACATCGTTTATCGCCTGACAGTCATTATCGATGATCGCTACGAATCGCTGAAAAACCTGATT
NdeI           TDoT
T  L  R  A  D  R  L  E  M  I  I  N  D  N  V  S  T  I  L  A  S  I  T  S  I  E  G  R  A  S
ACCTTACGTGCAGATCGCTTGGAGATGATCATCAATGACAATGTGTCCACCATTCTCGCGAGCATTACTAGTATTGAAGGCCGTGCTAGC
                                                                  SpeI     Xa       NheI
G  G  G  S  G  G  G  S  G  G  G  S  G  S  M  N  I  I  A  I  M  G  P  H  G  V  F  Y  K  D
GGCGGTGGGTCTGGAGGCGGCTCAGGTGGTGGGTCGGGATCCATGAACATCATCGCTATCATGGGCCCTCACGGTGTTTTCTACAAGGAT
3xGGGS-Linker                  BamHI                    EcLDC
E  P  I  K  E  L  E  S  A  L  V  A  Q  G  F  Q  I  I  W  P  Q  N  S  V  D  L  L  K  F  I
GAGCCAATCAAGGAGCTGGAATCCGCACTAGTTGCACAGGGCTTTCAGATCATCTGGCCCCAGAACTCCGTTGACCTTCTCAAATTCATC
E  H  N  P  R  I  C  G  V  I  F  D  W  D  E  Y  S  L  D  L  C  S  D  I  N  Q  L  N  E  Y
GAGCACAATCCTCGCATTTGTGGTGTGATTTTTGACTGGGACGAGTACTCTCTTGATTTATGCTCCGACATCAACCAGCTCAACGAGTAC
L  P  L  Y  A  F  I  N  T  H  S  T  M  D  V  S  V  Q  D  M  R  M  A  L  W  F  F  E  Y  A
CTGCCACTCTACGCATTCATCAACACTCACTCCACCATGGACGTTTCCGTGCAGGACATGCGTATGGCACTCTGGTTCTTTGAATACGCT
L  G  Q  A  E  D  I  A  I  R  M  R  Q  Y  T  D  E  Y  L  D  N  I  T  P  P  F  T  K  A  L
CTGGGCCAGGCTGAGGACATCGCGATCCGCATGCGTCAGTACACCGACGAGTACCTGGACAACATCACCCCTCCATTCACCAAGGCTCTC
F  T  Y  V  K  E  R  K  Y  T  F  C  T  P  G  H  M  G  G  T  A  Y  Q  K  S  P  V  G  C  L
TTCACCTACGTAAAGGAACGCAAGTACACTTTCTGCACCCCAGGCCACATGGGCGGCACCGCCTACCAGAAGTCCCCAGTCGGATGCCTC
F  Y  D  F  F  G  G  N  T  L  K  A  D  V  S  I  S  V  T  E  L  G  S  L  L  D  H  T  G  P
TTCTACGACTTCTTCGGCGGTAACACTCTTAAGGCAGATGTCTCCATTTCCGTCACCGAGTTGGGCTCTCTGCTGGACCACACCGGCCCT
H  L  E  A  E  E  Y  I  A  R  T  F  G  A  E  Q  S  Y  I  V  T  N  G  T  S  T  S  N  K  I
CACCTGGAGGCAGAAGAGTACATCGCTCGTACCTTCGGTGCTGAACAGTCCTACATCGTCACCAACGGTACTTCCACCAGCAACAAGATC
V  G  M  Y  A  A  P  S  G  S  T  L  L  I  D  R  N  C  H  K  S  L  A  H  L  L  M  M  N  D
GTTGGTATGTACGCAGCTCCTTCTGGCTCCACCCTGTTGATCGACCGCAACTGTCACAAGTCCCTCGCGCATCTTCTTATGATGAACGAT
V  V  P  V  W  L  K  P  T  R  N  A  L  G  I  L  G  G  I  P  R  R  E  F  T  R  D  S  I  E
GTGGTCCCTGTATGGCTGAAGCCAACCCGTAACGCTCTGGGCATCCTTGGCGGTATCCCCCGTCGCGAGTTCACCCGTGATTCCATCGAG
E  K  V  A  A  T  T  Q  A  Q  W  P  V  H  A  V  I  T  N  S  T  Y  D  G  L  L  Y  N  T  D
GAAAAGGTTGCAGCCACTACCCAGGCACAGTGGCCTGTCCACGCTGTCATTACCAACTCGACCTACGACGGCCTGCTCTACAACACCGAT
W  I  K  Q  T  L  D  V  P  S  I  H  F  D  S  A  W  V  P  Y  T  H  F  H  P  I  Y  Q  G  K
TGGATCAAGCAGACCCTAGATGTTCCTTCCATTCACTTCGACAGCGCATGGGTTCCTTACACTCACTTCCACCCAATCTACCAGGGTAAG
S  G  M  S  G  E  R  V  A  G  K  V  I  F  E  T  Q  S  T  H  K  M  L  A  A  L  S  Q  A  S
TCCGGAATGTCCGGCGAGCGTGTCGCTGGCAAGGTTATCTTCGAAACCCAATCAACCCACAAGATGCTGGCTGCTCTCTCCCAGGCTTCT
L  I  H  I  K  G  E  Y  D  E  E  A  F  N  E  A  F  M  M  H  T  T  T  S  P  S  Y  P  I  V
CTGATCCACATCAAGGGCGAGTACGACGAGGAAGCTTTCAACGAGGCTTTCATGATGCACACCACCACCTCCCCATCCTACCCTATCGTC
A  S  V  E  T  A  A  A  M  L  R  G  N  P  G  K  R  L  I  N  R  S  V  E  R  A  L  H  F  R
GCGTCCGTCGAGACTGCTGCCGCAATGCTTCGCGGTAACCCAGGTAAGCGCCTCATCAACCGTTCCGTTGAGCGCGCTCTTCACTTCCGT
K  E  V  Q  R  L  R  E  E  S  D  G  W  F  F  D  I  W  Q  P  P  Q  V  D  E  A  E  C  W  P
AAGGAAGTGCAGCGCCTGCGTGAGGAATCTGACGGTTGGTTCTTCGACATTTGGCAGCCACCTCAGGTTGATGAGGCCGAGTGCTGGCCA
V  A  P  G  E  Q  W  H  G  F  N  D  A  D  A  D  H  M  F  L  D  P  V  K  V  T  I  L  T  P
GTTGCTCCAGGTGAACAGTGGCACGGATTCAACGATGCAGATGCTGACCACATGTTTTTGGACCCGGTCAAGGTCACCATTCTTACTCCT
G  M  D  E  Q  G  N  M  S  E  E  G  I  P  A  A  L  V  A  K  F  L  D  E  R  G  I  V  V  E
GGTATGGATGAGCAGGGCAACATGTCTGAGGAGGGTATCCCAGCTGCTCTGGTTGCAAAGTTCCTCGACGAACGTGGCATCGTTGTTGAG
K  T  G  P  Y  N  L  L  F  L  F  S  I  G  I  D  K  T  K  A  M  G  L  L  R  G  L  T  E  F
AAGACCGGACCATACAACCTGCTGTTCCTGTTCAGCATCGGCATCGACAAAACCAAGGCAATGGGTCTGCTGCGCGGCCTTACCGAGTTC
K  R  S  Y  D  L  N  L  R  I  K  N  M  L  P  D  L  Y  A  E  D  P  D  F  Y  R  N  M  R  I
AAGCGCTCCTACGACCTGAACCTTCGCATCAAGAATATGCTGCCGGACCTGTACGCTGAAGATCCTGATTTCTACCGCAACATGCGCATC
Q  D  L  A  Q  G  I  H  K  L  I  R  K  H  D  L  P  G  L  M  L  R  A  F  D  T  L  P  E  M
CAGGACCTCGCACAGGGCATCCACAAGCTCATTCGCAAGCACGACCTGCCAGGCCTTATGCTCCGTGCATTCGATACCCTCCCAGAGATG
I  M  T  P  H  Q  A  W  Q  R  Q  I  K  G  E  V  E  T  I  A  L  E  Q  L  V  G  R  V  S  A
ATCATGACCCCTCACCAGGCTTGGCAGCGCCAGATCAAGGGCGAGGTGGAAACCATCGCACTGGAGCAGCTGGTTGGTCGTGTCTCCGCC
N  M  I  L  P  Y  P  P  G  V  P  L  L  M  P  G  E  M  L  T  K  E  S  R  T  V  L  D  F  L
AACATGATCCTGCCATATCCACCTGGCGTTCCGCTGCTGATGCCAGGCGAGATGCTCACCAAGGAGTCCCGCACCGTATTGGACTTCCTT
L  M  L  C  S  V  G  Q  H  Y  P  G  F  E  T  D  I  H  G  A  K  Q  D  E  D  G  V  Y  R  V
CTCATGTTGTGCTCTGTTGGCCAGCACTACCCAGGCTTCGAGACCGACATCCACGGCGCTAAGCAAGATGAAGACGGCGTTTACCGCGTT
R  V  L  K  M  A  G  *
CGCGTCCTTAAGATGGCAGGCTAAGTCGACAAGCTTGCGGCCGCACTCGAG
          SalI      NotI     XhoI
```

***Ec*LDC-L-TDoT**

```
.  M  M  N  I  I  A  I  M  G  P  H  G  V  F  Y  K  D  E  P  I  K  E  L  E  S  A  L  V  A
CATATGATGAACATCATCGCTATCATGGGCCCTCACGGTGTTTTCTACAAGGATGAGCCAATCAAGGAGCTGGAATCCGCACTAGTTGCA
NdeI           EcLDC
Q  G  F  Q  I  I  W  P  Q  N  S  V  D  L  L  K  F  I  E  H  N  P  R  I  C  G  V  I  F  D
CAGGGCTTTCAGATCATCTGGCCCCAGAACTCCGTTGACCTTCTCAAATTCATCGAGCACAATCCTCGCATTTGTGGTGTGATTTTTGAC
W  D  E  Y  S  L  D  L  C  S  D  I  N  Q  L  N  E  Y  L  P  L  Y  A  F  I  N  T  H  S  T
TGGGACGAGTACTCTCTTGATTTATGCTCCGACATCAACCAGCTCAACGAGTACCTGCCACTCTACGCATTCATCAACACTCACTCCACC
M  D  V  S  V  Q  D  M  R  M  A  L  W  F  F  E  Y  A  L  G  Q  A  E  D  I  A  I  R  M  R
ATGGACGTTTCCGTGCAGGACATGCGTATGGCACTCTGGTTCTTTGAATACGCTCTGGGCCAGGCTGAGGACATCGCGATCCGCATGCGT
Q  Y  T  D  E  Y  L  D  N  I  T  P  P  F  T  K  A  L  F  T  Y  V  K  E  R  K  Y  T  F  C
CAGTACACCGACGAGTACCTGGACAACATCACCCCTCCATTCACCAAGGCTCTCTTCACCTACGTAAAGGAACGCAAGTACACTTTCTGC
T  P  G  H  M  G  G  T  A  Y  Q  K  S  P  V  G  C  L  F  Y  D  F  F  G  G  N  T  L  K  A
ACCCCAGGCCACATGGGCGGCACCGCCTACCAGAAGTCCCCAGTCGGATGCCTCTTCTACGACTTCTTCGGCGGTAACACTCTTAAGGCA
D  V  S  I  S  V  T  E  L  G  S  L  L  D  H  T  G  P  H  L  E  A  E  E  Y  I  A  R  T  F
GATGTCTCCATTTCCGTCACCGAGTTGGGCTCTCTGCTGGACCACACCGGCCCTCACCTGGAGGCAGAAGAGTACATCGCTCGTACCTTC
G  A  E  Q  S  Y  I  V  T  N  G  T  S  T  S  N  K  I  V  G  M  Y  A  A  P  S  G  S  T  L
GGTGCTGAACAGTCCTACATCGTCACCAACGGTACTTCCACCAGCAACAAGATCGTTGGTATGTACGCAGCTCCTTCTGGCTCCACCCTG
L  I  D  R  N  C  H  K  S  L  A  H  L  L  M  M  N  D  V  V  P  V  W  L  K  P  T  R  N  A
TTGATCGACCGCAACTGTCACAAGTCCCTCGCGCATCTTCTTATGATGAACGATGTGGTCCCTGTATGGCTGAAGCCAACCCGTAACGCT
```

```
L  G  I  L  G  G  I  P  R  R  E  F  T  R  D  S  I  E  E  K  V  A  A  T  T  Q  A  Q  W  P
CTGGGCATCCTTGGCGGTATCCCCCGTCGCGAGTTCACCCGTGATTCCATCGAGGAAAAGGTTGCAGCCACTACCCAGGCACAGTGGCCT
V  H  A  V  I  T  N  S  T  Y  D  G  L  L  Y  N  T  D  W  I  K  Q  T  L  D  V  P  S  I  H
GTCCACGCTGTCATTACCAACTCGACCTACGACGGCCTGCTCTACAACACCGATTGGATCAAGCAGACCCTAGATGTTCCTTCCATTCAC
F  D  S  A  W  V  P  Y  T  H  F  H  P  I  Y  Q  G  K  S  G  M  S  G  E  R  V  A  G  K  V
TTCGACAGCGCATGGGTTCCTTACACTCACTTCCACCCAATCTACCAGGGTAAGTCCGGAATGTCCGGCGAGCGTGTCGCTGGCAAGGTT
I  F  E  T  Q  S  T  H  K  M  L  A  A  L  S  Q  A  S  L  I  H  I  K  G  E  Y  D  E  E  A
ATCTTCGAAACCCAATCAACCCACAAGATGCTGGCTGCTCTCTCCCAGGCTTCTCTGATCCACATCAAGGGCGAGTACGACGAGGAAGCT
F  N  E  A  F  M  M  H  T  T  T  S  P  S  Y  P  I  V  A  S  V  E  T  A  A  A  M  L  R  G
TTCAACGAGGCTTTCATGATGCACACCACCACCTCCCCATCCTACCCTATCGTCGCGTCCGTCGAGACTGCTGCCGCAATGCTTCGCGGT
N  P  G  K  R  L  I  N  R  S  V  E  R  A  L  H  F  R  K  E  V  Q  R  L  R  E  E  S  D  G
AACCCAGGTAAGCGCCTCATCAACCGTTCCGTTGAGCGCGCTCTTCACTTCCGTAAGGAAGTGCAGCGCCTGCGTGAGGAATCTGACGGT
W  F  F  D  I  W  Q  P  P  Q  V  D  E  A  E  C  W  P  V  A  P  G  E  Q  W  H  G  F  N  D
TGGTTCTTCGACATTTGGCAGCCACCTCAGGTTGATGAGGCCGAGTGCTGGCCAGTTGCTCCAGGTGAACAGTGGCACGGATTCAACGAT
A  D  A  D  H  M  F  L  D  P  V  K  V  T  I  L  T  P  G  M  D  E  Q  G  N  M  S  E  E  G
GCAGATGCTGACCACATGTTTTTGGACCCGGTCAAGGTCACCATTCTTACTCCTGGTATGGATGAGCAGGGCAACATGTCTGAGGAGGGT
I  P  A  A  L  V  A  K  F  L  D  E  R  G  I  V  V  E  K  T  G  P  Y  N  L  L  F  L  F  S
ATCCCAGCTGCTCTGGTTGCAAAGTTCCTCGACGAACGTGGCATCGTTGTTGAGAAGACCGGACCATACAACCTGCTGTTCCTGTTCAGC
I  G  I  D  K  T  K  A  M  G  L  L  R  G  L  T  E  F  K  R  S  Y  D  L  N  L  R  I  K  N
ATCGGCATCGACAAAACCAAGGCAATGGGTCTGCTGCGCGGCCTTACCGAGTTCAAGCGCTCCTACGACCTGAACCTTCGCATCAAGAAT
M  L  P  D  L  Y  A  E  D  P  D  F  Y  R  N  M  R  I  Q  D  L  A  Q  G  I  H  K  L  I  R
ATGCTGCCGGACCTGTACGCTGAAGATCCTGATTTCTACCGCAACATGCGCATCCAGGACCTCGCACAGGGCATCCACAAGCTCATTCGC
K  H  D  L  P  G  L  M  L  R  A  F  D  T  L  P  E  M  I  M  T  P  H  Q  A  W  Q  R  Q  I
AAGCACGACCTGCCAGGCCTTATGCTCCGTGCATTCGATACCCTCCCAGAGATGATCATGACCCCTCACCAGGCTTGGCAGCGCCAGATC
K  G  E  V  E  T  I  A  L  E  Q  L  V  G  R  V  S  A  N  M  I  L  P  Y  P  P  G  V  P  L
AAGGGCGAGGTGGAAACCATCGCACTGGAGCAGCTGGTTGGTCGTGTCTCCGCCAACATGATCCTGCCATATCCACCTGGCGTTCCGCTG
L  M  P  G  E  M  L  T  K  E  S  R  T  V  L  D  F  L  L  M  L  C  S  V  G  Q  H  Y  P  G
CTGATGCCAGGCGAGATGCTCACCAAGGAGTCCCGCACCGTATTGGACTTCCTTCTCATGTTGTGCTCTGTTGGCCAGCACTACCCAGGC
F  E  T  D  I  H  G  A  K  Q  D  E  D  G  V  Y  R  V  R  V  L  K  M  A  G  A  S  G  G  G
TTCGAGACCGACATCCACGGCGCTAAGCAAGATGAAGACGGCGTTTACCGCGTTCGCGTCCTTAAGATGGCAGGCGCTAGCGGCGGTGGG
                                                                        NheI
S  G  G  G  S  G  G  G  S  G  S  I  I  N  E  T  A  D  D  I  V  Y  R  L  T  V  I  I  D  D
TCTGGAGGCGGCTCAGGTGGTGGGTCGGGATCCATCATTAACGAAACTGCCGATGACATCGTTTATCGCCTGACAGTCATTATCGATGAT
3xGGGS-Linker                  BamHI          TDoT
R  Y  E  S  L  K  N  L  I  T  L  R  A  D  R  L  E  M  I  I  N  D  N  V  S  T  I  L  A  S
CGCTACGAATCGCTGAAAAACCTGATTACCTTACGTGCAGATCGCTTGGAGATGATCATCAATGACAATGTGTCCACCATTCTCGCGAGC
I  *
ATTTAAGCGGCCGCACTCGAG
      NotI     XhoI
```

*Ec*LDC-L-3HAMP

```
.  M  M  N  I  I  A  I  M  G  P  H  G  V  F  Y  K  D  E  P  I  K  E  L  E  S  A  L  V  A
CATATGATGAACATCATCGCTATCATGGGCCCTCACGGTGTTTTCTACAAGGATGAGCCAATCAAGGAGCTGGAATCCGCACTAGTTGCA
NdeI          EcLDC
Q  G  F  Q  I  I  W  P  Q  N  S  V  D  L  L  K  F  I  E  H  N  P  R  I  C  G  V  I  F  D
CAGGGCTTTCAGATCATCTGGCCCCAGAACTCCGTTGACCTTCTCAAATTCATCGAGCACAATCCTCGCATTTGTGGTGTGATTTTTGAC
W  D  E  Y  S  L  D  L  C  S  D  I  N  Q  L  N  E  Y  L  P  L  Y  A  F  I  N  T  H  S  T
TGGGACGAGTACTCTCTTGATTTATGCTCCGACATCAACCAGCTCAACGAGTACCTGCCACTCTACGCATTCATCAACACTCACTCCACC
M  D  V  S  V  Q  D  M  R  M  A  L  W  F  F  E  Y  A  L  G  Q  A  E  D  I  A  I  R  M  R
ATGGACGTTTCCGTGCAGGACATGCGTATGGCACTCTGGTTCTTTGAATACGCTCTGGGCCAGGCTGAGGACATCGCGATCCGCATGCGT
Q  Y  T  D  E  Y  L  D  N  I  T  P  P  F  T  K  A  L  F  T  Y  V  K  E  R  K  Y  T  F  C
CAGTACACCGACGAGTACCTGGACAACATCACCCCTCCATTCACCAAGGCTCTCTTCACCTACGTAAAGGAACGCAAGTACACTTTCTGC
T  P  G  H  M  G  G  T  A  Y  Q  K  S  P  V  G  C  L  F  Y  D  F  F  G  G  N  T  L  K  A
ACCCCAGGCCACATGGGCGGCACCGCCTACCAGAAGTCCCCAGTCGGATGCCTCTTCTACGACTTCTTCGGCGGTAACACTCTTAAGGCA
D  V  S  I  S  V  T  E  L  G  S  L  L  D  H  T  G  P  H  L  E  A  E  E  Y  I  A  R  T  F
GATGTCTCCATTTCCGTCACCGAGTTGGGCTCTCTGCTGGACCACACCGGCCCTCACCTGGAGGCAGAAGAGTACATCGCTCGTACCTTC
G  A  E  Q  S  Y  I  V  T  N  G  T  S  T  S  N  K  I  V  G  M  Y  A  A  P  S  G  S  T  L
GGTGCTGAACAGTCCTACATCGTCACCAACGGTACTTCCACCAGCAACAAGATCGTTGGTATGTACGCAGCTCCTTCTGGCTCCACCCTG
L  I  D  R  N  C  H  K  S  L  A  H  L  L  M  M  N  D  V  V  P  V  W  L  K  P  T  R  N  A
TTGATCGACCGCAACTGTCACAAGTCCCTCGCGCATCTTCTTATGATGAACGATGTGGTCCCTGTATGGCTGAAGCCAACCCGTAACGCT
L  G  I  L  G  G  I  P  R  R  E  F  T  R  D  S  I  E  E  K  V  A  A  T  T  Q  A  Q  W  P
CTGGGCATCCTTGGCGGTATCCCCCGTCGCGAGTTCACCCGTGATTCCATCGAGGAAAAGGTTGCAGCCACTACCCAGGCACAGTGGCCT
V  H  A  V  I  T  N  S  T  Y  D  G  L  L  Y  N  T  D  W  I  K  Q  T  L  D  V  P  S  I  H
GTCCACGCTGTCATTACCAACTCGACCTACGACGGCCTGCTCTACAACACCGATTGGATCAAGCAGACCCTAGATGTTCCTTCCATTCAC
F  D  S  A  W  V  P  Y  T  H  F  H  P  I  Y  Q  G  K  S  G  M  S  G  E  R  V  A  G  K  V
TTCGACAGCGCATGGGTTCCTTACACTCACTTCCACCCAATCTACCAGGGTAAGTCCGGAATGTCCGGCGAGCGTGTCGCTGGCAAGGTT
I  F  E  T  Q  S  T  H  K  M  L  A  A  L  S  Q  A  S  L  I  H  I  K  G  E  Y  D  E  E  A
ATCTTCGAAACCCAATCAACCCACAAGATGCTGGCTGCTCTCTCCCAGGCTTCTCTGATCCACATCAAGGGCGAGTACGACGAGGAAGCT
F  N  E  A  F  M  M  H  T  T  T  S  P  S  Y  P  I  V  A  S  V  E  T  A  A  A  M  L  R  G
TTCAACGAGGCTTTCATGATGCACACCACCACCTCCCCATCCTACCCTATCGTCGCGTCCGTCGAGACTGCTGCCGCAATGCTTCGCGGT
N  P  G  K  R  L  I  N  R  S  V  E  R  A  L  H  F  R  K  E  V  Q  R  L  R  E  E  S  D  G
AACCCAGGTAAGCGCCTCATCAACCGTTCCGTTGAGCGCGCTCTTCACTTCCGTAAGGAAGTGCAGCGCCTGCGTGAGGAATCTGACGGT
W  F  F  D  I  W  Q  P  P  Q  V  D  E  A  E  C  W  P  V  A  P  G  E  Q  W  H  G  F  N  D
TGGTTCTTCGACATTTGGCAGCCACCTCAGGTTGATGAGGCCGAGTGCTGGCCAGTTGCTCCAGGTGAACAGTGGCACGGATTCAACGAT
A  D  A  D  H  M  F  L  D  P  V  K  V  T  I  L  T  P  G  M  D  E  Q  G  N  M  S  E  E  G
GCAGATGCTGACCACATGTTTTTGGACCCGGTCAAGGTCACCATTCTTACTCCTGGTATGGATGAGCAGGGCAACATGTCTGAGGAGGGT
I  P  A  A  L  V  A  K  F  L  D  E  R  G  I  V  V  E  K  T  G  P  Y  N  L  L  F  L  F  S
ATCCCAGCTGCTCTGGTTGCAAAGTTCCTCGACGAACGTGGCATCGTTGTTGAGAAGACCGGACCATACAACCTGCTGTTCCTGTTCAGC
I  G  I  D  K  T  K  A  M  G  L  L  R  G  L  T  E  F  K  R  S  Y  D  L  N  L  R  I  K  N
ATCGGCATCGACAAAACCAAGGCAATGGGTCTGCTGCGCGGCCTTACCGAGTTCAAGCGCTCCTACGACCTGAACCTTCGCATCAAGAAT
```

```
M  L  P  D  L  Y  A  E  D  P  D  F  Y  R  N  M  R  I  Q  D  L  A  Q  G  I  H  K  L  I  R
ATGCTGCCGGACCTGTACGCTGAAGATCCTGATTTCTACCGCAACATGCGCATCCAGGACCTCGCACAGGGCATCCACAAGCTCATTCGC
K  H  D  L  P  G  L  M  L  R  A  F  D  T  L  P  E  M  I  M  T  P  H  Q  A  W  Q  R  Q  I
AAGCACGACCTGCCAGGCCTTATGCTCCGTGCATTCGATACCCTCCCAGAGATGATCATGACCCCTCACCAGGCTTGGCAGCGCCAGATC
K  G  E  V  E  T  I  A  L  E  Q  L  V  G  R  V  S  A  N  M  I  L  P  Y  P  P  G  V  P  L
AAGGGCGAGGTGGAAACCATCGCACTGGAGCAGCTGGTTGGTCGTGTCTCCGCCAACATGATCCTGCCATATCCACCTGGCGTTCCGCTG
L  M  P  G  E  M  L  T  K  E  S  R  T  V  L  D  F  L  L  M  L  C  S  V  G  Q  H  Y  P  G
CTGATGCCAGGCGAGATGCTCACCAAGGAGTCCCGCACCGTATTGGACTTCCTTCTCATGTTGTGCTCTGTTGGCCAGCACTACCCAGGC
F  E  T  D  I  H  G  A  K  Q  D  E  D  G  V  Y  R  V  R  V  L  K  M  A  G  A  S  G  G  G
TTCGAGACCGACATCCACGGCGCTAAGCAAGATGAAGACGGCGTTTACCGCGTTCGCGTCCTTAAGATGGCAGGCGCTAGCGGCGGTGGG
                                                                        NheI
S  G  G  G  S  G  G  G  S  G  S  M  G  L  F  N  A  H  A  V  A  Q  Q  R  A  D  R  I  A  T
TCTGGAGGCGGCTCAGGTGGTGGGTCGGGATCCATGGGCCTGTTTAACGCCCATGCAGTTGCGCAGCAACGCGCGGATCGCATTGCGACT
   3xGGGS-Linker                    BamHI                3HAMP
L  L  Q  S  F  A  D  G  Q  L  D  T  A  V  G  E  A  P  A  P  G  Y  E  R  L  Y  D  S  L  R
CTCCTGCAGTCCTTTGCGGATGGTCAGTTGGACACCGCCGTGGGTGAAGCGCCAGCACCTGGTTACGAACGCCTGTATGACTCGCTTCGC
A  L  Q  R  Q  L  R  E  Q  R  A  E  L  Q  Q  V  E  S  L  E  A  G  L  A  E  M  S  R  Q  H
GCCCTTCAGCGCCAACTGCGCGAACAACGTGCGGAGTTACAACAGGTTGAGAGCCTGGAAGCAGGCTTGGCTGAAATGAGTCGGCAGCAT
E  A  G  W  I  D  Q  T  I  P  A  E  R  L  E  G  R  A  A  R  I  A  K  G  V  N  E  L  V  A
GAAGCAGGGTGGATTGACCAGACGATTCCGGCTGAACGGTTAGAGGGCCGTGCAGCACGTATCGCCAAAGGCGTGAATGAGCTGGTTGCT
A  H  I  A  V  K  M  K  V  V  S  V  V  T  A  Y  G  Q  G  N  F  E  P  L  M  D  R  L  P  G
GCGCACATTGCGGTGAAAATGAAAGTCGTGAGCGTAGTCACCGCGTATGGCCAAGGGAACTTCGAACCGCTCATGGATCGCCTGCCGGGT
K  K  A  Q  I  T  E  A  I  D  G  V  R  E  R  L  R  G  A  A  E  A  T  S  A  Q  L  A  T  A
AAGAAAGCCCAGATCACGGAGGCCATTGATGGCGTACGTGAACGCCTGCGTGGAGCTGCTGAAGCGACCTCTGCGCAGCTGGCCACAGCC
A  Y  N  *
GCCTACAATTAAGCGGCCGCACTCGAG
            NotI    XhoI
```

6 Chapter 6

Acknowledgement

I have put a lot of thought into this.
The outcome is what I would normally call 'cheesy'.
But on this one special occasion, I feel it is justified.

Thanks to the Chiefs

First of all, I would like to thank Prof. Dr. Karl-Erich Jaeger for giving me the opportunity of a doctoral thesis, for providing me with this appealing and interesting topic, and also for welcoming me in the IMET where, all-in-all, I had a pretty good time.

Furthermore, I am grateful to Prof. Dr. Martina Pohl, not only for the acceptance as co-referee, but even more for all her helpful advice in numerous meetings and all the concern she put in our CatIBs-project.

By far, the biggest gratitude goes to Dr. Ulrich Krauss. He is one of the most intelligent and most chilled people I have yet met. His kind guidance over almost four years was equally both supporting and demanding. By encountering his protégés on eye level and his fatherly concerns he achieves authority without even noticing. For me he has become an awe-inspiring role model, which I think, embarrasses him, whenever he notices. Anyway, having a boss who looks like a pirate is simply awesome.

Thanks to the Institute

Colleagues are most important for an enjoyable work-space. Therefore, I am very lucky that I had not only colleagues, but also friends at work. Judith, Timo, Katrin, and I made a great team. Timo supplied the whole Institute with Döner and taught me American Football, Katrin is the best motivation trainer, and Judith even became a roommate. Since they all left by now, I fervently hope, that our friendship can survive beyond the 'Biophotonics' group. Fortunately for me, Jenny was still in the Lab and with her reserved vigour she brightened a lot of gruelling days.

Through the long years of lab experience, technicians become strolling libraries of know-how and deserve to be decently acknowledged. Here, I want to thank Maja and Ester who taught me more than they know. I was competently supported and sometimes motherly shepherded, which felt surprisingly comfortable.

At this point I must not forget all the students I had over the years. Above all they taught me patience, serenity, and yes, anger management. This is not meant to sound fretful at all. Instead I think, that apart from endurance and persistence, these are the most important soft-skills I learned as a doctoral student. Anyway, especially with my long-term students Stefanie and Michael, who, incidentally, did a lot of work for me, I had a good time and a lot of fun as well. And while they were good students, I hope, I could proof to be a good teacher as well.

Thanks to the Project Partners

At first, I want to put a big thanks to Ramona Kloss, my 'Inclusion-Buddy'. She not only made my start in Jülich much funnier. Over the years we brewed beer, dressed as Vikings, and haunted the streets of Budapest. It is a good thing when project partners become friends.

Furthermore, I thank Robin Lamm, the third doctoral student in our CatIBs-project, as well as Prof. Dr. Jochen Büchs for the great cooperation and the helpful meetings we had over the years.

For their recurring help with fluorescence microscopy pictures and videos and especially for the further processing of those, I thank Prof. Dr. Alexander Grünberger and Eugen Kaganovitch of the 'Microscale Bioengineering' group at the IBG-1.

Further I want to thank the technicians of the 'Catalysis' group of the IBG-1 for all the assistance they gave me in the implementation of the cascade reaction. Without their unremitting help with laboratory equipment and the HPLC, I would have gotten much more grey hair than I actually did.

And also, thanks to Steffen Köhler, from the Center for Advanced Imaging (CAi) at the Heinrich-Heine University Düsseldorf, who did his best, to take high resolution SEM-images, while constructions where performed next door.

Thanks to my Family and Friends

To my mother, who made me wonder about the universe when I was a little girl and to my father, who I am proud to call the oldest punk in the world.

And to Lisa. Having a big sister and a friend in personal union is a rare gift. She is my Madita and I am her Pims. Come what may, I know she will always look out for me.

And to Arthur. To use a chemical term, I would call him my buffer. Whatever side I kick out, he grounds me. He puts up with all my craziness and still sees more goodness in me, than I ever will. So I have no choice, but to become a better version of myself.

Finally, I want to thank Aster, Smret, Ruta, Saba, and Weghata for proving that friendship can overcome any border. And Karola, Ute, Max, and all my other friends. They taught me that quality means infinite more than quantity. Over the years, they stood by me through some pretty rough times. And day by day they endorse my trust in friendship.



7 Chapter 7
Erklärung

Hiermit versichere ich an Eides Statt, dass die vorgelegte Dissertation von mir selbstständig und ohne unzulässige fremde Hilfe unter Beachtung der „Grundsätze zur Sicherung guter wissenschaftlicher Praxis an der Heinrich-Heine-Universität“ erstellt worden ist. Wörtliche wie inhaltliche Zitate wurden vollständig als solche kenntlich gemacht.

Die vorgelegte Dissertation wurde in dieser oder in ähnlicher Form noch bei keiner anderen Institution eingereicht. Bisher habe ich keine erfolglosen Promotionsversuche unternommen.

Ort, Datum

Vera D. Jäger